SUMMARY TECHNICAL REPORT
OF THE
NATIONAL DEFENSE RESEARCH COMMITTEE

This document contains information affecting the national defense of the United States within the meaning of the Espionage Act, 50 U.S.C., 31 and 32, as amended. Its transmission or the revelation of its contents in any manner to an unauthorized person is prohibited by law.

This volume is classified RESTRICTED in accordance with security regulations of the War and Navy Departments because certain chapters contain material which was RESTRICTED at the date of printing. Other chapters may have had a lower classification or none. The reader is advised to consult the War and Navy agencies listed on the reverse of this page for the current classification of any material.

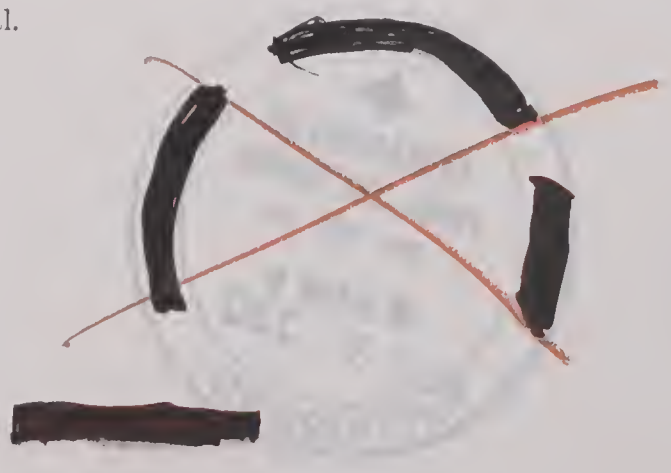

Manuscript and illustrations for this volume were prepared for publication by the Summary Reports Group of the Columbia University Division of War Research under contract OEMsr-1131 with the Office of Scientific Research and Development. This volume was printed and bound by the Columbia University Press.

This volume, like the seventy others of the Summary Technical Report of NDRC, has been written, edited, and printed under great pressure. Inevitably there are errors which have slipped past Division readers and proofreaders. There may be errors of fact not known at time of printing. The author has not been able to follow through his writing to the final page proof.

Please report errors to:

JOINT RESEARCH AND DEVELOPMENT BOARD
PROGRAMS DIVISION (STR ERRATA)
WASHINGTON 25, D. C.

A master errata sheet will be compiled from these reports and sent to recipients of the volume. Your help will make this book more useful to other readers and will be of great value in preparing any revisions.

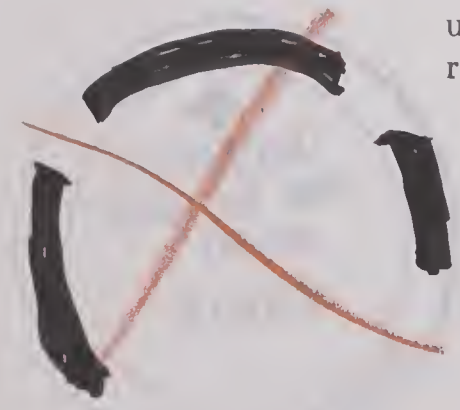

SUMMARY TECHNICAL REPORT OF DIVISION 4, NDRC

VOLUME 2

BOMB, ROCKET, AND TORPEDO TOSSING

OFFICE OF SCIENTIFIC RESEARCH AND DEVELOPMENT
VANNEVAR BUSH, DIRECTOR

NATIONAL DEFENSE RESEARCH COMMITTEE
JAMES B. CONANT, CHAIRMAN

DIVISION 4
ALEXANDER ELLETT, CHIEF

WASHINGTON, D. C., 1946

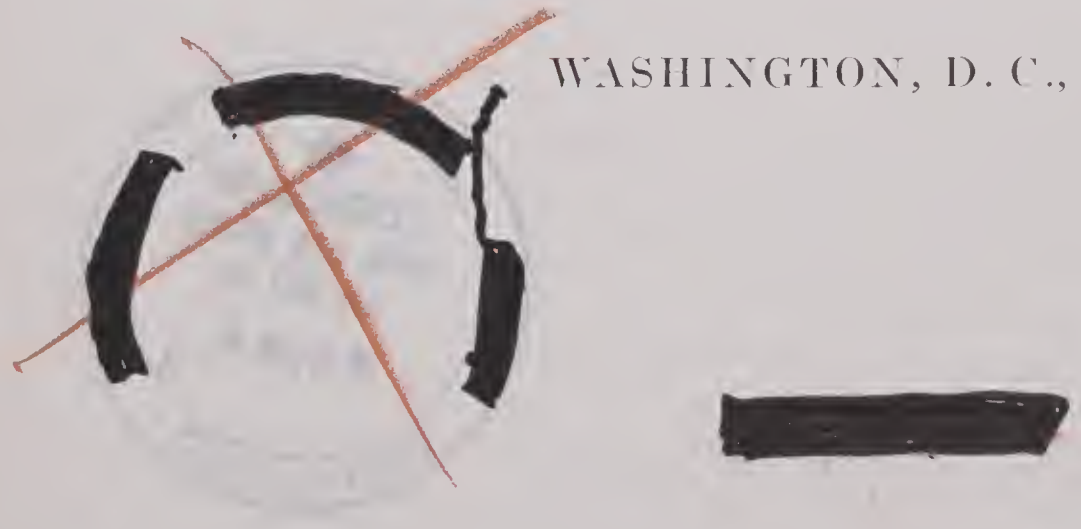

NATIONAL DEFENSE RESEARCH COMMITTEE

James B. Conant, *Chairman*

Richard C. Tolman, *Vice Chairman*

Roger Adams	Army Representative [1]
Frank B. Jewett	Navy Representative [2]
Karl T. Compton	Commissioner of Patents [3]

Irvin Stewart, *Executive Secretary*

[1] *Army representatives in order of service:*

Maj. Gen. G. V. Strong — Col. L. A. Denson
Maj. Gen. R. C. Moore — Col. P. R. Faymonville
Maj. Gen. C. C. Williams — Brig. Gen. E. A. Regnier
Brig. Gen. W. A. Wood, Jr. — Col. M. M. Irvine
Col. E. A. Routheau

[2] *Navy representatives in order of service:*

Rear Adm. H. G. Bowen — Rear Adm. J. A. Furer
Capt. Lybrand P. Smith — Rear Adm. A. H. Van Keuren
Commodore H. A. Schade

[3] *Commissioners of Patents in order of service:*

Conway P. Coe — Casper W. Ooms

NOTES ON THE ORGANIZATION OF NDRC

The duties of the National Defense Research Committee were (1) to recommend to the Director of OSRD suitable projects and research programs on the instrumentalities of warfare, together with contract facilities for carrying out these projects and programs, and (2) to administer the technical and scientific work of the contracts. More specifically, NDRC functioned by initiating research projects on requests from the Army or the Navy, or on requests from an allied government transmitted through the Liaison Office of OSRD, or on its own considered initiative as a result of the experience of its members. Proposals prepared by the Division, Panel, or Committee for research contracts for performance of the work involved in such projects were first reviewed by NDRC, and if approved, recommended to the Director of OSRD. Upon approval of a proposal by the Director, a contract permitting maximum flexibility of scientific effort was arranged. The business aspects of the contract, including such matters as materials, clearances, vouchers, patents, priorities, legal matters, and administration of patent matters were handled by the Executive Secretary of OSRD.

Originally NDRC administered its work through five divisions, each headed by one of the NDRC members. These were:

Division A — Armor and Ordnance
Division B — Bombs, Fuels, Gases, & Chemical Problems
Division C — Communication and Transportation
Division D — Detection, Controls, and Instruments
Division E — Patents and Inventions

In a reorganization in the fall of 1942, twenty-three administrative divisions, panels, or committees were created, each with a chief selected on the basis of his outstanding work in the particular field. The NDRC members then became a reviewing and advisory group to the Director of OSRD. The final organization was as follows:

Division 1 — Ballistic Research
Division 2 — Effects of Impact and Explosion
Division 3 — Rocket Ordnance
Division 4 — Ordnance Accessories
Division 5 — New Missiles
Division 6 — Sub-Surface Warfare
Division 7 — Fire Control
Division 8 — Explosives
Division 9 — Chemistry
Division 10 — Absorbents and Aerosols
Division 11 — Chemical Engineering
Division 12 — Transportation
Division 13 — Electrical Communication
Division 14 — Radar
Division 15 — Radio Coordination
Division 16 — Optics and Camouflage
Division 17 — Physics
Division 18 — War Metallurgy
Division 19 — Miscellaneous
Applied Mathematics Panel
Applied Psychology Panel
Committee on Propagation
Tropical Deterioration Administrative Committee

NDRC FOREWORD

As events of the years preceding 1940 revealed more and more clearly the seriousness of the world situation, many scientists in this country came to realize the need of organizing scientific research for service in a national emergency. Recommendations which they made to the White House were given careful and sympathetic attention, and as a result the National Defense Research Committee [NDRC] was formed by Executive Order of the President in the summer of 1940. The members of NDRC, appointed by the President, were instructed to supplement the work of the Army and the Navy in the development of the instrumentalities of war. A year later, upon the establishment of the Office of Scientific Research and Development [OSRD], NDRC became one of its units.

The Summary Technical Report of NDRC is a conscientious effort on the part of NDRC to summarize and evaluate its work and to present it in a useful and permanent form. It comprises some seventy volumes broken into groups corresponding to the NDRC Divisions, Panels, and Committees.

The Summary Technical Report of each Division, Panel, or Committee is an integral survey of the work of that group. The report of each group contains a summary of the report, stating the problems presented and the philosophy of attacking them, and summarizing the results of the research, development, and training activities undertaken. Some volumes may be "state of the art" treatises covering subjects to which various research groups have contributed information. Others may contain descriptions of devices developed in the laboratories. A master index of all these divisional, panel, and committee reports which together constitute the Summary Technical Report of NDRC is contained in a separate volume, which also includes the index of a microfilm record of pertinent technical laboratory reports and reference material.

Some of the NDRC-sponsored researches which had been declassified by the end of 1945 were of sufficient popular interest that it was found desirable to report them in the form of monographs, such as the series on radar by Division 14 and the monograph on sampling inspection by the Applied Mathematics Panel. Since the material treated in them is not duplicated in the Summary Technical Report of NDRC, the monographs are an important part of the story of these aspects of NDRC research.

In contrast to the information on radar, which is of widespread interest and much of which is released to the public, the research on subsurface warfare is largely classified and is of general interest to a more restricted group. As a consequence, the report of Division 6 is found almost entirely in its Summary Technical Report, which runs to over twenty volumes. The extent of the work of a Division cannot therefore be judged solely by the number of volumes devoted to it in the Summary Technical Report of NDRC; account must be taken of the monographs and available reports published elsewhere.

The program of Division 4 in the field of electronic ordnance provides an excellent example of the manner in which research and development work by a civilian technical group can complement and supplement work done by the Armed Services. The greatest responsibility of Division 4, under the leadership of Alexander Ellett, was to undertake the development of proximity fuzes for nonrotating or fin-stabilized missiles, such as bombs, rockets, and mortar shells.

Early work on fuzes of various types indicated that those operating through the use of electromagnetic waves offered the most promise; the eventual device depended on the doppler effect, combining the transmitted and received signals to create a low frequency beat which triggered an electronic switch. During the last phases of the war against Japan, approximately one-third of all the bomb fuzes used by carrier-based aircraft were proximity fuzes. For improving the accuracy of bombing operations the Division developed the toss bombing technique, by which the effect of gravity on the flight path of the missile is estimated and allowed for. The success of this technique is demonstrated by its combat use, when a circle of probable error as low as 150 feet was obtained.

The Summary Technical Report of Division 4 was prepared under the direction of the Division Chief and has been authorized by him for publication. We wish to pay tribute to the enterprise and energy of the members of the Division, who worked so devotedly for its success.

Vannevar Bush, Director
Office of Scientific Research and Development

J. B. Conant, Chairman
National Defense Research Committee

FOREWORD

The attempt to get proximity fuzed projectiles into air-to-air combat was responsible for the development of toss bombing. This technique arose out of conversations between Colonel H. S. Morton of the Army Ordnance Department and the Chief of Division 4 in January 1943. That these discussions ultimately led to the evolution of a successful technique is due very largely to Colonel Morton's enthusiastic and effective support during the early stages of the development. Through the cooperation of the Ordnance Department, planes and testing facilities were made available at Aberdeen at a time when toss bombing was merely an idea. Without the assistance of the Ordnance Department throughout the early and often disappointing trials with breadboard equipment, the technique could not have been developed to a useful form.

When the development had progressed to such a state that the feasibility of the technique was fairly evident, the Army Air Forces and later the Navy offered cooperation. Testing in connection with pilot production and production models was carried out very largely under Navy auspices at Patuxent and Inyokern. Much credit is due to personnel of both these stations for enthusiastic and effective cooperation.

Development of equipment for toss bombing was carried on in the Division's Central Laboratory at the National Bureau of Standards and at the State University of Iowa. The personnel primarily responsible were William B. McLean, J. Rabinow, W. L. Whitson, and W. S. Hinman, Jr., of the National Bureau of Standards and James A. Jacobs and I. H. Swift of the University of Iowa.

Alexander Ellett

Chief, Division 4

PREFACE

This volume of the Division 4 Summary Technical Report covers work done on the development and evaluation of equipment for tossing bombs, rockets, and torpedoes.

The toss technique was conceived and initiated by Colonel Harold S. Morton, of the Army Ordnance Department, and by Dr. Alexander Ellett, Chief of Division 4. The principle of the toss technique is explained in the introduction to the volume, Chapter 1. The introduction also includes a brief summary of the achievements of the program.

A simplified theory of the toss technique is given in Chapter 2, including the principle of instrumentation. A description of the equipment designed and produced is given in Chapter 3, "Instrumentation."

Considerable space is devoted to describing the early experimental models, which are now obsolete. These descriptions are included primarily because almost all of the evaluation studies which were made on the equipment were carried out with experimental models. Production models, which incorporated a number of desirable improvements, were not available until just before the end of the war, at which time Division 4 transferred sponsorship of the project to the Navy.

The problems of installation and maintenance of the equipment in aircraft under Service conditions are presented in Chapter 4.

A summary of the evaluation tests on bomb, rocket, and torpedo tossing is given in Chapter 5.

The theoretical formulation of the toss technique is presented in some detail in Chapters 6 and 7, supplementing Chapter 2. Inclusion of this material is considered important in providing a basis for future work.

The newest ideas for tossing equipment, some of which have not reached the stage of development where they could be evaluated by field tests, are included in Chapter 8.

This volume is based to a very appreciable extent on a comprehensive summary prepared jointly by members of Division 4's central laboratories, the Ordnance Development Division at the National Bureau of Standards, and of the State University of Iowa under the editorship of A. G. Hoyem, formerly of the latter institution and now at the Naval Ordnance Test Station, Inyokern, California, and of Francis B. Silsbee, of the National Bureau of Standards. The material from that summary has been appreciably revised and rearranged for the purposes of this volume. In this process, invaluable assistance was rendered by Emma U. Rotor, of the National Bureau of Standards, and William B. McLean, formerly of the National Bureau of Standards and now at the Naval Ordnance Test Station, Inyokern, California. The authors of the separate chapters are named in the table of contents and as footnotes to the chapter and section headings. Where authorship is not specifically indicated, the material was prepared jointly by one or more of the aforementioned and the editor.

Art work in the volume, unless credit is otherwise indicated, was prepared by Theodore C. Hellmers, photographer for Division 4's central laboratories, and E. W. Hunt and his staff of draftsmen at the National Bureau of Standards. The Bibliography was compiled and checked by Mrs. Rotor and Catherine Pike.

Very appreciable credit for this volume is due Mrs. Rotor not only for the contributions mentioned above but also for her diligent supervision of the review and assembly of the final manuscript. In the latter work she was given able and generous assistance by S. H. Lackenbruch, R. L. Eichberg, and Betty Hallman.

A. V. Astin

Editor

CONTENTS

Frontispiece

Strike photograph of the first combat mission using the toss-bomb technique. The target was a stores depot in Germany; the aiming point was the center of the quadrangle formed by the four rectangular buildings within the circle. Of twelve 500-pound bombs dropped, six struck within 125 feet of the aiming point and the maximum displacement was 310 feet. (Army Air Force photograph.)

Chapter 1

INTRODUCTION

1.1 THE DIVE-TOSS TECHNIQUE

TOSS BOMBING provides a method of improving the accuracy of bombing operations. The method can be used with bombs, rockets, and torpedoes, and although applicable primarily to dive attacks, it is also effective in level, plane-to-plane attacks. In fact, the method can be employed wherever a collision course with the target can be flown for a short period prior to release of the missile. The object of the toss technique is to estimate and allow for the effect of gravity on the flight path of the missile. The latter is accomplished by releasing the missile from the aircraft with sufficient upward velocity above a line of sight to compensate for the gravity drop of the missile during its flight to the target. The release conditions are determined by an instrument which measures the time integral of the transverse acceleration of the aircraft during a pull-out above the line of sight and then releases the missile when this integral has reached the appropriate value as required by the time-of-flight of the missile. The time-of-flight is computed by the instrument prior to pull-out, while the aircraft is flying a collision course toward the target.

A typical toss bombing attack is illustrated in Figure 1. The airplane enters a dive 2,000 to 5,000 feet above the point at which the projectile will be released and attains speed as rapidly as feasible during this dive. When the speed has reached a value sufficiently high for operation, and with the sight properly oriented on the target, the normal bomb release switch is closed by the pilot. Two or three seconds after the beginning of the timing run, a light near the sight comes on, indicating that the pilot may commence pulling out of the dive. When the angle through which the airplane has pulled up reaches the proper size, as determined automatically by the instrument, the release of the missile occurs. At this instant, the signal light goes out, indicating to the pilot that release has occurred and that thereafter he can employ any evasive action he desires.

If, after the timing run has begun, the pilot decides not to complete the maneuver, the action of the instrument can be stopped by merely opening the bomb release switch. This restores the electrical circuits to a standby condition. The equipment can be made operative again, even in the same dive, remaining altitude and other conditions permitting, by closing again the bomb release switch.

The development of the toss bombing instrument was originally undertaken as a means of attacking bomber formations by using fighter airplanes carrying bombs. It was initially planned to use a head-on approach with high closing speeds and relatively small gravity drops of the bombs after release. The development was carried far enough to demonstrate that the technique offered excellent advantages as a defensive weapon against formations of bombers (see Chapter 6; also reference 265). However, in view of the rapidly increasing scale of the Allied air offensive at that time (late summer of 1943), the weapon was considered potentially more dangerous to Allied than to enemy operations. Work on the

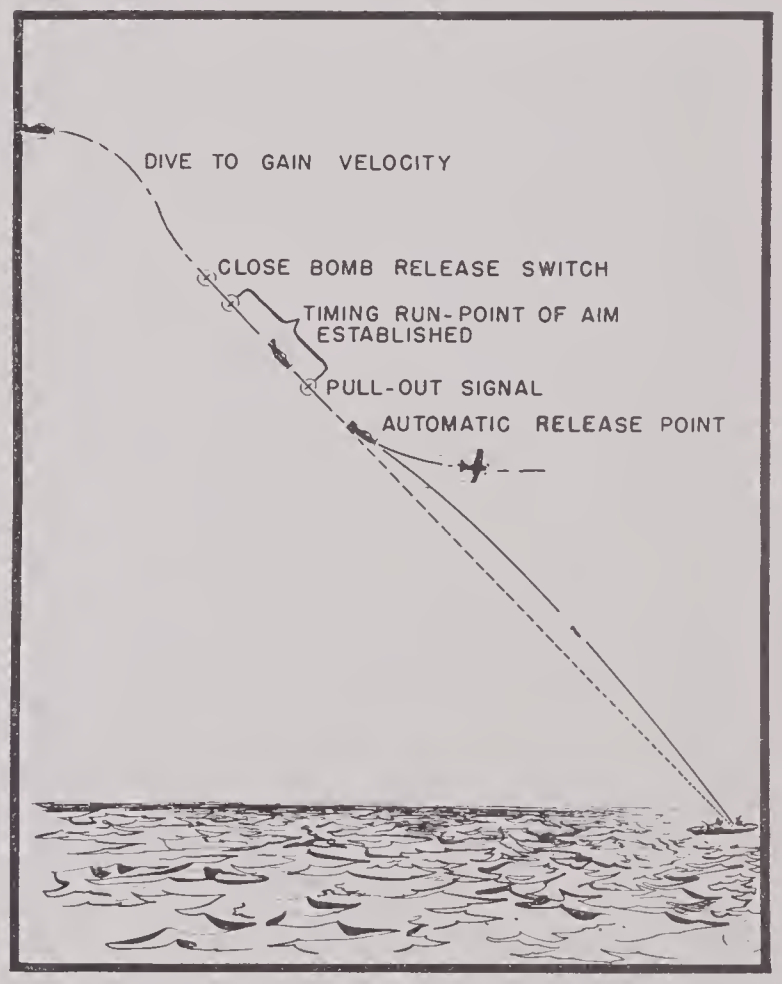

FIGURE 1. Typical toss bombing maneuver.

air-to-air portion of the project was therefore curtailed, and further development was directed toward applying the toss technique to dive bombing.

1.2 COMPARISON WITH ORDINARY DIVE BOMBING

The difference between the toss bombing technique and ordinary (depressed sight) dive bombing is shown schematically in Figure 2. In a dive bombing attack (Figure 2A), the airplane is flown in a line AB passing over the target, and the bomb is released manually by the pilot at a point A, which, in his judgment, is so related to the speed, dive angle, and range, that the gravity drop will carry it down to the target. In a toss bombing attack (Figure 2B), the plane first dives directly at the target to give the automatic computer the necessary data. It then pulls out of the dive with the bank indicator centered, and when the angle BAT attains the necessary size, as determined by the automatic computer, the latter causes the release of the bomb. The same method is used in torpedo and rocket tossing.

With the use of the toss technique, much less skill is required of the pilot. No visibility below the nose of the plane is needed, the range at which a given accuracy can be attained is much greater, the time during which the airplane flies a predetermined course is very short (usually about three seconds), and the pull-up preceding release constitutes an effective preliminary for evasive maneuvers should they be necessary.

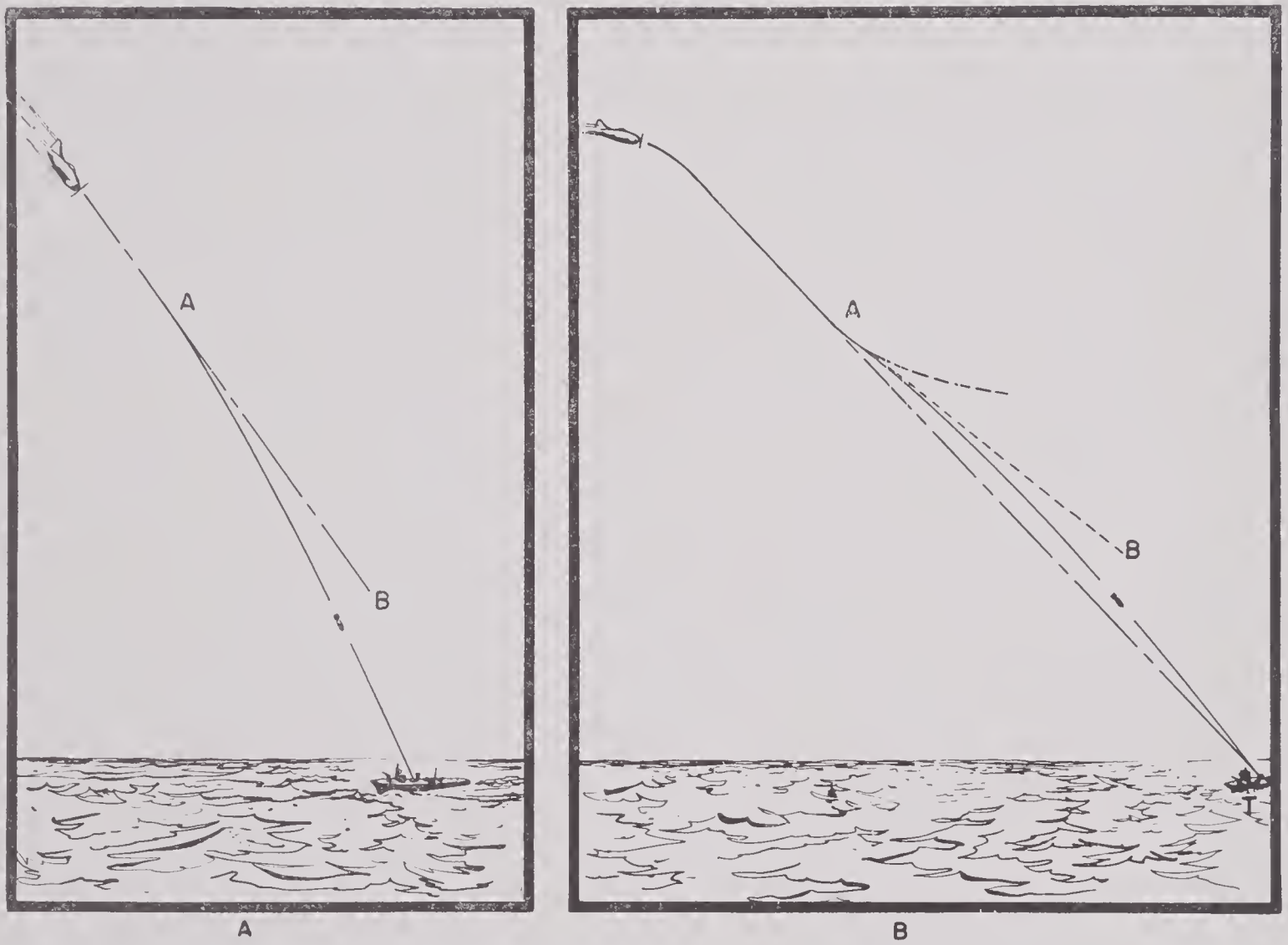

FIGURE 2. Comparison between ordinary dive bombing and toss bombing: (A) normal dive bombing maneuver; (B) toss bombing maneuver.

The tossing technique is particularly useful in the case of low-velocity, fin-stabilized projectiles, such as bombs and the 11.75-in. aircraft rockets, since it removes the restriction on range which, in the case of the depressed sight technique, is imposed by limited visibility over the nose of the airplane. In Figure 3 are graphs which show the range restrictions imposed by various visibility angles when the de-

pressed sight technique is used in launching bombs from an airplane traveling with a speed of 300 knots.[87] In the same figure, the dotted curve indicates the ranges up to which bombs have been successfully released by one of the models of the toss bombing instrument.

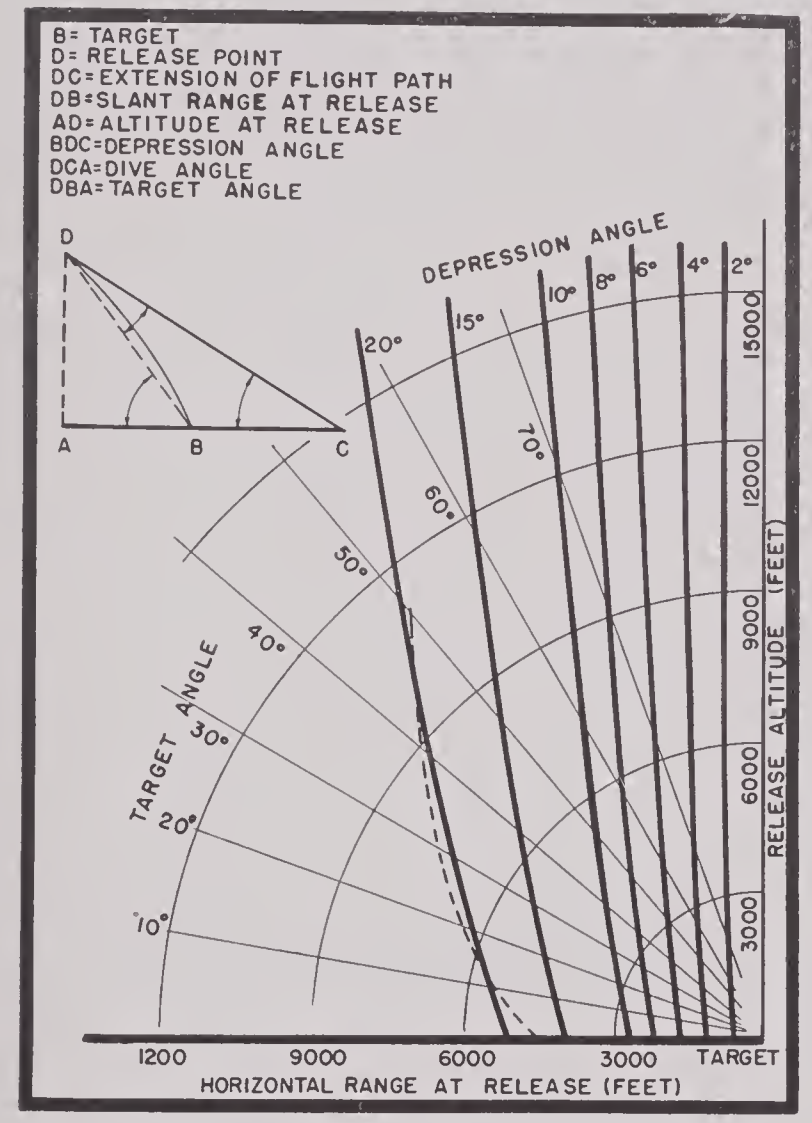

FIGURE 3. Theoretical ranges for given sight depression angles in normal dive bombing (plane velocity = 300 knots). Dashed curve indicates ranges up to which bombs have been successfully released by toss bombing equipment.

The toss equipment provides for the automatic release of missiles in dives between 15 and 60 degrees at ranges which are subject to the limits imposed by the speed of the airplane. Table 1 shows the range of operating conditions recommended in toss bombing.

In the case of rockets, the maximum tossing distance is not restricted by plane speed, since the rocket has an additional velocity of its own. Tossing distances up to 4,500 yards and dive angles ranging from 15 to 60 degrees were used with rockets with satisfactory results.[189]

In the tests conducted with torpedoes and using airspeeds up to 300 knots, best results were obtained when release altitudes were less than 2,000 feet, and dive angles between 15 and 25 degrees.

TABLE 1. Recommended release conditions for toss bombing. Maximum altitudes * (in feet) for (1) closing bomb release switch and (2) initiating pull-up (shown in italics) as a function of dive angle and airspeed.

Angle of dive	True airspeed (knots) 250	300	350	400
15°		1,900	2,300	2,700
		1,390	*1,668*	*2,000*
20°	1,900	2,700	3,200	3,900
	1,390	*2,000*	*2,400*	*2,880*
30°	3,200	4,700	5,600	6,800
	2,400	*3,450*	*4,150*	*4,980*
40°	4,700	6,800	8,100	11,000
	3,450	*4,980*	*5,975*	*8,600*
50°	6,800	9,500	11,000	11,000
	4,980	*7,170*	*8,600*	*8,600*
60°	11,000	11,000	11,000	11,000
	8,600	*8,600*	*8,600*	*8,600*

* The minimum operating altitude at which the bomb release switch may be closed is 1,700 feet, and the corresponding altitude below which pull-up may be initiated is 1,390 feet.

1.3 SUMMARY OF PERFORMANCE

Extensive field tests have been made with the tossing equipment, using several types of bombs and rockets. In the case of bombs, it has been possible to conduct overall tactical evaluation tests as well as equipment evaluation tests. In the tactical evaluation tests, errors occurring in the allowance for wind are superimposed upon equipment errors. In the case of rockets, the results of tests on the accuracy of the equipment only are available. Conclusions regarding the overall accuracy of the tossing equipment may be drawn from these tests, with due allowance made for the effect of wind.

Figure 4 shows the distribution of the impacts of 747 bombs dropped during a series of evaluation tests in which slant ranges varied from 5,400 to 9,300 feet. The pilots allowed for wind, using aerological data and the wind error indicated by the first bomb. In general, five bombs were dropped in succession. For all the bombs, the 50 per cent circle about the target had a radius on the ground of 100 feet. If the pattern of impacts is projected onto a plane normal to the line of flight, 50 per cent of the

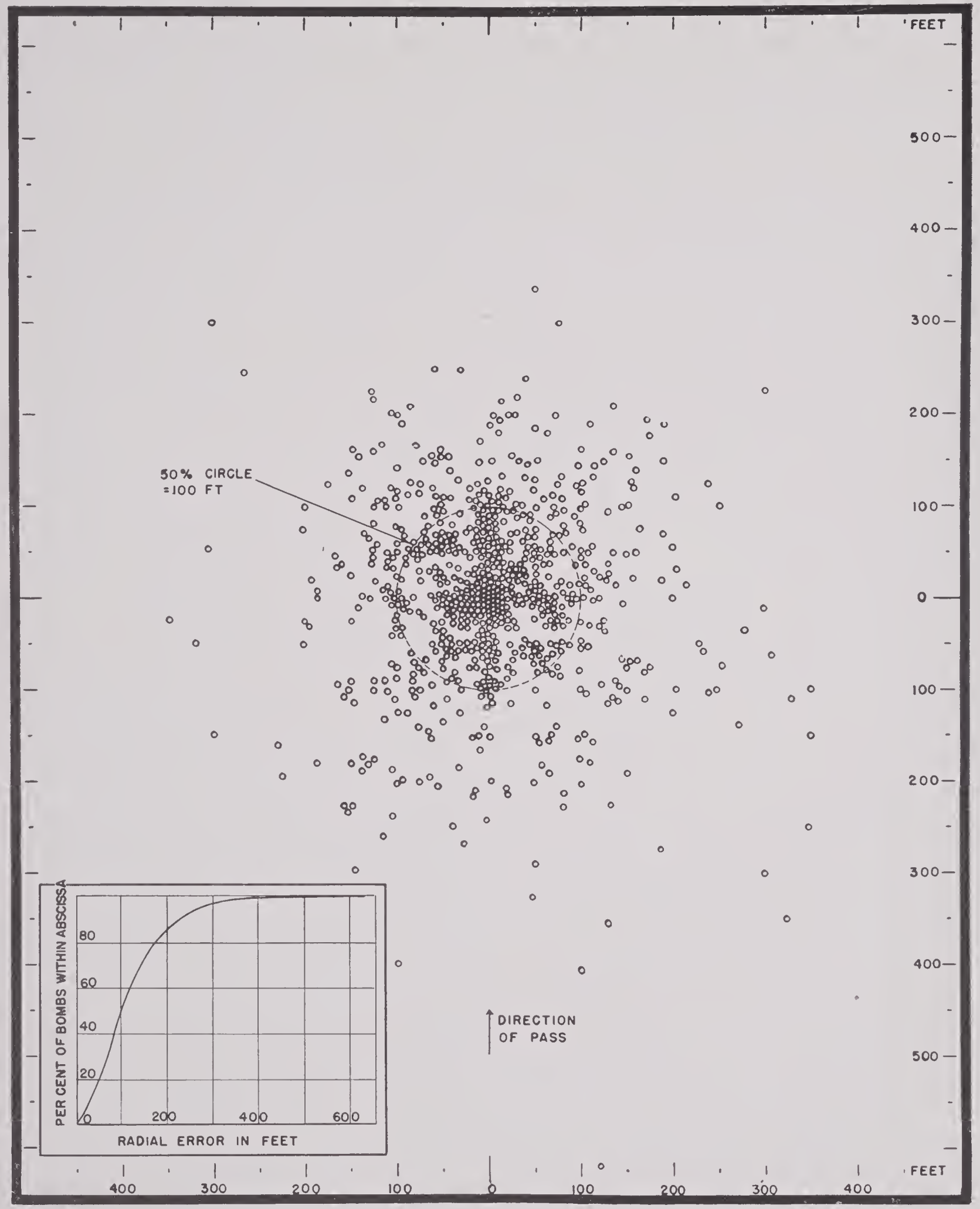

FIGURE 4. Impact pattern of 747 bombs dropped in pilots' evaluation tests at Naval Air Station, Patuxent River, Maryland, October 1944 to August 1945. Slant ranges used varied from 5,400 to 9,300 feet. Distribution of radial errors is given in graphical form in inset.

impacts fall within a circle having a radius of 11.5 mils. As for the errors in range, 50 per cent of the impacts show an error of less than 61 feet on the ground, or 5.8 mils normal to the line of dive. The corresponding deflection errors are 52 feet on the ground and 7.8 mils normal to the line of dive. A more detailed analysis of these data is given in Chapter 5.

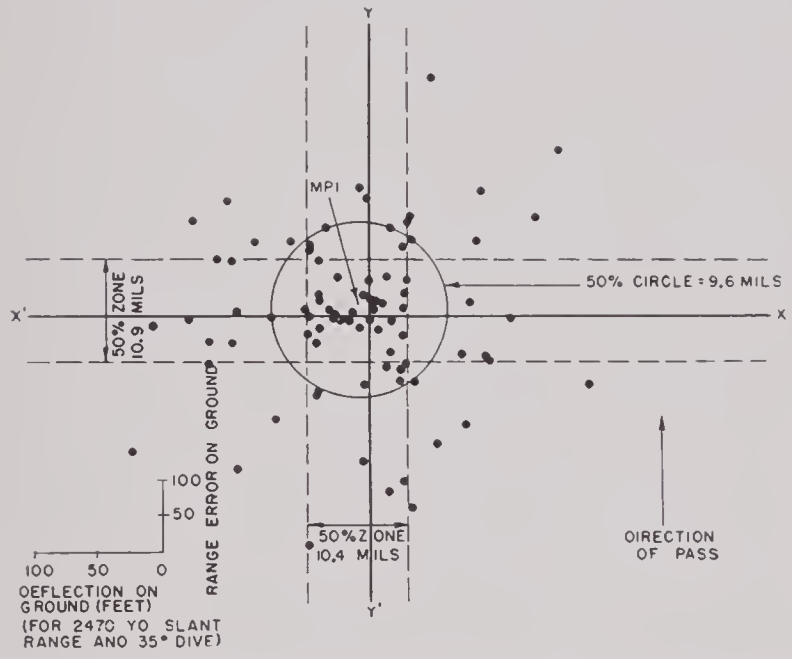

FIGURE 5. Impact pattern of 82 high-velocity 5.0-inch aircraft rockets launched from F6F-5 airplane at Naval Ordnance Test Station, Inyokern, California (plotted in plane perpendicular to line of flight and corrected to no-wind conditions). Test conditions were as follows:

Slant range	2,050–2,820	yards	(avg 2,470)
Dive angle	30–40	degrees	(avg 35)
True airspeed	300–400	knots	(avg 350)

Figure 5 shows the impact pattern of 82 high-velocity 5.0-in. aircraft rockets launched in pairs from dives aimed directly at the target. The pattern has been corrected to no-wind conditions and hence shows where the rockets would have hit if the pilot had made proper compensation for wind. Fifty per cent of the rockets lie within a circle of 9.6 mils radius normal to the line of dive. The dashed lines in this figure show the limits within which 50 per cent of the rockets are located in range and deflection respectively. Fifty per cent deviate from the mean point of impact by less than 6.3 mils in range and 7.4 mils in deflection. A more detailed analysis of these data also is given in Chapter 5.

The toss equipment was used on a limited number of combat missions, in which it gave a *circle of probable error* [CPE] of 200 feet for all rounds released. Throwing out several rounds where misidentification of the target was established, the CPE drops to 150 feet.[269] Further discussion of the operational experience is included in Chapter 5.

1.4 MODELS DEVELOPED

All the data given in the rocket evaluation tests and about half the data in the bomb evaluation tests just described were obtained using experimental equipment designated as bomb director Mark 1 Model 0, AN/ASG-10XN. Modifications were made to the equipment to enable it to release rockets. The other half of the data in the bomb evaluation tests was obtained using production equipment for the release of bombs, designated as bomb director Mark 1 Model 1, AN/ASG-10. Production equipment for the release of either bombs or rockets is designated as bomb director Mark 1 Model 2, AN/ASG-10A. The first production model was Service-tested, just before the end of the war, with satisfactory results. A later model, designated as bomb director Mark 3, AN/ASG-10B, had reached the experimental stage at the end of the war. The first three equipments are described in Chapter 3, and the Mark 3 in Chapter 8.

The Mark 1 Model 0 equipment was manufactured as rapidly as possible in order to serve as a pilot model to work out production difficulties, as well as to get equipment into the hands of the Services for immediate use. Of this model, 500 sets were delivered to the Navy, which, in turn, transmitted 300 of them to the Army. Half of these 300 were sent to the European theater, where some were used on thirteen combat missions in P-47 airplanes.[96,269]

The Mark 1 Model 1 equipment was developed on a contract basis by the Magnavox Corporation during the production of the Model 0 units.[202] Delivery under this contract began on March 10, 1945, and by June 30, about 200 sets had been turned over to the Navy. Facilities were set up for production at an ultimate rate of one thousand per month. This rate was not reached due to the conclusion of the war. Division 4 withdrew from the project during August of 1945, at which time the Navy Department took over sponsorship of further development and production.

Chapter 2

THEORY OF THE TOSS METHOD

2.1 BOMB TOSSING[a]

2.1.1 Introduction

CHAPTER 2 GIVES a simplified exposition of the mathematical theory underlying the toss technique, together with its application to the tossing of bombs, rockets, and torpedoes. The basic equations are set up and the results of the mathematical treatment are given. Detailed mathematical developments are given as supplementary material in Chapters 6 and 7. Section 2.1 deals with bomb tossing, and the succeeding sections deal with rocket and torpedo tossing and with wind correction.

2.1.2 The Basic Toss Bombing Equations

Figure 1 is a diagram representing the toss bombing maneuver, together with the coordinate axes commonly used. The point N represents the position

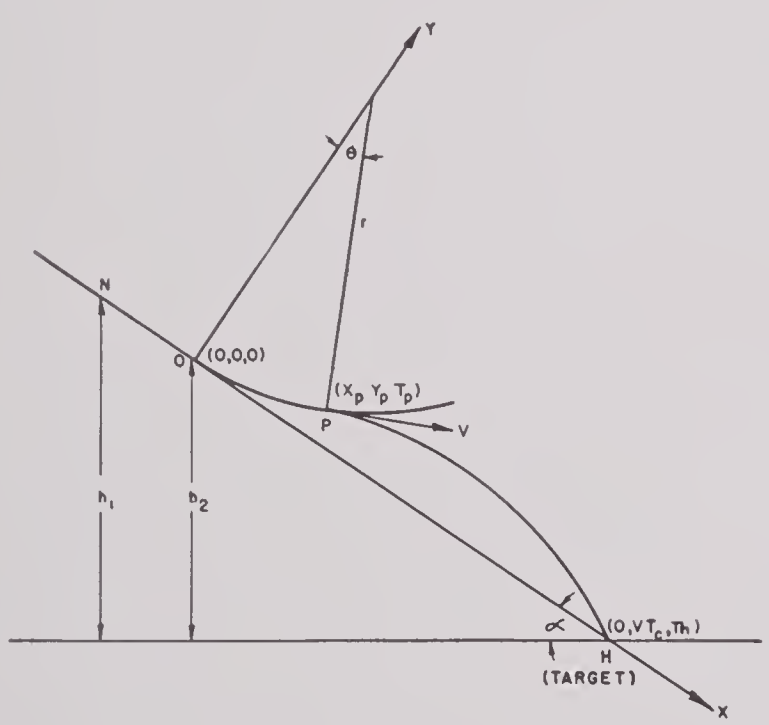

FIGURE 1. Diagrammatic representation of toss bombing maneuver. (For explanation of symbols, see text.)

where the bomb release switch is closed, O the point where pull-up is begun, and NO the flight path before pull-up. The extension OH of NO constitutes a collision course to the target at H, assumed stationary. The line NOH is used as the x axis; the y axis is perpendicular to NOH at O, slanting upward.

Since the airplane is supposed to reach its approximate final velocity in the dive before the bomb release switch is closed, we assume the velocity of the airplane to be constant in the theoretical developments; this velocity is denoted throughout by V. The slant range from O to H can then be represented by the product VT_c, where T_c is the closing time or time to target at pull-up. This time is one of the physical quantities computed by the equipment. The actual time interval measured is T_{12}, the time required to fly from N to O. Because of the assumed constant velocity of the airplane between points N and O, the time T_c is proportional to the time T_{12}. The proportionality constant is fixed by designing the equipment to measure an arbitrary fraction of the closing time or time to target. In the Mark 1 and Mark 3 bomb directors, $T_c = 5T_{12}$.

A fixed ratio between T_{12} and T_c is obtained by altitude measurements. If h_1 and h_2 are the altitudes of the points N and O, then the ratio of h_1 to h_2 must be 6:5 in order that $T_c = 5T_{12}$. Further discussion of the altitude measurements will be given in Section 2.1.4.

We assume in this development that the pilot begins to pull up at O. The arc OP in Figure 1 represents the path of the airplane during the pull-up. Since this path is curved, the airplane has an acceleration normal to its direction of motion at each instant. It has no acceleration in its direction of motion since the velocity is assumed to remain constant.

Let μg be the acceleration normal to the path at any instant. Here, g is the acceleration of gravity, μ is a number, and the product μg is what has been called the *spatial acceleration*. Let r be the radius of curvature at any instant. Then $r = V^2/\mu g$. Since also $r = ds/d\theta$ where ds is the differential of arc on the pull-up path and θ is the angle the tangent to this path makes with the x axis, it follows that

$$d\theta = \frac{ds}{r} = \frac{\mu g}{V^2} ds = \frac{\mu g}{V} dt . \qquad (1)$$

[a] Section 2.1 was prepared by Dr. L. E. Ward, of the Naval Ordnance Test Station, Inyokern, California, and Dr. Albert London, of the National Bureau of Standards.

Consequently, at any time during the pull-up period, the angle θ will be given by the integral

$$\theta = \frac{g}{V}\int_0^t \mu dt, \tag{2}$$

where time is measured from the point O.

Let the letter p be used as a subscript to denote the instant of release of the bomb, so that T_p is the pull-up time, that is, the time to fly from the beginning of pull-up to the point where the bomb is released; θ_p is the pull-up angle; et cetera. Then,

$$\theta_p = \frac{g}{V}\int_0^{T_p} \mu dt. \tag{3}$$

Let the time average of the number μ, taken from the beginning of pull-up to the release of the bomb, be $\bar{\mu}$; i.e.,

$$\bar{\mu} = \frac{1}{T_p}\int_0^{T_p} \mu dt.$$

In terms of $\bar{\mu}$, equation (3) can be written

$$\theta_p = \frac{gT_p}{V}\bar{\mu}. \tag{4}$$

A standard aircraft accelerometer mounted in an airplane shows at each instant during pull-up the number K of g's present at that instant and acting normal to the direction of motion. If α is the dive angle, then approximately

$$\mu g \cong (K - \cos\alpha)g. \tag{5}$$

This relation is sufficiently accurate to be useful for small pull-up angles. It is exact at the beginning of pull-up since in the dive, $K = \cos\alpha$ and $\mu = 0$. The error in subsequent calculations based on equation (5) will be considered in more detail in Chapter 6.

If x and y are the coordinates of the bomb at any time, t, always measured from the beginning of pull-up, then the components of velocity on the coordinate axes at any instant during pull-up are

$$\dot{x} = V\cos\theta$$

and

$$\dot{y} = V\sin\theta.$$

Hence, (6)

$$x = V\int_0^t \cos\theta dt$$

and

$$y = V\int_0^t \sin\theta dt.$$

By using equation (1) to eliminate dt, those equations become[b]

$$x = \frac{V^2}{g}\int_0^\theta \frac{\cos\theta}{\mu}d\theta$$
$$y = \frac{V^2}{g}\int_0^\theta \frac{\sin\theta}{\mu}d\theta. \tag{7}$$

By placing $t = T_p$ in these relations, expressions are obtained for x_p, y_p, $\dot{x}_p$, and $\dot{y}_p$.

After the bomb has been released, the important force acting on it is gravity. Hence, for this phase of the motion, the components of velocity and the coordinates are

$$\begin{aligned}
\dot{x} &= \dot{x}_p + g(t - T_p)\sin\alpha,\\
\dot{y} &= \dot{y}_p - g(t - T_p)\cos\alpha,\\
x &= x_p + \dot{x}_p(t - T_p) + \tfrac{1}{2}g(t - T_p)^2\sin\alpha,\\
y &= y_p + \dot{y}_p(t - T_p) - \tfrac{1}{2}g(t - T_p)^2\cos\alpha.
\end{aligned} \tag{8}$$

In order to secure a hit, x must equal VT_c when $y = 0$. Let this occur when $t = T_h$, so that, from equations (8),

$$\begin{aligned}
VT_c &= x_p + \dot{x}_p(T_h - T_p) + \tfrac{1}{2}g(T_h - T_p)^2\sin\alpha,\\
0 &= y_p + \dot{y}_p(T_h - T_p) - \tfrac{1}{2}g(T_h - T_p)^2\cos\alpha.
\end{aligned} \tag{9}$$

On replacing x_p, y_p, $\dot{x}_p$, and $\dot{y}_p$ by their values from equations (6) and (7), equations (10) are obtained.

$$\begin{aligned}
VT_c &= \frac{V^2}{g}\int_0^{\theta_p}\frac{\cos\theta}{\mu}d\theta + V(T_h - T_p)\cos\theta_p\\
&\quad + \tfrac{1}{2}g(T_h - T_p)\sin^2\alpha;\\
0 &= \frac{V^2}{g}\int_0^{\theta_p}\frac{\sin\theta}{\mu}d\theta + V(T_h - T_p)\sin\theta_p\\
&\quad - \tfrac{1}{2}g(T_h - T_p)^2\cos\alpha.
\end{aligned} \tag{10}$$

Equations (10) are the basic equations from which the toss bombing computer determines the proper release time T_p. The procedure in general is to eliminate T_h from the equations, obtaining an expression for T_p in terms of T_c, V, θ, and α. The value for T_c is obtained during the timing run, α is given by a dive angle indicator, and θ is determined in terms of pull-up acceleration. V occurs only as a minor correction term and the equipment is set for an average operating value. When values for these parameters are fed into the computer, the release time is automatically determined.

[b] Certain details concerning the convergence of these improper integrals are slurred over here.

A first step in solving the equations is to eliminate the quantity $(T_h - T_p)$ between the pair of equations (10). Solving the second of equations (10) for $(T_h - T_p)$ and substituting the expression thus obtained into the first gives

$$T_h - T_p = \frac{V}{g\cos\alpha}\cdot \left[\sin\theta_p + \sqrt{\sin^2\theta_p + 2\cos\alpha\int_0^{\theta_p}\frac{\sin\theta}{\mu}\,d\theta}\right], \quad (11)$$

and

$$\frac{gT_c}{V} = \frac{\cos\alpha\cos\theta_p + \sin\alpha\sin\theta_p}{\cos^2\alpha}\cdot \left[\sin\theta_p + \sqrt{\sin^2\theta_p + 2\cos\alpha\int_0^{\theta_p}\frac{\sin\theta}{\mu}\,d\theta}\right] + \int_0^{\theta_p}\frac{\cos\theta}{\mu}\,d\theta + \tan\alpha\int_0^{\theta_p}\frac{\sin\theta}{\mu}\,d\theta. \quad (12)$$

In equation (11), the positive sign, as written, is the only sign which can be associated with the radical, since the use of a negative sign would make T_h less than T_p.

Equation (12) can be regarded as fundamental to further discussion. While it could be written in a slightly more compact form as regards the trigonometric functions, the present form is more useful for the purpose of the approximations to be made in Section 2.1.3.

2.1.3 Approximate Solution for Release Time

An approximate solution of equation (12) will be developed in this section. This solution is called the zero order solution,[153] and it is mechanized by the Model 0 bomb tossing equipment. In Section 6.1.2 is found a more accurate solution, called the first order solution,[34] which is mechanized by the Model 1 equipment, while in Sections 6.1.3, 6.1.4, and 6.1.5 is found an exact solution of the equation.[72]

In obtaining the zero order solution of equation (12), the first step is to replace μ in the integrals by $\bar{\mu}$. Approximate values for the integrals can then be found. The resulting form of the relation is

$$\frac{gT_c}{V} = \frac{\cos\alpha\cos\theta_p + \sin\alpha\sin\theta_p}{\cos^2\alpha}\cdot \left[\sin\theta_p + \sqrt{\sin^2\theta_p + 2\cos\alpha\frac{1-\cos\theta_p}{\bar{\mu}}}\right] + \frac{1}{\bar{\mu}}\sin\theta_p + \frac{1-\cos\theta_p}{\bar{\mu}}\tan\alpha. \quad (13)$$

Next, the trigonometric functions $\sin\theta_p$ and $\cos\theta_p$ are replaced by θ_p and $1 - \frac{1}{2}\theta_p^2$, respectively, on the assumption that pull-up angles will be small. The resulting equation in θ_p has the form

$$\frac{gT_c}{V} = \theta_p\frac{(1-\frac{1}{2}\theta_p^2)\cos\alpha + \theta_p\sin\alpha}{\cos^2\alpha}\left[1 + \sqrt{1 + \frac{1}{\bar{\mu}}\cos\alpha}\right] + \frac{1}{\bar{\mu}}\theta_p + \frac{1}{2\bar{\mu}}\theta_p^2\tan\alpha. \quad (14)$$

This equation is seen to be an equation of degree 3 in θ_p. However, since the solution sought is expected to be valid only for small pull-up angles, we may ignore the term of degree 3 in θ_p, at least if $\cos\alpha$ is not too small. This leaves the following quadratic equation in θ_p.

$$(1+2\sigma)\theta_p^2\tan\alpha + 2(1+\sigma)\theta_p - \frac{2gT_c\bar{\mu}}{V} = 0, \quad (15)$$

where

$$\sigma = \frac{\bar{\mu} + \sqrt{\bar{\mu}(\bar{\mu}+\cos\alpha)}}{\cos\alpha}.$$

The corresponding equation for T_p, obtained by using equation (4), is

$$\frac{1+2\sigma}{2V}g\bar{\mu}T_p^2\tan\alpha + (1+\sigma)T_p - T_c = 0. \quad (16)$$

The positive solution of equation (16), designated by T_{p0} (to indicate the zero order solution for T_p) is

$$T_{p0} = \frac{2T_c}{\left[1+\sigma+\sqrt{(1+\sigma)^2 + 2\frac{1+2\sigma}{V}g\bar{\mu}T_c\tan\alpha}\right]},$$

or

$$T_{p0} = \frac{T_c\cos\alpha}{\bar{\mu}+\cos\alpha+\sqrt{\bar{\mu}(\mu+\cos\alpha)}}\cdot\frac{2}{1+\sqrt{1+2\beta}}, \quad (17)$$

where

$$\beta = \frac{1+2\sigma}{(1+\sigma)^2}\cdot\frac{g\bar{\mu}T_c}{V}\tan\alpha = \frac{gT_c\sin\alpha}{V}\cdot\frac{\bar{\mu}}{\bar{\mu}+\cos\alpha}.$$

Let $\bar{K}$ designate the time average of K from the beginning of pull-up until the release of the bomb. From equation (5) it follows that $\bar{K} \cong \bar{\mu} + \cos\alpha$, so that equation (17) can be expressed in the form

$$T_{p0} = \frac{T_c\cos\alpha}{\bar{K}+\sqrt{\bar{K}(\bar{K}-\cos\alpha)}}\cdot\frac{2}{1+\sqrt{1+2\beta}}, \quad (18)$$

where

$$\beta = \frac{gT_c\sin\alpha}{V}\cdot\frac{\bar{K}-\cos\alpha}{\bar{K}}.$$

In mechanizing equation (18) by means of the Model 0 equipment, it was found desirable to rewrite it in the form

$$T_{p0} = \frac{T_c}{\bar{K} + \sqrt{\bar{K}^2 - \bar{K}}}\,\psi_0\,, \tag{19}$$

where

$$\psi_0 = \frac{\bar{K} + \sqrt{\bar{K}^2 - \bar{K}}}{\bar{K} + \sqrt{\bar{K}\,(\bar{K} - \cos\alpha)}} \cdot \frac{2\cos\alpha}{1 + \sqrt{1 + 2\beta}}\,.$$

The particular property of the ψ_0 function which makes it useful in this connection is that, although it is a function of the three variables $\bar{K}$, α, and T_c/V, it is chiefly a function of α, showing but little variation with $\bar{K}$ and T_c/V over the ranges of values of $\bar{K}$ and T_c/V which occur in bomb tossing. This point is discussed in detail in Section 6.1. However, Figures 2 and 3 show how the dependence of ψ_0 on the major variable, α, is affected by different representative values of T_c/V and $\bar{K}$.[153]

Since ψ_0 reduces to unity when $\alpha = 0$, and since

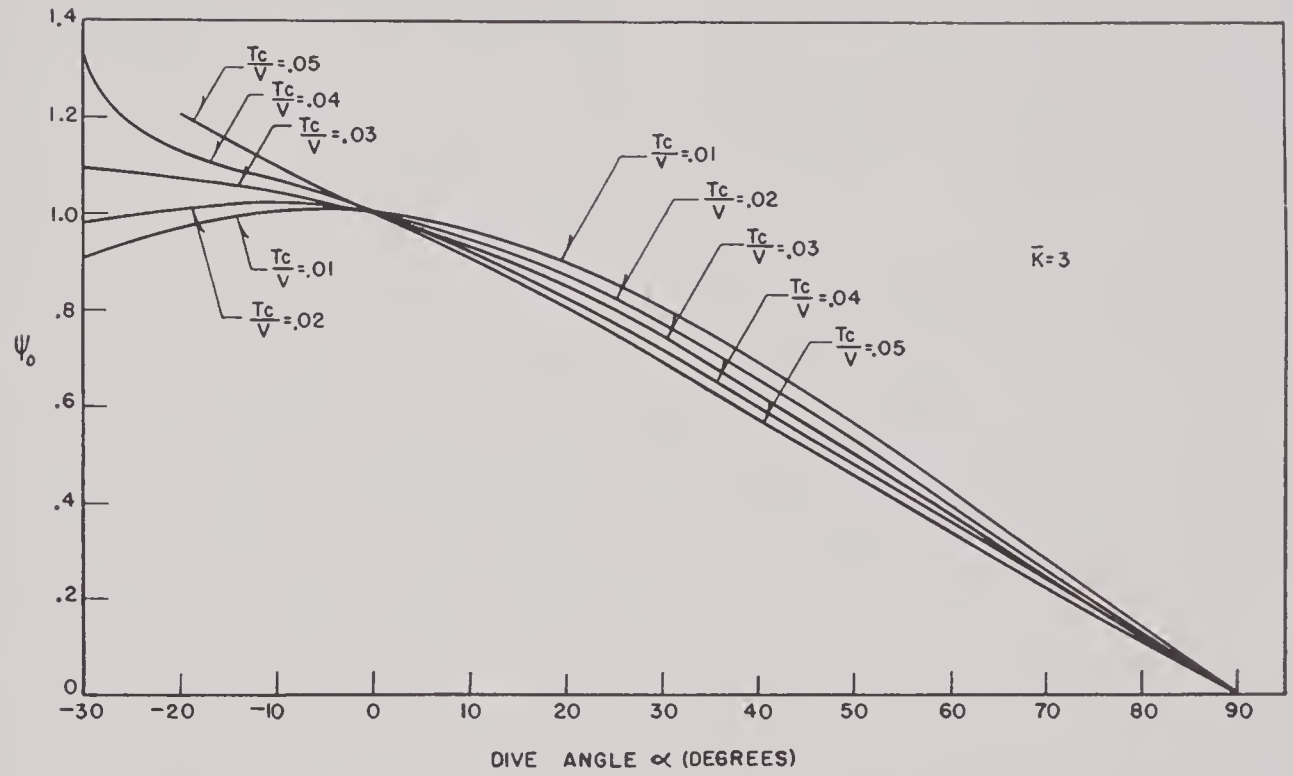

FIGURE 2. ψ_0 versus dive angle for different values of T_c/V, $\bar{K}$ being constant (= 3).

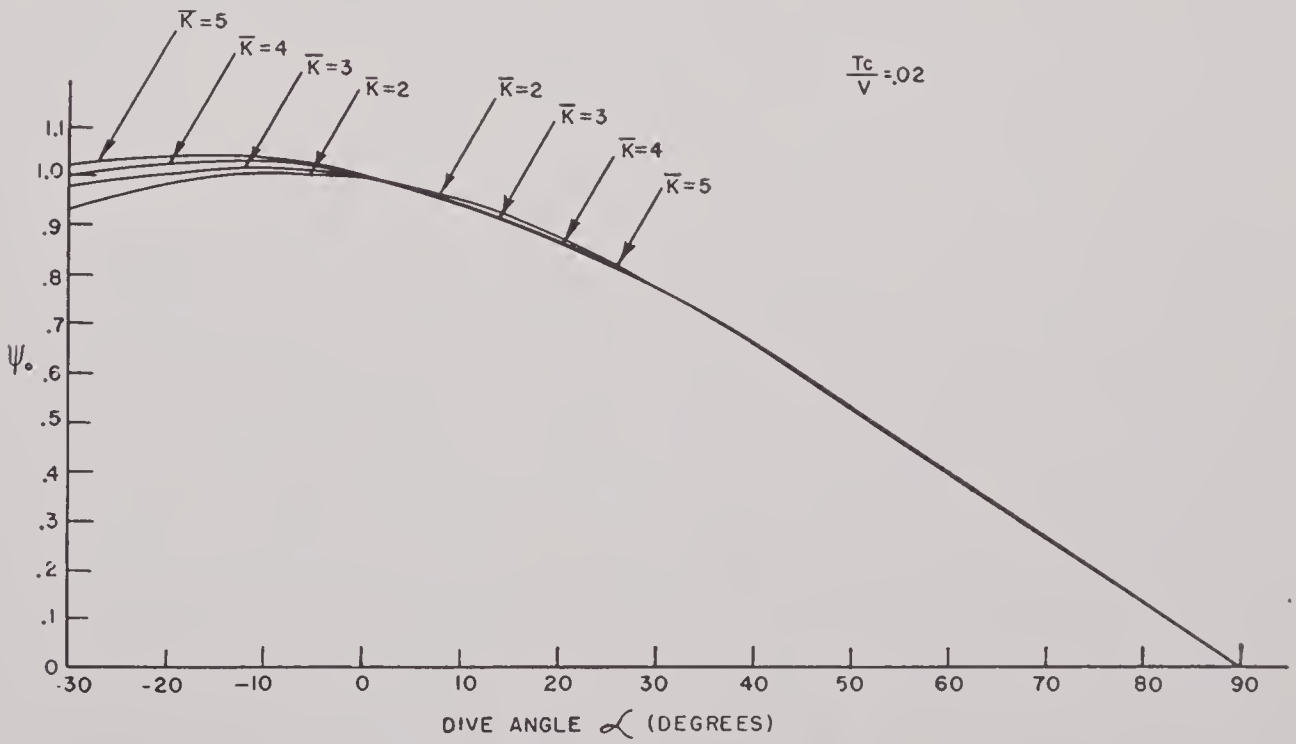

FIGURE 3. ψ_0 versus dive angle for different values of $\bar{K}$, T_c/V being constant (= 0.02).

ψ_0 shows relatively little change when $\bar{K}$ and T_c/V are varied, equation (19) shows that ψ_0 can be regarded as a factor whose purpose is to reduce the pull-up time from that for horizontal bombing to the correct value for bombing from a dive.

2.1.4 Mechanization of the Basic Equation

On referring to equation (19), it is clear that if the physical quantities T_c, K, and α can be measured or computed while in the dive and the pull-up and then combined according to this equation, the correct release time will have been found. Some means should also be provided to take care of the effect on T_{p0} of changes in the ratio T_c/V.

mechanization is shown in Figure 4. A full description of the circuits is given in Chapter 3.

The altimeter is arranged so as to cause a condenser of capacity $C_1 = 2\mu$f to charge for the period T_{12} or $T_c/5$, corresponding to the time required for the altimeter reading to drop to five-sixths of its initial value. Initiation of this charging process occurs at "the first altitude point" of the altimeter. The charging voltage, v_a, applied to this capacitor, is obtained from a potentiometer built into the artificial horizon. This voltage decreases as the dive angle increases as determined by the ψ_0 function. The voltage v_1 built up across C_1 is given by the equation

$$v_1 = v_a \left(1 - e^{-T_c/5R_1C_1}\right), \tag{20}$$

where $R_1 = 2$ megohms.

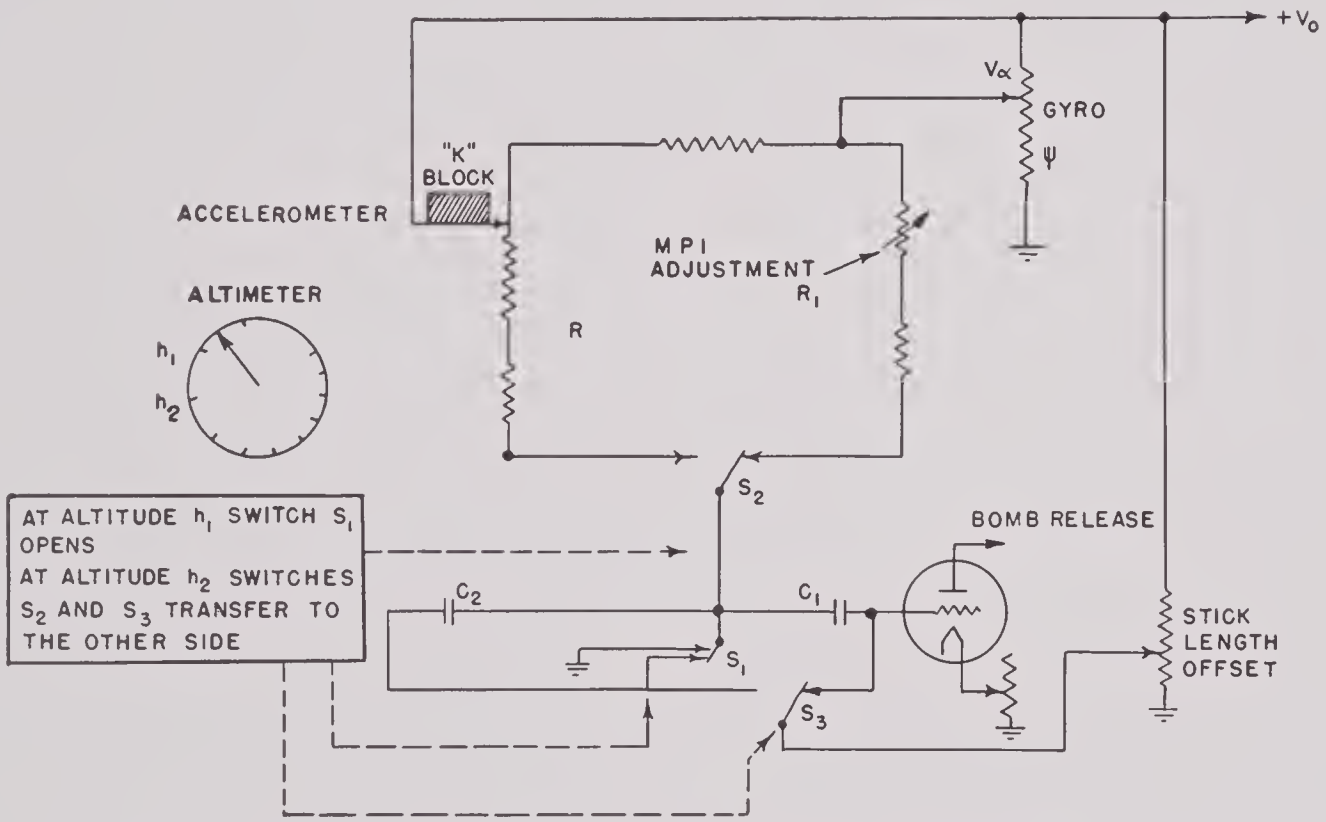

FIGURE 4. Simplified schematic diagram of toss bombing circuit.

The instrumentation of the Mark 1, Models 0 and 1 bomb directors consists of an electronic computer which receives the values of T_c, K, and α from three electromechanical components and combines them in accordance with equation (19) so as to furnish automatically the value of T_{p0} and T_{p1}, respectively. (T_{p1} is the first order solution for T_p mechanized in the Model 1 equipment.) The value of T_c is obtained from a suitably modified altimeter, the value of K from an accelerometer, and the value of α from an artificial horizon modified so as to measure the dive angle. A simplified schematic arrangement of the

After the completion of this operation, which is accomplished during the timing run (N to O in Figure 1), a second condenser of capacity $C_2 = 2\mu$f is charged, starting at the "second altitude point" of the altimeter; charging continues during pull-up from a voltage v_0 applied through a resistor $R(K)$ which varies in accordance with the acceleration present at each instant during the pull-up. The charge q, acquired by C_2 at time, t, is the solution of the differential equation

$$R\dot{q} + \frac{q}{C_2} = V_0, \tag{21}$$

where R is to be regarded as a function of t, since K varies with t.

The solution of equation (21), which is zero when $t = 0$, is

$$q = C_2 v_0 \left[1 - e^{-(1/C_2)\int_0^t dt/R} \right].$$

Hence, the voltage across C_2 is

$$v = v_0 \left[1 - e^{-(1/C_2)\int_0^t dt/R} \right]. \tag{22}$$

The release of the bomb is effected by the firing of a thyratron when the voltage across C_1 equals that across C_2; that is, the release of the bomb occurs when

$$v_a \left(1 - e^{-T_c/5R_1C_1} \right) = v_0 \left(1 - e^{-(1/C_2)\int_0^t dt/R} \right). \tag{23}$$

The resistor R consists of a stack of 84 resistors, each resistor being connected between two successive conducting segments which are separated by thin mica washers. For $K > 1.3$, this resistor obeys the relation in the Model 0:

$$R = \frac{10}{K + \sqrt{K^2 - K}} \text{ in megohms,}$$

so that as K increases, R decreases nearly proportionally. Thus, the right-hand member of equation (23) becomes

$$v_a \left(1 - e^{-T_c/5R_1C_1} \right) = v_0 \left(1 - e^{-(1/10C_2)\int_0^t (K + \sqrt{K^2 - K})dt} \right). \tag{24}$$

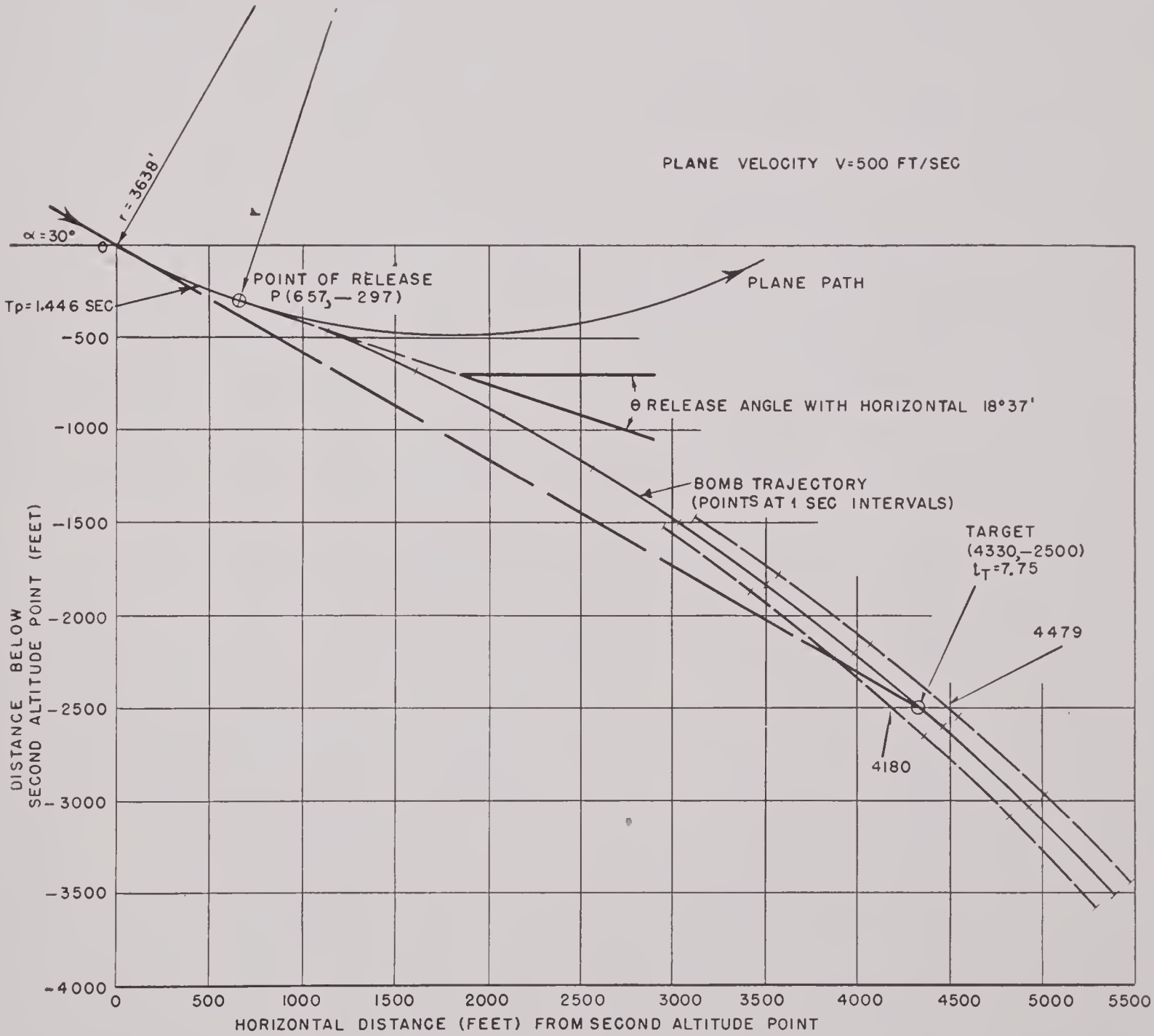

FIGURE 5. Toss bombing trajectories (theoretical) for perfect release time and for release times in error by ±10 per cent. (Latter are represented by broken curves on either side of unbroken curve.) Dive angle = 30 degrees; t_T = time of arrival at target, in seconds, measured from release.

The potentiometer card in the artificial horizon is designed so that

$$v_a = v_0 \frac{1 - e^{-(T_c\psi_0/5R_1C_1)}}{1 - e^{-T_c/5R_1C_1}} = v_0\psi_0 \frac{1 - \frac{\psi_0}{2!}\frac{T_c}{5R_1C_1} + \cdots}{1 - \frac{1}{2!}\frac{T_c}{5R_1C_1} + \cdots}. \tag{25}$$

For $T_c << 5R_1C_1$, this is nearly equivalent to $v_a = v_0\psi_0$. Using this value to eliminate v_a in equation (24) and remembering that the exponential terms are small, gives

$$T_c\psi_0 = \int_0^{T_p} (K + \sqrt{K^2 - K})\, dt. \tag{26}$$

Equation (26) gives the same value for T_p as does equation (19) since $\bar{K} + \sqrt{\bar{K}^2 - \bar{K}}$ is the average value of the K function.

The actual potentiometer card in the artificial horizon, the so-called ψ card, must be designed to give perfect agreement with the theoretical value of ψ for one particular design value of $\bar{K}$, and T_c/V. In the Model 1 bomb director, as explained in detail in Chapter 7, the design centers of $\bar{K} = 3$ and $T_c/V = 0.028$ have been chosen.[57] The variation of the theoretical value of ψ with $\bar{K}$ is quite negligible (Figure 3). However, ψ does vary to some extent with T_c/V, since ψ decreases with increasing T_c/V (Figure 2). The nonlinear charging characteristic of the condensers used in the computing circuit is of assistance here, since less proportionate charge accumulates on the condenser with increasing charging time and hence with increasing T_c or T_c/V at a fixed V. As a result of this nonlinear characteristic, there is considerable agreement between the instrumental ψ and the theoretical ψ for values of T_c/V different from 0.028, as shown in Figure 8 in Chapter 6.

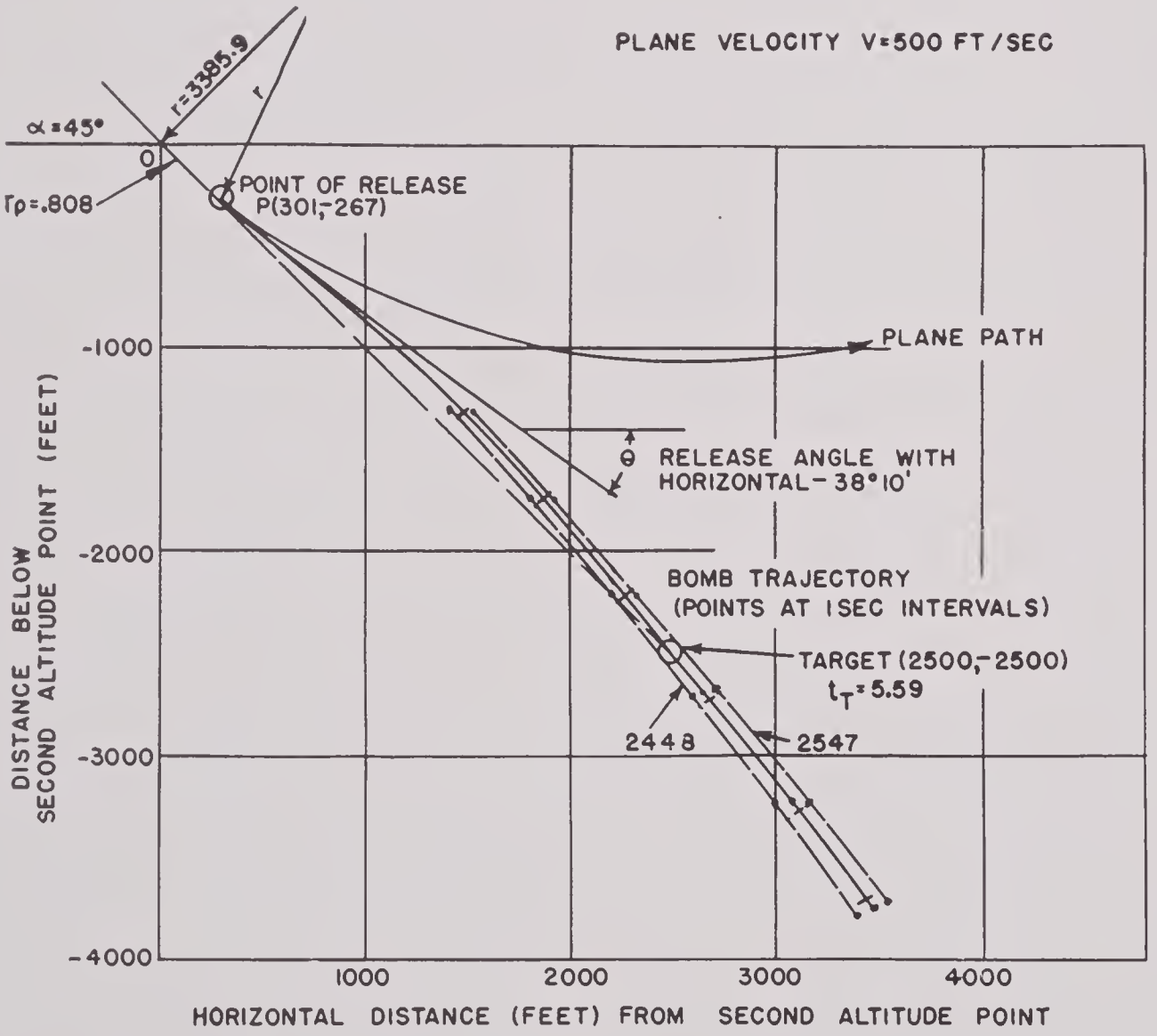

FIGURE 6. Toss bombing trajectories (theoretical) for perfect release time and for release times in error by ±10 per cent. (Latter are represented by broken curves on either side of unbroken curve.) Dive angle = 45 degrees; t_T = time of arrival at target, in seconds, measured from release.

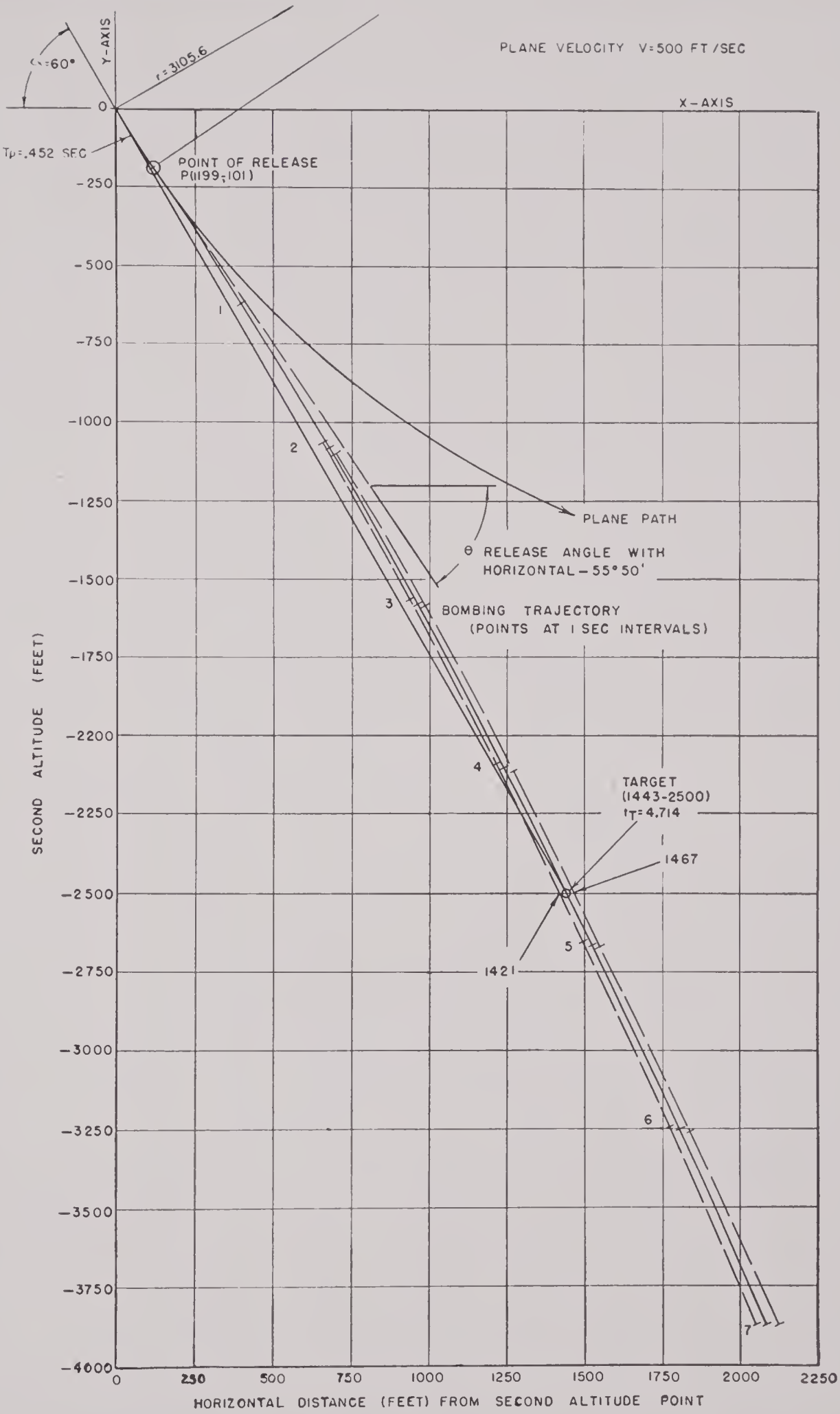

FIGURE 7. Toss bombing trajectories (theoretical) for perfect release time and for release times in error by ±10 per cent. (Latter are represented by broken curves on either side of unbroken curve.) Dive angle = 60 degrees; t_T = time of arrival at target, in seconds, measured from release.

2.1.5 Trajectories, Release Conditions, and Restrictions

Figures 5, 6, and 7 show computed trajectories for dive angles of 30, 45, and 60 degrees, respectively, other conditions being indicated on the figures and in the captions.[120]

The indicated trajectories are for perfectly estimated release times, T_p. Shown also in the curves (in the neighborhood of the target only) are the theoretical trajectories for release times in error by

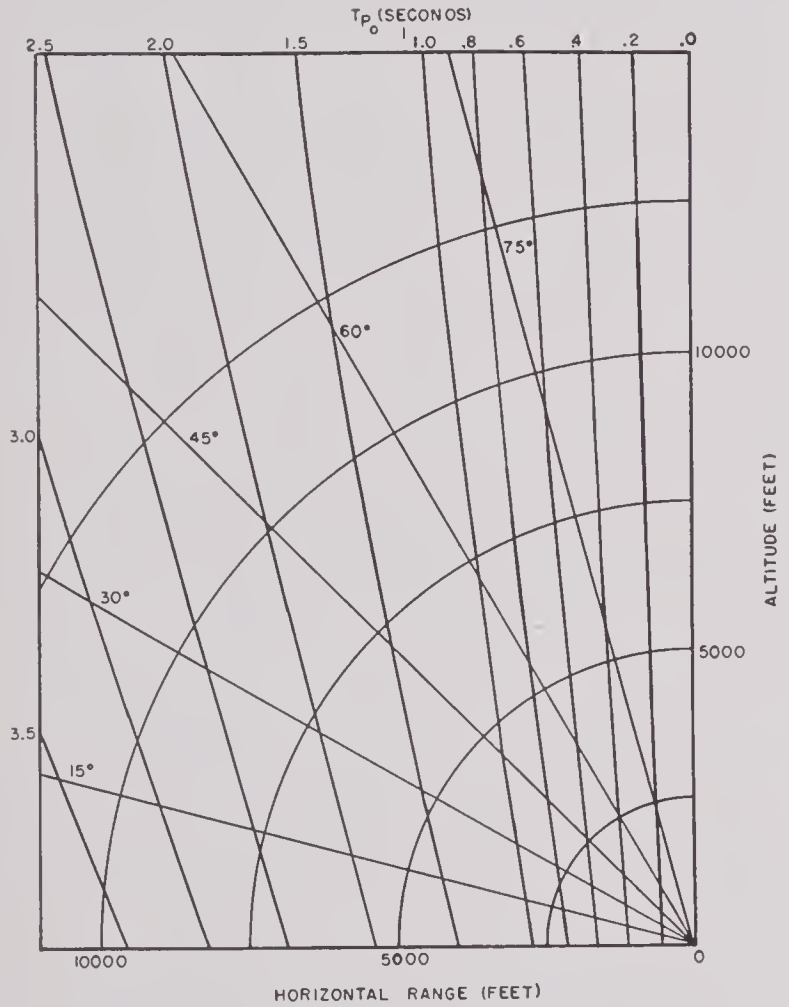

FIGURE 8. Curves of constant pull-up times, $V = 500$ feet/second, $K = 3$.

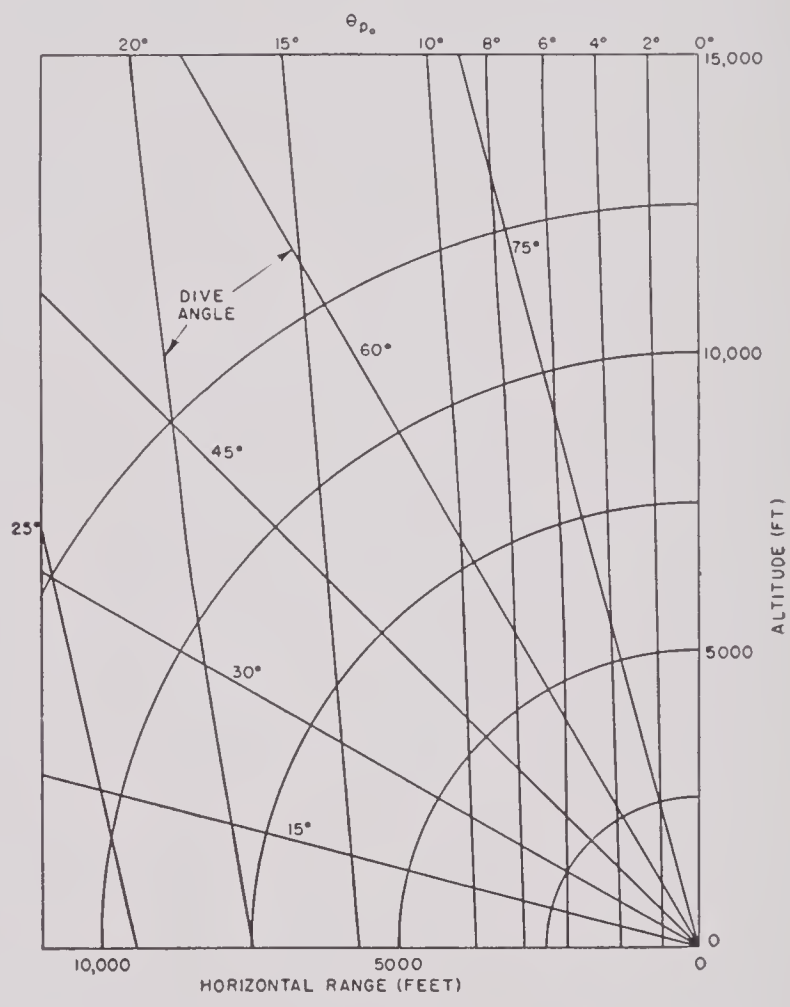

FIGURE 9. Curves of constant pull-up angles, $V = 500$ feet/second, $K = 3$.

plus and minus 10 per cent. The horizontal range errors decrease rapidly with increased angle of dive, and for the three cases shown, are approximately 150, 50, and 25 feet, corresponding to 3.5 per cent, 2 per cent, and 1.5 per cent of the total horizontal range. The curves are extended both above and below the theoretical horizon so that the variation of the error with the altitude of release may be estimated.

For certain evaluations, it is of interest to determine the range of operating conditions for various pull-up times and pull-up angles.[56] Figure 8 is a chart showing contours of constant pull-up times, i.e., each chart represents the spatial coordinates (at the start of pull-up) of various maneuvers which result in the same value of T_p. By following, for example, the curve labeled 2.0, the various conditions requiring a pull-up time of 2 seconds are found. The conditions $K = 3$ and $V = 500$ feet/second are assumed. In the same way, Figure 9 is a chart showing contour curves of constant pull-up angles.

Not all of the ranges shown in Figures 8 and 9, corresponding to a given pull-up time, are feasible. For the Model 0 bomb director, pull-up angles less than about 12 degrees and pull-up times less than 1.5 seconds are normally used. This restriction is chiefly a consequence of the approximations made in deriving the equations in Section 2.1.3.

Because of these approximations, principally the omission of those terms in the series for $\sin \theta_p$ and $\cos \theta_p$ which would result in terms of degree 3 or more in the equation for θ_p, the automatic computer determines a pull-up time which is somewhat too small. The consequence of an early release time is to cause the bomb to fall short of the target, as is

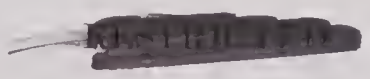

demonstrated, in an exaggerated form, in Figure 10. In the figure, P' represents the actual release point and P the correct point. The bomb therefore crosses the collision course OH at a point H' and hits the ground at a point K' short of the target H. Means of compensating for such errors are described briefly in Section 2.1.6, and in detail in Section 6.4.

Denoting by ΔT_c an error in the determination of T_c, and by ΔT_p the error thereby caused in T_p, the bomb will cross the collision course a distance nearly equal to $V \cdot \Delta T_c$ from the target. This is true because the slant range is VT_c. Since the arc $H'K'$ of the trajectory is nearly a straight-line segment, it follows from the law of sines that

$$\frac{\delta}{\sin \theta_h'} = \frac{V\Delta T_c}{\sin (\alpha + \theta_h')}. \tag{27}$$

Equation (27) is basic in the error calculations considered in Chapter 6.

Figure 11 is a chart based on equation (27), from which can be determined all pull-up conditions which will result in a miss on the target 100 feet short.[79] These curves represent theoretical operational limits on the Model 0 bomb director if 100-foot accuracy is required. As will be seen from the figure, these maximum range curves depend on the velocity of the aircraft. For any given velocity, say 350 knots, all pull-ups conducted to the right of the 350-knot curve will have instrument errors *less* than 100 feet short of the target, while all pull-ups to the left will correspond to errors *greater* than 100 feet. The horizontal distance by which the bomb misses the target is approximately proportional to the cube of the range for a fixed velocity and dive angle.[79] Consequently, the error increases rapidly when the maximum ranges of Figure 11 are exceeded and decreases rapidly for ranges less than this value. Figure 12 illustrates this for horizontal errors of 50, 100, 150, and 200 feet.

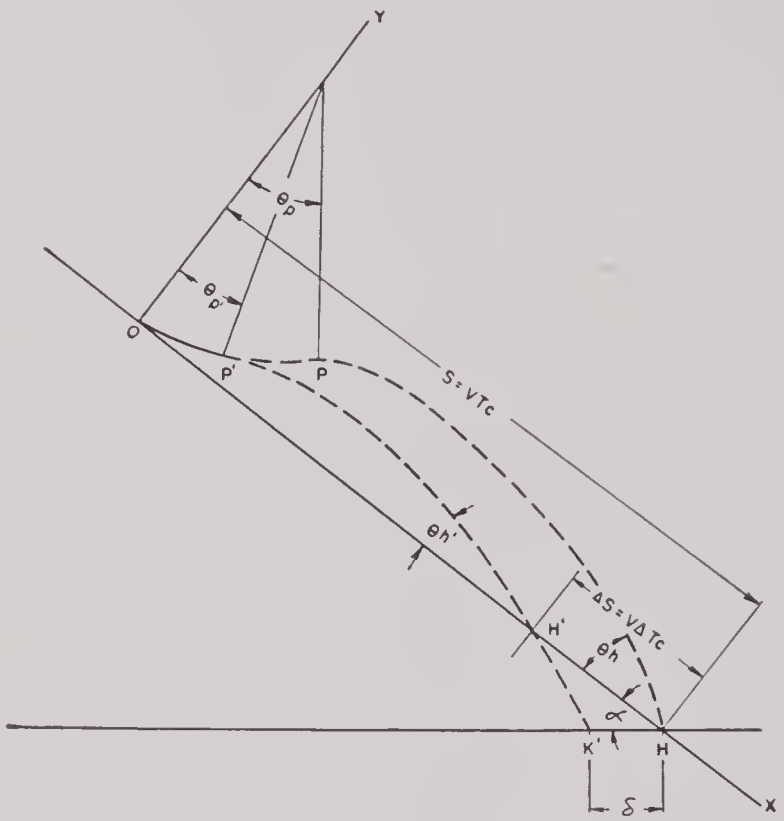

FIGURE 10. Diagrammatic representation of toss bombing maneuver showing effect (exaggerated) of early release time.

The recommended operating limits, given in Chapter 1, are based on the curves of Figure 11 and have been found to be in close agreement with the results of field tests.[150] Inasmuch as the limitations in range discussed in the preceding paragraph are a result of approximations used in solving the bomb tossing equations, it is to be expected that the mechanization of a more accurate solution of these equations would make possible longer maximum ranges.

The first order solution on which the Model 1 bomb director is based is a more accurate approximation to the exact solution, so that it results in theoretical maximum ranges which are somewhat greater than those of the Model 0 bomb director.[79] Further

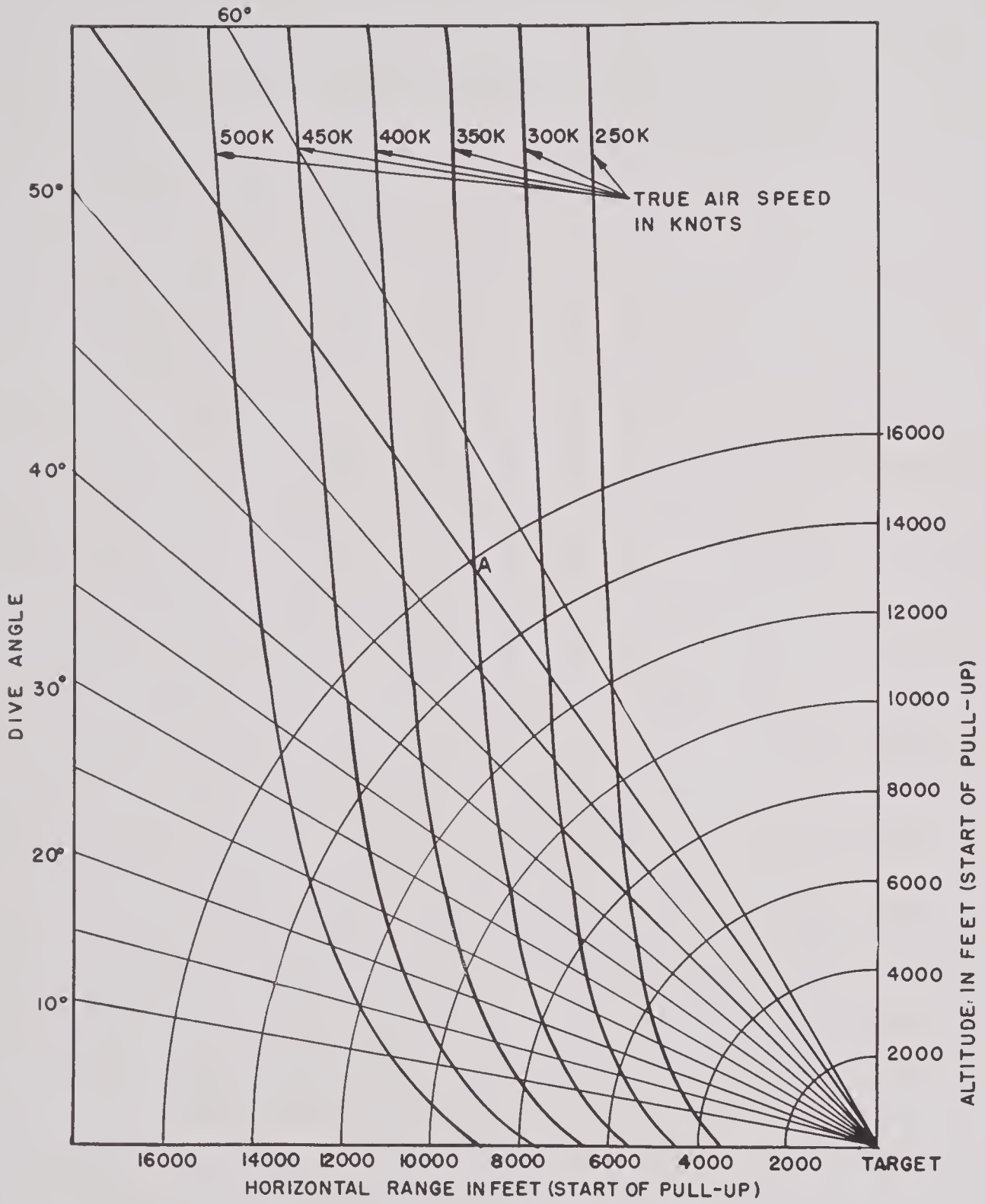

FIGURE 11. Curves (theoretical) of maximum allowable ranges (for different aircraft velocities) corresponding to horizontal errors less than 100 feet, for bomb director Mark 1 Model 0 (ψ_0 function). Example: if plane's speed is 300 knots, bomb will hit ground 100 feet short of target if pull-up begins at any point (determined by dive angle) on the 350-knot curve, such as A. Dive angle, 55 degrees, slant range 15,800 feet, altitude 13,000 feet.

[redacted]

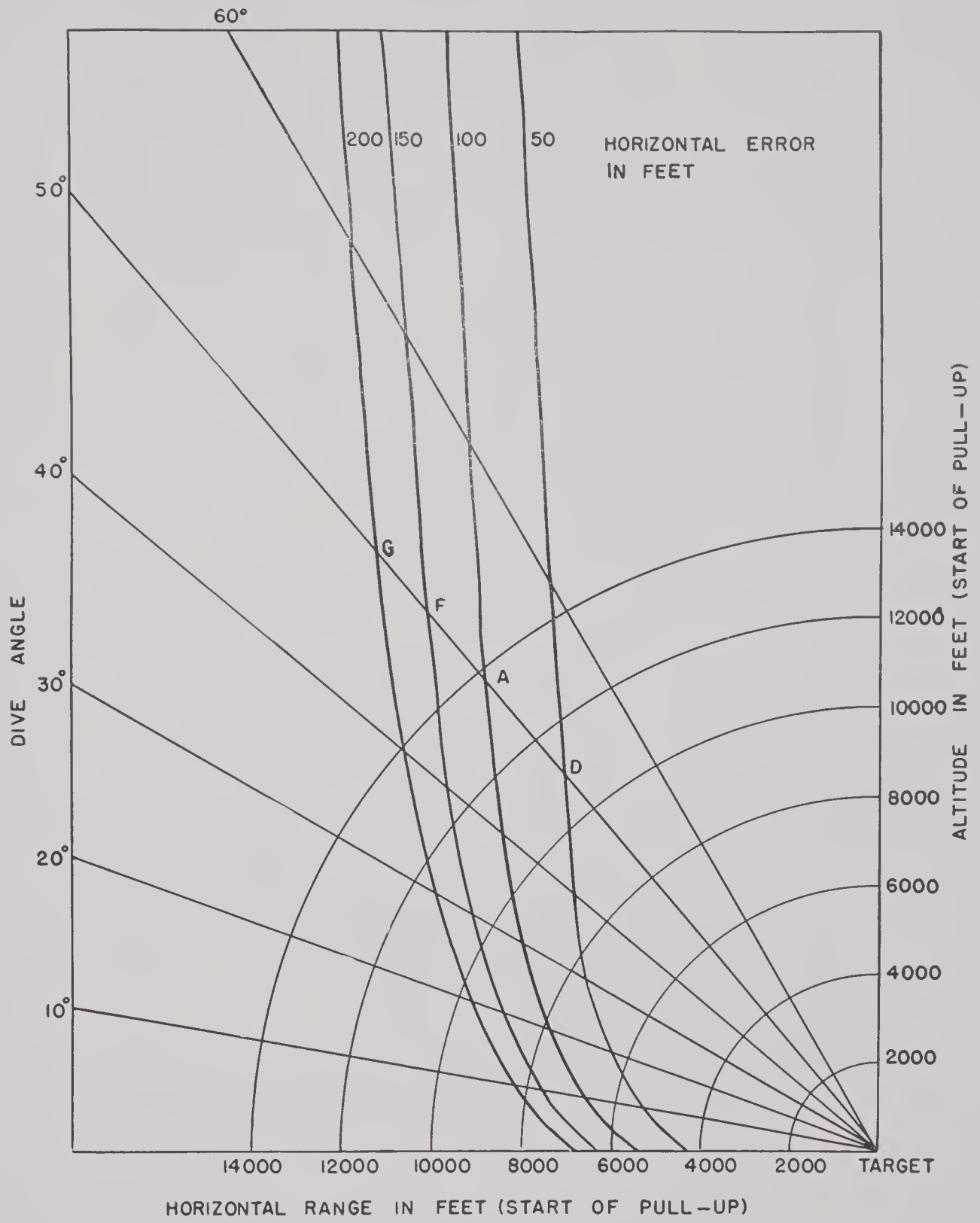

FIGURE 12. Curves (theoretical) of maximum allowable ranges corresponding to different horizontal errors for aircraft velocity of 350 knots, for bomb director Mark 1 Model 0 (ψ_0 function). If plane's speed is 350 knots and dive angle is 50 degrees, bomb will hit ground 50, 100, 150, or 200 feet short of target for pull-ups beginning at *D*, *A*, *F*, or *G* respectively.

details of the corrections made in the Mark 1 director are given in Chapter 6. It should be emphasized, however, that these theoretical maximum ranges may not be identical with the practical limits because of the presence of other errors to be discussed. Practical range limitations have to be determined experimentally.

2.1.6 Instrumental Adjustments

The two primary instrumental adjustments by means of which the impact point of the bomb may be changed are the *mean point of impact* [MPI] adjustment and the *stick-length offset*. The diagrammatic location of these adjustments is shown in Figure 4. In the former, the slant range is changed by a fixed percentage $\Delta T_c/T_c$, while in the latter, the range may be reduced by a fixed amount, i.e., by the amount $V\Delta T_c$, where ΔT_c is a time offset introduced by the stick-length offset circuit.[44,144] The MPI dial may be used to bring the point of impact on the target as in flight calibration procedures, or in the tactical situation in which a miss is obtained on the first bombing run; or it may be used in correcting for the different ballistic coefficients of the different types of bombs.

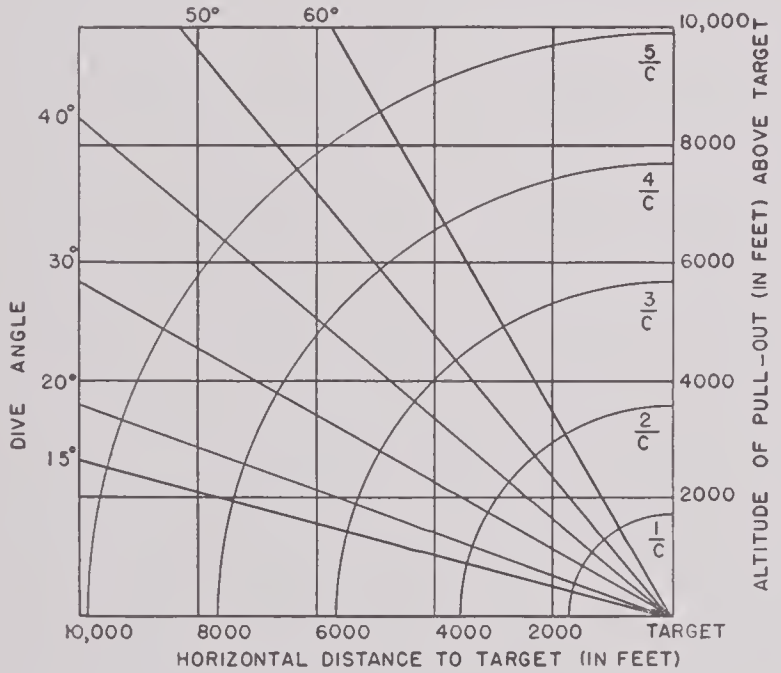

FIGURE 13. MPI adjustment for bomb ballistic compensation (for bomb director Mark 1 Model 1). Example: for pull-up altitude of 6,650 feet, dive angle of 60 degrees, and ballistic coefficient (C) of 2, MPI setting should be increased by $4/2 = 2$ divisions. (1 division is equivalent to $\Delta T_c/T_c = 0.034$.)

Figure 13 is a chart of the MPI adjustment for the Model 1 bomb director, which may be used for compensating for ballistic coefficient effects.[55,140] From this chart it will be seen that this adjustment is constant for a fixed slant range and a given ballistic coefficient. For a fixed slant range, the MPI setting must be increased when a bomb with a smaller ballistic coefficient is substituted for a bomb whose ballistic coefficient is larger. This is the case because bombs with small ballistic coefficients are subject to greater air resistance and tend to fall short. The air resistance effect may be approximately compensated for by an MPI adjustment of the amount

$$\frac{\Delta T_c}{T_c} = 1.73 \times 10^{-5} \times \frac{S}{C}, \qquad (27a)$$

where C is the ballistic coefficient and S the slant range in feet. Figure 13 is based on equation (27a).

2.2 ROCKET TOSSING[c]

2.2.1 Introduction

The principles involved in the application of the bomb director to rocket tossing are essentially the same as for bombs. The differences in the theory and instrumentation are due to the fact that the high projectile velocity results in a smaller angular drop from the direction of launching. This requires the use of a shorter pull-up time.

In Section 2.2, the physical relations will be emphasized in the derivations of the formulas; more detailed and exact derivations will be found in Chapter 7. The theory applies to fin-stabilized rockets launched from "zero-length" launchers according to standard Navy practice.

2.2.2 Rocket Trajectories

The angular trajectory drops of rockets can be approximated by a linear function of slant range in the form $m + nR$.[169,170,172,174,177] The constants m and n depend upon the particular rocket type and propellant temperature, as well as plane velocity and dive angle. The constant m is essentially the drop occurring during the burning period and therefore depends upon the burning time in addition to the dive angle and airplane speed, whereas n is determined by the trajectory after burning.

[c] This section was prepared by I. H. Swift, formerly of the State University of Iowa, now at Naval Ordnance Test Station, Inyokern, California.

The nature of n is indicated by the following considerations. The angular drop in radians of a projectile launched at an angle γ with the horizontal and a velocity $V + V_R$, where V is the airplane velocity and V_R the velocity of the rocket relative to the airplane, is the ratio of the linear drop normal to the dive path to the coordinate along the dive path. Thus, if ϵ is the angular drop and t is the time after launching,

$$\epsilon = \frac{\frac{1}{2}gt^2 \cos\gamma}{(V + V_R)t + \frac{1}{2}gt^2 \sin\gamma}$$

$$\cong \frac{gR}{2(V + V_R)^2} \cdot \frac{\cos\gamma}{1 + \frac{gR}{2(V + V_R)^2}\sin\gamma}, \qquad (28)$$

where R replaces the approximately equivalent quantity $(V + V_R)t$. This relation can be transformed as follows, where ϵ_0 is the drop at zero dive angle,

$$\epsilon \cong \frac{gR}{2(V + V_R)^2} \cdot \frac{\cos\gamma}{1 + \epsilon_0 \sin\gamma}$$

$$\cong A_1 \cdot \frac{g}{2V^2} R\,(1 - \epsilon_0 \sin\gamma)\cos\gamma, \qquad (29)$$

and

$$A_1 = \left(\frac{V}{V - V_R}\right)^2.$$

The dive angle factor $(1 - \epsilon_0 \sin\gamma)\cos\gamma$ is the same as that given in reference 215 and derived therein from geometric considerations. This shows that n, the trajectory drop per unit slant range, depends for a given rocket upon the velocity of the airplane and the dive angle.

A more accurate expression for the trajectory drop of a rocket will now be indicated. The trajectory drop tables, published by CIT for a number of rockets,[216-218] have been fitted with an empirical formula of the type

$$\epsilon = \left[aRe^{-V/b} + \frac{ch(T)}{V}\right]F(\gamma), \qquad (30)$$

where a, b, and c are constants for a particular type of rocket, $h(T)$ is a function of the propellant temperature T, and $F(\gamma)$ is a function of the dive angle γ of the rocket which is defined graphically and is the same for all rockets. The values of these constants and formulas for the function $h(T)$ for several types of Service rockets will be found Section 7.5. Equation (30) can be written

$$\epsilon = \left[A_2 \cdot \frac{g}{2V^2} \cdot R + \frac{ch(T)}{V}\right]F(\gamma), \qquad (31)$$

where

$$A_2 = \frac{2V^2}{g} ae^{-V/b}. \qquad (31a)$$

It is seen that the parameters enter in the first term of equation (31) in the same way they do in equation (29). The functions A_1 and A_2 play corresponding roles in the two formulas, as do $F(\gamma)$ and $(1 - \epsilon_0 \sin\gamma)\cos\gamma$.

Since formula (31) is based on trajectory calculations which take into account air resistance, yaw, motion during burning, etc., it is a more accurate representation of the rocket trajectory than is equation (29). In addition, it includes a term which represents the effect of temperature variations of the propellant on the trajectory.

2.2.3 Launching Characteristics of Rockets

A rocket launched from a zero-length launcher has immediately after release a small velocity with respect to the airplane. As a result, the stabilizing action of the fins tends to cause the rocket to align itself with the airflow or flight line. Accordingly, it is assumed that the rocket leaves the airplane in the direction of the flight line at release. This assumption is further justified by the following considerations. In the usual installation, the launchers are aligned with the boresight datum line and thus are about 25 mils below the flight line during the dive. During the pull-up, however, the angle of attack of the airplane increases. This tends to offset the angle which exists between the launchers and the flight line during the dive, resulting in a close enough alignment of the launchers and the flight line at release so that negligible error is introduced by this assumption.

2.2.4 The Equation for the Pull-Up Time[176]

An equation will now be obtained which determines the pull-up time, T_p, which will result in a hit. The equation will be set up with a delay time of T_d seconds between the release of the rocket and the

ignition of the propellant; thus it is applicable not only to rockets launched from zero-length launchers ($T_d = 0$), but also to the launching of large rockets in which a lanyard or a short time delay fuse is used to insure that the round is a safe distance from the airplane at ignition. The derivation will make use of formula (31); in this way, account is taken of variations in propellant temperature.

The following list itemizes the assumptions made:

1. The target is stationary.
2. The extension of the flight line beyond the point of initiation of pull-up intersects the target.
3. The acceleration during pull-up is perpendicular to the direction of the flight line immediately preceding pull-up.
4. The rocket leaves the airplane in the direction of the flight line *at release*.
5. During the delay period, gravity is the only external force acting on the rocket.
6. Yaw during the delay period has a negligible effect upon the motion.

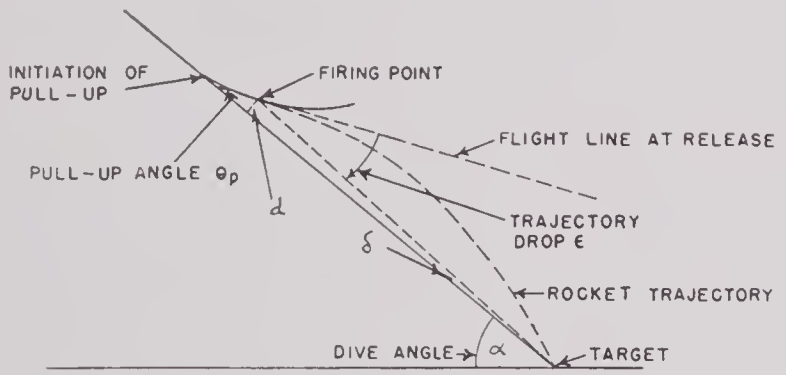

FIGURE 14. Representation of condition for hit (greatly exaggerated). From this diagram, it may be seen that condition for hit is that pull-up angle θ_p be equal to angular trajectory drop ϵ minus angle δ.

Figure 14 shows for the case of no-delay period the principal lines and angles related to the pull-up and the path of the rocket after release.

From this sketch it is seen that a hit is obtained if, and only if,

$$\theta_p = \epsilon - \delta. \tag{32}$$

This relation between angles is made to yield an equation for pull-up time by expressing both members in terms of the physical quantities which constitute the input to the director and the pull-up time.

In radians, the angle δ is given by d/R. The angle ϵ is given by equation (31), but in order to allow for the gravity drop during the delay period between release and ignition, ϵ must be increased by the amount $gT_d \cos\alpha/V$, i.e., the ratio of velocity components perpendicular to and along the collision course. Thus, equation (32) becomes

$$\theta_p = \left[\frac{g}{2V^2}A_2R + \frac{ch(T)}{V}\right]F(\gamma) + \frac{gT_d\cos\alpha}{V} - \frac{d}{R}. \tag{33}$$

In this formula, R is the slant range at the ignition point and is nearly equal to the quantity $V(T_c - T_p - T_d)$. In the small terms ($gT_d \cos\alpha/V$) and d/R, it is sufficiently accurate to take VT_c for R and to replace $\cos\dot{\alpha}$ by $F(\gamma)$. This permits equation (33) to be written in the form

$$\theta_p = \frac{g}{2V}A_2\psi_R(T_c - T_p - T_d) + \frac{ch(T)}{V}\psi_R + \frac{gT_d}{V}\psi_R - \frac{d}{VT_c}, \tag{34}$$

where $\psi_R = F(\gamma)$.

As in Section 2.1, the pull-up angle, θ_p, is given by

$$\theta_p = \frac{g}{V}\int_0^{T_p}(K - \cos\alpha)\,dt. \tag{35}$$

The distance d is given by the double integral

$$d = g\int_0^{T_p}\left[\int_0^t (K - \cos\alpha)\,dt\right]dt.$$

When these are substituted into equation (34), that equation becomes

$$\frac{2}{A_2}\int_0^{T_p}\left[K - \cos\alpha + \frac{A_2\psi_R}{2} + \frac{1}{T_c}\int_0^t (K - \cos\alpha)dt\right]dt = \psi_R T_c + \frac{\psi_R}{A_2}\left[\frac{2ch(T)}{g} + T_d(2 - A_2)\right]. \tag{36}$$

The inner integral $\int_0^t (K - \cos\alpha)dt$ will now be approximated. For this purpose, the expression $K - \cos\alpha$ will be replaced by pt, where p is a constant time rate of change of K during pull-up. This is justifiable since (1) in the normal pull-up it has been found that rockets are released while K is still increasing, (2) K increases nearly linearly, and (3) the term in which this replacement is made is small in relation to the terms to which it is added. It follows, then, that

$$\int_0^t (K - \cos\alpha)dt \cong \int_0^t ptdt = \tfrac{1}{2}pt^2,$$

and

$$\int_0^{T_p}\left[\int_0^t (K - \cos\alpha)dt\right]dt \cong \int_0^{T_p}\frac{pt^2}{2}dt = \frac{pT_p^3}{6}.$$

From equation (32) of Chapter 7,

$$T_p^2 \cong \frac{A_2\psi_R T_c}{p}.$$

Hence,

$$\int_0^{T_p}\int_0^t (K - \cos\alpha)\, dtdt \cong \frac{A_2\psi_R}{6}\, T_p T_c$$

$$= \int_0^{T_p} \tfrac{1}{6}\, A_2\psi_R T_c dt.$$

When this result is put into equation (36), it is found that the relation can be written in the form

$$\frac{2}{A_2}\int_0^{T_p} (K - \cos\alpha + \tfrac{2}{3}A_2\psi_R)dt$$

$$= \psi_R T_c + \frac{\psi_R}{A_2}\left[\frac{2ch(T)}{g} + T_d(2 - A_2)\right]. \quad (37)$$

This equation is fundamental for the bomb director as applied to rockets.

The bomb director measures the quantities K, α, and T_c. It must now be made to integrate the quantity $(K - \cos\alpha + 2A_2\psi_R/3)$ in a satisfactory manner. The number A_2, or *A factor*, depends upon the type of rocket and the velocity of the airplane. It might appear, therefore, that the equipment for rocket tossing should measure also the velocity of the airplane. This is found not to be necessary since the A factor is set for a median airspeed and any variation from this median velocity is partially compensated by anopposite error resulting from the change in angle of attack; this will be referred to again in Sections 2.2.9 and 2.2.10. The final result, as proven by field tests (see Section 5.3), is that the equipment is insensitive to variations in airplane velocity.

2.2.5 Comparison with T_p for Bombs

In order to compare the pull-up time for a rocket with that for a bomb released under similar conditions, the left-hand member of equation (37) may be written

$$\frac{2}{A_2}[\bar{K} - \cos\alpha + \tfrac{2}{3}A_2\psi_R]T_p,$$

where $\bar{K}$ is the time average of K from the beginning of pull-up until the release of the rocket. This permits equation (37) to be written as a linear equation for T_p, and the solution of that equation is

$$T_p = \frac{A_2\psi_R T_c + \psi_R\left[\frac{2ch(T)}{g} + T_d(2 - A_2)\right]}{2[\bar{K} - \cos\alpha + \tfrac{2}{3}A_2\psi_R]}. \quad (38)$$

In order to effect the comparison, the temperature term will be omitted, and T_d will be taken as zero. Equation (38) becomes

$$T_p = \frac{A_2\psi_R T_c}{2(\bar{K} - \cos\alpha + \tfrac{2}{3}A_2\psi_R)}. \quad (39)$$

The corresponding formula for bombs is

$$T_{pB} = \frac{\psi_1 T_c}{\bar{K} + \sqrt{\bar{K}^2 - \bar{K}}}.$$

Recalling that $\psi_R = F(\gamma)$, the similarity of these two formulas provides the justification for the notation ψ_R and for regarding $F(\gamma)$ as the ψ function for rockets. This function is discussed in more detail in Section 7.2.8. The graphs in Figures 15 and 16 show how the values assumed by ψ_1 for bombs and ψ_R for rockets differ.

The denominator $\bar{K} + \sqrt{\bar{K}^2 - \bar{K}}$ is very nearly a linear function of $\bar{K}$, being represented well by $2(\bar{K} - 0.3)$ for the range of values of $\bar{K}$ occurring in rocket tossing. Thus, it is seen that the two denominators are essentially the same. The chief difference in the two formulas is the presence in equation (39) of the factor A_2. It has a value between 0.1 and 0.35, depending upon the type of rocket and the airplane velocity.[179]

2.2.6 Mechanization of the Rocket Tossing Equation

Equation (37) is the relation upon which the instrumentation is to be based. In this article, the temperature variations of the propellant and the effect of the delay period will be ignored. They are treated in detail in Section 7.5. The relation to be mechanized is therefore

$$\frac{2}{A_2}\int_0^{T_p} (K - \cos\alpha + \tfrac{2}{3}A_2\psi_R)dt = \psi_R T_c. \quad (40)$$

The Mark 1, Model 2, bomb-rocket director (Section 3.3) accomplishes the solving of the above equation with a few modifications to the circuit used for bombs. The principal modification is the provision for introducing the A factor.

The equation actually solved by the computer is

$$\frac{2}{A_2}\int_0^{T_p} \frac{dt}{R(t)} = \psi T_c,$$

where $R(t)$ is a resistor whose value is determined by K.

From examination of the circuit constants for the

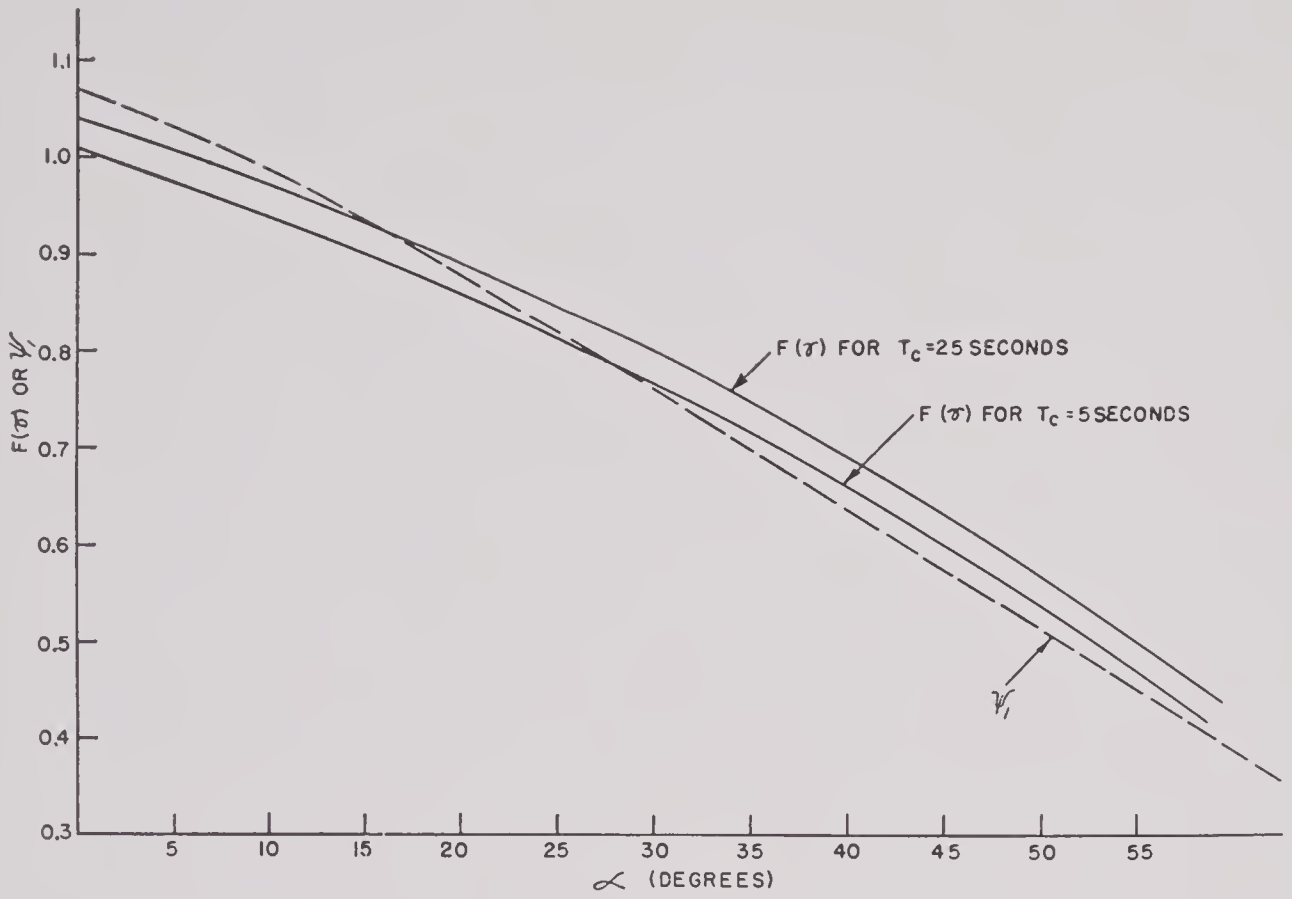

FIGURE 15. Comparison of $F(\gamma)$ (ψ function for rockets) with ψ_1 for bombs. $F(\gamma)$ curves are for 5.0-inch HVAR; bomb function ψ_1 is for $T_c/V = 0.03$. Plane velocity = 500 feet/second.

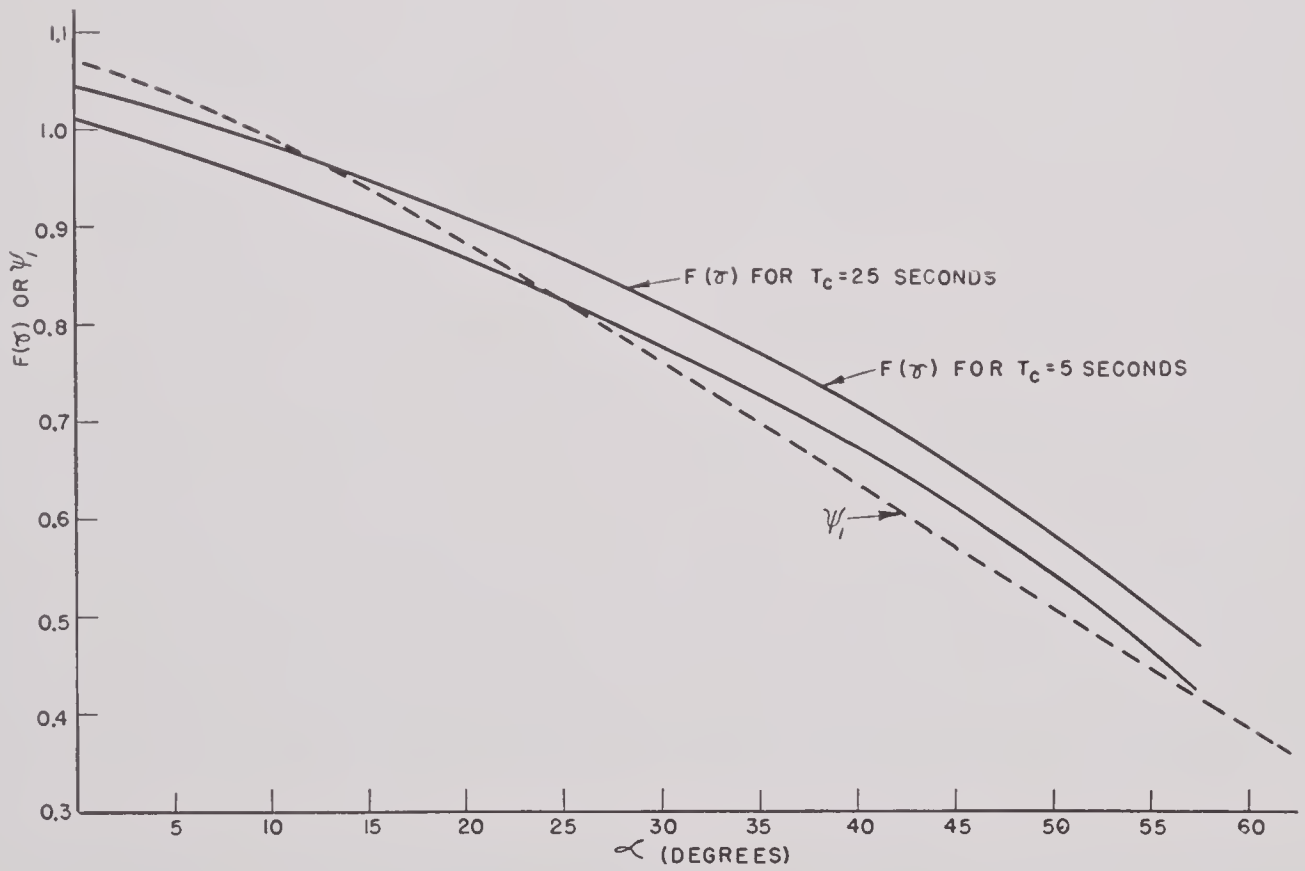

FIGURE 16. Comparison of $F(\gamma)$ (ψ function for rockets) with ψ_1 for bombs. $F(\gamma)$ curves are for 11.75-inch aircraft rockets; bomb function ψ_1 is for $T_c/V = 0.03$. Plane velocity = 500 feet/second.

Mark 1, Model 2, director, it is evident that the resistor $R(t)$ should satisfy the equation

$$R(t) = \frac{5/3}{K - \cos\alpha + \frac{2}{3}A_2\psi_R} \text{ megohms.} \qquad (41)$$

This choice of $R(t)$ will result in computer performance in accordance with equation (40).

The actual construction of $R(t)$ provides that

$$R(t) = \begin{cases} \dfrac{10}{3\psi A_2} & \text{when } \cos\alpha < K < 1.3 \\ \dfrac{10/3}{K + \sqrt{K^2 - K}} & \text{when } 1.3 < K. \end{cases}$$

Consequently, the equation actually solved by the computer is

$$T_{1.3}\psi + \frac{1}{A_2}\int_{T_{1.3}}^{T_p} [K + \sqrt{K^2 - K}]\, dt = T_c\psi, \qquad (42)$$

where $T_{1.3}$ is the time at which K equals 1.3.

The integrands in equations (40) and (42) will now be compared. For convenience, write

$$F_R(K, \alpha, A) = 2(K - \cos\alpha + \tfrac{2}{3}A_2\psi_R).$$

Then, replacing ψ_R by $\cos\alpha$, to which it is roughly equal,

$$F_R(K,\alpha,A) \cong 2K - 2\cos\alpha\,(1 - \tfrac{2}{3}A_2).$$

A median value 0.825 of $\cos\alpha$ is selected, corresponding to $\alpha = 34.4$ degrees, so that $F_R(K,\alpha,A)$ becomes

$$F_R(K, A) = 2K - 1.65(1 - \tfrac{2}{3}A_2). \qquad (43)$$

As a result of this simplification of F_R, the pull-up time determined by the computer will be too short if $\alpha < 34.4$ degrees and too long if $\alpha > 34.4$ degrees. This error is compensated for by use of the ψ function for bombs. As seen from Figures 15 and 16, $\psi_R > \psi$ if $\alpha > 34.4$ degrees. Consequently, the right-hand member of equation (42) is somewhat too small, leading to a value of T_p as determined by the computer which will be too small. In the same way, for small dive angles, a similar compensation occurs.

If A_2 is taken equal to unity in equation (43), an expression essentially equal to $K + \sqrt{K^2 - K}$ is obtained. The following table shows the close agreement between these functions.

K	$K + \sqrt{K^2 - K}$	$F_R(K,1)$	Difference
1.3	1.92	2.05	0.13
2.0	3.41	3.45	0.04
3.0	5.45	5.45	0.00
4.0	7.46	7.45	—0.01
5.0	9.47	9.45	—0.02
6.0	11.48	11.45	—0.03

2.2.7

The A Factor

In Section 2.2.2 two expressions were given for the A factor, namely

$$A_1 = \left(\frac{V}{V + V_R}\right)^2$$

and

$$A_2 = \frac{2V^2}{g} ae^{-V/b}.$$

Graphs of these two expressions show that for the ranges of the parameters occurring in rocket tossing, each is nearly linear in V. A comparison of numerical values furnished by these formulas is given in Section 7.4.4.

Both A_1 and A_2 are to be compared with an A factor determined experimentally. Satisfactory agreement has been obtained between the theoretical and the experimental values (see Section 7.4.5) except in the case of the 11.75-inch AR, for which the experimental A factor is about 40 per cent larger than the theoretical value. The reason for this discrepancy is presumed to lie in conditions obtaining at the release of the rocket.

2.2.8

Compensation for Propellant Temperature and Lanyard

Firing Delay Time. Experimental tests tossing the 5-inch HVAR show approximately a 15-mil shift in mean impact point as the propellant temperature is varied from 0 F to 100 F, other variables being kept the same.[178] It is evident, therefore, that this variable must be taken into account. The trajectory mil drop occurring before firing with a lanyard is of the same order of magnitude as the mil drop due to extreme temperature variations. Both of these drops are to be added to the mil drop after burning, and both are independent of range; it is precisely these drops which determine the value of m in the expression $m + nR$ for total mil drop. In fact, adding the part of equation (30) which pertains to temperature to the gravity drop during the delay period results in the formula

$$m = \frac{ch(T)F(\gamma) + gT_d\cos\alpha}{V} \cong \frac{\omega}{V}[ch(T) + gT_d].$$

The temperature and lanyard control on the Mark 1, Model 2, bomb director[186] provides for the term m. This control is a potentiometer across the output of the gyro. The voltage from the control is

used in the circuit to increase the pull-up time, and consequently, the pull-up angle by the amount m mils. The increase in pull-up angle obtained is proportional to ψ since the voltage is obtained from the gyro and inversely proportional to airplane velocity because the rate of change of pull-up angle is proportional to $1/V$.

A more complete discussion of the theory and operation of this control, together with calibration data and comparison with field results, is given in Section 7.5.

2.2.9 Shift of Impact Point with the A Factor

In equation (33), the term which shows the greatest variation when the A factor is changed and the other parameters kept the same is the term in A_2. Accordingly, a change of amount dA in the A factor results in a change in pull-up angle given by

$$d\theta_p(\text{mils}) \cong \frac{gRF(\gamma)}{2V^2}\, dA \times 10^3. \qquad (44)$$

Since the rocket trajectory deviates but little from the flight line at release, the mil error at the target will be nearly equal to the change in pull-up angle. Thus, equation (44) may be used to find the angular shift in impact point at the target resulting from the change dA in the A factor.

Formula (44) shows that the effect on mil error of increasing the A factor slightly is proportional to the range, inversely proportional to the square of the airplane velocity, and in such a sense that the shot falls long. For R = 2,300 yards, α = 35 degrees, V = 320 knots = 540 feet/second, a change of 0.01 in A corresponds to an error of 2.8 mils at the target. An experimental check at Inyokern with the 5.0-inch HVAR fired from an F4U-1D gave a shift of 2.2 mils under the same conditions.[187] This is regarded as satisfactory agreement with the theory. Roughly, a change in A of 0.01 shifts the impact point 1 mil per thousand yards slant range.

2.2.10 Shift of Impact Point with Plane Velocity

In the Model 2 rocket tossing equipment, no provision is made for measuring and taking into account the plane velocity. Instead, a mean value of the airplane velocities expected to be used is set into the equipment. A considerable variation of airplane velocity from the present value will be shown in this section to have little effect upon the overall dispersion; i.e., the equipment is insensitive to airplane velocity.

Except for smaller terms, the angle δ (see Figure 13) is given by

$$\delta = \epsilon - \theta_p \cong aR\psi_R e^{-V/b} - \frac{gA_2R\psi_R}{2V^2}.$$

If V is increased to V' and a corresponding increase made in A_2 so as to secure a hit, the new δ will be given by

$$\delta' = aR\psi_R e^{-V'/b} - \frac{gA_2'R\psi_R}{2V'^2}.$$

If, however, A_2 is not changed, the angular drop of the rocket from its line of motion at release will still be $aR\psi_R e^{-V'/b}$, but the pull-up angle will now be $gA_2R\psi_R/2V'^2$. The failure to increase A_2 results in the rocket's falling short, the angular error being given by the negative quantity

$$-\frac{gR\psi_R}{2V'^2}(A_2' - A_2). \qquad (45)$$

Since the angle of attack of the airplane during the dive is given by[d]

$$\eta = \frac{CW\cos\alpha}{V^2} - C',$$

the change in angle of attack caused by increasing the velocity by the amount $dV = V' - V$ is

$$d\eta = -\frac{2CW\cos\alpha}{V'^3}\, dV.$$

In order to keep the sight line on the target, this requires a rise in the flight line of amount

$$\frac{2CW\cos\alpha}{V'^3}\, dV, \qquad (46)$$

and the direction of motion of the rocket upon release is elevated by this amount. Combining equations (45) and (46) gives for the total change in the pull-up angle

$$d\theta_p = \frac{2CW\cos\alpha}{V'^3}\, dV - \frac{gR\psi_R}{2V'^2}(A_2' - A_2) \times 10^3. \qquad (47)$$

Since

$$A_2 = \frac{2V^2}{g} ae^{-V/b},$$

it follows that

$$dA_2 = A_2\left(\frac{2}{V'} - \frac{1}{b}\right) dV,$$

[d] In this discussion, no differentiation is made between *indicated* airspeed and *true* airspeed.

and thus equation (47) becomes

$$d\theta_p = \left[\frac{2CW\cos\alpha}{V'} - gR\psi_R A_2\left(\frac{1}{V'} - \frac{1}{2b}\right)\times 10^3\right]\frac{dV}{V'^2}. \tag{48}$$

Figure 17 shows a graph of $d\theta_p/dV$, that is, of the rate of change of mil error for each foot/second change in airplane velocity. In the construction of

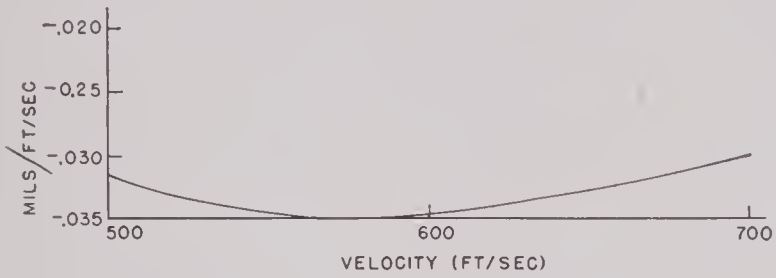

FIGURE 17. Rate of change of rocket impact with airplane velocity. (Computations are based on range of 7,680 feet, dive angle of 35 degrees, and constants for F6F-5 airplane and 5.0-inch HVAR.)

this graph, a dive angle of 35 degrees was used and a range of 7,680 feet was assumed, and the other constants are those of an F6F-5 airplane and the 5.0-inch HVAR. This graph shows that a change of 10 feet/second in airplane velocity causes a shift of less than ½ mil in impact error.

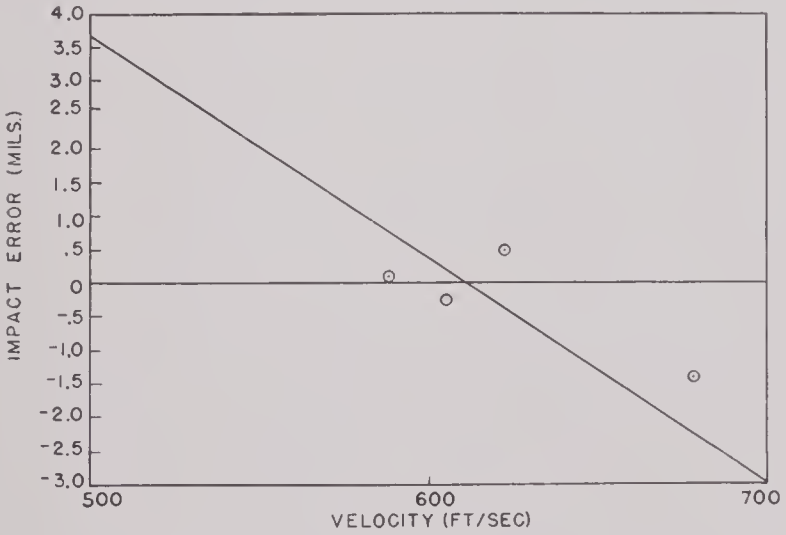

FIGURE 18. Rocket impact error as function of airplane velocity when sight is calibrated at 608 feet/second. (Computations are based on F6F-5 airplane and 5-inch HVAR, slant range of 7,680 feet, and dive angle of 35 degrees. Zero error is assumed for airplane velocity of 608 feet/second. Isolated points represent data from field tests using same type of airplane and rocket.

Figure 18 shows the theoretical mil error for a slant range of 7,680 feet and a dive angle of 35 degrees, again with an F6F-5 airplane and the 5.0-inch HVAR. The graph was obtained by computing the integral of equation (48) with the constant of integration chosen so that the error would be zero at 360 knots = 608 feet/second. The isolated points on the graph are from data obtained at Inyokern with the same combination of airplane and rocket.[17s] Within the accuracy of the test, the agreement with theory is satisfactory. In this typical case, the graph shows that a shift in velocity of about 30 feet/second or 18 knots is required to produce a shift of 1 mil at the target.

The fact that the MPI shift with velocity is small does not mean that the A factor need not be set accurately. It means that when the A factor has been correctly set so as to produce a hit, then a small change in the velocity of the airplane will not lead to large errors at the target.

2.3 TORPEDO TOSSING[e]

In the normal method of releasing torpedoes from aircraft, the distance by which the torpedo falls short of the target may be as much as 3,000 yards. As a consequence, the total travel time of the torpedo in the water is large, and the target may have sufficient time to engage in evasive maneuvers. In order to reduce this travel time to a minimum, it is desired to be able to locate accurately the point of impact of the torpedo in an interval between 450 and 900 feet short of the target. This minimum distance short is required to allow sufficient water travel to arm the torpedo.

The bomb director may be utilized to toss torpedoes by introducing instrumentally a ΔT_c of such an amount as to cause the torpedo to fall the required distance short. The ΔT_c required to place the torpedo exactly 450 feet short for a toss bombing maneuver initiated at a dive angle of 25 degrees and at a second altitude point of 1,395 feet was computed and found to be 3.719 seconds. Using this value of ΔT_c, the minimum and maximum altitudes were determined for dive angles between 15 and 25 degrees, such that the torpedo falls between 450 feet and 1,350 feet short of the target.[40] The results are summarized in graphical form in Figure 19, vacuum trajectories being plotted. This makes it possible to approximate visually the angle of release of the torpedo with respect to the horizon, the angle of entrance into the water, the distance short from the target, and the limits on range and dive angle. In the figure, the lower area shaded with the single

[e] Sections 2.3 and 2.4 were written by Dr. Albert London, of the National Bureau of Standards.

diagonal lines includes all toss bombing pull-ups for which the torpedo will have an impact point within the interval of 450 to 900 feet short, while the upper cross-hatched region corresponds to an interval of 900 to 1,350 feet short. It should be emphasized that these areas on the graph represent the limiting values of the second altitude point, and initiation of the dive occurs, of course, at correspondingly higher altitudes. All important physical quantities may be read from the graph. The values of some are tabulated in the table below for $V = 250$ knots, $K = 3$, and $\Delta T_c = 3.719$ seconds.

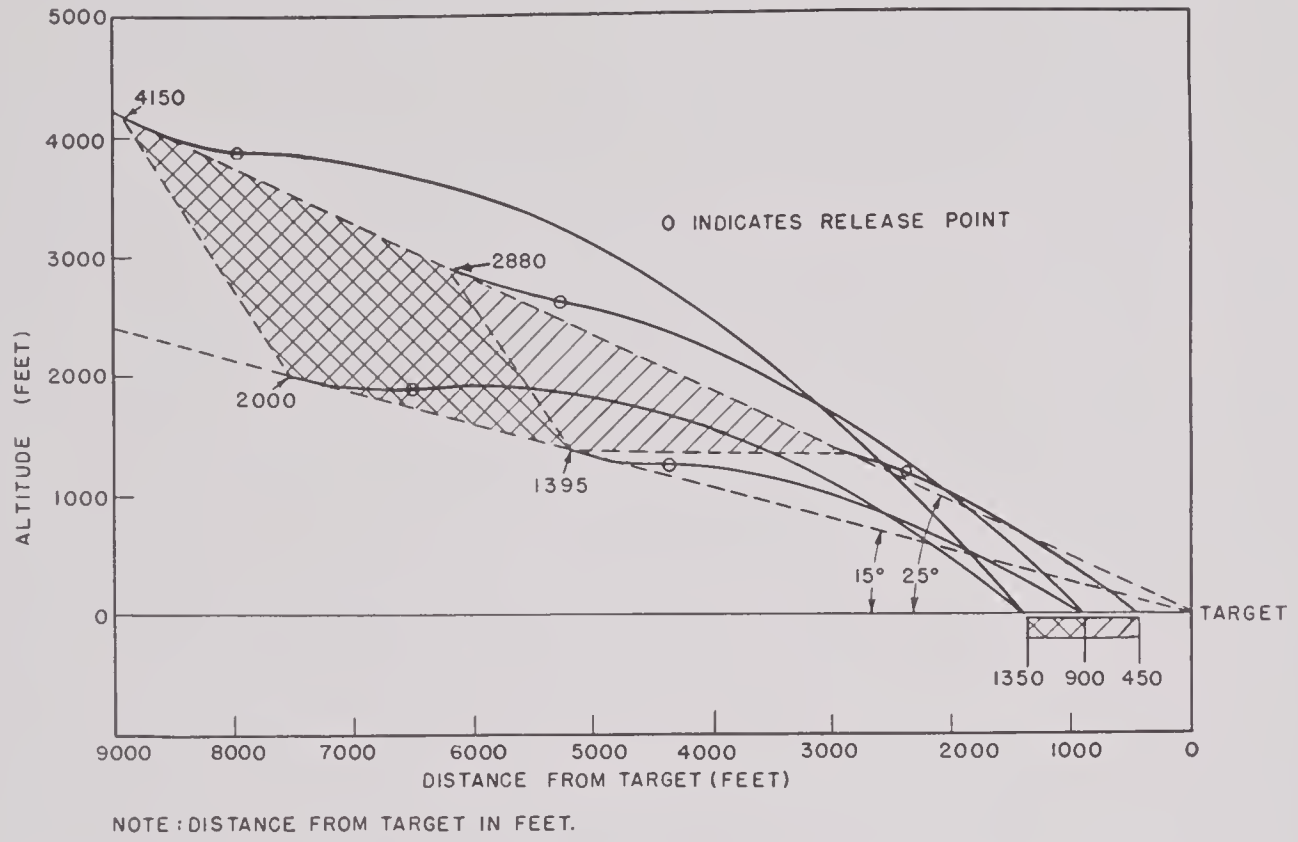

FIGURE 19. Torpedo tossing chart (vacuum trajectories) for $V = 250$ knots, $K = 3$, and $\Delta T_c = 3.719$ seconds. Area shaded with single diagonal lines shows range of values of dive angle and second altitude which will place torpedo 450 to 900 feet short of target; cross-hatched area corresponds to interval of 900 to 1,350 feet.

2.4 WIND CORRECTION

2.4.1 Toss Bombing: Wind Correction Procedure

In order to compensate for the effect of wind, a number of different methods are available. However, practically all of them may be classified under two main headings:

1. Methods involving special sighting procedures.
2. Instrumental methods which compute the magnitude of the wind and automatically make the required correction.

2.4.2 Sighting Method

In the sighting method of compensating for wind, if an estimate of the magnitude and direction of the wind is not available, a preliminary bombing run may be made. The mil errors, both in range and deflection, are noted and on the second run, the aiming point is changed to correspond to the observed error in the first run. An application of this principle is the squadron method in which a group of planes all make the same approach on a target. The

Dive angle (degrees)	Second altitude point (feet)	Pull-up altitude (feet)	Slant range (feet)	Release angle (degrees)	Entrance angle (degrees)	Impact point from target (feet)
25	1,395	1,210	3,301	— 20	37	450
	2,880	2,880	6,760	— 9	44	887
	4,150	4,150	9,820	— 1	50	1,362
15	1,395	1,360	5,390	— 2	34	900
	2,000	2,000	7,727	6	41	1,361

first plane makes the preliminary run. The following planes note the impact point and change their aim accordingly. Experimental results obtained by this method show a marked improvement in accuracy.

to construct similar sighting charts for any type of sight reticle. In this method of sighting, the bombing run is made, keeping the target located at a fixed point in the sight field. This point will be the center

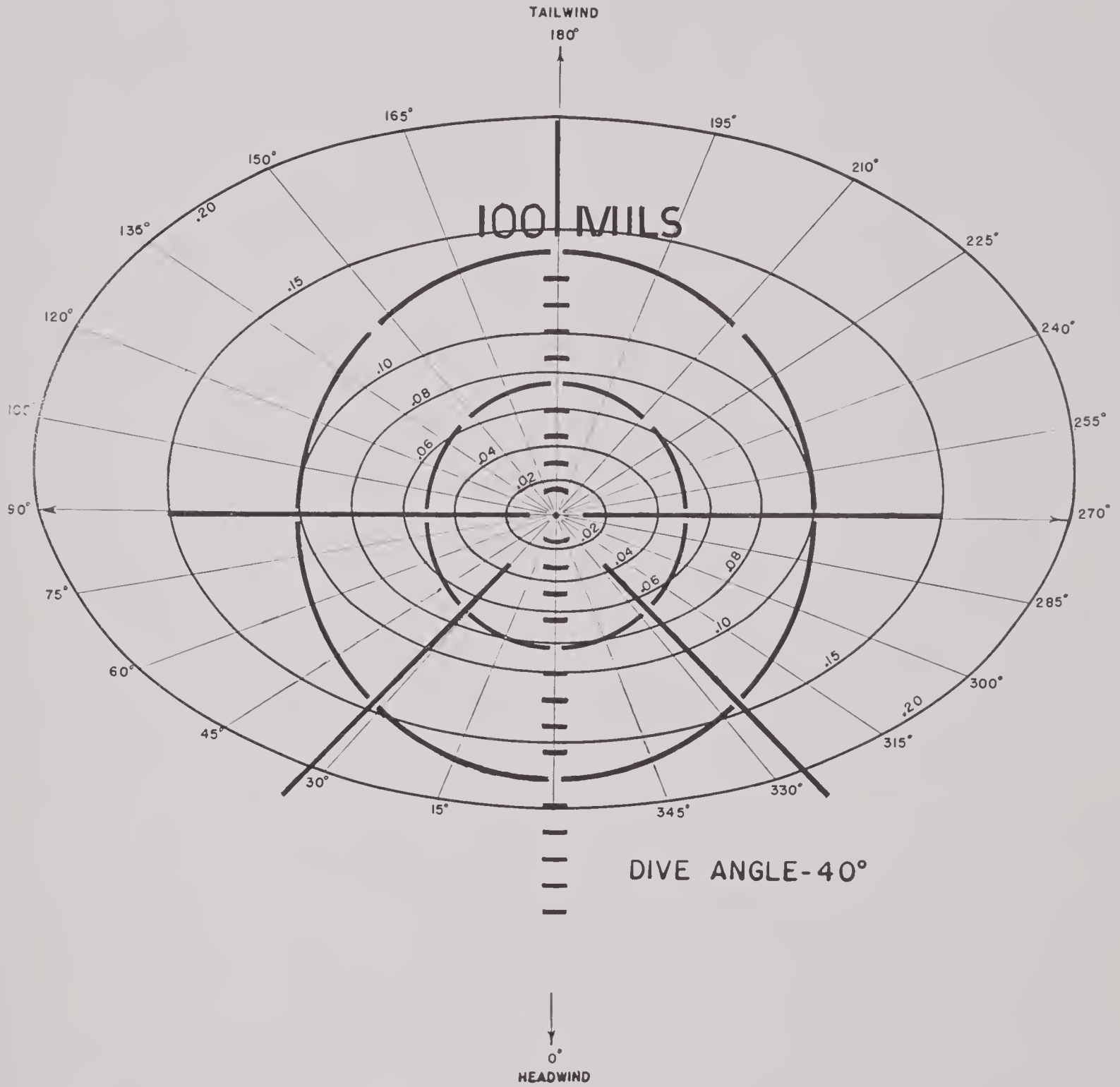

FIGURE 20. Wind correction chart for 40-degree dive angle, with superimposed Mark 8 gunsight reticle. (See text for directions as to use.)

If the magnitude and direction of the wind relative to the intended direction of approach of the airplane are known approximately, it is possible to use the sighting grids, [71, 80] an example of which is shown in Figure 20, to determine the aiming point required. These wind correction charts are drawn with the Mark 8 gunsight reticle superimposed. It is possible

pip of the sight in the zero-wind case only. If this aiming point is used, a collision course approach will be established for the bombing run. Instructions for using the charts follow:

1. Select the wind-correction chart corresponding to the approximate dive angle at which the toss

bombing maneuver is to be conducted. (Figure 20 is for a 40-degree dive angle.)

2. The wind-correction ellipses on the chart correspond to different values of the ratio of wind velocity to airplane dive velocity, each ellipse corresponding to a fixed value of this ratio. Thus, if the wind velocity is 30 knots, and airplane velocity 300 knots, the ratio is .10 and the ellipse marked .10 should be used.

3. The required sighting point may then be determined from the direction of the wind relative to the intended heading of the airplane in the dive, this point being determined by the intersection of the wind-airplane velocity ratio ellipse with the wind direction radius. Thus, if the ratio is .10 and the direction of the wind is 15 degrees relative to the heading of the airplane, the target should be kept fixed in the sight at the point which is the intersection of the .10 ellipse with the 15-degree line.

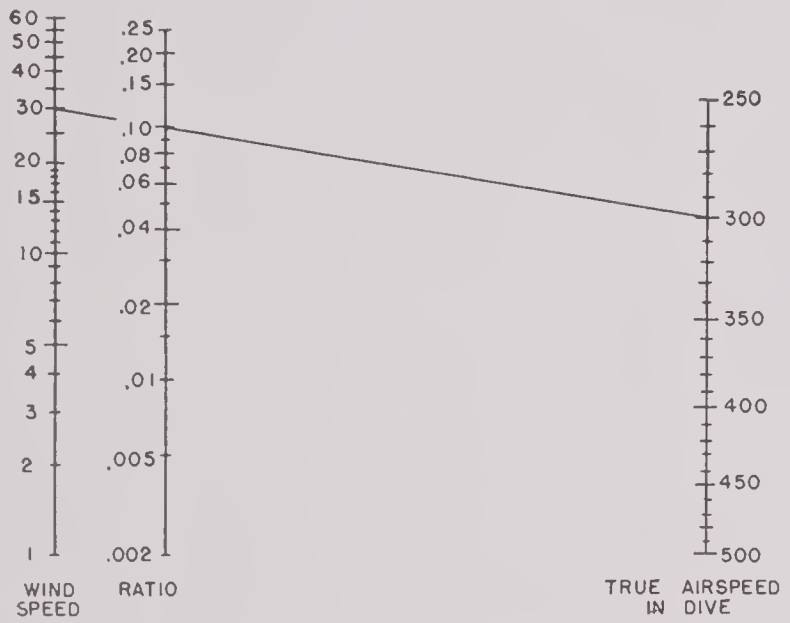

FIGURE 21. Nomogram to determine ratio of wind speed to airspeed. (To use, set straight edge through proper values of wind speed and airspeed in dive and read off ratio. Speeds are in knots.)

4. The pull-up should be made in the vertical plane; i.e., the target or aiming point should move downward in a direction parallel to the vertical line of the sight reticle.

Figure 21 is a nomogram which may be used for determining the ratio of wind velocity to airplane velocity. A mathematical discussion of the nature of the wind correction grids is given in Section 6.6.

The same grids may be used in firing rockets if the plane velocity is replaced by the final rocket velocity in computing the value of the wind-projectile velocity ratio. A nomogram similar to that of Figure 21 can be used to give the desired ratio as a function of rocket type and wind velocity. *It is assumed that the speed of the plane is 375 knots, but the results can be applied with negligible error at other speeds.* Having determined the appropriate ratio, the correction is made as in the case of bombs.[182]

2.4.3 Instrumental Method of Wind Correction

The instrumental method of correcting for wind (or equivalent target motion) was in its preliminary developmental stage at the end of the war. At that time it had been proposed to compensate for range winds only, i.e., head or tail winds. In this method,[51] the pilot flies a pursuit course, keeping his sight pip fixed on the target. Consequently, in the presence of wind, the flight path is curved, the dive angle varying with time. The rate of change of dive angle with time is measured by a rate-of-turn or pitch gyro and is a function of the wind velocity. The voltage output from the gyro may be used to decrease or increase the no-wind bomb release time by the amount necessary to obtain a hit. Further details of this method will be found in Chapter 6.

Chapter 3

INSTRUMENTATION[a]

3.1 INTRODUCTION

THE OPERATION of the bomb director Mark 1 Model 1, AN/ASG-10, which provides for bomb and torpedo tossing, and of the bomb director Mark 1 Model 2, AN/ASG-10A, which provides also for the tossing of rockets, is described in Sections 3.2 and 3.3. The pilot production units which were designated as Mark 1 Model 0, AN/ASG-10(XN) are described briefly in Section 3.4 and further in Section 3.5. The circuit diagrams changed considerably during development, but the operating principles which are embodied in the Mark 1 Model 1 and Mark 1 Model 2 circuits are essentially the same as in the Mark 1 Model 0. (Detailed instructions as to installation and maintenance of the bomb director Mark 1 Model 0 are given in reference 220; of the bomb director Mark 1 Model 1 in reference 232c.)

Problems connected with the actual construction and assembly of the bomb director are discussed in Section 3.5 and, with laboratory testing, in Section 3.6.

The most advanced developmental work which did not reach the stage of production by the end of the war is given in Chapter 8.

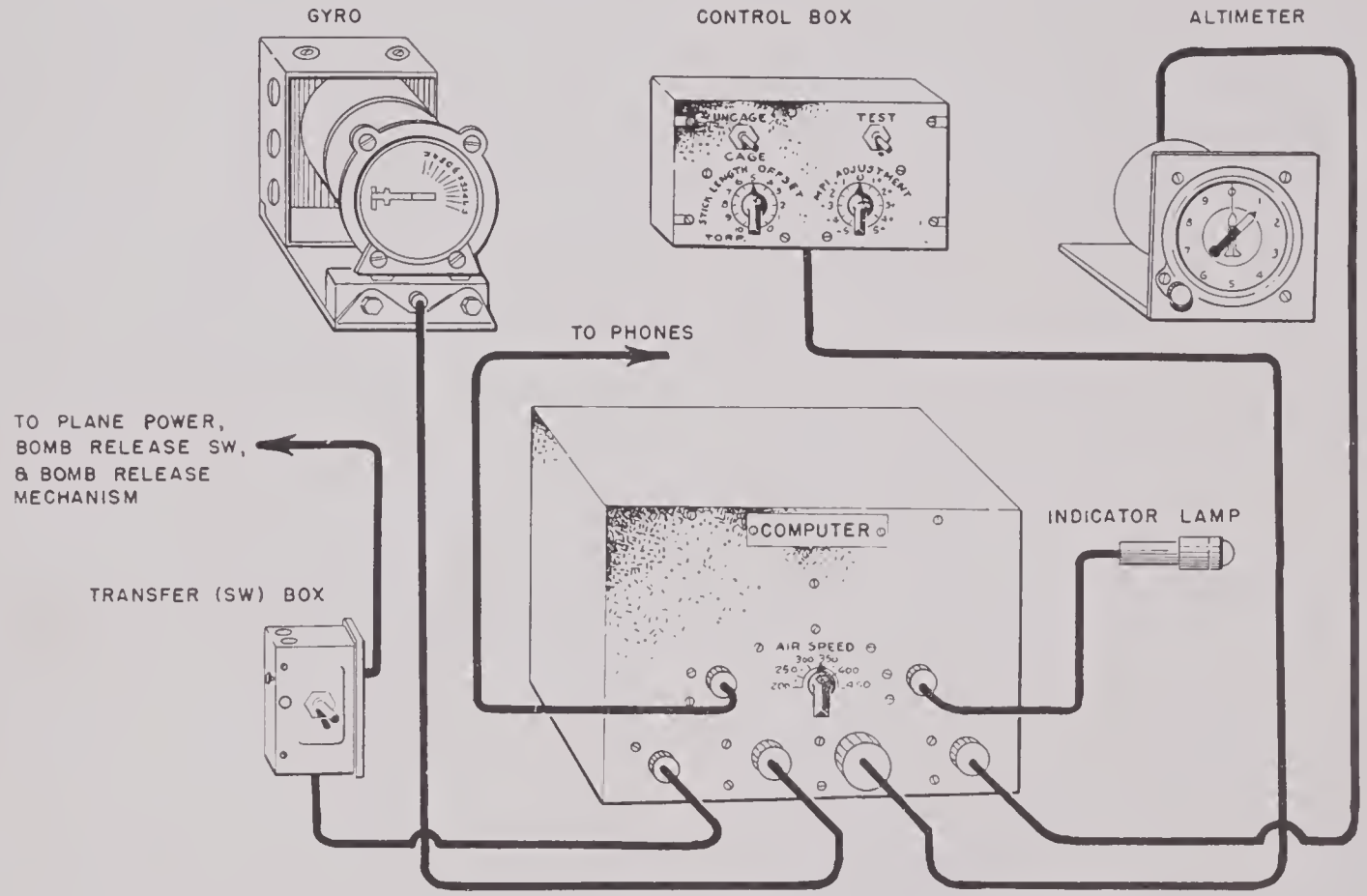

FIGURE 1. Bomb director Mark 1 Model 1 AN/ASG-10, components and interunit cabling.

3.2 BOMB DIRECTOR MARK 1 MODEL 1, AN/ASG-10

3.2.1 Assembly

The bomb director Mark 1 Model 1 consists of an altimeter unit, a gyro unit, computer, control box, switch box, and an indicator lamp which are electrically interconnected by cables. Figure 1 shows a sketch of the components. A functional diagram of its circuit is given in Figure 2. This equipment is so designed that it determines the required release instant on the basis of the time to target T_c, the angle of dive α, and number of g's pull-up acceleration K.

[a] Chapter 3 is based on material compiled by V. W. Cohen and F. M. Defandorf, of the National Bureau of Standards, and on the final report of the Magnavox Company.[202]

The manner in which it performs this operation will be discussed by describing the function of each unit separately, starting with the altimeter.

around the periphery of the dial extending from an altitude indication of 10,328 feet down to 1,390 feet in steps which are in the ratio of 6 to 5. The contacts

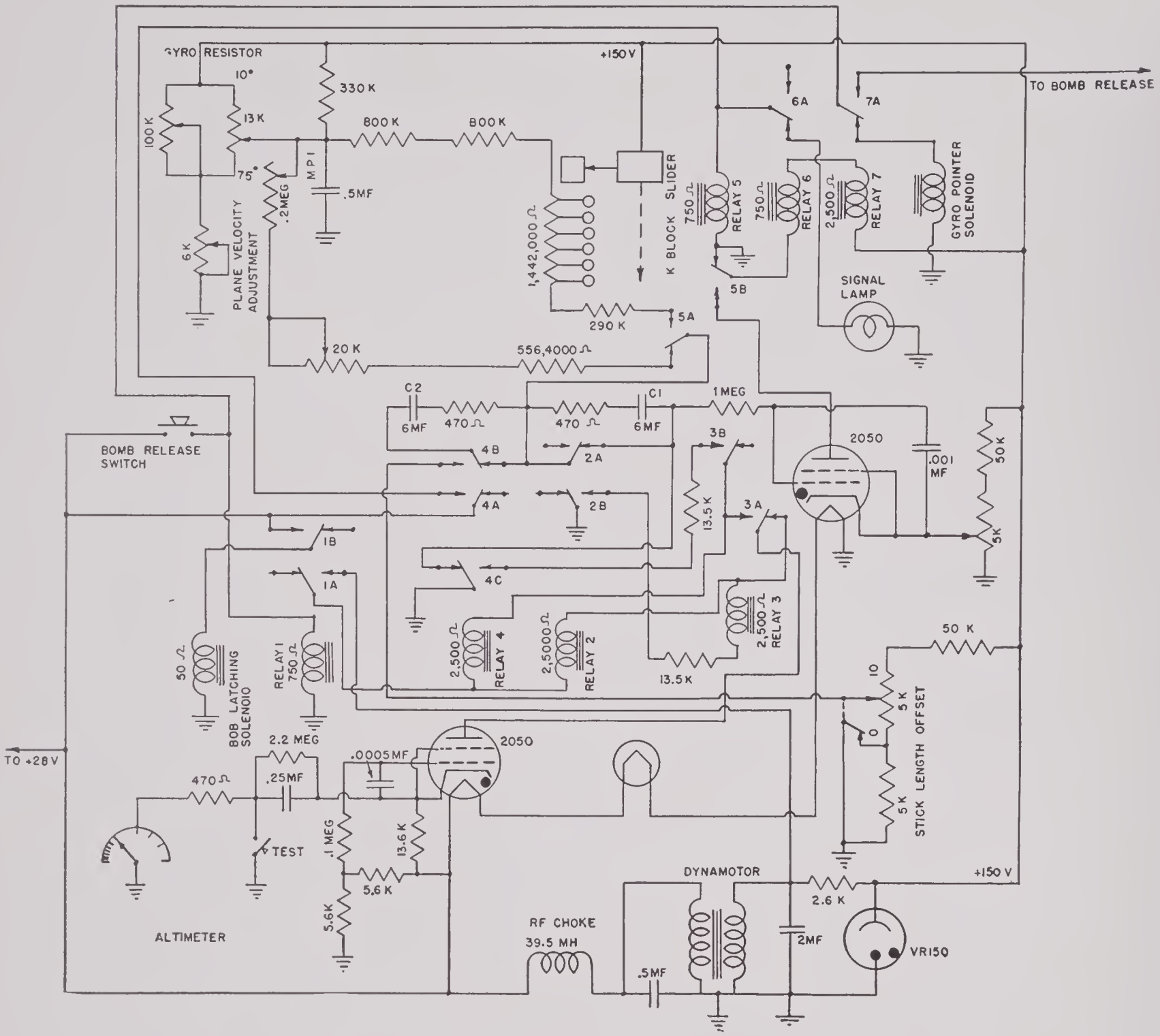

FIGURE 2. Functional circuit diagram of bomb director Mark 1 Model 1, AN/ASG-10.

3.2.2 Altimeter Unit Mark 1 Model 1, ID-112/ASG-10

The altimeter unit supplies the electrical computer with time-to-target information. The instrument is a Kollsman sensitive altimeter which has been modified through the addition of a fine ribbon contact on its 1,000-foot hand and a series of contacts on the altimeter may be seen in Figure 3. In Figure 3 the Model 0 altimeter is shown with the glass face removed to show the fixed contacts around the periphery. There is no significant difference between the Model 0 and Model 1 altimeters. As indicated in Figure 2 the operations within the altimeter consist in merely grounding the various altitude points. Discussion of subsequent operations is given in

Section 3.2.4. In all cases the altimeter is preset to indicate altitude above the target to be attacked. Thus, for a uniform-speed constant-angle dive, the elapsed time between any two altimeter contacts will be one-fifth the time it would take the plane to reach the target from the second-altitude point.

FIGURE 3. Altimeter unit, Mark 1 Model 0, with cover glass removed. Note fine ribbon contact on 1,000-foot hand and contacts on rim at following altitudes: 1,390, 1,668, 2,002, 2,402, 2,882, 3,459, 4,151, 4,981, 5,977, 7,172, 8,607, and 10,328 feet. Model 1 (see assembly drawing, Figure 1 of Chapter 4) is essentially same as Model 0.

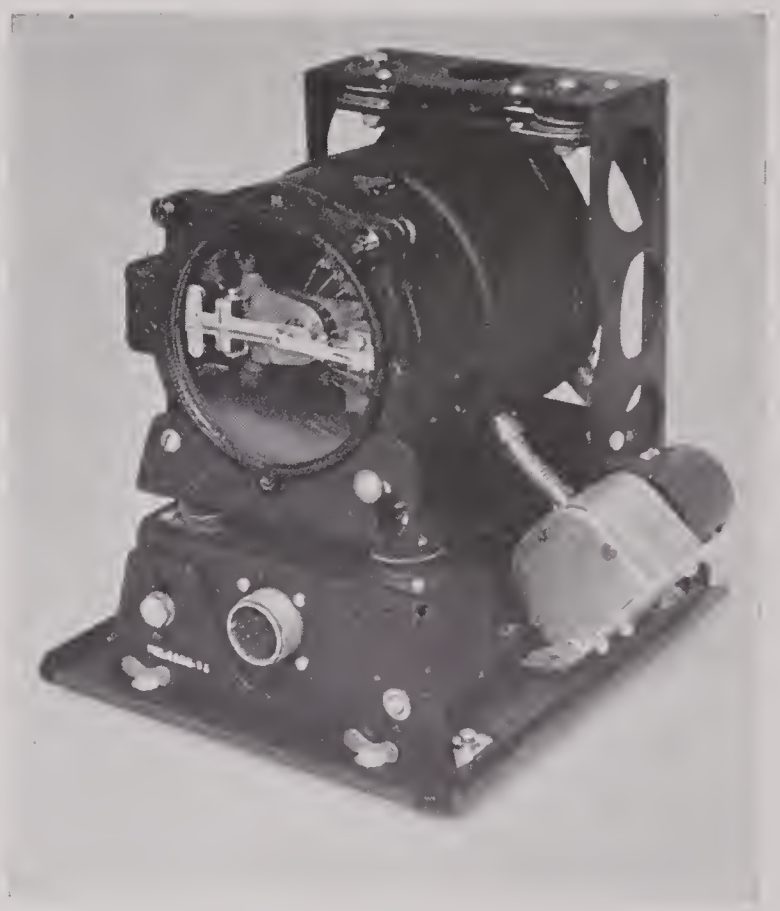

FIGURE 4. Gyro Mark 20 Model 0 (XN2), shock-mounted and equipped with electric motor for caging and uncaging. Model 1 (see assembly drawing, Figure 1 of Chapter 4) is essentially same as Model 0.

3.2.3 Gyro Mark 20 Model 1, MX-329/ASG-10

The gyro furnishes the intelligence related to the angle of dive. It is a Sperry Artificial Horizon indicator with a 60-degree sector of a circular tapered wire-wound potential divider mounted inside its case. Contact with the resistance strip is made through a contact arm mounted on the gyro's gimbal ring and operated by a solenoid in the arming circuit of the plane. A modified gyro is shown in Figure 4. The resistance strip, commonly referred to as the ψ card, is composed of three linear segments (see Section 6.3.3) and is so designed that it provides the required dive-angle correction for a plane speed of 500 feet/second. A ψ card in various stages of assembly is shown in Figure 5. Adjustment to compensate for other plane velocities (T_c/V corrections) is made through a variable resistor which is connected in series with the strip. This adjustment is not critical since the ψ factor is mainly a function of the dive angle and varies only slightly with plane speed. It is not intended to adjust this control

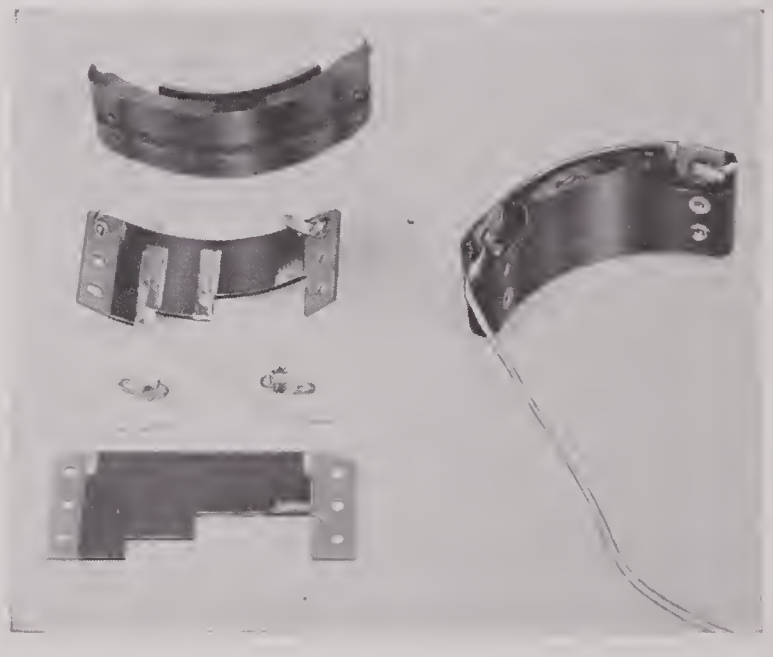

FIGURE 5. A 3-step wire-wound ψ card in two stages of assembly. At bottom left is shown straight wire-wound card; above it is shown card after it has been heat-formed to proper radius. At top left is molded bakelite card holder. At right is ψ card mounted on holder.

except in such extreme cases as would result when changing the equipment from fighters to torpedo bombers.

The instrument is uncaged in level flight before the plane enters the dive toward the target. When the pilot closes the bomb release switch to start computer operation, the gimbal arm contact is brought into contact with the resistance strip.

3.2.4 Computer Mark 20 Model 1, CP-15/ASG-10

The computer combines the information from the different intelligence sources and automatically triggers the bomb release circuit at the proper time.

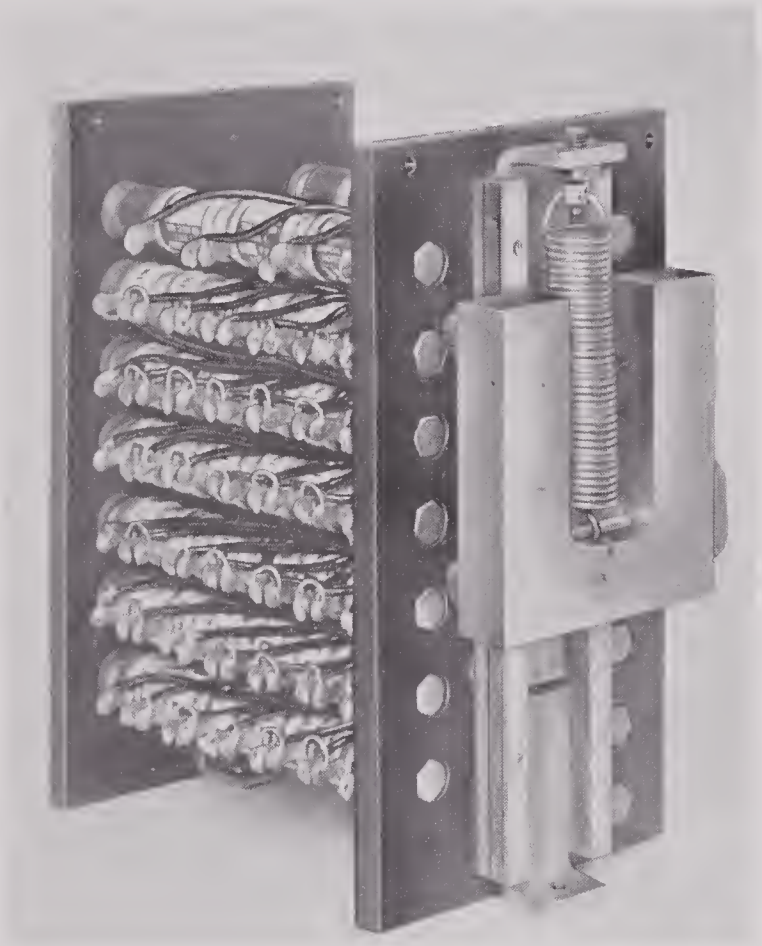

FIGURE 6. Accelerometer or *K*-block assembly of Model 0 computer, showing spring-supported weight (or bob) in position. Contact carried by bob (see Figure 7) slides over segmented commutator (or *K* block) connected to network of precision resistors.

One intelligence source, the acceleration integrator, is so intimately related to the computing action that it is built into the complete unit and generally is considered part of it.

Acceleration is indicated by a spring-supported weight, such as is shown in Figure 6. The weight carries a sliding contact over a commutator block (generally called the *K* block) consisting of 83 insulated metal disks. These are shown in Figure 7, which is another view of the object shown in Figure 6, but with the spring supported weight removed. The segments of the commutator are connected to a network of precision resistors (shown in Figure 6). Figure 6 is actually of a Model 0 computer, but the basic operations are the same as in the Model 1. The latter is shown in Figure 11.

The computer assembly contains, in addition to the acceleration integrator, the timing capacitors, the altimeter circuit and release circuit thyratrons, a dynamotor which supplies 285 volts d-c, and relays.

The sequence of operations in the computer is as follows: (all circuit references are to Figure 2).

1. Placing the power switch in the *ON* position starts the dynamotor, heats the cathode in each of the thyratrons, establishes the proper thyratron grid biases, and places 150 volts between the 0-degree position on the gyro resistor and ground. This

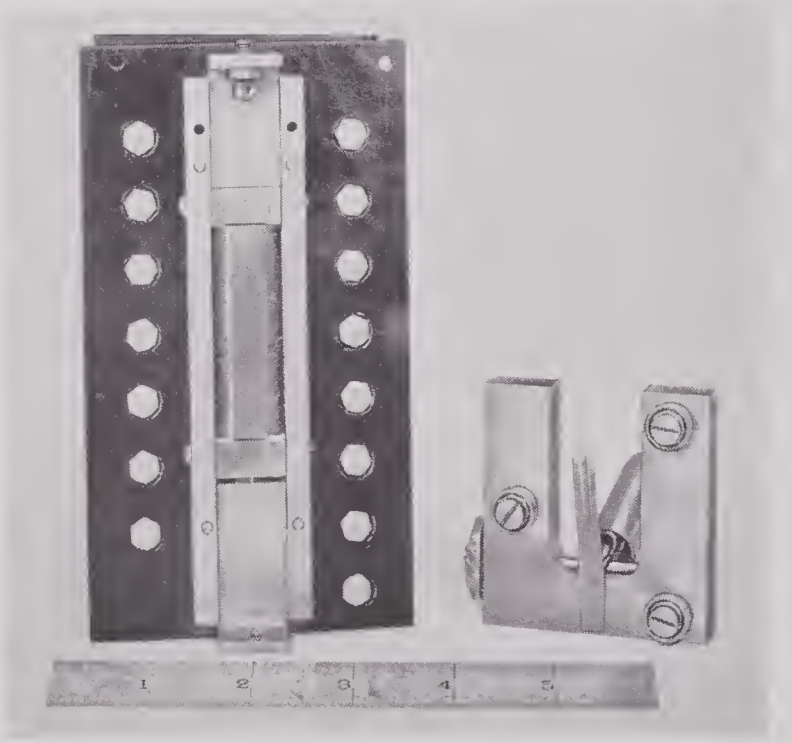

FIGURE 7. Another view of *K*-block assembly with spring-actuated weight removed to show commutator segments.

switch is closed far enough in advance of the dive to enable circuit elements to become stabilized.

2. Closing the bomb release switch operates relay No. 1. This energizes the gyro solenoid, applies +285 volts to the plate of the altimeter thyratron, and operates the bob latching solenoid to free the acceleration bob.

3. The actual computing operation starts at the

first altimeter contact following the closing of the bomb release switch. The altimeter hand ribbon, in sweeping across this peripheral contact, fires the thyratron by grounding its cathode and thereby dropping its potential momentarily to a potential which is several volts below the potential of the grid. The resultant plate current operates relay No. 2 which removes the short from the first 6-mfd capacitor, C_1, and applies the gyro output voltage to it through a resistance having a nominal value of 2/3 megohm. (In the Model 0 this capacitor as well as C_2 had a 2-μf value.) Relay No. 2 simultaneously operates relay No. 3 which locks relay No. 2 and quenches the thyratron by breaking its plate circuit briefly at the 3A contact. Relay contact 3A again applies +285 volts to the thyratron plate.

4. When the second altimeter contact is made, the thyratron again fires because its cathode is grounded momentarily. The resultant plate current now operates relay No. 4. This applies current to the signal lamp notifying the pilot to commence pull-up. It simultaneously ungrounds the negative side of condenser C_1 (isolating its charge), removes the short from the second 6-mfd capacitor C_2, and connects one side of the latter to ground (except for the small amount of bias produced by the stick-length offset). The charge acquired by C_1 was acquired during the time it took the plane to travel between the two altimeter points; hence, it is proportional to T_c. Since the negative side of this capacitor is connected to the grid of the release circuit thyratron, and the mid-point between C_1 and C_2 is essentially at ground potential through C_2 at this instant, the voltage associated with the above charge lowers the thyratron grid a corresponding amount below ground. Relay No. 4 furthermore operates relay No. 5 which causes the charging current to capacitor C_2 to pass through the K block circuit whose resistance is nominally 10/3 megohm. At the same time relay No. 5 puts + 150 volts on the plate of the release circuit thyratron.

Should the dive continue toward the target without pull-up, these two equal capacitors will have equal charges when the target is reached, since the same charging voltage would be used for both, while the resistances of the two circuits bear the same ratio as the corresponding charging times. As the charge on C_2 increases, the thyratron grid becomes less and less negative, the difference between the voltages on the two capacitors being proportional to the remaining time to target.

5. When pull-up begins, the K block bob moves downward under the action of the imposed pull-up acceleration. This applies the 150-volt supply directly to one of the K block segments through the contact attached to the bob. The resistors connected to the K block are chosen so that for an acceleration of Kg's, the effective resistance in the circuit is

$$\frac{10}{3\,(K+\sqrt{K^2-K})} \text{ megohm.}$$

The thyratron fires when the charges accumulated on the two capacitors become equal at T_p seconds and the following equation is satisfied:

$$\int_0^{T_p} (K+\sqrt{K^2-K})\,dt = T_c\psi.$$

(See Section 2.1.)

6. Firing of the release circuit thyratron operates two relays, No. 6 and No. 7. The latter energizes the bomb release mechanism and at the same time frees the gyro arm contact. No. 6 extinguishes the signal lamp to indicate that the bomb has been released.

7. Consistent computer operation is assured by means of the following provisions. (a) Firing of the altimeter thyratron by closing the bomb release switch while the altimeter ribbon is on a peripheral contact is prevented by the 0.25-mf capacitor in the altimeter-cathode lead. Closing the altimeter contact quickly charges this capacitor and prevents the passage of another pulse until the altimeter contact is open for about 0.3 second. If the altimeter contact closes before plate voltage is applied to the thyratron, the thyratron will not fire until the next altitude point is reached. This capacitor also prevents more than one pulse per contact since it retains its charge for sufficient time to allow the altimeter hand to travel completely across the contact. (b) A 0.3-megohm resistor placed between the 150-volt terminal and the gyro contact arm insures that the computer will receive a charge corresponding to a 40-degree dive angle in case of any failure in the gyro circuit. (c) Releasing the bomb release switch at any time prior to bomb release automatically restores the circuit to its normal standby condition.

3.2.5 Control Box Mark 8 Model 1, C-200/ASG-10 for Console Installation, C-203/ASG-10 for Other Installations

This unit houses switches and controls operated by the pilot as follows:

1. *A switch* to cage or uncage the gyro electrically.

2. *A momentary test switch.* This provides the pilot with a check on the operation of the computer. The switch is wired across the altimeter contacts. If the equipment is operating properly, it should require five times the time between two operations of the switch to release the bomb.

3. *Stick-length offset.* This adjustment is used in releasing a stick of bombs to cause the first bomb to hit short of the target. It imposes an initial positive bias on the second capacitor. This shortens its charging period by a definite time and produces the desired reduction in T_p. One position of this switch is used for torpedo tossing. This control is shown in simplified form in Figure 4, Chapter 2.

4. *MPI adjustment.* This control provides a means of increasing or decreasing the pull-up time. The adjustment changes the resistance in the first capacitor circuit. Increasing the resistance decreases the charging rate and thus decreases the charge which will be stored in the first capacitor during the timing run. The adjustment is adequate to compensate for small errors in sight setting and differences in the ballistic coefficients of different types of bombs. (This control is shown in simplified form in Figure 4 of Chapter 2.)

5. *Torpedo tossing.* In tossing torpedoes (see Section 2.3) the stick-length offset control is turned to its maximum counterclockwise position, marked TORP. This applies a positive bias to the second capacitor, and consequently shortens the pull-up time sufficiently to cause the torpedo to enter the water 150 to 450 yards short of the target when the release altitude is less than 2,000 feet, and dive angles are between 15 and 25 degrees. The amount the torpedo will strike short is dependent on dive angle and altitude of release.

3.2.6 Switch Box (Transfer) Mark 2, Model 1, J-108/ASG-10

This component houses the off-on switch which simultaneously connects the bomb director to the plane power supply and to the bomb release circuit. The connection is so made that the switch in its off position returns the release mechanism to conventional electrical operation. This unit also contains a 5-ampere circuit breaker.

3.2.7 Indicator Lamp, MX-339/ASG-10

This lamp lights when the second altimeter contact is made, indicating to the pilot that he may pull up; and this lamp remains lit until the bomb is released. A buzzer, which is wired in parallel with the lamp and which produces an audible signal in the phone circuit, was also provided in a number of Model 1 computers.

3.3 BOMB DIRECTOR MARK 1 MODEL 2, AN/ASG-10A

3.3.1 Assembly

The circuit of the Model 2 bomb director is so arranged that bombs, rockets, or torpedoes can be tossed. When set for bombs, the circuit is identical with the bomb director Mark 1 Model 1 discussed in Section 3.2. A sketch of its components is shown in Figure 8, and a functional diagram of its circuit in Figure 9. Components which are used solely for rocket tossing are indicated with heavy lines. The changes which have been made consist of adding a rocket calibration capacitor, a temperature and lanyard-length control, and a relay to the computer circuit, and of combining the transfer switch box with the control box. The altimeter and gyro units remain unchanged.

3.3.2 Computer Mark 20 Model 2, CP-15A/ASG-10

1. *Rocket calibration capacitor,* C_0. This is a capacitor bank which provides the A factor correction (see Section 2.2.7) by reducing the capacitance of the second charging circuit at the beginning of pull-up. It thereby shortens the pull-up time T_p, to compensate for the smaller trajectory drop in the case of rockets. The capacitor setting is controlled by the *coarse* rocket calibration dial and is determined by the type of rocket to be tossed and the velocity of the plane (i.e., the A factor). The *fine* control, which corresponds to the MPI adjustment for bombs, is a vernier on the coarse control. The matter of placing the rocket capacitor in series with the second capacitor at the beginning of pull-out is brought about through the action of relay No. 8 which is de-energized when the K block bob contact reaches the 1.3 segment in its downward motion.

2. *Temperature and lanyard-length control.* The larger trajectory drop of the rockets at low ambient temperature of cold as compared with that of rockets at high ambient temperature, and the drop which occurs between release and firing when rockets are launched with a lanyard are compensated for by

placing an appropriate negative charge on the C_0 capacitor prior to the beginning of pull-up. This has the effect of increasing the pull-up time by the required amount.

3. *Relay No. 9.* This relay serves merely to eliminate the effect of the rocket calibration capacitor and relay No. 8 when the equipment is used for toss bombing.

differed in a number of important mechanical design details. Some of the changes in the production models were made to facilitate their manufacture (see Section 3.5), others were made to improve the reliability of operation (see Chapter 4). The major difference, in the ψ potentiometer design, has been discussed in Chapter 2 and is discussed further in Chapter 6. Essentially, this change improved the

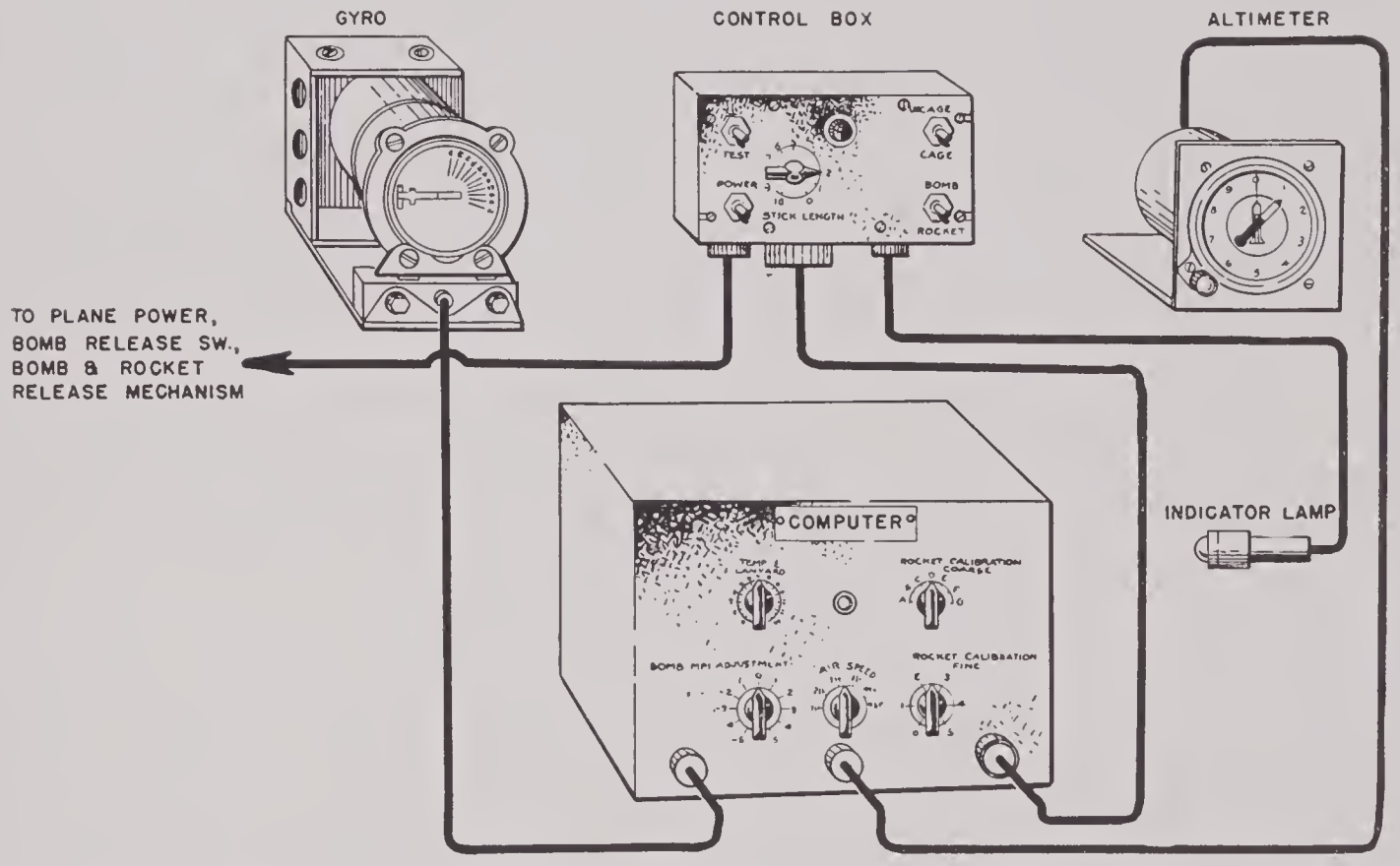

FIGURE 8. Bomb director Mark 1 Model 2, AN/ASG-10A, components and interunit cabling.

3.3.3 Control Box Mark 8 Model 2, C-200A/ASG-10 for Console Installation, C-203A/ASG-10 for Surface Installation

The control box for the Mark 1 Model 2 contains the power on-off switch, test switch, gyro cage-uncage switch, stick-length offset, and the bomb-rocket transfer switch. The latter switch is set for whatever type of ammunition is to be used. The MPI adjustment for bombs is located on the computer.

3.4 BOMB DIRECTOR MARK 1 MODEL 0, AN/ASG-10(XN)

The experimental or pilot model of the bomb director (Mark 1 Model 0) was essentially the same in principle as the two models just described, but accuracy of the intelligence fed into the computer for dive angle correction and permitted satisfactory performance at longer ranges.

The major mechanical design changes from the Model 0 were (1) improved contacts in both the altimeter and K block, (2) improved support of the gyro, (3) improved sealing of the computer against moisture and attendant electrical leakage, and (4) modifications in the physical dimensions of the equipment to facilitate installation.

3.5 PRODUCTION

3.5.1 Arrangement for Production

The experimental production of bomb directors was done largely in the development laboratories at Division 4's Central Laboratories at the National Bureau of Standards and at the State University of

Iowa (Contract No. OEMsr-769).[197] Because of urgent requests for bomb directors for operational use, an appreciable number (500) of the experimental models (Mark 1 Model 0) were built. The

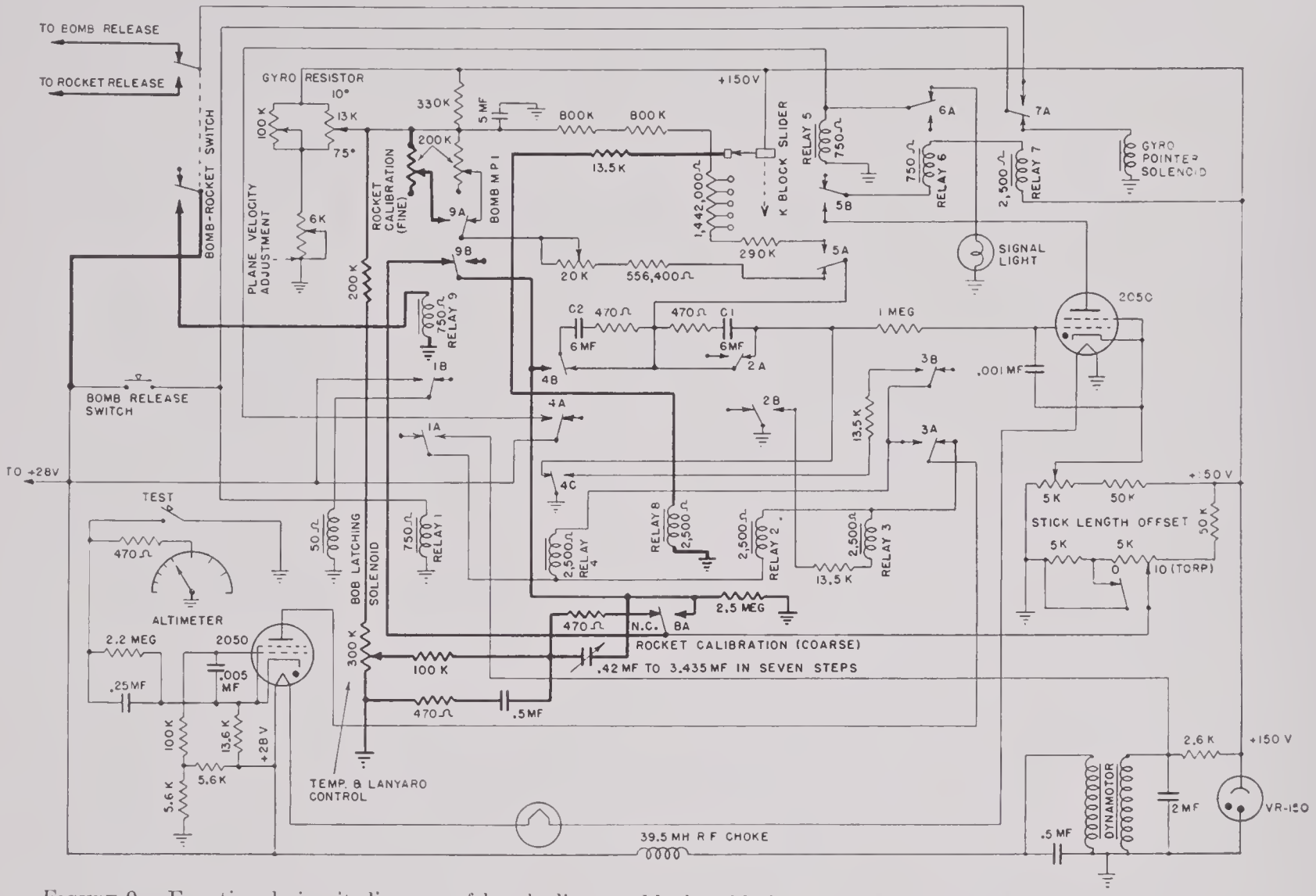

FIGURE 9. Functional circuit diagram of bomb director Mark 1 Model 2, AN/ASG-10A. Heavy lines denote circuit components used in rocket tossing.

only operational use (see Chapter 4) was with experimental models. Also, the major installations at the end of the war in both Army and Navy aircraft were with Model 0 bomb directors. Commercial laboratories and factories furnished considerable assistance on the experimental production program largely through development and pilot construction of altimeters (Contract No. OEMsr-1378)[207] and of modified gyros (Contract No. OEMsr-1227[208] and No. OEMsr-1378).

A number of changes were made in the Model 0 Directors during the experimental production period so that there were minor differences among the 500 which were built. The nature of some of these differences is indicated in the following sections.

Because of the urgency of the Service requests for the bomb directors, tooling for large-scale production (Contract No. OEMsr-1417)[202] was started before the experimental production program was complete. This meant that a number of changes in tooling and materials were inevitable, but it insured that production facilities for an acceptable model would be ready at the earliest possible date. Actually the first production models (Model 1) became available about the time the last experimental units (Model 0) were completed.

The bomb director, as explained in Sections 3.2 and 3.3, consisted of a number of distinct units connected by cables. A single unit was considered impracticable mainly because of installation and serviceability requirements. (These problems are discussed in Chapter 4.) Such breakdown of the bomb directors simplified the production program since various facilities could be used for the different components. The general plan, which was later justified by operational experience, was to build an excess number of altimeters and gyros for field replacement.

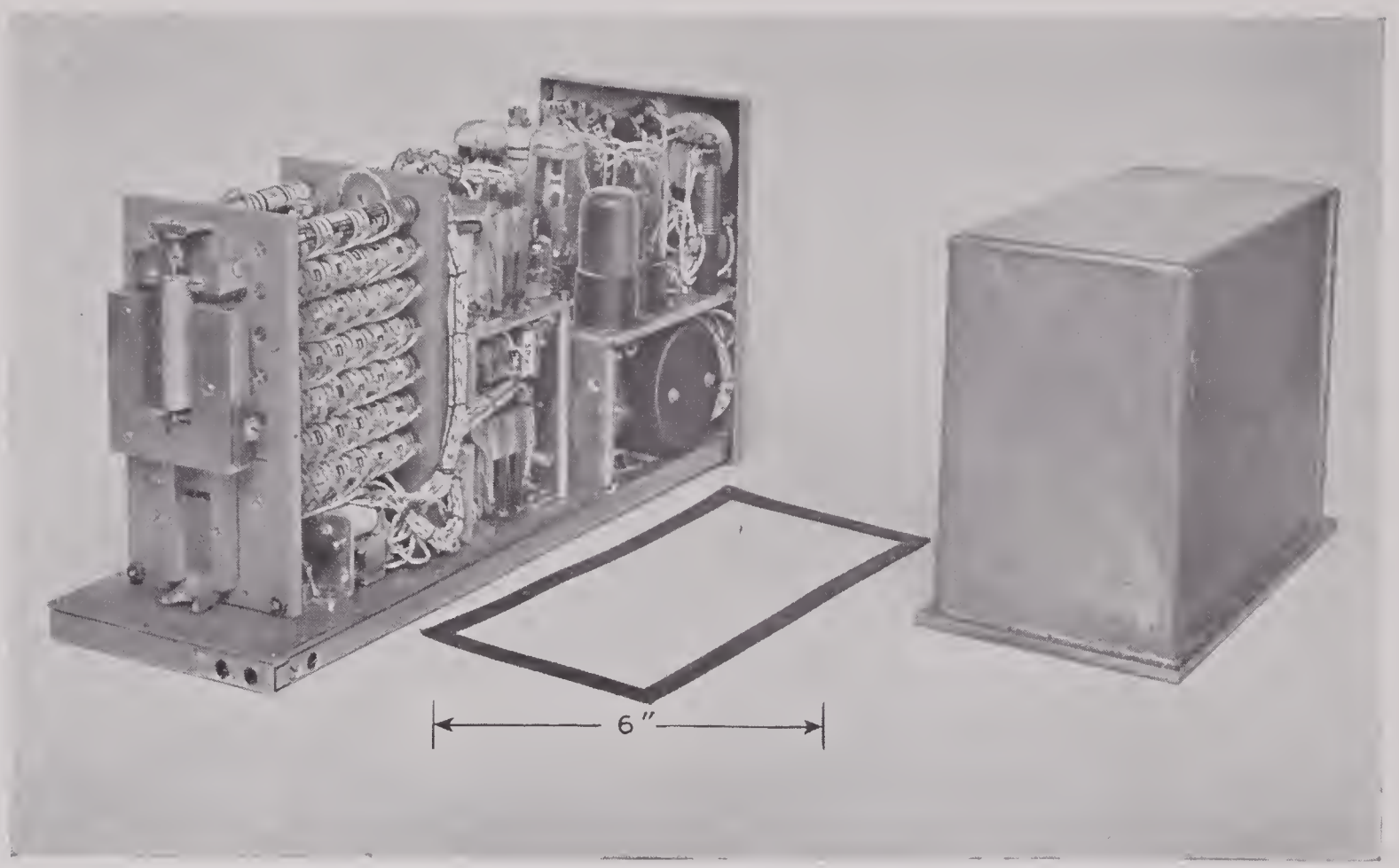

FIGURE 10. NBS experimental model of computer, with gasket sealing.

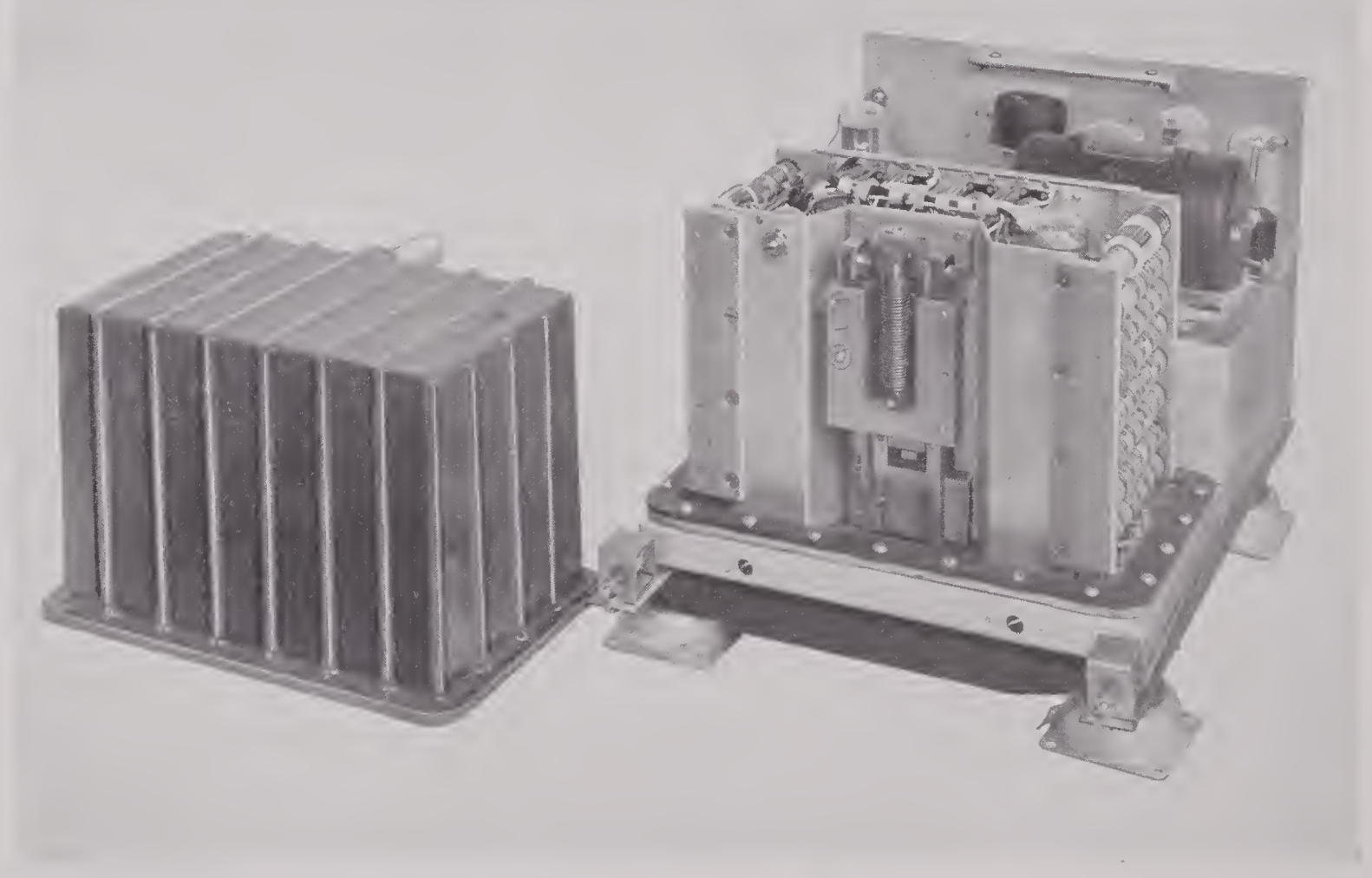

FIGURE 11. Computer Mark 20 Model 1, with case and cover for sealed chamber removed to show accelerometer.

Since the essential differences in the Model 0 and Model 1 units were in the structural design of the major components, the production problems will be presented by component headings rather than by model. The general breakdown of the bomb director into a number of separate subassemblies further justifies such presentation.

3.5.2

Computer

The major production problems in the computer were (1) sealing and drying the elements in the high-resistance circuits to prevent leakage resistance from altering the equivalent resistance values, (2) design of the contacts in the *K* block to insure reliable operation over extended periods, (3) design and mounting of relays to secure continuing reliable operation, and (4) selection of resistors and capacitors of proper quality and within close tolerances as to value.

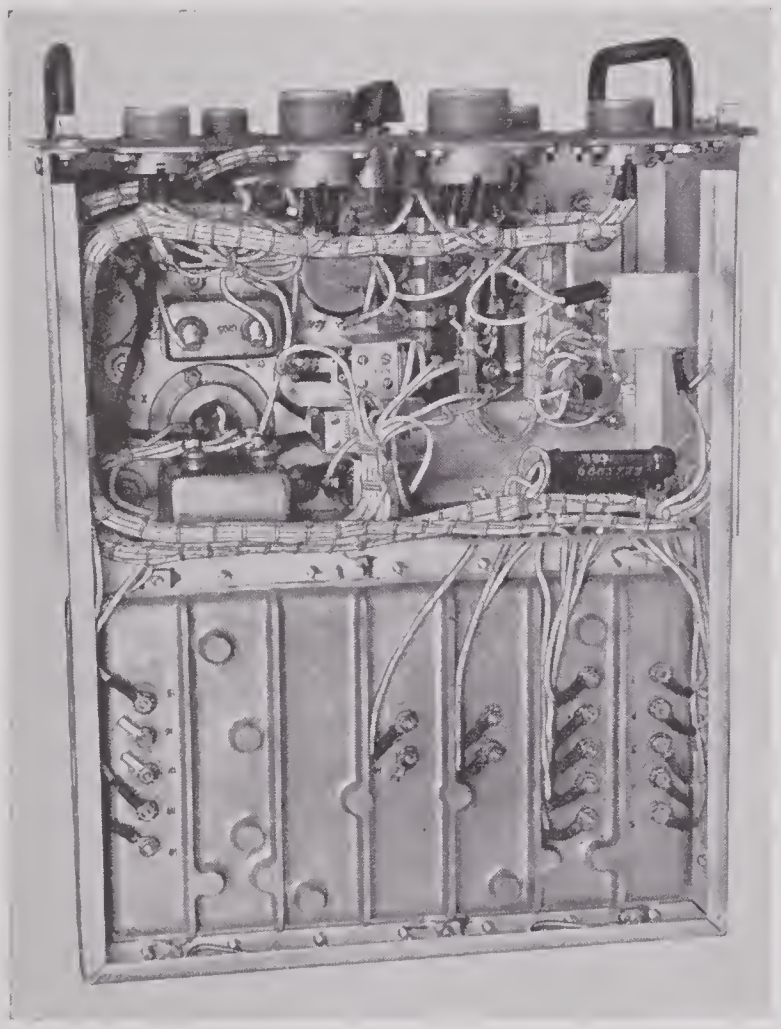

FIGURE 12. Bottom view (with case removed) of computer Mark 20 Model 1.

1. *Sealing.* The capacitors C_1 and C_2 and associated charging circuits, including the *K* block and connected resistors, certain critical relays, and the bomb release thyratron, were housed in a sealed container. Silica-gel drier was included in the container.

The first experimental units used a gasket sealing as shown in Figure 10. Later Model 0 units used solder sealing, but difficulties in removing the soldered cover for repair or adjustment led to a return to gasket sealing for production models.

The cover for the sealed chamber in the Model 1 was a heavy aluminum permanent-mold pressure casting to withstand the pressure changes encountered in high-altitude operation (see Figure 11). The best method of sealing the casting against small air leaks was an application of phenol formaldehyde high-temperature baking enamel. This enamel did not lose its sealing properties when subjected to wide ranges of temperature cycling. Buna S was used as the gasket material for Mark 1 production.

The feed-through terminals were sealed with bakelite washers with neoprene bonded to both sides. Rubber cement was applied to the screw terminals before assembly. See Figure 12.

2. *Commutator.* Probably the most serious defect of the Model 0 computer was the short-circuiting of the mica segments of the *K* block stack by metal particles which were ground off the brushes by vibration in shipment and flight. A three-leaf phosphor bronze brush, in which the contacting surface was formed by raising bosses on the contacting ends, was first used to bear against the mica-insulated brass-segment commutator. Initially the commutator surface was machined flat so as to leave the mica flush. Low insulation resistance between the brass segments was found to occur as an effect either of high humidity or of metal dust resulting from wear of the brushes and commutator. However, in properly sealed computers the metal dust proved to be the principal source of insulation trouble. Undercutting of the mica insulation was incorporated in practically all Model 0 computers. This step proved helpful in eliminating this defect. It was also found that replacement of the phosphor bronze bosses by either Bell No. 1 alloy or Sumet metal[37a] as a contact metal against the brass segments practically eliminated wear, and thus the production of the metal dust which shorted out the mica insulation. This change was incorporated in Model 0 computers about half way through production (Serial No. 266).

In the Model 1 computer the *K* block was built of 0.015-in. coin silver segments with 0.010-in. mica spacers. Undercutting, as with the later Model 0

units, was tried at first but the small dimension made the operation very difficult. In final production the mica was shaped with a flat on one side of such dimensions as to eliminate the need for undercutting. The brush on the spring-supported bob was made of Elkonium (gold) No. 18 alloy. Extensive testing of the brush sliding over the commutator showed that materials became burnished with use rather than worn.

In order to reduce further the possible wear of the brush on the commutator, the Model 1 was provided with a solenoid latch for the bob. Thus the excursions of the bob were limited to the actual periods of use.

3. *Capacitors.* The Model 0 units used 2-μf mica capacitors of selected high-insulating properties. Later investigations[49a] showed that impregnated paper capacitors (Sprague Vitamin Q) could be obtained with excellent insulating properties. Furthermore, the 6-μf paper capacitor was of about the same size as the 2-μf micas. Since the larger capacitors allowed the use of smaller resistors, the special paper capacitors were used in the Model 1 computers. Capacitors were ordered with plus or minus 5 per cent tolerance and then measured and segregated into pairs with tolerance of 2 per cent.

4. *Resistors.* Precision wire-wound resistors on ceramic forms (see Figure 6) were used in the capacitor-charging circuits. It was essential that the resistors be stable under wide temperature and humidity cycles and also under severe vibration. It was found that some of the resistors developed open circuits under vibration. The defective units were eliminated by requiring all resistors to pass a vibration test.

In the Model 0 computers the resistors used were obtained from the single manufacturer whose product stood up well under temperature cycling and humidity tests.[33a,51a,192] In the case of the Model 1 equipment, it was necessary to have several sources of resistors, and it was found necessary by the production company to temperature-cycle all resistors for four cycles, and to sort out for use only those resistors which did not change excessively in resistance. Resistance values were measured to within 0.1 per cent and those which changed more than 0.5 per cent after cycling were discarded. This procedure insured reliable components but required extensive resistor testing (several thousand measurements per day) for the estimated production rate of 1,000 computers per month.

Final exact adjustment of the *RC* ratio of the two charging circuits was made in a 20,000-ohm potentiometer shown below the MPI adjustment in Figure 2.

5. *Relays.* No relays were available commercially with adequate current carrying capacity and leakage resistance, small enough weight, short enough operating time.[38a] The Magnavox Company, in cooperation with the North Electric Company, developed a special relay for the computer. Current capacity of 10 amperes and an operating time of less than 0.012 second were required.

6. *Thyratron.* The thyratrons in computer circuits were the 2050 type specially selected for high grid impedance.[62,69,193] It was also necessary to select thyratrons for the altimeter control circuit with deionization times of less than a millisecond.

7. *Accelerometer.* The material selected for the spring in the accelerometer was an alloy known commercially as Iso-elastic. It consisted of 36 per cent Ni, 8 per cent Cr, 0.5 per cent Mo, and the balance Fe.[146a]

In the Model 0 units the weights were adjusted individually to match the springs. In the Model 1 units all the weights were the same and an arrangement was devised to adjust the spring constant and the spring position. These two independent adjustments permitted a straightforward assembly and testing technique for production.

3.5.3 Gyro

The gyro component of the tossing equipment was a Sperry Artificial Horizon Gyroscope modified to slide a contact over a potentiometer. This operation fed to the computer a voltage which was a function of the angle of dive. The production of this component disclosed a number of problems, particularly in the design and adjustment of the contacting element, in proper shock mounting, in securing a simple and reliable caging mechanism, and in insuring that the necessary alterations to the gyro did not impair its reliability in operation.[202,207,208,136a,137a,137b] describe the gyro problems in detail. They will be summarized briefly here.

ψ *Card Potentiometer.* The first experimental ψ card was wound on a simple rectangle of bakelite. The Model 0 and Model 1 ψ cards consisted of a three-step sheet; and the former is pictured in Figure 5. They are further described in Section 6.3.3. Various methods were developed for winding, shap-

ing, and installing the card in the potentiometer. The first models employed an aluminum envelope or card holder which held the resistance card. The latter was wound on a straight piece of bakelite and then flexed so that it could be forced into the pocket of the card holder. The aluminum card holder was shaped to a definite radius of curvature. It was soon found desirable to eliminate the aluminum card holder, and use a heat-formed card provided with metal end fittings for attachment to the gyro case. A more satisfactory production technique was established by using a special, partially cured plastic material. Suitable hard-drawn Advance wire was wound on a straight card which was subsequently heat-formed to the proper radius and cured in this shape. The necessary adjustment for correct angular positioning of the card was provided by using slotted holes in the case. These were sealed against air leakage by using external rubber washers. A further improvement in late Model 0 units (subsequent to serial number 525 and designated as AN/ASG-XN2) was secured by devising a molded bakelite card holder provided with metal inserts for the attachment screws. Also, a potentiometer card approx-

FIGURE 13. Interior view of gyro Mark 20 Model 0 (XN2), showing potentiometer card (at right) and contact arm.

imating the Model 1 card was used. This type of construction insured high electrical insulation resistance to the case and held the card to a fixed radius of curvature, while the molded holder insured that the card would not warp to such an extent that the pointer might not make contact.

The Model 1 units were provided with a cam adjustment for locating the card in its correct angular position. Metal end fittings were used for clamping the card in its final position after it was properly located. Slots to permit adjustment of the card were located in the card end fittings rather than in the case, as was done in the early Model 0 units.

The technique of winding and cleaning the contacting edge portion of the card was considerably improved during pilot production and the final production units showed greatly improved performance. Gyro units were only considered acceptable if the continuity of contact along the contacting edge of the card showed very small variations when tested with a low-voltage ohmmeter. Properly cleaned cards were found to maintain this condition over an extended period of time. An interior view of a modified gyro showing the potentiometer card, contacting arm, and leads is given in Figure 13.

Contact arm difficulties with early pilot models disclosed that the contact finger was poorly balanced. Vibration of the gyro caused the silver V-shaped contact to hammer on the potentiometer until it cut through the resistance wire of the strip. Smaller

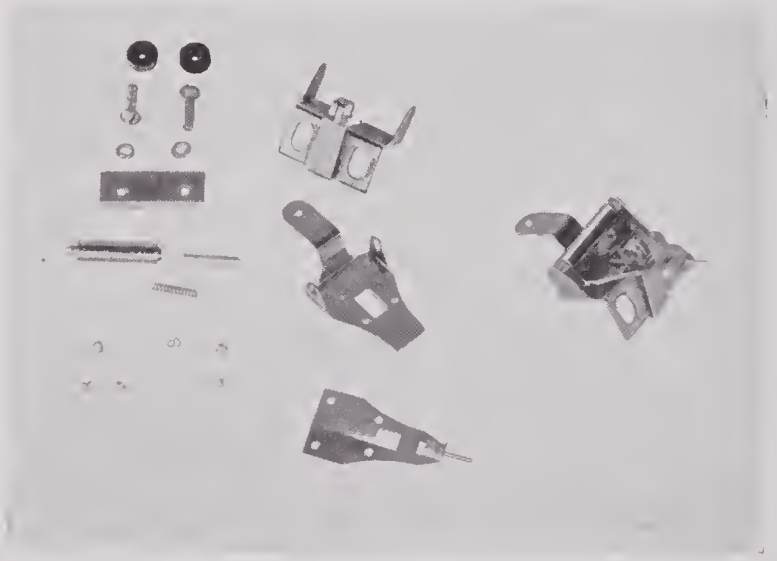

FIGURE 14. Components of gyro contact arm. (Assembled contact arm shown at right.)

contact points and better balanced assemblies eliminated the difficulty.

In production models the contact finger was further modified to allow exact assembly on a production-line basis. Provision was made to permit a bending of the contact finger for good contact without affecting clearances. Bell No. 1 gold alloy

was substituted for silver as a contact material. Details of the contact elements are shown in Figure 14 and the method of assembling the contact arm on the gimbal ring of the gyro is shown in Figure 15.

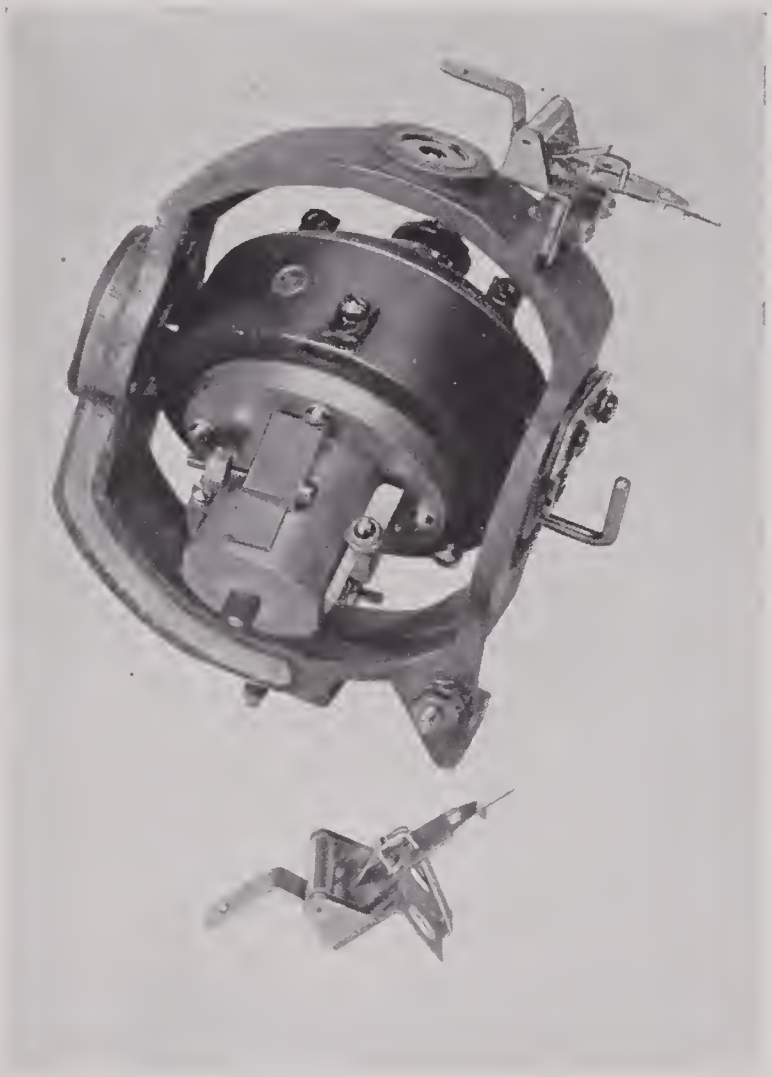

FIGURE 15. Gyro with case removed, showing pendulous housing, gimbal ring and contact arm.

It was felt that the simple interchangeability of resistance card assembly provided in the Model 0 design should have been retained in the production design. However, considerable progress had been made in the manufacture of tools for the production model before the last Model 0 design was completed. Later it was found expedient to incorporate certain of the features of the later Model 0 design in the Model 1.

Early models of the gyros developed defects due to air leakage at the point where the electrical leads were brought through the case. The later Model 0 design included a lead-through in the form of a rubber button molded around the insulated wires. This insulating button was clamped against the case to minimize air leakage. The Model 1 design employed a molded bakelite lead-through with through metal inserts to which the wires were soldered. This lead-through was clamped to the case and cemented.

Caging. The first few Model 0 units were equipped for manual caging of the gyroscope. A flexible drive a few feet long permitted mounting the gyro at a convenient distance from the pilot's control panel, at the same time permitting the caging knob to be located where it would be accessible to the pilot in flight. However, the flexible drive shaft could not be removed easily and its installation, adjustment, and removal from the plane proved to be quite troublesome. An electrical caging mechanism, consisting of a 28-volt series motor with a gear box and suitable limit switches was designed and incorporated in an improved type of shock mounting for the gyro. This new arrangement permitted caging and uncaging the gyro by the flip of a switch as compared with a pull, twist, and locking into position of the earlier manual caging knob.

The caging mechanism consisted, in part, of a series motor which had two field windings wound in opposite directions. One side of the armature was grounded and the other side connected to one end of each field winding. By connecting the live side of the grounded power source to the free end of one or the other field winding, either direction of rotation was obtained. Limit switches were provided in series with each field winding. These limit switches were operated by a cam in the gear box. One was adjusted to insure that the circuit would be opened when the gyro was uncaged to such an extent that the caging dogs would not interfere with the gyro within its normal operating limits. The other limit switch was adjusted to open when the gyro was caged. The wind-up torque on the drive spring was sufficient to keep the gyro caged.

Trouble was experienced with some of the first electrical caging motors because of excessive speeds in caging and uncaging. It was found expedient to correct any trouble arising from motors giving excessive speeds, by shunting the armature with a fixed resistor of approximately 15 ohms. This shunt insured that the starting torque would not be greatly reduced, and at the same time limited the maximum speed of the caging motor at the expense of a slight increase in power requirements. The shunt method was used in the Model 1 units.

An alternative speed reducing technique, incorporated in the later Model 0 units, consisted of a solenoid-operated brake. This was superior to the

shunt method in that over-travel of motors could be reduced to a minimum. Because of the urgency of the program, it was not feasible to redesign the motor and incorporate a brake; so for expediency, a brake bearing on the armature was added to the available motor.

Tests of some of the first mechanisms at low temperature (−40 C) revealed erratic performance due to large variations in the torque required to cage and uncage different gyros. This led to specification of tolerances for the caging torque which when followed insured a more uniform production and satisfactory operation of the caging mechanism at low temperatures.

Shock Mounting. Best operation of the contacts in the potentiometer in the gyro required that vibration induced by the aircraft be minimized. In addition, the gimbal bearings in the gyro were susceptible to shock so insulation of the equipment from shock was important. Changing from manual to electrical caging simplified the problem of insulating the gyro from external disturbances.

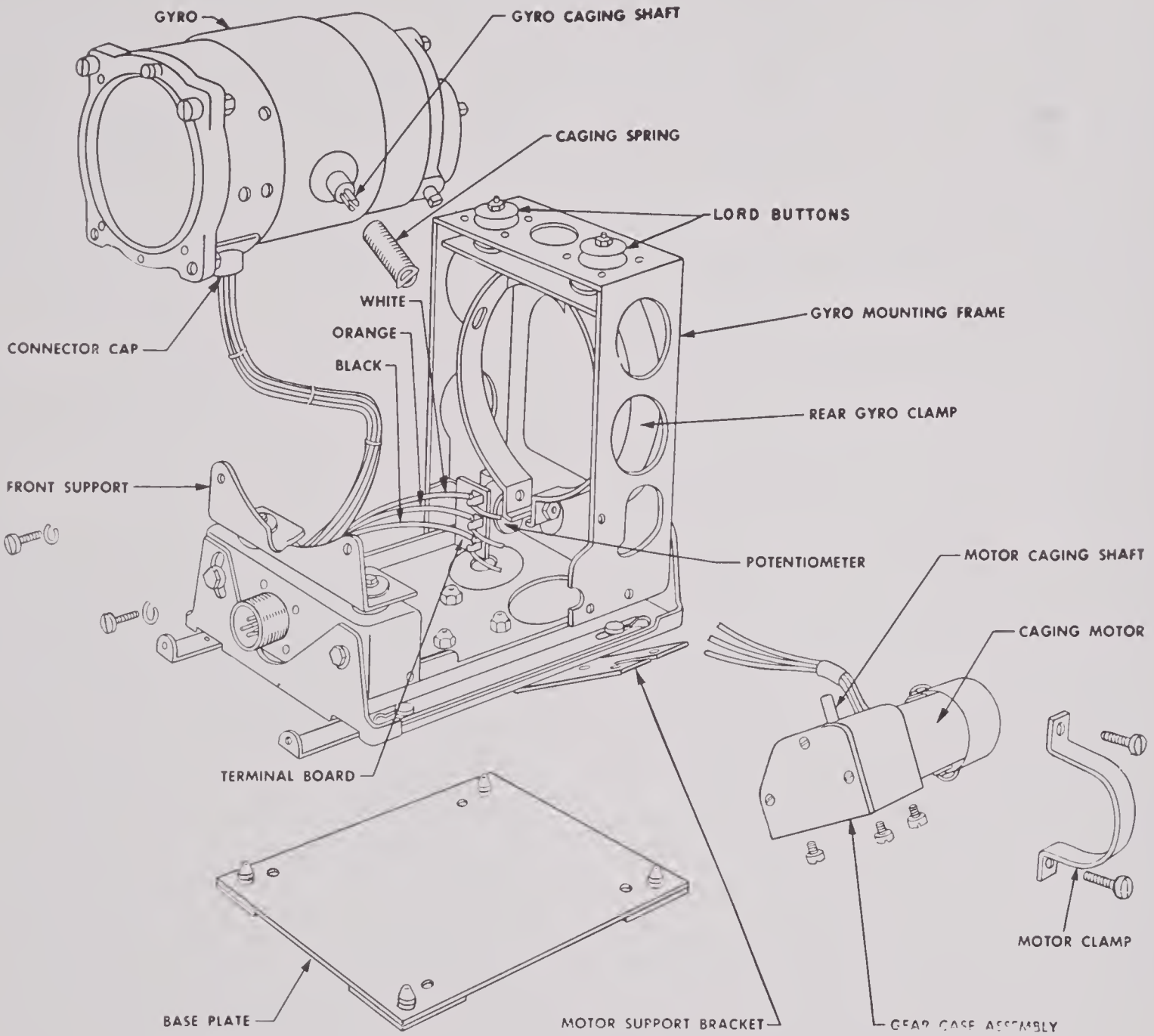

FIGURE 16. Components of gyro Mark 20 Model 1 (Magnavox drawing).

Various shock mounting systems were tried both in the pilot and final production. It proved necessary to incorporate a snubbing action in order to limit excursion under extreme shock.

The Model 0 design of shock mounting for the gyro consisted essentially of a framework which

carried four Lord buttons, two located in front and below the gyro and two above at the rear of the gyro. The design of this mount insured that the center of gravity of the modified gyro was located in the plane of the four buttons. Buttons of 1-pound rating were used, although 2-pound buttons, which were not available, were preferred.

The Model 1 design used 2-pound buttons, which had become obtainable. The final design used two of these buttons in tandem at each point of support. The location of these buttons may be seen on the mounting frame and front support in Figure 16. This figure illustrates the general arrangement of the Mark 1 gyro-mounting system.

Some difficulty was experienced from bearing failures in the gyro during shipment. This apparently was due to bending of the frame lug which carried the gimbal assembly, part of which had been milled away to accommodate the changes made to the gyro. An improved, cushioned package for shipping the gyros eliminated the failures.

In order to reduce the possibility that the vibration of the potentiometer contact would cause voltage fluctuations during operations, a 0.5-μf capacitor was added between the pointer and ground (see Figure 2). A further precaution was a 330,000-ohm resistor by-passing the potentiometer, to provide charging voltage in case of an open circuit in the potentiometer. This provided a charging voltage corresponding to a 40-degree dive. Although this precaution appeared desirable on very early models, it was probably superfluous on the production models.

Banking Limitation. The original design of the caging mechanism was such that in the uncaged condition a roll of 70 degrees would disturb the inner gimbal (spill the gyro). This imposed a serious tactical limitation on the use of the bomb director since common dive bombing tactics call for a sharp turn prior to the dive, with a bank of about 80 degrees or more. (To avoid disturbing the gyro, pilots had been using a push-over type of entry into the dive.)

A number of simple modifications devised to remove this limitation were put into production toward the end of the program.[112] These changes were: (1) Removing the bumper on the bottom of the pendulous housing; (2) sliding a piece of rubber tubing over the caging arm; (3) installing on the gimbal ring a metal plate with tabs turned up at right angles (this plate, in conjunction with the rubber tubing, acts as a stop); (4) careful filing of the supporting fin on the inside of the gimbal ring to allow clearance for one pendulous vane; (5) adjusting the new stops and rebalancing the gyro.

Gyros so modified successfully underwent flight tests in which the pilot made (a) 85-degree banks, (b) 85-degree banks followed by 90-degree turns, (c) 85-degree to 90-degree banks simultaneously with 50- to 55-degree dives and 90-degree turns. In no case was the gyro spilled.[102,104]

In view of this performance and of the fact that the required changes were of such a nature that they could easily be made in the field, a program of this conversion was begun in August 1945.

3.5.4 Altimeter Unit

The first altimeter units were 50,000-foot sensitive Kollsman altimeters which were modified by the addition of electrical contacts in the laboratory.[41] Considerable effort was spent in devising a delicate contact which would not seriously affect the altitude indication of the altimeter.[138] A number of models were made before the contact mechanism was finally considered adequate. It was found desirable to use a gold alloy "whisker" 1 inch long with its inner end mounted on and electrically connected to the 1,000-foot pointer, which was grounded through the gear mechanism of the instrument. In order to increase the initial contact force of this fine whisker on the altitude prongs, the whisker, 0.01 inch wide by 0.001 inch thick, was threaded through a small loop projecting beyond the end of the pointer to within 0.1 inch of the end of the whisker (see Figure 3). This loop acted as a fulcrum so that when the tip of the whisker came in contact with the prong the contact force was initially fairly high and remained high until the contact was broken. It was important that the whisker have sufficient initial set to make it press against the trailing edge of the loop, even when free of the prong. Approximately constant pressure was insured by this design so that with properly cleaned platinum or gold alloy prongs the "continuity of contact" was good for the complete duration of contact. In order to reduce burning of the tip of the whisker, a 500-ohm resistor was connected in series with the prong ring to limit the current flowing through the tip of the whisker as a result of discharge of the capacitor when the circuit was broken.

Twelve wedge-shaped noble metal prongs were placed at altitude points around the periphery as shown in Figure 3. The prongs were supported and electrically connected by a brass ring. The pressure exerted by the gold whisker on the wedge-shaped prongs was so low that it was found necessary to take great care in cleaning the metal prongs. The most satisfactory method evolved for cleaning the prongs consisted in a final operation of removing metal by scraping or filing along the contact edge. For this reason plated prongs did not prove satisfactory. Other attempts at cleaning chemically, by metallographic paper, etc., did not always leave an adequately clean contact surface.

In order to minimize "first button release" trouble which might be the result of intermittent contact between the whisker and the prong, a circuit having a time constant of ½ second was introduced between the prong ring and the grid of the thyratron to which it was connected. This circuit consisted of a ¼-μf capacitor shunted by a 2-megohm resistor (see Figure 2).

Simple electrical insulation of the prong ring by means of varnished cambric and varnished glass cloth proved inadequate under high humidity conditions. In fact, the introduction of the time delay element having the capacitor and 2-megohm resistor required that the insulation resistance between the altimeter prong ring and ground be at least three megohms. Several designs of bakelite molded prong rings were tried before a satisfactory one was evolved. Better insulation was secured by molding the ring and its prongs as an insert in the bakelite molding. The bakelite ring incorporated an electrical lead-through to permit external connections and at the same time an airtight seal of the altimeter. The prongs were threaded through holes in the brass ring and soft-soldered to it. The prongs were shaped in such a way that they could be bent so as to permit adjustment to the precise altitude positions desired. The insulation material in the late Model 0 units was BM 14726. After curing at 300 F for three hours the ring assembly would withstand repeated temperature cycling between the limits −60 and +65 C without cracking. The design of the Model 1 incorporated straight prongs placed in the prong ring and subsequently swaged to have a wedge shape toward the contacting edge.

The design of the contacting mechanism in the altimeter unit was such that the altimeter indications were not appreciably affected; except that it was necessary to adjust the altimeter to indicate zero at the target, the altimeter unit was available in use as a flight instrument. In the experimental models it was found convenient to mount the altimeter in the panel in the bombardier's cockpit and thereby make use of the shock mounting already provided in the panel. However, the very lightweight design of the contact mechanism incorporated in the altimeter made it desirable to provide even better shock mounting for the altimeter than that provided for the instrument panel. The best procedure seemed to be installation of the altimeter unit on a specially isolated instrument panel.

The general assembly layout of the Model 1 altimeter is shown in Figure 17.

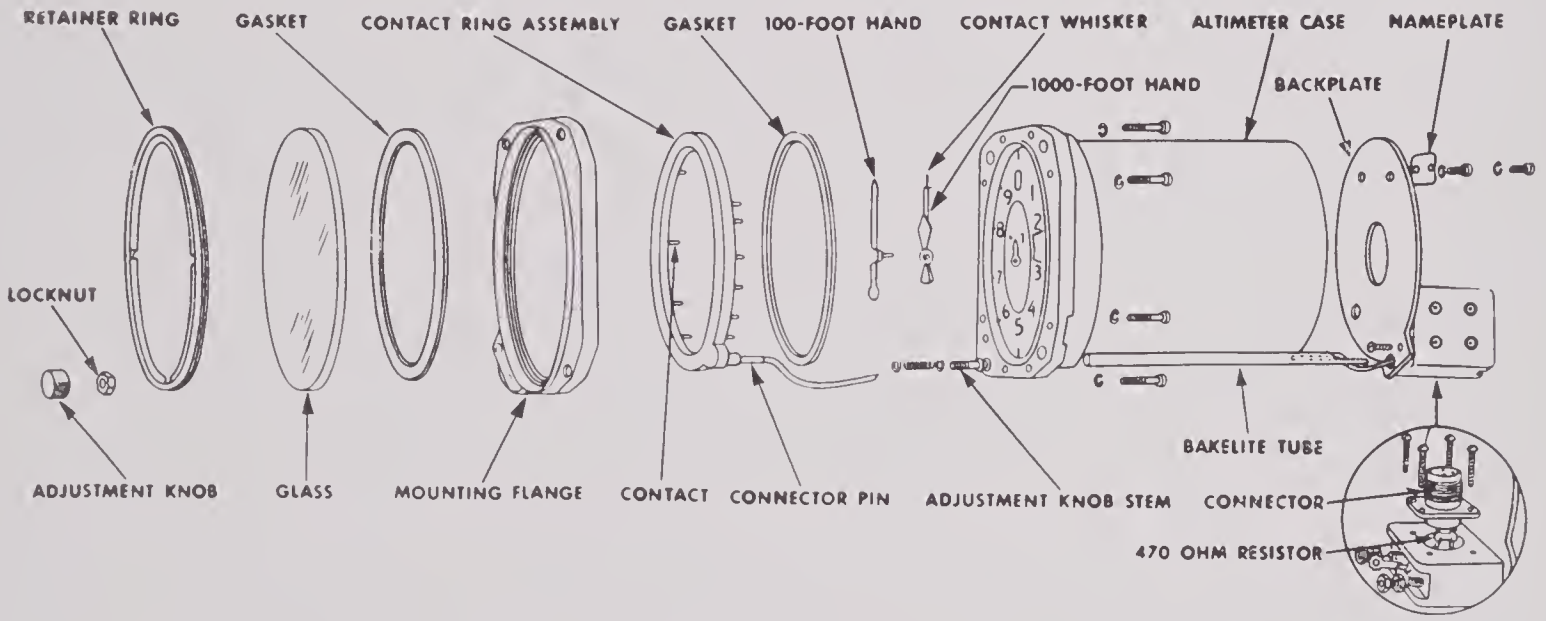

FIGURE 17. Components of altimeter unit Mark 1 Model 1 (Magnavox drawing).

3.6 LABORATORY TESTING

3.6.1 Objective

In view of the experimental nature of the production of the bomb director Mark 1 Model 0 and the initial 500 Mark 1 Model 1 equipment, it was considered advisable to inspect and test all major components individually before issue to the Services. Accordingly, Division 4 carried on, at its central laboratories at the National Bureau of Standards, acceptance type tests on all Model 0 units and Model 1 units up until the time the project was turned over to the Navy.

An attempt was made wherever possible to apply overall functional tests to the equipment, rather than to check individual parts. The inspection proved to be of definite value in uncovering defects in factory inspection and in design.

The details of testing equipment procedures and acceptance limits are given in the following sections. While the exact limits and certain details of procedure varied during the course of the program, the summary given here represents the final requirements.

The final specifications given in reference 138 are based on experience gained in acceptance testing of the Model 0 and the initial 500 Model 1 equipment.

3.6.2 Computer

1. *Features tested.* The computer was put through a series of overall performance cycles while placed in a centrifuge oriented with respect to the acceleration as it would be in service. No gyro was connected. The computer was tested at rest and under eight different values of acceleration. The output time was measured in each case for a 2-second input.

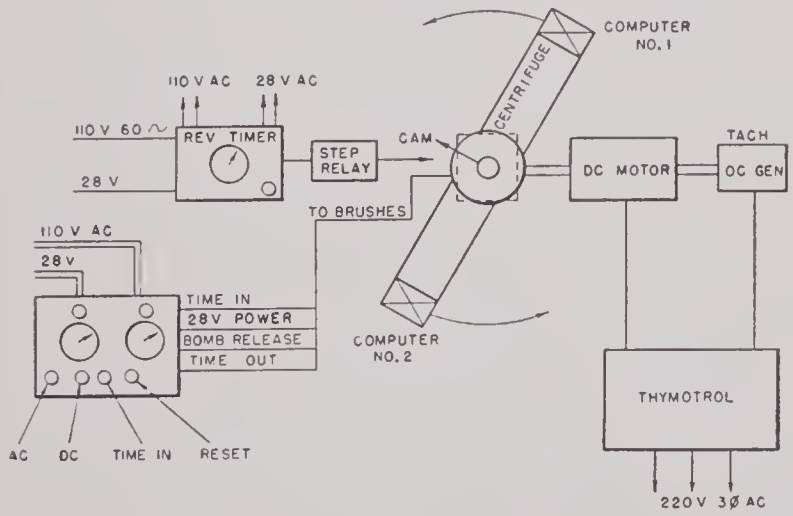

FIGURE 18. Block diagram of centrifuge test set to check operation of computers under acceleration.

2. *Equipment.* The testing equipment consisted of the following principal components arranged schematically as shown in Figure 18 and in photographs, Figures 19 and 20. (a) Centrifuge arranged to carry two computers and rotate them to obtain accelerations similar to Service conditions. (b) A 1-hp d-c motor to drive the centrifuge through a 20 to 1 reduction gear box. (c) A tachometer of permanent magnet type which gave a voltage proportional to speed. Its armature was fastened to the motor shaft. (d) The GE tachometer signal Thymotrol was a thyratron system of current control in which the motor was brought up to a speed such that the voltage output of the tachometer generator balanced a network involving a set of voltage regulator tubes, a d-c amplifier, and a pair of adjustable wire-wound resistors. These resistors served as adjustments of the centrifuge running speed. One served as a coarse and the other as a fine adjustment. An eight-point switch served to cut in any one of eight pairs of such resistors. Each pair of resistors was adjusted to give one arbitrary centrifuge speed. It was then necessary only to turn the multiple point switch to get any one of the eight standard

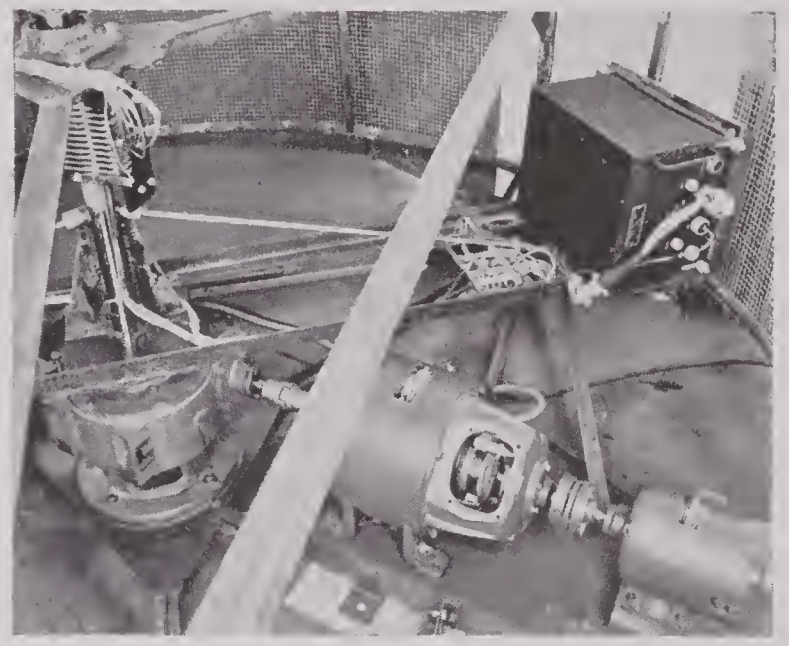

FIGURE 19. Photograph of centrifuge showing computer mounted on one arm of centrifuge. Note 11 brushes and slip rings at top left for bringing test leads to two computers. Lowest spring on brush block is contact for cam used for two computers; right-hand timer times 10 revolutions of computer.

running speeds. Once the system was warmed up for an hour the speed remained constant to about 0.2 per cent. (e) A computer test set to put time into both computers simultaneously and to measure output time with one timer for each computer. This circuit was essentially similar to that described in

FIGURE 20. Control panel for Thymotrol. Lower section contains timers for two computers; right-hand timer times 10 revolutions of centrifuge.

reference 65. (f) A revolution timer which measured the time for ten revolutions of the centrifuge. This was operated by a cam, mounted on the shaft, which closed a circuit which actuated a rotating switch at each revolution. This relay energized the timer clutch during the time interval of the ten revolutions.

3. *Acceptance limits.* The units were checked at rest with supply of 24, 27, and 30 volts. Accuracy of plus or minus 1 per cent of theoretical values was required. The unit was required to operate, without regard to accuracy, with a 20-volt supply. With the centrifuge in motion the unit was tested at eight particular speeds corresponding to values of acceleration approximately equally spaced between $1.41g$ and $5.77g$. The acceptance limits at each speed allowed an error of plus or minus 1 per cent due to resistance values in the charging circuits and an error due to the K block making contact with the segment adjacent to the theoretically correct one.

The value of rotational speed required for any given K value was calculated from the equation

$$K = \frac{4\pi^2 RN^2}{g},$$

where K is the acceleration in g units, R is the radius to the center of gravity of the K block, N is the number of revolutions per second, and g the acceleration of gravity.

The acceptance time limits were rounded off to multiples of 0.01 second in order to widen the limits.

Less than 5 per cent of the Model 1 computers failed to pass the centrifuge test.

3.6.3

Gyro

The gyro unit was an item of such a nature that defects in manufacture were very likely to slip by undetected. Tests were made as follows:

1. *A caging test* to insure that: (a) Both caging and uncaging operations took less than five seconds at 28 volts. (b) The operations were satisfactory with a 20-volt supply. (c) When uncaging, the caging dogs did not strike the stops. (d) When caging, the overtravel of the motor should be about 90 degrees to provide proper tension to keep the gyro caged. (e) The limit switches on the caging motor operated positively at each end of the motor stroke. This was done with an ammeter in the caging circuit. (f) The gyro was caged in the 45-degree climb position to insure that the coupling spring did not snap out of place. With the gyro in the climb position the spring suffered its maximum elongation. In some cases, where the clearance was excessive, the spring was found to jump out of place.

2. *A check* to insure that the contactor made contact with the resistance card at all points and that the pointer, if energized either at a climb angle or a dive angle of over 75 degrees, would ride properly onto the card. The solenoid was expected to operate the pointer on a 20-volt supply.

3. *Contact continuity.* Failure to obtain electrical continuity between the pointer and the resistance

card was the most frequent source of rejection. A tilt table, provided with a coarse worm gear drive, was used for this test. The gyro was leveled and the solenoid energized. An electronic ohmmeter was then used to measure the resistance between the leads. As the gyro was tilted slowly, the resistance was required to change continuously. If at any point the resistance jumped up to infinity the gyro was rejected. The contact continuity was checked with the gyro tilted first slowly in the dive direction, then back to the level position.

4. *Precession test.* In order to insure that the gyro would not precess excessively due either to high contact pressure or to a rough card, the pointer was energized with the gyro leveled. The gyro was then tilted slowly and uniformly to the 75-degree dive position in one minute. The gyro would then precess in the roll direction. The solenoid was then de-energized, the gyro brought back quickly to the horizontal position and rotated through 90 degrees about a vertical axis. The roll precession was then transferred to the pointer and was read directly on the glass scale. The acceptable limit for this precession was 23 degrees.

5. *Voltage distribution.* The distribution of voltage over the potentiometer card was measured[26] in a setup arranged to show directly in volts the departure from the nominal resistance. Tolerances were as follows:

Fractions of the Total Voltage

Angle	Fraction	Tolerance
0–10°	1.00	1.5v
14.6	0.960	1.5
21.9	0.896	1.0
31.2	0.814	1.0
40.6	0.712	1.0
50.6	0.592	1.5
60.4	0.4587	2.0

The test set was originally designed for the Model 0 XN-1 gyro card which gave the above voltages at angles of even multiples of 10 degrees. However, when the XN-2 and the Model 1 gyros were tested, the voltage values were retained, but the angles were changed slightly to conform to the new card design.

6. *Voltage proof test.* This test measured the insulation resistance between the pointer and case, both with and without the solenoid energized. A test was also made of the resistance between the strip and case. The lowest acceptable value was 200 megohms in an atmosphere of 60 per cent relative humidity.

3.6.4 Altimeter Unit

The most critical features of the altimeter unit were the duration of contact, the continuity of contact, and the accuracy of the altitude at which each contact was made. These features were checked as well as electrical leakage resistance from the contact ring to case, air leakage of the case, and the so-called position error, i.e., the shift in reading due to changing orientation of the instrument.

The particular tests follow:

Calibration. The calibration was performed in two stages. First, the indicated altitude was read at the instant that contact was made, i.e., the reading of the altimeter itself was taken without regard to its own instrumental correction. The second stage consisted of placing the instrument in a low-pressure chamber and checking the instrumental error, or the pressure at which each contact was made.

1. The indicated reading was determined as follows: The altimeter was adjusted by turning the adjustment knob until the reading was well over 10,328 feet.

The adjustment knob was then rotated so that the instrument read decreasing altitude. The point of contact was then indicated by an ohmmeter. As the whisker made contact with each prong in succession, the indicated altitude was read. These readings were required to agree with the theoretical altitude within 15 feet.

2. The second stage of calibration was done by placing the altimeter in a steel low-pressure chamber. A vibrator was mounted on the rack which held the instrument. Its purpose was to shake out most of the friction in the altimeter mechanisms. The chamber held six altimeters simultaneously.

A pair of leads was brought out of the chamber from each instrument. By means of a multiple-point switch each one in turn was connected with a computer so modified that a relay operated and a neon light flashed each time the whisker made contact with a prong.

The chamber was evacuated five times to the pressure equivalent of 20,000 feet and then brought back slowly to atmospheric pressure. The purpose

of the five pressure cycles was to get the instruments into a standard condition with respect to hysteresis.

The pressure of the chamber was read with an unmodified Kollsman altimeter which was periodically checked by the Aeronautical Instruments Section of the National Bureau of Standards.

A reading was made of the standard altimeter each time the test altimeter made contact.

The instrumental error, the theoretical altitude minus the indicated altitude, was kept within limits as specified in Joint Army-Navy Specification AN GG 461, except that when the error was appreciable at the low altitudes, the zero was shifted to reduce all values by a constant amount.

The calibration of the altimeter unit Mark 1 Model 1 was adjusted by the manufacturer so that the altimeter scale error was as small as possible over the range 0 to 16,000 feet. It had been hoped that by doing so and by making slight compensation for the scale error in locating the contact pins, a higher order of accuracy could be obtained. However, difficulties in absolute calibration raised serious questions as to the advisability of making pin adjustments to compensate for scale error.

Contact Duration and Continuity. Along with the first part of the calibration test a reading was taken of the altitude at which contact was broken. The difference between the "break" and the "make" points was required to be between 40 and 60 feet for the altitudes 1,390 to 2,402 feet, and between 40 and 75 feet for the points 2,882 to 10,328.

Over the range between the make and the break, continuous low-resistance contact was required. Unless the contact pins were properly shaped and scraped, and the proper whisker design and tension maintained, the whisker could make *mechanical* contact while the resistance between elements would be of the order of several hundred megohms.

Air Leakage. The instrument case was connected to a vacuum line and exhausted to 1,000 feet. The vacuum connection was then closed. If air leaked into the case fast enough to drop the reading by 100 feet per minute, the instrument was rejected.

Insulation Resistance. The resistance between the contact ring and the case was measured as a function of ambient humidity. The tolerance limits follow:

Relative humidity per cent	Lower limit megohms
30	10,000
40	4,000
50	2,000
60	600
70	300
80	120
90	50
95	30

Position Error. The instrument was placed with its face in a vertical plane and adjusted to an integral multiple of 1,000-foot reading, with the 100-foot hand vertical. The instrument was then tapped gently by the operator until the 100-foot hand settled at one point. The operation of tapping was twice repeated rotating the instrument first 120 degrees, then 240 degrees about its axis. If the maximum difference between any two readings exceeded 20 feet, the altimeter was rejected.

This test was repeated for two other altitudes of about 250 and 500 feet greater than the first.

3.6.5

Control Box

This control box was inspected in a special test set which checked continuity of each circuit and the approximate values of the MPI and stick-offset resistors. The acceptable limits were approximately plus or minus 10 per cent of the nominal value of the resistance at each indicated point. At the three lowest resistance values the correct resistance was to be obtained with the pointer set within one division of the correct one.

The control box Mark 8 Model 1 was not checked as an acceptance control since the production inspection was considered satisfactory.

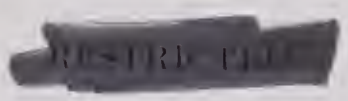

Chapter 4

INSTALLATION, OPERATION, AND MAINTENANCE[a]

IN THE FOLLOWING PARAGRAPHS a picture of the general problem of installation is given, with a rather more detailed discussion of the flight tests required following installation.

Published information, such as installation and operating manuals,[220,223–225,232a,b,c,250–254,270,272–274] gives a still greater detailed description of the problems. A photograph of the items to be installed, less connecting cables, is shown in Figure 1. Placement of the components in typical Navy planes is shown in Figure 2.

[a]This chapter was written by P. V. Johnson of the National Bureau of Standards.

4.1 INSTALLATION

4.1.1 Computer

The computer is so installed that the enclosed accelerometer measures the component of spatial acceleration perpendicular to the flight line. This is accomplished when the base of the unit is in a geometrical plane that is parallel with the flight line and the line joining the wing tips, i.e., its base is level during level flight. Whether the computer is positioned lengthwise or athwartship does not affect its operation. It is preferable, but not imperative,

FIGURE 1. Bomb director Mark 1 Model 1 components, minus interunit cabling.

that the computer be near the center of gravity of the airplane.

4.1.2

Gyro

The gyro is located within 9 feet of the center of gravity of the airplane, and positioned athwartship with its glass face plate facing to starboard (right). Vacuum line and electrical connections are so made that no interference with free movement of the gyro in its shock mounting is caused. It is of prime importance that the gyro be so leveled that the indicated zero angle is that of the flight line of the airplane in an average or typical dive under operational speeds or loads. A vacuum of $4 \pm \frac{1}{4}$ inch of mercury is required for proper operation.

4.1.3

Altimeter

The altimeter is variously installed as a replacement for the regular flight instrument or as a separate flight instrument in single-place airplanes and as a replacement for the bombardier's altimeter in two place aircraft. It is positioned so as to be readily accessible to the pilot (or bombardier) for adjust-

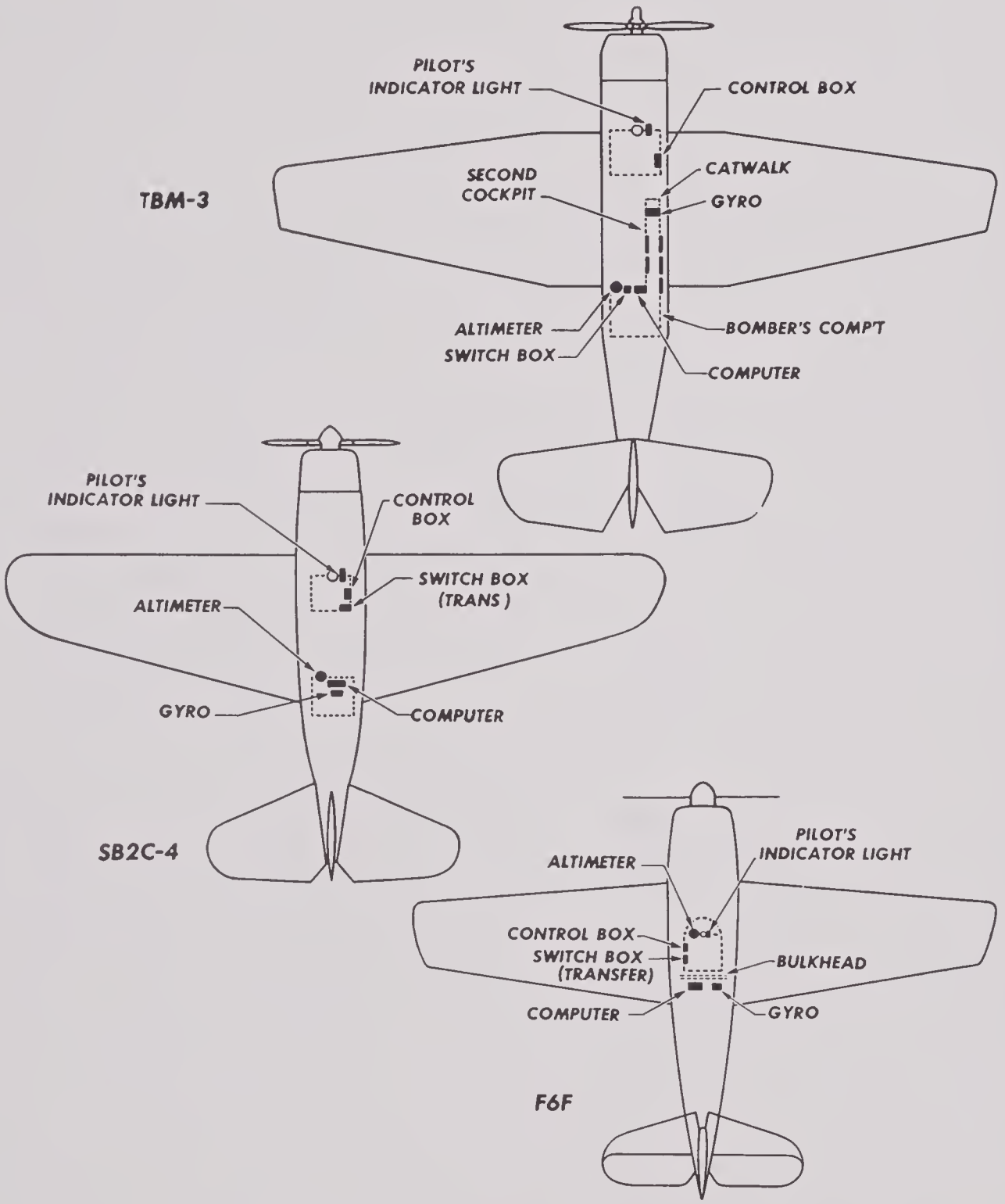

FIGURE 2. Placement of bomb director equipment in 3 Navy aircraft (U. S. Navy drawing).

ment. Special care is taken to insure that there is no restriction to free movement on its shock mount.

4.1.4 Control Boxes

The pilot's control box is either surface mounted or is mounted as part of a console installation. No particular requirements are to be met other than accessibility to either the pilot or bombardier.

The transfer switch box is generally located so as to be readily accessible to the pilot in all types of airplanes.

4.1.5 Indicator Lamp

The indicator lamp is mounted near the pilot's gunsight and aligned with the pilot's eye during glide bombing so that the light may be observed without shifting attention from the sight.

4.1.6 Gunsight

Any standard-type gunsight is satisfactory[242] provided due consideration is given to the problem of alignment so that the sight line and flight line coincide in a dive under median conditions of dive angle, airspeed, and loading. This subject is treated in Section 4.2.1.

4.2. EXPERIMENTAL FLIGHT TEST PROCEDURES

4.2.1 Calibration Tests for Toss Bombing

Normal procedure in alignment[b] of the gunsight in airplanes such as are used in toss bombing calls for the sight line to be adjusted for use in gunnery. Since conditions considered as median for gunnery are quite different from those for toss bombing, a problem of proper sight alignment is presented. For gunnery, the sight and guns are harmonized for flight conditions encountered in level flight and at considerably lower speeds than those used in toss bombing; the difference in angle of attack may be as much as 40 mils in the two techniques.

If a gunsight with a fixed reflector plate is used, its suitability for either gunnery or toss bombing can be accomplished by use of a reticle modified to contain two pips so positioned that when the plane is boresighted for gunnery using the central pip, the other then becomes the sighting line for median toss bombing conditions. Median conditions are usually considered as 400 mph in a 40-degree dive. If a gunsight with an adjustable reflector is available, it is obvious that a mere turn of the adjusting knob will properly align the sight for whichever use is desired.

The primary problem, then, is one of determining the proper alignment to insure coincidence of the sight line and flight line for each plane or an average setting for all planes of one type. There can be considerable variation in the angle of attack of a number of planes even of one type, which may, in part, account for the difficulty encountered in using engineering data supplied by manufacturers, or found in aircraft manuals, to determine accurately the difference between sight and flight lines. Some published data, such as those in reference 214, proved fairly reliable and useful for some plane types, but unsuitable for other types when used in toss bombing. Thus, it is deemed advisable to calibrate each airplane following installation of toss bombing equipment.

Two methods of calibration in flight have been used, both of which appear to be satisfactory. In one, a stationary theodolite is used as an aiming point toward which a plane dives.[78] An arbitrary sight setting is previously made from engineering data or past experience, the plane is loaded with an average combat load, and a dive is made using predetermined dive angle and airspeed corresponding to average toss bombing conditions. If the sight is properly set, an observer at the theodolite determines when the plane is flying a straight course relative to the cross hairs toward the target. If the flight path is not straight, but the plane appears to rise or fall, this information is transmitted to the pilot and the sight raised or lowered for subsequent dives. A number of such dives are necessary from headings 180 degrees apart; the average of the two sight settings, one for each heading, is taken as a no-wind value. Accurate determinations by this method are difficult and probably unsatisfactory if made under conditions where the wind exceeds 10 knots.

The other method consists of dropping bombs and adjusting the sight setting until the no-wind MPI with respect to the point of aim is within desired limits. Calibration flights in naval stations and army fields for tests mentioned in this volume were done using median conditions of dive angle, altitude,

[b] The importance of sight alignment and angle of attack variations is discussed later in Section 6.4.11.

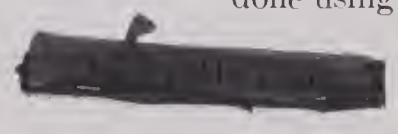

airspeed, and plane loading. Sight settings thus obtained were found satisfactory. In calibrating P-47 aircraft of the Ninth Air Force in the European Theater of Operations [ETO], however, it was found more desirable to calibrate the sight at low altitudes (two lowest altimeter contacts), low dive angles (15–20 degrees) and indicated airspeeds [IAS] of about 350 mph. Since impact errors are greatest under these conditions, sharper adjustment to the sight setting could be made, and fewer bombs were required to complete the calibration.

Since wind errors must be eliminated from calibration results, it is desirable that runs be made on dead crosswind headings where wind effect will appear only in deflection errors and can be disregarded. However, if this condition cannot be met, runs may be made on up and downwind headings, and the no-wind MPI computed by using the method illustrated in Table 5 of Chapter 5.

Using a preliminary sight setting based on experience or available data, a minimum of three bombs are dropped from each of two headings, 180 degrees apart. Scoring range errors only, the no-wind MPI should be within 50 feet of the point of aim. If this is not the case, the sight may be adjusted; any adjustment so made, however, should be confirmed by dropping additional bombs with the new sight setting.

After calibrating by either method, the relationship between the sight setting and the thrust line or bore sight datum line should be recorded for periodic checking of the sight alignment.

4.2.2 Calibration Tests for Rocket Tossing

The same condition of coincidence of sight line and flight path is required when tossing rockets as in toss bombing. Either of the two methods pre-

TABLE 1. Relation between flight path and boresight datum line [BSDL] or thrust line for Navy planes.

Plane		Weight of plane (lb)	IAS (knots)	Dive angle (deg.)	(1) Angle of BSDL above thrust line (mils)	(2) Flight path above BSDL (theodolite tests) (mils)	Flight path above BSDL (from CIT manuals) (mils)	Flight path above thrust line (from wind tunnel data) (mils)	Flight path above thrust line [from (1) and (2)] (mils)	Reference No.
TBM or TBF		15,000	300	30				30		126
TMB–1C	45473	14,300	290–300	18	0	29	28		29	132
TBM–3E	85862	. . .	315	30	0	35	. .		35	
F4U, FG, F3A		12,000	350	40				31		126
F4U–1D	57369	11,650	340	35–40	9	28	32		37	
F4U–1D	57181	12,000	305	35	. .	26	26		. .	198(2/21/45)
F4U–4	81032	. . .	320	30–35	. .	30	. .		. .	198(5/8/45)
F4U–4	80860	10,000	380	39–43	28	35	. .		63	94
F6F		12,000	350	40				55		126
F6F–5	77555	10,122	360	34–37	38	37	26		75	84
F6F–5	77555	10,300	385	40–45	38	41	28		79	94
F6F–5	70179	12,000	340	40	44	17	27		61	131
F6F–5	72679	12,400	320	30	. .	27	23		. .	198(2/13/45)
SB2C		14,000	320	40				9		126
SB2C–4	19717	13,600	280	33–37	— 23	32	27		9	165
SB2C–4	20354	12,350	350	43–47	— 23	45	43		22	78
SB2C–5	83135	12,100	315	32–40	— 23	39	39		16	94

viously described may be used, although if rockets are fired in the determination of a no-wind MPI, a sufficient number must be used to eliminate the effects of ammunition dispersion.

4.2.3 Sight Setting Data on Various Planes Used for Bomb and Rocket Tossing

Sight setting calibration data for a number of Navy airplanes are given in Table 1. It should be noted that the longitudinal level line coincides with the thrust line in such aircraft as TBM's, SB2C's and F4U's, while in the F6F's, it is along the wing chord line which is 3 degrees above the thrust line.

The experimental data obtained by diving on the theodolite agree fairly well with the theoretical data obtained from wind tunnel experiments for the TBM's, F4U-1's, F6F-5 No. 70179, and the SB2C's, if the expected variation of ±9 mils between planes of the same type is considered. The F6F-5 No. 77555 does not agree with the theoretical value but a repetition of theodolite tests checked the experimental figures.

Better correlation is shown between the theodolite sight settings and the sight settings based on CIT angle of attack values. The latter were computed using equation (82) of Chapter 6, which is based on reference 214. Therefore, when no data on individual planes are available, a first approximation of the correct sight setting may be obtained from the CIT values.[168]

TABLE 2. Sight settings on P47–D airplanes.

Plane No.	Sight setting (degrees)	Plane No.	Sight setting (degrees)
541	1.3	360	2.5
201	2.5	180	2.5
281	2.5	952	2.5
444	2.0	295	2.3
284	2.5	458	2.5
141	2.8	103	2.0
219	2.8	334	2.5
000	3.0	524	2.5
485	2.0		

Table 2 gives sight settings used as a result of calibration tests by the bomb dropping method, for 17 P47-D aircraft in Ninth Air Force in ETO. While the majority of settings lie within a fairly narrow range, the extremes agree with a maximum anticipated variation of ±1 degree.

Machine guns are harmonized at a sight setting of 2.0 degree, which is 3 mils above the thrust line.

Sight settings 2.0 degrees, or above, indicate a nose-up flight attitude, while those below 2.0 degrees indicate the plane flies nose down.

4.2.4 Altimeter Lag Problem

The use of a pressure altimeter in the bomb director creates a problem which can produce errors of considerable magnitude. The presence of altimeter lag causes the bombs to overshoot the target, since the range-to-target information set into the computer is longer than the actual range. Solution of this problem was not complete at the end of the war.

One method of measuring altimeter lag in a dive is to install a flash bulb in the diving plane, connected to fire at one of the altimeter contact points (usually the 4,980-foot point), and then to dive this plane past an observation plane flying at constant altitude. By observing or photographing the diving plane against the horizon from the observation plane and noting where the flash bulb fires with respect to the horizon, the altimeter lag at one point in the dive can be determined.

Probably the most accurate and useful altimeter lag experiments were those performed by Tactical Test Unit of the Patuxent Naval Air Station under BuAer project 3312. The planes being used were equipped with Model 0 altimeters which interrupted a radio signal at each of the eleven contact points. The planes were dived on three photographing theodolites on the range station at Dahlgren, Va. The true altitude of the plane at any instant in the dive was completed from the theodolite data. By synchronizing the interruption of the plane's radio signal with the theodolite records, the true altitude of the plane at each altimeter contact was obtained. By comparing these data with the altimeter reading (corrected for temperature and barometric pressure) at each contact point, the altimeter lag in a dive is obtained at each contact point.

Because of the complexity of these experiments and the time required to compute the theodolite data, only a limited amount of data was on hand at the time NDRC withdrew from the project. Tests on TBM-3E and F6F-5 planes indicated altimeter lags of 360 and 300 feet respectively.

It could be expected that if the altimeter lag should happen to decrease in the ratio of 6/5 between the first and second altitudes, the true as well as the indicated altitudes could be in the correct ratio and no error would be introduced in the tossing operation. On the other hand, if the lag should increase during the timing run, as it might as the result of an increase in speed and a corresponding change in angle of attack, its effect would be exaggerated. As an example of what appears to be such an effect, it was found that accurate impacts were obtained with a particular P-38 when the zero adjustment of the altimeter was set off by 1,300 feet, although the lag measured for this plane was 650 feet.

Apparently the major cause of these effects lies in the aerodynamic conditions at the static orifice. Such errors will affect (in dives) not only the bomb director equipment but any other device whose operation depends on barometric altitude or airspeed. The desirability of a more complete study of the phenomenon is obvious.

4.3 OPERATION

The correct release time for a bomb or torpedo tossing attack is a function of the following four basic quantities: distance from airplane to target, velocity of the airplane, angle of dive toward the target, and the amount of pull-up acceleration (number of g's). The release time for rocket tossing is a function of all the above factors, plus these additional ones: propellant temperature prior to launching, velocity acquired by the rocket after launching, and the length of the launching lanyard (for large-caliber rockets).

By measuring three basic quantities, the computer takes into account the necessary factors to determine correctly the release time. These three quantities are the time to target (slant range divided by plane velocity), measured by the altimeter unit; the dive angle, measured by the gyro unit; and the pull-up acceleration, measured by an accelerometer enclosed in the computer.

The trajectory drop of rockets is taken to be a linear function of range, i.e., $m + nR$, times a dive angle correction factor. The constant n is determined by the type of rocket and the plane velocity, and is taken into account by the *rocket calibration* settings. The constant m is determined by the setting of the *temperature-lanyard* control.

4.3.1 Optimum Operating Conditions

The range of flight conditions for which the director can be used and the optimum operating conditions are given in Table 3 (for rockets).

TABLE 3. Operating range for rocket tossing.

	Min.	Max.	Optimum
Dive angle	15°	60°	30° – 45°
Max. g's	2.5	6.0	4 to 6
Airspeed	200 knots	...	See below
Range	....	...	1,500 – 3,500 yd.

The *rocket calibration* adjustment on the computer can be set for the most probable speed of attack, and the optimum, of course, will be this speed. In the case of rockets at airspeeds below 300 knots, the permissible variation from the preset speed is about 15 knots. As the airspeed increases, however, the adjustment becomes less critical until a variation of 30 to 40 knots from a setting of 350–400 knots is permissible.

In tossing bombs there is no manual adjustment to compensate in flight for variations in airspeed. The maximum usable range is increased greatly, however, by the use of higher airspeeds, as shown in the table in Chapter 1. The maximum bombing range for an airspeed of 400 knots is about 4,500 yards (at a 40-degree dive angle). The range of values of dive angle, pull-up g's and airspeeds as shown for rockets will also apply for bombs.

Minimum range for either bombs or rockets is determined either by the recovery distance above the target, or by the lowest contact on the altimeter.

4.3.2 Adjustment and Use of the Director

Section 4.3.2 deals with the adjustments which must be made, and the procedure followed by the pilot in making a successful attack. It covers only the operations connected with the director after it is installed and tested. Normal procedure for arming the plane will be followed in addition to the points listed here.

1. *Adjustment before take off.* It will be assumed that the plane is armed with both bombs and rockets. Each adjustment on the director should then be set as shown below.

Set the *altimeter* so that it will read zero at the altitude of the target. This setting is accomplished

by means of the setting knob beside the altimeter face. Any method which permits setting to an accuracy of about 100 feet is suitable.

Set the *airspeed* adjustment on the computer to read the speed for which the sight line is parallel to the flight line.

Set the *MPI adjustment* according to the ballistic coefficient of the bombs. Consult Figure 13 in Chapter 2 for MPI adjustment for bomb ballistic compensation.

Set the *rocket calibration* controls on the computer according to Table 4, using the speed for which the sight line and flight line are parallel. The *fine* control is a vernier on the *coarse* control, one rotation of the *fine* control (0 to 5) giving the same effect as one step, *C* to *D*, say, on the *coarse* control. A clockwise rotation of either control shifts the point of impact away from the plane.

Set the *temperature and lanyard* control to the expected temperature of the rocket propellant at launching. Table 5 contains the information necessary to do this properly.

2. *Adjustments made during flight.* The following operations are necessary to prepare the director for an attack while the plane is in flight.

Turn the *power* switch on at least five minutes, before the equipment is to be used, so that the tubes will become stabilized. When this switch is off, the normal bomb and rocket release circuits are operative.

TABLE 4. Dial settings for rocket calibration controls.[186]

Plane speed (knots) (TAS)	3.5-in. AR		5.0-in. AR		11.75-in. AR		5.0-in. HVAR		2.25-in. AR (Fast)	
	Coarse	Fine	Coarse	Fine	Coarse	Fine	Coarse	Fine	Coarse	Fine
260	D	$2\frac{1}{2}$	E	2	F	4	B	$1\frac{1}{2}$	D	$4\frac{1}{2}$
280	D	4	E	$3\frac{2}{3}$	F	4	B	$3\frac{1}{2}$	E	$1\frac{1}{2}$
300	E	1	F	$\frac{2}{3}$	F	4	C	$\frac{2}{3}$	E	$3\frac{1}{3}$
320	E	$2\frac{1}{2}$	F	2	F	4	C	$2\frac{1}{2}$	E	$4\frac{1}{2}$
340	E	$3\frac{2}{3}$	F	$3\frac{1}{2}$	F	4	C	4	F	$1\frac{1}{3}$
360	E	5	F	$4\frac{2}{3}$	F	4	D	$\frac{1}{2}$	F	$2\frac{2}{3}$
380	F	$1\frac{1}{3}$	G	$1\frac{1}{3}$	F	4	D	$1\frac{2}{3}$	F	$3\frac{2}{3}$
400	F	$2\frac{1}{2}$	G	$2\frac{1}{2}$	F	4	D	3	F	$4\frac{2}{3}$
420	F	$3\frac{2}{3}$	G	$3\frac{1}{2}$	F	4	D	4	G	1
440	F	$4\frac{2}{3}$	G	$4\frac{1}{3}$	F	4	D	5	G	$2\frac{1}{3}$

TABLE 5. Settings for temperature and lanyard control.[186]

Propellant temperature (F)	Plane* velocity (knots)	Dial Settings 2.25-in. AF (Fast)	3.5-in. AR	5.0-in. AR	5.0-in. HVAR	11.75-in. AR 77-in. Lany.	11.75-in. AR 36-in. Lany.
0°	300	20	32	18	43	57	45
	350	16	26	15	34	53	41
	400	14	22	12	28	51	39
20°	300	14	24	13	31	51	39
	350	11	19	10	24	49	37
	400	9	16	9	20	47	35
40°	300	9	16	8	20	46	34
	350	7	13	7	16	45	33
	400	6	11	6	13	43	31
70°	300	3	7	3	7	41	29
	350	2	6	3	6	40	28
	400	2	5	2	5	40	28
100°	300	0	0	0	0	38	26
	350	0	0	0	0	38	26
	400	0	0	0	0	38	26

* Use plane velocity nearest the speed at which the flight line and sight line match.

If a train of bombs is to be released, adjust the *stick-length offset* so that the first bomb will land short of the target by one-half the stick length. For single rounds or salvo, this control should be set on *zero*.

Select *bomb* or *rocket* on the *transfer* switch. If a torpedo is to be launched, the *transfer* switch should be set on *bomb*, and the *stick-length offset* should be turned completely counterclockwise, to the *torp* position.

The gyro must be *uncaged* during an attack. If there is any doubt as to whether it is erect, it should be caged, then uncaged while the plane is in level flight.

3. *Sequence of operations during attack.* The pilot should dive from an altitude which will allow time to attain fairly constant speed before the director begins to operate. Because of the gyro 60-degree bank limitation, the split-S type of attack may not be used. The straight-in approach is not mandatory, however, as it is possible to pass the target to one side and turn into the attack with a bank of less than 60 degrees.

Early Model 0 gyros would spill in banks over 60 degrees. The later Model 1 gyros were modified to permit banks up to 85 degrees. This modification was also introduced in a number of Model 0 and early Model 1 gyros after release to the Service.[145]

When the point of aim is correct and airspeed has stabilized, the pilot should press and hold down the bomb release switch and continue the dive toward the target with the point of aim steady and the bank indicator ball in the center. In a few seconds, the pilot's indicator lamp will light, indicating that the pilot should then pull up immediately. The pull-up should be sudden, and the bank indicator ball should be kept in the center until the pilot's indicator lamp goes out. Thereafter the course of the plane is at the discretion of the pilot.

4.3.3 MPI Errors and Remedies

Use of a director which computes the release time reduces to a minimum some of the errors normally associated with bombing or forward firing of rockets from aircraft, such as incorrect estimation of range, dive angle, and airplane speed. However, errors due to the following sources are still present.

1. *Factors other than the director.*

a. *Wind or target motion.* The pilot must make allowance for wind or target motion in the same way as for a strafing attack with bullets. The longer flight time of bombs and rockets requires a greater lead.

b. *Skidding or side slipping.* If the pull-up is not made in a plane perpendicular to the wings, or if the airplane skids consistently to one side during the approach, a deflection error will result according to the amount of side-slip.

c. *Error in sight setting.* An error in sight setting will cause the projectile to miss the target by the number of mils between the sight line and the flight line.

d. *Faulty bomb racks* or *rocket launchers* will cause erratic operation which is difficult to trace.

e. *Ammunition dispersion.* Errors from this source are always present, and account for the larger part of the error in rocket firing when this director is used. The mean ammunition dispersion for aircraft rockets (Navy) is about 5 mils at operational plane speeds. It decreases with higher airplane speeds.

2. *Director difficulties and remedies.* Some of the sources of erratic behavior of the bomb director and the suggested remedies are listed below. A comprehensive discussion of errors is given in Section 6.4.

a. *MPI* considerably *over* the target. This may be caused by a tumbled or caged gyro, an altimeter incorrectly set to read zero at an altitude considerably below that of the target, a sight set incorrectly below the flight line, a premature pull-up, or (for rockets only) the *transfer switch* set on *bomb*.

b. *MPI* considerably *short* of target. This type of inaccuracy may be the result of a tumbled gyro, a sight setting above the flight line, an altimeter set at zero considerably above the altitude of the target, or (for bombs only) the *transfer switch* on *rocket*.

c. *Errors in deflection* may be the result of a gunsight improperly boresighted in deflection, or an improper pull-up.

d. *Small*, consistent errors in *range* MPI (5 to 10 mils) may be due to a slight error in sight setting or to such other causes as variation in rocket launcher installations, etc. In bomb tossing they can be taken care of by changing the sight setting, or changing the MPI adjustment, as shown in Figure 3. Small range errors in rocket tossing can be corrected with the *rocket calibration* control or with the *temperature and lanyard* control. Ten divisions on the latter will shift the MPI about 10 mils for the slower rockets and about 5 mils for the 5.0-inch HVAR.

Clockwise rotation of either of these controls will cause the MPI to be longer. The shift in mils obtained per 1,000 yards of slant range for a change of one division on the *fine rocket calibration* control is given below:

Coarse setting	A	B	C	D	E	F	G
Mils/1,000 yd	0.4	0.5	0.7	1.0	1.2	1.7	2.0

The values are correct for a 35- to 40-degree dive angle and 350 knots TAS, and approximately correct for other conditions.

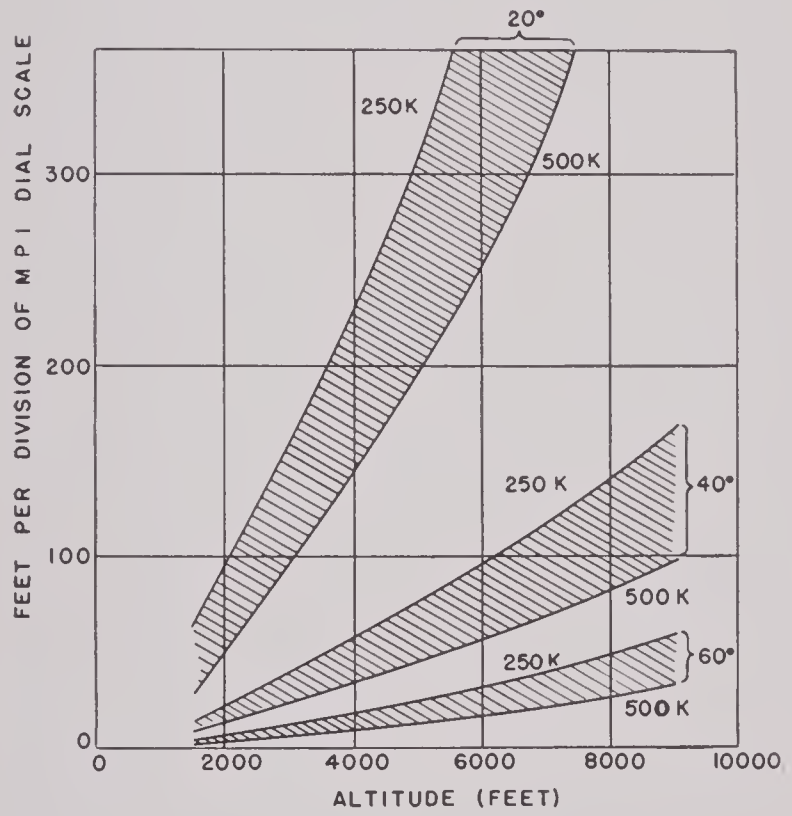

FIGURE 3. Calibration curves for MPI dial, bomb director Mark 1 Model 1, for various altitudes, dive angles, and plane speeds. Example: to increase point of impact by +300 feet at airspeed of 250 knots, dive angle of 40 degrees, and pull-up altitude of 6,000 feet, read up on chart from 6,000-foot designation to 250-knot line for 40-degree dive angle. Read calibration at left side of chart, which is 100 feet per scale division. Thus +300-foot offset requires +3 setting of MPI control knob.

Since the effect of the *rocket calibration* control is proportional to range, this control is not ideal in compensating for sight errors. Any necessary adjustments should be made in the sight setting or, as a second alternative, in the *temperature and lanyard* control. In no case should the *rocket calibration* control be set more than three divisions on the *fine* control from the settings given in Table 4.

4.4 MAINTENANCE

4.4.1 Field Adjustments

Maintenance in the field is generally considered to be limited to trouble shooting to the extent of locating and replacing a faulty component. Beyond this, only minor repairs to a faulty component, such as replacement of tubes or circuit breakers, or repairs to cables and connectors, should be attempted. Major repairs should be undertaken only at proper repair depots by competent personnel.

The following test schedule is recommended for use at squadron levels:

1. Daily timing of the equipment in the plane by counting or watching the instrument panel clock. This is accomplished in the following manner: a. Throw switch to *bomb director* position. b. Cage gyro. c. Press and hold bomb release button. d. Close test switch on *pilot's control box* momentarily. Two seconds (or counts) later, close the test switch again, at which time the indicator light should come on. e. Ten seconds (or counts) later the light should go out and the bomb release relay operate. f. Release bomb release button and uncage gyro.

2. Timing of the equipment in the plane using the Mark 16 Model 0 test set after each 25 hours of operation. Operation of this equipment is described in Section 4.5.

3. After each 25 hours of operation the gyro should be removed from the plane and complete instrument shop tests made, including a starting test, erection rates and coasting time tests. At this time the resistor strip should be tested for cleanness and continuity by using an ohmmeter to measure the resistance at all points on the strip. This is done by tilting the gyro to cause it to read 60 degrees, and with the lever arm in contact with the strip, slowly returning the gyro to a level position. Circuit continuity should be shown at all positions of the arm on the strip.

4. *Trouble shooting.* Detailed instructions on miscellaneous trouble shooting are given in the maintenance manual, reference 232c and in reference 273.

4.4.2 Maintenance Experience

The only available basis for judging the reliability of the equipment is the amount of servicing which has been required to keep it in operating condition

on aircraft. Records of such servicing are available, mainly from two sources. (1) Tactical Test Group at Naval Air Station, Patuxent, where experimental equipment in various stages of development has been in use on relatively few planes for seven months,[74,243-254] and (2) ETO, where 28 sets of equipment (of a very early type) were in use under field conditions for six months.[269-274]

It must be considered that all the listed experience was gained on either strictly experimental models or an interim production type. Obviously, troubles are to be expected with such equipment, and since corrective measures may be taken as a result of such experience it may be assumed that much less difficulty would be encountered with final production models.

1. The result of six months experience at Naval Air Station, Patuxent, is summarized as follows.[74]

During the period from October 28, 1944, to June 1, 1945, no adjustments on computers, such as resetting the cathode bias on the release thyratron, were found necessary. Definite faults developed in only 3 out of 27 computers and only one of these was such that it could not readily be repaired. One computer had over 100 hours in the air, 4 had over 60 hours, 10 had over 40 hours, 20 had over 20 hours, and 24 had over 10 hours without trouble or adjustments.

No adjustments were made on any altimeters during this period. Five out of 26 altimeters were removed from planes because of faults. Two altimeters had over 100 hours in the air, 10 had over 50 hours, and 16 had over 25 hours without trouble or adjustment.

No adjustments or repairs were made on gyros during this period. Seven out of 25 gyros were removed from planes because of faults (4 mechanical faults and 3 electrical). Three gyros had over 100 hours in the air, 11 over 50 hours, and 19 over 25 hours without trouble or adjustment.

2. Following are summaries from reports regarding experience in ETO.

a. About May 15, 1945, thirteen P-47 aircraft equipped with bomb directors were transferred from 368th Fighter Group at R-42 Buschwabach, to the 367th Fighter Group at Y74 near Frankfort. At the time of transfer the toss bombing equipment had a total flying time of 2,500 hours, ranging from 61 hours in one aircraft to a maximum of 267 hours in another aircraft, as indicated in the accompanying report.

b. Flying time of bomb director sets.

Plane	Installed	Time (hours)	
Operational Planes (13)			
D-544	14 Feb.	244	
E-458	2 Mar.	254	
F-952	14 Feb.	241	
H-360	2 Mar.	203	
J-040	14 Feb.	168	
L-485	29 Dec.	267	
L-284	27 Feb.	228	
P-589	29 Dec.	217	
Q-444	23 Mar.	146	
R-103	30 Mar.	61	
T-180	14 Feb.	197	
U-390	28 Mar.	109	
W-007	23 Mar.	132	
Planes Lost (6)			
G-258	25 Feb.	31	Crashed 27 March. Set total loss.
J-769	14 Feb.	200*	Crashed 25 April. Set recovered. Records 7th. ADG.
M-734	29 Dec.	200*	Battle damage. 8 April. Records 7th. ADG.
N-542	29 Dec.	53	Crashed 21 March. Set ruined.
T-151	14 Mar.	143	Destroyed in battle, 24 April. Total loss.
Y-439	29 Dec.	50*	Transferred to U.K. with records.
-584	29 Dec.	10*	Crashed 3 Feb. Set recovered. Records at 10th. ADG.
	Total flying time		3,154 hours.

* Estimated time as records are not available.

c. Prior to the transfer indicated in (a) the maintenance of the equipment was not excessive, as indicated by the following excerpts from the maintenance report of the 396th Squadron of the 368th Group.

Twenty-eight sets of Mark 1 Model 0 bomb director equipment were originally received for installation, of which 20 were installed. Since then, 3 sets have been lost in crashes, and 2 sets have been released for experimental purposes. The sets which were installed have been maintained in operational status at all times since then. Following is a list of all maintenance problems encountered and replace-

ments necessary on these sets in approximately 3 months of use.

Maintenance required, listed by components, is as follows.

Computer Mark 20 Model 0
13 *K* blocks cleaned
1 *K* block wiper loose
4 voltage regulator tubes replaced
1 thyratron tube replaced
2 grid bias adjusted
1 loose connection inside

Relay box Mark 11 Model 00
3 thyratrons replaced
1 loose wire

Gyro Unit Mark 20 Model 0
12 defective caging handles
1 defective caging cable
2 defective caging gears
5 bad contact on strip
3 broken wires on strip
3 pointer arms binding
4 bad erection rates
1 out of balance
1 bearing fell out
1 defective bearing

Altimeter Unit Mark 1 Model 0
6 poor insulation on contact ring
1 cracked contact ring
2 poor contacts
3 stick on contacts
3 whiskers out of place
1 adjusting knob binds

Pilot's control box
1 defective DPDT switch
1 grounded resistor

Dive angle indicator
2 burned out

Signal lights
2 grounded

Cables
5 caused compass deviation
4 poor insulation at altimeter
5 wires broken in plugs

However, when flight operations started again at the 367th Group several pilots noticed immediately that their dive angle indicators would not function properly. Inspection showed that 9 out of the 13 aircraft had gyro trouble, mainly bad rotor bearings.

Of the total of 27 manually caged gyros which were brought to the theater, 17 or 18 required 4th echelon repairs.

However, the normal life of the gyro bearings should be more than the average 200 hours on these planes. Inspection showed that the air filters were very dirty.

3. The most frequent source of trouble was the abrasion of the bob-contact and the top segment block, which produced an accumulation of metal particles sufficient ultimately to short circuit the top mica segment. This trouble has been very greatly reduced in Model 0 equipments made after serial number 266 by using a gold alloy contact in place of the phosphor bronze used in the earlier computers (see Section 3.5.2). Elimination of another source of trouble has been accomplished by replacement of hand caging of gyros by an electric caging mechanism.

Trouble from poor altimeter contact ring insulation has been remedied by a redesign of the ring.

4.5 TEST EQUIPMENT

4.5.1 Test Unit Mark 16 Model 0

The test unit Mark 16 Model 0 was designed to incorporate the minimum features necessary for field servicing of the bomb director Mark 1 Model 0. By using a set of special adapter cables, supplied with the unit, tests may be made on the Mark 1 Model 1 equipment. The principal function of the unit is to put an accurately timed pulse into the computer and measure the resulting output time. For this purpose an a-c operated electric timer, Type S1, of the Standard Electric Time Co., Springfield, Mass., was modified to close one pair of contacts each second. This may be used to introduce timing pulses exactly one second apart. A second pair of contacts is used to flash a neon lamp each time the first pair is closed.

The schematic arrangement of the timer is shown in Figure 4. If switch S_2 is held down for one flash, up for the next, and down for a third, a 2-second signal will be introduced.

The timer actuated by the *J* or signal light circuit, measures the time from second altimeter contact to release.

The timer operates on 110 volts alternating current at a nominal 60 cycles. Since time ratios are the only precise requirements, exact frequency control is not essential. The unit may be operated either directly from alternating current, or by 24 to 30 volts direct current, by use of a vibrator-transformer combination.

In addition to operating the computer, as discussed above, the test unit has a voltmeter for

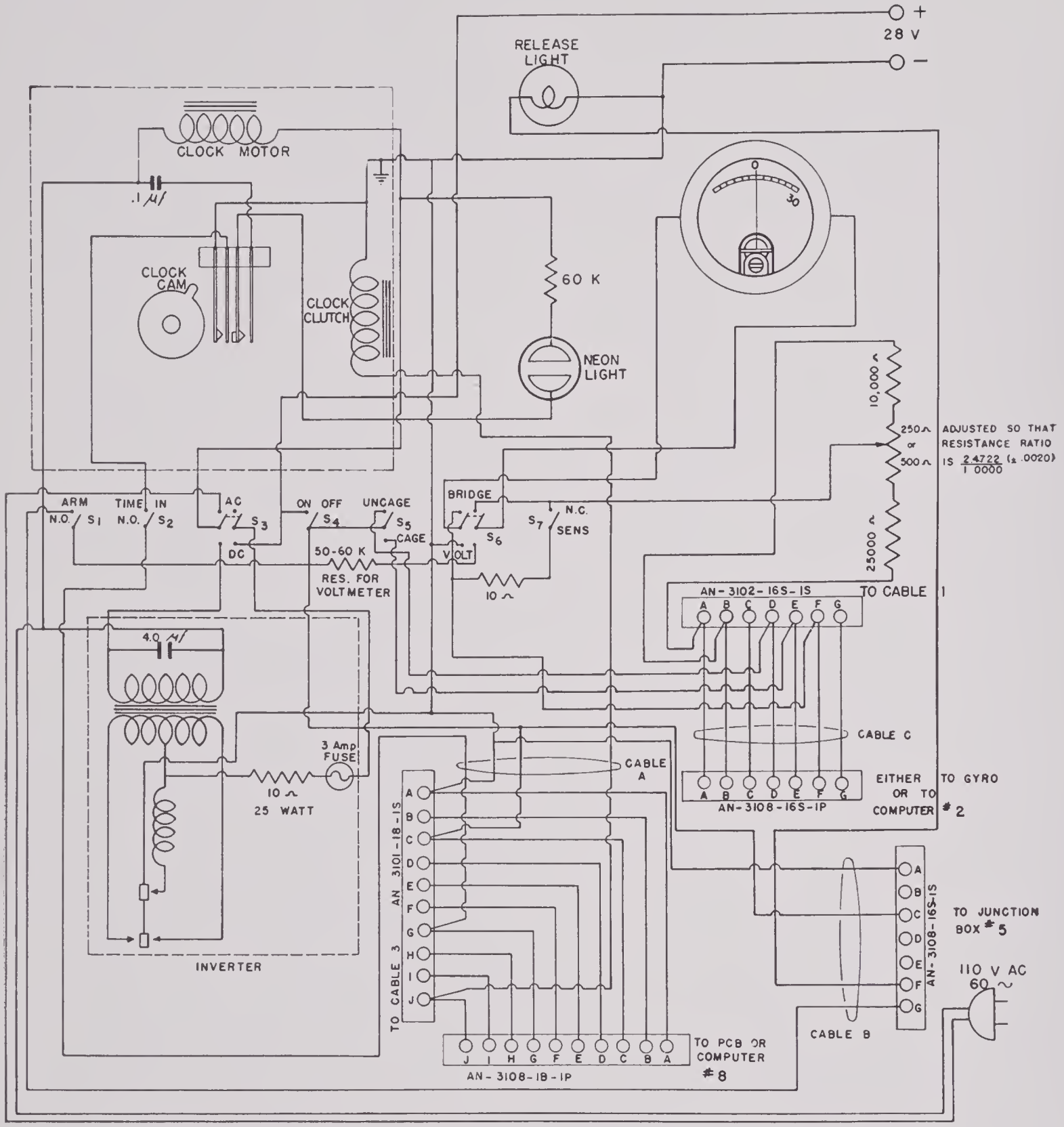

FIGURE 4. Schematic circuit diagram of field test unit Mark 16 Model 0.

checking the supply voltage, and a bridge for adjusting the gyro end resistor.

Detailed operating instructions for the equipment were supplied with it.[65]

4.5.2 Test Unit Mark 17 Model 0

This test unit, Mark 17 Model 0 (TS-362/ASG-10), is considerably more elaborate than the test unit Mark 16. It incorporates the timing system similar to that of the Mark 16 but the a-c timer power is derived solely from a d-c operated vibrator inverter. Weighing approximately forty pounds, it is more a complete bench tester rather than a portable set to be used in aircraft.[202] It incorporates the following features.

1. A timer which may introduce an accurately timed input and measure the output time.

2. Pilot control box with MPI settings of 0 and −5, and a stick offset of 10. A double-throw switch may throw in either the internal "pilot control box" or an externally connected one.

3. A set of lights to indicate continuity of the cage-uncage circuits, the solenoid circuit, a terminal to check resistance of the gyro end resistor, and a switch to open the pointer circuit so that the 0.33-megohm resistor in the computer may be checked for continuity.

4. Signal light.

5. Bomb release indicator light.

6. A switch to enable an adjustment to be made of the grid bias of the output thyratron.

7. A simple megohm meter with a range of 2 to 1,000 megohms.

8. A thyratron tester which can measure grid current and firing bias.

Chapter 5

EVALUATION OF THE TOSS TECHNIQUE

5.1 TOSS BOMBING FIELD TESTS[a]

SECTION 5.1 SUMMARIZES all significant flight tests on production equipment, Mark 1 Model 0 and Mark 1 Model 1, together with tests on some special applications. The major portion of the testing program was carried out at the Naval Air Station, Patuxent River, Maryland, by Navy personnel, with technical assistance from Division 4, NDRC. About 5,000 bombs were dropped at this station between October, 1944, and August, 1945. During the same period, tests were conducted at the Antisubmarine Development Detachment, Naval Air Station, Quonset, Rhode Island; but the smaller number of planes used, and the generally unfavorable weather conditions prevalent at that station, resulted in a smaller amount of data. A limited amount of flight testing was also done at other naval stations and army fields.

In this summary, tests are arbitrarily classified into the following groups: (1) Tactical evaluation tests, (2) equipment evaluation tests, (3) special tests.

5.1.1 Tactical Evaluation Tests

A measure of the effectiveness of the Mark 1 Bomb Director is given by the results of pilots' evaluation tests[244-248] carried out at the Naval Air Station, Patuxent River, during the period October 1944 to August 1945. The object of the test was to obtain the highest percentage of target hits at the particular slant ranges and dive angles designated for each group of flights, the values of which fell within the tactical limitations of both plane and equipment. In all cases, correction for wind error was introduced by the pilot by aiming off the target, using the sight mil rings as reference. The amount of aim offset for the first bomb of a flight was calculated by the pilot, using the wind correction charts and local aerological data. The location of the bomb impact determined any correction necessary in the aiming allowance for the rest of the bombs. Usually five or six bombs were dropped on each flight. The bombing runs were made upwind, downwind, or crosswind to facilitate wind correction. In general, the bombing approach was made in a slight turn up to the pushover point in order to keep the target in sight. When the proper position was attained, the nose was swung over the target and a straight pushover entry made into the dive. Pushover was usually started at an altitude about 5,000 feet above the pull-up altitude in order to reach the desired speed.

Test features are summarized in Table 1. Previous to the pilots' evaluation tests, all planes underwent sight calibration flights (see Section 4.2.1). Two targets were used: (1) Point-No-Point target — a platform 30 feet square in shallow water with pile markers giving reference points at 50, 100, 200, and 300 feet radius from the center in four directions 90 degrees apart; (2) Sharp's Island target — a platform 10 feet square in shallow water with pile markers giving a circular reference 15 feet in radius from the center, plus pile markers giving reference points at 50, 100, 200, and 300 feet radius from the center in four directions 90 degrees apart, plus additional pile markers at 100-foot intervals on the north leg of the target extending to a distance of 1,000 feet from the center. Impact data were based on either visual or photographic observations. In the first case, recorded data were obtained independently by both pilot and observer; in the second case, a photo-observation plane accompanied the test plane and photographed each impact. The accuracy of measurements in the latter case was about plus or minus 5 feet. A comparison of the values obtained from photographic assessment and from visual observation of the same impacts showed no large discrepancies, the difference rarely exceeding 25 feet and averaging about 15 feet. Dive angles between altitude points were read by the observer from the gyro. When this was impossible because of the location of the gyro, dive angles were read by the pilot or an observer from a dive angle repeater instrument especially installed for the purpose. In the first case, measurements were accurate to about plus or minus 3 degrees; in the second case, the accuracy was slightly less. Indicated airspeeds were read by the pilot from his instrument panel in the

[a]Sections 5.1 and 5.2 were written by Emma U. Rotor of the Ordnance Development Division, National Bureau of Standards.

TABLE 1. Pilots' evaluation tests.

Aireraft	Bomb direc-tor	Sight setting (mils)	Number of pilots	Type of bomb and ballistie eoeffieient	Number of bombs seored	Impaet data obtained	Direction of approach	General weather eondition	Max. g at pull-up	Second altitude eontact (ft)	Dive angles	Average slant range at 2nd altitude (ft)	Average pull-up IAS (knots)	Average altitude (ft) and IAS at pushover (knots)	Average lowest altitude in pull-up (ft)	Average radial error (ft)	Average radial error (mils)
*SB2C-3 #18605 SB2C-4 #20354 SB2C-4 #20381	Mk 1 Mod 0	+17½	4	Mk 15, 60-lb water fill-ed; 0.8 and Mk 19, miniature; 2.3	475	Visual	Downwind 32% Upwind 35% Crosswind 33%	Avg. wind velocity 24 mph	2.6-5.7 Avg. 4.2	2,000 (133 bombs)	30°-35°	3,700	320	7,000 ft	....	53	10 6
										3,450 (201 bombs)	35°-40°	5,700	325	9,000 ft	....	95	12.9
										5,970 (141 bombs)	40°-45°	8,900	340	12,000 ft	....	128	14.7
†SB2C-5 #83135	Mk 1 Mod 1	+16	2	Mk 15, 95-lb sand and water filled; 1.3	101	Photo	Downwind 50% Crosswind 50%	Fair to good. Avg. wind velocity 11 mph	4.8-6.6 Avg. 5.4	4,975	38°-60° Avg. 49°	6,800	335	10,000 ft 145 k	3,200	115	15.1
‡F4U-1D #57369	Mk 1 Mod 0	+30	2	Mk 15, 60-lb water fill-ed; 0.8	104	Visual	Downwind 29% Upwind 38% Crosswind 33%	Avg. wind velocity 25 mph	4.0-5.9 Avg.4.7	4,975	38°-45° Avg. 40°	6,800	340	10,000 ft	...	153	15.9
§F4U-4 #80860	Mk 1 Mod 1	+40	2	Mk 15, 95-lb sand and water filled; 1.3	99	Photo	Downwind 50% Crosswind 50%	Good. Avg. wind velocity 25 mph	4.0-6.7 Avg. 5.0	5,970	42°-57° Avg. 48°	8,100	380	10,000 ft 165 k	3,500	123	13.3
¶TBM-3E #86046	Mk 1 Mod 1	+34	2	Army M-38-A2 practice, 100-lb; 1.35	101	Photo	Downwind 50% Crosswind 50%	Fair to good. Avg. wind velocity 13 mph	2.9-3.9 Avg. 3.4	3,450	29°-36° Avg. 35°	6,300	315	8,500 ft 135 k	2,200	110	13.1

*See referenee 245.
†See referenee 248.
‡See referenee 244.
§See referenee 247.
¶See referenee 246.

early part of his pull-up and were accurate to about plus or minus 10 knots. The maximum acceleration reached during pull-up was read by the pilot from the plane accelerometer and was accurate to about plus or minus 0.2g. The lowest altitude reached in pull-up was read by the pilot or observer and was accurate to about plus or minus 200 feet.

Test results are illustrated in Figure 4 of Chapter 1, wherein are shown impact points of 747 bombs dropped from medium slant ranges, and in Figure 1,

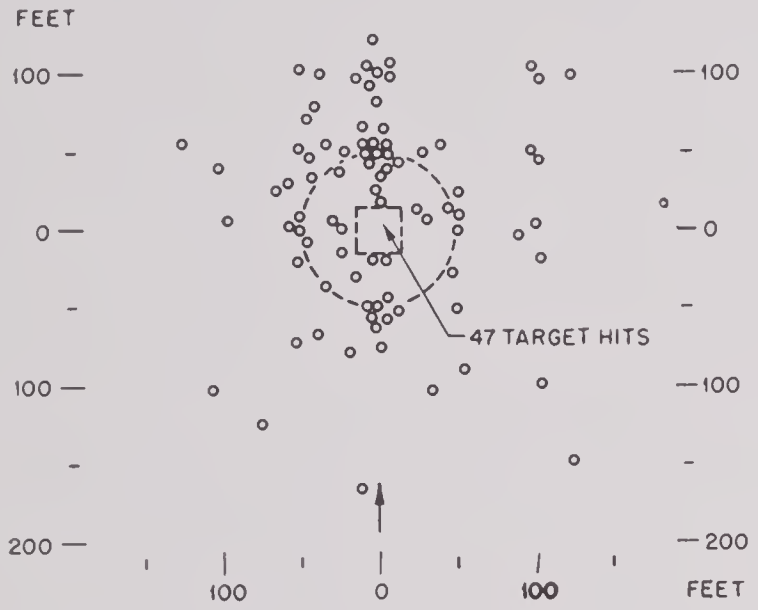

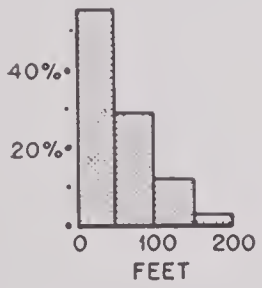

FIGURE 1. Impact pattern of 133 bombs dropped in pilots' evaluation tests at Naval Air Station, Patuxent River, Maryland, using short slant ranges of 5,400 to 9,300 feet. (See Figure 4 of Chapter 1 for impact pattern at longer ranges.)

which gives the impact points of 133 bombs dropped from short slant ranges. A number of bombs were not scored for such reasons as defective bomb racks, defective bombs, caged gyro, spilled gyro, defective gunsight, poor visibility, slant ranges, and plane speeds being outside the limitations of the equipment.

Further analysis of the data is given in tabulated form in Table 2 and graphically in Figures 2 and 3. Bombs which hit the center 30-foot square platform of Point-No-Point target were given a radial error of 11 feet, a 7.8-foot range error and a 7.8-foot deflection error, since in the case of a hit the actual distance

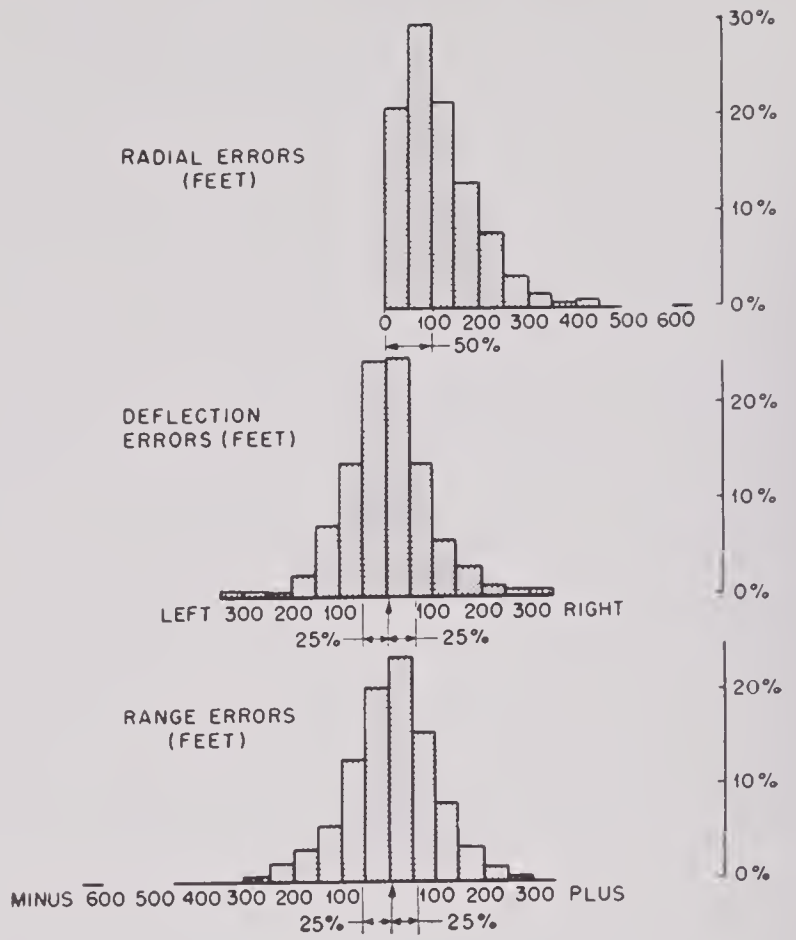

FIGURE 2. Distribution of impact errors in feet of 747 bombs tossed at slant ranges of 5,400 to 9,300 feet. (See Figure 4 of Chapter 1 for impact pattern.)

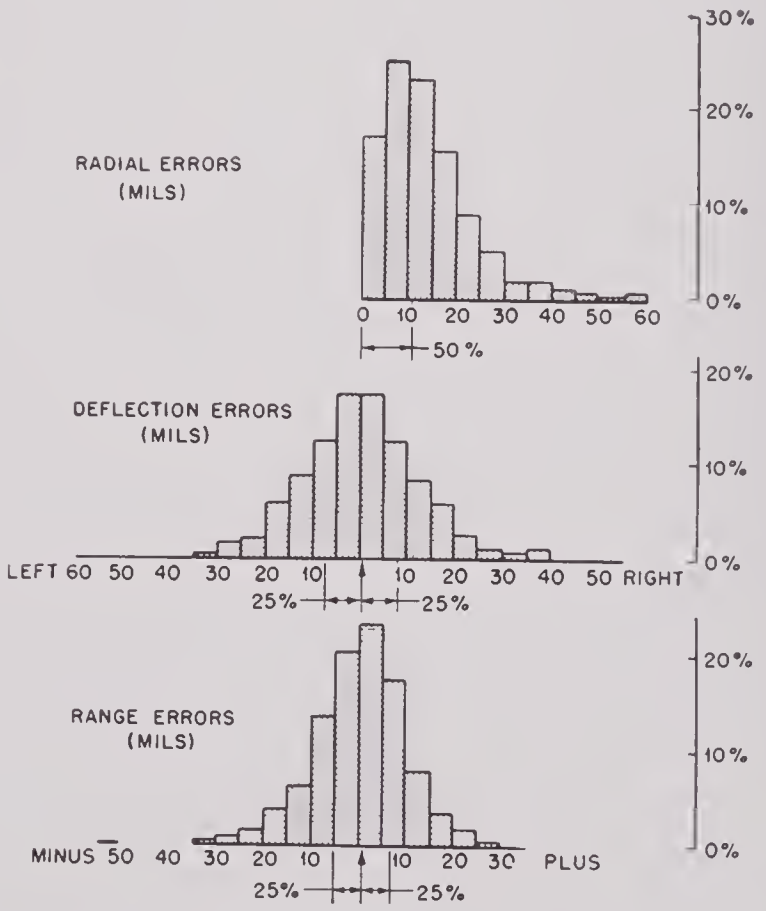

FIGURE 3. Distribution of impact errors in mils (same bombs as in Figure 2.)

from the center of the target could not be determined. Mil errors were calculated on a plane at the target perpendicular to the line of sight by the following formulas:

$$\text{Range mil error} = \frac{\text{Ground error in feet} \times \text{Sine of dive angle} \times 1000}{\text{Slant range at second altitude}}.$$

$$\text{Deflection mil error} = \frac{\text{Ground error in feet} \times 1000}{\text{Slant range at second altitude}}.$$

$$(\text{Radial mil error})^2 = (\text{Range mil error})^2 + (\text{Deflection mil error})^2.$$

of the SB2C-4 and F4U-1D planes, provide some means of comparing the relative accuracy of dive bombing with that of the toss bombing technique under approximately the same conditions of release.[245,249a] Project PTR-1204, NAS Patuxent, consisted of dive bombing tests at an average release altitude of 2,000 feet at steep dive angles. By taking the results of the pilots' evaluation tests at a second or pull-up altitude of 2,000 feet, comparison as shown in Table 3 is possible. It should be noted, however,

TABLE 2. Results of pilots' evaluation tests.

(a) *At medium slant ranges*

Total number of bombs: 747 — Slant range: 5,400–9,300 ft

	Average error		Median (absolute) error	
	ft	mils	ft	mils
Radial	118	13.5	100	11.5
Range	79	7.2	61	5.8
Deflection	70	9.8	52	7.8

Results according to direction of plane approach

	Crosswind	Downwind	Upwind
Avg. radial error (mils)	14.2	12.7	13.4
Avg. range error (mils)	7.5	6.7	7.3
Avg. deflection error (mils)	10.5	9.1	9.9
Number of bombs	289	291	159

(b) *At short slant ranges*

Total number of bombs: 133 — Slant range: 3,500–4,000 ft

	Average error		Median (absolute) error	
	ft	mils	ft	mils
Radial	53	10.6	50	7.6
Range	37	5.3	18	2.6
Deflection	28	7.5	8	2.1

(c) *Results* (a) *and* (b) *according to slant range*

Slant range at second altitude	Number of bombs	Average radial error	
		ft	mils
7,100–9,300 ft	375	134	13.3
5,400–7,000 ft	372	101	13.7
3,500–4,000 ft	133	53	10.6

Comparison of Toss Bombing with Standard Dive Bombing. The data furnished by the pilots' evaluation tests at low altitudes when used in conjunction with the results of Project PTR-1204, a test to determine the comparative dive bombing accuracy that the dive angles in toss bombing were between 30 and 45 degrees, whereas those in dive bombing were much steeper, so that although altitudes involved are comparable, the slant ranges for toss bombing were considerably longer.

Low Ceiling Tests.[244,245] The SB2C-3, SB2C-4 and F4U-1D planes used in the pilots' evaluation tests made special flights to determine the minimum ceiling conditions under which the toss bombing maneuver could be successfully made without sacrificing accuracy. Results showed that low ceiling attacks could be accurately made in both types of planes from a starting altitude of 3,000 feet in level flight at high entry speed (200 or more knots) with recovery from the dive above 800 feet. A dive angle of 25 to 30 degrees with a speed of 280 knots could be attained if the 1,660/1,390 feet altitude contacts were used.

TABLE 3. Comparison of toss bombing with ordinary dive bombing.

Total average radial error in dive bombing for 4 pilots, average release altitude 2,000 ft (270 bombs)	83 ft
Total average radial error in toss bombing for 3 pilots, second altitude 2,000 ft (133 bombs)	53 ft
Improvement in bombing efficiency = $(83)^2/(53)^2$ = 2.5 times. Bombs required for given effect using toss bombing = 40% of those needed using conventional dive bombing.	

Evaluation Tests in Army Aircraft, Eglin Field, Florida.[256] During the period January 24 to May 12, 1945, the Mark 1 Model 0 bomb director was tested in P-47D, P-38J and P-51D aircraft at Eglin Field, Florida. The tests were conducted to determine the accuracy and practicability of the bomb director in fighter-type aircraft for release altitudes of 4,000 feet and above, and to determine what improvement, if any, the bomb director gave over standard dive bombing at the same altitudes of release. The bomb director was found unsuitable in P-38J aircraft because the pitot static installation resulted in excessive altimeter lag — more than 600 feet. Toss bombing with the P-51D aircraft was successful but tests were discontinued because the Model 0 equipment, installed between the engine and fire wall, was being subjected to high ambient temperatures. (The dimensions of the Model 1 equipment permit a more suitable location.) Most of the tests were therefore made in a P-47D aircraft.

Six pilots, three experienced in dive bombing and three inexperienced, participated in the tests. Three release altitudes were used — 4,000, 6,000, and 8,000 feet, approximately — corresponding to second-altitude contacts at 4,980, 7,160, and 8,600 feet, respectively. Average dive angle was about 40 degrees; indicated airspeed, 400 to 440 mph. Each pilot made two releases from a P-38 plane using conventional dive bombing and two releases from a P-47 plane equipped with the bomb director. Different headings were used for each of the two runs in a flight. No pilot made more than one flight in the same plane on the same morning or afternoon. Missions were repeated daily until a representative sample at the three altitudes was obtained.

TABLE 4. Results of comparison test — Eglin Field, Florida.[256]

	4,000 ft		6,000 ft		8,000 ft	
Release altitude	P–38 No computing sight	P–47 Bomb director	P–38 No computing sight	P-47 Bomb director	P–38 No computing sight	P–47 Bomb director
Number of releases	106	129	65	75	52	85
Average range error	346 ft	211 ft	414 ft	301 ft	497 ft	464 ft
Average deflection error	167 ft	178 ft	274 ft	238 ft	292 ft	283 ft
Average circular error	416 ft	306 ft	542 ft	433 ft	632 ft	591 ft
Circular probable error	382 ft	302 ft	500 ft	409 ft	589 ft	510 ft
Range MPI	+ 143 ft	− 28 ft	+ 55 ft	− 62 ft	− 116 ft	− 182 ft
Deflection MPI	− 12 ft	+ 5 ft	− 60 ft	− 33 ft	− 46 ft	− 130 ft
Percentage of hits (100-ft radius)	9.4	14.0	1.9	4.0	1.9	4.7

The equipment in the P-47 plane was a Mark 1 Model 0 bomb director. Bombs used were M38A2, 100-lb practice bombs. Dive angles and indicated air speeds increased from 37 degrees, 400 mph at 4,000-ft release altitude to 42 degrees, 440 mph at 8,000-ft release altitude.

The results of the tests are summarized in Table 4.

On the basis of the *circular probable error* [CPE], the bomb director was found to be more accurate by 20.9, 18.2, and 13.4 per cent at 4,000, 6,000, and 8,000 feet release altitude, respectively. The average dive angles used ranged from 37 degrees at 4,000 feet to 42 degrees at 8,000 feet. These are based on on the whole, the bomb director scores of the inexperienced pilots were 29 per cent poorer than those of the experienced pilots. The scores obtained at Eglin Field are definitely less favorable than those obtained in pilots' evaluation tests at Patuxent Naval Air Station; however, they are not surprising

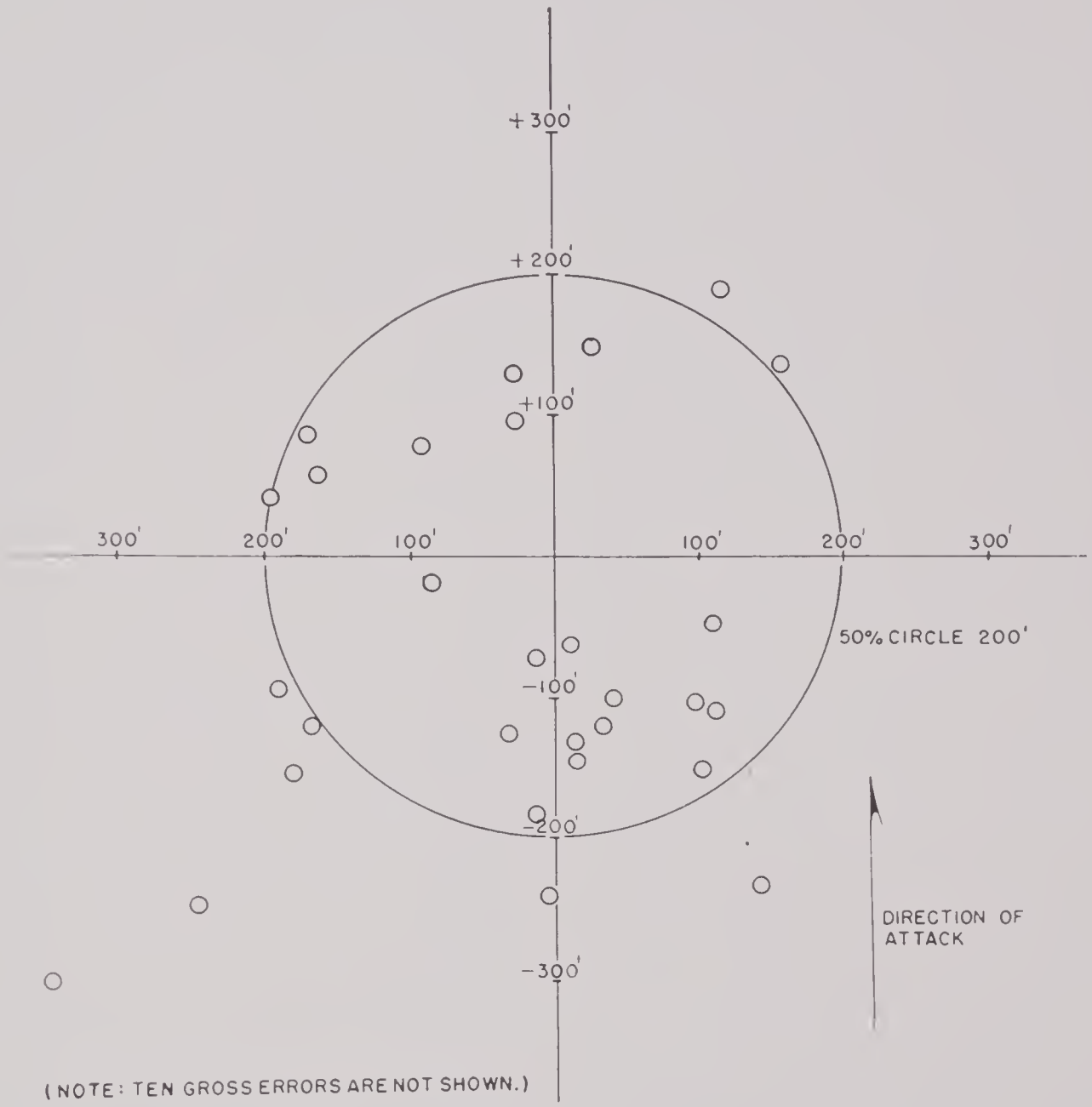

FIGURE 4. Plot of all (39) bombs identified in combat toss bombing missions with P-47 aircraft, 368th Fighter Group, Nineteenth Tactical Air Command, Ninth Air Force. Average conditions at release: altitude 3,000 feet, dive angle 40 degrees, speed 350 to 400 mph, and range 4,700 feet. The 50 per cent circle was 200 feet for all bombs, including 10 gross errors not shown. (Diagram reproduced from ORS report, reference 269.)

pilots' estimates minus 5 degrees, the approximate amount of pilot estimate error. These give second-altitude slant ranges of 8,300 feet at the low altitude and 13,000 feet at the high altitude. The use of dive angles shallower than those required for accurate operation of the bomb director at high altitudes caused many bombs to fall short by large amounts. This was especially true of the inexperienced pilots; in view of the particular test conditions used.

While it is true that a strict tactical evaluation of the bomb director should give the results of flights under combat conditions, an analysis of flights conducted at testing stations can give a measure of the expected performance of the equipment in Service use. The pilots' evaluation tests at Patuxent may be said to represent the expected results under

optimum conditions — the same pilot and plane make five or six successive runs on the target and thus can benefit from the information given by the first bomb impacts as regards the amount of aim offset needed to compensate for wind. On the other hand, the tests conducted at Eglin Field might be said to represent the opposite set of conditions. Here, the pilot makes only two successive runs, with different headings, so that he has to base his aim offset estimates purely on whatever aerological data are available. The toss bombing technique is designed for use in squadron attack and the location of the bomb dropped by the leader would give the required wind compensation information to the rest of the group.[b] Therefore, it is not unreasonable to expect that in Service use, the performance of the bomb director would be somewhere between those indicated by the results of the Patuxent and Eglin Field tests. The results of limited operational use do lie between these extremes, as shown in the next paragraph.

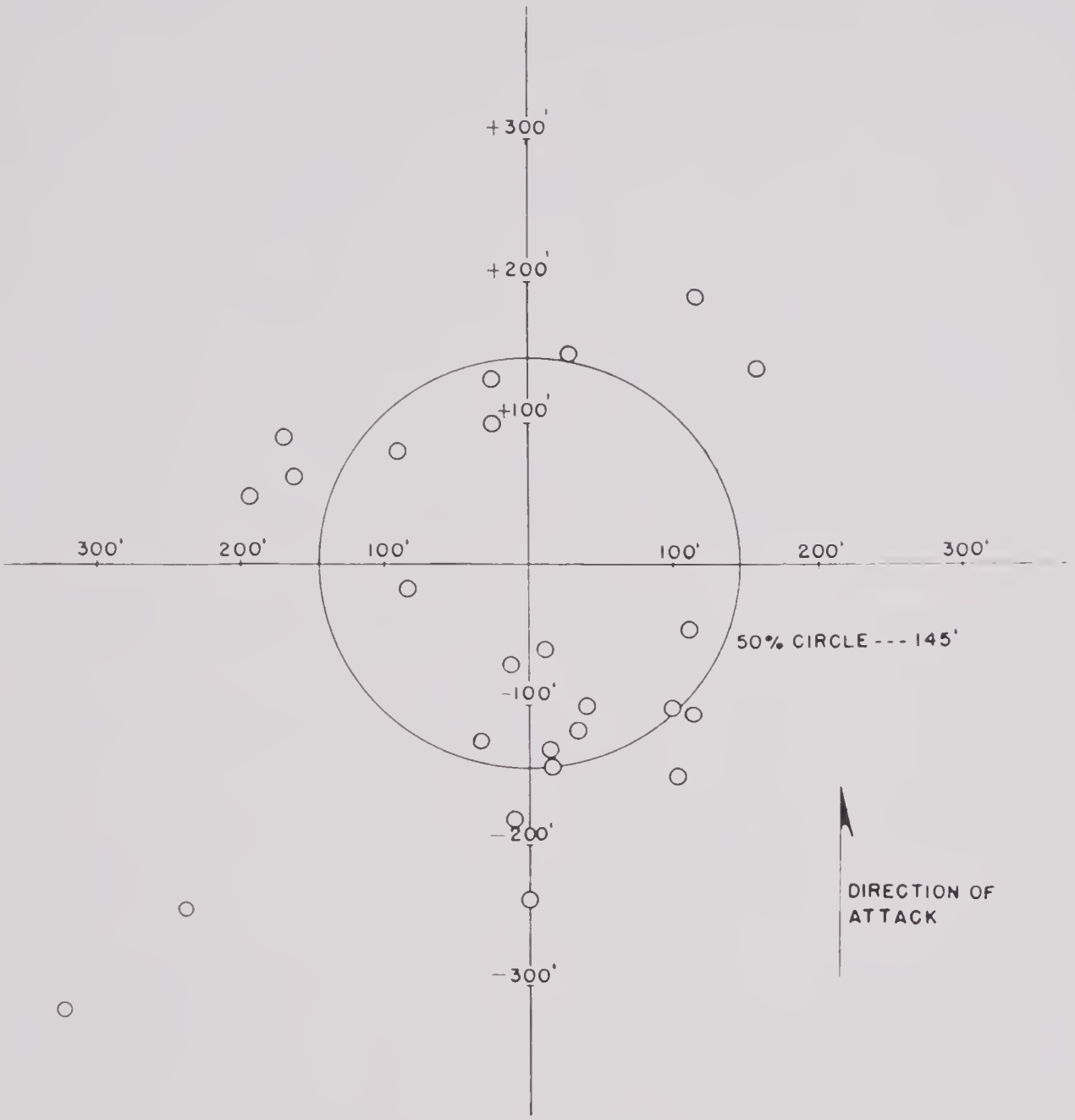

FIGURE 5. Plot of all (25) bombs scored, after discarding releases in which bombs hung up, or where pilot aimed at wrong target, etc. The 50 per cent circle was 145 feet. (See Figure 4 for average conditions at release and for plot of all identified bombs.)

[b] In the course of the Eglin Field evaluation project, two-plane team toss bombing was given a limited test. The first pilot aimed on the target, the second observed the impact and made his corrected run on the same heading. Eighteen pairs of bombs dropped from 4,000 feet release altitude by four different teams gave an average circular error of 281 feet for the second bomb as compared to 493 feet for the uncorrected bomb.

Operational Evaluation by Ninth Air Force. Thirteen operational missions using Model 0 bomb tossing equipment were carried out during the last half of March 1945. These were conducted over Germany by the 368th Fighter Group of the Nineteenth Tactical Air Command of the Ninth Air Force. Evaluation of the missions was made by the Operational Research Section of the Ninth Air Force.[269] Photographic coverage was made on all missions but only four of these were assessable. From four to twelve P-47 aircraft carrying two bombs apiece participated in each mission.

The impact distributions of the four assessable missions are plotted in Figure 4, which shows a CPE about the target of 200 feet (Figure 4 does not show 10 gross errors). It was established that in a few cases, the bombs hung up momentarily in the racks or the pilots had aimed at the wrong target. If these rounds are discarded, the impact pattern shown in Figure 5 is obtained. Here the CPE is 145 feet. Figures 4 and 5 are from the ORS report[269] referred to above.

The general conclusion of this report was that further data were needed to establish the possible advantage ratio of the bomb tossing equipment in combat. However, it was estimated that with the Model 0 equipment, the accuracy would not exceed that shown in Figures 4 and 5. The reference report noted that the reaction of the aircraft pilots to the equipment was very favorable. Their nonquantitative evaluation was that the accuracy of fighter-bomber operations would be appreciably improved with the tossing equipment.

5.1.2 Equipment Evaluation Tests

Overall Operation of the Mark 1 Bomb Director

A measure of the reliability of the Mark 1 bomb director is afforded by studying the results of all recorded flights made with this equipment at the Naval Air Station, Patuxent River.[39,46,50,53,60,68,76,85,88,97] Since these flights were made under all conditions, varying according to the type of test being conducted, results of the group as a whole cannot be analyzed from the standpoint of location of no-wind MPI, magnitude of radial error, dispersion, or other similar means of scoring.

The operation of the equipment was considered satisfactory in all cases where the point of impact was within the area which conditions of the particular test indicated as proper. This does not mean that all satisfactory impacts fell within any fixed distance from the target. In cases where bombs were dropped in tests involving upwind and downwind runs, with no adjustments made in the equipment or gunsight to bring the impact point nearer the target, the bombs should fall in approximately the same place regardless of the heading, provided the instrument settings are constant and no sudden variation in wind conditions occurs. Such impacts are considered satisfactory, although with respect to the target or point of aim, they may be a considerable plus or minus distance away. Figure 6 is an illustration of impacts of this type. In general, unsatisfactory drops are easily classified, normally deviating from the common impact area by a considerable amount. In most cases, they miss the common impact area by several hundred feet.

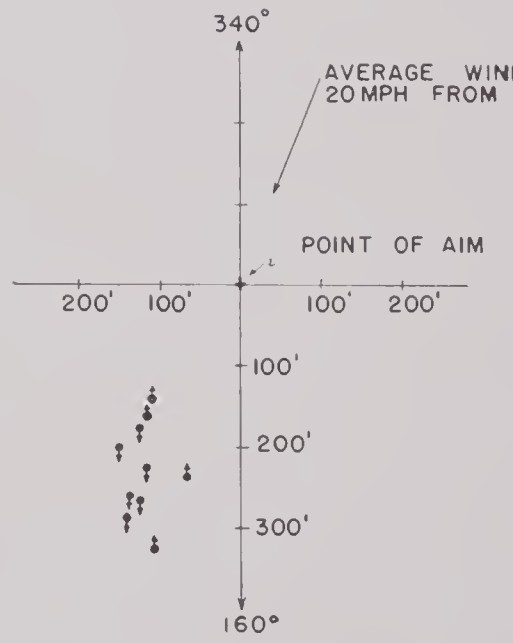

Figure 6. Results of typical test flight to check no-wind MPI. Shown are bomb impacts of two flights made in quick succession. Slant range at second altitude was approximately 6,000 feet. Each flight consisted of 5 runs, runs being made with alternate plane headings 180 degrees apart. Small arrows indicate plane heading used for each run. (For methods of computing no-wind MPI, see Table 5.)

The method of calculating the no-wind *mean point of impact* [MPI] is demonstrated in Table 5, using the data from Figure 6.

Since the object of this survey is the appraisal of the functioning of the Mark 1 bomb director, obviously impacts which are unsatisfactory due to some factor outside the equipment were not scored. Some

of these factors are rack lag, frozen bombs, pilot error, and adverse weather conditions, such as clouds hiding the target during the bombing run. In many of the tests, especially during the early part of the production program, it was found desirable to continue, for a limited time at least, the use of equipment which occasionally or even frequently malfunctioned. This was done since it is often true that malfunctioning which occurs in flights is not readily duplicated in laboratory tests and thus its cause can be more readily diagnosed through flight tests. This lowers a "score" but is justified from a developmental standpoint.

Table 6 summarizes the results of tests with the Mark 1 bomb director at NAS, Patuxent, from the point of view of satisfactory operation of the equipment.

Table 5. Methods of computing no-wind MPI.

Plane heading	Range error	Deflection error	No-wind range impacts (computed)	Alternative method of computing no-wind MPI	
160°	+ 200	150R	− 18 ft		
340°	− 235	65L			
160°	+ 285	140R		Average impact	
340°	− 325	105L	− 35 ft	point for runs	
160°	+ 225	115R		at 340° heading	− 215 ft
340°	− 160	115L	+ 8 ft	Average impact	
160°	+ 175	125R		point for runs	
				at 160° heading	+ 235 ft
340°	− 140	110L			
160°	+ 260	135R	+ 62 ft		
160°	+ 265	125R			
		No-wind MPI	+ 8 ft	No-wind MPI	+ 10 ft

Table 6

Date of tests: November 7, 1944, to July 31, 1945.

Planes: 15, as follows: two SB2C–3's, four SB2C–4's, one SB2C–5, one F4U–1D, one F4U–4, two P–47's, two F6F–5's, one TBM–1C, and one TBM–3E.

Total number of bombs tossed 4,226
Total number of bombs scored 3,998
Total number of satisfactory impacts . . . . . 3,883 or 97.1%.

Total number of unsatisfactory drops, 115 or 2.9%, as follows:

89, or 2.2%, premature releases
8, or 0.2%, late releases
12, or 0.3%, defective gyro operation
6, or 0.2%, defective altimeter operation.

Most of these unsatisfactory operations occurred during the early part of the developmental program. Their causes, being mainly small defects in design and workmanship, were localized and eliminated.

Total number of bombs not scored, 228, as follows:

35% Unobserved impact point.
24% Wrong technique, e.g., premature pull-up, changing dive angle during aiming run, leaving gyro caged, low speed.
18% Defects outside of toss bombing equipment, e.g., rack lag, frozen bombs, bomb bay doors closed.
15% Adverse weather conditions — poor visibility.
6% Bombs dropped in salvo of two or more, only one of which was scored.
2% Bomb director switch in off position.

Constancy of No-Wind MPI

Mark 1 Model 0 Equipment. Tests were carried out at NAS, Patuxent, during November and December 1944 to determine the effect of changing slant range and dive angle on the no-wind MPI.[47,52] Prior to the tests proper, each plane made calibration flights at 3,450 feet second altitude and 40 degrees dive angle. The sight and MPI adjustment settings which placed the no-wind MPI reasonably near the target under these conditions were adopted for the whole test. In no case was any correction for wind introduced by the pilot. The plane approached the target alternately from two opposite directions. A no-wind impact was calculated for each pair of drops at alternate headings, using the method illustrated in Table 5. The no-wind MPI was computed for each combination of dive angle and second altitude by taking the algebraic average of all no-wind impacts at this dive angle and altitude. The mean absolute error about the no-wind MPI was computed by using standard equations based on normal distribution laws, and was taken as 0.8 of the standard error.

The corresponding mil value for each impact, projected on a plane perpendicular to the line of sight, was computed, and similar calculations made.

Test results are summarized in Table 7. It is noted that with the variations of dive angle and slant range defined by the test, the shift of no-wind MPI was insignificant in magnitude and smaller than variations introduced by, say, air bumps. It is noted, however, that (1) the MPI tends to shift in a minus direction as the altitude increased, the dive angle remaining constant, and (2) the MPI tends to shift in a minus direction as the dive angle is decreased from 40 to 20 degrees, the slant range remaining approximately the same.

Mark 1 Model 1 Equipment. The same test was carried out on a set of Mark 1 Model 1 equipment in

TABLE 7. No-wind MPI tests with Mark 1 Model 0 bomb director.

Plane	Settings		2nd alt.	Avg. dive angle	Avg. slant range at 2nd alt.	Avg. IAS at pull-out (knots)	No. of bombs	No. of no-wind impacts	No-wind MPI (ft)	Mean abs. dispersion (ft)	No-wind MPI (mils)	Mean abs. dispersion (mils)
	Sight	MPI										
SB2C-4 #20381	19.5°	0	4,150	38°	6,700	320	19	9	+ 1	62	+ 2.6	4.7
			2,880	37°	4,800	320	19	7	+ 98	40	+ 17.1	3.8
			2,000	23°	5,100	310	18	8	− 11	44	+ 0.9	4.7
			1,390	22°	3,700	310	16	7	+ 88	39	+ 9.9	4.7
SB2C-4 #20354	19.5°	+ 5	4,150	38°	6,700	315	15	6	− 53	46	− 0.2	6.9
			2,880	35°	5,000	325	15	7	− 35	46	+ 3.4	5.3
			2,000	23°	5,100	315	15	7	− 58	53	− 4.8	3.2
			1,390	21°	3,900	315	13	4	− 23	71	− 1.2	6.6
SB2C-3 #18604	19.5°	0	4,150	39°	6,600	315	14	6	− 45	38	− 0.3	5.7
			2,880	38°	4,700	320	18	7	+ 32	45	+ 7.4	7.0
			2,000	23°	5,100	310	16	7	− 102	80	− 6.8	6.9
			1,390	24°	3,400	310	16	7	− 49	70	− 3.4	5.2
F6F-5 #70179	47.5°	− 5	4,150	42°	6,200	365	16	8	+ 25	26	+ 3.7	2.8
			2,880	40°	4,500	360	8	4	− 9	10	− 0.6	1.6
			2,000	21°	5,600	340	10	5	− 63	60	− 3.7	3.5
			1,390	21°	3,900	340	10	4	+ 48	8	+ 5.6	3.0
SB2C-4 #20381	19°	0	7,160	43°	10,500	320	15	6	− 44	104	+ 0.1	6.6
			5,970	41°	9,100	315	20	7	− 25	73	− 1.1	5.0
			4,980	38°	8,100	325	13	5	− 23	67	− 0.2	6.5
			2,880	37°	4,800	300	10	4	+ 14	14	+ 1.9	1.6
SB2C-4 #20354	19°	0	5,970	44°	8,600	340	16	8	− 31	75	+ 0.4	6.4
			4,980	44°	7,200	340	17	7	+ 25	35	+ 6.1	2.5
			2,880	38°	4,700	310	12	5	+ 94	18	+ 12.3	1.1

TABLE 8. Range no-wind MPI tests with Mark 1 Model 1 bomb director.

Plane: SB2C-4 #20381 MPI setting: 0 Sight setting: 17.5°

2nd alt. (ft)	Avg. dive angle	Avg. slant range at 2nd alt. (ft)	Avg. IAS at pull-out (knots)	No. of bombs	No. of no-wind impacts	No-wind MPI (ft)	Mean abs. dispersion (ft)	No-wind MPI (mils)	Mean abs. dispersion (mils)
2,000	22°	5,300	300	42	20	− 16	35	− 0.3	2.5
2,400	22°	6,400	300	30	14	− 173*	51	− 9.3	4.5
3,450	43°	5,000	325	10	5	+ 7	37	+ 1.5	4.3
4,150	41°	6,300	335	10	5	+ 24	35	+ 2.9	3.5
4,980	41°	7,600	320	12	5	+ 1	31	+ 1.4	4.3
5,970	36°	10,100	330	10	5	+ 37	58	+ 2.0	2.8
7,160	40°	11,100	325	10	5	+ 83	34	+ 5.0	1.5

* Short MPI explained by combined effects of change in angle of attack (sight was calibrated at 40°) air resistance, relatively low speed at slant range involved, limitations of ψ function. Subsequent flights with the MPI dial setting moved to +2 gave a range no-wind MPI of −11 feet (−0.3 mil) for 34 bombs. Mean absolute dispersion was 49 feet (3.4 mils).

[redacted]

an SB2C-4 airplane during June and July 1945.[118] The test procedure was the same as outlined above, with improvements in some test features. For example, bombs with better ballistic coefficient were used, ten bombs were dropped on each flight, and the bomb racks had been especially wired so that it was possible to measure the time lag between the reception of the release pulse and the actual time of release of the bomb.[106] It was thus possible to discard several abnormal impacts which were due to excessive rack lag.

The test results are given in Table 8. The no-wind MPI remained fairly constant, except for the group of bombs dropped at 2,400 feet second altitude, 20 degrees dive angle. The short MPI under these conditions may be explained by the combined effect of several factors (see Table 8). There was no tendency for the no-wind MPI to shift in a minus direction as the altitude was increased, dive angle remaining constant; on the contrary, there seemed to be an unexplained positive shift at the higher altitudes.

5.1.3

Special Tests

Tests at NAS, Quonset, Rhode Island

In this heading are placed the tests carried out at the Antisubmarine Development Detachment, Naval Air Station, Quonset, Rhode Island, for the purpose of determining the value of the Mark 1 bomb director in relation to other forms of bombing attack on submarines and comparable targets. The low-altitude tests are divided into two groups, the first comprising flights in which bombs alone were tossed at low altitudes, and the second comprising flights designed to test a new tactic, namely, the use of toss bombing for very low-altitude or "masthead" attack combined with machine gun and rocket fire on the same pass. Another group of tests involved the simultaneous tossing of bombs and rockets. These three groups of tests used the bomb director in a way not originally provided for, so that some modification of the standard equipment was necessary in each case.

Bomb Tossing at Low Altitudes. A set of Mark 1 Model 0 equipment was used with special modifications to allow toss bombing at altitudes below those provided by the standard equipment. Altimeter contacts were installed below 1,390 feet — at 965, 670, and 465 feet — each contact being 25/36 of the next higher contact instead of the standard ratio of 5/6. The altitude difference timed by the computer is thus 11/25 of the lower altitude. An extra resistance was added to the integrating circuit to conform with this change in altitude ratio. This change in ratio was necessary since the use of the standard value of 5/6 at very low altitudes would place the altimeter contacts very close to each other; the timing interval would in that case be so short that any small irregularities in the movement of the altimeter catwhisker would result in large errors.

Prior to the tests proper,[257] the gunsight of the TBM-1C airplane was calibrated so that the sight line was on the flight path of the airplane for a dive angle of 30 degrees, second altitude 2,000 feet, and airspeed of 260 knots. The target for about half the bombs dropped was a hut 20 feet wide and 12 feet high at the center, located on a small island, with circular markers of 50- and 100-foot radius. The rest of the bombs were tossed at a towed sea target consisting of a line of five spars moving at 8 knots and spaced 100 feet apart.

Eighty-five Mark 15 water-filled bombs were dropped singly at three different altitudes and dive angles. All runs were made crosswind to minimize the effect of wind on the range error. K-24 vertical photographs were taken of the impact points by the bombing aircraft when passing directly over the target. A summary is given in Table 9.

Table 9. Summary of low altitude toss bombing tests, ASDevLant, Quonset.

No. of bombs	Avg. dive angle	2nd alt. (ft)	Avg. slant range (ft)	Mean point of impact (MPI) (range component) (ft)	(mils)	Mean deviation about range MPI (ft)	(mils)	Standard deviation (ft)	(mils)
22	16°	670	2,440	+ 7	+ 1.0	42	5.0	56	6.0
50	30°	2,000	4,070	− 8	− 1.0	68	8.5	86	10.5
13	33°	3,450	6,420	− 28	− 2.5	66	5.0	86	6.0

Note. The mil error was measured from slant range at second altitude. It was computed for each bomb impact and averaged to give the value in the above table. Mean deviation is the average scatter about the MPI. Standard deviation is root mean square.

Toss Bombing Combined with Machine Gun Fire and Rocket Fire. Flights were made to test a proposed tactic for antisubmarine low-altitude attack which entails the use of machine guns, rockets, and bombs on the same run.[255a] The machine guns and rockets were fired by "ballistic aiming" and the bombs, by tossing with the Mark 1 bomb director. The technique consisted of making a well-executed strafing run, in the course of which rockets were fired in salvo at a predetermined range, after which bombs were released automatically by the bomb director during the normal pull-up. The sight was not used except as an initial guide in aiming machine guns at 6,000 feet and as a check to keep the flight path undeviating during intervals between machine gun bursts early in the attack run. A predetermined glide angle (15 to 18 degrees) was used. The range of rocket firing became a function of temperature alone, the other variables being held constant (speed, glide angle, angle of attack, launcher line, machine gun boresight). The pilot's principal concern was simply to hold the machine gun fire steadily on the target.

The target consisted of a towed line of five spars moving at 8 knots. A spacing of 100 feet between spars was observed so that photographs from the aircraft could be analyzed to give accurate readings of the slant range at the instant of rocket firing. The center spar represented the gun platform of a submarine, 10 feet above the water line. To pass through such a point, bullets fired at 15 degrees glide should strike 40 feet beyond the spar. Rockets, to be lethal, should strike from zero to 70 feet short of the spar. The first depth bomb (of a stick of two) should strike 70 feet short of the target and the second bomb should hit the target.

Calibration runs were made in order to adjust the fall of bombs to the machine gun trajectory. The toss bombing equipment was also calibrated to produce a hit 70 feet short of the target, with the pip of the sight held on the target. The purpose of this was to provide for a stick of two depth bombs spaced at 70 feet. Allowing 35 feet of underwater travel before detonation of the hydrostatic fuse, the impact point of number one bomb should be 70 feet short of the target. The intervalometer was calibrated to produce a ground spacing of 70 feet between bombs.

Twenty-four successive runs were made on two days. The records were obtained by measurements on photographs. Results are given in Table 10.

TABLE 10. Results of combined bomb tossing, machine gun fire, and rocket fire.

Plane: TBM-1C. Glide angle: 15 to 18 degrees. Range at rocket firing: 1,300 to 2,000 feet (approximate). Average altimeter contact points (2-pt. Kollsman): 890/570 ft.

	Desired range impact point (ft)	Actual MPI Range (ft)	Actual MPI Deflection (ft)	Average deviation about range MPI (ft)
Machine gun fire	+ 40	+ 32	4R	11
Rocket fire	− 40	− 41	5L	24
First bomb	− 70	− 80	9L	37
Desired spacing between bombs:			70 ft	
Actual average spacing between bombs:			77 ft	
Deviation about the mean (bomb spacing):			17 ft	

Simultaneous Tossing of Bombs and Rockets with Mark 1 Model 0 Bomb Director. Tests were conducted at Antisubmarine Development Detachment, Naval Air Station, Quonset, to determine the feasibility of simultaneous tossing of bombs and rockets with the use of the Mark 1 Model 0 bomb director.[259] Pretest flights were made to determine the most satisfactory values of the sight setting, the bomb MPI setting, and the rocket MPI setting. A TBM-3 aircraft was used with a Mark 1 Model 0 bomb director modified so as to give, for the same input time, two different output times during the same pull-up, one for rockets and one for bombs. A stationary target was used and flight and impact data were obtained photographically. Two 3.5-inch AR rockets and one water-filled bomb were dropped on each run. In order to eliminate as many sources of error as possible, only those rounds were analyzed which met certain rigid specifications. Only photographed impacts were considered, and only of those runs which were made consecutively from opposite headings.

Results indicated that under conditions of zero wind and no target motion, the bomb director would toss bombs and rockets simultaneously with approximately the same accuracy as either can be fired alone. However, because of the large difference in time of flight between bombs and rockets, the impact separation became excessive with as little as 5 knots wind or target motion. For the same reason, the sight-offset method could not be used to compensate for the effect of wind on both bombs and rockets.

Tests on Electrical Indicating Altimeter. The electrical indicating altimeter was developed (see

Chapter 8) to provide a more flexible timing device than the multiple-contact Kollsman altimeter used in Mark 1 directors. It is essentially an aneroid altimeter provided with a potentiometer such that it continuously gives a voltage output proportional to altitude. This altimeter, together with its associated relay circuits, provides that (1) "first-button" operation of the computer circuit occurs simultaneously with the pressing of the bomb release switch, and (2) "second-button" operation automatically follows when the aircraft reaches an altitude which is a preset fraction of the "first-button" altitude. Such a device obviously affords the pilot greater operational freedom.

Test on Accuracy of Altitude Ratio of Electrical Indicating Altimeter.[128] The electrical indicating altimeter was installed in an SB2C-4 airplane at NAS, Patuxent. It was set so that "second-button" operation would occur at five-sixths of the first altitude—altitude at which the bomb release switch is pressed. A test was then made to determine how accurately and consistently the altimeter would select one-sixth of any slant range. The plane made dry dives using different values of the first altitude, dive angle and plane speed. Motion pictures were taken of the instrument panel during dives to furnish accurate readings of the altitudes of operation of the bomb release switch and the second button. The values as read from the film are given in Table 11A. The variation in the ratio of the second altitude to the first altitude was found to be less than 1 per cent.

Toss Bombing Runs with Electrical Indicating Altimeter. The electrical indicating altimeter, with a specially constructed relay box, was installed in an SB2C-3 plane together with a standard Mark 1 Model 0 bomb director on February 1, 1945. Flights were made to determine whether or not the use of this altimeter, as compared to the production model in use, would give improved accuracy, mainly from the point of view of dispersion. The equipment was installed so that either type of altimeter could be connected to the computer. Toss bombing runs were made alternately using the experimental altimeter and the standard altimeter. The plane heading, altitude points, dive angle, and airspeed were kept as constant as possible for each flight. The sight was kept fixed on the target on all runs. In view of the accuracy with which the electrical indicating altimeter gave the timing signals for first- and second-button operation at a ratio of 6/5 (see

TABLE 11A. Altitude ratio test of electrical indicating altimeter.

Dive No.	First altitude (photo) (ft)	Second altitude (photo) (ft)	Dive angle (observ'd) (degrees)	Airspeed (observ'd) (knots)	Ratio of second altitude to first altitude
1	8,980	7,570	41	335	0.843
2	8,970	7,570	41	325	0.844
3	8,960	7,560	40	325	0.844
4	5,960	4,990	40	330	0.837
5	5,930	4,960	40	325	0.836
6	5,975	5,000	40	320	0.837
7	5,960	4,990	25	290	0.837
8	5,965	4,995	25	290	0.837
9	5,950	5,000	25	290	0.840
10	5,980	5,010	20	260	0.838
11	2,985	2,515	20	290	0.843
12	2,995	2,525	20	285	0.843
13	2,980	2,510	19	280	0.842

TABLE 11B. Test to compare dispersion of bomb impacts using electrical indicating altimeter and Mark 1 Model 0 altimeter.

Dive number	Second altitude (ft)	Dive angle (degrees)	Avg. dispersion about MPI: Electrical indicating altimeter (ft)	Avg. dispersion about MPI: Mark 1 Model 0 altimeter (ft)	Plane heading	Remarks
1	4,150	40	40 (4)*	10 (3)	Upwind	Winds rough; average velocity, 38 mph.
2	2,880	30 – 35	80 (4)	180 (3)	Upwind	Winds rough; average velocity, 32 mph.
3	2,880	25 – 30	45 (8)	45 (7)	Downwind	Average wind velocity, 10 mph.

* Figures in parentheses show number of bombs dropped.

[redacted]

Section 5.1.3, "Test on Accuracy of Altitude Ratio of Electrical Indicating Altimeter"), this flight test did not seek to compare the location of the no-wind MPI for both altimeters, but rather the relative dispersion of the bomb impacts under approximately identical toss bombing conditions. The results are summarized in Table 11B grouped according to flights made under approximately the same conditions.

On the basis of the results of the third flight shown in Table 11B (the rough and variable winds during the first two flights render the dispersion data less reliable), it may be concluded that the dispersion obtained with the electrical indicating altimeter is of the same order of magnitude as that obtained with the standard Mark 1 Model 0 altimeter.

This conclusion, although based on a limited amount of data, is strengthened by the results of additional flights in which 20 bombs tossed with the use of the electrical indicating altimeter, gave an average dispersion of 55 feet about the MPI. The second altitude was 4,150 feet; the dive angle, 30 to 50 degrees.

5.2 TORPEDO TOSSING FIELD TESTS

The efficacy of the Mark 1 Model 0 bomb director in launching torpedoes was tested at Gould Island Naval Detachment, Naval Air Station, Quonset, Rhode Island, during January and February 1945. An early model of the toss bombing equipment was used in which had been introduced circuit changes identical to those incorporated in all later models intended for Service use. These changes were based on calculations made of the amount by which the output time, T_c, must be reduced in order to place a torpedo 450 feet short of the target for a toss bombing maneuver at 1,395 feet second altitude, a glide angle of 25 degrees, and 250 knots velocity. Using a value of ΔT_c of 3.72 seconds, calculations were made of the limiting values of altitude for glide angles between 15 and 25 degrees, such that the torpedo will fall between 450 and 1,350 feet short of the target (see Sections 2.3 and 6.4.10). The purpose of the tests at Gould Island was to determine how close the agreement was between predicted and actual torpedo impacts.

An SB2C-1 aircraft was used for all flights. Torpedoes were Mark 13 Model 2. Prior to torpedo tests, flights with Mark 15 bombs were made to insure that the airplane sight setting was proper and that the equipment was functioning normally. Seven torpedoes were tossed, using the normal bomb output time; four of these fell within 60 feet of the target; the average range error was −100 feet. Second altitude was 1,390 feet; glide angle, 20 degrees.

Then, using the torpedo setting mentioned above, 26 torpedoes were tossed, 20 at altitude points 1,670/1,390 feet, and 6 at 2,000/1,670 feet, dive angles 15 to 25 degrees, indicated airspeeds 250 to 280 knots. No allowance was made for wind in sighting. Most of the runs were made crosswind. Values of impact points were obtained by triangulation. All torpedoes fell within the range predicted by theory, as shown by the following summary of results.

Second altitude (ft)	Dive angle (degrees)	Range component of impact point: Observed values (ft)	Range component of impact point: Theoretical values
1,395	18 to 23	− 870 to − 435	− 900 to − 450 ft (for 15 to 25 degrees dive)
1,670	16 to 20	− 900 to − 705	− 1200 to − 750 ft (for 15 to 20 degrees dive)

The shift of the impact point with variation in glide angle agreed with theory, as illustrated by the following tabulation of the same results.

Second altitude (ft)	Dive angle (deg)	Range component of impact point: Range of values (ft)	Range component of impact point: Avg. value (ft)	Avg. deviation (ft)	Number of torpedoes
1,395	15-17	− 870 to − 600	− 715	110	4
	18-20	− 825 to − 450	− 670	85	10
	21-23	− 705 to − 435	− 605	80	6
1,670	16-18	− 900 to − 720	− 810	60	3
	20	− 780 to − 705	− 745	30	3

The amount of data on hand does not warrant more detailed analysis; it is sufficient, however, to demonstrate the feasibility of employing the Mark 1 bomb director for tossing torpedoes. One feature which marred the torpedo tests and which was mainly responsible for the discontinuance of tests at Gould Island was the frequency with which torpedoes sank instead of making a normal straight run toward the target. Of the total number dropped, about 55 per cent

had normal runs, 35 per cent sank, and 10 per cent had erratic runs. This high incidence of sinkings was ascribed to the fact that the target range at Gould Island was too shallow for the dive angles used in the tests.

A few tests were made at NAS, Patuxent, just before the end of the war, in an SB2C-4 plane, in order to check the operation of the torpedo setting in the Mark 1 Model 1 bomb director. Miniature bombs (ballistic coefficient about 2.3) were dropped from a second altitude of 2,880 feet, indicated airspeed 310 knots. The MPI dial setting was at 0 and the *stick-length* dial knob was set at *torpedo*. The results showed good agreement with the expected values of the impact points.

5.3 ROCKET TOSSING FIELD TESTS[c]

5.3.1 Equipment and Procedure

The first rocket tossing field tests were made with a bomb director Mark 1 Model 0, AN/ASG-10XN which had been adapted to rocket tossing by replacing the second capacitor by one of smaller size, and increasing the resistance of the range MPI control so as to allow adjustment for rocket and plane speeds. This was shortly replaced by another modification of the Mark 1 Model 0 which transformed it into a combination bomb and rocket director. The appropriate pull-up time for rockets was obtained by inserting a capacitor (adjustable in seven steps) in series with the second capacitor at the beginning of pull-up. Insertion of the capacitor was accomplished through action of a micro-switch operated by the *K*-block bob when the selector switch was on *rockets*. This latter switch in the *bomb* position restored the circuit to that of the Mark 1 Model 0. This combination bomb-rocket director, Mark 1 Model 0, AN/ASG-10XN, served as the basic test equipment for all tests considered in this section. Circuit refinements and controls to compensate for propellant temperature and for launching with a lanyard, added during the course of field tests, are incorporated in the bomb director Mark 1 Model 2, AN/ASG-10A, which was discussed in Chapter 3. The results cited can, therefore, be taken as indicative of the performance which the Model 2 should give.

[c] Section 5.3 was written by A. G. Hoyem, formerly of the State University of Iowa and now at the Naval Ordnance Test Station, Inyokern, California.

Field tests were conducted at the Naval Air Test Stations at Patuxent River, Maryland, and Quonset, Rhode Island, and at the Naval Ordnance Test Station at Inyokern, California, by Navy personnel who were assisted by technical advisers supplied by Division 4.[189] Tests were also made at the Army Air Base, Dover, Delaware. The testing facilities and procedures used at each of these field stations are described below. These descriptions are followed by a consideration of the tests proper under the Sections: 5.3.2 "Preliminary Calibration Tests"; 5.3.3 "Equipment Evaluation Tests"; 5.3.4 "Special Tests."

NATS Patuxent River, Maryland

Approximately 1,400 rounds (mainly 3.5-inch aircraft rockets and 5.0-inch high-velocity aircraft rockets) were launched with rocket tossing equipment during the course of the test program at NATS, Patuxent River, Maryland. TBM, F6F and SB2C aircraft were used.[160,166,181]

Tests were made to determine the effect of the no-wind MPI produced by changing slant range, release *g*'s, and airspeed. On account of various difficulties, some due to tossing equipment and others extraneous, the work done with the SB2C and F6F aircraft served mainly to determine the proper *A* factor and sight setting, and to locate the sources of the troubles. The Patuxent equipment evaluation data included in this report are therefore limited to those obtained with a TBM-1C.

The rocket tossing equipment used did not have temperature and lanyard controls. Aircraft were equipped with Mark 8 gunsights with Mark 2 adjustable reflector heads.

Tossing Procedure. The TBM and SB2C planes carried four rocket pairs per flight, and the F6F, three pairs. One pair was tossed on each dive at the target, and the passes were alternated between the 160- and 340-degree directions. Impact points were, in all cases, scored visually by the pilot (also by the observer in the SB2C and TBM planes), and recorded in terms of displacement from the target along the direction of approach (range), and displacement in the direction perpendicular thereto (deflection). As in toss bombing tests, impact points which fell short of the target were designated with a negative sign, and those which fell long with a positive sign.

Method of Evaluating Data. All range impact points were expressed in mils based on slant ranges measured from the beginning of pull-up. No photographic records of cockpit instruments were made during the tests on MPI variation with slant range and airspeed; hence, exact information as to when pull-up occurred during these flights was lacking. Film records for the tests on the effect of release g's indicated, however, that as a rule 2 seconds elapsed during those flights between second altitude and the initiation of pull-up. Since the same pilot made all test flights, all slant ranges were accordingly based on such a time lapse. Thus, the mil value ϵ_y corresponding to a range impact point of y feet, was obtained from the relation $\epsilon_y = 1{,}000\ y \sin \alpha / R$, where α is the angle of dive and R (feet) is the slant range measured from the point at which pull-up was assumed to have been initiated. This slant range is given by $(h/\sin \alpha) - 1{,}000$, where h is the second-altitude point and 1,000 feet is the distance the plane would, on the average, cover in the 2 seconds which elapsed between second altitude and the initiation of pull-up.

The pilot occasionally compensated for deflection due to wind by sighting to the right or left of the target so the impacts would lie within the target array. He made no attempt, however, to correct for range errors due to wind.

True airspeeds were determined by a BuAer U. S. Navy Aircraft Navigational Computer, Mark 8. When the temperature at flight altitude was not listed in the original data, the normal lapse rate of 20 C decrease in temperature per 1,000-foot increase in altitude was assumed.

Rocket pairs having range separations greater than 22 mils were not included, on the basis that such separations would be due mainly to causes other than normal ammunition dispersion. This was statistically permissible since this group comprised only 2 per cent of the total number tossed.

Flight Conditions. The pilot, as a rule, held the angle of dive to 30 $\pm$ 5 degrees, and the indicated airspeed at second altitude to 280 $\pm$ 10 knots (indicated airspeed varied during the test for shift in no-wind range MPI with true airspeed). The 2,400-, 5,000-, and 7,200-foot second-altitude points were used for tests on the effect of slant range; the 5,000-foot second-altitude point, for velocity tests; and the 4,200-foot second-altitude point, for the tests on the effect of release g's.

NATS Quonset, Rhode Island

Testing at NATS Quonset[258] was done with a TBM-1C and a total of 283 3.5-inch aircraft rockets were launched during the test period. Of these rounds, 222 were launched as pairs, 40 in groups of four, 7 singly, 6 in one salvo, and 8 in another salvo. Mark 8 sights were used, set 2 degrees 12 minutes above the thrust line. Launchers were latch-type Mark 5 Model 3. The target was the center spar of five spars 100 feet apart, which were towed at 7 knots into or with the wind.

Tossing Procedure. Passes at the target were made crosswind whenever possible to eliminate range-wind error. Impacts were photographed from the plane as it passed over the target, by means of a K-24 camera, mounted vertically. Photographs were also made by a photo plane equipped with an F-56 camera. In addition, the pilot and the observer who accompanied him made visual estimates of the impact points. Flight data were obtained from GSAP photographs of the instrument panel. Tests were made specifically to observe what effect, if any, the tossing distance and the angle of dive had on the performance of the equipment. An attempt was also made to examine the data thus obtained for the effect produced by changes in propellant temperature associated with variations in air temperatures during the testing period.

Method of Evaluating Data. The rounds which were analyzed were limited to 159 by rejecting those for which: (1) the prescribed test conditions were not met, (2) the head or tail wind component was in excess of two knots, or (3) no photographic impact data were obtained. Ten rounds were also excluded because their impact points were sufficiently far removed from those of their group to indicate that some factor outside the equipment, such as bumpy air, abnormal pilot error, or dislocation of the gunsight, had been present.

Impact points were expressed above, except that slant range was measured from the second-altitude point. Slant range was so measured because the pilot generally began pulling up shortly after passing the second-altitude point, and this point thus represented the end of dive toward the point of aim. (If slant ranges had been measured from the actual release point rather than second altitude, the mil values would have been increased between 5 per cent and 15 per cent.)

NOTS, Inyokern, California

This section includes the results obtained at NOTS, Inyokern, up to approximately June 1, 1945.[178,181,259a,b] Since testing at Inyokern continued after NDRC withdrew from the program, and the transfer of personnel was gradual, the setting of a boundary date for the inclusion of data is somewhat arbitrary Approximately 1,700 rockets were tossed during the period covered in this report, and of these, 1,550 were 5.0-inch HVAR and 94 were 11.75-inch AR. The balance were 3.5-inch AR, 5.0-inch AR, and 2.25-inch AR (fast). Most of the testing was done with F6F-5 and an F4U-1D. Tests were also made with an F4U-4.

The Model 0 directors were equipped with temperature and lanyard compensation controls during the latter part of the test period. The sights used were Mark 8 gunsights.

Three target areas, located in the Mojave Desert, were used for rocket tossing tests at this base. Each target consisted of a 600-foot square area with a bull's-eye in its center and four camera markers each 300 feet from the center and spaced 90 degrees apart. Two of these markers were on the flight line which was formed by additional markers spaced over a distance of several miles on each side of the target. An observation station with a harp was located 1,000 yards from the target in a direction perpendicular to the flight line. The station was in charge of the range officer who controlled traffic and directed the pilots into the angle of dive prescribed for a given test. This limitation on the angle of dive was imposed so that the tossing ranges for consecutive passes during a flight would be essentially the same.

Tossing Procedure. Passes at the target were made along the flight line in opposite directions, NS and SN, alternately. Two rockets were tossed simultaneously during each pass at the target, and their impact points immediately marked with numbered stakes. At the completion of the flight, the stake positions were measured by transit and stadia rod and recorded in polar coordinates. Other data pertaining to the flight were obtained from the pilot's flight report, loading area data, and the range officer's data.

A torpedo camera mounted in the starboard wing and boresighted parallel to the line of sight provided a picture of the target area from second altitude, which could be used in determining the point of aim, the slant range, and the angle of dive. Energizing of the camera was done by wiring it in parallel with the second-altitude light.

A GSAP gun camera was mounted in the port wing of the plane and operated by the bomb release switch. It thus provided a sequence of pictures which showed the point of aim throughout the critical portion of the dive.

Another GSAP cockpit camera photographed the instrument panel so as to record the airspeed meter, g-meter, and altimeter readings, and the operation of the first- and second-altitude lights.

Method of Evaluating Data.[162] Slant range was normally obtained from the torpedo camera film. As already stated, the target areas had two on-course markers 300 feet on each side of the target and two off-course markers similarly located on a line perpendicular to the course. If on the torpedo camera film the distances between the images of the on-course markers is designated by d_y, and the distances between the images of the off-course markers by d_x, then

$$\frac{R_2}{600\ (\text{feet})} = \frac{\text{Focal length}}{d_x},$$

where R_2 is the distance in feet from the second-altitude point to target. Using this value of R_2, the slant range is then given by $R_2 - VT$, where V is the aircraft velocity at the second-altitude point in feet per second and T is the time in seconds from second altitude to the rocket release point. The dive angle is also obtained from this film by the relation $\sin\alpha = d_y/d_x$. If the torpedo camera film was defective, the slant range was obtained by dividing the altitude at release by the sine of the angle of dive, using values taken from the cockpit camera film. If the film from the cockpit camera was not sufficiently clear to allow reading of the release altitude, the time which elapsed between the second-altitude point and release (as shown by number of frames the pilot's indicator light stayed on) was multiplied by the true airspeed. This distance was then subtracted from the known range at second altitude to give the correct slant range. If this film was entirely obscured, the slant range was obtained by subtracting from the second-altitude range an average of the distance to release for similar conditions of dive angle, speed, range, and pull-up acceleration.

The range and deflection coordinates (X,Y) of the impact points were obtained from the polar coordinates (r,θ) by the simple transformations $X = r\sin\theta$,

$Y = r \cos \theta$, when the direction of flight is taken into consideration. Thus, an impact point to the right of the target and beyond it had positive X and Y values. The coordinates (X,Y) in feet were finally changed to coordinates (ϵ_x,ϵ_y) in mils by the formulas

$$\epsilon_x(\text{mils}) = \frac{X \text{ (ft)}}{\text{Slant range (in thousands of feet)}},$$

$$\epsilon_y(\text{mils}) = \frac{Y \text{ (ft)} \sin \alpha}{\text{Slant range (in thousands of feet)}}.$$

Army Air Base, Dover, Delaware

The work at this base was carried on under arrangements similar to those for toss bombing tests at various Army bases. Tests were conducted in a P47-D aircraft equipped with four rocket rails. Rockets tossed were 3.5-inch AR. A total of 124 rockets were launched during this period, of which 84, launched from opposite directions, are analyzed in this summary.

The tossing equipment used was without temperature and lanyard compensation controls. The sight was a K-14 fixed gunsight.

The target was a 50-foot circle, formed by markers, with a bull's-eye center consisting of a red pyramid approximately 10 feet along its base. The area was marshy ground. A road which passed through the target in a 115-degree to 295-degree direction served as the flight line on all passes.

Tossing Procedure. Rockets were tossed singly on all flights and the passes alternated between opposite approaches along the flight line. (A few preliminary tosses were made from only one direction at the request of Army officers to ensure that a nearby farmhouse would not be endangered.) Impacts were scored from three observation stations grouped around the target, which determined the azimuth of each rocket impact point. An automatic device known as HARP was used to guide the plane into 30-degree dives on all flights.

Method of Evaluating Data. The azimuth readings of impact points were plotted on a chart of the range, drawn to scale, and their positions expressed in range and deflection coordinates. Slant ranges and mil values were determined by the same methods as were used at Patuxent.

5.3.2 Preliminary Calibration Tests

Preliminary calibration tests were made to determine the sight setting required to make the plane fly a straight course during its dive at a target, and to determine the A factor which would produce on-target impacts under no-wind conditions.

The sight setting was in most cases determined by the theodolite method, as explained in Section 4.2.1. In some instances, however, poor visibility, air roughness, and high-velocity winds prevented use of this method. In such cases, recourse was made to sight setting data given in CIT manuals, [213,214] and the value so chosen checked by determining the no-wind MPI for bombs and rockets using the procedure described in Section 4.2.1. After the correct setting had thus been found, the plane was boresighted, and the angle between the sight line and the boresight datum line recorded for future convenience in checking or resetting the sight.

The A factor, or rocket calibration (coarse and fine) setting, used in tossing the first rockets of a given type, was obtained from theoretical A factor curves similar to those shown in Section 7.5 by estimating the true airspeed which would be attained by the plane during the timing portion of its dive. A sufficient number of rockets were then tossed to establish a no-wind MPI for the group, using, as nearly as possible, the same dive angle and true airspeed as were employed in calibrating the gunsight. Changes in rocket calibration setting necessary to bring the no-wind MPI on target were then made and this corrected setting maintained throughout the subsequent equipment evaluation and special calibration tests.

5.3.3 Equipment Evaluation Tests

Included under this heading are the tests which were made in investigating the variation in no-wind MPI with tossing distance, angle of dive, plane speed, pull-out acceleration, and propellant temperature using the A factors and sight settings determined during the preliminary calibration work. The results of these tests are summarized in Tables 12 to 21, inclusive, and are grouped according to test station. Average values of each variable are given for all passes made during a given test. These are followed by the mean dispersion of the individual values about the average, e.g., 32 ± 2. Columns

TABLE 12. Variation in MPI with slant range (Patuxent).

Number of rockets	A	Maximum g's	Second altitude (ft)	Dive angle (deg)	Slant range (ft)	True airspeed (knots)	Range dispersion (mils)	No-wind range MPI (mils)
28	0.192	3.0 ± 0.1	2,400	29 ± 2	4,300 ± 500	285 ± 15	6.6	+ 3.3
39	0.192	3.1 ± 0.1	5,000	33 ± 2	8,300 ± 600	305 ± 15	4.0	+ 0.6
29	0.192	3.2 ± 0.1	7,200	32 ± 3	12,500 ± 1,000	315 ± 5	5.2	− 2.8

(TBM-1C #45473—3.5-in. AR)

TABLE 13. Variation in MPI with true airspeed (Patuxent).

Number of rockets	A	Maximum g's	Second altitude (ft)	Dive angle (deg)	Slant range (ft)	True airspeed (knots)	Range dispersion (mils)	No-wind range MPI (mils)
72	0.192	2.9 ± 0.1	5,000	29 ± 2	9,300 ± 700	275 ± 5	5.9	6.8
66	0.192	3.1 ± 0.2	5,000	29 ± 2	9,300 ± 800	305 ± 10	3.4	3.0

(TBM-1C #45473—3.5-in. AR)

TABLE 14. Variation in MPI with release g's (Patuxent).

Number of rockets	A	Maximum g's	Second altitude (ft)	Dive angle (deg)	Slant range (ft)	True airspeed (knots)	Range dispersion (mils)	No-wind range MPI (mils)
40	0.192	2.0 ± 0.1	4,200	30 ± 2	7,300 ± 600	300 ± 10	6.0	− 4.7
26	0.192	2.4 ± 0.1	4,200	32 ± 3	7,200 ± 600	295 ± 5	6.5	+ 4.7
18	0.192	2.7 ± 0.1	4,200	29 ± 2	7,600 ± 400	295 ± 5	3.6	+ 5.1

(TBM-1C #45473 — 3.5-in. AR)

TABLE 15. Summary of Quonset data.

Number of rockets	A	Second altitude (ft)	Rocket temperature (°F)	Dive angle (deg)	Slant range (ft)	True airspeed (knots)	Range	
							Dispersion (mils)	No-wind MPI (mils)
19	.188	1,390	32	17	5,200	253	6.1	− 1.0
14	.188	1,390	23	25	3,000	270	3.1	3.8
4	.188	1,670	23	32	3,100	268	3.5	0.9
8	.188	2,000	59	25	4,900	265	1.5	2.4
24	.188	2,000	14	29	4,200	245	5.9	2.7
14	.188	2,000	30	15	7,400	255	6.6	− 2.2
16	.188	2,400	41	27	5,100	260	5.3	0.2
22	.188	2,900	32	28	6,300	240	7.1	2.7
16	.188	3,460	14	28	7,500	250	4.3	13.5
10	.188	3,460	64	26	7,800	222	6.5	4.5
4	.188	3,460	61	19	10,800	...	4.5	4.5
8	.188	5,000	28	26	11,200	248	7.5	0.8

(TBM-1C — 3.5-in. AR)

TABLE 16. Variation in MPI with slant range (Inyokern).

Number of rockets	A	Release g's	2nd Alt. (ft)	Rocket temp. (°F)	Dive angle (deg)	Slant range (ft)	TAS (knots)	Deflection (mils) Disp.	Deflection (mils) MPI	Range (mils) Disp.	Range (mils) MPI
					(F6F-5 #72679 — 5.00-in. HVAR)						
24	0.148	2.0 ± .2	2,400	59 ± 5	33 ± 2	3,530 ± 280	356 ± 16	5.9	1.7	5.0	− 2.7
36	0.148	2.2 ± .3	5,000	53 ± 8	34 ± 5	7,800 ± 1,000	364 ± 20	7.0	− 1.0	6.8	− 1.9
30	0.148	2.6 ± .5	7,200	52 ± 7	36 ± 5	10,750 ± 1,300	369 ± 14	8.0	4.4	7.4	− 3.8
					(F4U-1D #57181 — 5.00-in. HVAR)						
24	0.140	.....	2,400	57 ± 3	36 ± 1	3,420 ± 150	320 ± 11	9.6	13.1	7.1	− 4.2
45	0.140	3.0 ± .2	5,000	64 ± 10	35 ± 2	7,890 ± 390	343 ± 9	6.5	11.2	7.4	1.4
16	0.140	3.1 ± .2	7,200	52 ± 2	36 ± 1	11,400 ± 243	352 ± 8	6.9	15.1	5.3	− 1.8
16	0.140	2.3	4,200	77	45 ± 0	5,400 ± 210	338 ± 8	8.8	6.6	6.9	11.5
30	0.140	(Max.) 4.9	7,200	61	48 ± 5	8,850 ± 1,000	365 ± 19	8.0	7.2	7.8	2.4
15	0.140	(Max.) 4.9	8,500	73	45 ± 3	10,500 ± 660	400 ± 6	10.3	10.5	5.6	0.9

TABLE 17. Variation in MPI with angle of dive (Inyokern).

Number of rockets	A	Release g's	2nd alt. (ft)	Rocket temp. (°F)	Dive angle (deg)	Slant range (ft)	TAS (knots)	Deflection Disp. (mils)	Deflection MPI (mils)	Range Disp. (mils)	Range MPI (mils)
					(F6F-5 #72679 — 5.00-in. HVAR)						
43	0.148 & 0.158	2.6 ± 0.3	3,500	57 ± 4	22 ± 3	8,230 ± 600	325 ± 13	11.4	2.5	7.4	− 4.2
36	0.148	2.2 ± 0.2	5,000	53 ± 4	34 ± 4	7,800 ± 800	359 ± 15	7.0	− 1.0	6.7	− 1.8
30	0.148	2.1 ± 0.1	7,200	55 ± 10	50 ± 4	7,740 ± 600	368 ± 11	11.4	4.7	10.3	− 0.2
					(F4U-1D #57181 — 5.00-in. HVAR)						
47	0.140	3.0 ± 0.4	2,900	68 ± 6	22 ± 2	7,170 ± 600	313 ± 15	9.1	7.5	8.1	− 8.7
16	0.140	3.0 ± 0.2	5,000	54 ± 0	35 ± 1	7,710 ± 500	347 ± 6	6.1	10.9	6.7	1.8
30	0.140	4.9 ± 0.3	7,200	61 ± 5	48 ± 5	8,850 ± 960	365 ± 19	8.0	7.2	7.8	2.4

TABLE 18. Variation in MPI with true airspeed (Inyokern).

Number of rockets	A	Release g's	2nd alt. (ft)	Rocket temp. (°F)	Dive angle (deg)	Slant range (ft)	TAS (knots)	Deflection (mils) Disp.	Deflection (mils) MPI	Range (mils) Disp.	Range (mils) MPI
					(F6F-5 #72679 — 5.00-in. HVAR)						
7	0.158	3.0 ± .6	5,000	60 ± 14	33 ± 2	8,160 ± 291	309 ± 3	6.5	− 9.1	5.1	7.3
4	0.158	.....	5,000	72 ± 0	37 ± 0.5	7,875 ± 135	310 ± 3	5.7	2.3	3.5	7.0
12	0.158	.....	5,000	72 ± 0	34 ± 1	7,950 ± 282	348 ± 0	2.8	− 1.5	1.6	0.1
4	0.158	2.5 ± .5	5,000	65 ± 2	36 ± 2	6,870 ± 990	358 ± 22	5.5	− 6.5	3.3	− 0.3
18	0.158	2.7 ± .6	5,000	65 ± 2	35 ± 2	7,410 ± 309	368 ± 6	7.6	− 6.3	4.9	0.5
18	0.158	2.0 ± .1	4,200	62 ± 2	35 ± .5	6,300 ± 111	402 ± 5	4.9	2.3	7.2	− 1.4

TABLE 19. Variation in MPI with pull-up g's (Inyokern).

Number of rockets	A	Release g's	2nd alt. (ft)	Rocket temp. (°F)	Dive angle (deg)	Slant range (ft)	TAS (knots)	Deflection (mils) Disp.	Deflection (mils) MPI	Range (mils) Disp.	Range (mils) MPI
					(F6F-5 #72679 — 5.00-in. HVAR)						
18	0.158	2.7 ± .6	5,000	65 ± 2	36 ± 2	7,410 ± 309	368 ± 6	7.6	− 6.3	4.9	0.5
22	0.158	2.5 ± .2 (Max. g's)	5,000	58 ± 5	36 ± 1	7,680 ± 330	357 ± 10	9.5	1.9	10.9	− 5.2
					(F4U-1D #57181 — 5.00-in. HVAR)						
19	0.140	2.0 ± .1	5,000	59 ± 5	38 ± 3	7,533 ± 903	350 ± 17	8.8	8.3	5.7	− 9.1
16	0.140	3.0 ± .2	5,000	54 ± 0	35 ± 1	7,710 ± 510	347 ± 6	6.1	10.9	6.7	1.8

TABLE 20. Variation in MPI shift with propellant temperature (Inyokern).

Number of rockets	A	Release g's	Second altitude (ft)	Rocket temp. (°F)	Dive angle (deg)	Slant range (ft)	TAS (knots)	Deflection (mils) Disp.	Deflection (mils) MPI	Range (mils) Disp.	Range (mils) MPI
12	0.158	.....	5,000	100 ± 3	34 ± 0	7,755 ± 120	367 ± 6	6.8	2.0	6.8	6.3
12	0.158	.....	5,000	—2 ± 1	34 ± 0	8,190 ± 240	363 ± 2	4.8	— 3.5	4.3	— 8.8
(F6F-5 #72679 — 5.00-in. HVAR)											

TABLE 21. Variation in MPI with slant range (Dover).

Number of rockets	A Factor	Maximum g's	Second altitude (ft)	Dive angle (deg)	Slant range (ft)	True airspeed (mph)	Range dispersion (mils)	No-wind MPI (mils)	No-wind MPI for A = 0.240 (mils)
31	0.225	4.5 ± .1	2,900	30 ± 0	4,500 ± 400	365 ± 5	9.6	— 5.4	— 2.4
6	0.225	5.0 ± .2	5,000	30 ± 0	9,000 ± 0	375 ± 5	3.6	— 8.5	— 2.5
47	0.240	4.0 ± .2	5,000	30 ± 0	9,000 ± 0	373 ± 3	9.1	— 1.3	(— 1.3)
(P47-D #42-28612 — 3.5-in. AR)									

labeled "dispersion" give the average deviation of each impact of a group from the center of impact for that group.

RESULTS ON THE VARIATION IN MPI WITH SLANT RANGE

The results obtained in varying the slant range or tossing distance are condensed and grouped together in Table 22. The analysis of the Quonset data given in the table is based on reference 258. Considering the results in the order of listing, it is noted that:

TABLE 22. MPI variation with slant range at median dive angle (32°).

Test station	Number of rockets	Slant range (ft)	No-wind MPI (mils)
Patuxent			
(TBM-1C)	28	4,300	3.3
	39	8,300	0.6
	29	12,500	— 2.8
Quonset			
(TBM-1C)	4	3,100	0.9
	33	4,300	1.0
	16	5,100	0.2
	46	5,300	1.2
	22	6,300	2.7
	30	8,000	9.3
	8	11,250	— 0.8
Inyokern			
(F6F-5)	24	3,500	— 2.7
	36	7,800	— 1.9
	30	11,000	— 3.8
(F4U-1D)	24	3,400	— 4.2
	45	7,900	1.4
	16	11,400	— 1.8
Dover			
(P-47D)	31	4,500	— 2.4
	53	9,000	— 1.4

1. *The Patuxent data* indicate that the no-wind range MPI decreases with increase in slant range if the differences in true airspeed at the different ranges is neglected. The A factor, however, is essentially an airspeed correction factor. Also, for the 3.5-inch AR, the value used, 0.192, corresponds to a 300-knot true airspeed. If account is taken of the shifts in MPI which would be caused by the differences in airspeeds, which at 300 knots is about 1 mil decrease in MPI for each 10-knot increase in airspeed, the shift in MPI becomes negligible.

2. *The Quonset data* show no significant shift in MPI. The large range error for the releases at 3,480 feet second altitude is considered to have been at least partially caused by altimeter error.

3. *The Inyokern F6F data* similarly show no shift in MPI. The error in the MPI's, averaging almost 3 mils short of the target, was corrected in the tests which followed by increasing the A factor.

4. *The Inyokern F4U data* are less conclusive in view of the short MPI and low airspeed for the close range tosses. The MPI's are, however, adequately on-target for the medium and long ranges.

5. *The Dover data* also show no significant shift in MPI within the limits of range considered. By referring back to Table 21, it will be observed that two different values of A were used in acquiring these data. The MPI's for the smaller A value were corrected so as to correspond to the larger value and higher velocity by the formula:

$$d\theta_p(\text{mils}) = \frac{gR}{2V^2} F(\gamma) dA \times 1{,}000.$$

This formula is discussed in Section 2.2.

It is thus concluded, on the basis of the above evidence, that the performance of the equipment in tossing rockets is not affected by variations in tossing distance.

Results on the Variation in MPI with the Angle of Dive

The results of the work done under this heading at Quonset and at Inyokern in varying the angle of dive are condensed in Table 23.

Table 23. MPI variation with angle of dive.

Test station	Number of rockets	Average angle of dive (degrees)	No-wind MPI (mils)
Quonset	35	16	− 1.4
(TBM-1C)	61	24	4.7
	63	31	3.2
Inyokern	43	22 (low-*g* pull-up)	− 4.2
(F6F-5)	36	34	− 1.8
	30	50	− 0.2
(F4U-1D)	23	24 (low-*g* pull-up)	− 12.7
	23	20 (high-*g* pull-up)	− 2.4
	16	35	1.8
	30	48	2.4

Conclusions from the foregoing table are: (1) that the performance of the equipment in tossing rockets is insensitive to the angle of dive for angles between 30 and 50 degrees; (2) that at dive angles below 25 degrees, the MPI is short if the pull-up is gentle enough so that the maximum *g*'s attained are less than 3.0 (this shortcoming is not tactically significant, however, as during combat the pull-up would probably be made with high *g*'s); (3) that the MPI will be over the target at dive angles above 45 degrees and slant ranges below 2,000 yards.

Results on the Variation in MPI with Plane Speed

The results of these tests showing variation of MPI with plane speed are condensed in Table 24.

1. *The Patuxent data* on the effect of changing the speed of the plane indicate a definite shift in MPI amounting to approximately 1 mil decrease in MPI for each 10-knot increase in speed when the plane speed averages 290 knots.

2. *The work done at Inyokern with the F6F*, which involved a greater spread in speed, also indicates a similar type of shift. The shift, however, is seen to be a function of the plane velocity and is relatively insignificant at the higher speeds. This is in agreement with theory which indicates that the rate of shift in MPI should vary inversely as the square of the plane velocity (see Section 2.2.10).

Table 24. MPI variation with plane speed.

Test station	Number of rockets	True airspeed (knots)	No-wind MPI (mils)
Patuxent	72	275	6.8
(TBM-1C)	66	305	3.0
Inyokern	11	310	7.2
(F6F-5)	12	350	0.1
	4	360	− 0.3
	18	370	0.5
	18	400	− 1.4

Results on the Variation of MPI with Pull-Up Acceleration

The results of the tests dealing with the effect of varying pull-up acceleration are condensed in Table 25.

Table 25. MPI variation with pull-up acceleration.

Test station	Number of rockets	Pull-up acceleration (*g*'s)	No-wind MPI (mils)
Patuxent	40	2.0	− 4.7
(TBM-1C)	26	2.4	4.7
	18	2.7	5.1
Inyokern	22	2.5 (max. *g*'s)	− 5.2
(F6F-5)	18	2.7	0.5
(F4U-1D)	19	2.0	− 9.1
	16	3.0	1.8

1. *The Patuxent data*, taken at low dive angles, indicate that there is a decided decrease in MPI when low release *g*'s, less than approximately 2.1, are used, whereas there is no apparent shift at higher values.

2. *The Inyokern data* obtained with each of the two planes substantiate the Patuxent findings. No data on the number of *g*'s at rocket release were available for the F6F flights in which a slow rate of pull-up was used, due to the fact that the cockpit

camera films were obscured. The exceedingly low maximum *g*-meter reading listed indicates, however, that the low-*g* type of pull-up was attained.

It thus follows that, in rocket tossing, best performance is obtained if a sharp pull-up, such as would be used in combat, is executed.

Results on the Variation of MPI with Propellant Temperature

The results of the work done at Quonset and at Inyokern on the effect of propellant temperature are condensed in Table 26.

Table 26. MPI variation with propellant temperature.

Test station	Number of rockets	Propellant temperature (F)	No-wind MPI (mils)
Quonset	95	18	2.4
(TBM-1C)	42	40	3.0
3.5-in. AR	22	59	3.7
Inyokern	12	−2	−8.8
(F6F-5)	12	100	6.3
5.0-in. HVAR			

1. *The Quonset data* given here are the result of an analysis which was made of the data acquired in the tests on slant range and angle of dive, in which variation in the temperature of the propellant resulting from variations in air temperatures were taken into account. No tests were actually made in which propellant temperature was the lone variable. Thus, though the values given in the summary show no appreciable shift in MPI with temperature for the 3.5-inch AR, the variations due to other factors may be masking the effect of the temperature.

2. *The Inyokern tests,* in which 5.0-inch HVAR's were used, were run specifically for the purpose of observing the effect of propellant temperature. Heating and cooling of the rockets prior to loading was carefully done and a correction, to allow for the change in the temperature of the propellant prior to firing, was applied. The results show that, in the case of the 5.0-inch HVAR, the shift in MPI is 15 to 16 mils when the propellant temperature is changed from 0 to 100 F. This shift is about 50 per cent greater than the shift produced by CIT mil drop tables.

These results of tests on the effect of temperature showed the need for the temperature compensation control which was introduced in the Model 2 equipment. The effectiveness of the compensation which was added is shown in Table 27 in the Section 5.3.4.

Overall Performance of the Rocket Tossing Equipment

In Figures 7 to 12, are shown the range distribution of no-wind impact points for all rockets considered in the analysis of equipment evaluation tests conducted at Patuxent, Inyokern, and Dover. The amount of wind error for a given flight, or for a group of flights made under similar wind conditions was estimated by computing half the difference between the MPI's for the two approaches, e.g., the NS MPI and the SN MPI. This correction was then added to or subtracted from the impact point value for each rocket comprising the group to determine where the rockets would have hit had there been no range wind component or had the pilot made proper compensation for wind error.

1. The distribution of 332 individual impacts, corrected for wind, of 3.5-inch aircraft rockets launched at Patuxent is shown in Figure 7. This

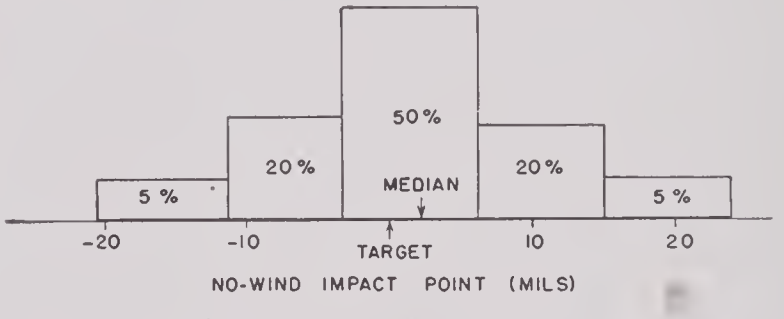

Figure 7. Distribution of range errors, corrected for wind, of 332 3.5-inch aircraft rockets launched from TBM-1C aircraft at Patuxent. A factor used was 0.192. Height of each block is proportional to concentration of rockets in area.

graph shows that the 50 per cent and 90 per cent regions are centered at 1.8 mils and have a total width of 9.6 mils and 26.0 mils, respectively. Thus, the mean range dispersion with respect to the center of impact for the entire group is approximately 5 mils.

2. Figure 8 gives a corresponding distribution of 110 3.5-inch aircraft rockets launched at Dover. For these, the mean dispersion is seen to be approximately 6.5 mils. Included in this graph are 26 rockets fired on flights where all passes were from the same direction. These were corrected for wind error by applying a correction based on the second altitude wind component and the mean flight times of the rockets fired on a given flight.

3. The Inyokern data for 5.0-inch HVAR'S are similarly shown in Figures 9, 10, 11, and 12. Figures 10 and 11 give the distribution obtained using A factors of 0.148 and 0.158, respectively, to show the shift in range with change in A factor. These impacts are combined in Figure 12. Mean dispersions are 7 mils for the F4U data and 6.5 mils for the F6F.

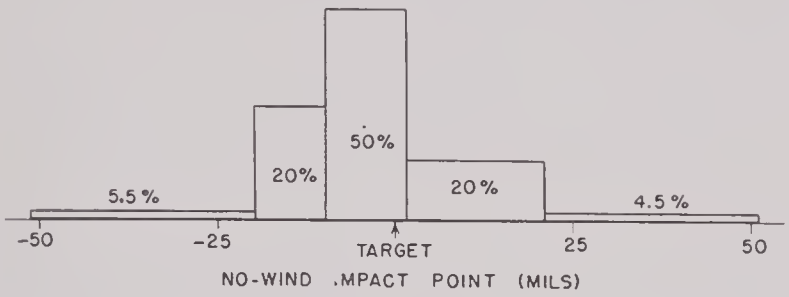

FIGURE 8. Distribution of range errors of 110 3.5-inch aircraft rockets launched from P47-D aircraft at Dover. A factors were 0.240 and 0.225. Height of each block is proportional to concentration of rockets in area.

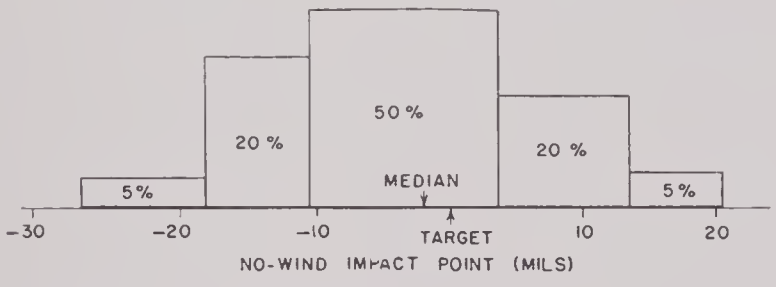

FIGURE 9. Distribution of range errors of 170 5-inch high-velocity aircraft rockets launched from an F4U-1-D aircraft at Inyokern. A factor used was 0.148. Height of each block is proportional to concentration of rockets in area.

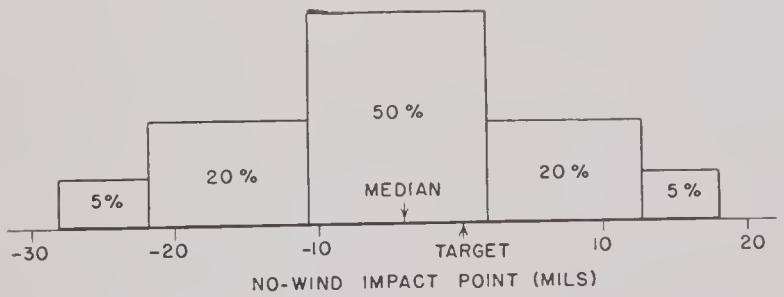

FIGURE 10. Distribution of range errors of 164 5-inch high-velocity aircraft rockets launched from F6F-5 aircraft at Inyokern. A factor used was 0.148. Height of each block is proportional to concentration of rockets in the area.

The actual impact points of the rounds launched by the F6F, plotted in a plane perpendicular to the line of flight, are shown in Figure 13. When these are corrected for wind error, both in deflection and range, the pattern is as shown in Figure 14. If the impacts are limited to median values of slant range, dive angle, and plane speed, the pattern is the one given in Figure 5 of Chapter 1. Under the latter conditions, the impacts are seen to have a mean

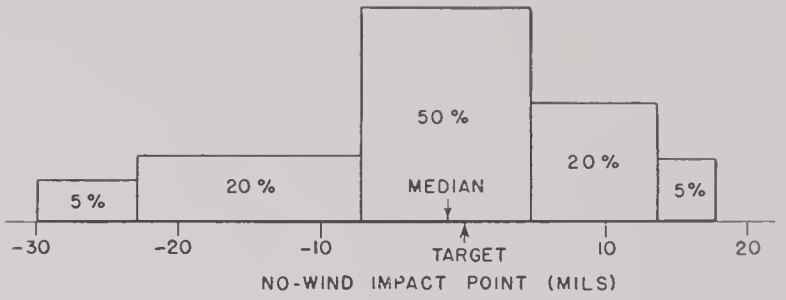

FIGURE 11. Distribution of range errors of 151 5-inch high-velocity aircraft rockets launched from same F6F-5 aircraft but with A factor of 0.158. Compare with Figure 10 and note shift in MPI with change in A factor.

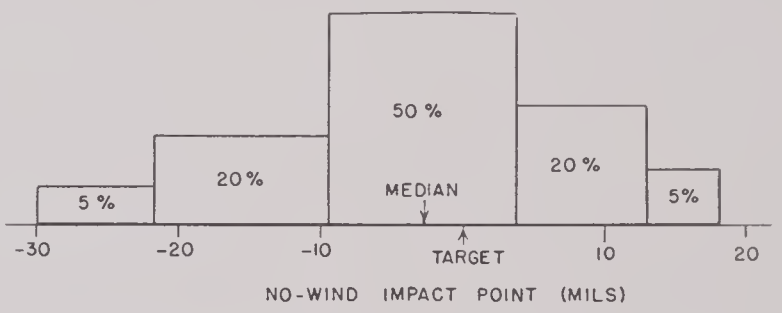

FIGURE 12. Distribution of range errors of 315 5-inch high-velocity aircraft rockets (Figures 10 and 11 combined).

dispersion of 5.2 mils in range and 5.45 mils in deflection. Figure 15 shows a corresponding impact pattern, corrected for wind, for the F4U data. It is to be noted that the impacts are centered on the target in range but are to the right of it in deflection. This would indicate that the pilot who made these flights had a consistent tendency to pull to the right in executing the pull-up maneuver.

5.3.4

Special Tests

The special test classification includes (1) the tests made to check the calibration of the temperature compensation controls, (2) the tests to correct the decrease in MPI at long range which resulted from use of temperature compensation, (3) the work on launching 11.75-inch AR's to determine the proper lanyard control setting and the effect of dive angle and slant range on their MPI, (4) the tests to check the theoretical A factor values for 2.25-inch AR, 3.5-inch AR, and 5.0-inch AR, and (5) the tests to determine the amount of dispersion associated

with salvo firing. All these tests were conducted at Inyokern.[178, 187]

Calibration of Temperature Compensation Control

Two types of tests were made in evaluating the required temperature control setting: (1) with the rockets all at about the same temperature, the control voltage was changed to find the shift in MPI which this change would produce, and (2) the rockets were heated or cooled to the extreme allowable temperatures and the temperature control set according to the theoretical curves given in Chapter 7.

The results are shown in Table 27. The first test showed the shift to be of the proper magnitude (first four rocket groups). When compensation for temperature was then made (last three groups), the MPI was somewhat short at both temperature extremes, but the small number of rockets tossed makes the significance of this error doubtful.

Correction for Decrease in MPI at Long Ranges When Compensation Is Made for Temperature

A decrease in MPI at long range became apparent when a smaller A factor was used in conjunction with the temperature controls. This decrease was corrected by adding a 7.5-megohm resistor in parallel with the rocket calibration condenser. This effectively increased pull-up time, particularly for

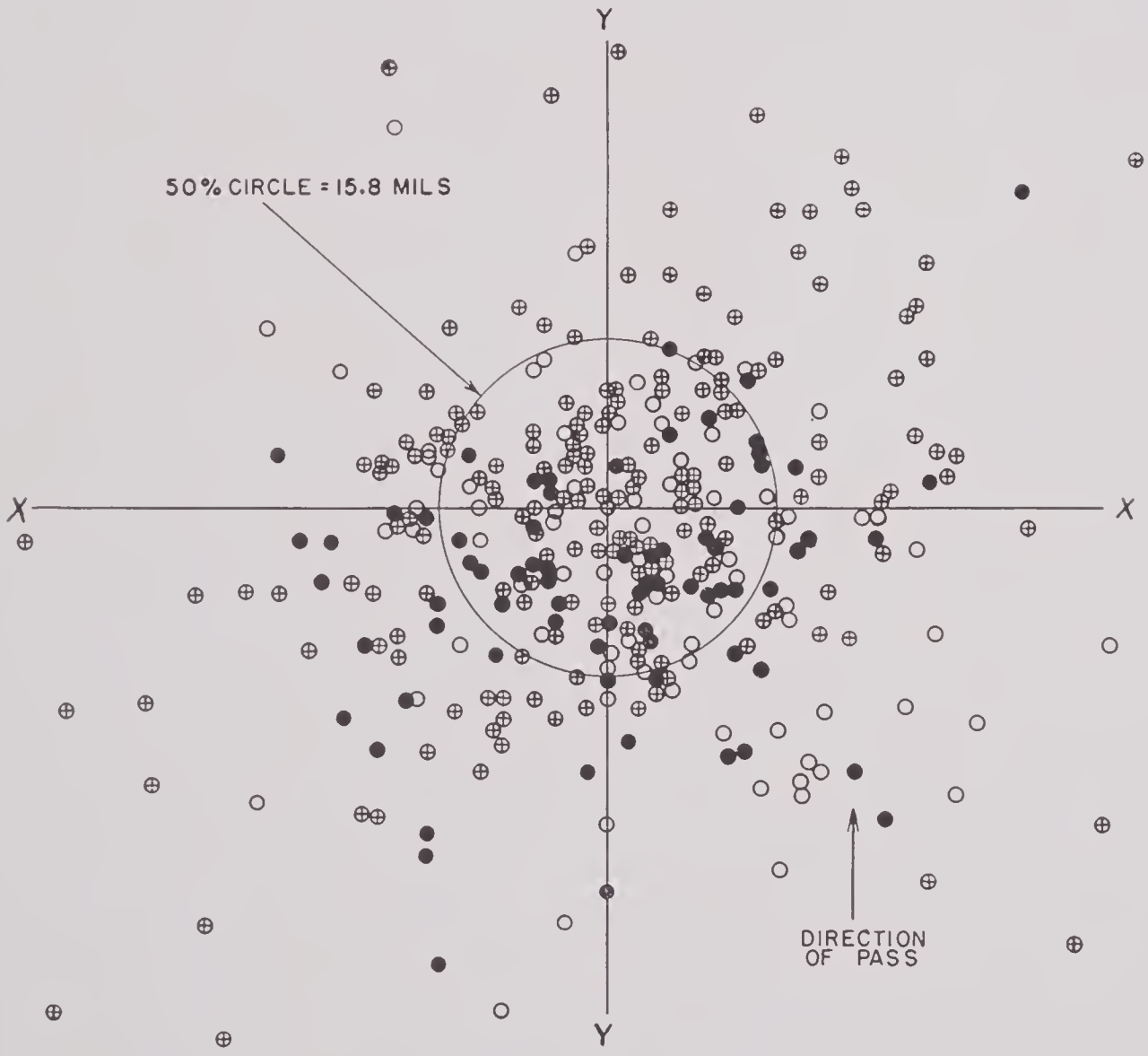

● Impacts of rockets released at slant ranges below 2,000 yards.
⊕ Impacts of rockets released at slant ranges of 2,000 to 2,800 yards.
○ Impacts of rockets released at slant ranges over 2,800 yards.

Figure 13. Impact pattern of all 5-inch high-velocity aircraft rockets launched from F6F-5 airplane, plotted in plane perpendicular to line of flight. No correction has been made and no attempt was made by pilots to compensate for wind error. They always sighted on target. (For distribution of range errors, see Figure 12.)

TABLE 27. Effect of temperature controls on the MPI ($A = 0.128$).
(F4U-1D, 5.0-in. HVAR)

Number of rockets	Temp. control volts	Rel. g's	Second altitude (ft)	Rocket temp. (°F)	Dive angle (deg)	Slant range (yd)	TAS (knots)	Deflection Disp. (mils)	Deflection MPI (mils)	Range Disp. (mils)	Range MPI (mils)
22	0	2.6 ± .4	5,000	45 ± 1	37 ± 3	2,500 ± 280	345 ± 8	7.6	8.5	4.7	— 2.9
6	8	.....	5,000	46 ± 0	36 ± 1	2,600 ± 190	348 ± 4	5.3	11.3	2.9	8.4*
6	30	2.6 ± .3	5,000	54 ± 4	40 ± 4	2,450 ± 260	336 ± 9	3.9	14.6	5.8	9.0*
16	30	3.2 ± .3	5,000	42 ± 2	38 ± 4	2,550 ± 240	344 ± 4	11.2	6.4	4.7	14.0
9	0	2.8 ± .3	5,000	102 ± 0	35 ± 1	2,800 ± 150	342 ± 7	9.4	8.7	2.3	— 5.1
14	8	.....	5,000	63 ± 7	37 ± 3	2,800 ± 150	335 ± 7	6.4	15.3	6.5	3.1
15	30	3.0 ± .2	5,000	11 ± 0	35 ± 1	2,600 ± 70	340 ± 9	5.1	12.3	3.0	— 2.2

* Only one pair from one direction. Thus, the fairly high wind which existed makes these data of small value.

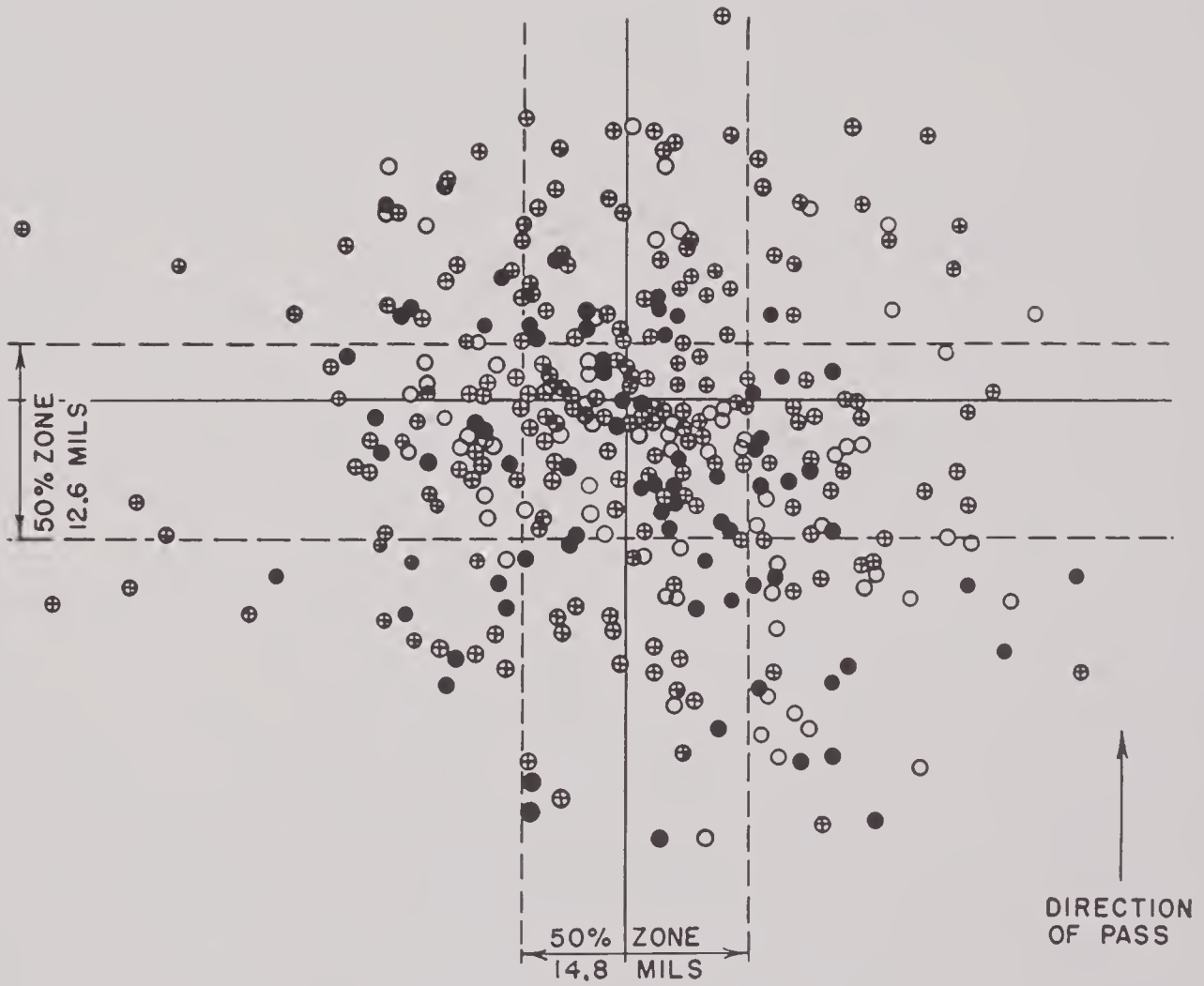

● Impacts of rockets released at slant ranges below 2,000 yards.
⊕ Impacts of rockets released at slant ranges of 2,000 to 2,800 yards.
○ Impacts of rockets released at slant ranges over 2,000 yards.

FIGURE 14. Impact pattern of all (343) 5-inch high-velocity aircraft rockets launched from F6F-5 airplane, plotted in plane perpendicular to line of flight. This is pattern which would have resulted if pilot had accurately compensated for wind. (For uncorrected impact pattern, see Figure 13.) At all ranges, true airspeed varied from 265 to 410 knots, and dive angle from 18 to 58 degrees.

long-range tosses. The progress of this improvement is shown in Table 28.

LAUNCHING THE 11.75-INCH AR

A series of tests was conducted in which 11.75-inch AR's were launched from F6F-5 and F4U-4 airplanes. Of a total of 94 rockets launched, 26 were used to find the correct A factor. The rest were used to determine the variation in impact point with variations in flight conditions, e.g., dive angle and range.

It was intended that, on each flight, two rockets would be carried and that they would be launched from opposite headings, thereby giving indication of wind error and permitting its determination and removal. Trouble with defective launchers, and with

TABLE 28. Effect of leakage resistor on impact point (temp. setting = 8 volts).

(F4U-1D, 5.0-in. HVAR)

Number of rockets	A	Maximum g's	Second altitude (ft)	Rocket temp. (F)	Dive angle (deg)	Slant range (yd)	TAS (knots)	Deflection Disp. (mils)	Deflection MPI (mils)	Range Disp. (mils)	Range MPI (mils)
16	0.118	(Rel.) 2.5 ± .2	5,000	74 ± 6	36 ± 0	2,400 ± 70	337 ± 5	7.0	7.7	4.5	2.0
16	0.118	(Rel.) 2.8 ± .5	7,200	69 ± 1	35 ± 0	3,550 ± 190	349 ± 7	8.1	11.8	8.3	− 7.2
8*†	0.100	4.9 ± .3	5,000	44 ± 0	39 ± 5	2,400 ± 230	343 ± 4	9.0	8.8	8.3	− 2.8
16*†	0.118	4.7 ± .4	5,000	71 ± 1	36 ± 1	2,380 ± 60	332 ± 5	8.9	16.4	6.3	6.4
13*†	0.118	4.8 ± .3	8,500	80 ± 5	36 ± 3	3,470 ± 270	343 ± 17	10.1	10.3	7.1	13.7
19*‡	0.103	4.9 ± .5	7,200	72 ± 3	36 ± 2	3,570 ± 320	351 ± 18	8.1	13.9	8.4	2.1
6*‡	0.118	5.0 ± .4	8,500	78 ± 0	39 ± 2	3,550 ± 240	363 ± 21	9.9	15.4	4.9	1.8
16‡	0.128	4.8 ± .4	7,200	73 ± 13	35 ± 1	3,740 ± 140	344 ± 4	11.0	8.1	7.7	− 3.5

* The MPI's have been corrected to correspond to $A = 0.128$, by the formula $d\theta$ (mils) $= g/2V^2\, RdAF(\gamma) \times 1{,}000$.

† Leakage resistance = 5.0 megohms.

‡ Leakage resistance = 7.5 megohms.

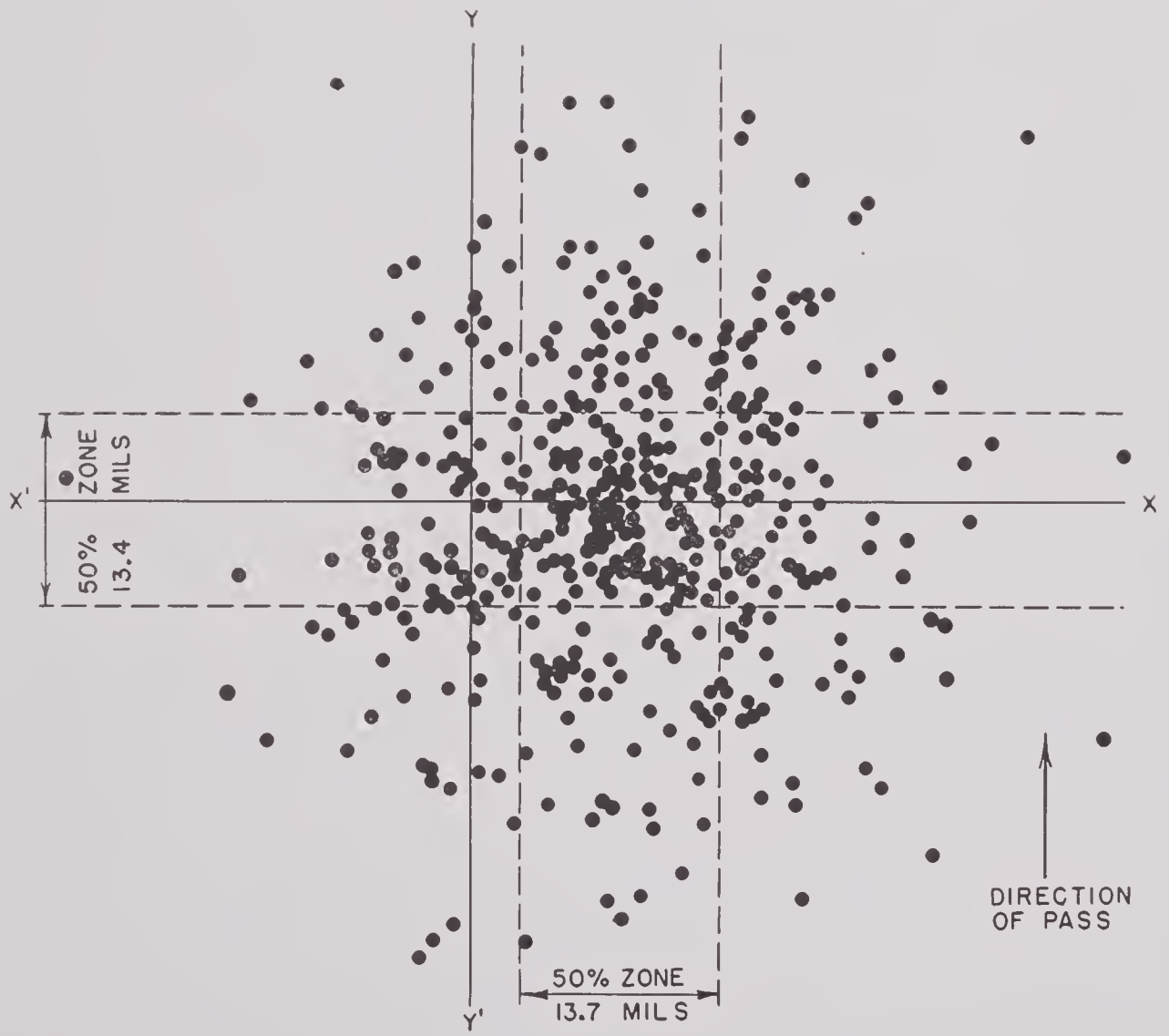

FIGURE 15. Impact pattern, corrected for wind, of all (440) 5-inch high-velocity aircraft rockets launched from F6F-1D airplane, Inyokern, plotted in plane perpendicular to line of flight. This is pattern which would have resulted if pilot had made perfect compensation for wind error.

misfires on 16 flights interfered with the determination of the wind error present, so the single rounds which were launched satisfactorily on these 16 flights will not be considered in the analysis of the data.

TABLE 29. Shift in MPI with dive angle for 11.75-inch AR.

Number of rockets	Max. g's	Second altitude (ft)	Dive angle (deg)	TAS (knots)	Slant range (yd)	MPI Defl. (mils)	MPI Range (mils)
8	5.1	2,000	20	320	1,500	4.6	− 0.1
20	5.2	2,900	36	341	1,360	− 5.4	1.6
4	4.2	6,000	51	411	2,105	− 18.0	4.6

TABLE 30. Shift in MPI with range (at two dive angles) for 11.75-inch AR.

Number of rockets	Max. g's	Second altitude (ft)	Dive angle (deg)	TAS (knots)	Slant range (yd)	MPI Defl. (mils)	MPI Range (mils)
20	5.2	2,900	36	341	1,360	− 5.4	1.6
10	4.9	6,000	36	369	2,725	5.4	− 4.6
8	4.8	6,000	36	352	3,155	− 5.8	− 4.1
8	5.1	2,000	20	320	1,500	4.6	− 0.1
2	4.5	3,500	20	353	3,030	− 13.7	− 9.2

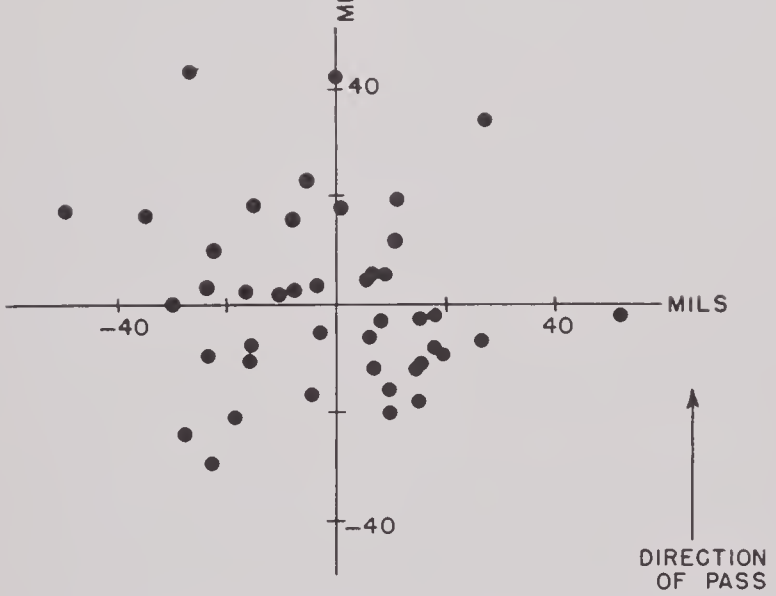

FIGURE 16. Impact pattern, uncorrected for wind, of 11.75-inch aircraft rockets launched from F6F-5 aircraft, Inyokern, plotted in plane perpendicular to line of flight. Test conditions were as follows:

Slant range 1,030–3,230 yards
A factor 0.215–0.295 (mostly 0.295)
True airspeed 307–410 knots
Dive angle 18–52 degrees
Average wind velocity at release altitude 7 knots

Table 29 shows the shift in no-wind MPI as the dive angle increases. It is apparent that some shift is present, but the amount of shift is probably reduced by the increase in true airspeed as the dive angle increases. These data indicate that a small increase in MPI can be expected as the dive angle increases.

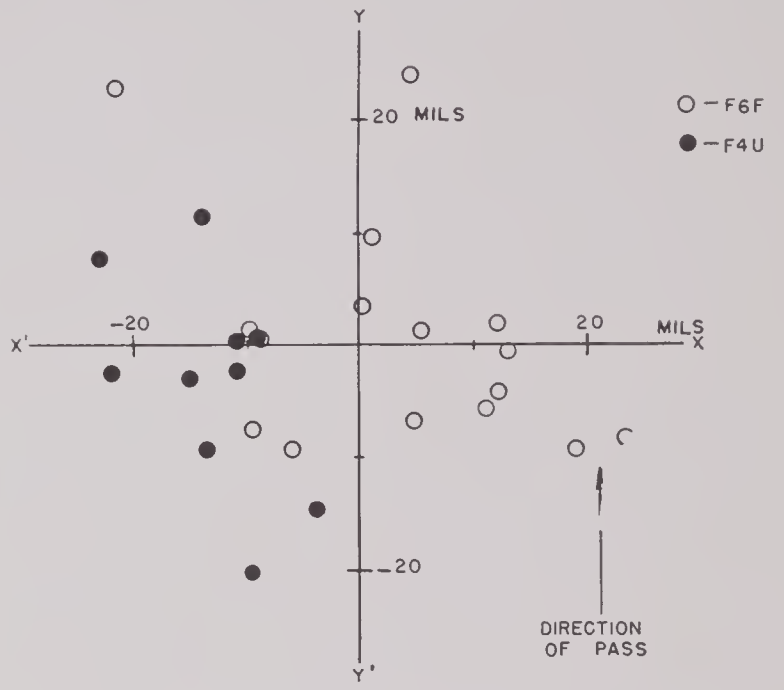

FIGURE 17. Impact pattern (corrected) of 11.75-inch aircraft rockets launched from F6F-5 and F4U-4 aircraft, Inyokern. Each point represents impact of two rounds launched in same flight from opposite directions, after effect of wind has been removed. (Removal of wind effect places both rounds at same point.) These impacts have also been corrected to correspond to $A = 0.295$ and temperature and lanyard setting of 40 volts.

Table 30 shows the shift in no-wind MPI as the range increases. Here, too, the true airspeed was not constant and probably had some effect on the MPI, but in this instance, the change in airspeed had an adverse effect. The data show that there is a slight decrease in MPI as the range increases at medium dive angles; and that there is a larger decrease in MPI as the range increases at low dive angles. This effect has been anticipated from previous tests with other rockets, and from laboratory tests. Use of a 7.5-megohm leakage resistance across the rocket calibration condenser probably reduced the shift which would have otherwise resulted.

The actual impact pattern of all 11.75-inch AR's launched by the F6F in the above tests is shown in Figure 16. Impact points are plotted perpendicular to the line of flight and have not been corrected for wind. The pattern of the impacts for the 11.75-inch AR's launched by the F4U as well as the F6F, after correction was made for wind, is shown in Figure 17. The mean dispersion of these rocket groups relative to their respective centers of impact under no-wind conditions averages 7.2 mils.

Check on Theoretical *A* Factor Values for 2.25-inch AR, 3.5-inch AR, and 5.0-inch AR

1. *A factor for 2.25-inch AR.* A total of 32 2.25-inch AR's were launched to find experimentally the proper *A* factor for this type rocket. The temperature control was set at 7 volts (from the theory) during all tests. The results are as shown in Table 31.

From these data it appears that the proper *A* factor for the 2.25-inch AR (fast) and a true airspeed of 340 knots is about 0.258. The theoretical *A* factor, which was obtained by extrapolating mil drop tables beyond 2,000 yards, is 0.221. In view of the data limitation in obtaining this theoretical value, it is not surprising that a larger factor is necessary in practice.

2. *A factor for 3.5-inch AR.* Sixteen 3.5-inch AR'S were launched to determine experimentally the *A* factor for this type rocket. The *A* factor and temperature controls were adjusted to the theoretical values of 0.216 and 7 volts, respectively, corresponding to an expected airspeed of 325 knots. The results are shown in Table 32, with a slightly larger airspeed than expected.

The correct *A* factor to employ for the 3.5-inch AR and a true airspeed of 344 knots is 0.232. Had this *A* factor been used instead of 0.216, the MPI would have been better still.

3. *A factor for 5.0-inch AR.* The results obtained in the test to check experimentally the *A* factor required in launching 5.0-inch AR's are shown in Table 33.

Twenty-four 5.0-inch AR's were launched. The temperature control was set at 8 volts from theory for all tests. The *A* factor was set at 0.250 (the theoretical value for 340 knots), but the MPI was short. From the above data, it would seem that an *A* factor of about 0.298 would be correct.

Results of Salvo Firing

Both the F6F and F4U airplanes were used to launch 5.0-inch HVAR in salvo for the purpose of checking dispersion. The values obtained for ammunition dispersion were: F4U, 6.64 mils in deflection, and 7.58 mils in range; F6F, 7.26 mils in deflection, and 6.28 mils in range. The complete summary is shown in Tables 34 and 35.

Table 31. F4U – 1D.

Number of rockets	*A* factor	Rel. *g*'s	Rocket temp. (°F)	Second altitude (ft)	Dive angle (deg)	Slant range (yd)	TAS (knots)	Deflection		Range	
								Disp. (mils)	MPI (mils)	Disp. (mils)	MPI (mils)
8	0.270	2.9±.2	——	5,000	36±1	2,530±60	341±9	6.0	– 2.3	4.3	6.3
8	0.260	2.9±.1	——	5,000	35±1	2,580±60	339±7	4.5	1.2	2.6	3.9
16	0.255	3.0±.2	——	6,000	35±1	2,980±280	347±9	6.6	6.6	5.0	– 4.6

Table 32. F4U – 1D.

Number of rockets	*A* factor	Rel *g*'s	Rocket temp. (°F)	Second altitude (ft)	Dive angle (deg)	Slant range (yd)	TAS (knots)	Deflection		Range	
								Disp. (mils)	MPI (mils)	Disp. (mils)	MPI (mils)
16	0.216	3.0±.2	68±4	5,000	36±1	2,800±100	344±5	6.6	13.7	5.0	– 2.2

Table 33. F4U – 1D.

Number of rockets	*A* factor	Max. *g*'s	Second altitude (ft)	Rocket temp. (°F)	Dive angle (deg)	Slant range (yd)	TAS (knots)	Deflection		Range	
								Disp. (mils)	MPI (mils)	Disp. (mils)	MPI (mils)
8	0.250	4.6±.2	6,000	60±0	35±0	2,480±70	339±8	3.9	11.7	6.2	– 16.6
16	0.287	4.5±.5	6,000	66±2	35±1	2,400±20	348±12	7.1	11.6	6.5	– 3.7

TABLE 34. Salvo firing summary (F4U).

Number of rockets	Course	A	Max. g's	Second altitude (ft)	Rocket temp. (°F)	Dive angle (deg)	Slant range (yd)	TAS (knots)	Deflection Disp. (mils)	Deflection MPI (mils)	Range Disp. (mils)	Range MPI (mils)
5	S–N	0.128	4.0	5,000	72	35	2,660	355	3.7	3.6	5.7	— 5.4
8	N–S	0.128	5.0	5,000	80	35	2,630	332	12.8	6.8	6.9	— 1.4
6	S–N	0.128	4.0	5,000	63	36	2,400	345	7.4	— 14.3	7.4	24.2
6	N–S	0.128	4.0	5,000	78	41	2,290	379	1.4	— 1.3	7.3	26.0
6	N–S	0.128	4.8	5,000	82	38	2,460	370	5.3	7.0	9.2	6.5
5	S–N	0.128	4.0	5,000	62	38	2,460	345	6.0	— 3.0	5.0*	— 23.8

* One rocket on this test landed 66.3 mils from the MPI of the other five, and was obviously defective. In order to give an unbiased view this rocket was omitted in the computation of MPI and dispersion.

TABLE 35. Results of salvo firing (F6F).

Number of rockets	Course	A	Rel. g's	Second altitude (ft)	Rocket temp. (°F)	Dive angle (deg)	Slant range (ft)	TAS (knots)	Deflection Disp. (mils)	Deflection MPI (mils)	Range Disp. (mils)	Range MPI (mils)
4	N–S	0.158	2.3	5,000	60	33	8,010	306	8.5	10	3	3
2	S–N	0.158	2.0	4,170	60	34	6,360	335	6.5	−21.5	3	— 6
6	S–N	0.158	——	4,170	50	32	7,140	331	5.8	1.8	5.0	−13.3
6	S–N	0.158	2.2	4,170	60	34	6,480	345	4.3	−18.0	12.3	— 7.0
6	N–S	0.158	2.2	5,000	——	40	6,690	367	10.5	— 0.5	9.7	21.0
6	N–S	0.158	2.0	5,000	——	50	5,370	378	2	— 7	3.7	16.3
6	N–S	0.158	2.4	4,170	——	23	9,930	354	9.1	1	5.2	— 2.2
6	S–N	0.158	2.1	5,000	54	44	6,030	372	7.9	— 3.2	4.1	19.3
6	N–S	0.158	2.0	2,000	——	36	2,940	374	10.1	19.2	2.8	28.3
2	S–N	0.158	2.0	1,395	——	19	3,420	348	1.0	−30.0	0.5	−21.5
4	S–N	0.158	2.0	1,395	——	19	3,540	343	5.9	−18.8	5.8	−22.3
6	S–N	0.158	1.6	2,000	——	43	2,490	385	5.0	−31.7	2.7	— 0.5

5.4 PLANE–TO–PLANE TESTS

5.4.1 The Technique

Toss bombing was initially proposed as a plane-to-plane operation in essentially level-flight bombing. The first computers built and tested were for this application. The results as shown below, were very promising — so promising, in fact, that the technique, when used with proximity-fuzed bombs, was considered too dangerous as a *defensive* weapon against aircraft for further development and risk of compromise. Development was stopped in the summer of 1943, when it was evident that the Allies were assuming air supremacy, and thus an outstanding defensive weapon against bomber formations would be of more value to the enemy, if compromised, than to the Allies.

The principle of the toss technique in level, plane-to-plane bombing is considerably simplified because there is no dive angle correction. The ψ term, discussed in Chapter 2, becomes unity and the computer requires intelligence only as to time to target and pull-up acceleration. In application, the bombing plane flies a head-on collision course toward the target plane and at a predetermined time, pulls up from the collision course. The equipment releases the bomb at the appropriate time to intersect the collision course at the target.[2, 11, 260–264]

Time to target was measured with an ARO radar equipment adapted for the purpose by representatives of Division 14, NDRC.[219, 265] The ARO measured range and range rate and was set to initiate the computing process when the time to target was 7 seconds. The acceleration integrator in the computer was similar in principle to the Mark 1 accelerometer.

Before the start of pull-up and after the 7-second point, the integrator circuit charged at a unit rate so that the time integral of the acceleration was equal to elapsed time. This provided that at any time after the start of integration, the part of the total integral remaining was proportional to the remaining closing time. Pull-up could start any time after the 7-second point; delay of pull-out

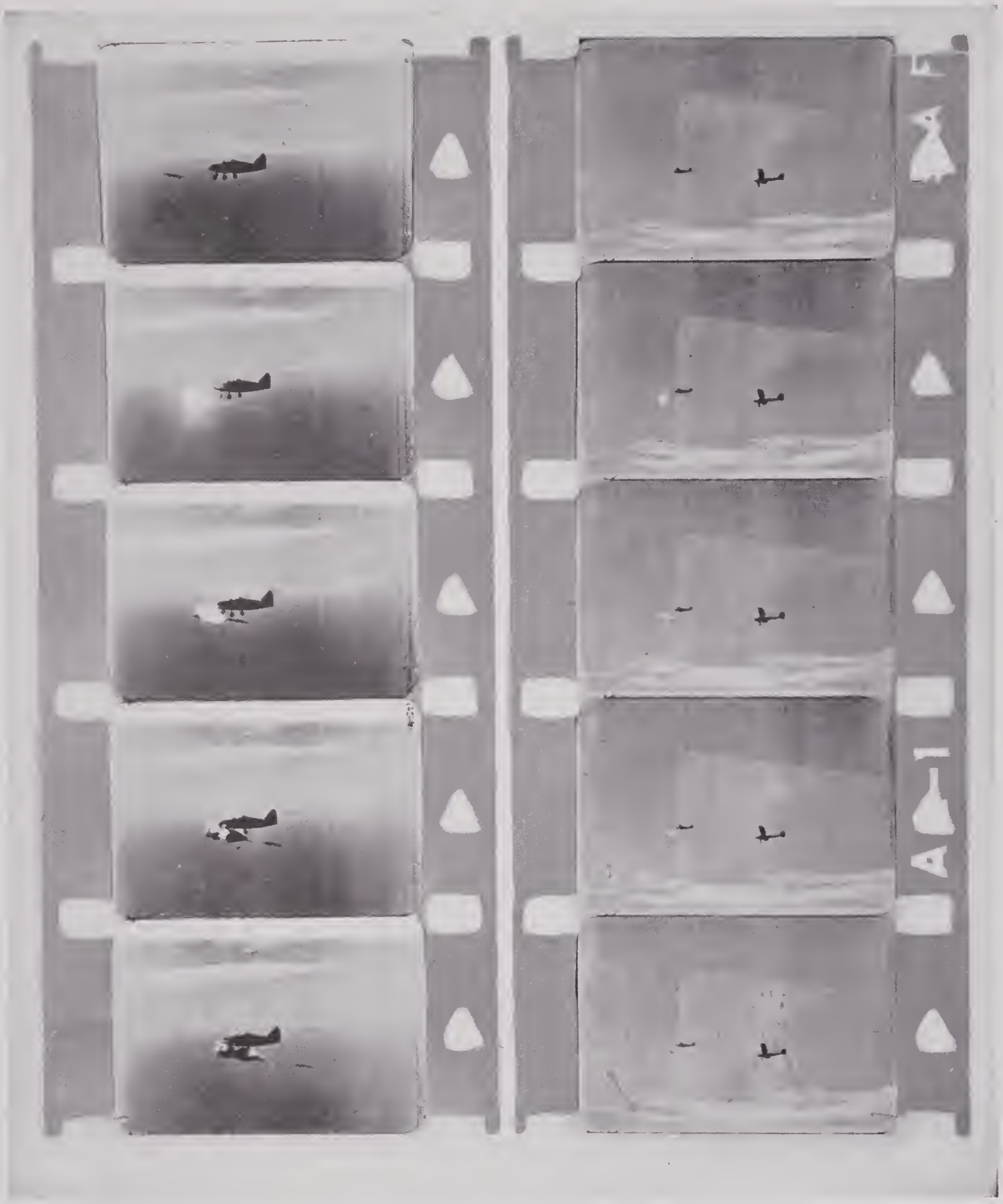

FIGURE 19. Toss bombing attack on PQ-8 target by B-25 bomber using radar range and 7-second acceleration integrator setup. 100-pound inert M-30 bombs were equipped with modified T-4 photoelectric fuzes and carried spotting charges. Photographs at left show passage of bomb and fuze function in close vicinity of radio-controlled target. Photographs at right show another round functioning on passage; at right is mother plane.

Altitude of attack 5,000 feet
True closing speed 325 mph

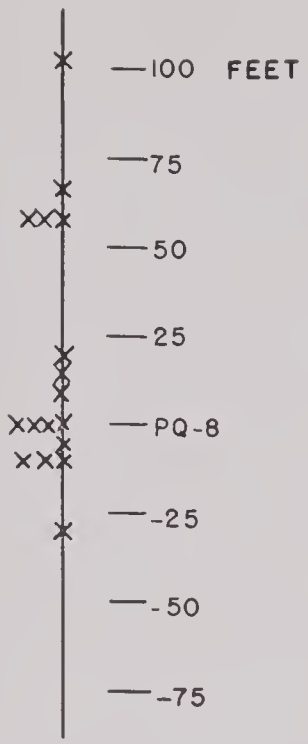

FIGURE 18. Plot of 17 bombs tossed by B-25 bomber in terms of minimum vertical passage distance above or below PQ-8 radio-controlled target.

beyond this point did not introduce error. Release of the bomb occurred when the time integral of the acceleration reached the appropriate value.

5.4.2

Performance

Tests of the plane-to-plane tossing technique were carried out using a B-25 bomber and a PQ-8 radio-controlled target. Closing speeds were about 400 mph, so that the range was about 4,100 feet at the 7-second point. A total of 27 bombs were tossed under these conditions. The results, plotted in terms of minimum vertical passage distance, are shown in Figure 18 for 17 of the bombs on which photographic data were obtained. Sixty per cent of the bombs were within 50 feet of the target and over 90 per cent were within 100 feet. One bomb scored a direct hit and another, a grazing hit.

A few rounds were tried with modified T-4 photoelectric fuses,[d] carrying spotting charges. Figure 19 shows the function of two of these rounds on passage.

[d] See Volume 3, Division 4.

Chapter 6

MATHEMATICAL ANALYSIS OF BOMB TOSSING[a]

6.1 SOLUTION OF THE BASIC BOMB TOSSING EQUATION

6.1.1 The ψ_0 Function

THE ψ_0 FUNCTION was defined in Section 2.1.2 as

$$\psi_0 = \frac{\bar{K} + \sqrt{\bar{K}^2 - \bar{K}}}{\bar{K} + \sqrt{\bar{K}(\bar{K} - \cos\alpha)}} \cdot \frac{2\cos\alpha}{1 + \sqrt{1 + 2\beta}}$$

where $\bar{K}$ is the time average of K from the beginning of pull-up to the release of the bomb, α is the dive angle, and

$$\beta = \frac{gT_0 \sin\alpha}{V} \cdot \frac{\bar{K} - \cos\alpha}{\bar{K}}.$$

In Tables 1, 2, 3, and 4 are given values of ψ_0 for $\bar{K} = 2, 3, 4, 5$; $T_c/V = 0.01, 0.02, 0.03, 0.04, 0.05$; and α from -30 to 90 degrees. (Figures in the tables are based on a value of $g = 32.2$ feet per second per second.) Figures 2 and 3 in Chapter 2 are graphical representations of ψ_0 based on typical values from the tables. The tabulated data, as well as Figure 2 of Chapter 2, show that for small values of T_c/V, that is, for short ranges or high airplane velocities, ψ_0 does not differ much from cos α, while for larger values of T_c/V the ψ_0 function is

TABLE 1. Values of ψ_0.
$K = 2$

α	$\frac{T_c}{V} = 0.01$	$\frac{T_c}{V} = 0.02$	$\frac{T_c}{V} = 0.03$	$\frac{T_c}{V} = 0.04$	$\frac{T_c}{V} = 0.05$
− 30°	0.886	0.939	1.008	1.110	1.299
− 20°	0.957	0.990	1.028	1.074	1.128
− 10°	0.995	1.011	1.027	1.045	1.062
0°	1.000	1.000	1.000	1.000	1.000
10°	0.968	0.955	0.943	0.932	0.920
20°	0.903	0.880	0.859	0.840	0.822
30°	0.808	0.778	0.752	0.728	0.708
40°	0.691	0.657	0.629	0.605	0.584
50°	0.558	0.525	0.498	0.476	0.457
60°	0.418	0.388	0.366	0.347	0.332
70°	0.275	0.253	0.237	0.224	0.213
80°	0.134	0.123	0.114	0.107	0.102
90°	0.000	0.000	0.000	0.000	0.000

TABLE 2. Values of ψ_0.
$K = 3$

α	$\frac{T_c}{V} = 0.01$	$\frac{T_c}{V} = 0.02$	$\frac{T_c}{V} = 0.03$	$\frac{T_c}{V} = 0.04$	$\frac{T_c}{V} = 0.05$
− 30°	0.906	0.984	1.095	1.324	Imaginary
− 20°	0.965	1.006	1.067	1.121	1.209
− 10°	1.002	1.022	1.046	1.070	1.098
0°	1.000	1.000	1.000	1.000	1.000
10°	0.965	0.949	0.933	0.919	0.905
20°	0.901	0.872	0.846	0.824	0.802
30°	0.809	0.773	0.742	0.716	0.692
40°	0.697	0.658	0.626	0.599	0.576
50°	0.568	0.531	0.501	0.477	0.456
60°	0.430	0.397	0.373	0.353	0.336
70°	0.286	0.262	0.245	0.231	0.219
80°	0.141	0.129	0.120	0.113	0.107
90°	0.000	0.000	0.000	0.000	0.000

TABLE 3. Values of ψ_0.
$K = 4$

α	$\frac{T_c}{V} = 0.01$	$\frac{T_c}{V} = 0.02$	$\frac{T_c}{V} = 0.03$	$\frac{T_c}{V} = 0.04$	$\frac{T_c}{V} = 0.05$
− 30°	0.919	1.006	1.149	Imaginary	Imaginary
− 20°	0.978	1.031	1.098	1.189	1.338
− 10°	1.005	1.029	1.055	1.084	1.118
0°	1.000	1.000	1.000	1.000	1.000
10°	0.964	0.945	0.928	0.912	0.898
20°	0.899	0.868	0.840	0.816	0.794
30°	0.809	0.770	0.737	0.709	0.685
40°	0.698	0.657	0.623	0.595	0.571
50°	0.572	0.532	0.501	0.476	0.455
60°	0.434	0.401	0.375	0.355	0.338
70°	0.290	0.266	0.248	0.234	0.222
80°	0.144	0.132	0.122	0.115	0.109
90°	0.000	0.000	0.000	0.000	0.000

TABLE 4. Values of ψ_0.
$K = 5$

α	$\frac{T_c}{V} = 0.01$	$\frac{T_c}{V} = 0.02$	$\frac{T_c}{V} = 0.03$	$\frac{T_c}{V} = 0.04$	$\frac{T_c}{V} = 0.05$
− 30°	0.925	1.021	1.185	Imaginary	Imaginary
− 20°	0.981	1.039	1.113	1.223	1.408
− 10°	1.006	1.032	1.060	1.092	1.130
0°	1.000	1.000	1.000	1.000	1.000
10°	0.963	0.943	0.925	0.909	0.893
20°	0.898	0.865	0.836	0.811	0.788
30°	0.809	0.768	0.734	0.705	0.680
40°	0.699	0.656	0.621	0.593	0.568
50°	0.574	0.533	0.501	0.475	0.454
60°	0.437	0.402	0.376	0.356	0.338
70°	0.293	0.268	0.250	0.235	0.223
80°	0.146	0.133	0.124	0.116	0.110
90°	0.000	0.000	0.000	0.000	0.000

[a] Chapter 6 is essentially appendix material to Section 2.1. It was prepared by Dr. L. E. Ward of the Naval Ordnance Test Station, Inyokern, California, and Dr. Albert London of the National Bureau of Standards.

more nearly linear in α. Figure 3 of Chapter 2 shows the very small change caused in ψ_0 by a change in $\bar{K}$, especially for $\bar{K} > 3$.

The tables and graphs establish the essential property of the ψ_0 function used in the bomb tossing equipment, namely, that ψ_0 is chiefly a function of α.

6.1.2 The ψ_1 Function

Referring to equations (13) and (14) in Chapter 2, it will be seen that one of the essential steps in obtaining the zero-order solution of equation (12), Chapter 2 is to replace $\sin \theta_p$ by θ_p and $\cos \theta_p$ by $1 - \frac{1}{2}\theta_p^2$. This results in a restriction on the range for which the Model 0 equipment can be used effectively.[79] This restriction is made the more severe by omitting the term of degree three in equation (14), Chapter 2.

The restriction of the range due to the use of these approximations can be partially removed by using in equation (13), Chapter 2, approximations to the trigonometric functions which result in an equation of degree three for θ_p. In order to obtain all terms of degree three in θ_p it is necessary to replace $\sin \theta_p$ by $\theta_p - \theta_p^3/6$, to replace the $\cos \theta_p$ which is under the radical by $1 - \frac{1}{2}\theta_p^2 + \theta_p^4/24$, and the other $\cos \theta_p$'s by $1 - \frac{1}{2}\theta_p^2$. The resulting equation of degree three in θ_p comes out to be[b]

$$\left(1 + 3\sigma + \frac{\frac{1}{4} + \sigma}{\sqrt{1 + \frac{\cos \alpha}{\bar{\mu}}}}\right)\theta_p^3 - 3(1 + 2\sigma)\,\theta_p^2 \tan \alpha - 6(1 + \sigma)\,\theta_p + \frac{6gT_c\bar{\mu}}{V} = 0. \qquad (1)$$

If equation (4) of Chapter 2 is used in order to eliminate θ_p, the following equation for T_p is obtained.[34]

$$\phi T_p^3 - \frac{g\bar{\mu}}{2V}(1 + 2\sigma)T_p^2 \tan \alpha - (1 + \sigma)\,T_p + T_c = 0 \qquad (2)$$

where

$$\phi = \frac{g^2\bar{\mu}^2}{6V^2}\left(1 + 3\sigma + \frac{\frac{1}{4} + \sigma}{\sqrt{1 + \frac{\cos \alpha}{\bar{\mu}}}}\right).$$

Comparison of equation (2) with equation (16), Chapter 2, shows that the above equation differs from the other only in the possession of a term in degree three. Since it is reasonable to expect that the solution of equation (2) does not differ greatly from the less exact solution it is desirable to write

$$T_p = T_{p0}(1 + \epsilon), \qquad (3)$$

where T_{p0} is given by equation (17), Chapter 2 and ϵ is a small quantity to be determined.

When equation (3) is substituted into equation (2), the terms containing ϵ to the second and third powers may be neglected, only terms containing ϵ to the first power and those not containing ϵ being retained. The resulting equation is a linear equation for ϵ, and if it turns out that ϵ is actually small for the values of the parameters of importance in bomb tossing, the validity of this method for solving equation (2) will be established.

The linear equation for ϵ is

$$\phi T_{p0}^3(1 + 3\epsilon) - \frac{g\bar{\mu}}{2V}(1 + 2\sigma)\,T_{p0}^2 \cdot (1 + 2\epsilon)\tan \alpha - (1 + \sigma)\,T_{p0}(1 + \epsilon) + T_c = 0$$

or, taking account of the fact that T_{p0} satisfies equation (16), Chapter 2

$$\phi T_{p0}^2(1+3\epsilon) - \frac{g\bar{\mu}}{V}(1+2\sigma)\cdot T_{p0}\epsilon\tan\alpha - (1+\sigma)\epsilon = 0. \qquad (4)$$

The solution of equation (4) for ϵ is

$$\epsilon = \frac{\phi T_{p0}^2}{1 + \sigma + \frac{g\bar{\mu}}{V}(1 + 2\sigma)T_{p0}\tan\,\alpha - 3\phi T_{p0}^2}. \qquad (5)$$

If the function ψ_1 is defined by the relation

[b] The ψ function as originally defined,[34] used in the Model 1 equipment, was primarily concerned with taking into account only one additional term in the expansion of $\cos \theta_p$ occurring as $V \cos \theta_p$ in the coordinate of the toss bombing equations. The procedure outlined in this chapter gives more accurate values of ψ_1 which will result from including all the degree-three terms. Consequently the ψ_1 for $T_c/V = 0.028$, which is the design value for Model 1 equipment, will not agree exactly with the procedure in Chapter 6. It should also be pointed out that the original design for ψ_1 agrees to within 1 per cent or less with corresponding values for ψ based on ψ_e = the exact ψ function.[72] The form of presentation given here is used because it appears a more logical presentation than the actual evolution of values for ψ during the development program. Most of the values in the tables and graphs in this chapter and in Chapter 2 are based on the original ψ_1 function rather than the ψ_1 function as derived herein; however the differences in the values for the ψ_1's can be disregarded.

$\psi_1 = \psi_0 (1 + \epsilon)$, it follows from equation (19), Chapter 2, and equation (3) that

$$T_p = \frac{T_c}{\bar{K} + \sqrt{\bar{K}^2 - \bar{K}}} \psi_1,$$

which is an equation of the type for which the bomb tossing equipment is designed.

TABLE 5. ϵ for different values of T_c/V.
$K = 3$

Dive angle (α)	T_c/V 0.01	0.02	0.03	0.04	0.05
0°	0.0062	0.0265	0.0661	0.1389	0.2835
10°	0.0057	0.0223	0.0509	0.0949	0.1617
20°	0.0048	0.0185	0.0392	0.0676	0.1049
30°	0.0043	0.0147	0.0296	0.0483	0.0706
40°	0.0034	0.0111	0.0214	0.0334	0.0470
50°	0.0025	0.0078	0.0144	0.0217	0.0296
60°	0.0016	0.0047	0.0085	0.0126	0.0167
70°	0.0008	0.0023	0.0040	0.0058	0.0076
80°	0.0002	0.0005	0.0011	0.0015	0.0020
90°	0.0000	0.0000	0.0000	0.0000	0.0000

Values of ϵ for $\bar{K} = 3$ are given in Table 5. It will be seen that for small dive angles and large values of the ratio T_c/V, the values of ψ_1 are appreciably greater than the corresponding values of ψ_0. The graph of ϵ based on Table 5 is shown in Figure 1.

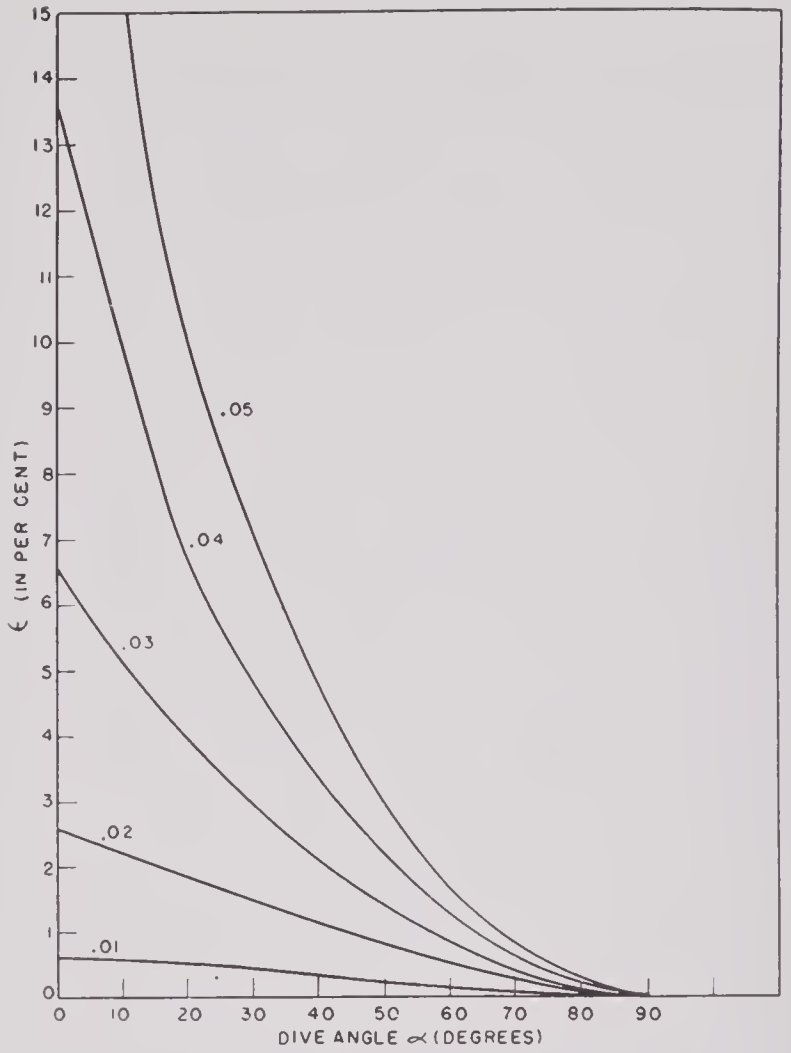

FIGURE 1. ϵ versus α for different values of T_c/V, $\bar{K}$ being constant (= 3).

6.1.3

The ψ_0 Function

In Section 6.1.3 an exact solution of equation (13) of Chapter 2 is obtained.[72] We find it convenient to go back to equations (10) of Chapter 2 which, after replacing μ by $\bar{\mu}$ can be written

$$\begin{aligned} VT_c - \tfrac{1}{2} gT_f^2 \sin\alpha &= \frac{V^2}{\bar{\mu}g} \sin\theta_p + VT_f \cos\theta_p, \\ \frac{V^2}{\bar{\mu}g} - \tfrac{1}{2} gT_f^2 \cos\alpha &= \frac{V^2}{\bar{\mu}g} \cos\theta_p - VT_f \sin\theta_p. \end{aligned} \tag{6}$$

where $T_f = T_h - T_p$ is the *time-of-fall*. Equations (6) can be regarded as a pair of simultaneous equations for the two unknowns, T_f and θ.

On squaring both members of each of the equations of (6) above and adding corresponding members of the resulting equations it is found that the angle θ_p drops out, leaving the relation

$$\frac{g^2}{4V^2} T_f^4 - \left(1 + \frac{\cos\alpha}{\bar{\mu}} + \frac{gT_c \sin\alpha}{V}\right) T_f^2 + T_c^2 = 0. \tag{7}$$

This equation is of degree two in the quantity T_f^2, and its solution is given in equation (8).

Of the four theoretically possible times-of-fall obtained by taking the square root of the right-hand member of equation (8) the one desired in bomb tossing is the smallest positive one [equation (9)].

$$T_f^2 = \frac{2V^2}{g^2}\left[1 + \frac{\cos\alpha}{\bar{\mu}} + \frac{gT_c \sin\alpha}{V} \pm \sqrt{\left(1 + \frac{\cos\alpha}{\bar{\mu}} + \frac{gT_c \sin\alpha}{V}\right)^2 - \frac{g^2 T_c^2}{V^2}}\right]. \tag{8}$$

$$T_f = \frac{V\sqrt{2}}{g} \sqrt{1 + \frac{\cos\alpha}{\bar{\mu}} + \frac{gT_c \sin\alpha}{V} - \left(1 + \frac{\cos\alpha}{\bar{\mu}} + \frac{gT_c \sin\alpha}{V}\right)^2 - \frac{g^2 T_c^2}{V^2}}$$

$$= \frac{V}{g}\left[\sqrt{1 + \frac{\cos\alpha}{\bar{\mu}} + \frac{gT_c}{V}(1 + \sin\alpha)} - \sqrt{1 + \frac{\cos\alpha}{\bar{\mu}} - \frac{gT_c}{V}(1 - \sin\alpha)}\right]. \tag{9}$$

[redacted]

It is now desired to solve equation (6) for θ_p. This can be done in a variety of ways, of which the following is adopted here.

Let $$\omega = \cot\frac{\theta_p}{2} = \frac{\sin\theta_p}{1-\cos\theta_p}.$$

If both members of the first of equations (6) be multiplied by $(1 - \cos\theta_p)$, both members of the second of equations (6) by $\sin\theta_p$, and the resulting equations added member by member, the equation (10) is obtained.

$$(VT_c - \tfrac{1}{2}gT_f^2\sin\alpha)(1-\cos\theta_p) - \tfrac{1}{2}gT_f^2\cos\alpha\sin\theta_p = VT_f(\cos\theta_p - 1). \quad (10)$$

Expressed in terms of ω, equation (10) is

$$VT_c - \tfrac{1}{2}gT_f^2\sin\alpha - \tfrac{1}{2}gT_f^2\omega\cos\alpha + VT_f = 0,$$

from which it follows that

$$\omega = \frac{VT_c + VT_f - \tfrac{1}{2}gT_f^2\sin\alpha}{\tfrac{1}{2}gT_f^2\cos\alpha}. \quad (11)$$

The right-hand member will now be expressed in a form free from T_f by making use of equation (9). After some algebraic reductions the following formula for ω is obtained.

$$\omega = \frac{V}{gT_c\cos\alpha}\left[1 + \frac{\cos\alpha}{\bar{\mu}} + \sqrt{1 + \frac{\cos\alpha}{\bar{\mu}} + \frac{gT_c}{V}(1+\sin\alpha)} + \sqrt{1 + \frac{\cos\alpha}{\bar{\mu}} - \frac{gT_c}{V}(1-\sin\alpha)} + \sqrt{\left(1 + \frac{\cos\alpha}{\bar{\mu}} + \frac{gT_c}{V}(1+\sin\alpha)\right)\left(1 + \frac{\cos\alpha}{\bar{\mu}} - \frac{gT_c}{V}(1-\sin\alpha)\right)}\right]. \quad (12)$$

But

$$\tan\theta_p/2 = \frac{1}{\omega},$$

so that

$$\theta_p = 2 \text{ arc tan } \frac{1}{\omega}, \quad (13)$$

and, from equation (4) of Chapter 2

$$T_{pe} = \frac{2V}{g\bar{\mu}} \text{ arc tan } \frac{1}{\omega}.$$

Further, defining ψ_e by

$$\psi_e = \frac{\bar{K} + \sqrt{\bar{K}^2 - \bar{K}}}{T_c} T_{pe}, \quad (14)$$

it follows that

$$\psi_e = \frac{2V}{gT_c} \cdot \frac{\bar{K} + \sqrt{\bar{K}^2 - \bar{K}}}{\bar{\mu}} \text{ arc tan } \frac{1}{\omega}. \quad (15)$$

Equations (12) and (13) provide the exact solution of equation (13), Chapter 2. Equations (12) and (15) provide a means for calculating values of the ψ_e function.

6.1.4 Discussion of the Exact Solution

It was noted in Section 6.1.3 that four times-of-fall can be computed from equation (8). To each of these corresponds a parabolic arc followed by the bomb after its release. In Figure 2 are shown these four arcs for a typical case: $\alpha = 20$ degrees, $\bar{K} = 4$, $T_c/V = 0.04$. In constructing Figure 2 it was assumed that the path of the airplane during pull-up is an arc of a circle. The parabolic arcs are tangent to the pull-up circle at the four points of release P_1, P_2, P_3, P_4. The point at which pull-up is commenced is labeled P_0. The tangent line at this point is the collision course. The parabola tangent at P_1 is the one used in bomb tossing at present; it has the shortest flight time to the target.

The parabola tangent at P_2 corresponds to a larger pull-up angle so that the projectile is lobbed onto the target after the fashion of a mortar shell. It will be noted that in the case of the lobbing trajectory, small errors in release time or pull-up angle will cause large errors at the target. For the trajectory tangent at P_1, which departs relatively little from the collision course, the impact point will be relatively insensitive to small errors in release time.

The two parabolas P_3 and P_4 correspond to negative values of T_f. They would be obtained if the airplane were to climb up the collision course away from the target, and pull away from the collision course in a clockwise sense around the circle until the release point were reached. This type of bombing maneuver is of theoretical interest only.

6.1.5 Calculation and Graphs of ψ_e

In calculating values of ψ_e, equation (12) is used to calculate ω first. Having ω, equation (15) yields the value of ψ_e. It was in this way that Table 6 was computed. Entries not given in the table correspond to complex values of ω; i.e., values of the parameters for which

$$\frac{gT_c}{V}(1-\sin\alpha) > 1 + \frac{\cos\alpha}{\bar{\mu}}. \quad (16)$$

For such values it is impossible to obtain a hit, however perfect the bomb director mechanism.

In Figure 3 are shown graphs of ψ_e for various values of T_c/V. Above the dashed curve, equation (16) is fulfilled. All trajectories used in bomb tossing up to the end of the war correspond to values of α and ψ_e which fall below this curve.

Maximum Slant Range. In order to obtain a

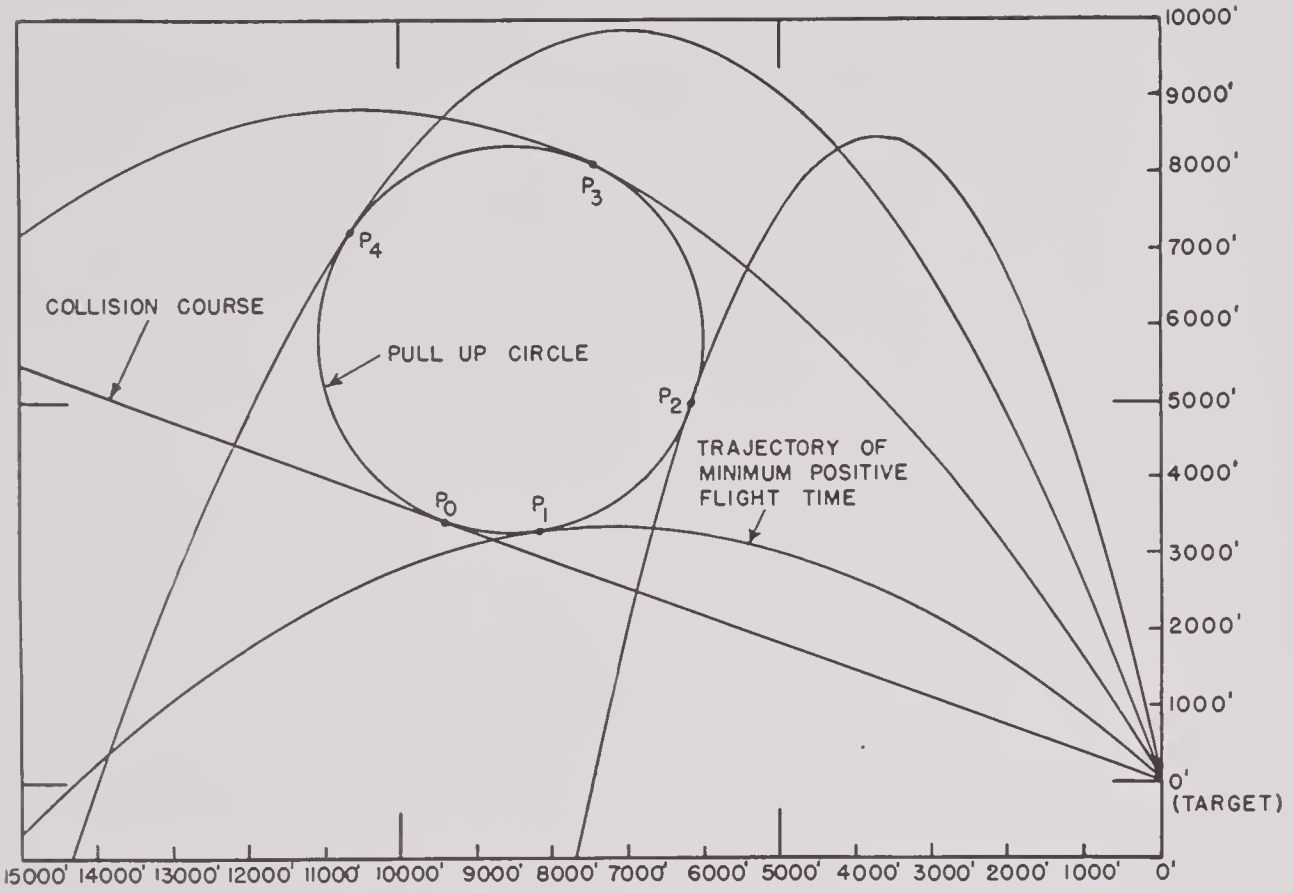

FIGURE 2. Four theoretically possible bomb trajectories corresponding to typical conditions $\alpha = 20$ degrees, $\bar{K} = 4$, $T_c/V = 0.04$. (Airplane is assumed to follow collision course to P_0, then pull up in circular arc, releasing bomb at P_1, P_2, P_3, or P_4. P_1 is usual release point; P_3 and P_4 correspond to negative pull-up time.)

TABLE 6. Values of ψ_e, $\bar{K} = 3$.

α \ $\frac{T_c}{V}$	0.00	0.01	0.02	0.03	0.04	0.05	0.06	0.07	0.08	0.09	0.10
0°	1.00000	1.00793	1.03398	1.08753	1.20513						
10°	0.99215	0.97241	0.97645	0.99720	1.04311	1.14843					
20°	0.93341	0.90626	0.89324	0.89156	0.90348	0.93189	0.99706				
30°	0.85339	0.81396	0.78860	0.77326	0.76627	0.76741	0.77813	0.80281	0.85746		
40°	0.74695	0.70000	0.66782	0.64494	0.62872	0.61775	0.61137	0.60942	0.61234	0.62141	0.64004
50°	0.61896	0.57029	0.53656	0.51155	0.49240	0.47736	0.46551	0.45621	0.44909	0.44392	0.44059
60°	0.47481	0.43057	0.40019	0.37753	0.35977	0.34539	0.33348	0.32346	0.31492	0.30760	0.30127
70°	0.32004	0.28630	0.26325	0.24626	0.23291	0.22203	0.21293	0.20515	0.19841	0.19249	0.18724
80°	0.16007	0.14145	0.12912	0.12005	0.11280	0.10717	0.10233	0.09819	0.09459	0.09142	0.08859
90°	0.00000	0.00000	0.00000	0.00000	0.00000	0.00000	0.00000	0.00000	0.00000	0.00000	0.00000

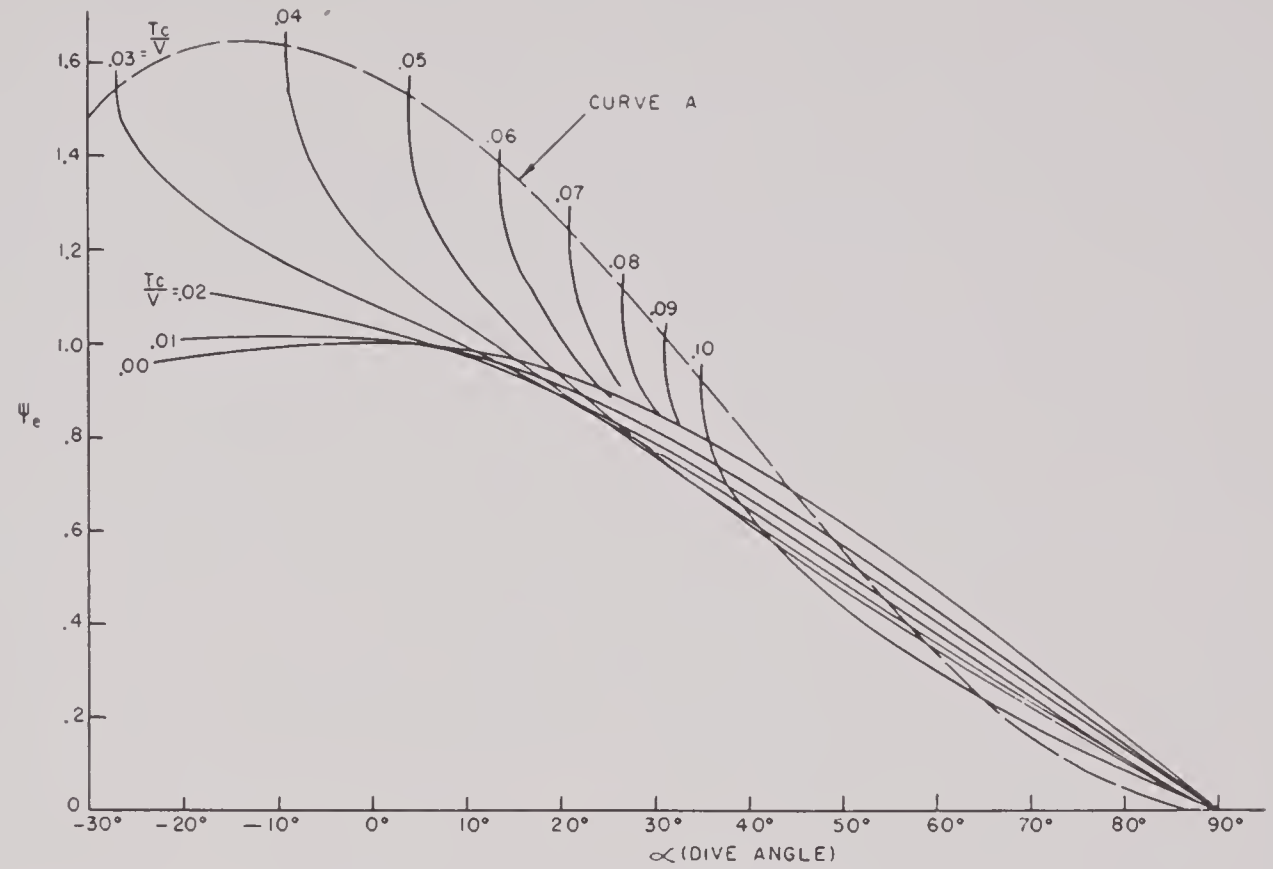

FIGURE 3. ψ_e versus α for different values of T_c/V, $\bar{K}$ being constant (=3). When parameter values correspond to points above dashed curve A, a hit is impossible, however perfect bomb director mechanism.

$$\text{Curve } A \text{ corresponds to } \frac{T_c}{V} = \frac{\bar{K}}{g\,(\bar{K} - \cos\alpha)\,(1 - \sin\alpha)}$$

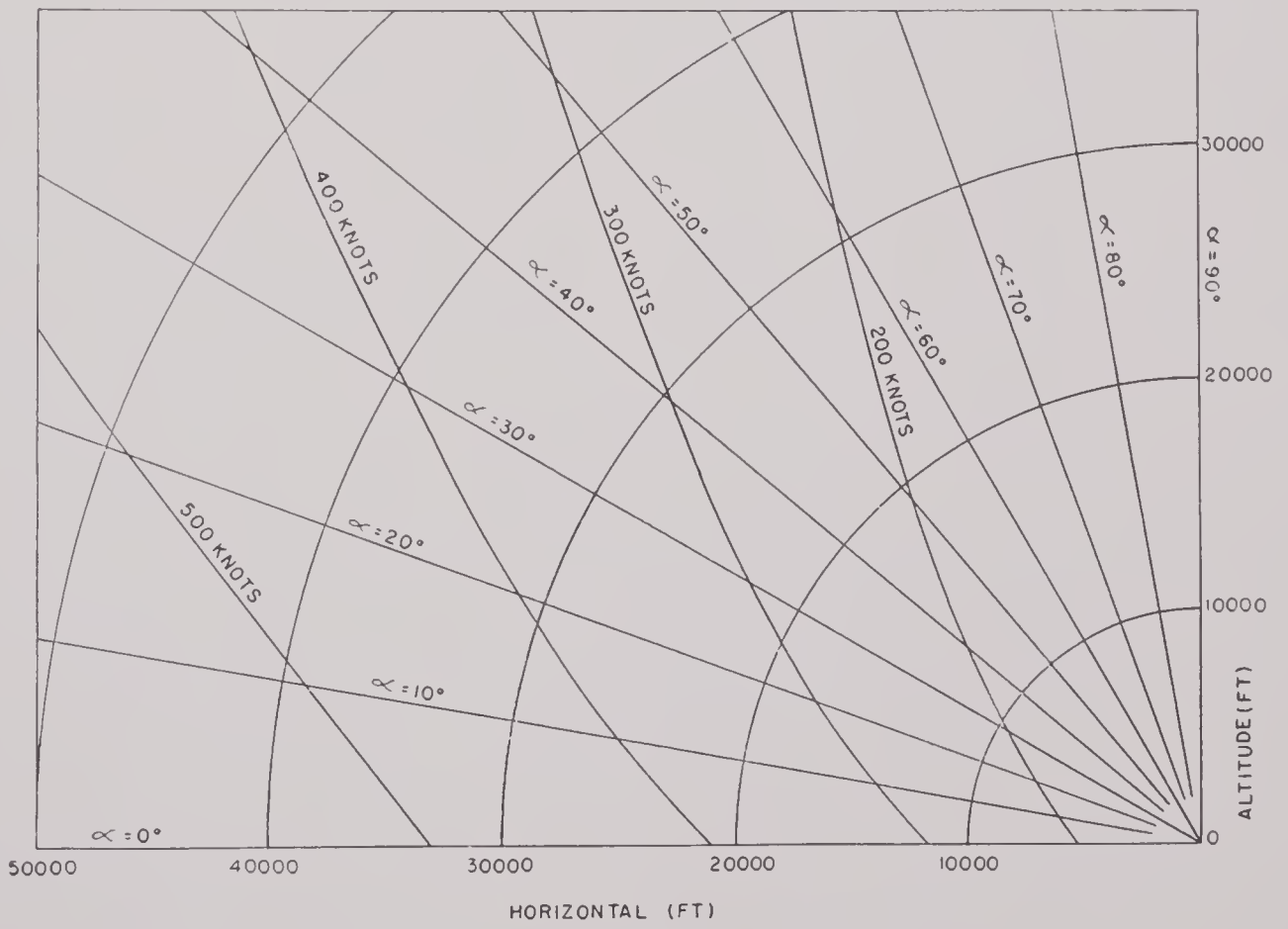

FIGURE 4. Curves of theoretical maximum attainable ranges in toss bombing at different aircraft velocities. $\bar{K} = 3$. (For theory see text, Section 6.1.5.)

formula for the maximum slant range, S_m, it is only necessary to make T_c in equation (16) as large as possible without having this relation fulfilled; that is

$$T_c = \frac{V\left(1 + \frac{\cos \alpha}{\bar{\mu}}\right)}{g\ (1 - \sin \alpha)} .$$

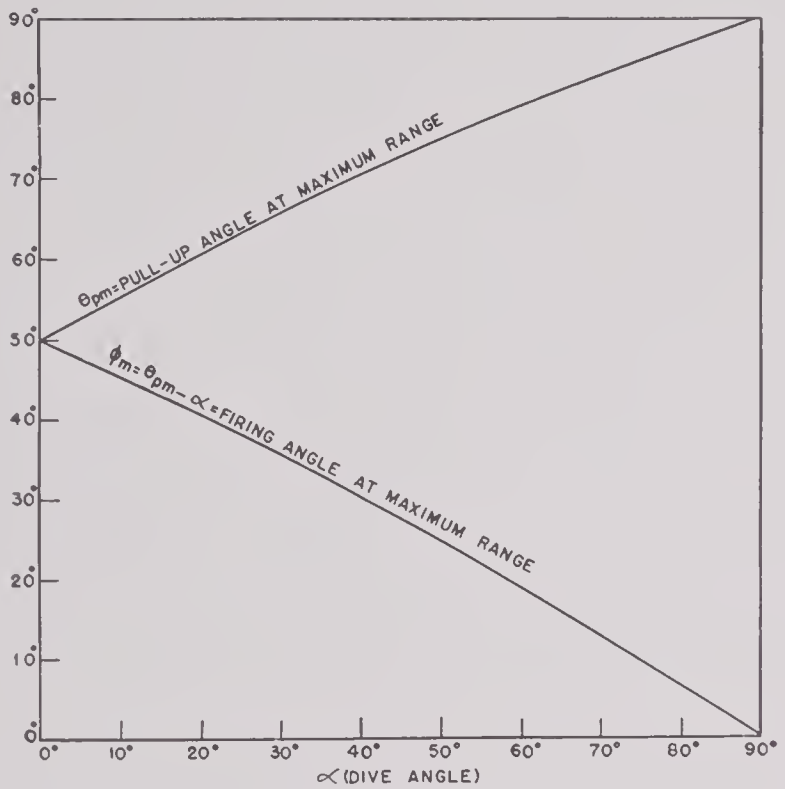

FIGURE 5. θ_{pm} and ϕ_m versus α. θ_{pm} is pull-up angle corresponding to theoretical maximum range of Figure 4.

Since slant range is given by $S = VT_c$, it follows that

$$S_m = \frac{V^2\left(1 + \frac{\cos \alpha}{\bar{\mu}}\right)}{g\ (1 - \sin \alpha)} . \qquad (17)$$

Figure 4, based on equation (17), provides a graphical means for determining the maximum slant range for the case $\bar{K} = 3$. For instance, with $\bar{K} = 3$, $\alpha = 20$ degrees, $V = 300$ knots, Figure 4 shows that $S_m = 17{,}600$ feet. This is, of course, the theoretical maximum slant range; in practice, instrumental errors, air resistance, etc., operate to reduce this maximum materially.

It is well known that for a gun firing down a hill having a declination α with respect to the horizontal, the maximum slant range is obtained if the gun is elevated at the angle $(45 - \alpha/2)$ degrees. In Figure 5 is shown the graph of the pull-up angle θ_{pm} against dive angle which, for $\bar{K} = 3$, secures the maximum range. The actual firing angle $\theta_{pm} - \alpha$ is somewhat greater than $(45 - \alpha/2)$ degrees because in bomb tossing the maximum range is referred to the beginning of pull-up, while in the case of firing from a fixed gun the range is referred to the point of release.

6.2 PULL-UP ACCELERATION

6.2.1 The Four Types of Acceleration

In Section 6.1 no special form was assumed for the pull-up acceleration. Observed pull-up accelerations are of four types as illustrated in Figure 6.

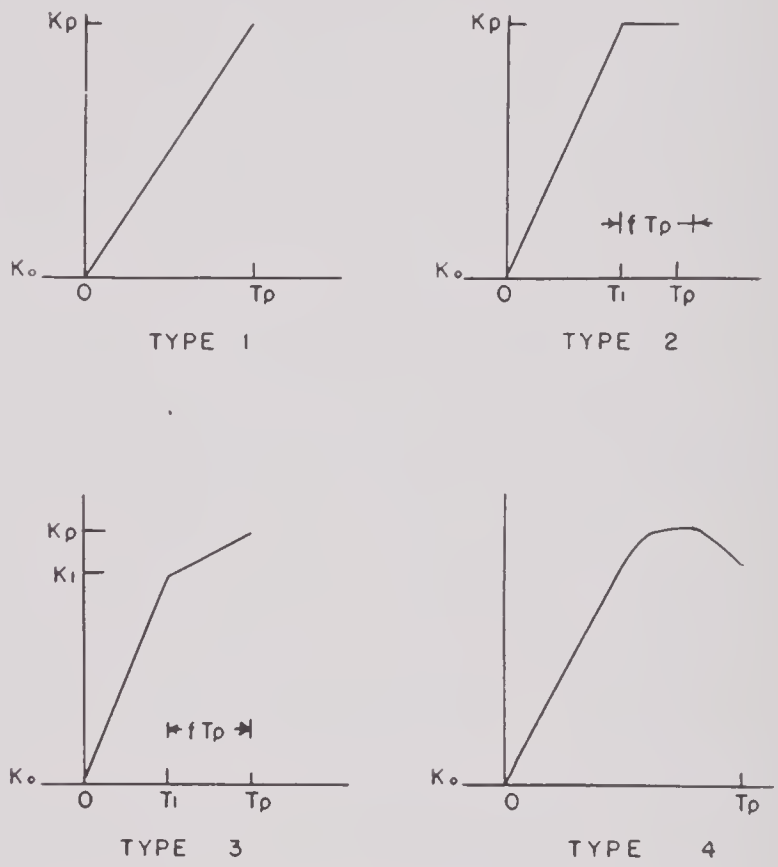

FIGURE 6. Four main modes of variation of pull-up acceleration with time. (Based on photographic records of accelerometer response.)

Some idea of the relative frequency of occurrence of each of these types is given in Table 7.[34]

TABLE 7. Summary of acceleration types experienced during pull-up.

Airplane	Total number of records	Percentage of total Type 1	Type 2	Type 3	Type 4
SB2C	36	33	22	45	0
TBM	28	18	54	14	14
Total	64	Average 27	36	31	6

The type 4 curves which have been observed are usually of such a nature that they may be reasonably well approximated by a type 2 curve. For this reason, and because pull-up acceleration of type

2 is most frequent, the theory will be developed for that type. (Type 3 is considered in reference 34.) While it is true that the exact solution in Section 6.1.3 applies in the case to be considered here, it is worth while to develop this case independently since a different function of K than the one in equation (15) is indicated as possibly desirable. (Also, a different ψ function will result, depending on the type of the acceleration function.[93])

6.2.2 The Condition for a Hit

The number K is assumed to be given by the pair of expressions

$$\begin{aligned} K &= pt + \cos\alpha \qquad 0 \leq t \leq T_1 \\ K &= K_1 = pT_1 + \cos\alpha \qquad T_1 \leq t \end{aligned}$$

where p is the constant rate of increase of K during the first phase of pull-up. It follows that

$$\begin{aligned} \mu &= pt \qquad 0 \leq t \leq T_1 \\ \mu &= \mu_1 = pT_1 \qquad T_1 \leq t. \end{aligned} \tag{18}$$

From equation (2), Chapter 2, and equation (18), the angle θ is found to be given by

$$\begin{aligned} \theta &= \frac{pgt^2}{2V} \\ \theta &= \frac{pgT_1}{V}\left(t - \frac{T_1}{2}\right) \end{aligned} \tag{19}$$

where

$$0 \leq t \leq T_1,\ T_1 \leq t.$$

It then follows that the components of velocity are

$$\dot{x} = V\cos\frac{pgt^2}{2V},\quad \dot{y} = V\sin\frac{pgt^2}{2V} \qquad 0 \leq t \leq T_1, \tag{20}$$

and

$$\begin{cases} \dot{x} = V\cos\dfrac{pgT_1}{V}\left(t - \dfrac{T_1}{2}\right) \\ \dot{y} = V\sin\dfrac{pgT_1}{V}\left(t - \dfrac{T_1}{2}\right) \end{cases} T_1 \leq t. \tag{21}$$

It is necessary to integrate these components of velocity in order to get the coordinates during pull-up. In order to carry out the integration by means of elementary functions the approximations

$$\cos\theta \cong 1 - \theta^2/2;\ \sin\theta \cong \theta$$

are made for $0 \leq t \leq T_1$. No approximations are necessary for $t = T_1$. In this way the equations (22) and (23) are obtained.

$$x = Vt - \frac{p^2g^2t^5}{40V},\ y = \frac{pgt^3}{6} \qquad 0 \leq t \leq T_1. \tag{22}$$

$$x = VT_1 - \frac{p^2g^2T_1^5}{40V} + \frac{2V^2}{pgT_1}\sin\frac{pgT_1(t - T_1)}{2V}\cos\frac{pgT_1t}{2V},$$
$$T_1 \leq t. \tag{23}$$

$$y = \frac{pgT_1^3}{6} + \frac{2V^2}{pgT_1}\sin\frac{pgT_1(t - T)}{2V}\sin\frac{pgT_1t}{2V}.$$

From equation (9), Chapter 2, and by elimination of the time-of-fall $T_f = T_h - T_p$, the condition for a hit is obtained in the form

$$VT_c = \frac{x_p\cos\alpha + y_p\sin\alpha}{\cos\alpha} + \frac{\dot{x}_p\cos\alpha + \dot{y}_p\sin\alpha}{g\cos^2\alpha}\cdot$$
$$(\dot{y}_p + \sqrt{\dot{y}_p^2 + 2gy_p\cos\alpha}). \tag{24}$$

Expressions for $\dot{x}_p$, $\dot{y}_p$, x_p, and y_p may now be placed in equation (24) which then becomes an equation for the determination of T_p.

The case $T_p = T_1$. If the bomb is released during the phase of pull-up in which the acceleration is increasing, equations (20) and (22) are used to get the components of velocity and the coordinates at release. At the same time the quantity p may be eliminated by use of the relation $pT_p = K_p - \cos\alpha$, where K_p is the value of K at release, so that

$$\dot{x}_p = V\cos\frac{pgT_p^2}{2V} \cong V - \frac{g^2T_p^2(K_p - \cos\alpha)^2}{8V},$$

$$\dot{y}_p = V\sin\frac{pgT_p^2}{2V} \cong \frac{gT_p(K_p - \cos\alpha)}{2}.$$

$$x_p = VT_p - \frac{p^2g^2T_p^5}{40V} = VT_p - \frac{g^2T_p^3}{40V}(K_p - \cos\alpha)^2,$$

$$y_p = \frac{pgT_p^2}{6} = \frac{gT_p^2(K_p - \cos\alpha)}{6}.$$

When these expressions are placed in (24), an equation of degree three in T_p results. Omitting the term in T_p^3, this equation is

$$K_p - \tfrac{1}{3}\cos\alpha + \sqrt{(K_p - \cos\alpha)(K_p + \tfrac{1}{3}\cos\alpha)} \times \frac{gT_p^2(K_p - \cos\alpha)\tan\alpha}{2V}$$
$$+ [K_p + \cos\alpha + \sqrt{(K_p - \cos\alpha)(K_p + \tfrac{1}{3}\cos\alpha)}]\,T_p - 2T_c\cos\alpha = 0. \tag{25}$$

If, for brevity, equation (25) is regarded as

$$AT_p^2 + \beta T_p - 2T_c\cos\alpha = 0,$$

the solution for T_p can be put into the form

$$T_p = \frac{4\,T_c \cos\alpha}{\beta + \sqrt{\beta^2 + 8A\,T_c \cos\alpha}},$$

or

$$T_p = \frac{2\,T_c \cos\alpha}{K_p + \cos\alpha + \sqrt{(K_p - \cos\alpha)\,(K_p + \tfrac{1}{3}\cos\alpha)}} \times \frac{2}{1 + \sqrt{1 + 2\beta'}}, \tag{26}$$

where

$$\beta' = \frac{4AT_c\cos\alpha}{\beta^2} = 2g\frac{T_c}{V}(K_p - \cos\alpha)\sin\alpha \times \frac{K_p - \tfrac{1}{3}\cos\alpha + \sqrt{(K_p - \cos\alpha)\,(K_p + \tfrac{1}{3}\cos\alpha)}}{[K_p + \cos\alpha + \sqrt{K_p - \cos\alpha)\,(K_p + \tfrac{1}{3}\cos\alpha)}]^2}.$$

The relation between K_p and $\bar{K}$ is given by

$$\bar{K} = \frac{1}{T_p}\int_0^{T_p} K\,dt = \frac{pT_p}{2} + \cos\alpha = \tfrac{1}{2}(K_p + \cos\alpha)$$

or

$$K_p = 2\bar{K} - \cos\alpha.$$

On replacing K_p by $2\bar{K} - \cos\alpha$, a formula is obtained which closely resembles that for T_{p0} in equation (18) of Chapter 2. The slight differences are due to the somewhat different methods used for the approximate computation of the integrals for x and y from the expressions for $\dot{x}$ and $\dot{y}$.

It is easily verified, using the relation

$$K = pt + \cos\alpha,$$

that

$$2p\int_0^{T_p}\left(K + K\sqrt{\frac{K - \cos\alpha}{K + \tfrac{1}{3}\cos\alpha}}\right)dt = (K_p - \cos\alpha)\times [K_p + \cos\alpha + \sqrt{(K_p - \cos\alpha)\,(K_p + \tfrac{1}{3}\cos\alpha)}]. \tag{27}$$

By virtue of equation (27) it is possible to write equation (26) in the form

$$T_c = \frac{1 + \sqrt{1 + 2\beta'}}{2\cos\alpha}\int_0^{T_p}\left(K + K\sqrt{\frac{K - \cos\alpha}{K + \tfrac{1}{3}\cos\alpha}}\right)dt. \tag{28}$$

This equation suggests the use of

$$K + K\sqrt{\frac{K - \cos\bar{\alpha}}{K + \tfrac{1}{3}\cos\bar{\alpha}}},$$

where $\bar{\alpha}$ is a mean value of the dive angles expected to be used, instead of $K + \sqrt{K^2 - K}$ as the accelerometer function, with, of course, ψ defined as follows:

$$\psi = \frac{2\cos\alpha}{1 + \sqrt{1 + 2\beta}} \cdot \frac{1 + \sqrt{\dfrac{K - \cos\bar{\alpha}}{K + \tfrac{1}{3}\cos\bar{\alpha}}}}{1 + \sqrt{\dfrac{K - \cos\alpha}{K + \tfrac{1}{3}\cos\alpha}}}.$$

6.3 THEORY OF INSTRUMENTAL DESIGN

6.3.1 Selection of T_c/V for ψ

In designing the gyro potentiometer card it is necessary to select a specific set of values of the ψ function, that is, the set of values corresponding to a particular value of T_c/V. The particular value of T_c/V selected should correspond to a mean of the values of range and velocity at which the bomb director is to be used, taking into account the fact that the tendency is to conduct bomb tossing maneuvers at approximately the maximum operational range.

Figure 11 in Chapter 2 shows the theoretical maximum ranges at which a bomb released by the Model 0 bomb director would fall within 100 feet of the target. When the loci of points for constant T_c/V values were superposed on this curve, it was found that the locus for $T_c/V = 0.028$ represented a good average for the operational conditions expected. Accordingly this value was chosen for the ψ_1 design of the Model 1.

The theoretical maximum ranges for the Model 1 are shown in Figure 7. By comparison with Figure 11, Chapter 2, it may be seen that these ranges are 33 to 60 per cent greater than for the Model 0.[79]

In Figure 8 are shown graphs of ψ_1 against α for $T_c/V = 0.014$, 0.028, and 0.042. The ψ card is designed so that the effective instrumental ψ fits the theoretical ψ for $T_c/V = 0.028$ between $\alpha = 20$ degrees and $\alpha = 70$ degrees. Below 20 degrees the theoretical ψ functions separate widely. For this reason, the design ψ is the one indicated by the dotted line from $\alpha = 10$ degrees to $\alpha = 20$ degrees, and is taken as 1.0 from $\alpha = 0$ degrees to $\alpha = 10$ degrees.[57]

It is necessary, then, to design a potential divider which, by equation (25), will provide a voltage v_α given by

$$v_\alpha = v_0\,\frac{1 - \exp[-T_c\psi(\alpha)/20]}{1 - \exp(-T_c/20)}. \tag{29}$$

Values of v_α obtained from equation (29) using for $\psi(\alpha)$ the values of ψ_1 corresponding to $T_c/V = 0.028$ and $V = 500$ feet/second, and based on $v_0 = 150$ volts, are shown in Table 8.

TABLE 8. ψ card voltages of various dive angles.

Dive angle	0°	10°	20°	30°	40°	50°	60°	75°
$\psi(\alpha)$	1.0	1.0	0.88	0.77	0.64	0.51	0.38	0.18
v_α (volts)	150	150	137	124	108	90	70	36

$v_0 = 150$ volts $T_c = 14$ seconds $V = 500$ ft/sec $T_c/V = 0.028$

6.3.2 Variations from Selected T_c/V

The voltages given in Table 8 are those required from the gyro card in order to obtain an instrumental ψ equal to the design ψ for $T_c/V = 0.028$. It is necessary to consider how to correct these values when T_c/V has other values. The rate at which charge accumulates on a capacitor decreases as the accumulated charge becomes greater. This means that for larger values of T_c, less charge will accumulate than would be the case if the rate of accumulating charge were constant. Consequently, for large

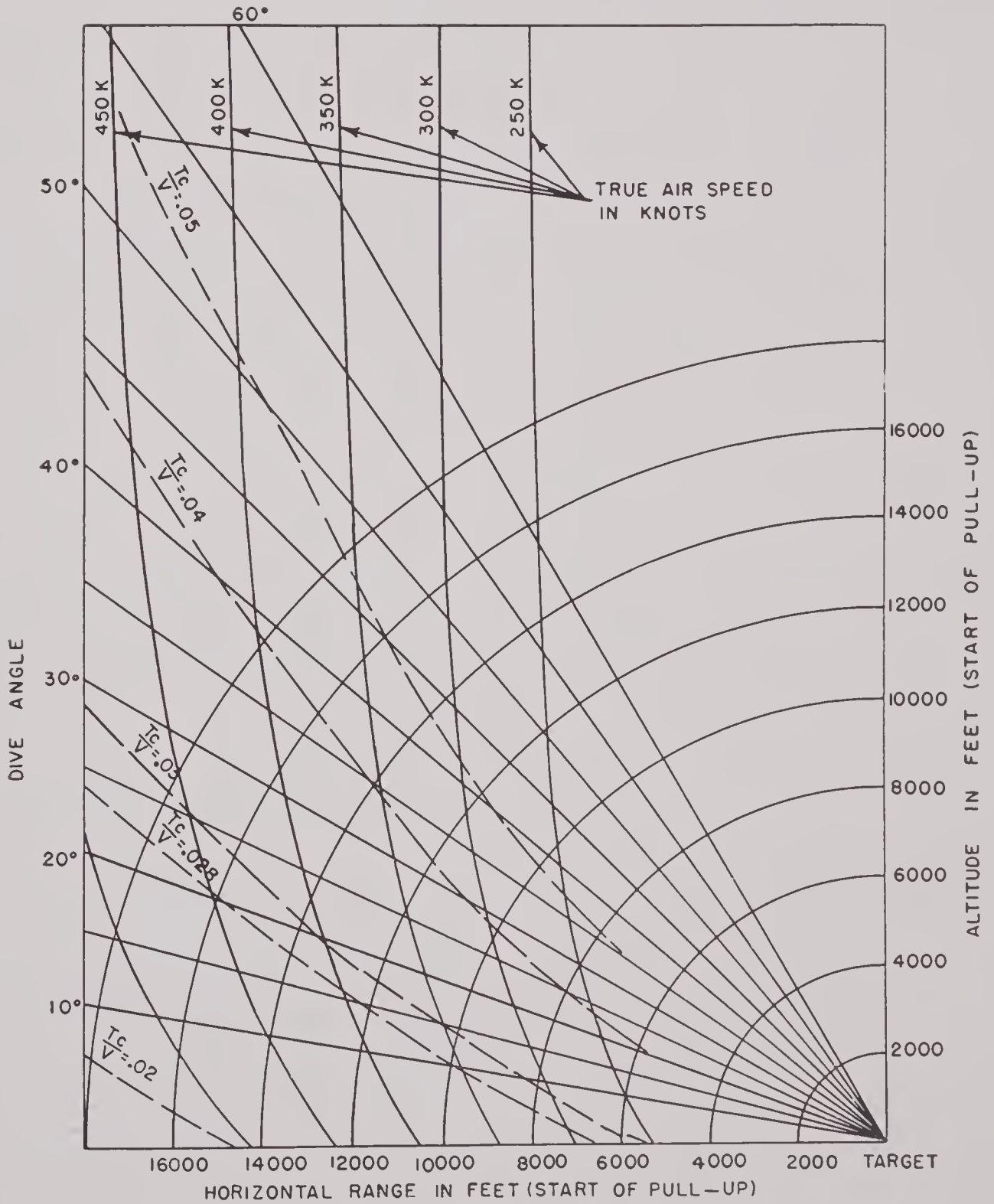

FIGURE 7. Curves of maximum allowable ranges (for different aircraft velocities) corresponding to horizontal errors of less than 100 feet for bomb director Mark 1 Model 1 (ψ_1 function).

[redacted]

values of T_c the effective ψ is smaller, and for smaller values of T_c it is larger. Thus, this nonlinear charging characteristic automatically provides some compensation for the variation of T_c/V from 0.028.

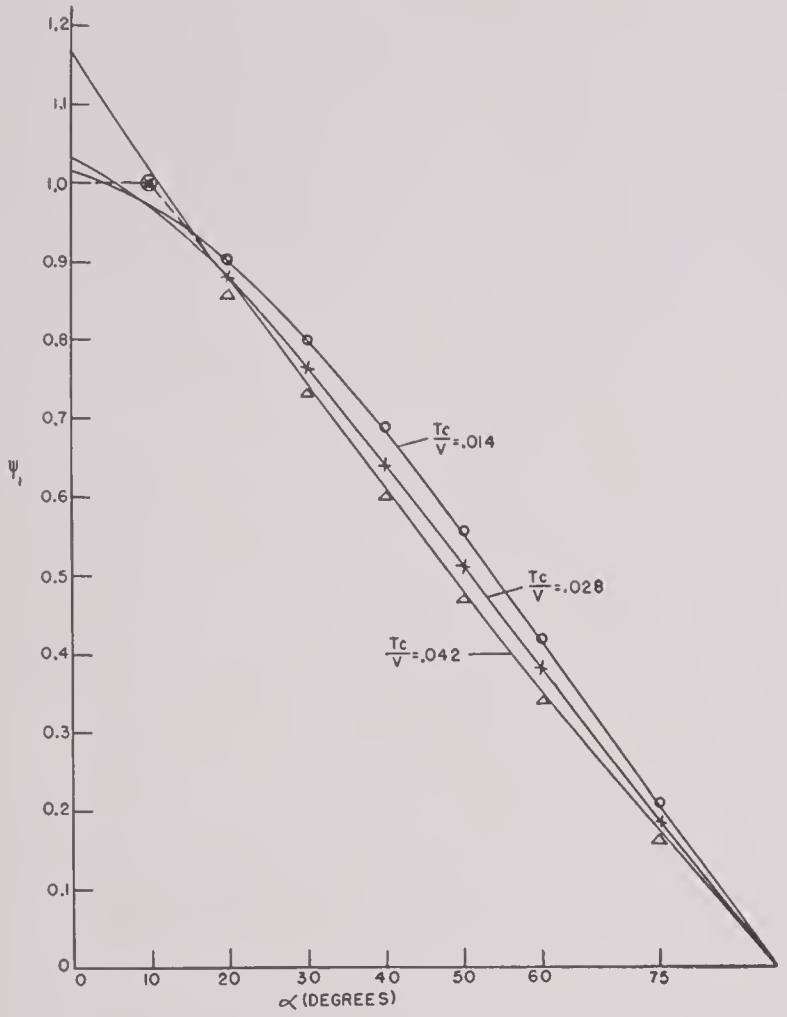

FIGURE 8. ψ_1 versus α for $T_c/V = 0.014$, 0.028, and 0.042, $\bar{K}$ being constant (= 3). Solid lines are theoretical values; points ($\odot$, $\times$, $\triangle$) are corresponding instrumental values obtained when ψ_1 card is designed to fit for $T_c/V = 0.028$ and $V = 500$ feet/second. Dashed lines are explained in text.

TABLE 9. ψ card voltage variation with speed.

Velocity (ft/sec)	T_c(sec) for $T_c/V = 0.028$	$V_{40°}$ (volts)
300	8.4	103.6
400	11.2	105.8
500	14.0	108.0
600	16.8	110.2
700	19.6	112.3
800	22.4	114.3

If V deviates from 500 feet/second, it is still desired that the ψ provided by the instrument agree with the theoretical ψ for $T_c/V = 0.028$ and over a considerable range of dive angle. In order to secure this adjustment, means must be provided to change v_α in accordance with variations in V. The voltage required at $\alpha = 40$ degrees for different velocities is shown in Table 9.

These values are found from (29) by taking $\psi(\alpha) = 0.643$, $T_c = 0.028V$, $v_0 = 150$ and calculating v_α for various values of V. Knowing these values of v_α it is possible to calculate the effective ψ for the different velocities. Figure 9 shows the results of such calculations for the extreme cases of $V = 300$ feet/second and 800 feet/second. For easy comparison the values of ψ for $V = 500$ feet/second are included.[57]

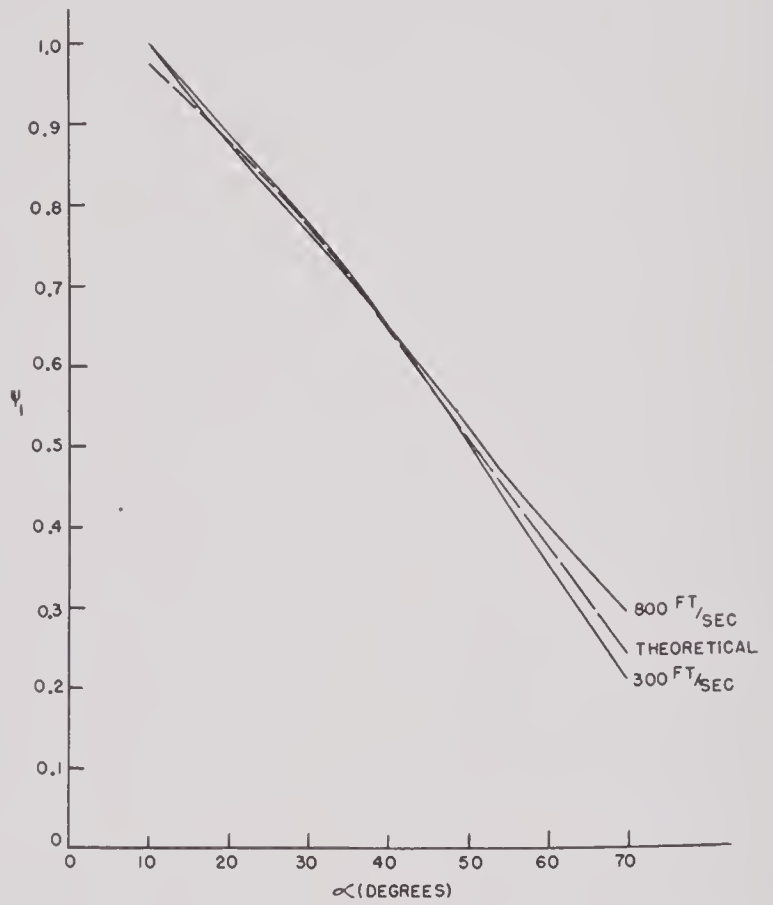

FIGURE 9. Curves showing extent of variation of instrumental ψ_1 functions between extremes of velocity, when ψ_1 card is designed to fit theoretical (dashed) curve at velocity 500 feet/second, T_c/V held constant at 0.028.

6.3.3 Physical Dimensions of ψ Card

In Figure 10 the voltage v_α as given in Table 9 is plotted against α. The curve thus obtained is approximated to by three line segments as shown, which correspond to the functional values of the curve within ½ per cent up to 70 degrees. It is therefore possible to make a potentiometer card with three different linear sections which will give an excellent fit. From the same figure the volts per degree required for each of the three linear resistance strips can be determined. See Figure 11 for dimensions.

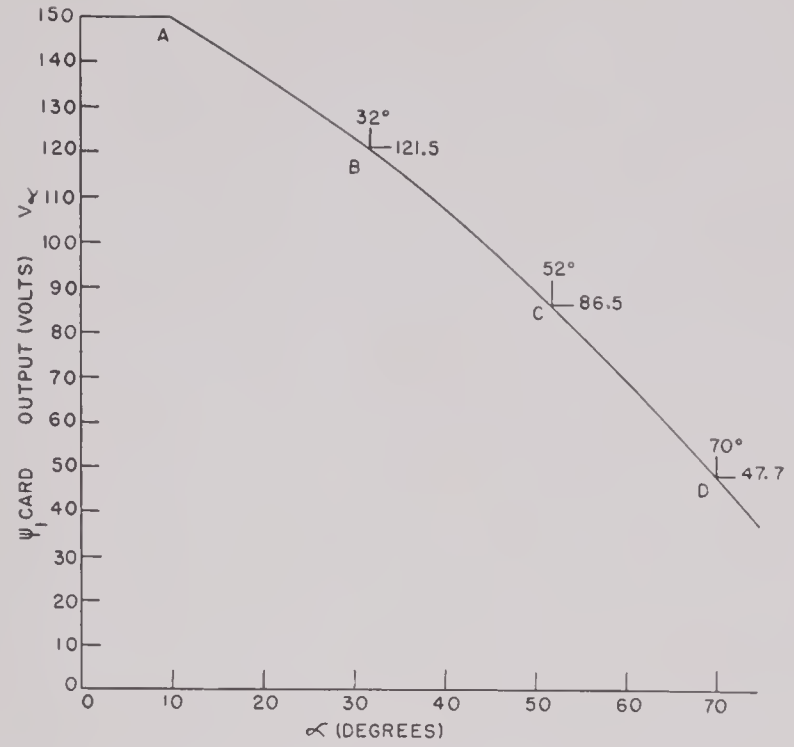

FIGURE 10. Curve of voltage V_α versus α. Instrumentally this curve is approximated by three straight line segments joining consecutive points A, B, C, and D.

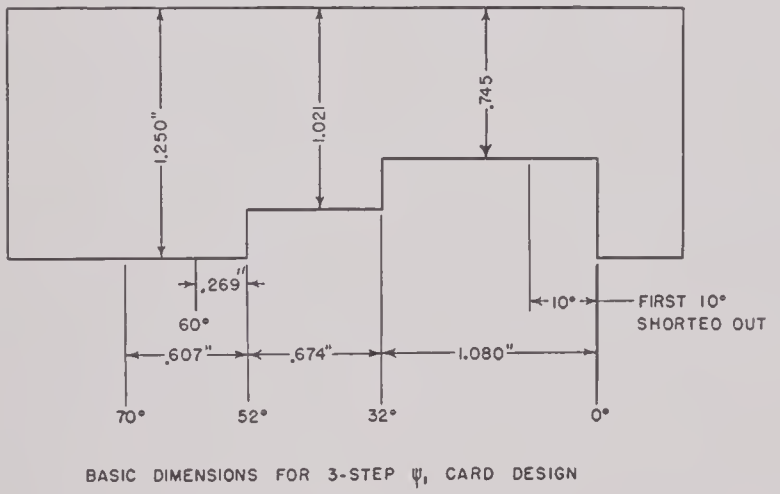

FIGURE 11. Basic dimensions for three-step ψ_1 card design.

6.3.4 Stick-Length Offset

As mentioned in Section 2.1.6, the stick-length offset is an adjustment by means of which the range can be reduced by an amount corresponding to a shortening of the input time T_c by the amount ΔT_c. In the Model 0 bomb director this was done by biasing both capacitors C_1 and C_2 by a voltage E selected by a setting of the stick-length offset dial. In the Model 1 equipment the circuit is arranged so that the second capacitor only is biased. This results in the decrease ΔT_c for the Model 0 director, being approximately twice as great as that obtained from the Model 1 circuit for the same biasing voltage. In the following discussion the Model 1 equipment, only, is considered.

The expression ΔT_c can be obtained from equation (20) of Chapter 2 for v_1 and equation (22) of Chapter 2 written in the form

$$v_2 = (v_0 - E)\left[1 - e^{-\frac{1}{c_2}\int_0^{T_p}\frac{dt}{R}}\right] \qquad (30)$$

together with the condition for firing of the thyratron, $v_2 = v_1 - E$, and the relation

$$(T_c - \Delta T_c)\,\psi_1 = 10\int_0^{T_p}\frac{dt}{R}. \qquad (31)$$

The result of eliminating the integral between the two above equations can be written

$$(T_c - \Delta T_c)\,\psi_1 = -20\ln\left(1 - \frac{v_2}{v_0 - E}\right).$$

Replacing v_2 in this equation by $v_1 - E$ and solving for ΔT_c yields the formula

$$\Delta T_c = T_c - \frac{20}{\psi_1}\ln\frac{1 - (E/v_0)}{1 - (v_1/v_0)}. \qquad (32)$$

Let $\overline{\Delta T_c}$ represent the value of ΔT_c corresponding to E on a bench test for which $\alpha = 0$ degree, $\psi_1 = 1$, and $v_\alpha = v_0$. It then follows that

$$\overline{\Delta T_c} = -20\ln\left(1 - \frac{E}{v_0}\right). \qquad (33)$$

Since $E << v_0$, this relation shows that $\overline{\Delta T_c}$ is nearly proportional to E. By means of equation (33) and equation (20), Chapter 2, equation (32) can be put into the form

$$\Delta T_c = \frac{\overline{\Delta T_c}}{\psi_1} + T_c + \frac{20}{\psi_1}\ln\left[1 - \frac{v_\alpha(1 - e^{-T_c/20})}{v_0}\right]. \qquad (34)$$

Figures 12A and 12B exhibit graphically the relation (34) between ΔT_c and $\overline{\Delta T_c}$ for the values of the parameters indicated.

6.4 ERRORS AND INSTRUMENTAL ADJUSTMENTS

6.4.1 Types of Error

For convenience, the problems to be studied in Section 6.4.1 are classified under four main headings, as follows:

1. Errors in the ψ function.
   a. Range limitations due to the use of ψ_0.
   b. Range limitations due to the use of ψ_1.
   c. Dive angle error.

2. Error in the pull-up time — range limitations corresponding to the degree of accuracy of the determination of T_p.
3. Errors in T_c.
   a. Altimeter error.
   b. Intervalometer characteristics.
   c. MPI adjustment.
   d. Torpedo tossing.
4. Error due to misalignment of sight.

so that

$$\tan \theta_h' = \frac{g(T_h' - T_p') \cos \alpha - \dot{y}_p'}{g(T_h' - T_p') \sin \alpha + \dot{x}_p'} \tag{37}$$

where T_h' is the time along the trajectory from P' to H'. In obtaining equation (37) from (36) the sign of the right-hand member was changed because θ_h' is the supplement of the angle given by (36).

The quantity $T_f' = T_h' - T_p'$ is now obtained

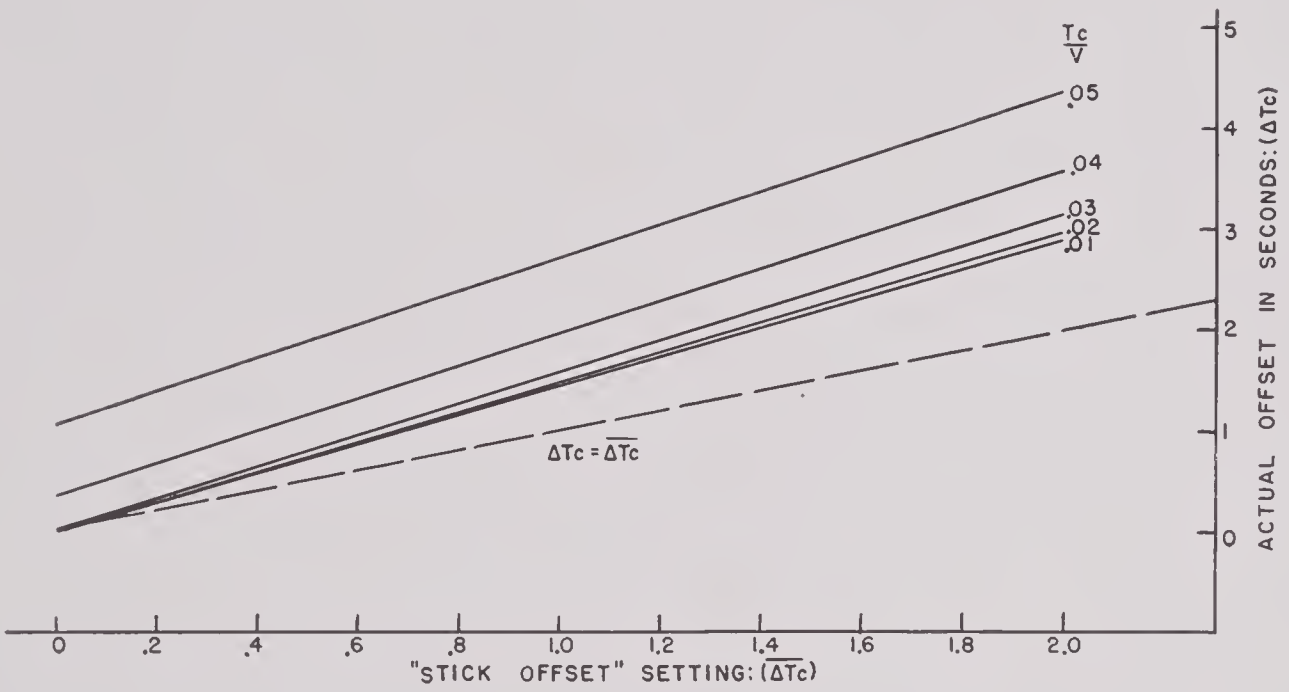

FIGURE 12A. Relation between "stick offset" setting ($\overline{\Delta T_c}$) and actual resulting offset (ΔT_c) for different values of T_c/V; α = 40 degrees, $\overline{K}$ = 3, V = 500 feet/second. Dashed curve is inserted as aid in comparing magnitudes of $\overline{\Delta T_c}$ and ΔT_c.

6.4.2 The Basic Equation

Equation (27) of Chapter 2, repeated here as equation (35), is basic in problems concerned with errors in bomb tossing.

$$\frac{\delta}{\sin \theta_h'} = \frac{V \Delta T_c}{\sin (\alpha + \theta_h')} . \tag{35}$$

The meanings of the symbols in equation (35) were previously defined with respect to Figure 10 of Chapter 2. Essentially the horizontal range error δ is expressed in terms of an error in release time ΔT_p.

It is necessary to obtain an expression for θ_h'. A starting point is equation (8) of Chapter 2, together with the corresponding equations for the components of velocity. If T_p' is the pull-up time from 0 to P', and θ the angle between a tangent line to the trajectory $P'H'K'$ and the collision course (refer to Figure 10, Chapter 2), then

$$\tan \theta - \frac{\dot{y}}{\dot{x}} = \frac{\dot{y}_p' - g(t - t_p') \cos \alpha}{\dot{x}_p' + g(t - t_p') \sin \alpha} , \tag{36}$$

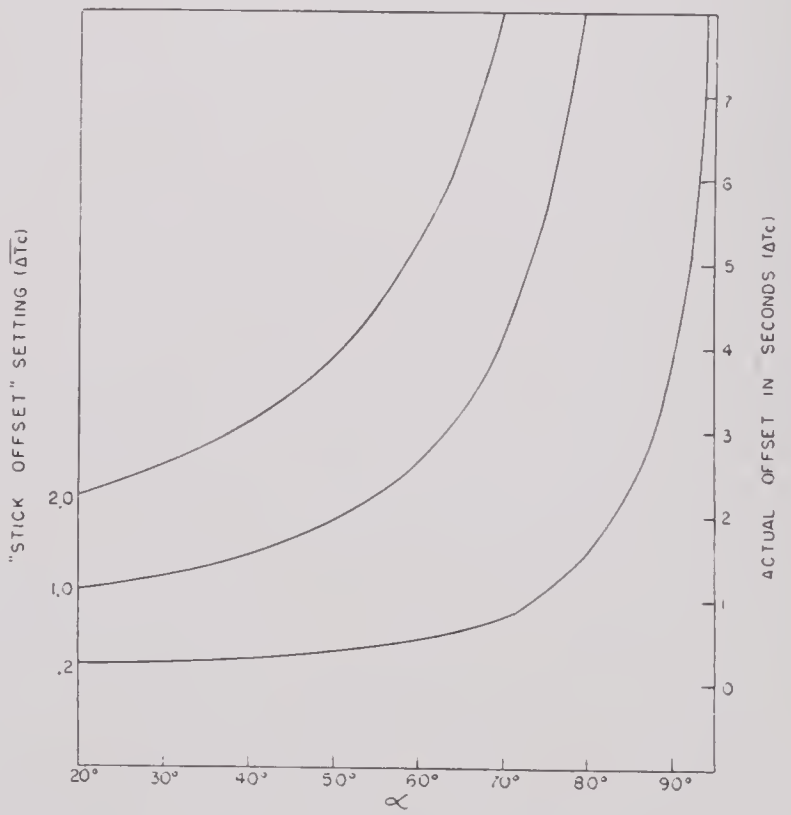

FIGURE 12B. Actual offset (ΔT_c), as function of α, corresponding to different instrumental "stick offset" settings ($\overline{\Delta T_c}$); T_c/V = 0.028, $\overline{K}$ = 3, V = 500 feet/second.

from equation (11) of Chapter 2 as

$$T_f' = \frac{v}{g \cos \alpha} \times \left[\sin \theta_p' \sqrt{\sin^2 \theta_p' + \frac{2 \cos \alpha}{\bar{\mu}} (1 - \cos \theta_p')}\right]. \quad (38)$$

This equation, and the relations $\dot{x}_p' = V \cos \theta_p'$, $\dot{y}_p' = V \sin \theta_p'$, bring equation (37) to the form

$$\tan \theta_h' = \frac{\sqrt{\sin^2 \theta_p' + \cos \alpha \frac{1 - \theta_p'}{\bar{\mu}}}}{\cos \theta_p' + \tan \alpha \left[\sin \theta_p' + \sqrt{\sin^2 \theta_p' + 2 \cos \alpha \frac{1 - \theta_p'}{\bar{\mu}}}\right]}. \quad (39)$$

For small θ_p' this is approximated to by

$$\tan \theta_h' \cong \frac{\theta_p' \sqrt{1 + \frac{1}{\bar{\mu}} \cos \alpha}}{1 + \theta_p' \tan \alpha \sqrt{1 + \frac{1}{\bar{\mu}} \cos \alpha}}. \quad (40)$$

Equation (35) can be written

$$\frac{\delta}{V \Delta T_c} = \frac{1}{\sin \alpha \cot \theta_h' + \cos \alpha}, \quad (41)$$

and it is a simple matter to replace $\cot \theta_h'$ by its value from equation (39). The resulting equation can be put into the form

$$\frac{\delta}{V \Delta T_c} = \frac{\sqrt{1 + \frac{2 \cos \alpha}{\bar{\mu}(1 + \cos \theta_p')}}}{\sin \alpha (\tan \alpha + \cot \theta_p') + \frac{1}{\cos \alpha} \sqrt{1 + \frac{2 \cos \alpha}{\bar{\mu}(1 + \cos \theta_p')}}}, \quad (42)$$

to which a good approximation is

$$\frac{\delta}{V \Delta T_c} \cong \frac{\sqrt{1 + \frac{1}{\bar{\mu}} \cos \alpha}}{\sin \alpha (\tan \alpha + \cot \theta_p') + \frac{1}{\cos \alpha} \sqrt{1 + \frac{1}{\bar{\mu}} \cos \alpha}}. \quad (43)$$

Finally, if $\cot \theta_p'$ is replaced by $1/\theta_p'$, we have

$$\frac{\delta}{V \Delta T_c} \cong \frac{\theta_p' \sqrt{1 + \frac{1}{\bar{\mu}} \cos \alpha}}{\sin \alpha + \theta_p' \frac{\sin^2 \alpha + \sqrt{1 + (1/\bar{\mu}) \cos \alpha}}{\cos \alpha}}. \quad (44)$$

A variant of equation (44) using the quantity β will be useful in Section 6.4.3. By the use of equations (4) and (17) of Chapter 2, the relation

$$\frac{2\beta}{1 + \sqrt{1 + 2\beta}} \cdot \frac{\cot \alpha}{1 + \sqrt{\frac{\bar{\mu}}{\bar{\mu} + \cos \alpha}}} = \theta_p'$$

is obtained, and thus equation (44) becomes

$$\frac{\delta}{V \Delta T_c} = \frac{\cos \alpha}{1 + \sin^2 \alpha \frac{1 + \sqrt{1 + 2\beta}}{2\beta} \sqrt{\frac{\bar{\mu}}{\bar{\mu} + \cos \alpha}} \left(\sqrt{1 + 2\beta} + \sqrt{\frac{\bar{\mu}}{\bar{\mu} + \cos \alpha}}\right)}. \quad (45)$$

6.4.3 Range Limitations from the Use of ψ_0[79]

For the discussion of range limitations due to the use of ψ_0, or of range errors due to errors in the measurement of ψ, a formula for δ in terms of ψ_e and ψ_0, or in terms of the error in ψ is needed. Equation (45) can be used to obtain such a formula.

In the first place, if $S = VT_c$ is the slant range OH, then

$$\frac{\delta}{S} = \frac{\delta}{V \Delta T_c} \cdot \frac{\Delta T_c}{\Delta T_p} \cdot \frac{\Delta T_p}{T_p} \cdot \frac{T_p}{T_c}. \quad (46)$$

Of the four factors comprising the right-hand member, the first is given by equation (45), the second and fourth are to be taken from the equations of Section 2.1.2, and the third will be retained in its present form.

From equation (16) of Chapter 2, in which $\bar{\mu}$ is assumed to change by an amount small enough to be ignored, it is found that

$$dT_c = \frac{1 + 2\sigma}{V} g \bar{\mu} T_{p0} \tan \alpha + (1 + \sigma)\, dT_{p0},$$

[redacted]

as well as

$$\frac{T_{p0}}{T_c} = \frac{1}{1 + \sigma + \dfrac{1 + 2\sigma}{2V} g\bar{\mu}T_{p0} \tan \alpha} .$$

It follows that

$$\frac{dT_c}{dT_{p0}} \cdot \frac{T_{p0}}{T_c} = \frac{1 + \sigma + \dfrac{1 + 2\sigma}{V} g\bar{\mu}T_{p0} \tan \alpha}{1 + \sigma + \dfrac{1 + 2\sigma}{2V} g\bar{\mu}T_{p0} \tan \alpha}$$

$$= 2 - (1+\sigma) \frac{T_{p0}}{T_c}. \qquad (47)$$

On replacing T_{p0} in the right-hand member by its value from equation (17) of Chapter 2, and expressing the result in terms of β, we obtain

$$\frac{dT_c}{dT_{p0}} \cdot \frac{T_{p0}}{T_c} = \frac{2\sqrt{1 + 2\beta}}{1 + \sqrt{1 + 2\beta}} . \qquad (48)$$

Substituting equations (48) and (45) into (46) results in

$$\frac{\delta}{S} = \frac{2\sqrt{1 + 2\beta}}{1 + \sqrt{1 + 2\beta}} \times \frac{\cos \alpha}{1 + \sin^2 \alpha \dfrac{1 + \sqrt{1 + 2\beta}}{2\beta} \sqrt{\dfrac{\bar{\mu}}{\bar{\mu} + \cos \alpha}} \left(\sqrt{1 + 2\beta} + \sqrt{\dfrac{\bar{\mu}}{\bar{\mu} + \cos \alpha}} \right)} \frac{\Delta T_p}{T_{p0}}$$

$$= \frac{1}{b_4} \frac{\Delta T_p}{T_{p0}} . \qquad (49)$$

The coefficient b_4 is plotted in Figure 13. The factor

$$\frac{\Delta T_p}{T_{p0}} = \frac{T_{pe} - T_{p0}}{T_{p0}} = \frac{\psi_e - \psi_0}{\psi_0}$$

is the relative error in release time due to the use of ψ_0 instead of ψ_e.

Figure 11 of Chapter 2 presents graphically the relation (49) connecting the variables S, α, V when δ and $\bar{K}$ are assigned the values 100 feet and 3, respectively. The figure was constructed as follows:

If a fixed value is assigned to T_c/V, the right-hand member of equation (49) becomes a function of α only. Hence for each α a value of S can be computed. By assigning α values from 0 degrees up to 60 degrees, and plotting S on a polar coordinate system, a curve is obtained along which α and S vary but T_c/V is constant. Eight such curves for T_c/V from 0.015 to 0.05 at intervals of 0.005 were plotted, and each labeled with the value of T_c/V to which it corresponded. Now $S = (T_c/V)V^2$. Hence for a constant V, eight values of S can be calculated, one for each T_c/V curve, for all eight of which V has the same value. These eight points are then connected. Repetitions of this procedure give the curves of constant V in Figure 11 of Chapter 2.

6.4.4 Range Limitations from the Use of ψ_1[79]

Equation (49) can be used to obtain curves for the Model 1 director (ψ_1 function) corresponding to those in Figure 11 of Chapter 2 but for the Model 0 bomb director. Such a graph was shown in Figure 7 of this chapter. It is unnecessary to change any part of equation (49) except $\Delta T_p/T_{p0}$, since the use of T_{p1} in the rest of the formula (instead of T_{p0}) will result in only a small percentage change in the whole expression. For T_p/T_{p0}, however, it is now necessary to use

$$\frac{T_{pe} - T_{p1}}{T_{p1}} = \frac{\psi_e}{\psi_1} - 1.$$

Since $\psi_e - \psi_1$ is much smaller than $\psi_e - \psi_0$, a great improvement is noted in the maximum range corresponding to a horizontal error of 100 feet at the target, especially for small dive angles and long ranges.

6.4.5 Errors from Incorrect Measurement of Dive Angle

An error in the measurement of dive angle means that an incorrect value of ψ will be used by the computer. This will cause an error in the release time.

Let $d\alpha$ and dT_p be the errors in α and T_p. From

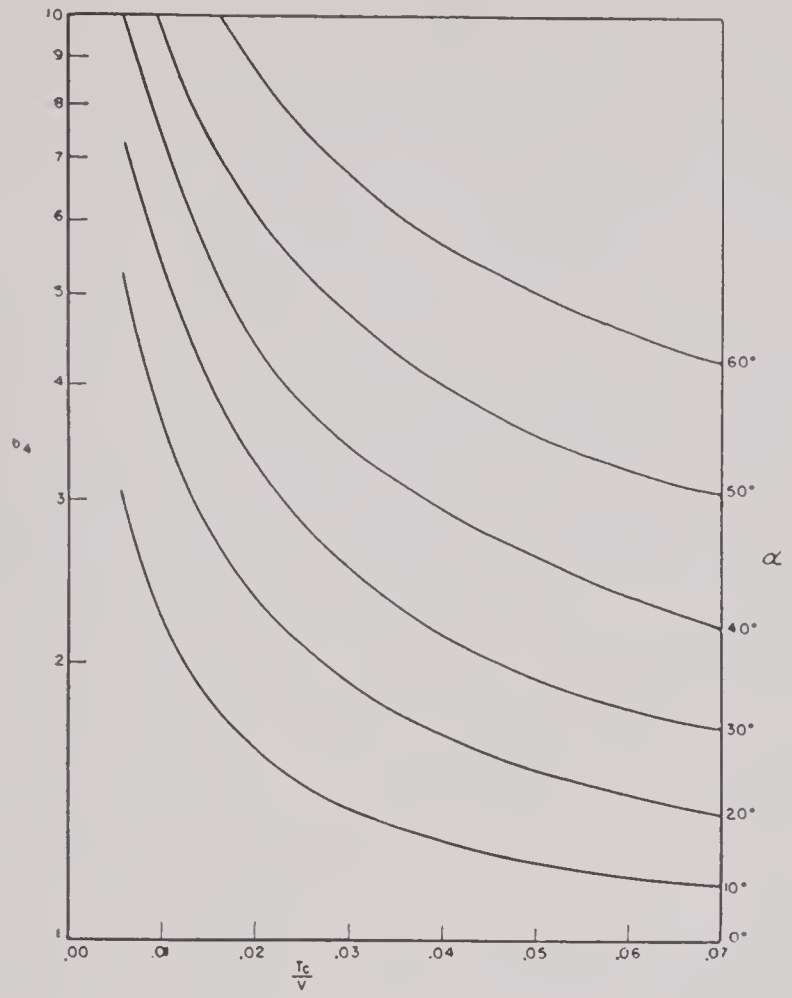

FIGURE 13. $b_4 = (\Delta T_p/T_p)/(\delta/S)$ versus T_c/V for different dive angles α; $\bar{K} = 3$; showing relationship between change or error ΔT_p in T_p and resulting horizontal impact error δ.

equation (18) of Chapter 2, using logarithmic differentiation, we have

$$\frac{dT_{p0}}{T_{p0}} = -\left[\tan\alpha + \frac{\sin\alpha}{2(\bar{K} - \cos\alpha + \sqrt{\bar{K}(\bar{K} - \cos\alpha)})} + \frac{\delta\beta/\delta\alpha}{(1 + \sqrt{1 + 2\beta})\sqrt{1 + 2\beta}}\right] d\alpha \qquad (50)$$

but

$$\frac{\delta\beta}{\delta\alpha} = \beta\left[\cot\alpha + \frac{\sin\alpha}{\bar{K} - \cos\alpha}\right],$$

and equation (50) becomes

$$\frac{dT_{p0}}{T_{p0}} = -b_\alpha d_\alpha \qquad (51)$$

where

$$b_\alpha = \tan\alpha + \tfrac{1}{2}\cot\alpha + \frac{\sin\alpha}{2} \times \left[\frac{1}{\bar{K} - \cos\alpha} + \frac{1}{\bar{K} - \cos\alpha + \sqrt{\bar{K}(\bar{K} - \cos\alpha)}}\right] - \frac{1}{2\sqrt{1 + 2\beta}}\left(\cot\alpha + \frac{\sin\alpha}{\bar{K} - \cos\alpha}\right).$$

Substitution from equation (51) into (49) gives the relation connecting δ/S with $d\alpha$ in the abbreviated form $\delta/S \cong (b_\alpha/b)\, d\alpha$, whence

$$\delta \cong -\frac{b_\alpha}{b} \cdot \frac{h_2}{\sin\alpha}\, d\alpha, \qquad (52)$$

where $h_2 = S\sin\alpha$ is the altitude at which pull-up began.

It follows from equation (52) that

$$-\frac{\delta}{d_\alpha} = \frac{b_\alpha}{b} \cdot \frac{h_2}{\sin\alpha}.$$

With $V = 250\sqrt{2}$ knots ($\cong 355$ knots) and $\bar{K} = 3$, the expression

$$\frac{b_\alpha}{b} \cdot \frac{h_2}{\sin\alpha}$$

is computed for several values of h_2 and $\alpha = 10$ degrees, 20 degrees, . . . 60 degrees, and the corresponding values of $-\delta/d\alpha$ are shown graphically in Figure 14.

Since b_α/b is independent of h_2 and V except as they occur in the expression h_2/V^2 (or T_c/V), it follows from equation (52) that if V is multiplied by a factor $\sqrt{n}$ and at the same time h_2 by n, then $-\delta/d\alpha$ will be multiplied by n. For this reason the use of the factor n, with V in knots, in both the h_2 and $-\delta/d\alpha$ scales of the graph makes the graph applicable to any airspeed. For $V = 250$, 350, and 500 knots, $n = \frac{1}{2}$, 1, and 2, respectively.

From Figure 14, reading values of h_2 corresponding to a given $-\delta/d\alpha$ at each dive angle, a spatial contour map (shown in Figure 15) of $-\delta/d\alpha$, or $-d\alpha/\delta$, as a function of the release point, can be constructed. The airspeed factor n is again used in all scales which involve linear units. Additional points were obtained for the contour map by direct calculation for the case $\alpha = 0$, when the relation

$$S = V\frac{2\bar{K}}{g(\bar{K} - 1)(-d\alpha/\delta)}$$

is valid.

It will be noted that the contours resemble slant range arcs with centers at the origin, and therefore that $d\alpha/\delta$ is almost independent of dive angle at constant slant range.

6.4.6 Range Error Due to Error in T_p

A certain range error must be expected because accumulated errors in the component parts of the bomb director result in an error in the release time. If a particular order of accuracy, such as one per

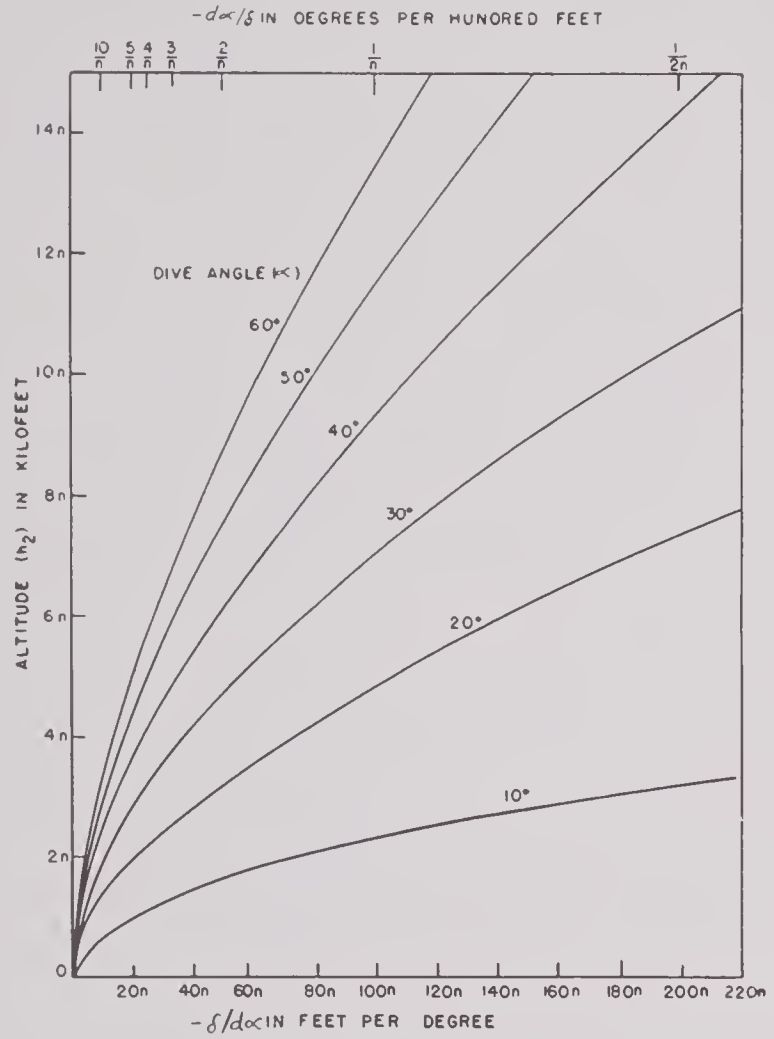

FIGURE 14. Relationship between error $d\alpha$ in dive angle and resulting horizontal impact error δ. Ratios $-\delta/d\alpha$ and $-d\alpha/\delta$ versus altitude $h_2 = S \sin \alpha$ for different values of α; $\bar{K} = 3$. Scale factor n is determined by velocity: $n = \frac{1}{2}$ when $V = 250$ knots, $n = 1$ when $V = 350$ knots; $n = 2$ when $V = 500$ knots.

cent in T_p, is demanded of the mechanism, it is possible to calculate from equation (49) the horizontal error δ.

Figure 16 shows graphically the results of such calculations. The curves in Figure 16 are strictly valid for the zero order solution and, except for second order terms, valid for the first order and exact solutions. The curves give the ranges corresponding to given percentage errors in the calculation of release time $\Delta T_p/T_p$, which will result in a ground error of 100 feet. At close ranges computer errors naturally can be permitted to be larger without affecting the ground accuracy adversely. A computer having one per cent accuracy permits slant ranges of the order of 15,000 feet.

The next consideration is whether toss bombing results are limited more by approximations involved in the early solutions of the equations, or by lack of instrumental accuracy. From Figure 16, it can be seen that an error of two per cent in T_p results in about the same error as is inherent in the ψ_0 solution at 350 knots, slant ranges being the same. In general, since the ψ error is negative, it can be reduced somewhat by depressing the sight slightly.

The relative importance of these two types of error depends strongly upon velocity, as Figure 16 shows. Figure 16 represents a superposition of the 100-foot error curves for ψ_0 on the computer accuracy

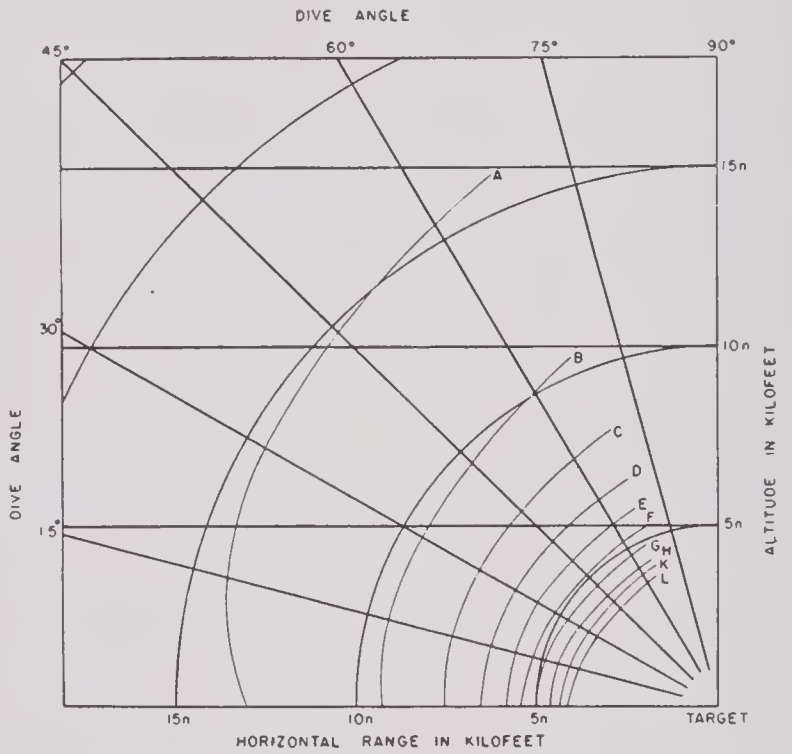

Curve	A	B	C	D	E	F	G	H	K	L
$-d\alpha/\delta$ in degrees per 100 ft	$\frac{1}{n}$	$\frac{2}{n}$	$\frac{3}{n}$	$\frac{4}{n}$	$\frac{5}{n}$	$\frac{6}{n}$	$\frac{7}{n}$	$\frac{8}{n}$	$\frac{9}{n}$	$\frac{10}{n}$

FIGURE 15. Pictorial chart of pull-up points corresponding to different ratios of dive angle error $d\alpha$ to resulting horizontal impact error δ; $\bar{K} = 3$. Scale factor n determined by velocity as in Figure 14.

curves. For small velocities the effect of ψ function variations will outweigh instrumental errors. However, if it is desired to take advantage of the long ranges theoretically possible at high velocities, the accuracy of the computer must be increased considerably.

6.4.7 Range Errors Due to Altimeter Errors[59]

In this section the effects produced by errors in altimeter indications on the time-to-target T_c are examined.

Let h_1 and h_2 be the true altitudes at which the altimeter operates. Also let h_{10} and h_{20} be the nominally correct altitudes; then $h_{10}/h_{20}=6/5$. Define ϵ_1 and ϵ_2 by the relations

$$h_1 = h_{10}(1 + \epsilon_1) \quad h_2 = h_{20}(1 + \epsilon_2); \tag{53}$$

ϵ_1 and ϵ_2 are the relative errors in the altitudes. Define ϵ_r by the relation

$$\frac{h_1}{h_2} = \frac{h_{10}}{h_{20}}(1 + \epsilon_r) = \frac{6}{5}(1 + \epsilon_r); \tag{54}$$

ϵ_r is the relative error in the measurement of h_1/h_2.

If T_{12} is the actual time it takes the aircraft to fly between the two altitude points, then

$$T_{12} = \frac{h_1 - h_2}{V \sin \alpha}.$$

By using equation (54) to eliminate h_1, we obtain:

$$T_{12} = \frac{h_2}{5V \sin \alpha}(1 + 6\epsilon_r). \tag{55}$$

Since

$$T_c = \frac{h_2}{V \sin \alpha},$$

it follows that

$$T_{12} = \frac{T_c}{5}(1 + 6\epsilon_r),$$

and

$$\Delta T_c = T_c - 5T_{12} = -6T_c \epsilon_r. \tag{56}$$

The presence of the negative sign shows that when ϵ_r is negative, i.e., $h_1/h_2 < 6/5$, then ΔT_c will be positive, so that the measured time-to-target $5T_{12}$ will be too small and the bomb will go short of the target. Moreover, any error ϵ_r is reflected in a relative error six times as large in T_c.

Range errors due to errors in ϵ_r are shown in Figure 17 for dive angles of 30 degrees and a plane speed of 250 knots. These range errors decrease for increasing dive angle and plane speed. In Figure 18

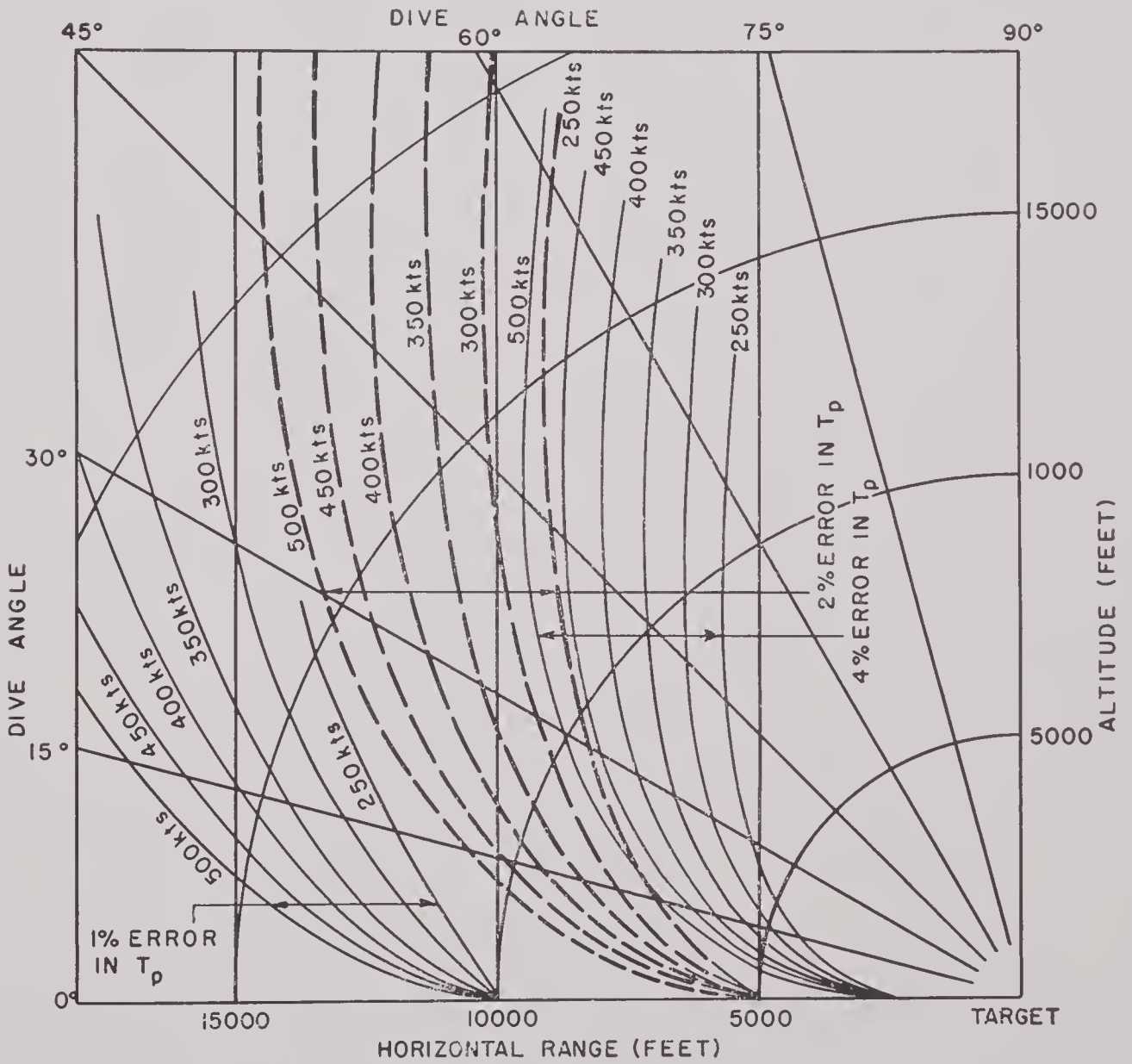

FIGURE 16. Pictorial chart of pull-up points for which 1, 2, and 4 per cent errors in T_p are required to produce 100-foot horizontal impact error, at different velocities; $\bar{K} = 3$.

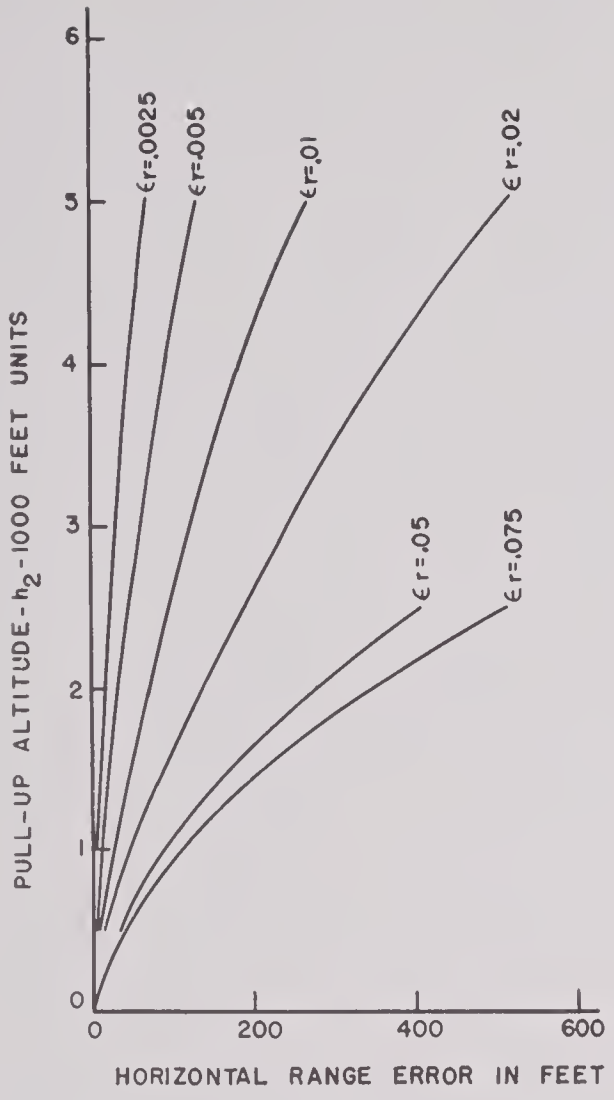

FIGURE 17. Graph of horizontal impact errors δ resulting from different relative errors ϵ_r in altitude ratio h_1/h_2, as function of h_2; $V = 250$ knots, $\alpha = 30$ degrees, $\bar{K} = 4$.

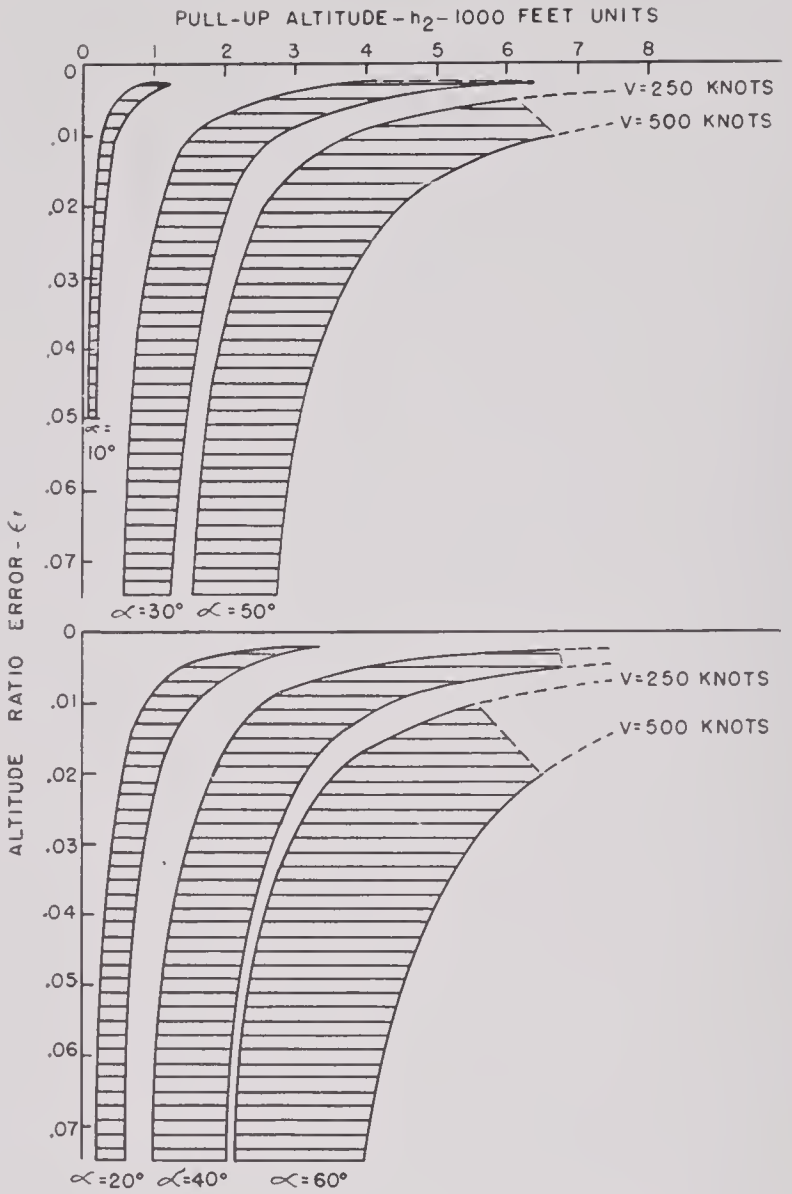

FIGURE 18. Graph of altitude ratio error ϵ_r required to produce 50-foot horizontal impact error, as function of h_2, for different dive angles and for velocities between 250 and 500 knots; $\bar{K} = 4$.

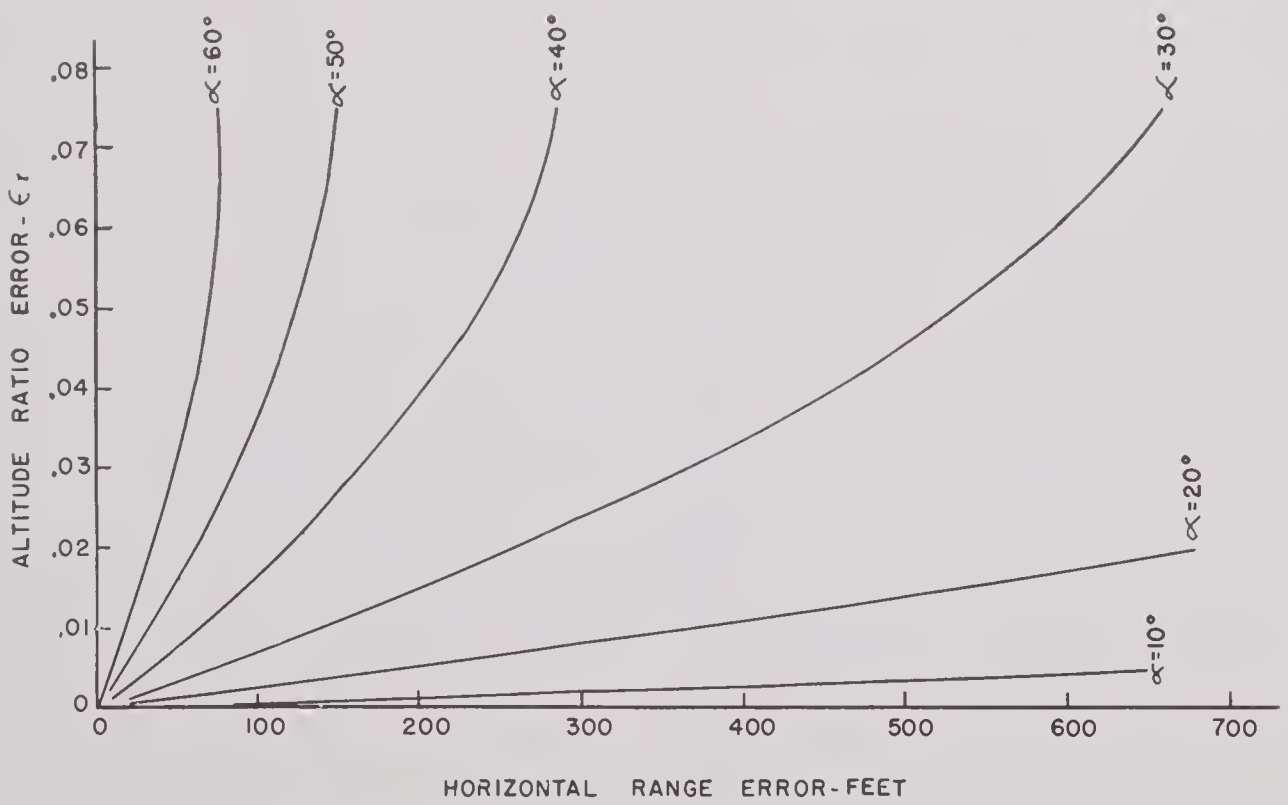

FIGURE 19. Altitude ratio error ϵ_r versus horizontal range error, resulting in horizontal impact error δ, for different dive angles α; $V = 500$ knots, $h_2 = 5{,}000$ feet, $\bar{K} = 4$.

are plotted contours corresponding to the altimeter ratio errors which will produce a horizontal range error of 50 feet at the various dive angles indicated. The shaded area is bounded by two curves, one for a plane velocity of 250 knots (the lower curve) and the other for a plane velocity of 500 knots (the upper curve).

Figure 19 shows how the altimeter ratio error affects the horizontal range error as the dive angle is increased from 10 degrees to 60 degrees.

From equations (53) and (54) it follows that

$$\epsilon_r = \frac{\epsilon_1 - \epsilon_2}{1 + \epsilon_2} \cong \epsilon_1 - \epsilon_2.$$

Hence, if $\epsilon_1 = \epsilon_2$, then ϵ_r must be zero. That is, equal relative errors in h_1 and h_2 cause ϵ_r to be zero, and therefore $\Delta T_c = 0$ by equation (56). However, if $\epsilon_1 = -\epsilon_2$, then $\epsilon_r \cong 2\epsilon_1$, so that $\Delta T_c = -12 T_c \epsilon_1$. This shows the importance of having errors which come into h_1 and h_2 in the same sense, both positive or both negative.

It is also possible to express ϵ_r in terms of target altitude error or, what amounts to the same thing, equal errors in h_1 and h_2. Thus, let $h_1 = h_{10} + e_1$ and $h_2 = h_{20} + e_2$. Then, by equation (54)

$$\epsilon_r = \frac{5e_1 - 6e_2}{6h_2}.$$

This shows that if $e_1 \cong e_2$, then ϵ_r will be quite small, but if

$$e_1 \cong -e_2,$$

then

$$\epsilon_r \cong \frac{11e_1}{6h_2}.$$

This brings out again the importance of preventing errors of opposite sign from occurring in h_1 and h_2.

Table 10 shows the maximum permissible errors in altitude that will produce a ground error of 50 feet

TABLE 10. Maximum permissible error in altitude that will produce error on ground of 50 feet or less.
(Case where errors have like signs at first and second altitudes.)

Altimeter prong No.	Second altitude (ft)	Plane velocity (knots)	Errors in altitude (ft) Dive angle (degrees) 10	20	30	40	50	60
11	1,389	250	< 21	40	90	224	431*	431*
		500	< 21	100	345	431*	431*	431*
10	1,667	250	< 25	39	85	210	518*	518*
		500	< 25	92	299	518*	518*	518*
9	2,000	250	< 30	37	81	175	359	621*
		500	< 30	66	224	621*	621*	621*
8	2,400	250	< 35	37	75	136	292	523
		500	< 35	60	173	455	745*	745*
7	2,880	250	< 43	43	71	135	259	444
		500	< 43	49	150	366	763	894*
6	3,456	250	< 52	< 52	67	122	223	391
		500	< 52	< 52	137	295	614	1,072*
5	4,157	250	< 74	< 74	< 74	109	204	355
		500	< 74	< 74	123	255	511	1,181*
4	4,977	250	< 74	< 74	< 74	97	192	314
		500	< 74	< 74	111	223	417	947
3	5,977	250	< 88	< 88	< 88	99	181	306
		500	< 88	< 88	92	192	402	767
2	7,200	250	< 106	< 106	< 106	< 106	173	293
		500	< 106	< 106	< 106	201	360	602

* This error in altitude will produce an error on the ground of less than 50 ft.
< Error in altitude should be less than given value in order to produce an error on the ground of 50 ft.
The range of values for which the curves in this report were plotted give rise to the above limitations in the use of Table 10.

TABLE 11. Maximum permissible error in altitude that will produce error on ground of 50 feet or less. (Case where errors have opposite signs at first and second altitudes.)

Altimeter prong No.	Second altitude (ft)	Plane velocity (knots)	Error in altitude (ft) Dive angle (degrees) 10	20	30	40	50	60
11	1,389	250	< 2	4	9	24	55*	55*
		500	< 2	10	40	55*	55*	55*
10	1,667	250	< 2	4	8	22	66*	66*
		500	< 2	9	33	66*	66*	66*
9	2,000	250	< 3	3	7	17	39	79*
		500	< 3	6	23	79*	79*	79*
8	2,400	250	< 3	3	7	13	30	59
		500	< 3	6	17	50	94*	94*
7	2,880	250	< 4	4	7	13	26	47
		500	< 4	5	14	38	91	113*
6	3,456	250	< 5	< 5	< 6	11	22	39
		500	< 5	< 5	13	29	66	136*
5	4,157	250	< 6	< 6	< 6	10	19	35
		500	< 6	< 6	12	25	52	145
4	4,977	250	< 6	< 6	< 6	7	9	18
		500	< 6	< 6	10	21	41	104
3	5,977	250	< 8	< 8	8	9	17	29
		500	< 8	< 8	9	18	39	79
2	7,200	250	< 10	< 10	< 10	< 10	16	28
		500	< 10	< 10	< 10	19	34	59

* This error in altitude will produce an error on the ground of less than 50 ft.
< Error in altitude should be less than given value in order to produce an error on the ground of 50 ft.
The range of values for which the curves in this report were plotted give rise to the above limitations in the use of Table 11.

or less if the errors have the same sign, while Table 11 gives corresponding figures if the errors have different signs.

The errors which may occur when using an altimeter with bomb tossing equipment may in general be classified as either instrumental errors or as errors inherent in the barometric method for measuring altitude. Among these errors are the following:

1. Scale errors.
2. Friction errors.
3. Position errors.
4. Lag in the static line.
5. Lag in the altimeter capsule.
6. Deviation of the temperature of the air column from that assumed in the standard atmosphere.
7. Atmospheric pressure at the target level.
8. Errors in the setting of the prongs.
9. Vibration.

In general, lag and scale errors have like signs at the first and second altitude points. Also, a shift in atmospheric pressure at the target level, from the assumed value, is of the nature of a lag (positive or negative). The other errors listed may cause errors of either sign at both altitude points.

Reference to Table 10 shows that for all prongs, all airspeeds, and for dive angles greater than 20 degrees, a net error in altitude at any one altitude point of 40 feet or less is permissible for a horizontal ground error of 50 feet or less provided the errors in adjacent altitude points are of like signs.

Table 11 serves to highlight the importance of eliminating random effects such as might be due to vibration. The bomb tossing altimeter was mounted on a suitable shock mount for this as well as for other reasons (see Section 3.5.4).

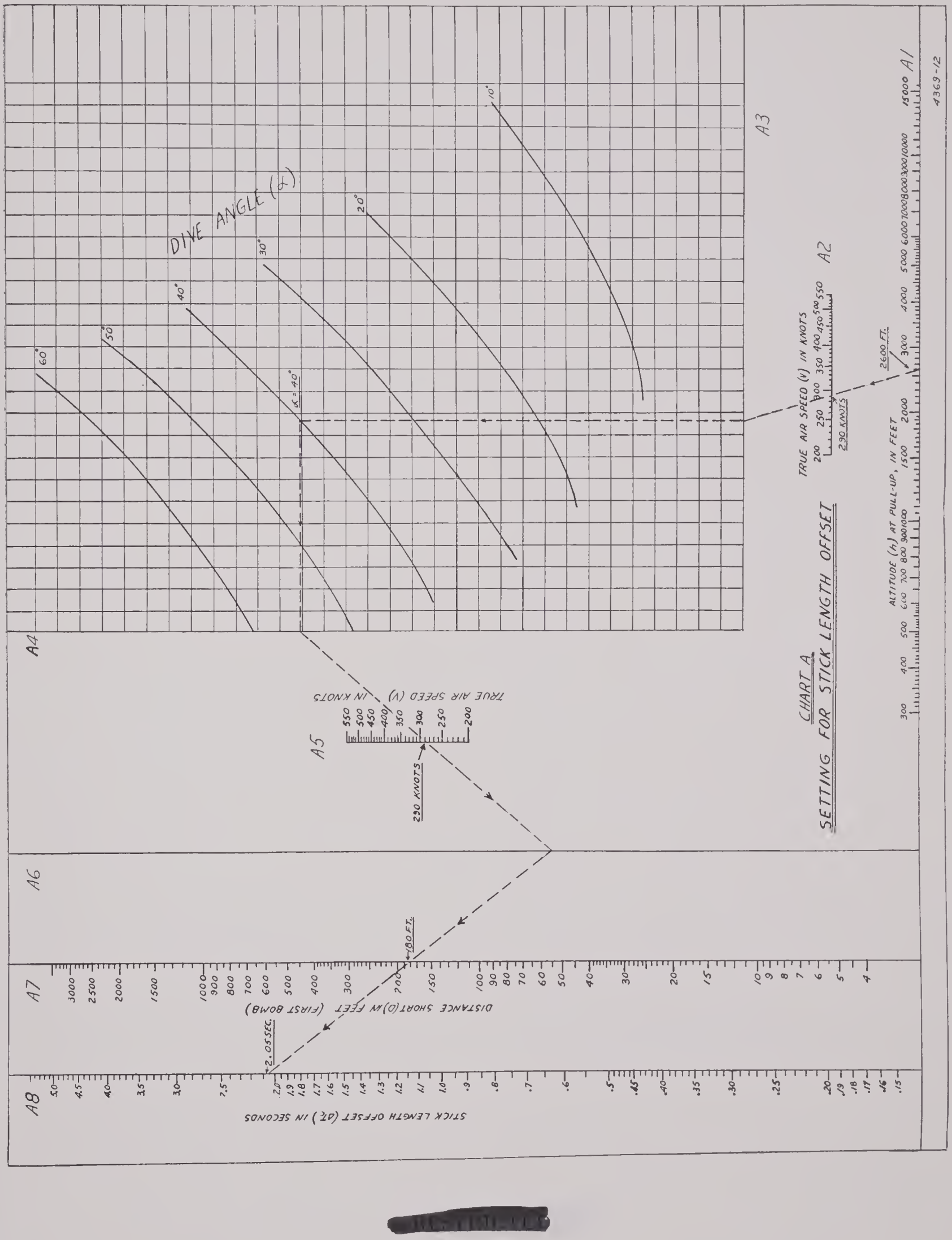

FIGURE 20. Nomographic chart for determining change ΔT_p in T_p corresponding to given shift δ in impact point (and vice versa).

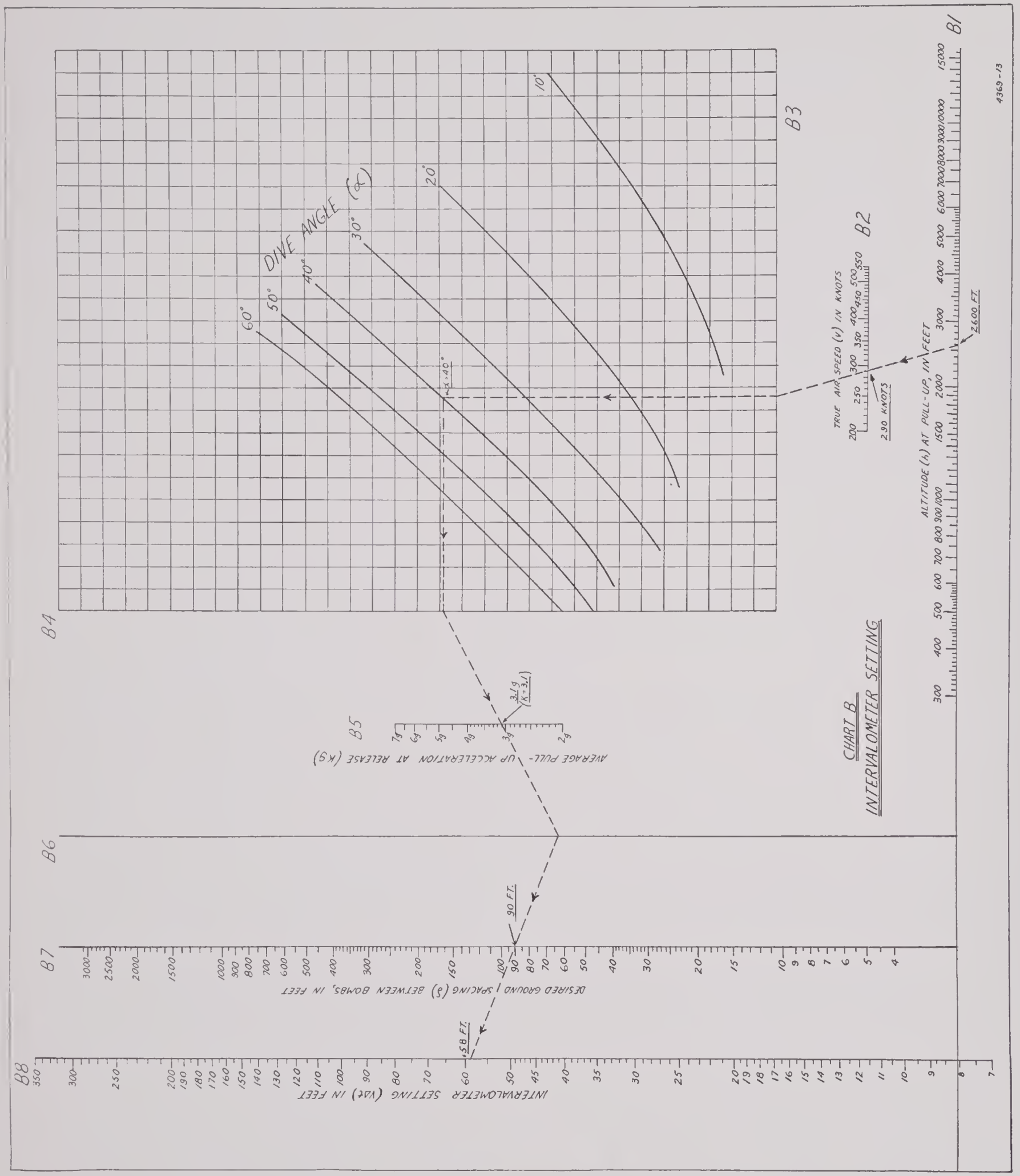

FIGURE 21. Nomographic chart for determining intervalometer setting required for given ground spacing of bombs.

6.4.8

Stick Offset[44]

The stick offset provides a means of systematically decreasing the release time to drop bombs short of the target. It is used when sticks or trains of bombs are released or when torpedoes are tossed (see Section 6.4.10). When sticks of bombs are released the stick offset provides for bracketing of the target by having the first bombs released to fall short of the target and the last one beyond. Controlling factors in selecting the setting are (1) the amount short of the target by which the first bomb should strike, and (2) the intervalometer setting which determines the time interval (or ground spacing) between the bombs in the train.

Computations for determining the settings are based on equation (35) in which horizontal error δ (or displacement in this case) is related to shift in release time ΔT_c. The details of the computations are given in reference 40. The summary of the calculations can be reduced to nomographic charts, as shown in Figures 20 and 21.

Short Impact Charts

Figure 20 allows the estimation of a short release time ΔT_c, to give an impact short of the target for the first bomb in the train. To use the chart proceed as follows:

1. Locate the point on line A1 corresponding to the altitude at the start of pull-up, and the point on line A2 corresponding to the plane's airspeed.

2. Join these two points with a straight line and extend this line until it intersects line A3.

3. From this point of intersection with A3 draw a vertical line up to the curve marked with the correct dive angle. (For intermediate dive angles, interpolate between two curves.)

4. Through the point so determined on the curve, draw a horizontal line to the left to intersect line A4.

5. Join this point on line A4 with the point on line A3 corresponding to the airspeed (same value as on line A2) and extend this straight line to intersect line A6.

6. Join this point on A6 with the point on line A7 corresponding to the desired amount by which the first bomb of the stick is to fall short of the target.

7. Extend to line A8 the line determined in 6 above. Where it intersects A8, read the value of the stick-length offset ΔT_c.

Intervalometer Chart

Figure 21 allows the selection of a stick spacing ($V\Delta T$) to give proper bracketing of the bombs on the target. To use the chart proceed as follows:

1. Using the intervalometer setting chart, proceed first as in paragraphs 1, 2, 3, under (1) above, using lines B1, B2, and B3. (Note that this second chart has a different set of curves.)

2. Through the point so determined on the curve, draw a horizontal line to the left to intersect line B4.

3. Join this point on B4 with the point on line B5 corresponding to the pull-up acceleration (K) of the plane at release. Where K varies, the value at release of the central bomb of the stick should be used. Extend this straight line to intersect line B6.

4. Join this point on B6 with the point on line B7 corresponding to the desired ground spacing δ between successive bombs. (The spacing between bombs will not be exactly uniform, but will center about the value used on line B7.)

5. Extend to line B8 the line so determined. At the intersection read the value of the intervalometer setting ($V\Delta T$). The intervalometer dial marked "spacing between bombs" should be set for this value, in order to obtain an actual spacing δ (as in 4 above).

The sample calculation (broken lines with arrows) on the two charts illustrates the method described above. A plane dives at an angle of 40 degrees with a true airspeed of 290 knots in the direction of the target, and starts to pull up when its altitude is 2,600 feet. A stick of 5 bombs is to be released, and it is desired to space these bombs 90 feet apart and to have the third bomb hit the target; hence the desired distance short (D) for the first bomb is 180 feet, and the desired ground spacing (δ) 90 feet. Moreover, it is estimated that the pull-up acceleration during the period of release of the 5 bombs will average $3.1g$. The calculations on the two charts show that the stick-length offset (ΔT_c) for this case must be 2.05 seconds, and the intervalometer setting ($V\Delta T$) 58 feet.

The charts may also be used in converse manner to determine one of the other quantities (e.g., δ, h, K, α) when ΔT_c or $V\Delta T$ is known.

In addition, Figure 21 may be used for determining the error on the ground resulting from a known error in release time, ΔT_p. In this case, $V\Delta T_p$ is entered in scale J and the ground error is read from scale I.

It should be pointed out that the construction of

the charts is based on the assumption that it is possible to provide an instrumental adjustment, ΔT_c, on the stick offset dial which will not vary as α, T_c/V, etc., vary. In actuality this is only approximately true, since the design of the biasing circuit used in the stick offset adjustment is such as to provide some variation of ΔT_c with α and T_c. The variation of the actual short offset in seconds as a function of $\overline{\Delta T_c}$, the stick offset setting, has been given in equation (34). In this connection the stick-offset nomograph given in reference 144 should be consulted. The reference chart uses the dial setting $\overline{\Delta T_c}$ instead of the theoretical offset ΔT_c.

6.4.9 MPI Adjustment

The MPI adjustment dial introduces a percentage change in release time which is independent of T_c and α. The effect of the MPI adjustment is shown in Figure 13 of Chapter 2 for the Mark 1 Model 1 bomb director. This figure was obtained from the chart in Figure 20 in the following way.

For a given airspeed, dive angle, and altitude, it was possible to calculate T_c. Since each division on the MPI dial corresponds to a fixed percentage change in T_c (3.4 per cent per division was used) ΔT_c could be computed. From Figure 20 the corresponding impact distance D was determined.

6.4.10 Torpedo Tossing Theory

Application of the bomb director to torpedo tossing is another example of the functional relationship between the impact point on the ground and the stick-offset or ΔT_c adjustment.

In order to toss torpedoes it is required to determine the ΔT_c which will give an optimum operational range of dive angle and altitude. This design value of ΔT_c was taken as the value which would place the torpedo exactly 450 feet short for a maneuver initiated at a dive angle of 25 degrees and a second altitude of 1,395 feet. The intervalometer chart does not provide sufficient accuracy to be useful in this connection, since the ΔT_c required is of the order of 50 per cent of T_c, so that curvature effects are no longer negligible.

Approximate Solution for Design Purposes

The following procedure was used to determine an accurate value of ΔT_c for this purpose.

The problem is to find the release time, T_p (references are to Figure 10, Chapter 2) required to make the torpedo hit the point K' which is located at a distance $\delta = -450$ feet from the target at point H.

The coordinates of the impact point K' are

$$x_{K'} = S + \delta \cos \alpha = V\left(T_c + \frac{\delta \cos \alpha}{V}\right) \qquad (57)$$

$$y_{K'} = + \delta \sin \alpha$$

where S is the slant range.

The y-coordinate of the torpedo at any time $t > T_p$, is given by the second equations (8), Chapter 2, which at time $t = T_{H'}$, $y = + \delta \sin \alpha$ becomes

$$\tfrac{1}{2} g \cos \alpha (T_{H'} - T_p)^2 - \mu g T_p (T_{H'} - T_p) - \tfrac{1}{2} \mu g T_p^2 + \delta \sin \alpha = 0. \qquad (58)$$

For $\delta = 0$, equation (58) leads to the usual solution given in Chapter 2. Similarly, the solution of equation (58) is taken as

$$T_{K'} - T_p = \sigma_{K'} T_p \qquad (59)$$

where

$$\sigma_{K'} = \frac{\mu + \left[\mu^2 + \cos \alpha \left(\mu - \dfrac{2\delta \sin \alpha}{g T_p^2}\right)\right]^{\frac{1}{2}}}{\cos \alpha} \qquad (60)$$

$$\sigma_{K'} = \frac{\mu + \mu^{\frac{1}{2}} \left(K - \dfrac{\delta \sin 2\alpha}{\mu g T_p^2}\right)^{\frac{1}{2}}}{\cos \alpha}.$$

Similarly the x-coordinate of the bomb at any time $t > T_p$ is

$$x = Vt + \tfrac{1}{2} g \sin \alpha (t - T_p)^2, \qquad (61)$$

where higher order terms in T_p arising from the expansion of the cosine of the pull-up angle have been neglected. For $t = T_{K'}$, $x = x_{K'}$. Using equations (59) and (60), (61) has the solution

$$T_p = \frac{l(\sigma_{K'} + 1)}{2\sigma_{K'}^2} \cdot \left\{-1 + \left[1 + \frac{4\sigma_{K'}^2}{l(\sigma_{K'} + 1)^2}\left(T_c + \frac{\delta \cos \alpha}{V}\right)\right]^{\frac{1}{2}}\right\}. \qquad (62)$$

Equation (62) will give the value of T_p which will cause the bomb to hit point K' provided the correct value of $\sigma_{K'}$ is used. The latter, in turn, is a function of T_p so that a method of successive approximations may be employed in evaluating T_p. That is, assume a value for T_p. Next, calculate $\sigma_{K'}$ using equation (60). Using this value of $\sigma_{K'}$, compute T_p from equa-

tion (62). This new value of T_p may then be inserted in (60), etc. The closer the originally assumed value of T_p is to the correct value, the more rapidly will the successive approximations of T_p converge to the correct value. The first approximate value may be that for which the trajectory crosses the collision course at an altitude equal to $\delta \tan \alpha$. Another possibility is to use the approximate value indicated from the intervalometer chart. The approximation method converges in either direction; i.e., the originally assumed T_p may be either larger or smaller than the correct value.

This approximation method was carried out for the case where $\delta = -450$ feet, $\alpha = 25$ degrees, $V = 250$ knots, $K = 3$, and a second altimeter contact at 1,395 feet. In order to allow for the time which elapses between the signal to start the pull-up and the initiation of the pull-up, the nominal altitude of 1,395 feet was changed to 1,210 feet which corresponds to an allowance of approximately one second for pilot and aircraft reaction time. For the above values, T_p turns out to be

$$T_p = 0.472 \text{ second } (\delta = -450 \text{ feet}).$$

From this value of T_p, the ΔT_c required may be determined from the equation

$$T_p = \frac{T_c - \Delta T_c}{K + \sqrt{K^2 - K}} \psi_0 \qquad (63)$$

where

$T_p = 0.472$ second

$T_c = 6.781$ seconds

$K = 3$

$\psi_0 = 0.84$ ($K = 3$, $\alpha = 25$ degrees, $T_c/V = 0.016$).

Solving for ΔT_c, the result is

$$\Delta T_c = 3.719 \text{ seconds.}$$

The operational limits resulting from the use of this value of ΔT_c are given in Figure 19 of Chapter 2.

One feature of the trajectories of this figure which requires further discussion is the fact that they do not all cross the collision course at the same point. That is, since $S = VT_c$ it is to be expected that $\Delta S = V\Delta T_c$. This would be true were it not for the fact that the Model 0 integrator computes a release time which is slightly in error. As a consequence there is an error in slant range in the amount of:

$$\epsilon_S = \frac{\mu^3 g^2}{2V} \cdot \frac{(1 - K^{\frac{1}{2}}/\mu^{\frac{1}{2}})}{\cos \alpha} T_{p0}{}^3. \qquad (64)$$

The actual intersection point with the collision course is then given by:

$$\Delta S = V\Delta T_c + \epsilon_S. \qquad (65)$$

The results given by the equation (65) are compared with those obtained from the trajectories in the following table for $V\Delta T_c = 1{,}570$ feet:

Dive angle	Pull-up altitude	(ft)	ΔS in feet Computed	From Figure 31
25°	1,210	30	1,600	1,650
	2,880	320	1,890	1,935
	4,150	830	2,400	2,550
15°	1,362	210	1,780	1,780
	2,000	570	2,140	2,160

It will be seen that equation (65) gives values for ΔS which are in reasonable agreement with the observed values.

Exact Solution for T_p (with Target off Collision Course)

On making the substitutions

$$x_p = \frac{V^2 \sin \theta_p}{g\bar{\mu}} \quad y_p = \frac{V^2(1 - \cos \theta_p)}{g\bar{\mu}}$$

$$\dot{x}_p = V \cos \theta_p \quad \dot{y}_p = V \sin \theta_p$$

in equations (8) of Chapter 2, and taking account of equation (57) we have:

$$VT_c - \tfrac{1}{2} g T_f'^2 \sin \alpha + \delta \cos \alpha = \frac{V^2 \sin \theta_p}{g\bar{\mu}} + VT_f' \cos \theta_p$$

$$\frac{V^2}{g\bar{\mu}} - \tfrac{1}{2} g T_f'^2 \cos \alpha - \delta \sin \alpha = \frac{V^2 \cos \theta_p}{g\bar{\mu}} - VT_f' \sin \theta_p \qquad (66)$$

where $T_f' = T_{K'} - T_p$ is the time from release to the point K'.

Squaring both members of each equation (66) and adding member by member, it is found that θ_p is eliminated, leaving

$$\frac{g^2}{4V^2} T_f'^4 - \left(1 + \frac{1}{\bar{\mu}} \cos \alpha + \frac{gT_c \sin \alpha}{V}\right) T_f'^2 + T_c^2 + \frac{\delta^2}{V^2} + \frac{2\delta T_c}{V} \cos \alpha - \frac{2\delta}{g\bar{\mu}} \sin \alpha = 0. \qquad (67)$$

As in the case of equation (7), the solution of equation (67) desired here is

$$T_f' = \frac{V}{g} (\sqrt{\Gamma_1} - \sqrt{\Gamma_2}), \qquad (68)$$

where

$$\Gamma_1 = 1 + \frac{\cos \alpha}{\bar{\mu}} + \frac{gT_c}{V}(D + \sin \alpha),$$

$$\Gamma_2 = 1 + \frac{\cos \alpha}{\bar{\mu}} - \frac{gT_c}{V}(D - \sin \alpha),$$

and

$$D = \sqrt{1 + \frac{\delta^2}{V^2 T_c^2} + \frac{2\delta \cos \alpha}{VT_c} - \frac{2\delta \sin \alpha}{g\bar{\mu}T_c^2}}.$$

It is now necessary to solve equations (66) for θ_p. Following the same procedure as before, let the first be multiplied by $1 - \cos \theta_p$, the second by $\sin \theta_p$, and the equations then be added member by member. The resulting relation is linear in the quantity

$$\omega' = \cot \frac{\theta_p}{2} = \frac{\sin \theta_p}{1 - \cos \theta_p},$$

and its solution is

$$\omega' = \frac{VT_c + \delta \cos \alpha + VT_f' - \frac{1}{2}gT_f'^2 \sin \alpha}{\delta \sin \alpha + \frac{1}{2}gT_f'^2 \cos \alpha}. \quad (69)$$

It remains to replace T_f' in equation (69) by its value from equation (68) and express the result in as simple a form as possible. After some algebraic reduction the formula (70) for ω' is obtained.

$$\omega' = \frac{1}{\delta \sin 2\alpha + \frac{g}{V^2}(\delta + VT_c \cos \alpha)^2} \times$$

$$\left\{ VT_c \cos \alpha \left[1 + \frac{\cos \alpha}{\bar{\mu}} + D(\sqrt{\Gamma_1} + \sqrt{\Gamma_2}) + \sqrt{\Gamma_1 \Gamma_2} \right] + \delta \left[\cos 2\alpha + \frac{\cos \alpha}{\bar{\mu}} + \sin \alpha (\sqrt{\Gamma_1} - \sqrt{\Gamma_2}) + \sqrt{\Gamma_1 \Gamma_2} \right] \right\}. \quad (70)$$

On setting $\delta = 0$, equation (70) reduces, as it should, to equation (12) of Chapter 2.

The pull-up angle is now given by

$$\theta_{Ke}' = 2 \text{ arc tan } \frac{1}{\omega'} \quad (71)$$

and the period from the beginning of pull-up until the release of the torpedo is given by

$$T_{pe}' = \frac{2V}{g\bar{\mu}} \text{ arc tan } \frac{1}{\omega'}. \quad (72)$$

6.4.11 Sight Misalignment and Angle of Attack Variations[101]

One of the fundamental requirements for utilizing the tossing technique is that the sight line and the flight line coincide. The standard sights used in most aircraft are aligned with the boresight datum line for use with machine guns. This standard sight alignment corresponds to a sight line which is approximately 25 to 35 mils below the flight line under average loading conditions of a number of fighter bomber aircraft at a dive angle of 40 degrees and average indicated airspeeds of 300 to 350 knots.

In Chapter 4, and particularly in Section 4.2.3, a standard flight test procedure is described for adjusting the sight line to coincidence with the flight line. In certain cases it may happen that complete adjustment is not possible, or that a residual misalignment error occurs. Such errors may be corrected instrumentally by making use of the MPI adjustment. Such an instrumental correction is ordinarily made only once, for the particular set of flight conditions existing during the sight alignment test. At other values of airspeed, dive angle, and range, it is not necessarily true that the instrumental adjustment will compensate for the sight misalignment. In addition, when dive angle, airspeed, and weight vary, the angle of attack of the aircraft changes, resulting in a change in the angle between the sight line and the flight line. The errors resulting from such misalignments and means for correcting them will be discussed here.

Figure 22 represents the flight of plane and bomb for the case in which the line of flight makes a constant angle ϕ with the sight line, the sight being kept on the target K' until pull-up. The vectors marked **S** represent instantaneous directions of the sight line, always directed toward the target; those marked **F**, making an angle ϕ with the **S** vectors, represent the corresponding instantaneous directions of flight. It will be noted that the path AO is slightly concave upward; it would be concave downward if ϕ had the opposite sense. For small angles, however, very little sacrifice of accuracy results from assuming that the arc AO is straight.

If A is the first altitude point, the values of dive angle, time to target, and airspeed which are fed into the computer are determined by conditions along AO, assuming that the dive angle gyro is aligned with respect to the flight line. Barring other errors, therefore, the release time will be so determined as to cause the bomb to pass through point H on the

extension of AO. The horizontal error due to the misalignment of the sight is then $\delta = K'H$.

As regards conventions of sign, the angle ϕ is considered positive when the sight line is above the flight line, and the error δ positive when the impact is beyond the target. In Figure 22, ϕ is positive and δ is negative.

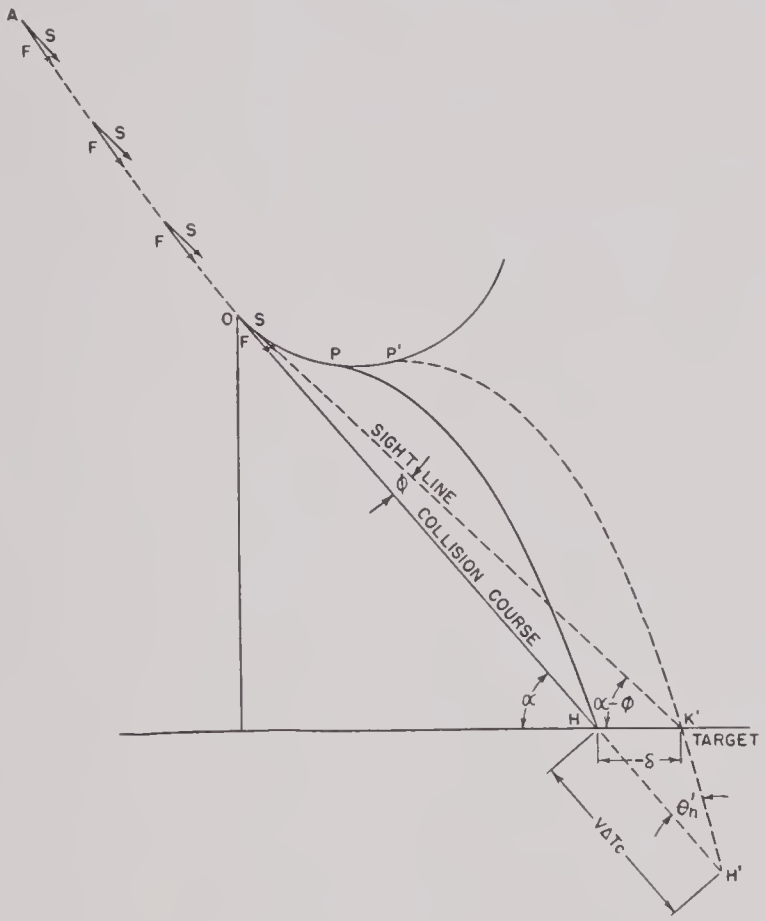

FIGURE 22. Flight and trajectory diagram with misaligned sight. Vectors marked S and F represent instantaneous directions of sight line and flight line, respectively.

The relation between ϕ and δ is obtained by applying the law of sines to the triangle OHK'. If $\overline{OH} = S = VT_c$, then

$$\frac{-\delta}{\sin\phi} = \frac{S}{\sin(\alpha-\phi)} \quad \text{or} \quad -\delta = \frac{S}{\sin\alpha(\cot\phi - \cot\alpha)}. \tag{73}$$

If $|\phi|$ is small compared with α, an approximation to (73) is

$$\delta = \frac{-S\phi}{\sin\alpha} \quad \text{or} \quad S = -\frac{\delta}{\phi}\sin\alpha, \tag{74}$$

ϕ being measured in radians. The relative error in δ, as given by equation (74), is slightly less than 5 per cent if $|\phi| \leq 1$ degree and $\alpha \geq 20$ degrees, and less than 10 per cent if $|\phi| \leq 1$ degree, and $\alpha \geq 10$ degrees.

If α and S as related in equation (74) are plotted in polar coordinates, a circle is obtained for each value of δ/ϕ, as shown in Figure 23. These circles have their centers on the line $\alpha = 90$ degrees, and the diameter of each is the corresponding value of $|\delta/\phi|$ as labeled in the figure.

From the exact equation (73) it is seen that δ is proportional not to ϕ but to $1/(\cot\phi - \cot\alpha)$, which differs significantly from ϕ when α is small or ϕ is large. The graphs of Figure 23, therefore, become accurate for all α and ϕ if the feet per mil values with which each circle is labeled are considered as values of $-1{,}000\delta(\cot\phi - \cot\alpha)$ instead of values of $-\delta/\phi$.

The error due to noncoincidence of sight and flight lines would be eliminated, causing a hit on the target K', if the value of T_c fed into the computer were adjusted to correspond to a target at H' instead of H. This would mean a relative increase $\epsilon_c = \Delta T_c/T_c$ (or a relative decrease $-\Delta T_c/T_c$), where $V\Delta T_c = HH'$ and $\Delta T_c/T_c = HH'/OH$.

Formulas for ϵ_c will now be obtained. An application of the law of sines to triangle $HH'K'$ in Figure 22 yields the relation

$$\frac{V\Delta T_c}{\sin(\alpha+\theta_h')} = \frac{-\delta}{\sin\theta_h'}.$$

It follows that

$$\epsilon_c = \frac{\Delta T_c}{T_c} = \frac{V\Delta T_c}{S} = \frac{-\delta\sin(\alpha+\theta_h')}{S\sin\theta_h'} = -\frac{\delta\Theta\sin\alpha}{S}, \tag{75}$$

where

$$\Theta = \frac{\sin(\alpha+\theta_h')}{\sin\alpha\sin\theta_h'} = \cot\alpha + \cot\theta_h'. \tag{76}$$

Taking the value of $\cot\theta_h'$ from (39) permits (76) to be brought to the form

$$\Theta = \frac{1}{\sin\alpha\cos\alpha} + \frac{\tan\alpha + \cos\theta_p'}{\sqrt{1 + \dfrac{2\cos\alpha}{\bar{\mu}(1+\cos\theta_p')}}}. \tag{77}$$

An approximate formula for Θ is obtained by replacing $1+\cos\theta_p'$ by 2, $\cot\theta_p'$ by $1/\theta_p'$, and making use of the formula for θ_p' immediately preceding (45); this formula is

$$\Theta = \frac{1}{\sin\alpha\cos\alpha} + \frac{\tan\alpha}{\sqrt{1+\dfrac{1}{\bar{\mu}}\cos\alpha}} \times \left[1 + \frac{1+\sqrt{1+2\beta}}{2\beta}\left(1 + \frac{1}{\sqrt{1+\dfrac{1}{\bar{\mu}}\cos\alpha}}\right)\right]. \tag{78}$$

When $|\phi|$ is small compared with α, equations (74) and (76) yield the approximate relation

$$\epsilon_c \cong \Theta\phi. \tag{79}$$

The remarks concerning the degree of accuracy of (74) as a formula for δ apply equally to (79) as a formula for ϵ_c.

With the notation expressed in equation (80), equation (78) in a form solved for β is equivalent to

$$\beta = M(1 + \tfrac{1}{2}M).$$

Since

$$S = VT_c = \frac{V^2\beta(\bar{\mu} + \cos\alpha)}{g\bar{\mu}\sin\alpha},$$

$$M = \frac{\tan\alpha}{\sqrt{1 + \frac{1}{\bar{\mu}}\cos\alpha}} \times \frac{1 + \frac{1}{\sqrt{1 + \frac{1}{\bar{\mu}}\cos\alpha}}}{\Theta - \frac{1}{\sin\alpha\cos\alpha} - \frac{\tan\alpha}{\sqrt{1 + \frac{1}{\bar{\mu}}\cos\alpha}}}, \tag{80}$$

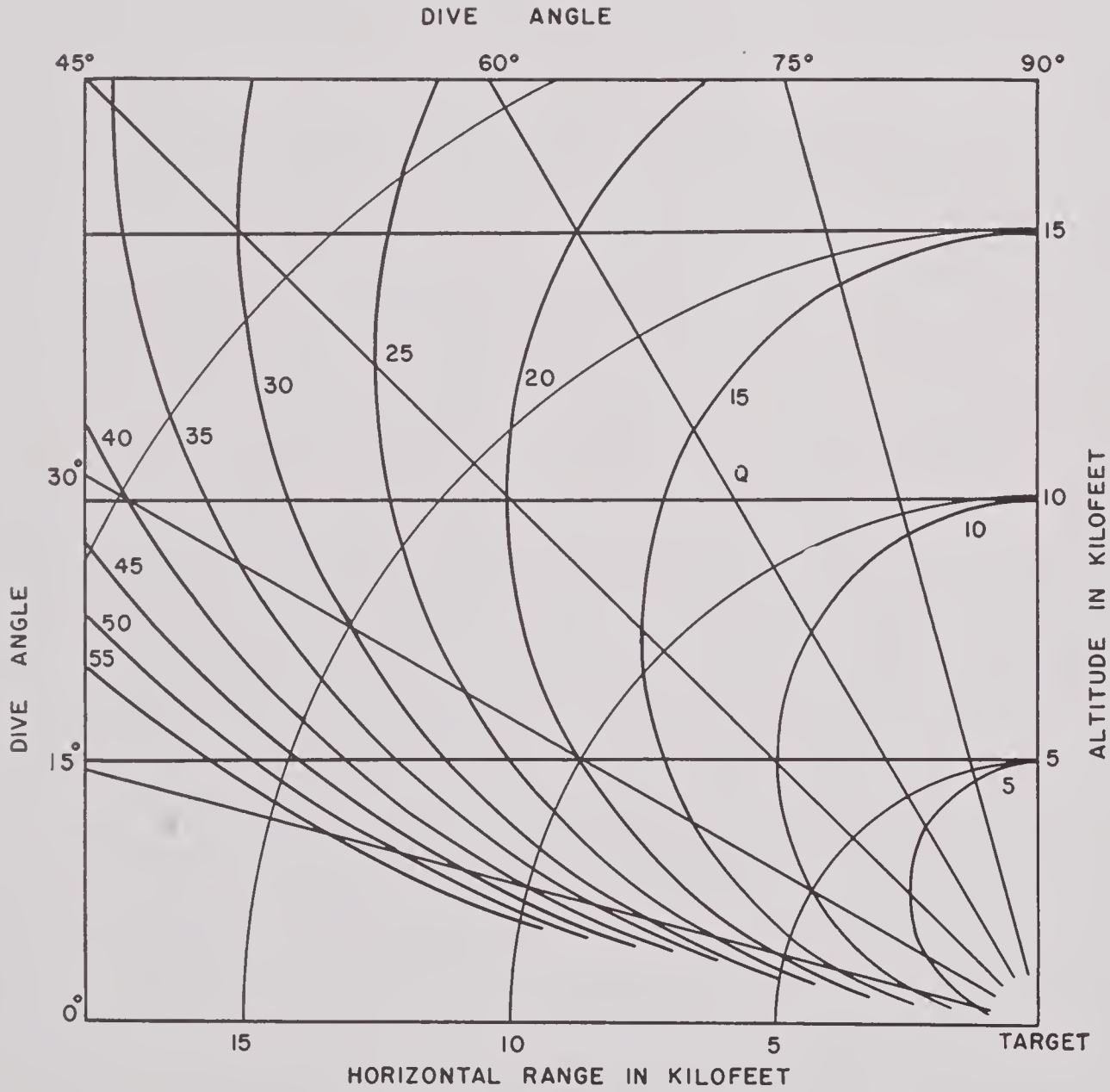

FIGURE 23. Effect of misaligned sight on impact point. Pictorial chart of pull-up points corresponding to different ratios of horizontal impact shift δ_ϕ to angle of misalignment ϕ producing shift (independent of V and $\bar{K}$). Each curve corresponds to constant value of $-\delta_\phi/\phi$, given in *feet/mil* by numerals on respective curves (5 to 55 feet/mil).

it follows that

$$S = \frac{V^2(\bar{\mu} + \cos\alpha)}{g\bar{\mu}\sin\alpha} M(1 + \tfrac{1}{2}M). \qquad (81)$$

Figure 24 is a contour map constructed from equation (81) using $\Theta = \epsilon_c/\phi$ in calculating the value of M in equation (80). Figure 24 shows the various slant ranges and dive angles which correspond to a given value of Θ.

As in the case of Figure 23, Figure 24 becomes inaccurate for very small α or very large ϕ, but becomes accurate for all α and ϕ if the figure attached to each curve is considered as the value of $1{,}000\,\epsilon_c(\cot\phi - \cot\alpha)$ instead of the value of ϵ_c/ϕ.

Figure 24 can be interpreted as a contour map of the function Θ. When so considered the "per cent per mil" figures must be converted by multiplication by $0.01/0.001 = 10$, since ϵ_c is a percentage and ϕ is in mils. The curve marked 0.8 per cent per mil, for example, is also the locus of $\Theta = 8$.

Figure 25 is a contour map constructed from equation (75) for the ratio δ/ϵ_c, i.e., the linear impact error for each per cent change in T_c. In Figure 25 both changes have the same sign. Furthermore, the reciprocals of the $|\delta/\epsilon_c|$ figures on the curves represent the per cent change in T_c required to offset each foot of impact error; and when so interpreted, δ and ϵ_c have opposite signs. Thus this figure is of a general nature, applicable not only to the sight error problem but to all problems involving correction of an impact error by adjustment of T_c. The curves of Figure 25 were plotted by noting that

$$\frac{\delta}{\epsilon_c} = \frac{\delta/\phi}{\epsilon_c/\phi},$$

and making use of Figures 23 and 24.

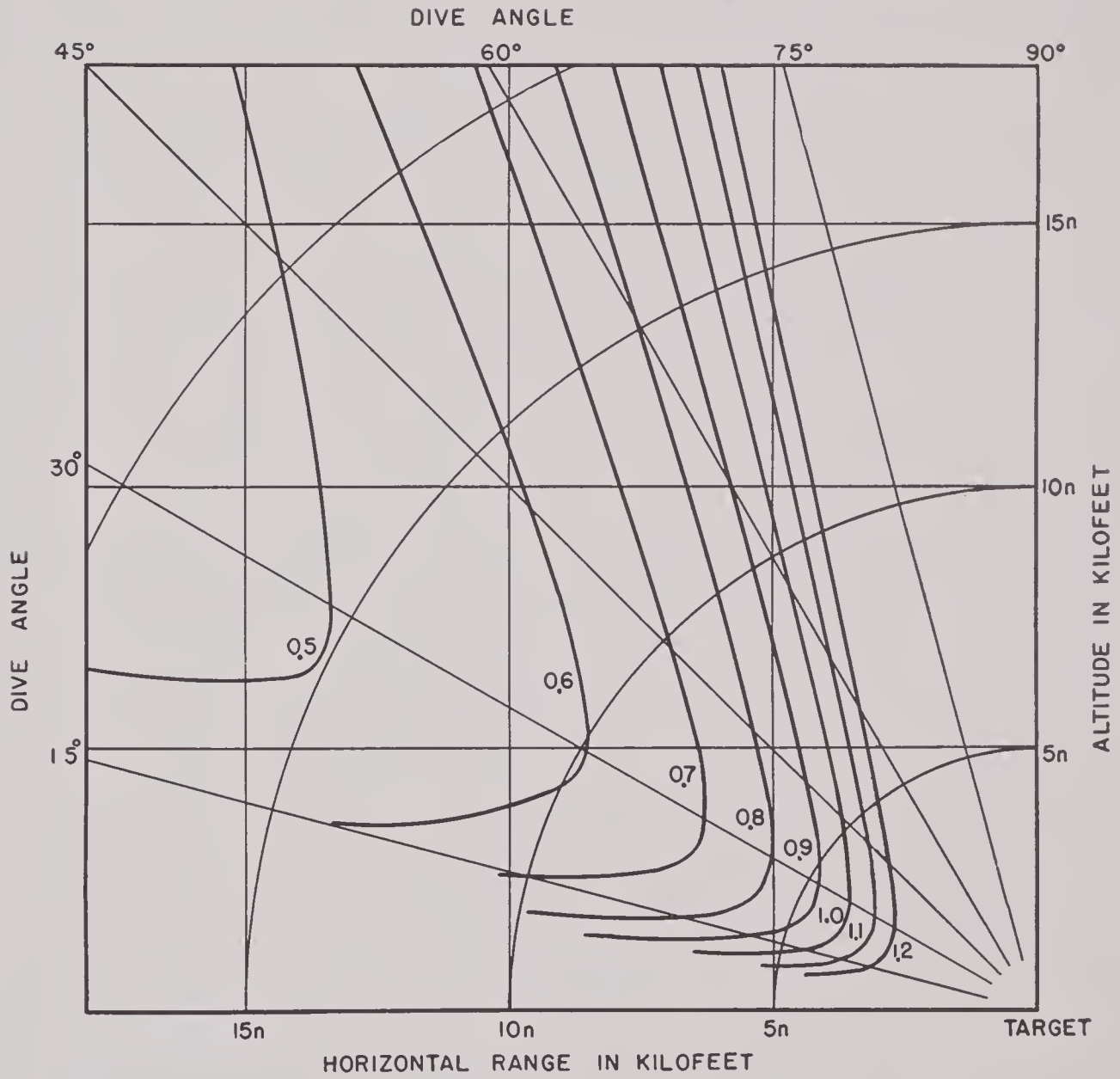

FIGURE 24. Relation between angle ϕ of sight misalignment and relative change $\epsilon = \Delta T_c/T_c$ required to offset its effect. Pictorial chart of pull-up points corresponding to different ratios ϵ_c/ϕ; $\bar{K} = 3$. Scale factor n determined by velocity: $n = \frac{1}{2}$ when $V = 350$ knots; $n = 2$ when $V = 500$ knots. Value of ϵ_c/ϕ represented by each curve is given in *per cent/mil* by numeral on curve (0.5 to 1.2 per cent/mil).

Application of the preceding discussion and of Figures 23 and 24 requires that the value of the sight error ϕ for any specific case, or at least the difference between ϕ values for two specific cases, be known. The effective sight error, however, depends not only on the fixed orientation of the sight with respect to the airplane, but also on the angle of attack, or orientation of the plane with respect to its flight line. The variation of the latter with airspeed and dive angle is appreciable and must be taken into account. depends on the choice of a reference line in the airplane, and for purposes of calculating *differences* in angles of attack one may set $k = 0$ with no loss of generality:

$$\phi_a = \frac{CW \cos \alpha}{V^2}. \tag{83}$$

It is found generally that C has the same value for all planes of a series, as TBM-1 and TBM-1C.

The nomogram of Figure 26 gives this relative

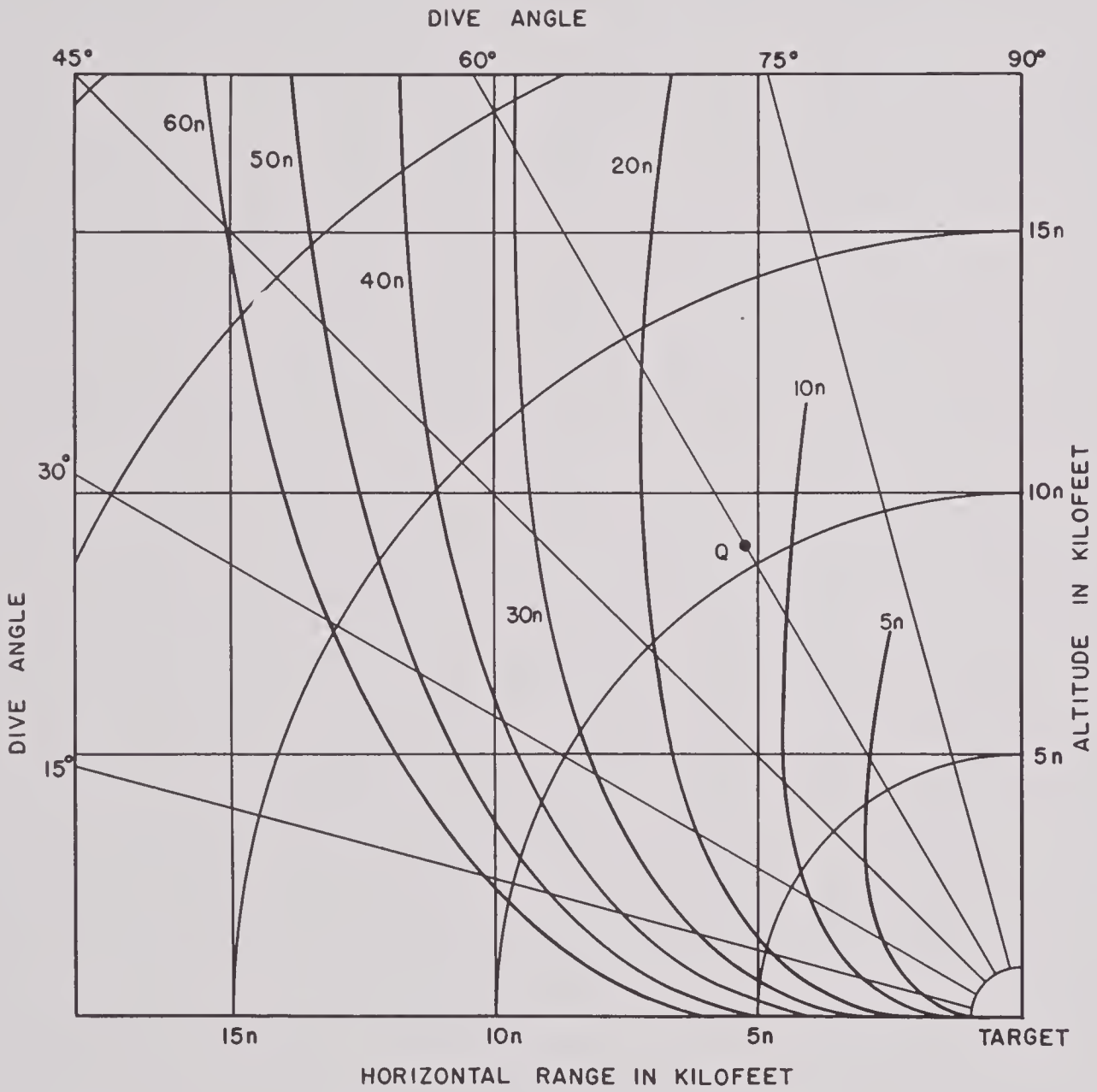

FIGURE 25. Relationship between relative change ϵ_c in T_c and resulting horizontal impact error δ_c. Pictorial chart of pull-up points corresponding to different ratios δ_c/ϵ_c represented by each curve is given in *feet/per cent* by numeral on curve ($5n$ to $60n$ feet/per cent).

The angle of attack ϕ_a is given by the formula

$$\phi_a = \frac{CW \cos \alpha}{V^2} - k, \tag{82}$$

where W is the gross weight of the plane, and C and k are constants for any one plane. The value of k also

angle of attack ϕ_a, as in equation (83), as a function of C, W, V, and α. The calibrations on lines G, H, K, and M, have been determined from values of log C, log W, log V, and log cos α, respectively. Points on line J have been predetermined for each plane at its nominal weight, thus obviating the use of lines G and

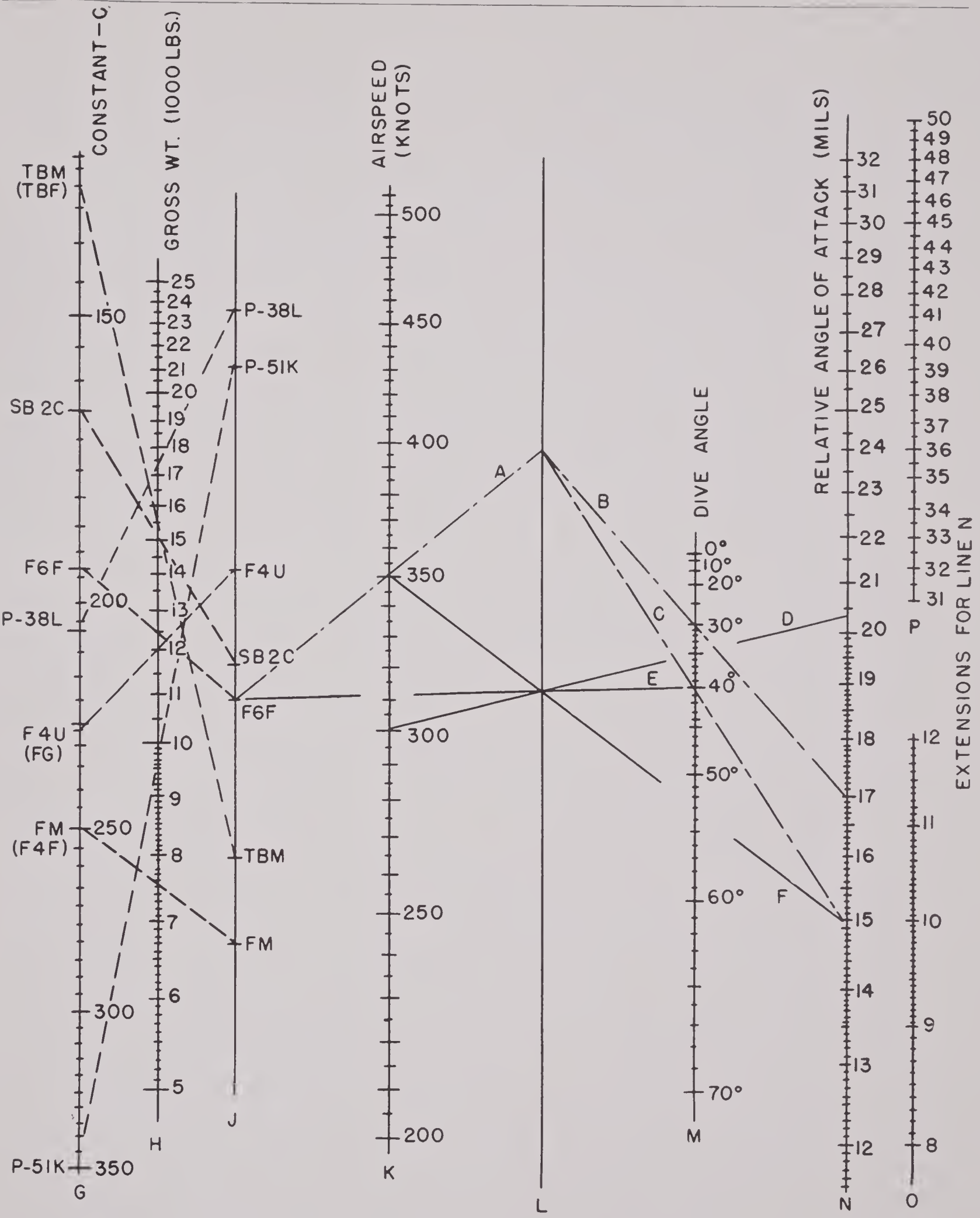

FIGURE 26. Nomogram for determining changes in angle of attack (ϕ_a). For planes at approximately nominal weight (e.g., F4U, 12,000 pounds), start with designated points on line J, already predetermined by dashed lines through lines G and H. Examples: for F6F plane at nominal weight, (1) if V = 350 knots (line A), decreasing α from 40 degrees (line C) to 30 degrees (line B) increases angle of attack by 16.9 − 14.9 = 2.0 mils; (2) if α = 40 degrees (line E), decreasing V from 350 (line F) to 300 knots (line D) increases angle of attack by 20.4 − 14.9 = 5.5 mils.

[redacted]

H whenever the gross weight is approximately nominal.

Lines G through N have been so spaced that airspeed, V, and dive angle, α, may be entered in either order. This property is illustrated by the example appearing on the nomogram. The intersection of line A and line L, corresponding to an F6F at 350 knots, may be joined with several points in turn on line M to obtain ϕ_a on line N for different dive angles at the fixed airspeed; this is illustrated by dashed lines B and C for dive angles of 30 and 40 degrees, respectively. On the other hand, the intersection of line E and line L, corresponding to an F6F at 40 degrees dive angle, may be joined with points on line K to obtain ϕ_a for different airspeeds at the fixed dive angle; this is illustrated by lines D and F for airspeeds of 300 and 350 knots, respectively. The relative convenience of the two methods depends on whether one is concerned more with variation of ϕ_a with dive angle or with airspeed.

According to equation (83), the angle of attack, while independent of range, is increased by a decrease in either airspeed or dive angle. Hence the range of variation in ϕ_a for any given plane is widened by the fact that decreases in dive angle are in practice usually accompanied by decreases in airspeed.

The preceding discussion suggests two alternative methods of correcting for sight misalignment at a *given* range, dive angle, and airspeeds: (1) direct adjustment of the *sight*, until flight and sight lines coincide; or (2) *computer* adjustment, i.e., changing T_c by a percentage ϵ_c determined from Figure 24.

The adjustment required, however, depends in either case on the values of α and V, and in case (2) on S as well. Since it is not feasible to make frequent readjustments of either type in any one plane, in practice a *fixed* adjustment must be made, such as would completely offset the sight error at some chosen intermediate or modal value of S, α, and V. At other values an impact error will generally result, the magnitude of which depends on the method used — a fixed sight adjustment, a fixed computer adjustment, or some combination of the two. The most efficient method is, of course, the one which minimizes this impact dispersion.

The following example illustrates the results of a fixed computer adjustment: The sight installed in an F6F plane at nominal weight (12,400 pounds) is misaligned by -20 mils at slant range $\bar{S} = 7{,}500$ feet, dive angle $\bar{\alpha} = 40$ degrees, and airspeed $\bar{V} = 350$ knots. A fixed per cent adjustment in T_c is made in an amount just sufficient to offset the -20-mil sight error at $(\bar{S}, \bar{\alpha}, \bar{V})$, causing a hit. It is desired to determine the resulting impact error at slant range $S_1 = 12{,}000$ feet, dive angle $\alpha_1 = 60$ degrees, and airspeed $V_1 = 375$ knots.

From Figure 24 the required per cent adjustment in T_c per mil at 7,500 feet, 40 degrees, and 350 knots (point $\bar{P}$) is $\epsilon_c/\phi = 0.75$ per cent per mil, so that for $\phi = -20$ mils, the fixed adjustment is $\epsilon_c = -15.0$ per cent. In other words, under these conditions a 15 per cent decrease in T_c, by itself, would displace the impact point by an amount equal and opposite to the displacement which would result from a -20-mil sight error alone.

At another range, dive angle, and airspeed, these two displacements, while oppositely directed, will generally be unequal in magnitude, and in addition, the angle of attack will generally be different. Thus the impact error at (S_1, α_1, V_1) will be the algebraic sum of three displacement components: (a) the difference $\Delta\phi_a$ between the angles of attack at $(\bar{\alpha}, \bar{V})$ and (α_1, V_1) is a change in sight error and therefore causes an impact displacement δ_a; (b) the original sight error $\phi = -20$ mils, by itself, would result in a positive (beyond-target) impact error δ_ϕ; (c) the adjustment $\epsilon_c = -15$ per cent, by itself, would give a negative (short-of-target) error δ_c.

1. The difference in angle of attack is determined from Figure 26. For an F6F plane at nominal weight, this nomogram gives $\phi_a = 14.9$ mils at $\bar{\alpha} = 40$ degrees, $\bar{V} = 350$ knots, and 8.5 mils (determined by extending line N and using lower extension scale O) at $\alpha_1 = 60$ degrees, $V_1 = 375$ knots. Hence, $\Delta\phi_a = -6.4$ mils. But from Figure 23, at $\alpha_1 = 60$ degrees and $S_1 = 12{,}000$ feet (point Q), $-\delta/\phi \cong 14$ feet per mil, so that the impact displacement due to change in angle of attack is $\delta_a = +90$ feet.

2. From this same ratio $-\delta/\phi = 14$ feet per mil, it follows that the -20-mil sight error in itself causes an impact error $\delta_\phi = +280$ feet.

3. Finally, at 12,000 feet, 60 degrees, and 375 knots, the value of δ_c/ϵ_c may be read from Figure 25. As there defined, $n = (375/350)^2 = 1.148$, so that at 375 knots, 12,000 feet $= (12{,}000/1.148)n = 10{,}450n$ feet. The point Q determined by this slant range and 60-degree dive angle lies between the curves marked $10n$ and $15n$, slightly nearer the latter, so that approximately $\delta_c/\epsilon_c = 13n = 14.9$ feet per per cent. The -15.0 per cent adjustment in T_c therefore displaces the impact point by about $\delta_c = -220$ feet.

The resultant impact error at (S_1, α_1, V_1) is then

[redacted]

$\delta_a + \delta_\phi + \delta_c = +90 + 280 - 220 = 150$ feet, i.e., the bomb may be expected to fall 150 feet beyond the target under the given conditions.

The effect of angle of attack variation may be seen to be of considerable importance. If δ_a were neglected in this example, (2) and (3) alone would yield an impact error of + 60 feet, or only 40 per cent of that given in the above. Quite often even the algebraic sign of the resultant error is changed by this effect.

According to the wording of the hypothesis, this example may at first appear to typify only the computer adjustment method. But if the original misalignment were given not as −20, but as −30 mils, of which 10 mils were corrected by a sight adjustment and the balance by a computer adjustment, the solution would be identical, yet the problem would appear more general, involving a combination of sight and computer adjustments. Further details are in reference 101.

6.5 AIR RESISTANCE IN BOMB TOSSING[1,55]

6.5.1 The Trajectory Equations in Air

The study of air resistance effects is facilitated by utilizing a coordinate system consisting of horizontal and vertical coordinates ξ and η with origin at the point of release as indicated in Figure 27. In this figure the solid curve PH is a vacuum trajectory through the target at H, $PH'K'$ an air trajectory with the same release conditions, and $P''H$ an air trajectory from a release point determined so that the bomb will hit the target. The percentage increase in T_c required to obtain the trajectory $P''H$ is

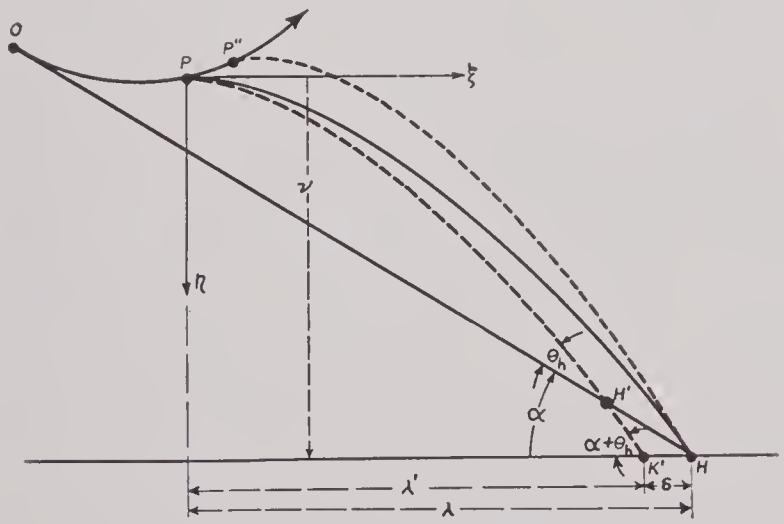

FIGURE 27. Flight and trajectory diagram of toss bombing maneuver, showing ξ,η coordinate system and three trajectories: solid curve PH: theoretical vacuum trajectory through target H; dashed curve $P'K'$: air trajectory with same release conditions; dashed curve $P''H$: air trajectory from release point so determined as to produce hit.

$$\frac{\Delta T_c}{T_c} = \frac{V\Delta T_c}{VT_c} = \frac{\Delta S}{S} = \frac{HH'}{OH}. \tag{84}$$

The equations of the vacuum trajectory, using ξ,η coordinates, are

$$\xi = U_p(t - T_p),$$

and

$$\eta = W_p(t - T_p) + \tfrac{1}{2}g(t - T_p)^2, \tag{85}$$

where U_p and W_p are the horizontal and vertical components of velocity at release. If the coordinates of the target are $\xi_h = \lambda$, $\eta_h = \nu$, elimination of the quantity $t - T_p$ between equations (85) yields the relation

$$\nu = \frac{W_p}{U_p}\lambda + \frac{g}{2U_p^2}\lambda^2. \tag{86}$$

The corresponding relation for the air trajectory $PH'K'$ will now be obtained. If $u = \dot{\xi}$ and $w = \dot{\eta}$, then the velocity of the bomb in its path is $v = \sqrt{u^2 + w^2}$. The retarding acceleration, a, due to the air, is assumed to be representable in the form

$$a = Bv^2, \tag{87}$$

where B is constant along the trajectory. The degree of accuracy of this assumption will be discussed in Section 6.5.2. The components of the retarding acceleration are

$$\begin{aligned} a_\xi &= Buv, \\ a_\eta &= Bwv. \end{aligned} \tag{88}$$

From equation (88) the equations of motion of the bomb are

$$\begin{aligned} \dot{u} &= -Buv, \\ \dot{w} &= g - Bwv. \end{aligned} \tag{89}$$

Let ϕ be the angle between a tangent at any point on the trajectory and the horizontal, so that

$$\tan\phi = \frac{w}{u}. \tag{90}$$

Differentiating both members with respect to t gives

$$(\sec^2\phi)\dot{\phi} = \frac{u\dot{w} - w\dot{u}}{u^2},$$

which, by use of equation (89) can be reduced to

$$\dot{\phi} = \frac{g\cos\phi}{v}. \tag{91}$$

Equating components of acceleration in the direction of the tangent to the path gives the relation

$$\dot{v} = g \sin \phi - Bv^2. \tag{92}$$

Between equations (91) and (92) the quantity dt can be eliminated. This yields the relation

$$\frac{dv}{d\phi} = v \tan \phi - \frac{Bv^3}{g \cos \phi}, \tag{93}$$

which is a differential equation for v as a function of ϕ. While this differential equation can be integrated in terms of the elementary functions of mathematics, its solution in this form is quite cumbersome when it comes to making applications in numerical computation. For this reason the approximation

$$B \cong B \frac{\cos \phi}{\cos \bar{\phi}}, \tag{94}$$

is made, in which $\bar{\phi}$ is a mean value of ϕ. This approximation is quite good when the total change in direction along the trajectory is not too large and when α (and hence ϕ) is not too close to 90 degrees.

With the use of equation (94), equations (89) become

$$\begin{aligned} \dot{u} &= - Bu^2 \sec \bar{\phi}, \\ \dot{w} &= g - Buw \sec \bar{\phi}. \end{aligned} \tag{95}$$

By integration of the first of equations (95) we have

$$\frac{1}{u} - \frac{1}{U_p} = B(t - T_p) \sec \bar{\phi}$$

or

$$u = \frac{U_p}{1 + BU_p(t - T_p) \sec \bar{\phi}}. \tag{96}$$

The use of this result in the second of (95) gives

$$\dot{w} = g - \frac{BU_p w \sec \bar{\phi}}{1 + BU_p(t - T_p) \sec \bar{\phi}}$$

whose solution is

$$w = \frac{W_p + [g(t - T_p) + (1/2)BU_p(t - T_p)^2 \sec \bar{\phi}]}{1 + BU_p(t - T_p) \sec \bar{\phi}}. \tag{97}$$

Equations (96) and (97) give the components of velocity in terms of time measured from the beginning of pull-up and the conditions at release. Further integration gives the coordinates ξ and η of the bomb after release in the form

$$\begin{aligned} \xi &= \frac{\cos \bar{\phi}}{B} \ln \left[1 + \frac{BU_p (t - T_p)}{\cos \bar{\phi}} \right] \\ \eta &= \tfrac{1}{4} g (t - T_p)^2 + \frac{g(t - T_p)}{2BU_p \sec \bar{\phi}} \\ &\quad + \frac{W_p - g \cos \bar{\phi}\ (2BU_p)}{BU_p \sec \bar{\phi}} \ln \left[1 + \frac{BU_p(t - T_p)}{\cos \bar{\phi}} \right]. \end{aligned} \tag{98}$$

The elimination of the quantity $t - T_p$ between these equations yields the Cartesian equation of the trajectory in the form

$$\eta = \frac{W_p}{U_p} \xi + \frac{g\xi}{2U_p^2} [1 + \epsilon(\xi)], \tag{99}$$

where

$$\begin{aligned} \epsilon(\xi) &= -1 - \frac{\cos \bar{\phi}}{B\xi} + \frac{\cos^2 \bar{\phi}}{2B^2\xi^2} (e^{2B\xi \sec \bar{\phi}} - 1) \\ &= 2 \sum_{K=1}^{\infty} \frac{(2B \sec \bar{\phi})^K}{(K + 2)!}, \end{aligned} \tag{100}$$

for which an approximate formula is

$$\epsilon(\xi) \cong \tfrac{2}{3} B\xi \sec \bar{\phi}. \tag{101}$$

Equation (99) is seen to differ from (86) only in the term $\epsilon(\xi)$ which is, therefore, the term due to air resistance.

6.5.2 The Constant *B*

The quantity B, in reciprocal feet, will now be expressed in terms of the ballistic coefficient C. Modern ballistics tables are based on the Gâvre function $G(v)$, defined as the retardation of a projectile of unit ballistic coefficient at velocity v. An examination of tables of $G(v)$ shows that $G(v)$ is very nearly proportional to v^2 in the range of velocities used in bomb tossing. Thus, in the interval from 350 feet/second to 800 feet/second the ratio $G(v)/v^2$ decreases from 4.51×10^{-5} at $v = 350$ feet/second to 4.14×10^{-5} at $v = 600$ feet/second and then increases to 4.51×10^{-5} at $v = 800$ feet/second. The value 4.25×10^{-5} may be selected as probably the best value for this ratio, so that

$$B \cong \frac{4.25 \times 10^{-5}}{C}.$$

6.5.3 The Ground Error

The ground error ($\delta = K'H$ in Figure 27) can now be found by placing $\eta = \nu$ and $\xi = \lambda - \delta$ in equation (99). This gives

$$\nu = \frac{W_p}{U_p} (\lambda - \delta) + \frac{g(\lambda - \delta)^2}{2U_p^2} [1 + \epsilon(\lambda - \delta)],$$

or, making use of equation (86)

$$O = - \frac{W_p \delta}{U_p} + \frac{g}{2U_p^2} [-2\lambda\delta + \delta^2 + (\lambda - \delta)^2 \epsilon(\lambda - \delta)]. \tag{102}$$

In equation (102) the unknown δ is obviously much smaller than λ. Hence the term δ^2 can be neglected in comparison with the term $-2\lambda\delta$. In the same way, and by using equation (101) the term $(\lambda - \delta)^2\epsilon(\lambda - \delta)$ can be replaced by

$$\tfrac{2}{3}B(\lambda^3 - 3\lambda^2\delta)\sec\overline{\phi}.$$

Thus equation (102) becomes

$$O = -\frac{W_p\delta}{U_p} + \frac{g}{2U_p{}^2}[-2\lambda\delta + \tfrac{2}{3}B(\lambda^3 - 3\lambda^2\delta)\sec\overline{\phi}]$$

whose solution for δ is

$$\delta = \frac{Bg\lambda^3\sec\overline{\phi}}{3(U_pW_p + g\lambda + Bg\lambda^2\sec\overline{\phi})}. \qquad (103)$$

For use in bomb tossing this equation may be expressed in terms of the dive angle α, the velocity of the airplane V, the slant range $S = VT_c$, the average pull-up acceleration $\bar{\mu}$, and the ratio $\tau = T_p/T_c$. For this purpose the following relations will be used:

$$U_p = V\cos(\alpha - \theta_p) \qquad W_p = V\sin(\alpha - \theta_p)$$

$$\lambda = S\cos\alpha - x_p\cos\alpha - y_p\sin\alpha \qquad \overline{\phi} \cong \alpha$$

$$x_p = \frac{V^2}{g\bar{\mu}}\sin\theta_p \qquad y_p = \frac{V^2}{g\bar{\mu}}(1 - \cos\theta_p).$$

It is found that

$$\lambda = S\cos\alpha\left(1 - \tau\frac{\sin\theta_p/2}{\theta_p/2}\cdot\frac{\cos(\alpha - \theta_p/2)}{\cos\alpha}\right), \qquad (104)$$

$$\delta = \tfrac{1}{3}BS^2\theta_p\cos^2\alpha\left(1 - \tau\frac{\sin\theta_p/2}{\theta_p/2}\cdot\frac{\cos(\alpha - \theta_p/2)}{\cos\alpha}\right)\times\left\{\tau\bar{\mu}\sin(\alpha - \theta_p)\cos(\alpha - \theta_p)\right.$$

$$\left. + \theta_p\cos\alpha\left[1 - \tau\frac{\sin(\theta_p/2)}{\theta_p/2}\cdot\frac{\cos(\alpha - \theta_p/2)}{\cos\alpha}\right] + \theta_pBS\cos\alpha\left[1 - \tau\frac{\sin(\theta_p/2)}{\theta_p/2}\cdot\frac{\cos(\alpha - \theta_p/2)}{\cos\alpha}\right]^2\right\}^{-1}. \qquad (105)$$

A good approximation to δ is obtained by replacing $\sin\theta_p$ by θ_p, $\cos\theta_p$ by unity, and discarding all terms of degree two or greater in the small quantities τ and θ_p. This approximate formula is

$$\delta \cong \frac{BS^2\theta_p\cos\alpha}{3[\tau\bar{\mu}\sin\alpha + (1 + BS)\theta_p]}. \qquad (106)$$

6.5.4 The Correction for Air Resistance

By using formula (106) to calculate the horizontal range error caused by air resistance, the percentage correction $\Delta T_c/T_c$ of T_c which will secure a hit can be found. Writing

$$\frac{\Delta T_c}{T_c} = \frac{V\Delta T_c}{\delta}\cdot\frac{\delta}{S},$$

the value of the first fraction is taken from equation (44) and the value of the second from equation (106). This results in the formula

$$\frac{\Delta T_c}{T_c} = \frac{\sin\alpha\cos\alpha + \theta_p[\sin^2\alpha + \sqrt{1 + (1/\bar{\mu})\cos\alpha}]}{\sqrt{1 + (1/\bar{\mu})\cos\alpha}}\times\frac{BS}{3[\tau\bar{\mu}\sin\alpha + (1 + BS)\theta_p]}. \qquad (107)$$

This formula gives the relative increase in T_c which will correct for air resistance. Formula (107) may be approximated to in a variety of ways. The approximation to be made here consists of the following:

1. First take $\alpha = 35$ degrees, $\overline{K} = 3$, leaving the formula

$$\frac{\Delta T_c}{T_c} \cong (.5675 \times 1.814\,\theta_p)\times\frac{10^{-5}\,S/C}{1.2517 + (1 + BS)\theta_p} = a\frac{S}{C}.$$

2. Next, take the B which remains in the formula to be $(4.25/2)\,10^{-5} = 2.125 \times 10^{-5}$, and calculate the value of a for $V = 500$ feet/second and $T_c = 5$ seconds. Then calculate a for $V = 500$ feet/second and $T_c = 20$ seconds. The average of the two values thus found will be used in an approximate formula for $\Delta T_c/T_c$.

It is found that when $T_c = 5$ seconds, $a = 2.697 \times 10^{-5}$, and when $T_c = 20$ seconds, $a = 2.103 \times 10^{-5}$. Consequently the value

$$\frac{2.697 + 2.103}{2}\,10^{-5} = 2.4 \times 10^{-5}$$

is chosen for a. This gives as a rough formula

$$\frac{\Delta T_c}{T_c} \cong 2.4\,\frac{S \times 10^{-5}}{C}. \qquad (108)$$

This correction differs slightly from the correction given in reference 140, because of a simplified presentation of the theory. Variations occur in the approximations for δ, starting with equation (105).

6.6 WIND CORRECTION AND TARGET MOTION

6.6.1 Introduction

In any consideration of the effect of wind or target motion on the bomb tossing maneuver, it is necessary to specify the type of course which is to be flown by the aircraft. Two types of approach are ordinarily most useful, the collision course and the pursuit course.

In the pursuit course the airplane flies in such a way as to keep the center of the sight on the target at all times. For a stationary target and under no wind the flight path will then be a straight line which is coincident with the collision course for this case. If wind is present, however, or if the target is in motion, the pursuit course will be curved. A collision course, on the other hand, will be a straight line characterized by the condition that the airplane, if it continues on this flight path, will ultimately collide with the target.

Other types of flight paths may be obtained if, instead of a fixed sight, a lead-computing sight is used, i.e., a sight which if kept on the target ultimately results in the flight line differing from the sight line by an amount sufficient to obtain a hit. All of these possibilities will be discussed in this section.

6.6.2 Collision Course in the Presence of Wind [71,80]

Figures 28 and 29 show the collision course approach in the presence of wind or target motion for the case in which the wind or target motion vectors lie in a vertical plane containing the velocity vector V of the aircraft, assumed to be constant during the dive. In order to establish a collision course for a target initially located at E_0 the pilot must offset his aiming point by the angle ϕ from the center of the sight. In Figure 28 it is shown schematically that, if the wind speed does not vary with altitude, the angle ϕ is constant as the target moves successively through points E_0, E_1, and E_2 at times $t = 0$, $t = T_1$, and $t = T_2$. The line OE_c is the collision course, of length VT_c, along which the airplane has the velocity V. The relative velocity between airplane and target is the vector **U**.

Figure 29 shows that target motion with velocity V_e is equivalent to a wind of velocity W, provided $W = -V_e$. Again the angle ϕ is constant and is the same as in the target motion case. The time to target is T_c, although the collision course length as

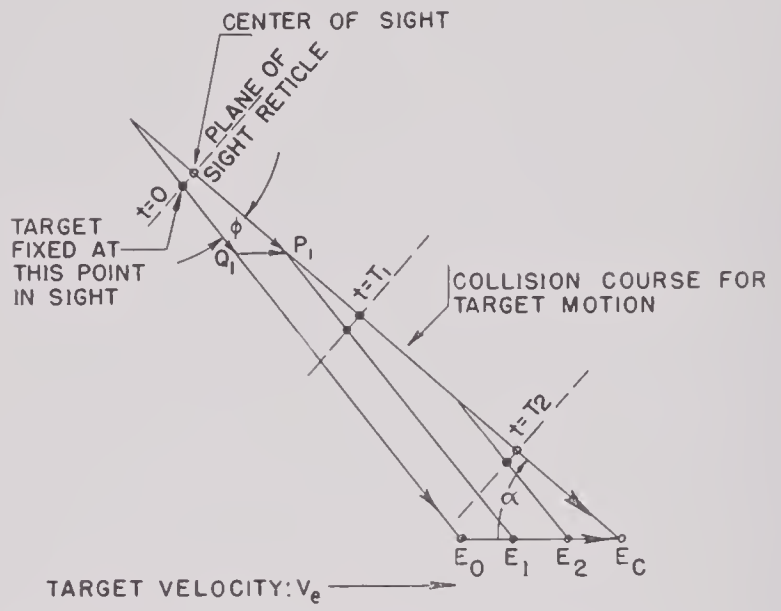

FIGURE 28. Diagram of collision course approach to moving target. (For details see text, Section 6.6.2.)

measured relative to the ground is UT_c. The relative velocity U is also the resultant velocity in this case. What was the dive angle α in the target motion case becomes the aircraft heading angle. Thus the equivalence between target motion with

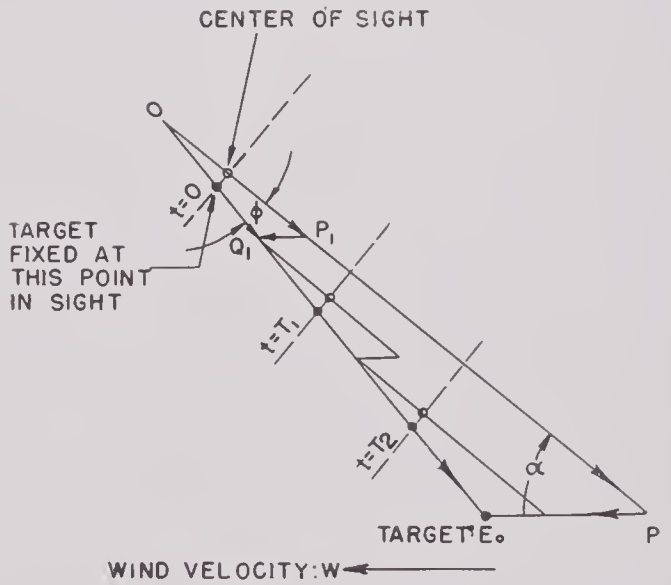

FIGURE 29. Diagram of collision course approach to stationary target in presence of wind. (For details see text, Section 6.6.2.)

velocity V_e and wind with velocity $W = -V_e$ consists in: (1) the same offset angle, ϕ; (2) the same time to target T_c; (3) the same aircraft velocity V; and (4) the dive angle in the first case being equal to the aircraft heading angle in the second case.

Accordingly, the wind correction sighting grids,[71,80] described in Section 2.4 may be used for both target motion and wind velocities, provided the target velocity vector is reversed in direction. The theory involved in the construction of these charts will now be developed.

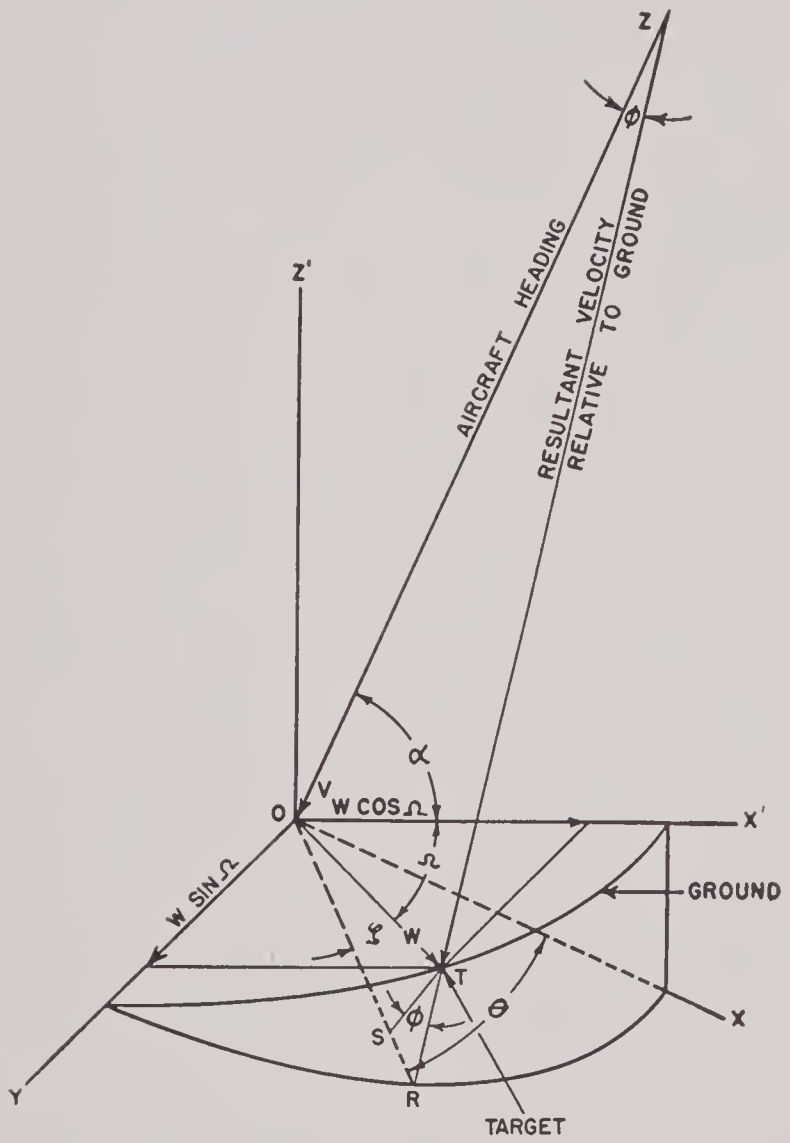

FIGURE 30. Velocity vector diagram illustrating method of construction of wind correction charts. (For details see text, Section 6.6.2.)

Referring to Figure 30, let W be the wind velocity, assumed horizontal, referred to the ground, and let V be the airplane velocity relative to the air mass. The plane $X'Y'$ is the horizontal plane of the ground and OZ' is vertical. The airplane is in the plane of X' and Z', headed along the direction $\overline{ZO}$ with a velocity V so that this direction coincides with the center pip of the sight reticle. However, the wind causes the airplane to follow a flight path along the direction of the resultant velocity. The plane of X and Y is normal to the aircraft's heading and hence constitutes a plane parallel to the sighting plane of the reticle. If the pilot flies so that the target is located at the fixed point R in his sight, the flight path will be along the line $\overline{ZT}$, which is the required collision course. The immediate objective is the locus of point R as the wind velocity vector varies in direction through 360 degrees.

Several relations between the angles marked in Figure 30 will be useful. These are all obtained by projecting the vector W in various ways. By projecting W onto OZ a length equal to $\overline{ST}$ or $W \sin \zeta$ is obtained. By projecting onto OZ the components $W \cos \Omega$ and $W \sin \Omega$ on the X' and Y axes respectively and adding these projections, the result $W \cos \Omega \cos \alpha$ is obtained. (The projection of $W \sin \Omega$ on OZ is zero.) It follows that

$$\sin \zeta = \cos \Omega \cos \alpha. \tag{109}$$

In the same way by projecting first W and then its components onto OX the relation

$$\cos \zeta \cos \theta = \cos \Omega \sin \alpha \tag{110}$$

is obtained, and similar projections onto OY result in

$$\cos \zeta \sin \theta = \sin \Omega. \tag{111}$$

Again from Figure 30, it is seen that

$$r = \overline{OR} = \overline{OS} + \overline{SR} = W \cos \zeta + \overline{ST} \tan \phi$$
$$= W \cos \zeta + \overline{ST} \cdot \frac{r}{V},$$

whence, solving for r,

$$r = \frac{W \cos \zeta}{1 - \dfrac{\overline{ST}}{V}}.$$

The matter of dimensions is ignored here.

But by equation (109)

$$\overline{ST} = W \sin \zeta = W \cos \Omega \cos \alpha.$$

Hence

$$r = \frac{W \cos \zeta}{1 - \omega \cos \Omega \cos \alpha}, \tag{112}$$

where $\omega = W/V$. Solving equations (110) and (111) as simultaneous equations for the angles ζ and Ω gives

$$\tan \Omega = \sin \alpha \tan \theta$$

$$\cos \zeta = \frac{\sin \alpha}{\sqrt{\cos^2 \theta + \sin^2 \alpha \sin^2 \theta}}. \tag{113}$$

By means of equation (113) equation (112) can be expressed in a form free of ζ and Ω, namely,

$$r = \frac{W \sin \alpha}{\sqrt{\cos^2 \theta + \sin^2 \alpha \sin^2 \theta - \omega \cos \alpha \cos \theta}}. \tag{114}$$

This is the polar equation of the locus of R.

On clearing equation (114) of fractions, and using the relations $x = r\cos\theta$ and $y = r\sin\theta$. The equation becomes

$$\sqrt{x^2 + y^2\sin^2\alpha} - \omega x\cos\alpha = W\sin\alpha,$$

which can be put into the form

$$\frac{\left(x - \dfrac{W\omega\sin\alpha\cos\alpha}{1-\omega^2\cos^2\alpha}\right)^2}{\dfrac{W^2\sin^2\alpha}{(1-\omega^2\cos^2\alpha)^2}} + \frac{y^2}{\dfrac{W^2}{1-\omega^2\cos^2\alpha}} = 1. \quad (115)$$

Equation (115) is recognized as the equation of an ellipse for each set of values of W, V, and α. One of these ellipses is shown in Chapter 2, Figure 20.

When x and y are nondimensional, say in mils, then the ellipses are functions of the nondimensional parameter ω. This is what makes possible the plotting of ellipses with ω as the only variable. Equation (115) assumes the nondimensional form if all W's are replaced by ω.

Several remarks of interest can be made from suitable interpretations of either equation (114) or (115). Among these are the following:

1. Since $\omega^2\cos^2\alpha << 1$, the major axes of the ellipses are nearly proportional to W, while the minor axes are shorter than the major axes by the factor $\sin\alpha$.

2. For very small ω, that is, small wind velocity, the center of each ellipse is near the origin.

3. For small positive α the ellipses are narrow, extending along the x axis, while for large α, they are nearly circular, the radius varying but little from W.

6.6.3

Ground Error in a Collision Course

A study of Figure 28 shows that the collision course which is established is such that the bomb director will cause the bomb impact to be at the point E_c. Let O be the point where pull-up is initiated and T_e the pull-up time plus the time-of-fall of the bomb. At time T_e the target will be a distance V_eT_e from E_o, but the bomb will strike at point E_c. Hence the ground error in a collision course approach is

$$\delta_c = V_e(T_c - T_e). \quad (116)$$

Using equation 11 of Chapter 2 as a source of T_e and approximating to the trigonometric functions in the usual way, it is found that

$$T_e \cong T_p + \frac{V\sin\theta_p}{g\cos\alpha}\left[1 + \sqrt{1 + \frac{1}{\bar{\mu}}\cos\alpha}\right],$$

or, by making use of equation (4) of Chapter 2

$$T_e \cong T_p\left[1 + \frac{\bar{\mu}}{\cos\alpha}\left\{1 + \sqrt{1 + \frac{1}{\bar{\mu}}\cos\alpha}\right\}\right]$$

$$= T_p\,\frac{\bar{K} + \sqrt{\bar{K}\,(\bar{K} - \cos\alpha)}}{\cos\alpha}. \quad (117)$$

Using the ψ_1 function as a means of expressing T_p this becomes

$$T_e \cong \frac{\bar{K} + \sqrt{\bar{K}\,(\bar{K} - \cos\alpha)}}{K + \sqrt{\bar{K}^2 - \bar{K}}} \cdot \frac{T_c\,\psi_1}{\cos\alpha} = nT_c \quad (118)$$

where

$$n = \frac{\bar{K} + \sqrt{\bar{K}\,(\bar{K} - \cos\alpha)}}{\bar{K} + \sqrt{\bar{K}^2 - \bar{K}}} \cdot \frac{\psi_1}{\cos\alpha}.$$

In terms of n, equation (118) becomes

$$\delta_c = (1 - n)V_eT_c. \quad (119)$$

Values of $1 - n$ are given in Table 12 and shown graphically in Figure 31, both based on $\bar{K} = 3$.

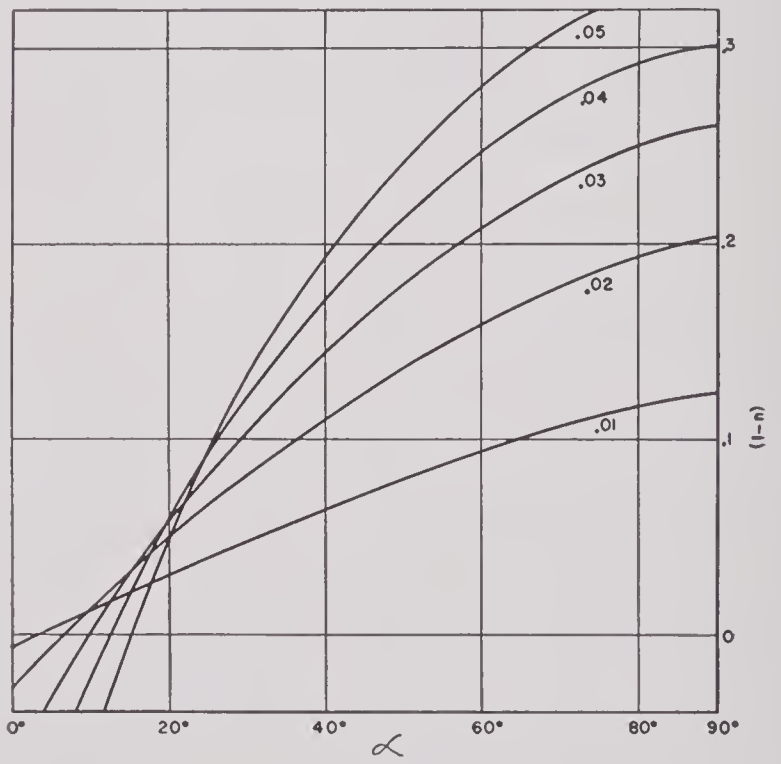

FIGURE 31. Curves for determining horizontal impact error δ_c resulting from collision course approach with wind or target motion. $(1 - n) = (\delta_c/V_cT_c)$ versus α for different values of T_c/V; $\bar{K} = 3$.

These show that for $\alpha > 12$ degrees, the bomb goes over the target. The use of Table 12 and equation (119) permits an easy determination of the range error. For example, if $\alpha = 30$ degrees, $V = 500$

feet/second, and $T_c/V = 0.03$, the table gives $1 - n = 0.104$. Assuming $V_e = 50$ feet/second, equation (119) gives

$$\delta_c = 0.104 \times 50 \times 15 = 78 \text{ feet.}$$

To obtain a hit under collision course conditions it is necessary to reduce the lead angle ϕ or to change operation of the bomb director so that it will compute a release time dependent on the target or wind velocity. An analysis of this problem is given in reference 5. The equation for the release time when flying a collision course in the presence of wind or target motion characterized by the lead angle ϕ_c is given by

$$T_{pc} = \Gamma\left[\left(1 + \frac{2T_c}{\Gamma}\right)^{\frac{1}{2}} - 1\right] \times \left[1 - \left(\frac{\mu}{K + \sin\alpha \tan\phi_c}\right)^{\frac{1}{2}}\right]$$

where

$$\Gamma = \frac{V(\sin\alpha \sin\phi_c + K\cos\phi_c)}{\mu g \sin(\alpha - \phi_c)}.$$

In this formula ϕ_c is positive if U is above V; that is, V_e is in a direction opposite to that in Figure 28.

Table 12. Values of $(1 - n)$.

α \ T_c/V	0.01	0.02	0.03	0.04	0.05
0°	− 0.006	− 0.026	− 0.066	− 0.139	− 0.284
10°	0.012	0.013	0.002	− 0.023	− 0.069
20°	0.031	0.062	0.058	0.058	0.050
30°	0.047	0.081	0.104	0.121	0.131
40°	0.064	0.110	0.144	0.171	0.193
50°	0.079	0.136	0.179	0.213	0.241
60°	0.094	0.159	0.208	0.247	0.280
70°	0.106	0.178	0.232	0.275	0.310
80°	0.116	0.194	0.250	0.292	0.331

6.6.4 Pursuit Course Approach[81]

For this type of approach the pip in the center of the sight is kept fixed on the target. It will be shown that in the presence of wind the flight line is curved, so that the dive angle varies with time.

In Figure 32, let (R, α) be the polar coordinates of the airplane during the dive, these coordinates referred to an origin at the target H. The angle ϕ is the angle between the sight line, which is along the radius R, and the flight line, which is tangent to the resultant velocity vector **U**. Thus at each instant the airplane is pointed along R at H but moving along a path making an angle ϕ with R.

Equating expressions for components of velocity yields the equations

$$-\frac{dR}{dt} = V + W\cos\alpha, \quad R\frac{d\alpha}{dt} = W\sin\alpha. \qquad (120)$$

Elimination of the quantity dt by division results in the differential equation

$$-\frac{dR}{R} = \left(\frac{\cos\alpha}{\omega} + \cot\alpha\right)d\alpha,$$

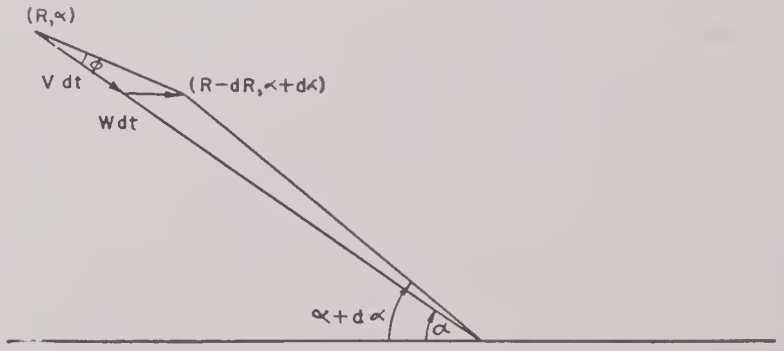

Figure 32. Instantaneous vector diagram for pursuit course approach. (For details see text, Section 6.6.4.)

where $\omega = W/V$. This differential equation is easily integrated to give

$$R = \frac{A}{\sin\alpha\,(\tan\alpha/2)^{\frac{1}{\omega}}}, \qquad (121)$$

where A is the constant of integration, which may be determined by conditions at the first altitude point. The relation (121) is the polar equation of a spiral resembling a logarithmic spiral.

From equation (120) the expression for ϕ is obtained.

$$\tan \phi = \frac{-Rd\alpha}{dR} = \frac{W \sin \alpha}{V + W \cos \alpha} = \frac{\omega \sin \alpha}{1 + \omega \cos \alpha}. \tag{122}$$

Since α varies during the timing run, it follows that ϕ will vary. The amount of variation in α will now be determined.

Using the subscripts 1 and 2 to designate values at the beginning and end of the timing run, and making use of equation (121) the following relations are obtained:

$$\frac{6}{5} = \frac{h_1}{h_2} = \frac{R_1 \sin \alpha_1}{R_2 \sin \alpha_2} = \left(\frac{\tan \alpha_2/2}{\tan \alpha_1/2}\right)^{\frac{1}{\omega}}.$$

It follows that

$$\frac{\tan \alpha_2/2}{\tan \alpha_1/2} = (1.2)^{\omega}. \tag{123}$$

Writing

$$\tan \frac{\alpha_2}{2} = \tan\left(\frac{\alpha_1}{2} + \frac{\alpha_2 - \alpha_1}{2}\right)$$

$$= \frac{\tan (\alpha_1/2) + \tan (\alpha_2 \alpha_1/2)}{1 - \tan(\alpha_1/2) \tan [(\alpha_2 - \alpha_1)/2]},$$

substituting into equation (123), and clearing of fractions, a linear equation for $\tan [(\alpha_2 - \alpha_1)/2]$ results. The solution of this linear equation is

$$\tan \frac{\alpha_2 - \alpha_1}{2} = \tfrac{1}{2} \sin \alpha_1 \frac{(1.2)^{\omega} - 1}{(1.2)^{\omega} \sin^2 \alpha_1/2 + \cos^2 \alpha_1/2}. \tag{124}$$

Since the right-hand member of equation (124) increases when ω increases, and since the largest value of ω due to wind is about 0.25 ($W = 60$ knots, $V = 240$ knots), it can be asserted that

$$\tan \frac{\alpha_2 - \alpha_1}{2} < \tfrac{1}{2} \sin \alpha_1 \frac{(1.2)^{\frac{1}{4}} - 1}{(1.2)^{\frac{1}{4}} \sin^2 \alpha_1/2 + \cos^2 \alpha_1/2}$$

$$< \tfrac{1}{2} \sin \alpha_1 [(1.2)^{\frac{1}{4}} - 1] = \frac{0.0467}{2} \sin \alpha_1.$$

Hence $\alpha_2 - \alpha_1 < 0.0467 \sin \alpha_1$. Taking $\alpha_1 = 60$ degrees as the largest dive angle to be used, it is found that $\alpha_2 - \alpha_1 < 0.0405$ rad < 2.4 degrees. Consequently the change in dive angle between the first and second altitude points is negligible.

6.6.5

Ground Error in a Pursuit Course

Figure 33 is a diagram of the timing run while flying a pursuit course (R_1, α_1) and (R_2, α_2) being the polar coordinates of the two altitude points referred to H as origin. The pull-up is assumed to begin at the second altitude point. The velocity of the airplane during pull-up is the constant resultant velocity U.

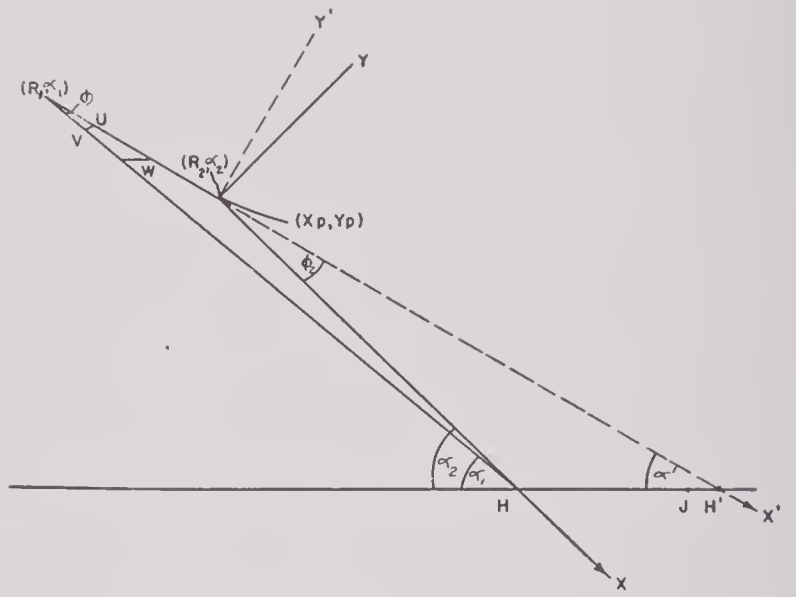

FIGURE 33. Flight diagram of timing run (first to second altitude) for pursuit course approach. (For details see text, Section 6.6.5.)

Let T_c be the time to target indicated by the altimeter. With this time to target the bomb impact would be at point H' if the dive angle gyro measured the angle α'. However, the dive angle actually measured is α_2, and since $\alpha_2 > \alpha'$, the bomb impact will be at J, somewhat short of H'.

Identifying $\overline{JH'}$ with the error caused by an error in measuring α (and hence ψ), equation (49) gives the relation

$$\frac{\delta}{S} = \frac{1}{b} \frac{\Delta T_p}{T_{p0}} = \frac{1}{b} \frac{\Delta \psi}{\psi} \cong \frac{1}{b} \frac{d\psi}{d\alpha} \cdot \frac{\alpha' - \alpha_2}{\psi}.$$

The instrumental ψ design function is very nearly linear for $\alpha > 20$ degrees, and its rate of change is such that $d\psi/d\alpha \cong -0.726$. Also by equation (122)

$$\alpha' - \alpha_2 = -\phi_2 \cong -\omega \sin \alpha.$$

Hence $$\frac{\overline{JH'}}{S} \cong \frac{0.726\ \omega \sin \alpha}{b\psi}.$$

Taking the case $\alpha = 40$ degrees, $T_c/V = 0.028$, it is found that $\psi_1 = 0.643$ and $b = 3.9$, so that for this case $\overline{JH'}/S \cong 0.19\omega$, and $\overline{JH}/S \cong 0.81\omega$. For

the same case it is found from equation (119) that

$$\frac{\delta_c}{S} = (1 - n)\omega = 0.14\omega.$$

Thus in this typical case the ground error is about six times as great with the pursuit course approach as with the collision course.

6.6.6 Automatic Range Wind Correction

Both the collision course and the pursuit course approaches require either a prior knowledge of, or some method of estimating, the magnitude and direction of the wind if a hit is to be obtained under wind conditions. For a collision course maneuver an appropriate sight-offset angle must be estimated. For a pursuit course approach the bomb release time must be changed by an amount dependent upon the magnitude and direction of the wind. It is seen that these methods burden the pilot with some additional duty and provide only approximate solutions to this problem. What is desired is an instrumental technique which automatically computes the desired wind correction and sets it into the bomb director.

Of the type of automatic wind correction procedures under consideration, two may be mentioned. (1) The use of a lead-computing sight which attempts to place the aircraft on a flight path involving the proper lead angle, and hence is of the nature of a collision course method of attack; and (2) the use of a rate-of-turn gyro or pitch gyro to measure the rate of change of dive angle during a pursuit course approach. The voltage output of the gyro is a function of the wind velocity and may be used to decrease or increase the no-wind bomb release time by the amount necessary to obtain a hit. Method (2) will be considered in Section 6.6.7, and method (1) in Chapter 8.

6.6.7 The Release Time for a Pursuit Course Approach[81]

In Figure 33 the $X'OY'$ coordinate system corresponds to the one commonly used in the analysis of the bomb tossing maneuver. Here, however, the XOY system is appropriate. The path of the bomb after release is given by the equations

$$\begin{aligned} x &= x_p + U(t - T_p)\cos(\theta_p + \phi_2) + \tfrac{1}{2}g(t - T_p)^2 \sin\alpha_2, \\ y &= y_p + U(t - T_p)\sin(\theta_p + \phi_2) - \tfrac{1}{2}g(t - T_p)^2 \cos\alpha_2, \end{aligned} \tag{125}$$

where θ_p is the pull-up angle as measured in the $X'OY'$ system and x_p and y_p are the coordinates of the release point in the XOY system.

If x_p' and y_p' are the coordinates of the release point in the $X'OY'$ system, then

$$x_p' = \frac{U^2}{\bar{\mu}g}\sin\theta_p,$$

and

$$y_p' = \frac{U^2}{\bar{\mu}g}(1 - \cos\theta_p), \tag{126}$$

and $\bar{\mu} = \bar{K} - \cos\alpha' \cong \bar{K} - \cos\alpha_2$. The equations connecting the coordinates of the release point are

$$\begin{aligned} x_p &= x_p'\cos\phi_2 - y_p'\sin\phi_2, \\ \text{and} \qquad & \qquad (127) \\ y_p &= x_p'\sin\phi_2 + y_p'\cos\phi_2. \end{aligned}$$

The slant range $R_2 = OH$ is given by

$$\frac{R_2}{UT_c} = \frac{\sin(\alpha_2 - \phi_2)}{\sin\alpha_2}. \tag{128}$$

The immediate problem is to combine the preceding equations of this article, together with the conditions for a hit, namely $x = R_2$, $y = 0$, so as to get an expression for the pull-up angle θ_p in terms of the measured parameters.

The first step is to express x_p and y_p in terms of θ_p by combining equations (126) and (127). This results in

$$\begin{aligned} x_p &= \frac{U^2}{\bar{\mu}g}[\sin(\theta_p + \phi_2) - \sin\phi_2], \\ y_p &= \frac{U^2}{\bar{\mu}g}[\cos\phi_2 - \cos(\theta_p + \phi_2)]. \end{aligned} \tag{129}$$

Next, in the second equation of (125) place $y = 0$, use the second equation of (129), and write T_f in place of $t - T_p$. This gives a quadratic equation for T_f, whose solution is

$$T_f = \frac{U\sin(\theta_p + \phi_2)}{\bar{\mu}g\cos\alpha_2}\sigma$$

where

$$\sigma = \bar{\mu} + \bar{\mu}\sqrt{1 + \frac{2\cos\alpha_2\,[\cos\phi_2 - \cos(\theta_p + \phi_2)]}{\bar{\mu}\sin^2(\theta_p + \phi_2)}}.$$

Placing this expression for T_f into the first equation of (125), at the same time using the first equation of (129), and replacing x by the value of R_2 as given

by equation (128) results in an equation which can be written

$$\frac{\sigma \sin\alpha_2 \sin^2(\theta_p+\phi_2)}{\cos^2\alpha_2} + \frac{\sigma \sin(\theta_p+\phi_2)\cos(\theta_p+\phi_2)}{\cos\alpha_2} + \sin(\theta_p+\phi_2) - \frac{\sin\alpha_2}{\cos\alpha_2}\cos(\theta_p+\phi_2) + \frac{\sin(\alpha_2-\phi_2)}{\cos\alpha_2} - \frac{\bar{\mu}gT_c\sin(\alpha_2-\phi_2)}{U\sin\alpha_2} = 0. \quad (130)$$

In order to solve this equation comfortably for θ_p certain approximations are made, the first of which is in the expression for σ. In this expression replacing $\cos\phi_2 - \cos(\theta_p+\phi_2)$ in the numerator by $1 - \cos(\theta_p+\phi_2)$ increases the expression slightly and permits it to be reduced to

$$\sigma \cong \bar{\mu} + \bar{\mu}\sqrt{1 + \frac{2\cos\alpha_2}{\bar{\mu}} \cdot \frac{1}{1+\cos(\theta_p+\phi_2)}}.$$

Next, replacing $\cos(\theta_p+\phi_2)$ by unity decreases the expression slightly. Hence the expression

$$\sigma \cong \bar{\mu} + \bar{\mu}\sqrt{1 + \frac{1}{\bar{\mu}}\cos\alpha_2} = \bar{\mu} + \sqrt{\bar{\mu}(\bar{\mu}+\cos\alpha_2)}, \quad (131)$$

which may be compared with the corresponding expression in Chapter 2, is an excellent approximation to σ for all values of ϕ_2 and θ_p which occur in bomb tossing.

The next two steps are to replace $\cos(\theta_p+\phi_2)$ by $1 - \frac{1}{2}\sin^2(\theta_p+\phi_2)$ and to omit the resulting term of degree three in $\sin(\theta_p+\phi_2)$. This leaves the quadratic equation (132) for $\sin(\theta_p+\phi_2)$,

$$\frac{\sin\alpha_2}{\cos\alpha_2}\left(\frac{1}{2}+\frac{\sigma}{\cos\alpha_2}\right)\sin^2(\theta_p+\phi_2) + \left(1+\frac{\sigma}{\cos\alpha_2}\right)\times \sin(\theta_p+\phi_2) - \frac{\sin\alpha_2 - \sin(\alpha_2-\phi_2)}{\cos\alpha_2} - \frac{\bar{\mu}gT_c\sin(\alpha_2-\phi_2)}{U\sin\alpha_2} = 0. \quad (132)$$

The solution of equation (132) for $\sin(\theta_p+\phi_2)$ is

$$\sin(\theta_p+\phi_2) = \frac{\dfrac{\sin\alpha_2 - \sin(\alpha_2-\phi_2)}{\cos\alpha_2} + \dfrac{\bar{\mu}gT_c\sin(\alpha_2-\phi_2)}{U\sin\alpha_2}}{\bar{K} + \sqrt{\bar{K}(\bar{K}-\cos\alpha_2)}} \times \frac{2\cos\alpha_2}{1+\sqrt{1+2\beta_\phi}}, \quad (133)$$

$$\beta_\phi = \frac{\sin\alpha_2}{\bar{K}} \times \frac{\sin\alpha_2 - \sin(\alpha_2-\phi_2)}{\cos\alpha_2} + \frac{\bar{\mu}gT_c\sin(\alpha_2-\phi_2)}{U\sin\alpha_2}.$$

On placing $\phi_2 = 0$, equation (133) gives the pull-up angle θ_J which will cause the bomb to land at J; that is,

$$\sin\theta_J = \frac{\bar{\mu}gT_c}{U[\bar{K}+\sqrt{\bar{K}(\bar{K}-\cos\alpha_2)}]} \cdot \frac{2\cos\alpha_2}{1+\sqrt{1+2\beta_J}}, \quad (134)$$

where

$$\beta_J = \frac{\bar{\mu}gT_c\sin\alpha_2}{U\bar{K}}.$$

Since ϕ_2 is small, it is clear that $\theta_p = \theta_J - C\phi_2$, where C is nearly equal to unity. The value of C can be calculated in a particular case by calculating $\theta_p+\phi_2$ from equation (133), θ_J from equation (134) and then using the defining equation $C = (\theta_J - \theta_p)/\phi_2$.

The fact that the difference between θ_p and θ_J is nearly equal to ϕ_2 means that the correct pull-up angle, which will secure a hit when making a pursuit course approach, is obtained by subtracting from the pull-up angle θ_J (normally determined by the bomb director) an angle nearly equal to ϕ_2. This can be interpreted in terms of the so-called theory of the rigidity of a trajectory in exterior ballistics, since the main part of the correction necessary to cause a hit at H is merely the rotation of the trajectory through an angle of size ϕ_2.

6.6.8 Instrumentation of the Wind Correction

The wind correction term may be introduced on the first charging network of the computer, appearing as a charge which is either subtracted from or added to T_c according as ϕ_2 is positive or negative. That is

$$T_{p\phi} = \frac{T_c\psi - E}{\bar{K} + \sqrt{\bar{K}^2 - \bar{K}}}.$$

Since

$$T_J = \frac{T_c\psi}{\bar{K} + \sqrt{\bar{K}^2 - \bar{K}}}$$

the value E should have is

$$E = (T_J - T_{p\phi})\ (\bar{K} + \sqrt{\bar{K}^2 - \bar{K}})$$
$$= \frac{U}{g\bar{\mu}}\ (\theta_J - \theta_p)\ (\bar{K} + \sqrt{\bar{K}^2 - \bar{K}})$$
$$= \frac{CU\phi_2}{g\bar{\mu}}\ (\bar{K} + \sqrt{\bar{K}^2 - \bar{K}}). \qquad (135)$$

The relation between ϕ_2 and the output from the rate-of-turn gyro will now be determined. The output of this gyro is merely the angle $\Delta\alpha$. Following the procedure used in Section 6.6.4 it is possible to express $\Delta\alpha$ in terms of α_2. From equation (123) the relation

$$\tan\frac{\alpha_2}{2} = (1.2)^{\omega}\frac{\tan(\alpha_2/2) - \tan(\Delta\alpha/2)}{1+\tan(\alpha_2/2)\tan(\Delta\alpha/2)}$$

is obtained. Solved for $\tan(\Delta\alpha/2)$ this relation becomes

$$\tan\frac{\Delta\alpha}{2} = \frac{(1.2)^{\omega} - 1}{(1.2)^{\omega} + \tan^2(\alpha_2/2)}$$

or

$$\tan\frac{\Delta\alpha}{2} \cong \frac{(1/5)\omega\tan(\alpha_2/2)}{1 + \tan^2\dfrac{\alpha_2}{2}} = \frac{1}{10}\omega\sin\alpha_2.$$

Hence

$$\Delta\alpha \cong 1/5\omega\sin\alpha_2. \qquad (136)$$

From equation (122) we have the relation

$$\tan\phi_2 = \frac{\omega\sin\alpha_2}{1 + \omega\cos\alpha_2}$$

which becomes upon using equation (136),

$$\tan\phi_2 \cong \frac{5\Delta\alpha}{1 + \omega\cos\alpha_2}. \qquad (137)$$

Since

$$U \cong V(1 + \omega\cos\alpha_2),$$

it follows that

$$\tan\phi_2 \cong \frac{5V\Delta\alpha}{U},$$

and hence equation (135) becomes

$$E \cong \frac{CU}{g\bar{\mu}}\ (\bar{K} + \sqrt{\bar{K}^2 - \bar{K}})\ \text{arc tan}\ \frac{5V\Delta\alpha}{U}$$
$$\cong \frac{5CV(\bar{K} + \sqrt{\bar{K}^2 - \bar{K}})\ \Delta\alpha}{\bar{\mu}g}. \qquad (138)$$

Some of the approximations made in the preceding discussion are admittedly crude. For numerical work recourse should be had to the exact equations.[81]

It is possible also to compensate for the wind by a fractional rather than an additive correction to the pull-up time. Thus, writing

$$T_{p\phi} = \frac{T_c\psi\ (1 - e)}{\bar{K} + \sqrt{\bar{K}^2 - \bar{K}}},$$

it is found that

$$e = \frac{T_J - T_{p\phi}}{T_J} = \frac{E}{T_c\psi}. \qquad (139)$$

The correction e shows less variation with dive angle than does E.

6.6.9 Wind Compensation Using a Photoelectric Accelerometer[81]

When flying a pursuit course in the presence of wind it has been seen that the flight path is curved. Because of this curvature there exists an additional force on the accelerometer which has not been taken into account in the preceding considerations. This force is in such a direction as partially to compensate for range errors due to wind. Thus, in a tail wind the path is concave downward, and the centrifugal force is upward. The net force on the unbalanced mass of the accelerometer is reduced, corresponding to a larger dive angle. Therefore a reduction occurs in the value of the ψ function and a corresponding reduction in the release time computed by the bomb director. Conditions are just reversed in the case of a head wind, resulting in an increase in the computed release time.

The object of Section 6.6.9 is a determination of the amount of compensation for wind effect provided by the use of the photoelectric accelerometer described in Chapter 8. To this end the following quantities are calculated.

1. Radius of curvature ρ of flight path.
2. Resultant centrifugal acceleration a.
3. Corresponding change in dive angle and ψ function.
4. Resulting change in release time, ΔT_p.
5. E_p, the correction obtained from the photoelectric accelerometer, as given by equation (135).
6. E_p/E, the fraction of the required correction which is obtained by using the photoelectric accelerometer.
7. $E - E_p$, the correction required from the rate gyro when used in conjunction with the photoelectric accelerometer.

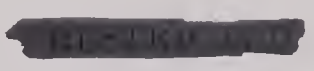

8. $e - e_p$, the fractional correction required from the rate gyro when used in conjunction with the photoelectric accelerometer.

Using the formula for radius of curvature in polar coordinates,

$$\rho = \frac{[R^2 + (dR/d\alpha)^2]^{\frac{3}{2}}}{R^2 + 2\,(dR/d\alpha)^2 - R\,d^2R/d\alpha^2}, \quad (140)$$

and taking the value of R from equation (121) it is found that equation (140) gives

$$\rho = \frac{R(1 + 2\omega\cos\alpha + \omega^2)^{\frac{3}{2}}}{\omega\,(1 + \omega\cos\alpha)\sin\alpha}. \quad (141)$$

The corresponding acceleration is

$$a = \frac{U^2}{\rho} = \frac{V^2\omega(1 + \omega\cos\alpha)\sin\alpha}{R\sqrt{1 + 2\omega\cos\alpha + \omega^2}}$$
$$= \frac{V\dot\alpha\,(1 + \omega\cos\alpha)}{\sqrt{1 + 2\omega\cos\alpha + \omega^2}} = \frac{V\dot\alpha}{\sqrt{1 + \left(\dfrac{\omega\sin\alpha}{1 + \omega\cos\alpha}\right)^2}}, \quad (142)$$

the expressions containing $\dot\alpha$ being obtained by using the second equation of (120). To a first approximation, $a \cong V\dot\alpha$.

The net force on the unbalanced mass of the photoelectric accelerometer is

$$F = mg\cos\alpha - ma \cong mg\left(\cos\alpha - \frac{V\dot\alpha}{g}\right).$$

Designating by $\alpha'' = \alpha + \delta\alpha$ the angle indicated by the accelerometer, it follows that

$$\cos(\alpha + \delta\alpha) = \cos\alpha - \frac{V\dot\alpha}{g\sqrt{1 + \left(\dfrac{\omega\sin\alpha}{1 + \omega\cos\alpha}\right)^2}}. \quad (143)$$

This is the equation which determines $\delta\alpha$. To a first approximation its solution, provided α is not too small, is

$$\delta\alpha \cong \frac{V\dot\alpha}{g\sin\alpha}. \quad (144)$$

The charge accumulated on the first capacitor is proportional to

$$5\int_0^{T_c/5}\psi(\alpha + \delta\alpha)\,dt \cong 5\int_0^{T_c/5}\left[\psi(\alpha) + \frac{d\psi}{d\alpha}\delta(\alpha)\right]dt$$
$$= T_c\,\psi(\alpha) + \frac{5V}{g\sin\alpha}\int_0^{T_c/5}\dot\alpha\,\frac{d\psi}{d\alpha}\,dt.$$

Using -0.726 as the value of $d\psi/d\alpha$, this gives

$$T_c\psi(\alpha) = \frac{3.63\;V\Delta\alpha}{g\sin\alpha}. \quad (145)$$

Hence the change in release time resulting from the use of the photoelectric accelerometer is

$$\Delta T_p \cong \frac{3.63\;V\Delta\alpha}{g(\bar K + \sqrt{\bar K^2 - \bar K})\sin\alpha}. \quad (146)$$

Consequently

$$\frac{E_p}{V\Delta\alpha} \cong \frac{3.63}{g\sin\alpha} \quad \text{and} \quad \frac{e_p}{\Delta\alpha} = \frac{3.63\;V}{gT_c\psi\sin\alpha}. \quad (147)$$

Since in the second equation of (147) the factor $\sin\alpha$ is multiplied by the ψ function, it follows that the wind correction supplied by the photoelectric accelerometer varies much less with dive angle when introduced as a fractional correction than when used as an additive correction. This means that if the rate gyro correction also is introduced on a fractional basis, the amount of correction required from it, $e - e_p$, will be roughly independent of dive angle.

Chapter 7

MATHEMATICAL THEORY OF ROCKET TOSSING[a]

7.1 EMPIRICAL EQUATIONS FOR TRAJECTORY DROPS OF AIRCRAFT ROCKETS[b]

7.1.1 Formulation of Equations Fitting CIT Data

EMPIRICAL EQUATIONS are found for the trajectory drop data on five Navy rockets and two British rockets given in California Institute of Technology booklets.[216–218]

The trajectory drop is the gravity drop from the effective launcher line in forward firing from an airplane, the rocket being fired from a zero-length launcher, and is a function of slant range (distance from rocket ignition point to target), dive angle, plane velocity (true airspeed), and rocket propellant temperature. The change in the trajectory drop caused by a change in propellant temperature (at a given dive angle and airplane speed) is, however, practically independent of slant range for slant ranges larger than 1,000 yards.

Examination of the graphs for the trajectory drops of the rockets indicates that a suitable general form of the empirical equations is

$$\epsilon_T = \epsilon_0(\alpha,V_p,T_0) + \epsilon_1(\alpha,R,V_p,T_0) + \Delta\epsilon(\alpha,V_p,T), \quad (1)$$

where T is the propellant temperature, ϵ_T is the trajectory drop at propellant temperature T, R is the slant range, α is the dive angle, V_p is the true airspeed of the airplane, and T_0 is a particular propellant temperature. The term $\epsilon_0(\alpha,V_p,T_0)$ is the value of ϵ_T when $R = 0$ and at the particular temperature T_0; $\epsilon_1(\alpha,R,V_p,T_0)$ is the increase in ϵ_T when the range increases from O to R, the temperature remaining at T_0; and $\Delta\epsilon\ (\alpha,V_p,T)$ is the difference between the trajectory drop at propellant temperature T and at T_0.

Taking $T_0 = 70$ F, equation (1) was evaluated for the various rockets and then reduced by one term. The simpler form was possible because of a common factor in the first and third terms. For all rockets considered, the simplified empirical equations of the trajectory drops at propellant temperature T are of the form

$$\epsilon_T = \left[pRe^{-V_p/\beta} + \frac{r}{V_p}h(T)\right]F(\gamma). \quad (2)$$

Table 1 gives the values of p, β, r, and $h(T)$ for each rocket considered. The superscripts refer to the reports listed in the bibliography giving the derivations of the respective equations. In connection with this table, the units for the various quantities are as follows: T in degrees Fahrenheit, ϵ_T in mils, R in yards, γ in degrees, V_p in knots, and the dimensionless function $F(\gamma)$ is graphically defined in Figure 1. This function is discussed further in Section 7.2.8.

TABLE 1

Rocket	p	β	r	$h(T)$
2.25-in.AR(Fast)[177]	0.060	550	0.25	$T^2 - 240T + 11{,}900$
3.5-in. AR[172]	0.062	550	0.195	$T^2 - 350T + 19{,}600$
RP3, 3.5-in.[177]	0.044	500	0.25	$T^2 - 240T + 36{,}900$
5.0-in. AR[177,170]	0.082	550	0.195	$T^2 - 350T + 19{,}600$
5.0-in. HVAR[174]	0.033	640	0.22	$T^2 - 264T + 28{,}730$
RP3, 5.0-in.[177]	0.063	500	0.25	$T^2 - 240T + 39{,}900$
11.75-in. AR (Pres. model)[169, 174]	0.0573	500	0.25	$T^2 - 240T + 31{,}900$

In order to show how well the empirical equations fit the data, graphs of corresponding values of the trajectory drops as determined empirically and from the CIT tables were made for small, medium, and large values of all variables involved. A typical case for the 5.0-inch HVAR is shown in Figure 2. These graphs show that the empirical equations, for useful values of the variables, fit the corresponding CIT data with about 3 mils maximum error and with an average error of 1 or 2 mils.

For all rockets studied, the CIT tables give trajectory drop data for true airplane speeds of 200 to 400 knots; propellant temperature of 0 F to 100 F; and dive angles of 0 to 60 degrees. The trajectory drop data for the 3.5-inch AR, 5.0-inch HVAR, and 11.75-inch AR were given for ranges of 500 to 4,000

[a] Chapter 7 is appendix material to Section 2.2.

[b] Section 7.1 was prepared by M. E. Rolfs of the State University of Iowa.

yards, whereas the data for the 2.25-inch AR (Fast), RP3 3.5 inches, RP3 5.0 inches, and 5.0-inch AR were only from 500 to 2,000 yards. Therefore, the degree of fit of the empirical equations for the latter four rockets depends upon the validity of extrapolations for ranges beyond 2,000 yards.

7.1.2 The Empirical Equations in Units Suitable for Theoretical Work

In theoretical analysis, it is desirable to use feet instead of yards, feet per second instead of knots, and radians instead of mils. When the variables are

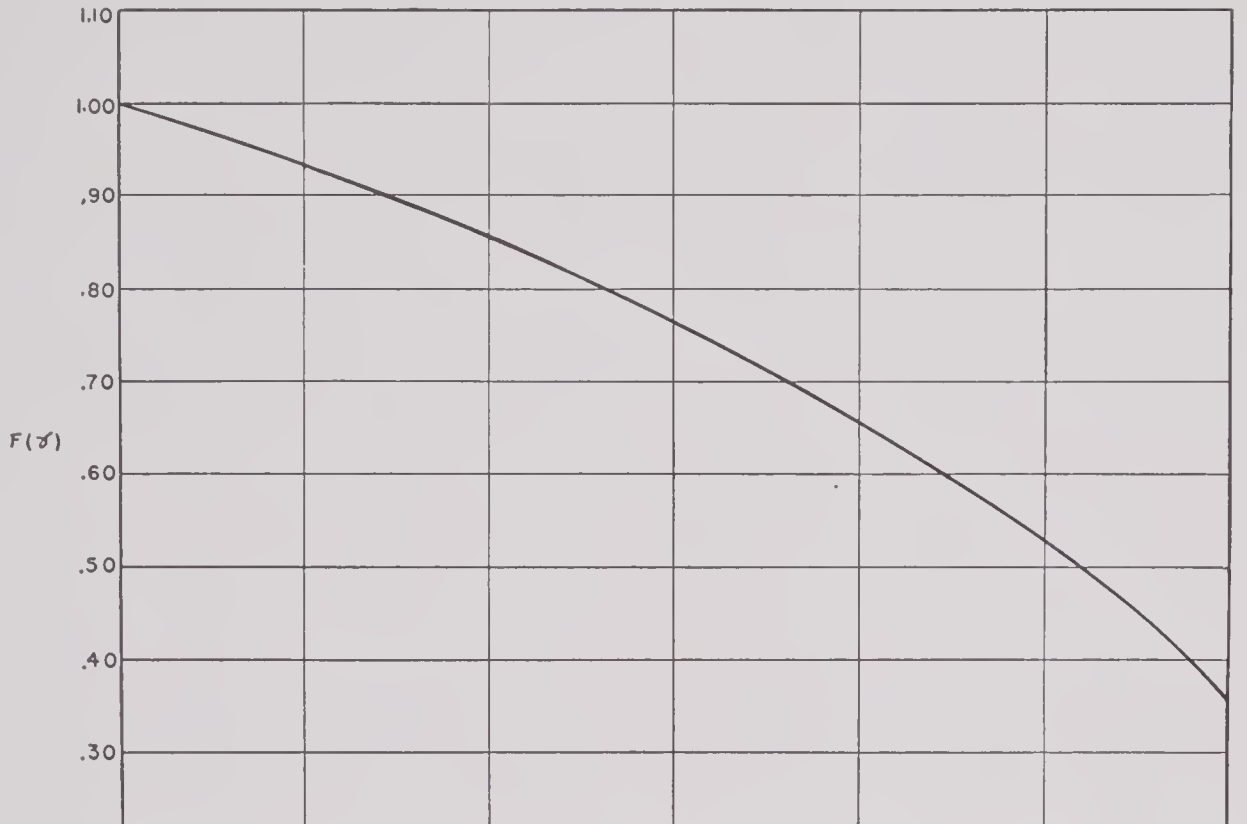

FIGURE 1. $F(\gamma)$ versus γ.

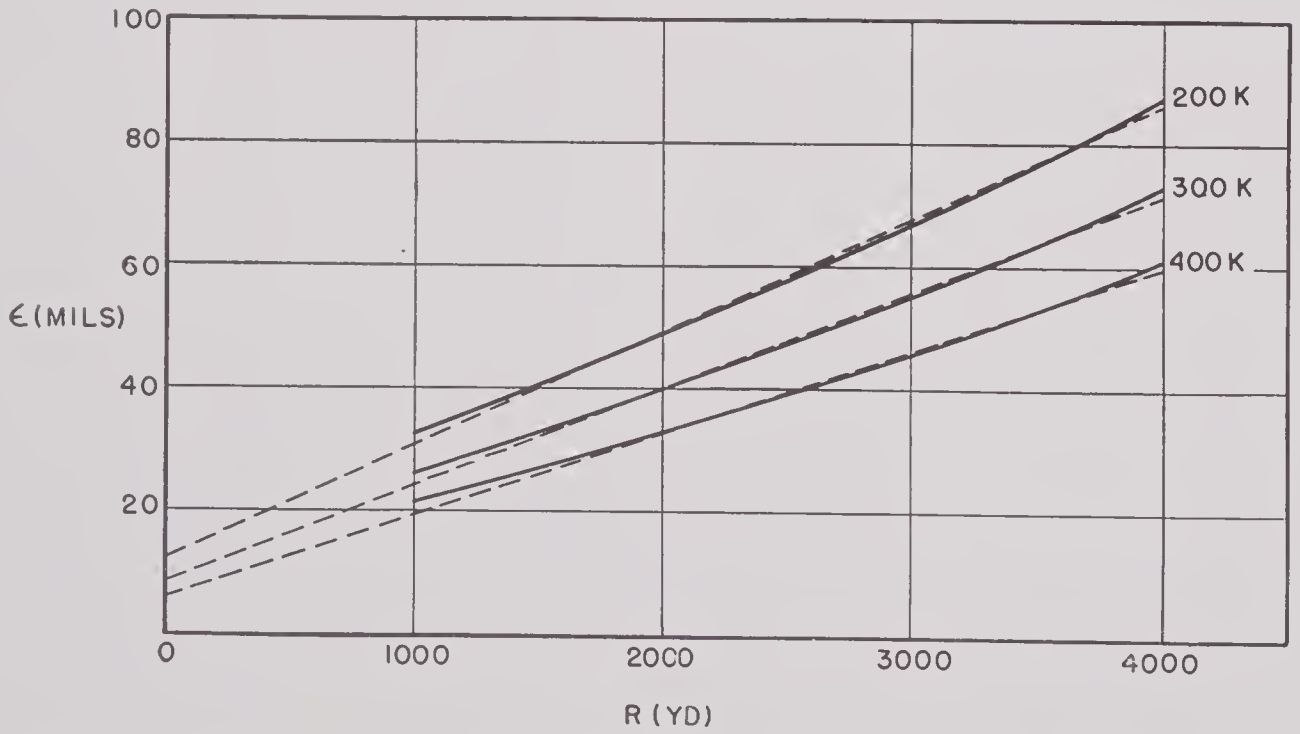

FIGURE 2. Trajectory drop ϵ versus slant range R for different values of airspeed V_p, for 5.0-inch HVAR at temperature $T = 70$ F and dive angle $\alpha = 30$ degrees. Solid curves are taken from tabulated experimental data at the three airspeeds specified; dashed lines are graphs of corresponding empirical equations, calculated from equation (2) and Table 1 of text. It is seen that for R between 1,000 and 4,000 yards, error in empirical equation does not exceed 3 mils.

expressed in the foot-second system, equation (2) may be written

$$\epsilon = \left[aRe^{-V/b} + \frac{ch(T)}{V} \right] F(\gamma). \qquad (3)$$

The values of the constants a, b, c, and of the function $h(T)$ are now those shown in Table 2.

TABLE 2

Rocket	a	b	c	$h(T)$
2.25-in. AR (Fast)	2.0×10^{-5}	930	4.22×10^{-4}	$T^2 - 240T + 11{,}900$
3.5-in. AR	2.07×10^{-5}	930	3.30×10^{-4}	$T^2 - 350T + 19{,}600$
RP3, 3.5-in.	1.5×10^{-5}	845	4.22×10^{-4}	$T^2 - 240T + 36{,}900$
5.0-in. AR	2.7×10^{-5}	930	3.30×10^{-4}	$T^2 - 350T + 19{,}600$
5.0-in. HVAR	1.1×10^{-5}	1,082	3.72×10^{-4}	$T^2 - 264T + 28{,}730$
RP3, 5.0-in.	2.1×10^{-5}	845	4.22×10^{-4}	$T^2 - 240T + 39{,}900$
11.75-in. AR (Present model)	1.9×10^{-5}	845	4.22×10^{-4}	$T^2 - 240T + 31{,}900$

7.2 EQUATIONS FOR ROCKET TOSSING PULL-UP TIME [c]

7.2.1 Introduction

In the mathematical treatment of the problem of rocket tossing, it is necessary at the outset to make a decision regarding the inclusion of the various parameters affecting the pull-up time, such as time to target, speed of airplane, dive angle, type of rocket, type of airplane (angle of attack, launcher angle), temperature of rocket propellant, manner of release (zero-length launcher, lanyard firing), manner of pull-up, etc. The simplest procedure which can be expected to give theoretical results which can be compared with experimental results is one in which the following assumptions are made:

1. The airplane dives, with constant velocity along a fixed straight line, directly toward a fixed target;

2. The airplane pulls out of the dive with a spatial acceleration which is constant in both direction and magnitude, being perpendicular to the line of the dive;

3. The rocket is released in such a manner that the initial direction of motion of its center of mass is the same as the direction of motion of the center of mass of the airplane;

4. The axis of the rocket is always tangent to the path of the center of mass of the rocket — no yaw;

5. The propellant is ignited at the instant of release. In general, the complexity of the equations increases as more of the factors affecting the flight of the rocket are included in the discussion.

In Section 7.2.1, equations describing the motion of the airplane during pull-up and of the rocket after release are set up subject to the assumptions listed in Section 7.2.2. No special assumption is made about the manner of variation of the *magnitude* of the spatial acceleration, $K - \cos\alpha$, of the airplane during pull-up, it being necessary at first only to be sure of the existence of certain integrals involving this acceleration. At appropriate points in the discussion, which will be specially indicated, definite assumptions about the manner of variation of this acceleration will be made.

If this acceleration varies directly as t^r, r being a constant, then in general the equation which determines the pull-up time T_p is of degree $r + 2$ in T_p.[180] It will be seen (see Section 7.2.11) that the effect of change in angle of attack can be included without raising the degree of this equation.[185] Motion pictures of the action of an accelerometer during pull-up show that the spatial acceleration of the airplane increases nearly as the first power of the time.[164] In this case, the equation for pull-up time is of degree three. Satisfactory approximate solutions of these equations of higher degree are obtained.

When the spatial acceleration is replaced by a mean value, the equation for pull-up time reduced to a quadratic equation in T_p. It is shown that a useful approximation to the solution of this equation can be put into the form

$$T_p = M_c T_c + M_d T_d + M_T,$$

in which the first term is the only one which varies with the time to target T_c, the second term the only one which varies with the duration T_d of the delay period, and the third the only one which varies with propellant temperature. Each term varies with the velocity of the airplane during the dive, the dive angle, and the number of g's present during pull-up. The second and third terms, respectively, show clearly the way in which a delay period and a change in propellant temperature affect the pull-up time.

7.2.2 Assumptions

The general assumptions which hold throughout Section 7.2 are listed here.

1. The sight line and the flight line are fixed in space and pass through the target.

[c] Section 7.2 was prepared by L. E. Ward, formerly of the State University of Iowa, now at Naval Ordnance Test Station, Inyokern, California.

2. During pull-up and until the ignition of the rocket propellant, the spatial acceleration of the airplane is in direction perpendicular to the line of dive.

3. There is a delay period between the release of the rocket and the ignition of the propellant.

4. The rocket is launched so that the path of its center of mass at release has the same direction as the line of flight of the airplane at the instant of release.

5. Upon release and at each instant thereafter, the axis of the rocket is tangent to the path of the center of mass of the rocket. This is the same as assuming that the rocket does not yaw.

6. The target is stationary.

7. The velocity of the airplane is constant during the dive.

7.2.3 Notation

Figure 3 is a sketch showing in grossly exaggerated form the principal lines and angles associated with the path of the airplane during pull-up and the flight of the rocket after release.

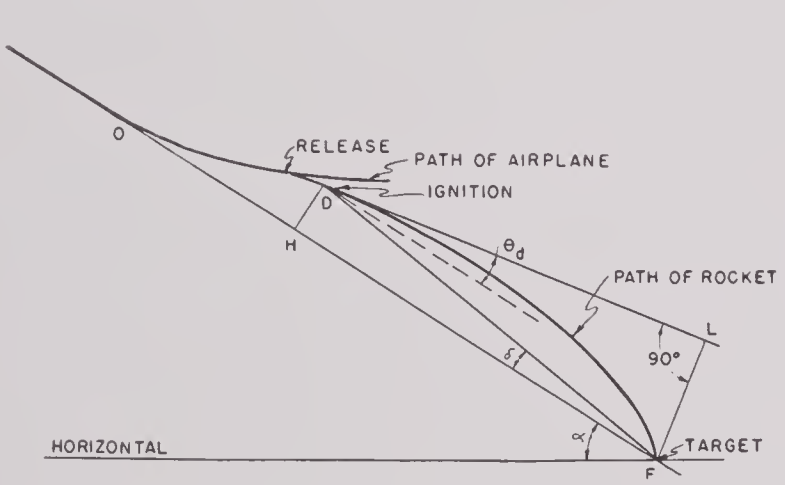

FIGURE 3. Diagrammatic representation of rocket tossing maneuver.

O is the point where pull-up began; the x axis is the line from O to the target; the y axis is upward and perpendicular to the x axis at O. T_p is the time-of-flight from O to the point where the rocket is released; T_d is the time it takes the rocket to go from the release point to the ignition point D; $T_c = \overline{OF}/V$, where V is the velocity of the airplane. The line DL is tangent to the path of the rocket at the ignition point. θ_d is the angle between DL and a line parallel to the x axis. α is the inclination of the line of dive to the horizontal. K is the number of g's registered on an accelerometer at any instant during pull-up; K equals $\cos\alpha$ during the dive, and K generally increases steadily during pull-up, tending to reach a maximum if pull-up is continued for several seconds.

Unless specifically indicated to the contrary, all times are in seconds; distances, in feet; velocities, in feet per second; accelerations, in feet per second per second; angles, in radians; and temperatures in degrees Fahrenheit.

7.2.4 The Equations of Motion

During pull-up, the components of the spatial acceleration of the airplane on the coordinate axes are

$$\ddot{x} = 0$$
$$\ddot{y} = (K - \cos\alpha)\, g.$$

It follows that at the point of release, the components of velocity are

$$\dot{x}_p = V$$
$$\dot{y}_p = g\int_0^{T_p} K(t)dt - gT_p\cos\alpha, \tag{4}$$

and the coordinates of the point of release are

$$x_p = VT_p$$
$$y_p = g\int_0^{T_p}\left[\int_0^t K(t)dt\right]dt - \tfrac{1}{2}gT_p^2\cos\alpha. \tag{5}$$

By means of integration by parts, the expression for y_p can be put into a form involving only single integrals,

$$y_p = g\int_0^{T_p}(T_p - t)\,K(t)dt - \tfrac{1}{2}gT_p^2\cos\alpha. \tag{6}$$

At the end of the delay period, the components of velocity of the rocket are

$$\begin{aligned}\dot{x}_d &= V + gT_d\sin\alpha,\\ \dot{y}_d &= g\int_0^{T_p} K(t)dt - g(T_p + T_d)\cos\alpha,\end{aligned} \tag{7}$$

and the coordinates of the rocket are

$$\begin{aligned}x_d &= V(T_p + T_d) + \tfrac{1}{2}gT_d^2\sin\alpha.\\ y_d &= -\tfrac{1}{2}g(T_p + T_d)^2\cos\alpha\\ &\quad + g\int_0^{T_p}(T_p + T_d - t)\,K(t)dt.\end{aligned} \tag{8}$$

From equations (7), the angle θ_d is given by

$$\tan\theta_d = g\frac{\int_0^{T_p} K(t)dt - (T_p + T_d)\cos\alpha}{V + gT_d\sin\alpha}. \tag{9}$$

The path of the rocket after ignition is given by

equation (3). In this application of equation (3), the slant range, R, is measured from the point D in Figure 3, and γ is the angle $\alpha - \theta_d$

7.2.5 The Equation for Pull-up Time

If the rocket is to hit the target, the angles ϵ, θ_d, δ of Figure 3 must satisfy the relation

$$\epsilon = \theta_d + \delta. \tag{10}$$

From this relation will be obtained the equation whose solution is the correct pull-up time.

The angle ϵ is given by equation (3); the angle θ_d, by equation (9); and the triangle FHD yields δ in the form

$$\tan \delta = \frac{y_d}{\overline{OF} - x_d}. \tag{11}$$

Instead of the exact expressions for θ_d and δ, their tangents as given by equations (9) and (11) are used. This approximation is considered to be acceptable since the trajectories of rockets are so flat that neither θ_d nor δ ever exceeds 10 degrees, and since the radian measure of an angle less than 9 degrees never differs from its tangent by more than 1 per cent. Moreover, because of the flatness of the trajectory, it is satisfactory to replace R by $\overline{HF} = (T_c - T_p - T_d)V$.

On making these approximations and using equations (8) and (9), equation (10) takes the form

$$\tfrac{1}{2}F(\gamma)A_2(V)(T_c - T_p - T_d) + \frac{cF(\gamma)h(T)}{g} = \frac{\int_0^{T_p} K(t)dt - (T_p + T_d)\cos\alpha}{1 + \mu} + \frac{\int_0^{T_p}(T_p + T_d - t)K(t)dt - \tfrac{1}{2}(T_p + T_d)^2 \cos\alpha}{T_c - T_p - \left(1 + \mu/2\right)T_d}, \tag{12}$$

where $\mu = (gT_d \sin\alpha)/V$, and the function $A_2(V)$ is as defined in equation (31a), Chapter 2. If equation (12) is cleared of fractions by multiplying both members by the product

$$(1 + \mu)\left[T_c - T_p - \left(1 + \mu/2\right)T_d\right],$$

it is found that certain combinations of terms can be made and the resulting equations put into the form

$$\frac{1 + \mu}{2} F(\gamma)A_2(V) \cdot \left[T_c - T_p - \left(1 + \frac{\mu}{2}\right)T_d\right](T_c - T_p - T_d) + \frac{c(1 + \mu)}{g} F(\gamma)h(T)\left[T_c - T_p - \left(1 + \frac{\mu}{2}\right)T_d\right] = \int_0^{T_p}\left[T_c + \mu T_p + \frac{\mu}{2}T_d - (1 + \mu)t\right]K(t)dt - (T_p + T_d)\left[T_c - \frac{1 - \mu}{2}T_p - \tfrac{1}{2}T_d\right]\cos\alpha. \tag{13}$$

It is seen that the unknown, T_p, enters this equation both algebraically and as the upper limit in the integral. Because of this fact, further investigation of the equation is restricted to several cases, each such that the integral in the equation can be easily evaluated and the resulting equation solved, at least approximately, for T_p.

7.2.6 Lanyard Firing

If a lanyard of effective length l is used to actuate the ignition mechanism, the propellant will be ignited when the rocket is at distance l from the airplane, that is, when

$$l^2 = (X - x_d)^2 + (Y - y_d)^2,$$

where X and Y are the coordinates of the airplane at $T_p + T_d$ seconds after pull-up was begun. Expressed by use of equations in Section 7.2.4, this relation becomes

$$l^2 = \tfrac{1}{4}g^2T_d^4 \sin^2\alpha + g^2\left(\int_{T_p}^{T_p+T_d}(T_p + T_d - t)K(t)dt\right)^2. \tag{14}$$

Equations (13) and (14) can be regarded as simultaneous equations for the determination of the two unknowns T_p and T_d. However, this point of view will not be followed up here.

If ignition occurs upon release of the rocket from the airplane, it is only necessary to place T_d equal to zero in equation (13), which is then the single equation for the determination of T_p.

If in equation (14) a mean value K_m of $K(t)$ during the delay period is used, that equation can be

brought to a form easily solved for T_d, resulting in the formula

$$T_d = \sqrt{\frac{2l}{g\sqrt{K_m^2 + \sin^2\alpha}}}. \tag{15}$$

It is noteworthy that T_p is not present explicitly in equation (15); it is present implicitly through K_m. A good approximation to this result is obtained by omitting the $\sin^2\alpha$ term and replacing K_m by K_d, the value of K when the propellant is ignited. This approximate formula is

$$T_d \cong \sqrt{\frac{2l}{gK_d}} \cong \tfrac{1}{4}\sqrt{\frac{l}{K_d}}. \tag{16}$$

7.2.7

Solution for T_p When a Mean Value of K Is Used

If a suitable mean value $\bar{K}$ of K over the pull-up period is used, a mean value theorem for integrals permits the integral in equation (13) to be written

$$\bar{K}\int_0^{T_p}\left[T_c + \mu T_p + \frac{\mu}{2}T_d - (1+\mu)t\right]dt$$
$$= \bar{K}\left[T_cT_p + \frac{\mu}{2}T_pT_d - \frac{1-\mu}{2}T_p^2\right].$$

When this is substituted into equation (13), that equation takes the form

$$B_2T_p^2 - B_1T_p + B_0 = 0, \tag{17}$$

where

$$B_2 = (1-\mu)(\bar{K} - \cos\alpha) + (1+\mu)F(\gamma)A_2(V).$$

$$B_1 = 2\left[\bar{K} - \cos\alpha + (1+\mu)F(\gamma)A_2(V)\right]T_c + \frac{2c(1+\mu)}{g}F(\gamma)h(T) + \left[2\cos\alpha + \mu(\bar{K} - \cos\alpha) - \frac{(1+\mu)(4+\mu)}{2}F(\gamma)A_2(V)\right]T_d,$$

$$B_0 = (1+\mu)F(\gamma)A_2(V)T_c^2 + \left[2\cos\alpha - (1+\mu)\frac{4+\mu}{2}F(\gamma)A_2(V)\right]T_cT_d - \left[\cos\alpha - (1+\mu)\frac{2+\mu}{2}F(\gamma)A_2(V)\right]T_d^2 + \frac{c(1+\mu)}{g}F(\gamma)h(T)\left[2T_c - (2+\mu)T_d\right].$$

The form of solution of the quadratic equation (17) best suited to present purposes is

$$T_p = \frac{2B_0}{B_1 + \sqrt{B_1^2 - 4B_0B_2}}. \tag{18}$$

When the values of B_2, B_1, and B_0 are substituted into equation (18), the resulting expression is so complex as to be unmanageable. It is therefore necessary to discard the terms which have relatively little influence on the value of T_p. When this is done (for details of this step, see reference 176), the resulting formula is

$$T_p = \frac{T_cF(\gamma)A_2(V) + 2T_d[\cos\alpha - F(\gamma)A_2(V)] + \frac{2c}{g}F(\gamma)h(T)}{\bar{K} - \cos\alpha + F(\gamma)A_2(V) + \sqrt{(\bar{K} - \cos\alpha)[\bar{K} - \cos\alpha + F(\gamma)A_2(V)]}}. \tag{19}$$

This formula is capable of being written in an obvious way as a sum of three terms, $T_p = M_cT_c + M_dT_d + M_T$, in which each term shows how the factors of time to target T_c, delay time T_d, and propellant temperature T, respectively, affect the value of T_p.

7.2.8

The Function $F(\gamma)$

Equation (19) is not ready for use in calculating the pull-up time in a numerical case because of the presence of the function $F(\gamma)$. Originally defined graphically (see Figure 1), tables of this function have been prepared and a representation of this function by means of trigonometric expressions has been obtained. The table and the trigonometric representation will be discussed first, and then the connection with the dive angle and the pull-up angle will be established.

Values of $F(\alpha)$ given in Table 3 were taken directly from the graph in Figure 1. Certain of these values have been changed slightly so that the differences in the tabular values will be regular.

Certain theoretical reasons connected with the

approximate computation of rocket trajectories (see reference 215, pp. 25, 26) indicate that $F(\alpha)$ may be represented with satisfactory accuracy by either of the formulas

$$\frac{\cos \alpha}{1 + C \sin \alpha}, \qquad \cos \alpha \ (1 - C' \sin \alpha). \tag{20}$$

This was found to be the case, the best value for C being 0.27 and for C', 0.2321.[171]

The function $F(\gamma)$ in formula (19) depends for its value on θ_d. Once θ_d has been determined, $\gamma = \alpha - \theta_d$ is found by subtraction, and the graph or the table for the F function then gives the value of $F(\gamma)$. The procedure to be used here is to solve approximately equations (9) and (19) as simultaneous equations for the two unknowns T_p and θ_d.

A sufficiently accurate formula for θ_d is obtained by starting with the approximate relation

$$T_p \cong \frac{T_c F(\gamma) A_2(V) + 2T_d \cos \alpha}{2 \ (\bar{K} - \cos \alpha)}, \tag{21}$$

obtained from equation (19). This is substituted into the right-hand member of (9), taken in the form

$$\theta_d \cong g \frac{(\bar{K} - \cos \alpha) T_p - T_d \cos \alpha}{V}.$$

The resulting relation is

$$\theta_d \cong \frac{gT_c}{2V} F(\alpha - \theta_d) A_2(V). \tag{22}$$

In order to solve (22) for θ_d, the first two terms of the Taylor's series for $F(\alpha - \theta_d)$,

$$F(\alpha - \theta_d) = F(\alpha) - \theta_d F'(\alpha) + \frac{\theta_d^2}{2!} F''(\alpha) - \cdots, \tag{23}$$

are used. This is permissible since θ_d is known to be small (never exceeding 10 degrees) and since it can be assumed that the higher derivatives of $F(\alpha)$ are small. The resulting relation,

$$\theta_d \cong \frac{gT_c A_2(V)}{2V} [F(\alpha) - \theta_d F'(\alpha)],$$

yields the approximate formula for θ_d,

$$\theta_d \cong \frac{gT_c F(\alpha) \dfrac{A_2(V)}{2V}}{1 + gT_c F'(\alpha) \dfrac{A_2(V)}{2V}} \tag{24}$$

Substitution from (24) into the first two terms of

TABLE 3. $F(\alpha)$.

α Radians	0	1	2	3	4	5	6	7	8	9	10
0	1.000	0.997	0.993	0.990	0.986	0.983	0.979	0.975	0.972	0.968	0.964
0.1	0.964	0.960	0.956	0.952	0.948	0.944	0.940	0.936	0.932	0.928	0.924
0.2	0.924	0.920	0.916	0.911	0.907	0.903	0.898	0.894	0.889	0.885	0.880
0.3	0.880	0.875	0.871	0.866	0.861	0.856	0.851	0.846	0.841	0.836	0.831
0.4	0.831	0.826	0.821	0.815	0.810	0.805	0.799	0.794	0.788	0.783	0.777
0.5	0.777	0.771	0.766	0.760	0.754	0.748	0.742	0.736	0.730	0.724	0.718
0.6	0.718	0.712	0.706	0.699	0.693	0.687	0.680	0.674	0.667	0.661	0.654
0.7	0.654	0.647	0.641	0.634	0.627	0.620	0.613	0.606	0.599	0.591	0.584
0.8	0.584	0.576	0.569	0.561	0.553	0.546	0.538	0.530	0.522	0.513	0.505
0.9	0.505	0.496	0.487	0.479	0.470	0.460	0.451	0.441	0.432	0.422	0.412

Approximate values of $F'(\alpha)$.

α Radians	0	1	2	3	4	5	6	7	8	9	10
0	— 0.34	— 0.34	— 0.35	— 0.35	— 0.35	— 0.36	— 0.36	— 0.37	— 0.37	— 0.37	— 0.38
0.1	— 0.38	— 0.38	— 0.39	— 0.39	— 0.39	— 0.40	— 0.40	— 0.41	— 0.41	— 0.41	— 0.42
0.2	— 0.42	— 0.42	— 0.43	— 0.43	— 0.43	— 0.44	— 0.44	— 0.45	— 0.45	— 0.45	— 0.46
0.3	— 0.46	— 0.47	— 0.47	— 0.48	— 0.48	— 0.49	— 0.49	— 0.50	— 0.50	— 0.51	— 0.51
0.4	— 0.51	— 0.52	— 0.52	— 0.53	— 0.53	— 0.54	— 0.54	— 0.55	— 0.55	— 0.56	— 0.56
0.5	— 0.56	— 0.57	— 0.57	— 0.58	— 0.58	— 0.59	— 0.59	— 0.60	— 0.60	— 0.61	— 0.61
0.6	— 0.61	— 0.62	— 0.62	— 0.63	— 0.63	— 0.64	— 0.64	— 0.65	— 0.65	— 0.66	— 0.66
0.7	— 0.66	— 0.67	— 0.68	— 0.69	— 0.69	— 0.70	— 0.70	— 0.71	— 0.72	— 0.73	— 0.74
0.8	— 0.74	— 0.75	— 0.76	— 0.77	— 0.78	— 0.79	— 0.80	— 0.81	— 0.82	— 0.84	— 0.85
0.9	— 0.85	— 0.87	— 0.88	— 0.89	— 0.91	— 0.92	— 0.94	— 0.95	— 0.97	— 0.98	— 1.00

the right-hand member of (23) gives the formula for $F(\gamma)$,

$$F(\gamma) = \frac{F(\alpha)}{1 + gT_cF'(\alpha)\ \dfrac{A_2(V)}{2V}}. \qquad (25)$$

From this formula it is seen that $F(\gamma)$ is chiefly a function of dive angle since the ratio of $A_2(V)$ to

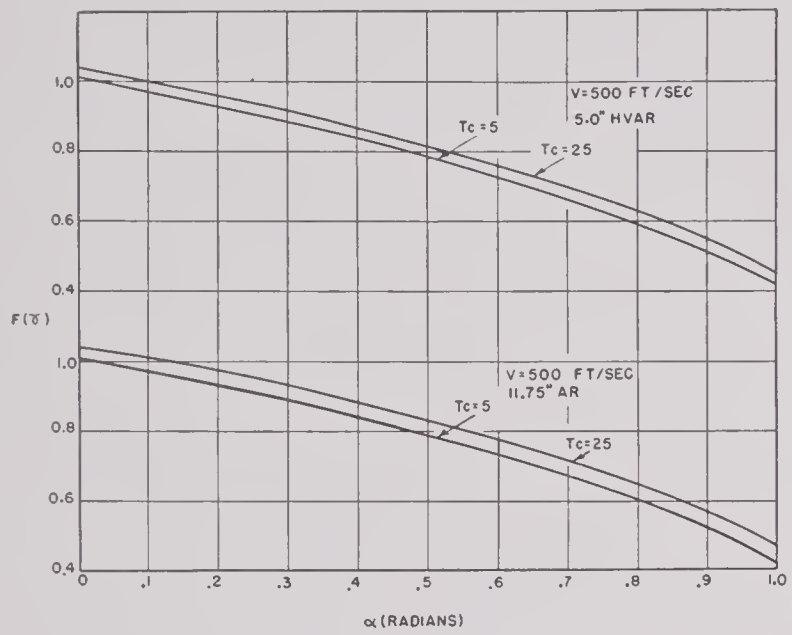

FIGURE 4. $F(\gamma)$ versus α for two values of T_c (5 and 25 sec) and for two types of rockets; $V = 500$ feet/second [based on equation (25) of text].

V shows little variation on the interval $450 < V < 700$ and since the term $gT_cF'(\alpha)\ [A_2(V)/2V]$ never exceeds $\frac{1}{4}$ in numerical value. Values of $F'(\alpha)$ are tabulated with those of $F(\alpha)$, and thus $F(\gamma)$ can be calculated from formula (25). Graphs of $F(\gamma)$ against α for several values of T_c and two types of rocket are shown in Figure 4.

7.2.9 Solution for Pull-up Time When $K = \cos\alpha + pt^r$

The solution of equation (13) for T_p when the spatial acceleration of the airplane during pull-up is of the form $\ddot{y} = pgt^r$, where p and r are positive constants, will now be considered.[180] In this case

$$K = \cos\alpha + pt^r. \qquad (26)$$

Substitution of the expression (26) into (13) permits the indicated integration to be carried out. The resulting equation is of degree $r + 2$ in T_p, and it can be put into the form

$$2p\frac{r+1-\mu}{(r+2)(r+1)}T_p^{\,r+2} - \frac{p}{r+1}(2T_c + \mu T_d)T_p^{\,r+1} + (1+\mu)F(\gamma)A_2(V)T_p^{\,2} - B_1'T_p + B_0 = 0, \qquad (27)$$

where

$$B_1' = 2(1+\mu)F(\gamma)A_2(V)T_c + [2\cos\alpha - (1+\mu)\frac{4+\mu}{2}F(\gamma)A_2(V)]T_d + \frac{2c(1+\mu)}{g}F(\gamma)h(T),$$

and B_0 is the same as in Section 7.2.7.

An approximate solution of equation (27) which is of value in rocket tossing theory is obtained as follows. For large values of T_c, at least, the important terms in the left-hand member of (27) are

$$-\frac{2pT_c}{r+1}T_p^{\,r+1} + F(\gamma)A_2(V)T_c^{\,2}.$$

If this expression is equated to zero, the resulting equation yields a value for T_p which can be regarded as a rough approximation to the correct value; this approximation is

$$T_{p0} = \left[\frac{r+1}{2p}F(\gamma)A_2(V)T_c\right]^{\frac{1}{r+1}}.$$

A much more accurate expression for T_p can now be obtained by the following procedure. Let equation (27) be written in the form

$$T_p = \left[2p\frac{r+1-\mu}{(r+2)(r+1)}T_p^{\,r+2} + \frac{(1+\mu)F(\gamma)A_2(V)T_p^{\,2} - B_1'T_p + B_0}{\dfrac{p}{r+1}(2T_c + \mu T_d)}\right]^{\frac{1}{r+1}}$$

and substitute T_{p0} for T_p in the right-hand member. After omitting certain parts of the resulting formula which have little influence on the value of T_p, it is possible to write finally

$$T_p \cong \left\{\frac{r+1}{2p}\left[F(\gamma)A_2(V)T_c + 2(\cos\alpha - FA_2)T_d + \frac{2cF(\gamma)h(T)}{g}\right]\left[1 - \frac{1}{T_c}\left(\frac{r+1}{2p}FA_2T_c\right)^{\frac{1}{r+1}}\right]\right\}^{\frac{1}{r+1}}. \qquad (28)$$

Formula (28) represents a useful approximate solution of equation (27) for any nonnegative value of r. If r is an integer, the quantity p can be replaced by a constant multiplied by a derivative of K.

Thus, if $r = 0$, then $p = \bar{K} - \cos\alpha$; if $r = 1$, then $p = dK/dt$; and generally, $p = (1/r!)\ (d^rK/dt^r)$. By means of this relation equation (28) can be brought to the form

$$T_p = \left\{ \frac{(r+1)!}{2\dfrac{d^rK}{dt^r}} \left[F(\gamma)A_2(V)T_c + 2\,(\cos\alpha - FA_2)T_d + \frac{2cF(\gamma)h(T)}{g} \right] H \right\}^{\frac{1}{r+1}} \tag{29}$$

where

$$H = 1 - \frac{T_{p0}}{T_c} = 1 - \frac{1}{T_c}\left[\frac{(r+1)!}{2\dfrac{d^rK}{dt^r}} F(\gamma)A_2(V)T_c \right]^{\frac{1}{r+1}}.$$

As in Section 7.2.7 it is necessary to obtain an expression for $F(\gamma)$ in terms of the observable quantities. If the method used in Section 7.2.8 is applied to equations (9) and (28), formula (25) is obtained again. Thus to the degree of accuracy used in this method it makes no difference in the value of $F(\gamma)$ whether a mean value of K be used or K assumed to vary in accordance with (26).

Tests have been made of the degree of accuracy possessed by formulas (25) and (29) as solutions of the equations for θ_d and T_p. This was done in numerical cases by calculating $F(\gamma)$ by use of (25), and then T_p from (29) on the one hand, and on the other setting up equation (27) and solving it by Horner's method. Of the corresponding values of T_p found in this way, no pair was found to differ by as much as 1.6 per cent.[180]

7.2.10 The Case $r = 1$

In this case K is a linear function of t, being given by (27) with $r = 1$. This is the most important case in rocket tossing theory since motion pictures of an accelerometer taken during pull-up show that the rocket is usually released while the spatial acceleration is increasing, and that this acceleration can be approximated reasonably well by a linear function of time.

When $r = 1$ equation (27) becomes the third degree equation

$$\frac{2-\mu}{3}pT_p^3 - \left[p\left(T_c + \frac{\mu T_d}{2}\right) - (1+\mu)F(\gamma)A_2(V) \right] T_p^2 - B_1'T_p + B_0 = 0. \tag{30}$$

Due to the fact that terms of degrees $r + 1$ and 2 in equation (27) are now both of degree 2, it is possible to give a solution of (30) which has features of interest and, at least in form, is different from (29).

Equation (30) can be written in the form

$$T_p = \sqrt{\frac{B_0 - B_1'T_p + \dfrac{2-\mu}{3}pT_p^3}{p\left(T_c + \dfrac{\mu T_d}{2}\right) - (1+\mu)F(\gamma)A_2(V)}}. \tag{31}$$

On referring to the values of B_0 and B_1' it is seen that from (31) a first approximation to T_p is

$$T_{p0} = \sqrt{\frac{F(\gamma)A_2(V)T_c}{p}}. \tag{32}$$

When this approximation is substituted into the right-hand member of (31), a better approximation to the value of T_p is obtained. After omitting relatively unimportant terms, the resulting formula can be written

$$T_p \cong \sqrt{\frac{\left[F(\gamma)A_2(V)T_c + 2(\cos\alpha - FA_2)T_d + \dfrac{2c}{g}F(\gamma)h(T) \right]\left(1 - \dfrac{T_{p0}}{T_c}\right) - \frac{1}{3}FA_2T_{p0}}{p - \dfrac{1}{T_c}F(\gamma)A_2(V)}}. \tag{33}$$

It can be seen that if r is taken equal to unity in formula (28), the latter becomes identical with (33) except for the terms in $F(\gamma)A_2(V)$ in both numerator and denominator. Since these terms are small in comparison with the terms from which they are

subtracted, it is concluded that formulas (28) and (33) will give essentially the same value for T_p in any numerical case which arises in rocket tossing.

It should be remarked that the methods used in deriving formulas (28) and (33) are capable of numerous variations, especially as to the manner in which the various approximations are made. Moreover, any approximate formula obtained by such methods must be tested as to its degree of accuracy before it can be used with any confidence to obtain numerical results.

7.2.11 The Effect on Pull-up Time of the Change in Angle of Attack During Pull-up [180,185]

In forward firing of fin-stabilized rockets from zero-length launchers the rocket is freed from the airplane after traveling about 1 inch on the launcher. Thus, relative to the airplane, it has a small velocity at release and the action of the airflow on the fins tends to align the axis of the round with the airflow. The degree to which the round aligns with the airflow is given by the "f" factor. This factor is obtained from theoretical calculations by CIT and is given in their publications dealing with the *trajectory drops of rockets*.[216,217,218]

If the round is launched at an angle λ with respect to the airflow, the end result of the motion during burning is the same as if the rocket had been launched along an "effective" launcher line without fin action.[173] The angle between the airflow direction (flight line) and the effective launcher line is given by $\lambda(1 - f)$. The value of f is usually from 0.90 to 0.95, and thus the rocket effectively leaves the airplane in the direction of the flight line if the launcher line is not too far from the flight line. As an example, if the launcher is 3 degrees from the flight line at firing, the round will leave in a direction within 2 to 4 mils of the flight line.

During the pull-up the angle of attack of the airplane increases in accordance with the formula[185]

$$\eta = \frac{C_1 w K}{v_i^2} - C_2, \tag{34}$$

where C_1 and C_2 are constants for any particular type of aircraft, w is the weight of the airplane, v_i the indicated airspeed, and K the number of g's registered on an accelerometer. This fact operates to raise the launcher line through an angle somewhat larger than the change in direction of the flight line during the same period.

Moreover, at the beginning of pull-up the flight line and the sight line usually differ slightly in direction due to a deviation of speed or dive angle or both from the standard conditions assumed in setting the sight. These two factors cause small changes in the pull-up time. The equation for pull-up time will be set up in a form which takes account of these factors and under the assumption that K obeys equation (26).

In rocket and bomb tossing the sight line is adjusted to be parallel to the flight line for a median value of dive angle, loading, and airplane speed, usually a high airspeed as obtains in a dive. Thus in the preliminary dive with the sight on target before the pull-up, the flight line is pointed toward the target at the median dive angle and airspeed, but for other flight conditions the flight line deviates from the target. The assumption is made in bomb and rocket tossing that the flight line is pointed toward the target, and thus there will be a possible mil error at the target equal to the angle between the flight line and the sight line. In the case of bombs this error is minimized by the use of high airplane speeds,[101] and for rocket tossing this error is opposite in sense to another error (see Section 2.2.10). Thus we are justified in assuming the sight line and the flight line to be coincident.

7.2.12 The Equation for Pull-up Time

Let the sight line at the beginning of pull-up be taken as the x axis, and let σ designate the angle from the x axis up to the datum line in the airplane. If $\bar{\alpha}$ and $\bar{v_i}$ are "standard" values of dive angle and indicated airspeed respectively under which the sight line and the flight line during a dive have the same direction, and if $\bar{\sigma}$ is the value of σ under these standard conditions, then from (34)

$$\bar{\sigma} = \frac{C_1 w \cos \bar{\alpha}}{\bar{v}_i^2} - C_2.$$

In a dive under nonstandard conditions, the angle from the x axis up to the flight line is given by

$$\bar{\sigma} - \eta = \frac{C_1 w}{v_i^2}\left[\left(\frac{v_i}{\bar{v}_i}\right)^2 \cos \bar{\alpha} - \cos \alpha\right]. \tag{35}$$

Let β be the angle from the datum line up to the launcher line and f the launching factor. Then the angle from the flight line at release of the rocket up

to the effective launcher line is $\gamma(\eta_p + \beta)$, where $\gamma = 1 - f$ and

$$\eta_p = \frac{C_1 w}{v_i^2}(\cos\alpha + pT_p^r) - C_2 = \frac{C_1 w p T_p^r}{v_i^2} + \eta.$$

Let θ_p be the "pull-up angle," that is, the angle through which the *flight line* turns from the beginning of pull-up until the release of the rocket. This is the angle measured by the computer. Then the angle in radians from the x axis up to the effective launcher line is

$$\theta_p + \gamma\left[\frac{C_1 w p T_p^r}{1{,}000 v_i^2} + \frac{\eta + \beta}{1{,}000}\right] + \frac{\bar\sigma - \eta}{1{,}000}. \qquad (36)$$

Let ϵ be the angular drop of the rocket from the effective launcher line until the target is hit. From Chapter 2, equation (31),

$$\epsilon = \frac{g}{2V}F(\gamma)A_2(V)(T_c - T_p) + \frac{c}{V}F(\gamma)h(T). \qquad (37)$$

If to expression (36) is added the angle δ (see Figure 3), given by

$$\tan\delta = \frac{y_p}{VT_c - VT_p\cos(\bar\sigma - \eta)},$$

the sum will equal ϵ.

Equations (4), (5), and (6) are replaced by

$$\dot x_p = V\cos(\bar\sigma - \eta)$$

$$\dot y_p = \frac{pg}{r+1}T_p^{r+1} + V\sin(\bar\sigma - \eta),$$

and

$$x_p = VT_p\cos(\bar\sigma - \eta)$$

$$y_p = \frac{pg}{(r+2)(r+1)}T_p^{r+2} + VT_p\sin(\bar\sigma - \eta).$$

It follows that

$$\theta_p \cong \frac{\dot y_p}{\dot x_p} - \frac{\bar\sigma - \eta}{1{,}000}$$

$$= \frac{\frac{pg}{r+1}T_p^{r+1} + V\sin(\bar\sigma - \eta)}{V\cos(\bar\sigma - \eta)} - \frac{\bar\sigma - \eta}{1{,}000}$$

$$\cong \frac{pg}{(r+1)V}T_p^{r+1}$$

and

$$\delta \cong \frac{y_p}{VT_c - VT_p\cos(\bar\sigma - \eta)}$$

$$\cong \frac{\frac{pg}{(r+2)(r+1)}T_p^{r+2} + VT_p\frac{\bar\sigma - \eta}{1{,}000}}{V(T_c - T_p)},$$

where the approximations made consist in replacing tangents and sines of small angles by their radian measures, and cosines by unity.

Using these expressions with (36) and (37) the condition for a hit becomes

$$\frac{pg}{(r+1)V}T_p^{r+1} + \gamma\left[\frac{C_1 w p}{1{,}000 v_i^2}T_p^r + \frac{\eta + \beta}{1{,}000}\right] + \frac{\bar\sigma - \eta}{1{,}000} + \frac{\frac{pg}{(r+2)(r+1)}T_p^{r+2} + VT_p\frac{\bar\sigma - \eta}{1{,}000}}{V(T_c - T_p)} = \frac{g}{2V}F(\gamma)A_2(V)(T_c - T_p) + \frac{c}{V}F(\gamma)h(T).$$

Arranged in the standard form of an algebraic equation for the unknown T_p, this relation is

$$\frac{pg}{r+2}T_p^{r+2} - p\left[\frac{gT_c}{r+1} - \frac{\gamma C_1 w V}{1{,}000 v_i^2}\right]T_p^{r+1} - \frac{\gamma p C_1 w V T_c}{1{,}000\, v_i^2}T_p^r + \frac{g}{2}F(\gamma)A_2(V)T_p^2 - \left[gF(\gamma)A_2(V)T_c + cF(\gamma)h(T) - \gamma V\frac{\eta + \beta}{1{,}000}\right]T_p + \frac{g}{2}F(\gamma)A_2(V)T_c^2 + cF(\gamma)h(T)T_c - VT_c\frac{\bar\sigma + \gamma\beta - f\eta}{1{,}000} = 0. \qquad (38)$$

It is now assumed that the spatial acceleration of the airplane between the beginning of pull-up and the release of the rocket is proportional to the time since pull-up began, i.e., $r = 1$. With the abbreviations

$$\delta_2 = \frac{\gamma p C_1 w V}{1{,}000 v_i^2},$$

$$\delta_1 = \delta_2 T_c - \gamma V\frac{\beta + \eta}{1{,}000},$$

and

$$\delta_0 = VT_c\frac{\bar\sigma + \gamma\beta - f\eta}{1{,}000},$$

equation (38) becomes the cubic equation

$$\tfrac{1}{3}pgT_p^3 - \left[\tfrac{1}{2}pgT_c - \tfrac{1}{2}gF(\gamma)A_2(V) - \delta_2\right]T_p^2 - \left[gF(\gamma)A_2(V)T_c + cF(\gamma)h(T) + \delta_1\right]T_p + \frac{g}{2}F(\gamma)A_2(V)T_c^2 + cF(\gamma)h(T)T_c - \delta_0 = 0. \qquad (39)$$

On the basis of values for T_p calculated by solving equation (39) for a 5.0-inch HVAR released from an

F6F airplane under "standard conditions," $\bar{\alpha} = 35$ degrees and $\bar{v}_i = 320$ knots, and for several values of T_c and T, it is concluded that for this combination of rocket and airplane the effect of change in angle of attack during pull-up on the computed pull-up time never exceeds 2 per cent and for most conditions is less than 1 per cent. The effect of a combination of a deviation from standard dive conditions of as much as 10 degrees and 40 knots and the increase in dive angle during pull-up on calculated pull-up time has been found to be nearly 4 per cent for $V = 310$ knots, $\alpha = 25°$, $T_c = 25$ seconds, and $T = 100$ F.

7.3 ROCKET TOSSING INTEGRATION ERRORS OF THE BOMB DIRECTOR WHEN PULL-UP ACCELERATION VARIES WITH TIME[d]

7.3.1 Introduction

Determination of the accuracy of the integration performed by the bomb director when pull-up acceleration varies with time involves the comparison of data which represent the instrumental operation with the theoretical formula for a hit. It is assumed in this section that the acceleration acting on the airplane during pull-up is given by $K = \cos\alpha + pt$. This is a close approximation to the actual conditions during a rocket tossing pull-up. If the analysis were extended to include bomb tossing, however, allowance would have to be made for the fact that K may reach its maximum value before the bomb is released. This analysis attempts to take into account all the physical and electrical conditions to which the unit is subject and determine the accuracy with which the computer calculates the solution. The general approach and methods are summarized as follows:

1. A formula representing the solution given by the computer was developed, taking into account the delay in integration until the value of K reaches 1.3. Since both theory and experiment show that the K block will oscillate as it descends, this oscillation was included, but tests have shown that its effect is negligible; therefore, the unwieldy complications introduced by oscillation will not be discussed here.[184]

2. A laboratory computer AN/ASG-10(XN), Mark 1 Model 0, was modified to act as it would during pull-up. The linear increase in acceleration was simulated by having a small electric motor pull the K block down at a constant rate, starting at the end of the first timing period; the correct starting point, corresponding to $K = \cos\alpha$, was computed and set for each operation. A potentiometer was used to vary the voltage on the first condenser according to the theoretical calibration for the gyro (Mark 20 Model 00) to be used with the bomb director AN/ASG-10(XN), Mark 1 Model 0. The modified unit was then tested by standard laboratory test equipment over the complete ranges of dive angles, instrumental A factors, and times to target anticipated in rocket tossing flights.

3. The results of laboratory measurements on the computer were compared with data from the derived formulas for several cases, and found to be in good agreement. A constant small difference was found to exist between the results for similar values of A, T_c, α, and p because of delay in the operation of relays and in the starting of the small motor. Addition of 0.02 second to the results of the formula was necessary to account for relay lag.

4. The release time given by the laboratory unit was compared with the theoretical pull-up time for a hit using rockets. A simplified formula for pull-up time was used with the instrumental A taken as A_2. In order to make the results represent more accurately the action of a computer in launching rockets, 0.04 second was added to the release time given by the integrator, to make allowance for the delay between firing of the thyratron and the moment at which the rocket actually leaves the airplane.

The comparison shows that the instrumental pull-up time is too short at low dive angles, and slightly long for very high dive angles, especially at short range. When the instrumental A is very small (0.100), or and at very short ranges (5 seconds to target), the instrumental pull-up time increases as the dive angle increases instead of decreasing as it should. At average values of T_c, A, and α as used in field testing with fast rockets, the instrumental and theoretical pull-up times agree very well. The discrepancies which exist are very noticeably reduced by increasing the value of p, which explains why a high pull-up rate has been found best in field tests.

5. The computer circuit was modified in an attempt to make its results agree more closely with the theoretical times. The performance at low dive

[d] Section 7.3 was prepared by P. G. Hubbard of the State University of Iowa.

angles with low g's can be improved noticeably by shunting the rocket calibration condenser with a resistor. A value of 7 megohms (for the Mark 1 Model 0 circuit) was found to give the best correction when the instrumental A is about 0.200. The optimum value experimentally agreed upon in field tests at Inyokern was 7.5 megohms.

The items just listed bring out the fact that the computer does not operate perfectly when used in rocket tossing. The shortcomings which have been brought to light in this investigation have also been evident in field testing, and this investigation brings out the reasons for them. The adverse operation at short ranges, high dive angles, or low instrumental A is partly due to a lack of integration until $K = 1.3$, together with a K block which was designed primarily for use in bomb tossing. The revised ψ card used in the Mark 1 Model 2 equipment will be of value in correcting both of these errors.

7.3.2 Derivation of Formula for Instrumental T_p

From Section 2.1.4 the voltage v_1 built up across the first capacitor during the timing run is

$$v_1 = v_0\left(1 - e^{-\frac{\psi T_c}{20}}\right). \tag{40}$$

The second capacitor acquires charge in two distinct steps. During the first stage $K < 1.3$, and this capacitor is charged through a resistor of 10 megohms. Since the length of this period is

$$t_1 = \frac{1.3 - \cos\alpha}{p}, \tag{41}$$

the voltage built up is $v_0\ (1 - e^{-t_1/20})$.

At time t_1 relays operate to change the second charging circuit so that the effective capacity of the second capacitor becomes $2A$, and the resistance through which it receives charge is $10/(K + \sqrt{K^2 - K})$. Consequently the charge present in the second capacitor at time t_1 is effectively $2Av_0$ $(1 - e^{-t_1/20})$, and it receives further charge as K becomes greater than 1.3 in accordance with the differential equation

$$\frac{dq}{2Av_0 - q} = \frac{K + \sqrt{K^2 - K}}{20A}\,dt. \tag{42}$$

In order to facilitate the integration of the right hand member of (42) the function $K + \sqrt{K^2 - K}$ is approximated by $2.1053K - 0.8053$. The error in this approximation is less than 1.7 per cent over the interval $1.3 \leqslant K \leqslant 3.5$. Thus $K + \sqrt{K^2 - K} \cong at + b$, where $a = 2.1053p$ and $b = 2.1053\cos\alpha - 0.8053$, and equation (42) becomes

$$\frac{dq}{2Av_0 - q} = \frac{at + b}{20A}\,dt. \tag{43}$$

The solution of (43) which meets the initial conditions $t = t_1$, $q = 2Av_0(1 - e^{-t_1/20})$ is

$$q = 2Av_0\left\{1 - e^{-(1/20A)\left[\frac{1}{2}a(t^2 - t_1^2) + b(t - t_1) + At_1\right]}\right\},$$

so that the instantaneous voltage across the terminals of the second capacitor is

$$v_2 = v_0\left\{1 - e^{-(1/20A)\left[\frac{1}{2}a(t^2 - t_1^2) + b(t - t_1) + At_1\right]}\right\}. \tag{44}$$

Firing occurs when $v_2 = v_1$. From (40) and (44) this is seen to occur at a time which makes the exponentials equal, i.e.,

$$-\frac{\psi T_c}{20} = -\frac{1}{20A}\cdot$$
$$[\tfrac{1}{2}a(t^2 - t_1^2) + b(t - t_1) + At_1]. \tag{45}$$

The solution of (45) for t is the instrumental pull-up time T_p'. It is readily found that this is

$$T_p' = -\frac{b}{a} + \sqrt{\frac{2A}{a}(\psi T_c - t_1) + \left(t_1 + \frac{b}{a}\right)^2}. \tag{46}$$

7.3.3 Laboratory Testing

A computer (Mark 1 Model 0 Director) was set up for standard laboratory testing with, however, the following additions.

1. The ψ voltage was varied by means of a potentiometer.

2. A small electric motor was attached so that it began pulling the K block down at the second altitude point with speeds corresponding to 1.08, 2.00, and 3.27 g's per second. The correct starting point, corresponding to $K = \cos\alpha$, was computed and set by hand before each run. A relay between the J lead and ground on the computer completed the power circuit for the motor at second altitude and stopped the motor after firing of the thyratron.

The effective ψ value for each value of T_c was determined by measuring the output times at 150 volts and reduced V_ψ voltage, K and A remaining constant. The ratio of output time at V_ψ to output time at 150 volts is the effective ψ.

The instrumental pull-up time was measured for dive angles of 10, 20, 30, 40, 50, and 60 degrees;

times to target, T_c, of 5, 15, and 25 seconds; instrumental A factors of 0.101, 0.138, 0.238, and 0.350; and g's increase per second, p, of 1.08, 2.00, and 3.27.

7.3.4 Comparison of Laboratory Results with Computer Equation

Figure 5 shows graphs of equation (46) and the instrumental T_p determined in the laboratory for similar values of A, p, and T_c. The effective values of ψ determined from the computer were used in the equation (46). It is evident that the character of each set of curves is similar, but that the experimental values are consistently greater. The difference may be ascribed to delays in the action of relays and the starting of the small motor. A total delay in relays

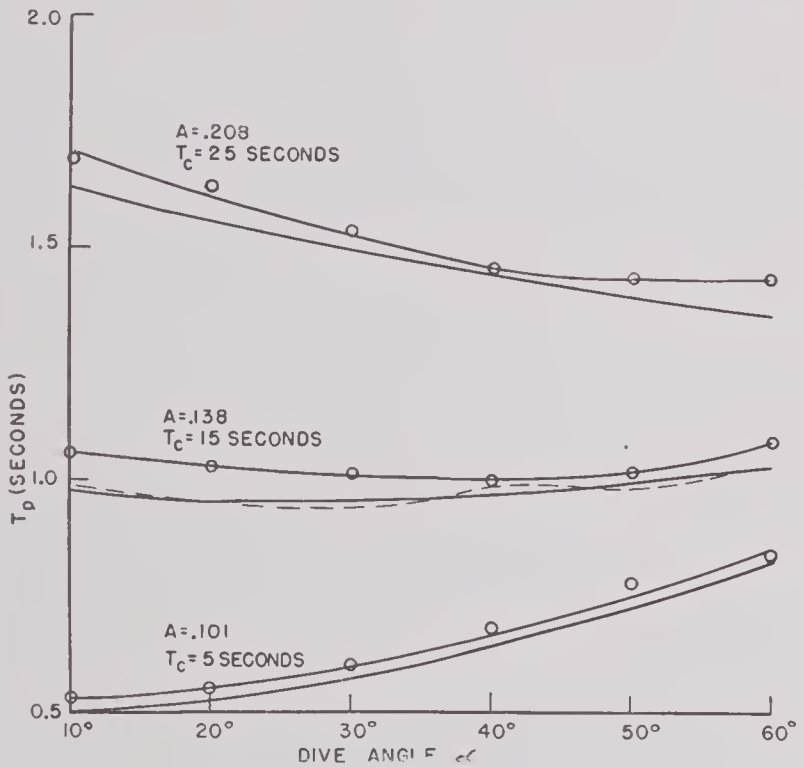

FIGURE 5. Comparison of theoretical rocket pull-up time T_p and instrumental T_p determined in laboratory, for typical values of A and T_c. Circles represent experimental points; unmarked solid curves and dashed curves are theoretical curves in nonoscillating and oscillating forms, respectively.

and motor of 0.05 second is easily possible. The effect of oscillation of the K-block bob in an average case is shown by the dashed curve.

7.3.5 Accuracy of Computer Solution

Formula (28) becomes for the case of no-delay-period, no-temperature-correction, and $r = 1$ the simplified formula

$$T_p = \left[\frac{A_2 F(\gamma) T_c}{p}\left(1 - \frac{T_{p0}}{T_c}\right)\right]^{\frac{1}{2}}. \tag{47}$$

The pull-up time given by this formula can be compared with the integrator pull-up time if the instrumental A is used in place of A_2.

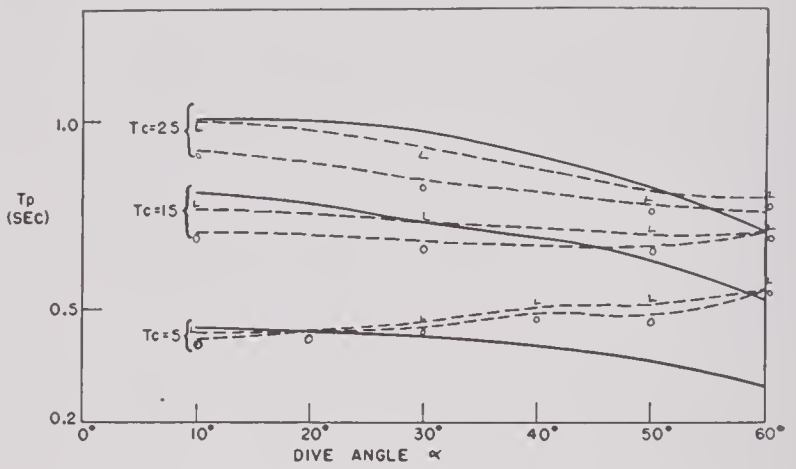

FIGURE 6. Comparison of theoretical T_p with computer results, for several values of T_c; $A = 0.101$, $p = 2.00$ g/second. Solid curves represent theoretical T_p; points O and L represent T_p of computer, without and with leakage resistance (7 megohms), respectively.

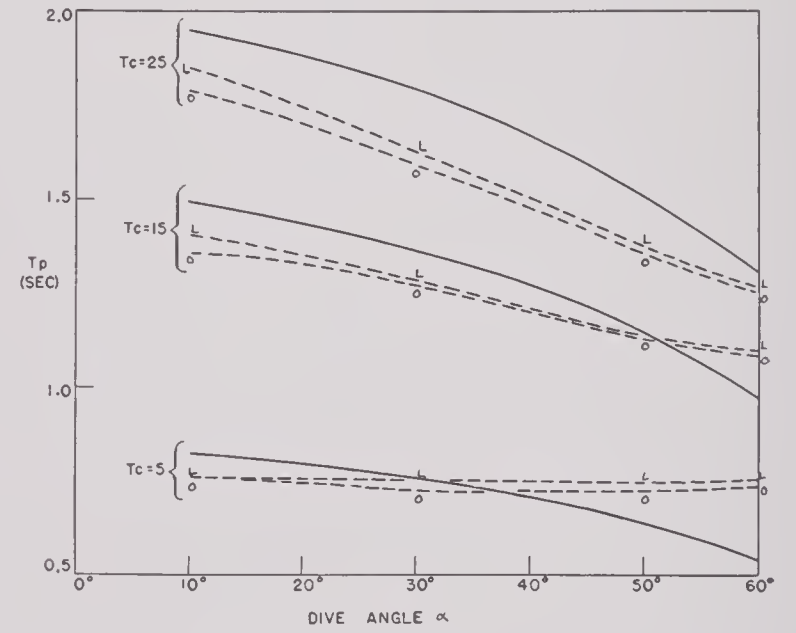

FIGURE 7. Comparison of theoretical T_p with computer results, for several values of T_c; $A = 0.350$, $p = 2.00$ g/second. Solid curves represent theoretical T_p; points O and L represent T_p of computer, without and with leakage resistance (7 megohms), respectively.

The representative graphs in Figures 6, 7, 8, and 9 show how the pull-up times given by (47) compare with the instrumental pull-up times.[184] An addition of 0.04 second has been made to the instrumental T_p because there is a delay of approximately that duration between firing of the thyratron and the instant when the rocket actually leaves the airplane. The

curves labeled L show the change in release time when a leakage resistance of approximately 7 megohms is put in parallel with the rocket calibration con-

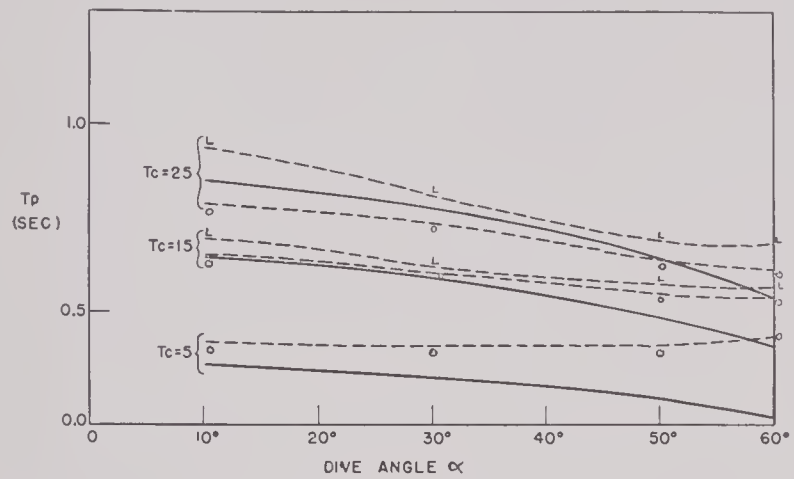

FIGURE 8. Comparison of theoretical T_p with computer results, for several values of T_c; $A = 0.101$, $p = 3.27$ g/second. Solid curves represent theoretical T_p: points O and L represent T_p of computer, without and with leakage resistance (7 megohms), respectively.

denser to improve the operation at low dive angles and long ranges.

From the curves in Figures 6, 7, 8, and 9 the following conclusions are drawn.

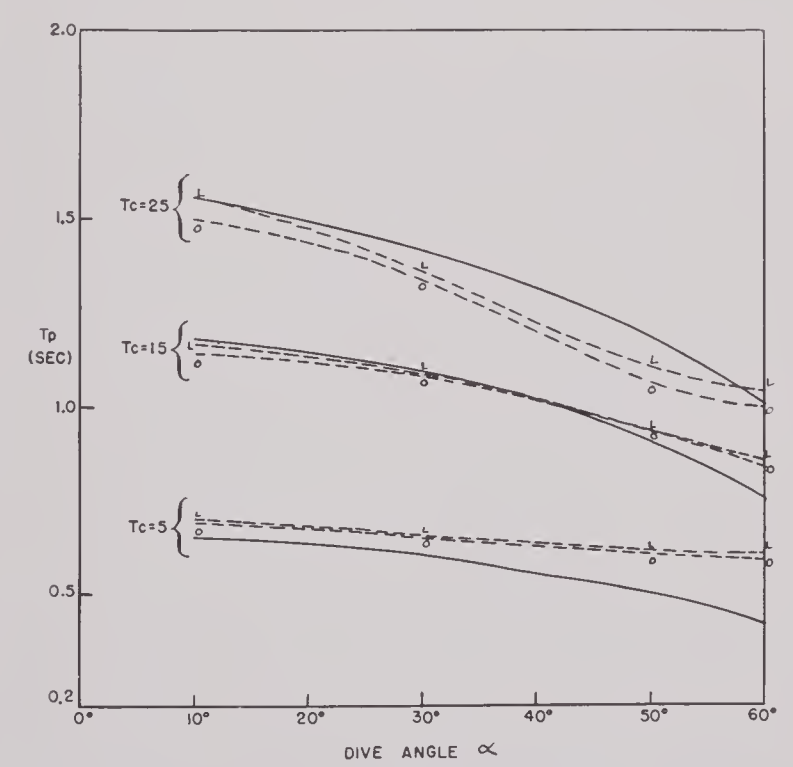

FIGURE 9. Comparison of theoretical T_p with computer results, for several values of T_c; $A = 0.350$, $p = 3.27$ g/second. Solid curves represent theoretical T_p; points O and L represent T_p of computer, without and with leakage resistance (7 megohms), respectively.

1. When the A factor or T_c is small, the integrator does not solve correctly for the pull-up time, but gives a longer pull-up time for high dive angles than it does for shallow dives. This causes the rocket to overshoot if the dive angle is large and undershoot when the dive angle is small. For intermediate dive angles the two curves agree very closely.

2. When a very large A factor is used, the release time is too small except at very high dive angles or very short ranges.

3. The curves emphasize the observation made in connection with field tests, namely, that a sudden pull-up is desirable. This corresponds to a large value of p, and had the effect of minimizing the discrepancies. A large value of p does not necessarily lead to a large number of g's because rockets are generally released before K reaches its maximum.

7.3.6 Analysis of Discrepancies

Formula (46) permits an analysis to be made of the reasons for inaccurate operation of the bomb director when used for rocket tossing. A critical examination of the formula shows that the instrumental T_p is influenced by three main factors.

1. The term $2A\psi T_c/a$. This is the most important term; when the quantities in the formula are such as to make this the preponderant term, the action of the computer is satisfactory.

2. The term b/a. This term is determined by the design of the K-block resistance strip.

3. The time t_1. This term represents the duration of the period before integration begins.

When A, ψ, or T_c is small, the term t_1 takes on relatively more importance. It is this term which gives many of the curves in Figures 6 to 9 the incorrect slope.

The explanation as to why the pull-up times are too small at longer ranges or higher instrumental A values is to be found in the term b/a. The resistances in the K block were designed for bomb tossing. The graphs in Figure 10 show how this design is not ideal for rocket tossing because of the decrease in pull-up time.

In Figure 10 the ordinates are proportional to the charging rate of the second capacitor, so that the total area under the curve is proportional to the voltage across the second capacitor. The solid curves give the theoretical rate for perfect integration, while the dotted ones correspond to the rate in the present computer. These diagrams show why the release time is somewhat short for small dive angles and somewhat long for large dive angles.

The same effects are shown in the earlier graphs in this section and have been observed in accurate analyses of field data.

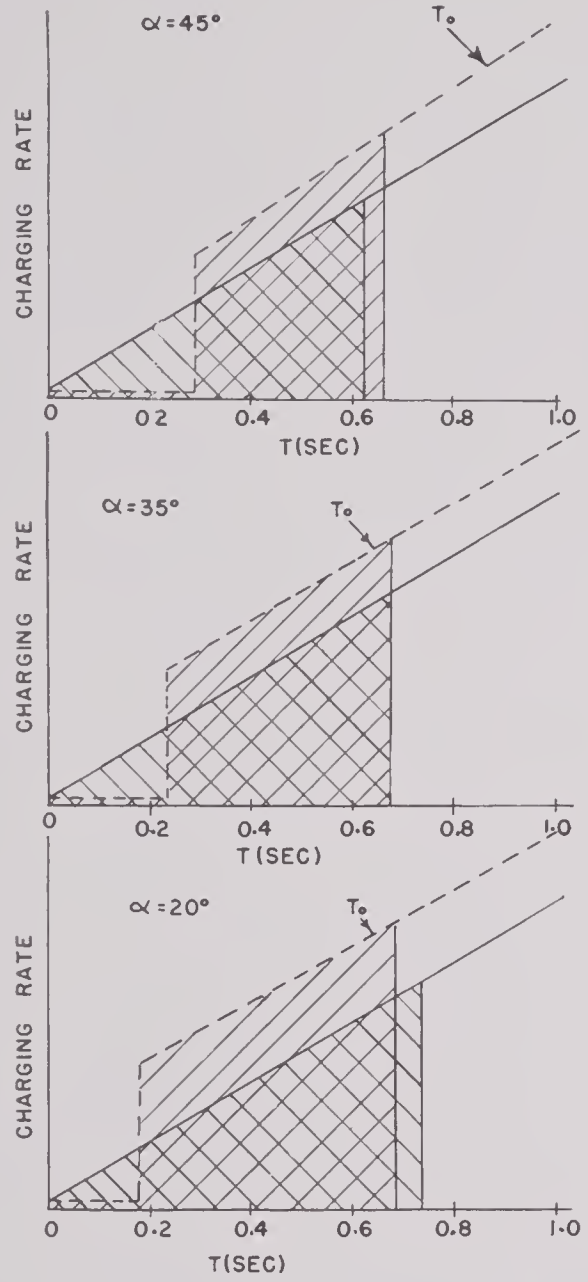

FIGURE 10. Comparison of theoretical (solid lines) and instrumental (dashed lines) charging rates of secondary condenser; both plotted as functions of time T for different values of α, with $A = 0.138$ and $p = 2.00\,g$/second. Shaded areas are proportional to voltages necessary for firing if $T_c = 10$ seconds. (Note difference in time T_p required to attain this area at theoretical and instrumental rates.) T_0 = time at which area under both curves is equal.

7.4 EVALUATION OF THE *A* FACTOR[e]

7.4.1 Introduction

Theoretical curves for the A factor as a function of plane speed are given for the following rockets: 5.0-inch AR, 3.5-inch AR, 2.25-inch AR (fast), 5.0-inch HVAR and 11.75-inch AR. The theoretical A factors are compared with experimental values determined by field tests and then new A factor curves are determined from the theoretical values modified by the field test results. These latter A factor curves are suitable for tossing rockets with the bomb director, Mark 1 Model 2, AN/ASG-10A.

7.4.2 Theoretical Values for *A* Factor

A derivation of the formula for the pull-up time for rocket tossing gives a theoretical expression for the A factor [equation (48)] which, with one exception, is in satisfactory agreement with values determined experimentally by field tests.[f] The derivation is based upon data on the gravity mil drops of rocket trajectories given in CIT publications [216,217,218] to describe the motion of the rocket after firing. These data on mil drops are used in the form of empirical equations which fit the data over usable ranges of the variables within about two mils (see Section 7.1). The theoretical expression for the A factor is given by equation (31a), Chapter 2:

$$A_2 = \frac{2V^2}{g}\, ae^{-Vb}, \tag{48}$$

where a and b are constants for each rocket type, V is the true airspeed of the airplane (feet/second), g is the acceleration due to gravity, and e the base of natural logarithms. The values of a and b for five Navy rockets now in use are given in reference 177.

Plots of theoretical values of A as given by equation (48) against true airspeed in knots are given in Figure 11 for five Navy rockets now in use.

The values for the A factor in Figure 11 are for firing from a zero-length launcher with rocket tossing equipment which has provisions for setting in the propellant temperature (and lanyard length in the case of lanyard firing of the 11.75-inch AR). The values for the A factor are good only when the gunsight is aligned along the flight line of the aircraft.

The data on mil drops of the rocket trajectories were obtainable only to 2,000 yards slant range for all of the rockets treated, except the 3.5-inch AR, 5.0-inch HVAR, and 11.75-inch AR. Thus the cal-

[e] Section 7.4 was prepared by I. H. Swift, formerly of the State University of Iowa, now at Naval Ordnance Test Station, Inyokern, California.

[f] The experimentally determined A factor for the 11.75-inch AR is considerably higher than the theoretical value. As yet no reason for this discrepancy has been found.

culated A factors given are partially dependent on extrapolations at ranges beyond 2,000 yards for the rockets not excepted in the previous sentence.

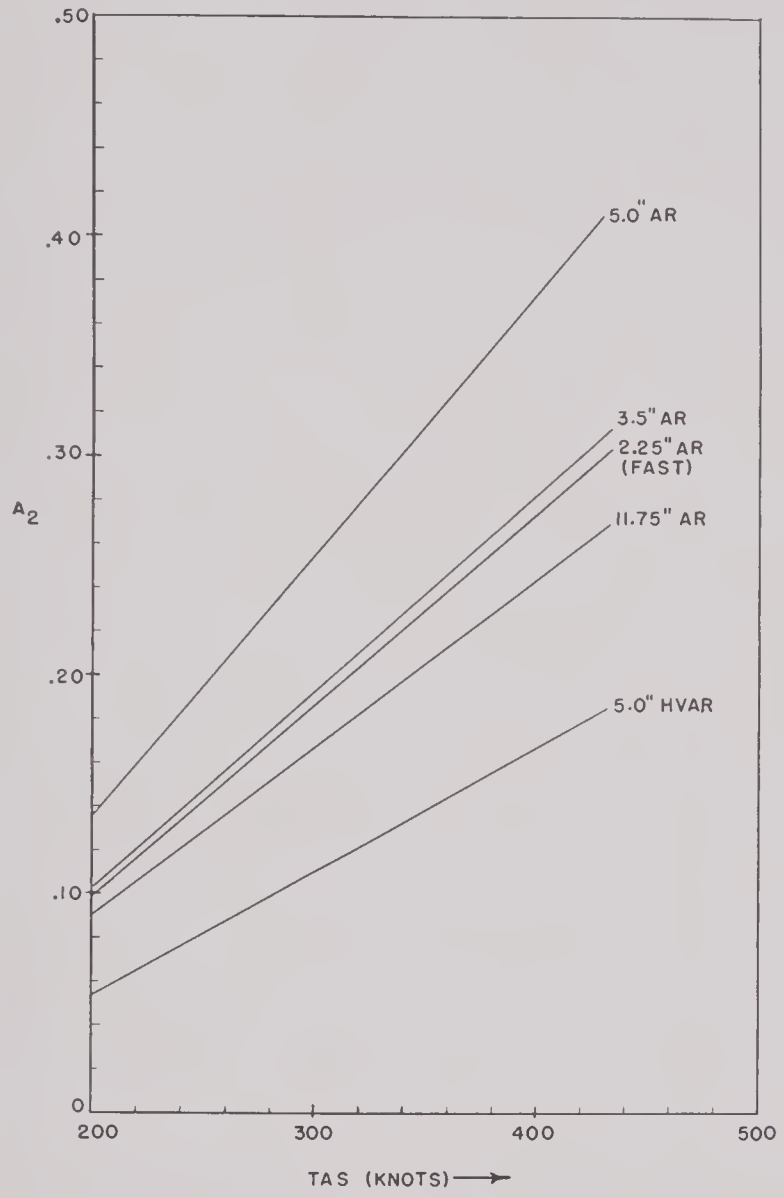

FIGURE 11. A factor (A_2) versus V for different types of rockets, for firing from zero-length launcher.

7.4.3 Effect of Plane Velocity on A Factor

As may be seen from Figure 11, the A factor increases nearly linearly with true airspeed of the plane. Field tests have shown that if the A factor for a particular plane speed is set into the equipment the shift in MPI obtained when a different plane speed is used is small — about 1 mil per 10 knots deviation from the set value (see Sections 2.2.10 and 5.3). Thus satisfactory results should be obtained at airspeeds within 20 or even 30 knots of the set value. The reason for the small MPI shift with velocity with the toss sight is that the change in attack angle of an airplane in a dive causes the MPI to go long as the airspeed increases, whereas the error due to having the A factor set too low at the higher speeds causes the rounds to land short. As a result the two effects partially cancel, and the error due to airspeed changes from the preset value is reduced.

7.4.4 A Factor as Based on Ratio of Plane to Rocket Speed

When the trajectory drop is evaluated by assuming that the rocket has a constant velocity V_r after firing (see Section 2.2.2), the A factor is given by A_1.

$$A_1 = \left(\frac{V}{V + V_R}\right)^2 \tag{49}$$

where V is the plane velocity and $(V + V_R)$ is essentially an average velocity of the rocket over the interval between the plane and target. The expression in equation (49) requires a known value for $(V + V_R)$ for evaluation. It will be shown in the following

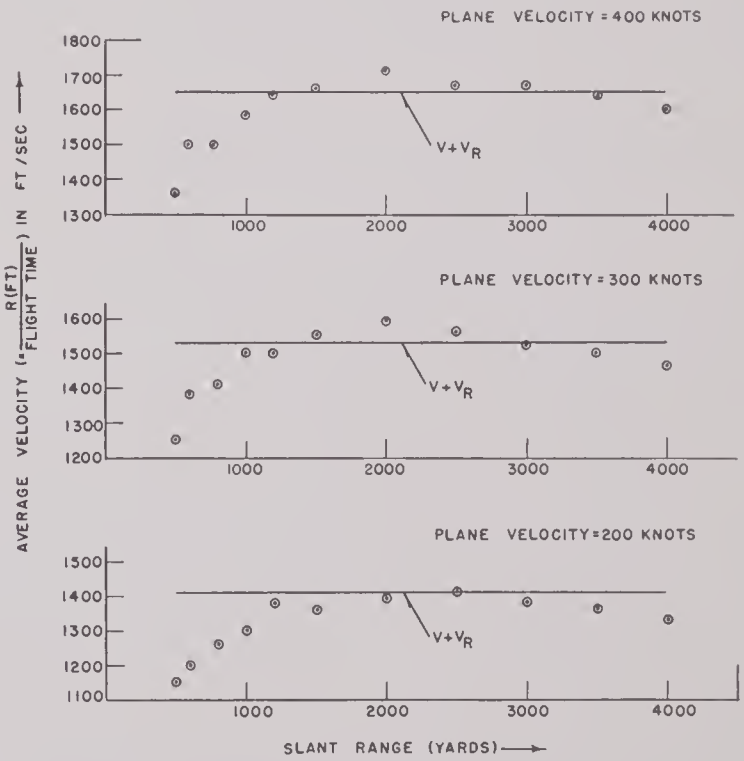

FIGURE 12. Average rocket velocity versus slant range at different plane velocities, as obtained from tabulated flight times for 5.0-inch HVAR (encircled points). Horizontal lines marked $V + V_R$ represent theoretical values.

paragraphs that if the quantity $(V + V_R)$ is obtained from the slant range divided by the rocket flight time given in CIT publications,[216,217,218] then the value of A_1 computed by equation (49) will give values comparable with those given by equation (48) and plotted in Figure 11. This will be shown by equating the two expressions (A_1 and A_2) for the

A factor and solving for $(V + V_R)$. Then the values of $(V + V_R)$ obtained will be compared with the total rocket velocity obtained from the flight times at various ranges. Equating A_1 and A_2 and solving for $(V + V_R)$ we have

$$V + V_R = \sqrt{\frac{g}{2a}}\, e^{V/2b}. \qquad (50)$$

In Figure 12 are shown plots of the average rocket velocity against slant range for the 5.0-inch HVAR. (Similar graphs for the 3.5-inch AR are given in Appendix D of reference 188. No velocity data are available for the 2.25-inch AR (fast)). The average rocket velocity is obtained from the flight time of the rocket [218] as a function of range at plane speeds of 200, 300, and 400 knots. Also given on the graphs is $(V + V_R)$ as calculated from equation (50). Thus it is seen that if $(V + V_R)$ is determined from an average value of the rocket flight time divided into the slant range, the values of A_1 given by the square of the ratio of plane velocity to rocket velocity are in substantial agreement with the values of A_2 given in Figure 11 from equation (48).

7.4.5 Comparison of Experimental and Theoretical A_2 Values

Table 4 gives values of A determined from field tests on rocket tossing, and the theoretical value of A_2 from equation (48) for the particular plane speed used.

TABLE 4

Rocket	Plane	Average TAS (knots)	Theoretical A_2 value from equation (48)	Experimental A value adjusted to give no-wind MPI on target	$A - A_2$
3.5-in. AR	TBM-1C	295	0.187	0.192	0.005
3.5-in. AR	TBM-1C	255	0.152	0.168	0.016
3.5-in. AR	F4U-1D	345	0.232	0.226*	−0.006
3.5-in. AR	P-47D	320	0.210	0.220	0.010
5.0-in. HVAR	F6F-5	360	0.146	0.158	0.012
5.0-in. HVAR	F6F-5	370	0.152	0.158	0.006
5.0-in. HVAR	F4U-1D	340	0.135	0.143	0.008
5.0-in. HVAR	SB2C-4	355	0.142	0.158	0.016
5.0-in. HVAR	F4U-1D	350	0.140	0.130*	−0.010
2.25-in. AR (fast)	F4U-1D	340	0.221	0.260*	0.039
5.0-in. AR	F4U-1D	340	0.301	0.307*	0.006
5.0-in. AR	F4U-1D	345	0.306	0.300*	−0.006
11.75-in. AR	F4U-4	355	0.210	0.305*	0.095
11.75-in. AR	F6F-5	345	0.202	0.290*	0.088

* With temperature compensation and a 7.5-megohm leakage resistor.

It will be noted from Table 4 that the theoretical A_2 was slightly lower than the experimental value when the equipment did not contain the temperature compensation feature. This is as expected, since a somewhat larger A factor was required to compensate for the increased mil drop due to the somewhat low temperatures of propellant used in the tests. For equipment containing the temperature compensation feature, the theoretical A_2 is more nearly the experimental A, except for the 2.25-inch AR (fast) and the 11.75-inch AR. In view of the data limitation in

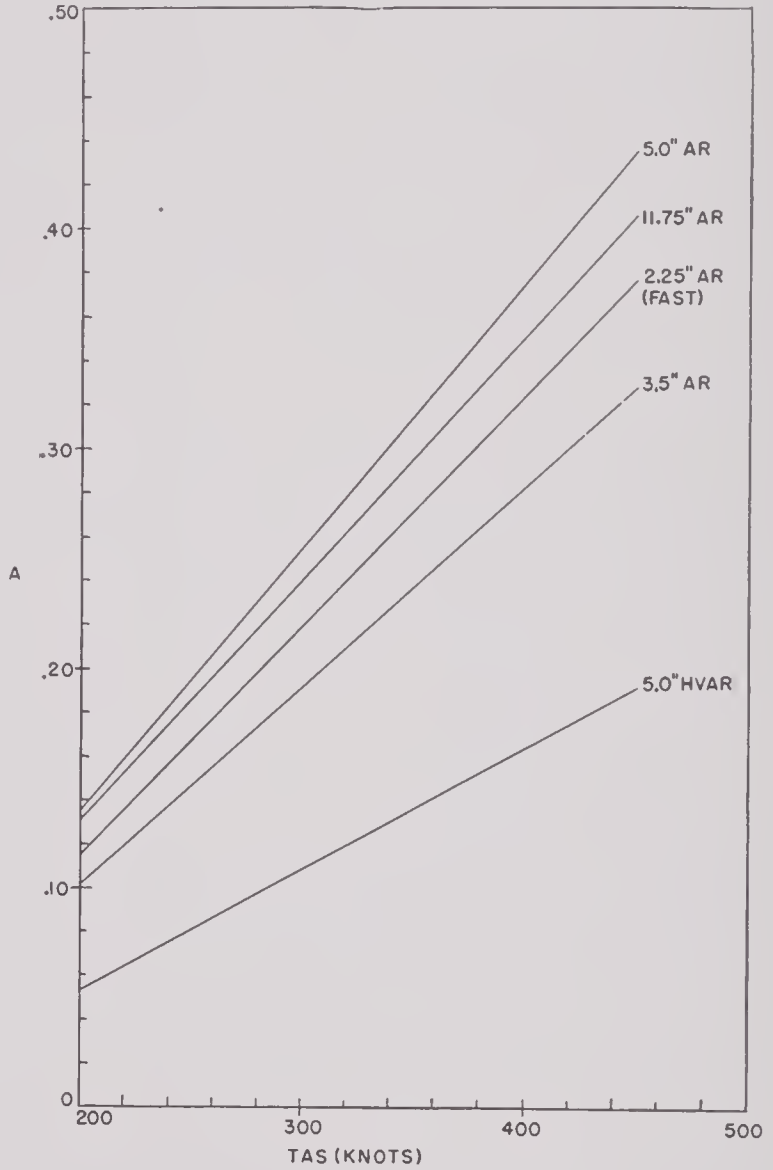

FIGURE 13. A factor versus V for different types of rockets from theoretical curves modified by field test results.

obtaining the theoretical A_2 for the 2.25-inch AR (fast), data available only to 2,000 yards, it is not surprising that a larger A factor is necessary in practice. As previously stated, no reason has yet been found for the large disagreement between the theoretical and experimental A values for the 11.75-inch AR.

Plots of the A factor as determined from equation

(48) and modified by field test results to give an on-target no-wind MPI under average conditions, are given in Figure 13 for five Navy rockets now in use. As noted by comparing Figures 11 and 13, there was a small modification for the 2.25-inch AR (fast) and the 5.0-inch HVAR; and a rather large modification for the 11.75-inch AR.[g] The A values for the 11.75-inch AR in Figure 11 are slightly higher than those used in determining the rocket calibration settings given in reference 186.

7.4.6

Conclusions

The A factors plotted in Figure 13 are sufficiently accurate to be used to predict results, and to set up the rocket tossing equipment, bomb director Mark 1 Model 2, AN/ASG-10A in a plane. It should be noted, however, that the values of A should be increased by about 0.01 at median temperatures if old style experimental equipment without temperature compensation is used.

The simplified picture of rocket tossing in which the A factor is given by the square of the ratio of plane velocity to rocket velocity is essentially correct. Also, if the average rocket velocity is obtained from the value of the slant range divided by the flight time required for the rocket to get to the target, and A is computed from it, the value obtained is essentially in agreement with field results.

7.5 COMPENSATION FOR PROPELLANT TEMPERATURE AND LANYARD LAUNCHING[h]

7.5.1

Introduction

It is necessary to take account of propellant temperature in rocket tossing, as the trajectory drop of a rocket is considerably increased at low propellant temperatures. The increased drop at lower temperatures is due to the fact that gravity has a longer time to act during the longer burning times which are obtained. In the launching of large rockets, a lanyard is used to fire the round a short time after release in order to minimize the damage to the plane from the rocket blast. In order to toss rounds when lanyard launching is used, as with the 11.75-inch AR, it is necessary to add to the pull-up angle an amount equal to the mil drop of the trajectory during the delay period between release and firing of the round. Since these two effects are similar in that an amount independent of slant range is to be added to the pull-up angle to compensate for a gravity mil drop occurring before the end of burning, they are treated together.

Section 7.5 will describe the function the computer is required to perform to compensate for temperature and to allow lanyard launching. The necessary modifications to the computer circuit will then be described. The theoretical calibration formulas for the temperature and lanyard compensation dial are given, and a section is devoted to the experimental data obtained recently as compared with the theoretical calibration.

7.5.2

Equation to be Solved by Computer

Equation (19) has been obtained as a formula for the pull-up time for rockets. The present rocket tossing equipment (Mark 1 Model 2) has a second capacitor charging rate which is proportional to ψ for $K < 1.3$, and to $(K + \sqrt{K^2 - K})/A$ for $K > 1.3$; that is, during the interval in which $K < 1.3$, the charging rate is much too small, while for $K > 1.3$, it is too large in the ratio

$$\frac{K + \sqrt{K^2 - K}}{K - \cos\alpha + F(\alpha)A_2(V) + \sqrt{(K - \cos\alpha)\,[K - \cos\alpha + F(\alpha)A_2(V)]}}.$$

This ratio is greater than unity for dive angles less than about 70 degrees, the exact angle depending upon A_2 and K. Thus, two errors of opposite sign are introduced in the pull-up time, the net error depending upon the relative durations of the conditions $K < 1.3$ and $K > 1.3$. For the remainder of this section, it will, therefore, be assumed that the

[redacted]

[g] See footnote f, Section 7.4.2.

[h] Section 7.5 was prepared by I. H. Swift, formerly of the State University of Iowa, now at Naval Ordnance Test Station, Inyokern, California.

equation to be solved by the computer is

$$T_p = \psi \frac{A_2(V)T_c + \dfrac{2ch(T)}{g} + 2T_d\left[\dfrac{\cos\alpha}{\psi} - A_2(V)\right]}{\bar{K} + \sqrt{\bar{K}^2 - \bar{K}}}, \tag{51}$$

this being obtained by replacing $F(\alpha)$ in the numerator of equation (19) by ψ for bombs (see Figures 2 and 3, Chapter 2), and replacing the denominator by $\bar{K} + \sqrt{\bar{K}^2 - \bar{K}}$.

7.5.3 Method of Compensating for Temperature and Lanyard Drop

The method of introducing the lanyard and temperature term into the equation for T_p solved by the computer, and the derivations of the theoretical calibration formulas, will be shown in Section 7.5.3.

1. *Method.* If the capacitor added to the bomb computer circuit to introduce the A factor is charged negatively with respect to ground by Δv volts at the initiation of pull-up, the T_p given by the computer is[161]

$$T_p = \frac{A\psi T_c + 20A \ln\left(1 + \dfrac{\Delta v}{v_0}\right)}{\bar{K} + \sqrt{\bar{K}^2 - \bar{K}}}, \tag{52}$$

where ψ is the ψ function for bombs, v_0 is the charging voltage for the condensers, and ln is the natural logarithm. According to equation (52), a term is added to T_p which is inversely related to $\bar{K}$ and directly proportional to A.

Since the pull-up angle associated with a change of amount ΔT_p in T_p is $(\bar{K} - \cos\alpha)g\Delta T_p/V$, the effect of the second term in the right-hand member of equation (52) is to increase the pull-up angle by an amount which is independent of range, and inversely proportional to airplane velocity. On the other hand, the angular trajectory drops associated with rocket propellant temperature and lanyard firing delay period are seen from equation (33), Chapter 2, also to be independent of range and inversely proportional to velocity. Thus, the desired type of correction is provided by equation (52).

In order for equations (51) and (52) to be equivalent, the relation (53) must hold.

$$20A \ln\left(1 + \frac{\Delta v}{v_0}\right) = \left[2T_d\left(\frac{\cos\alpha}{\psi} - A\right) + \frac{2ch(T)}{g}\right]\psi. \tag{53}$$

Equation (53) may be put into the equivalent form

$$\Delta v = v_0\left[e^{(r+s)\psi} - 1\right] = 150\left[e^{(r+s)\psi} - 1\right] \tag{53'}$$

where

$$r = \frac{1}{10} T_d\left(\frac{\cos\alpha}{A\psi} - 1\right),$$

and

$$S = \frac{ch(T)}{10Ag}.$$

Equation (53′) may be approximated by the equation

$$\Delta v \cong 179(r + s)\psi, \tag{54}$$

for the range of values of r, s, and ψ occurring in rocket tossing. This is shown in Table 5.

TABLE 5

$(r+s)\psi$	$179\,(r+s)\psi$	$150[e^{(r+s)\psi} - 1]$
0.1	17.9	15.78
0.2	35.8	33.21
0.3	53.7	52.48
0.4	71.6	73.77
0.5	89.5	97.31

2. *Determination of r.* The quantity r is zero for small rounds fired from zero-length launchers. For the 11.75-inch AR, which is fired with a lanyard, the A factor is approximately 0.30. At a dive angle of 35 degrees, the quantity $\cos\alpha/\psi$ equals 1.18 for the ψ corresponding to $T_c/V = 0.03$. This results in the formula

$$r = 0.29\, T_d. \tag{55}$$

The value for T_d to be used in equation (55) can be obtained from Table 6, which is based on equation (16).

TABLE 6

l	$K_d = 3$	$K_d = 4$
77″	0.365	0.317
36″	0.250	0.217

3. *Determination of s.* Considerable data have been taken at Inyokern[178] with the 5.0-inch HVAR with tossing equipment which did not include temperature compensation. These tests were made at propellant temperatures from 50 to 70 F, and they show no significant shift (less than 2 mils) in

MPI with variation in range out to 4,000 yards. Since the equipment without temperature compensation does not take account of the term of equation (51) which is independent of range, it is concluded either that the CIT theoretical mil drops[216,217,218] are in error, in that the constant term should be zero at field temperatures, or that some unknown factor adds a constant amount to all pull-up angles. Furthermore, as will be shown in a following paragraph, the field measurements on the shift in MPI with temperature give shifts considerably larger than those given in CIT tables. The CIT values have not been experimentally checked by firing rounds of different temperatures from airplanes. It should be noted that both of these discrepancies are the result of comparing deductions based on tossing results with theoretical calculations made by CIT on the trajectory of a rocket during the burning period, which is the most uncertain part of the trajectory. The toss results are in agreement with CIT calculations of the trajectory after burning.

The function $h(T)$ will now be altered so that it will vanish at $T = 100$ F; thus permitting compensation for temperature to be made for any temperature lower than 100 F. This change will require the use of a smaller A factor, and the MPI will be a few mils short at long ranges. This will be taken care of by inserting leakage resistance in the second charging circuit. The new functions are denoted by $H(T)$, and are given in Table 7.

TABLE 7

Rocket	$H(T)$
2.25-in. AR (fast)	$T^2 - 240T + 14{,}000$
3.5-in. AR	$T^2 - 350T + 25{,}000$
5.0-in. AR	$T^2 - 350T + 25{,}000$
5.0-in. HVAR	$T^2 - 264T + 16{,}400$
11.75-in. AR	$T^2 - 240T + 14{,}000$

The fact that the theoretical CIT mil drops do not agree with experimental firing tests as regards the magnitude of the MPI shift with temperature will now be considered. For example, the CIT tables give for the 5.0-inch HVAR a shift of 8.5 mils for a temperature change from 0 F to 100 F for flight conditions of 35-degree dive, TAS of 350 knots, and 2,500 yards slant range; whereas experimental data at Inyokern with both an F6F-5 and an F4U-1D give a shift of about 15 mils under the same conditions.[178,187] One way to take care of this discrepancy is to use the ratio $15/8.5 = 1.76$ as a factor to be multiplied into the values of c given in Table 2. Other later data gave, however, a slightly smaller MPI shift with temperature, indicating that a factor of about 1.5 should be used. These later tests consisted of use of the temperature compensation control to keep the MPI on target for various propellant temperatures, and therefore are more pertinent measurements. Hence, the value 1.5 will be used for the factor to be multiplied into c. Since field data are available only on temperature effect with the 5.0-inch HVAR, the same factor will be used for all rockets. This results in values for $C = 1.5c$ given in Table 8.

TABLE 8

Rocket	$C = 1.5c$
2.25-in. AR (fast)	6.3×10^{-4}
3.5-in. AR	4.95×10^{-4}
5.0-in. AR	4.95×10^{-4}
5.0-in. HVAR	5.6×10^{-4}
11.75-in. AR	6.3×10^{-4}

The value of s is now given by

$$s = \frac{CH(T)}{10Ag}. \tag{56}$$

In computing s for a given case, the value of A may be taken from Figure 13. It should be noted that the value of s given by equation (56) is not the same as the earlier s.

7.5.4 Instrumentation and Calibration

It is seen from equation (54) that the voltage Δv, to which the rocket calibration capacitor must be charged negatively, is proportional to ψ. The necessary initial voltage Δv can be obtained to a sufficient degree of approximation from the output voltage of the gyro, as this voltage is approximately proportional to ψ. The gyro voltage is positive with respect to ground but, by a suitable circuit arrangement, the rocket condenser is charged positively between arming and pull-up, and then reversed in the circuit at the initiation of pull-up. Thus, the capacitor is

negatively charged to a voltage proportional to ψ. The proportionality constant is determined by the setting of a potentiometer that applies a portion of the gyro output voltage to the capacitor. The setting of this potentiometer (the temperature and lanyard control) is determined by the values of r and s. The circuit of the present production model (Magnavox) of the Mark 1 Model 2 bomb rocket tossing equipment includes the features just described, and

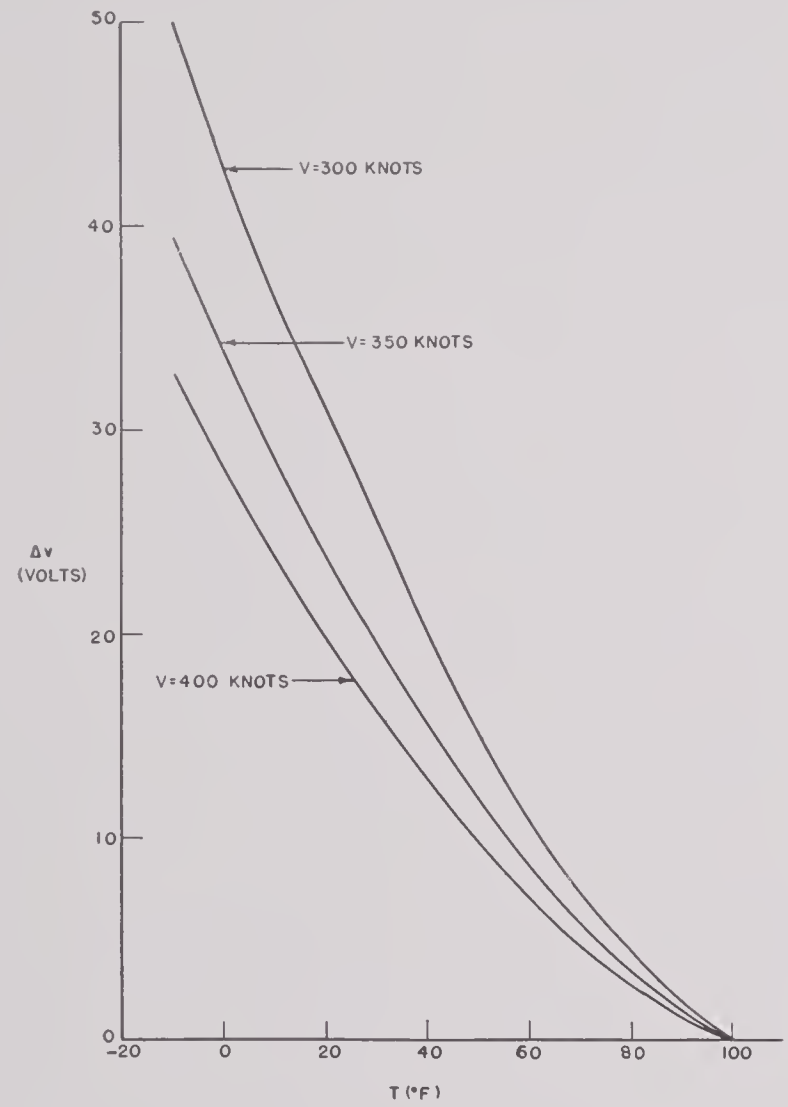

FIGURE 14. Temperature compensation voltage Δv versus temperature T for different velocities V for 5.0-inch HVAR.

is shown in Figure 9 of Chapter 3. The circuit for the Mark 1 Model 0 is identical in performance with the Magnavox circuit (Mark 1 Model 2).

If the gyro voltage is v_f, then

$$\Delta v = k v_f. \tag{57}$$

Comparison of this equation with equation (54) shows that k is given by

$$k = 179\ (r + s)\frac{\psi}{v_f}.$$

But at a mean dive angle of 35 degrees, the value of $150\,\psi / v_f$ is about 0.9. Hence,

$$k = \frac{179 \times 0.9}{150}\ (r + s) = 1.07(r + s).$$

The temperature-lanyard control dial is marked with numbers which designate the voltage Δv_0 when the dive angle is zero. Since $v_f = 150$ when the dive angle is zero, it follows from equation (57) that

$$\Delta v_0 = k \times 150 = 161(r + s) = 47 T_d + 161 s. \tag{58}$$

In equation (58), the delay time T_d may be taken from Table 6 or computed from formula (16), and the value of s is from (56).

For example, for the 11.75-inch AR fired using a lanyard of effective length 77 inches, the value of T_d may be taken as 0.3 second. If a propellant temperature of 60 F is assumed, and a velocity of 300 knots (corresponding to $A = 0.24$), the value of s from (56) is 0.026. Hence,

$$\Delta v_0 = 47 \times 0.3 + 161 \times 0.026 = 18.3.$$

Figures 14 and 15 show the temperature compensa-

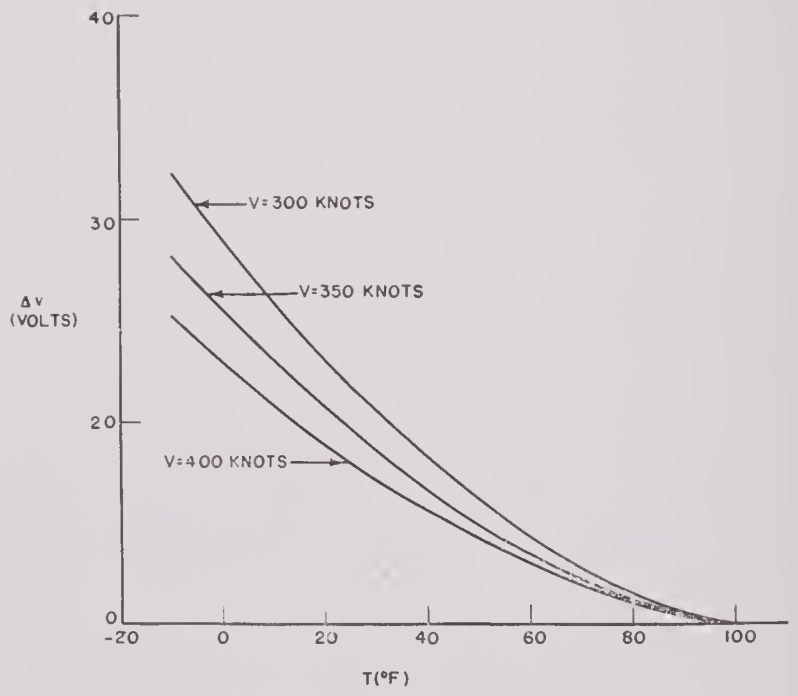

FIGURE 15. Temperature compensation voltage Δv versus temperature T for different velocities V for 11.75-inch AR.

tion voltages for the 5.0-inch HVAR and 11.75-inch AR, as obtained from equation (58). (For other types of rockets, see Appendix E of reference 188.)

7.5.5 Comparison of Experimental and Theoretical Values

Equipment containing the propellant temperature compensation control was used to fire 5.0-inch HVAR's at Inyokern, all at the same temperature, in order to determine the shift in MPI.[187] The following results were obtained.

Number of rockets	Temp. control (volts)	MPI (mils)
22	0	− 2.9
6*	8	8.4
6*	30	9.0
16	30	14.0

* Only one pair from one direction, together with a high wind, makes these data of small value. This series of tests showed a shift in the proper direction.

In a second series of tests,[187] rockets were heated or cooled to the extreme allowable temperatures, then compensation was made on the temperature controls according to the theory, all other factors remaining the same. The following results were obtained.

Number of rockets	Prop. temp. (degrees F)	Temp. control (volts)	MPI (mils)
9	102	0	− 5.1
14	63	8	3.1
15	11	30	− 2.1

The MPI is slightly short at both extremes, but the small number of rockets used makes the significance of this small error questionable.

Chapter 8

DEVELOPMENT OF IMPROVED TOSSING EQUIPMENT

8.1 ADVANTAGES AND LIMITATIONS OF THE MARK 1 BOMB DIRECTORS

As pointed out in the preceding chapters, the Mark 1 bomb director affords a definite improvement in the accuracy of dive-bombing operations. Quantitative measure of the advantage of the toss method varied with the Service branch conducting the evaluation, but all indicated some gain. The greatest advantage was indicated by Navy tests, probably on the basis of more extensive evaluation. This numerical advantage, as indicated in Section 5.1.1, was about two and one half times. A further advantage, difficult to express in quantitative terms, lay in the simplicity of the toss methods in actual use. The automatic properties of the equipment required only limited concentration from the pilot, and it was felt that under the stress of battle conditions this would show as a very decided advantage. The operational use of Model 0 established the latter factor if one accepts as pertinent the enthusiastic reception of the equipment by the pilots who used it in combat. (See Section 5.1.2, and reference 269.)

It was evident that there were a number of ways in which the Mark 1 equipments could be improved, and considerable effort was made to develop instrumentation of still greater accuracy and reliability. Probably the greatest difficulties in the production and maintenance of Mark 1 directors were encountered in the altimeter and gyro units and in the potentiometer which measured acceleration. In the case of the altimeter and gyro most of the difficulty was undoubtedly due to the fact that these were standard items modified to fit into the computer equipment and not specifically developed for the purpose. A common factor and limitation in all these items was the sliding or moving contact. Contact trouble could and did arise from a variety of sources such as vibration, dirt, pressure adjustment, and wear. A completely new computer circuit was designed, using new methods for indicating altitude, dive angle, and acceleration, and in which the sliding or variable contacts were either eliminated or greatly modified. This equipment, tentatively designated bomb director, Mark 3, Model 0, AN/ASG-10B, is described and discussed in Section 8.2. The Mark 3 director had not been evaluated in field tests at the end of the war.

Evaluations of the Mark 1 director showed that even though the equipment would inherently give excellent accuracy, this accuracy in Service use could be appreciably reduced through inadequate wind correction. Hence it became imperative to provide a method for estimating and making the proper trajectory correction for wind, if the full value of the instrument was to be utilized. The methods employed for this purpose with Mark 1 directors have been described in Chapters 2 and 6. These methods were, however, essentially improvements and appendages to the bomb director. In the Mark 3 director, the accelerometer to measure dive angle provides some correction for range wind error (see Section 8.2.4). The use of a lead-computing sight in conjunction with the director would provide a still greater correction. The principle of the use of this is described in Section 8.3.

The ψ function which represents the correction applied to the computing process for dive angle and other factors, was the least accurate intelligence fed to the computer. Although ψ can be formulated exactly (as shown in Chapter 6) instrumentation of the exact solution was not practicable. The ψ_1 function used in the Model 1 unit was an improvement of the ψ_0 function, but was still subject to a number of limitations as was shown in Chapter 6. More recently another formulation of the ψ function, designated as ψ_r, was devised, which offers even greater advantages. The ψ_r function is formulated and discussed in Section 8.4.

8.2 THE MARK 3 MODEL 0 BOMB DIRECTOR[a]

8.2.1 Altimeter Circuit

In the Mark 3 Model 0 (AN/ASG-10B) bomb director,[89] the time to target is measured by the use of two pressure capsules coupled to a potential

[a] Section 8.2 was written by William B. McLean, formerly of the Ordnance Development Division of the National Bureau of Standards, but now at the Naval Ordnance Test Station, Inyokern, California.

divider, $R26$ (Figure 1), in such a way as to provide a voltage which is proportional to the pressure altitude. This unit is approximately the size of a standard altimeter and is pictured in Figure 2. It has been

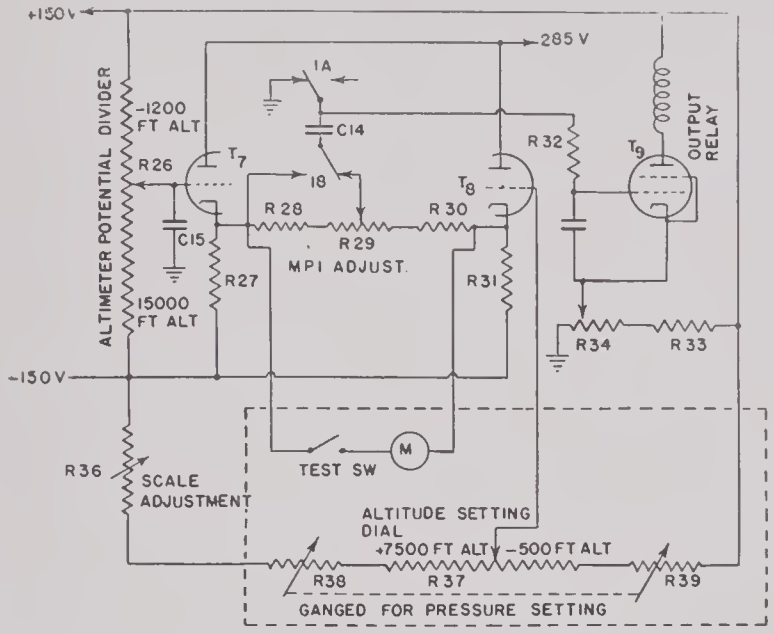

FIGURE 1. Schematic diagram of altimeter control circuit for Mark 3 bomb director.

tested in the Aeronautical Instruments section of the National Bureau of Standards and found to perform satisfactorily.[73] The barometric unit is used in conjunction with the electronic circuit shown in Figure 1. The unit is connected across a 300-volt source of d-c power. The voltage at the sliding contact is applied to the grid of a tube, T_7, used as a cathode follower. The high input impedance of this circuit insures that the effect of any contact resistance will be negligible. A capacitor, $C15$, connected to the grid of the cathode follower maintains the grid at a constant potential in the event that the sliding contact momentarily breaks contact with the potential divider.

The adjustment of the instrument for changes in pressure and target altitude is accomplished by means of the potential divider, $R37$, and the variable resistances, $R38$ and $R39$. The scale on resistor $R37$ is calibrated in feet of altitude and can be set at altitudes from -500 feet to $+7{,}500$ feet. Resistances $R38$ and $R39$ are ganged together so that $R38$ increases as $R39$ decreases. They permit the altitude scale to be set to compensate for varying atmospheric pressures. The dial controlling them is calibrated in inches of mercury.

To adjust the altimeter before starting a bombing mission, the altitude dial is set to the geographical altitude of the airplane. The test switch is closed to connect the meter between the cathodes of tubes T_7 and T_8. The pressure compensating resistors, $R38$ and $R39$, are adjusted until the meter reads zero current. The dial will then indicate sea level pressure. The altitude dial is reset to the altitude of the target and under these conditions the voltage between the two cathodes will be zero at the target altitude and the voltage difference between them will be proportional to the altitude above the target.

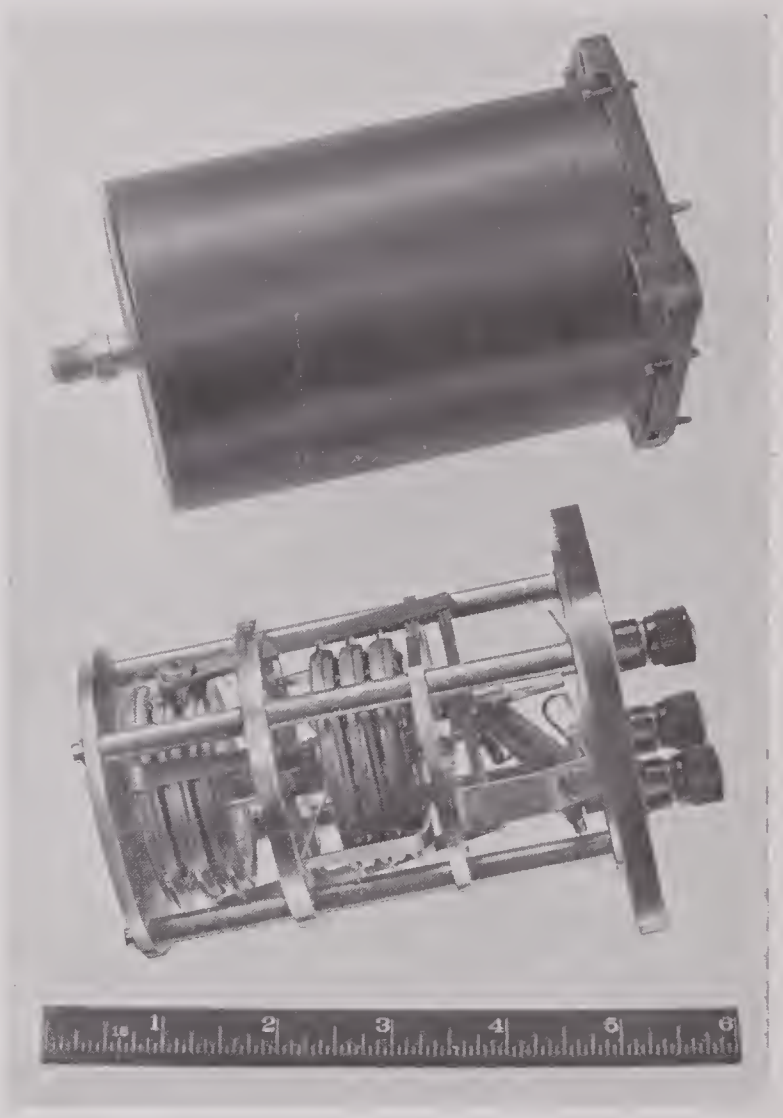

FIGURE 2. Altimeter control unit for Mark 3 Model 0 bomb director. Note the potentiometer and sliding contact at the right.

The capacitor, $C14$, is so arranged that the operation of relay contacts $1A$ and $1B$ will cause the grid of the thyratron T_9 to become negative by a voltage corresponding to one-sixth of the altitude above the target. As the altitude decreases, the contact on the altitude potential divider moves toward the positive end and the thyratron grid voltage rises. The thyratron grid reaches the zero firing potential when the altitude has decreased to five-sixths its original value. The interval between the time at which contacts $1A$ and $1B$ operate and the time at which

the thyratron fires is the time required for the plane to travel 1/5 of the distance to the target.

The altimeter described above has the following advantages over the contacting altimeter previously used:

1. The output is continuous so that the timing operation is started as soon as the bomb release switch is closed. This will result in shorter timing runs.

2. Its mechanical construction is materially simpler than that of the standard commercial altimeters which have hitherto been modified to produce the Mark 1 altimeter unit, and the force acting at the electrical contact can be much greater.

3. The adjustment of the altimeter for target altitude and pressure is accomplished electrically so

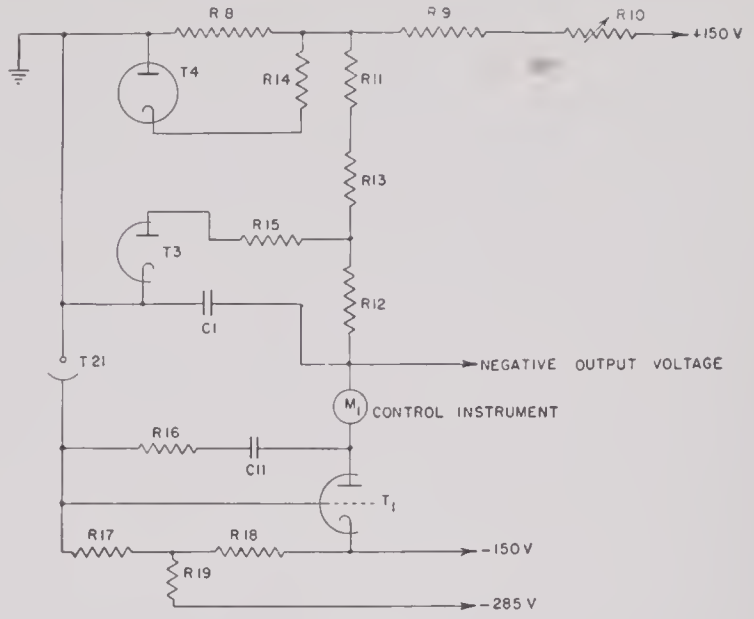

FIGURE 3. Schematic diagram of photoelectric accelerometer control circuit giving negative output voltage.

FIGURE 4. Photoelectric accelerometer unit. At the bottom right is photocell on its mount; at bottom left, condensing lens. At top left is case for 2½-inch milliammeter. At top center is shown meter movement; note, at end of pointer, flag partly covering aperture. At top right is back view of assembled unit, minus photocell and its mount.

that the controls may be located remote from the altimeter unit. This will result in a reduction of the amount of equipment which must be made accessible to the pilot.

8.2.2 Photoelectric Accelerometer

The photoelectric accelerometer unit consists of a 3½-inch panel milliammeter, the movement of which is unbalanced by the addition of a weight to the end of the pointer. The weight serves also as a shutter to cover a slot in the instrument face. A photocell (*T*21) is mounted behind the slot and is connected in a circuit of the type illustrated in Figure 3. The instrument is connected with such a polarity that an increasing current tends to move the hand in such a way as to decrease the light falling on the photocell, pictured in Figure 4. It is clear that the light falling on the photocell will adjust itself until the torque due to the current through the instrument coil just balances the torque due to the unbalance of the movement. If the acceleration normal to the plane containing the center of gravity of the movement and the two pivot points is changed, the current will immediately readjust itself until a balance is restored. The current through the instrument is therefore always proportional to the acceleration acting normal to the pointer. As long as there is sufficient amplification in the photocell circuit to maintain a balance, the circuit characteristics do not affect the output current. The output is also independent of variations in photocell sensitivity and light intensity.

Damping and Response

An electrical damping force is provided by the capacitor *C*1. If the pointer changes its position, the photocell circuit and capacitor immediately cause a high current to flow in the coil which opposes the motion. This transient current dies out as the motion ceases and is analogous to viscous damping in a purely mechanical system. It has a magnitude which depends on the angular velocity of the coil.

If the pointer bends, the motion of the coil is not in phase with the motion of the shutter controlling the photocell current. In this case the damping force described above may become a driving force and the moving system may oscillate. The oscillation is of such frequency that the pointer has a node about one-third the distance from the free end to the pivot, Such oscillations, which have a frequency of 250 cycles per second, can be prevented by decreasing the gain of the system for high frequencies and by increasing the stiffness of the pointer.

Capacitor *C*11 and resistor *R*16, Figure 3, are adjusted for any particular type of instrument movement so as to allow as much high frequency response as possible without running into danger of oscillation due to bending of the pointer.

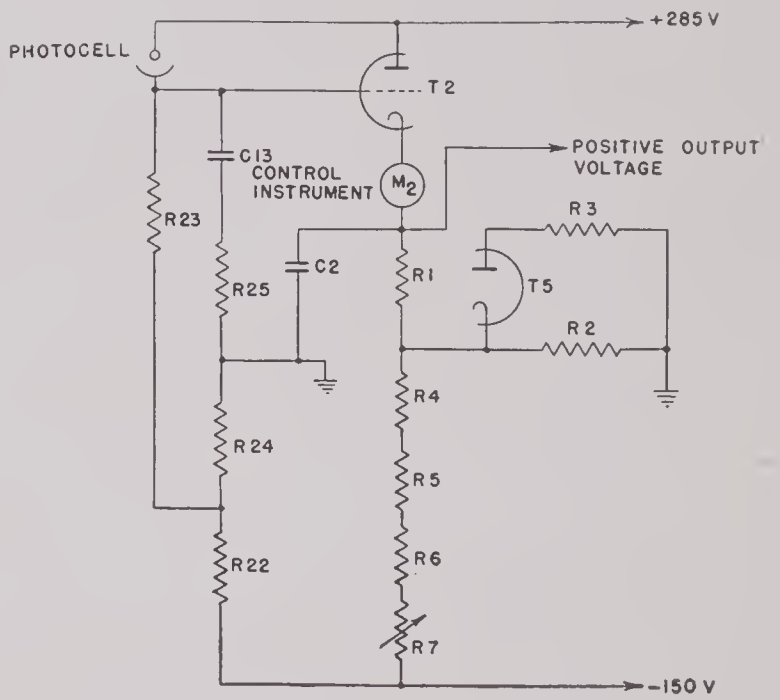

Figure 5. Schematic diagram of photoelectric accelerometer control circuit giving positive output voltage.

Figure 5 shows a similar circuit arrangement in which the instrument coil is in the cathode circuit of the control tube in place of the plate circuit. Both arrangements are used in the Mark 3 computer. The circuit of Figure 3 is adaptable to securing a negative output voltage with respect to ground and that of Figure 5 is more easily used to secure a positive voltage with respect to ground.

It should be noticed in both Figures 3 and 5 that if the output voltage is taken from the tube side of the control instrument coil, it will not be affected by changes in output load. If it is taken from the opposite side of the coil, it will be affected by changes in output load but will not be affected by changes in resistance of the instrument coil.

Centrifuge Tests

An accelerometer unit of the type described above was checked for linearity and stability by mounting it on the arm of a centrifuge. The speed of the

centrifuge was adjusted until the current through the instrument was a certain fixed value as determined by means of a standard 1-ohm resistor and a potentiometer. Then revolutions of the centrifuge were timed by means of an electric stopclock. Readings were the same to within the estimated accuracy of setting the potentiometer. The voltage output versus acceleration showed a high degree of linearity.[89]

Nonlinear Output

It is desired that the output voltage of the accelerometer be a nonlinear function of the acceleration. Since the current through the instrument is exactly a linear function of the acceleration it is necessary to make the resistance, across which the output voltage is developed, vary with the acceleration in order to obtain a nonlinear output voltage. By means of the diodes shown in Figures 3 and 5 it is possible to obtain voltage-current curves which will consist of a series of straight lines. The transition from one line to another occurs whenever the current through one of the branches containing a diode changes its direction. By properly selecting resistor values, it is possible to fit the desired curve with a series of straight lines.[113] The desired function of acceleration is shown in Figure 6. The dotted lines show the proposed straight line fit.

It is necessary to adjust the current through the meter movement under a standard acceleration to an exact value in order to obtain the proper curves by the above method. This is done by the use of a variable magnetic shunt which can be adjusted while the meter is operating under an acceleration of 1g.

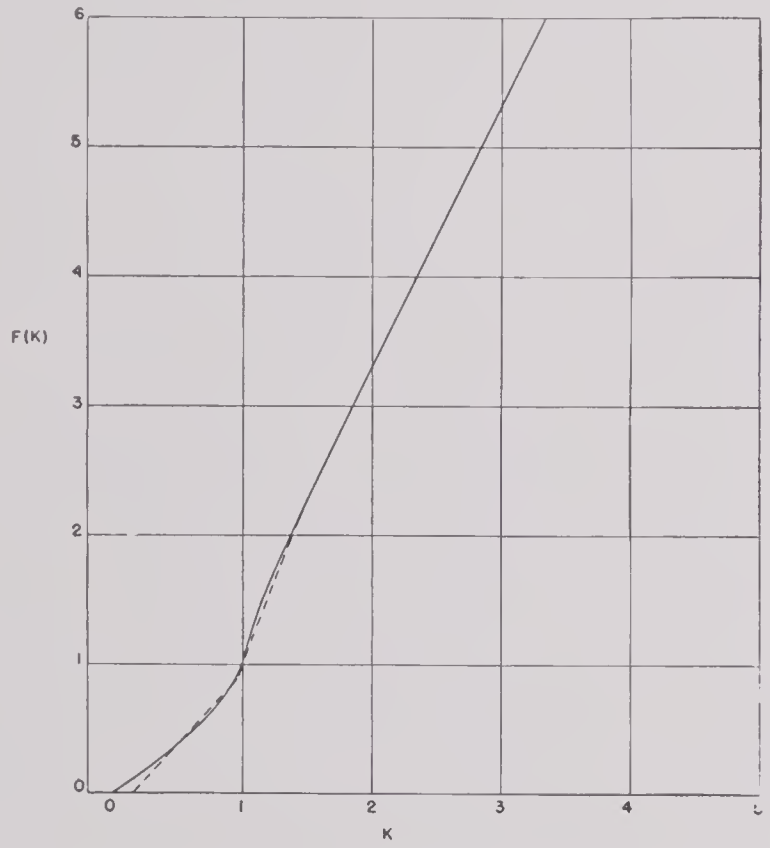

FIGURE 6. Graph of desired acceleration function:

$$F(K) = \begin{cases} \psi_1 \text{ (arc cos } K, 3, 0.028) & (0 < K < 1) \\ K\left(1 + \sqrt{\dfrac{3(K-1)}{3K-1}}\right) & (K > 1) \end{cases}$$

Dashed lines represent proposed straight line fit:

$$F(K) \cong \begin{cases} F_3(K) = 1.1207K - 0.19224 & (0 < K < 1) \\ F_2(K) = 2.6115K - 1.6115 & (1 < K < 1.5) \\ F_1(K) = 2.0069K - 0.7046 & (K > 1.5) \end{cases}$$

8.2.3 Dive Angle Indication

In bomb tossing, it is necessary to determine the component of gravity acting normal to the line of flight since this is one of the factors that will determine how long the bomb will stay above the line of flight. The Mark 3 director uses the sensitive accelerometer described above to measure this component of acceleration during the timing run. The current through the accelerometer during the timing run is

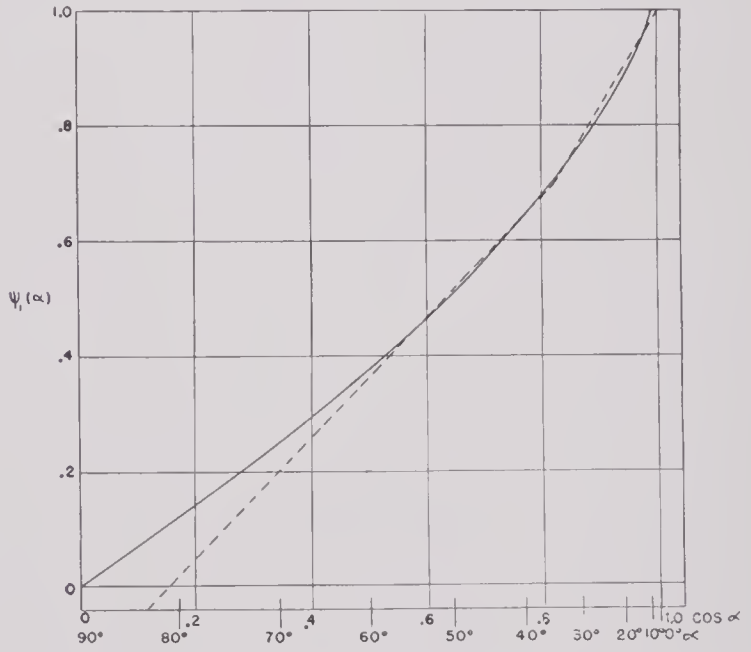

FIGURE 7. ψ function for Mark 3 director, as function of cos α, determined for $K = 3$ and $T_c/V = 0.028$ (solid curves); dashed lines give the straight line fit:

$$\psi_1(\alpha, 3, 0.028) \begin{matrix} 0.9906 \cos\alpha - 0.115 & (0 < \cos\alpha < 0.82) \\ 1.676 \cos\alpha - 0.676 & (0.82 < \cos\alpha < 1) \end{matrix}$$

proportional to $\cos\alpha$. A capacitor is charged in such a way that its voltage is proportional to:

$$\int_{-T_c/5}^{0} \psi\,(\alpha)\,dt.$$

Figure 7 shows a graph of $\psi(\alpha)$, as a function of $\cos\alpha$, together with the two straight lines used in fitting it.[113]

8.2.4 Wind Correction

The use of an accelerometer to measure dive angle provides some correction for the range-wind error as described in Section 6.6.9.[81] This is due to the fact that in tracking a target with a head or tail wind the plane will fly a curved course. The curvature of the path is such that it increases the reading of the accelerometer for a head wind, and thus increases the value of the acceleration integral set into the computer during the timing run. A longer toss results, which decreases the error due to the head wind. The converse conditions exist in the case of a tail wind.

It was suggested that this effect might be increased by the use of a lead-computing sight (see Section 8.3). In using such a sight the airplane must turn faster to keep the sight centered on the target. This will result in an accelerometer correction to the toss which may be sufficiently large to provide full wind correction, even though the computing sight does not have time to establish the proper lead.

8.2.5 Integrating Circuit

A linear integrating circuit[241] is incorporated in the Mark 3 computer. The circuit elements as used in the computer are shown in Figure 8. A positive voltage, proportional to the function to be integrated, is applied to the input lead. This causes a current to flow through resistor $R42$ to capacitor $C5$. Normally this would produce a rise in potential of the input side of this capacitor. Any rise of the grid voltage of tube $T11$, however, causes an amplified drop in its plate potential. By means of the cathode follower circuit, the potential of the opposite side of the capacitor $C5$ is lowered. The net effect is to maintain the grid of tube $T11$ at a very nearly constant potential while the condenser is charging. This means that the current flowing to capacitor $C5$ is always proportional to the applied voltage. The charge accumulated on the capacitor is a measure of the integral of the applied voltage during the charging period. It is expressed as a drop in potential of the cathode follower output. If the output is connected to a voltage of opposite polarity, the reverse operations will take place and the output voltage will rise by an amount which is proportional to the time integral of the new voltage.

The fact that the input grid remains at a constant potential makes it possible to compute the sum of several integrals with this circuit. If several resistors are connected to the input grid and their opposite ends connected to voltages proportional

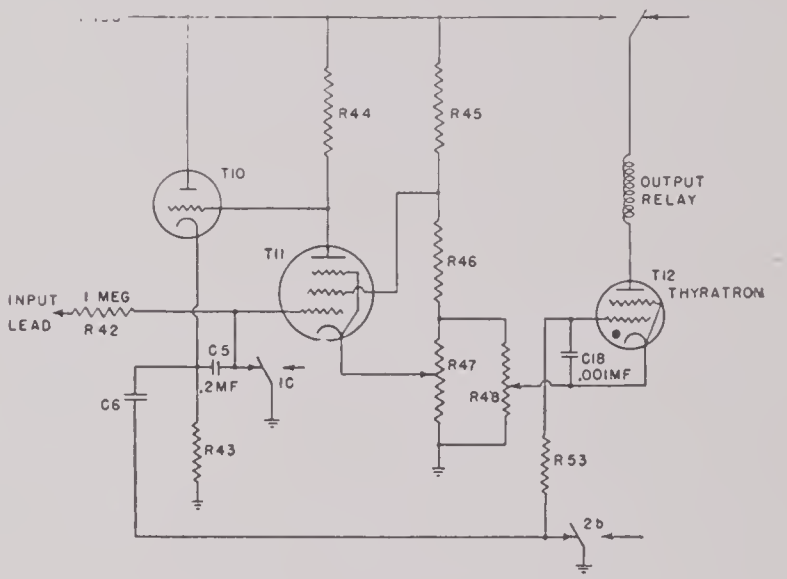

FIGURE 8. Schematic diagram of integrating circuit for Mark 3 computer.

to the functions to be integrated, the total current flowing to the capacitor will be proportional to the algebraic sum of all the functions. The total charge on the capacitor will be the sum of the integrals of these functions.

In the Mark 3 computer it is desired to determine when the integral of a function of pull-up acceleration is equal to the integral of the dive angle function over the timing run, i.e.,

$$5\int_{-Tc/5}^{0} \psi(\alpha)dt = \int_{0}^{T_p} F(K)dt. \qquad (1)$$

A positive voltage proportional to $\psi(\alpha)$ is applied to the input of the integrating circuit during the timing run. At the second altitude this input lead is connected to a negative voltage proportional to $F(K)$. A thyratron releases the bomb when the rise in voltage due to the pull-up acceleration is equal to the initial drop in voltage.

8.2.6 Provision for Firing Rockets

It is shown in reference 188 (pages 22–25) that the condition for release of rockets, as given by equation (25) of Chapter 2, can be converted to

$$\frac{2\psi(\alpha)}{A}\left(T_d + \frac{ch(T)}{g}\right) + 5\int_{-T_c/5}^{0} \psi(\alpha)dt = \int_0^{T_p} \frac{F_R(K,A)}{A}\,dt, \quad (2)$$

through the following assumptions (see also Chapter 2):

1. That $(2 - A)\ T_d$ is approximately equal to $2\,T_d$, A being a function of plane and rocket velocities;
2. That

$$F_R(K,A) \cong F_R(K,0) + m\,A, \quad (3)$$

reducing to the following relation for bomb tossing $A = 1$:

$$F_B(K) \cong F_R(K,0) + m, \quad (3a)$$

and

3. That $\psi\ (\alpha)$ is, to a sufficiently accurate approximation, the same function as for bomb tossing.

The above assumptions are justified in reference 188 by graphical methods.

Substituting equation (3) in equation (2), the condition for release becomes

$$\frac{2\psi}{A}\left(T_d + \frac{ch(T)}{g}\right) + 5\int_{-T_c/5}^{0} \psi(\alpha)dt = \int_0^{T_p} \frac{F_R(K,0) + mA}{A}\,dt \quad (4)$$

which can be expressed in the form

$$\underset{\text{I}}{\frac{2\psi(\alpha)}{A}\left(T_d + \frac{ch(T)}{g}\right)} + \underset{\text{II}}{5\int_{-T_c/5}^{0} \psi(\alpha)dt} = \underset{\text{III}}{\int_0^{T_p} F_B\,(K)dt} + \underset{\text{IV}}{\frac{1 - A}{A}\int_0^{T_p} F_R(K,0)\,dt}. \quad (5)$$

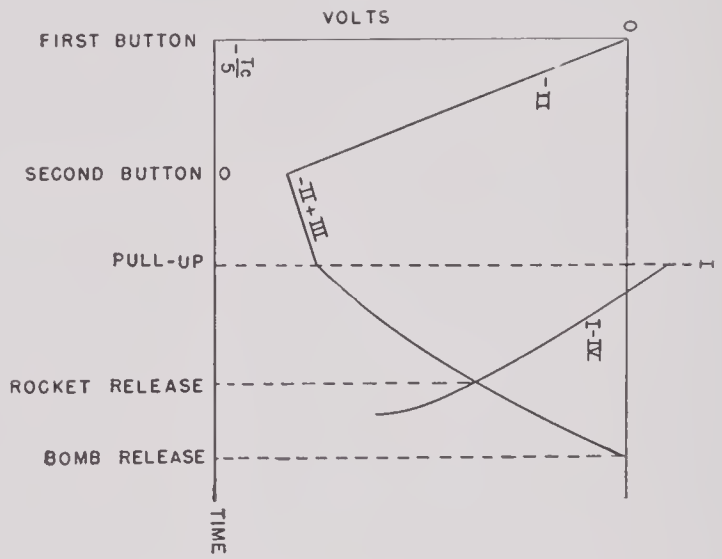

FIGURE 9. Graph of bias voltages corresponding to different terms of release equation (5).

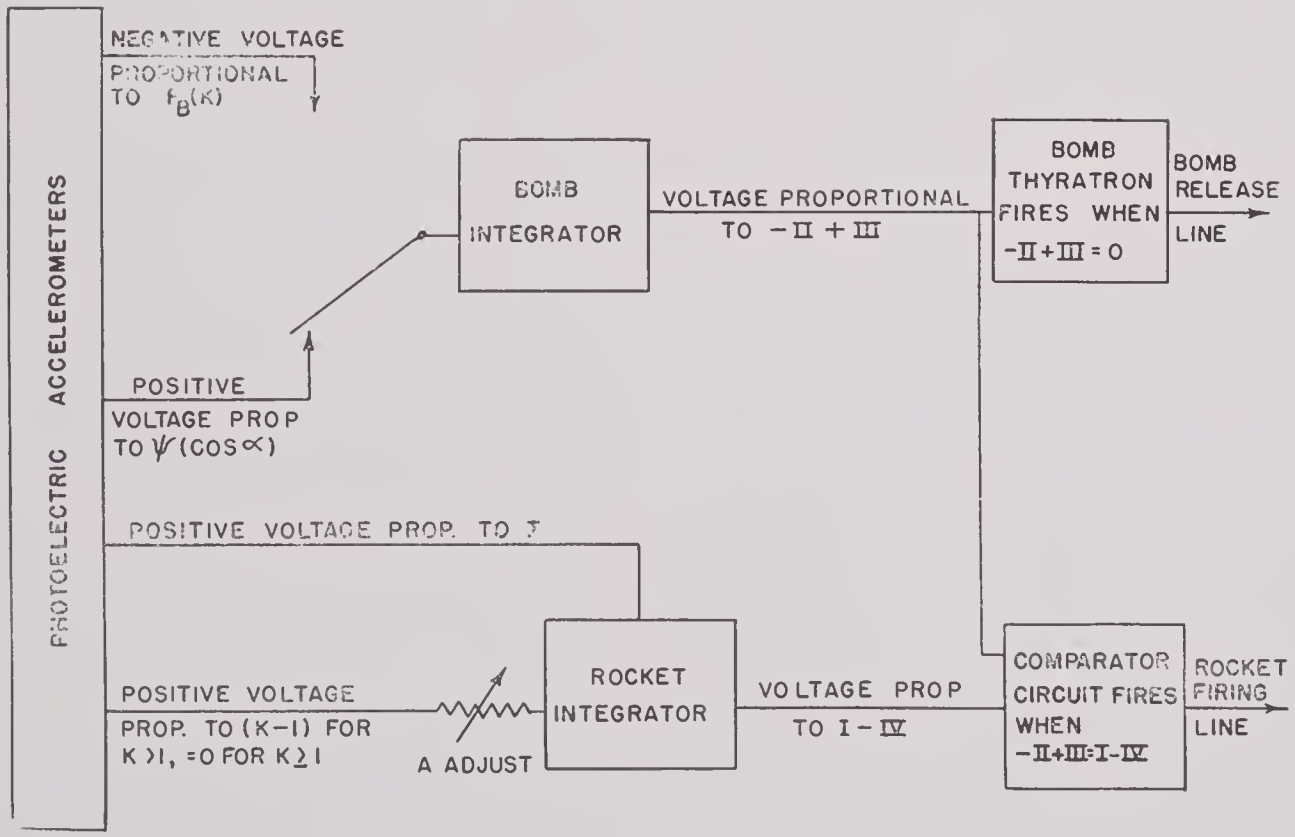

FIGURE 10. Schematic diagram of operation of Mark 3 computer, showing manner in which output voltage components are combined (for both bombs and rockets). For terms represented by I, II, III, and IV, see equation (5) in text, except that t instead of T_p is upper limit of integration in III and IV.

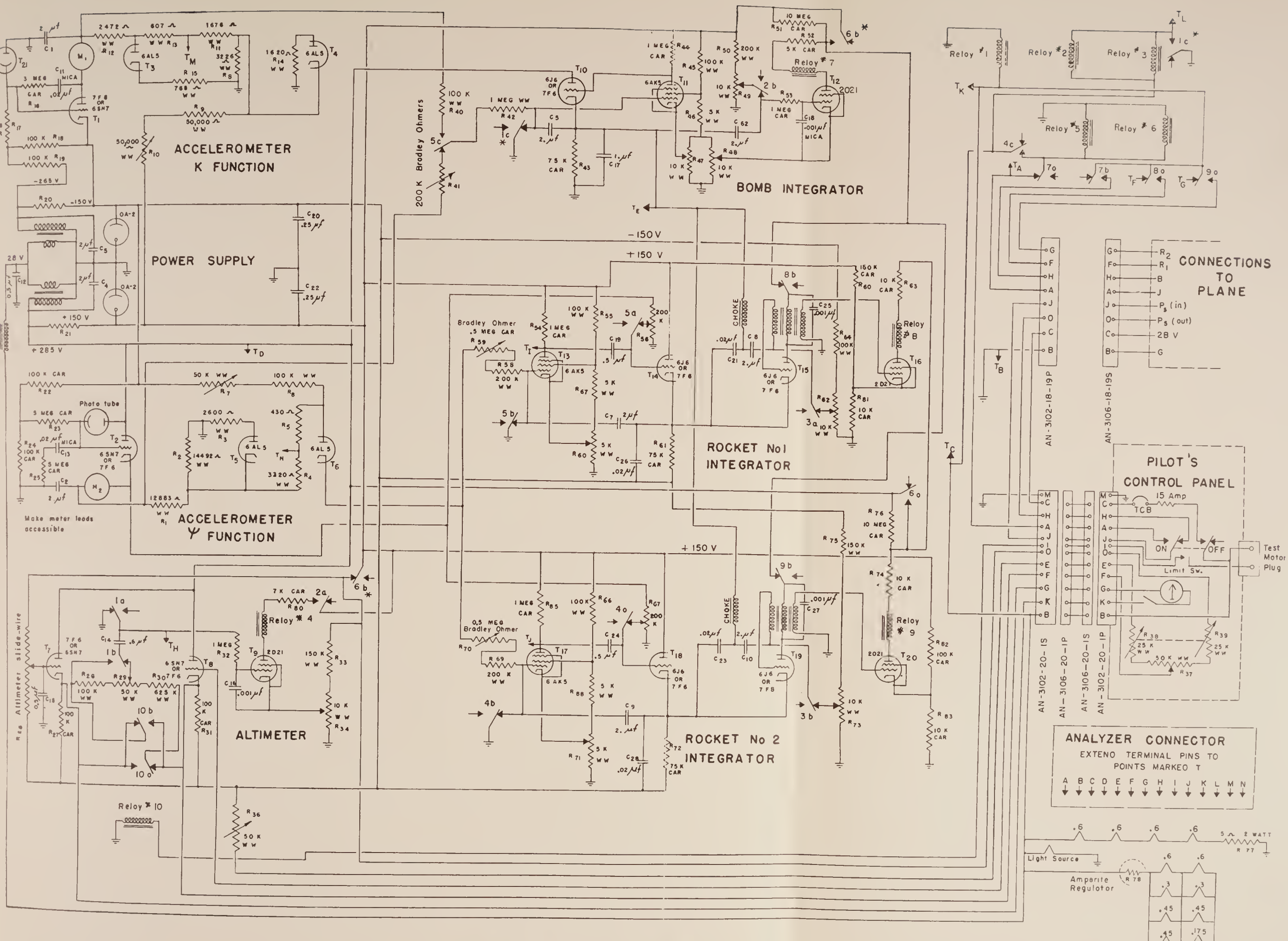

FIGURE 11. Circuit diagram of Mark 3 Model 0 bomb director.

[redacted]

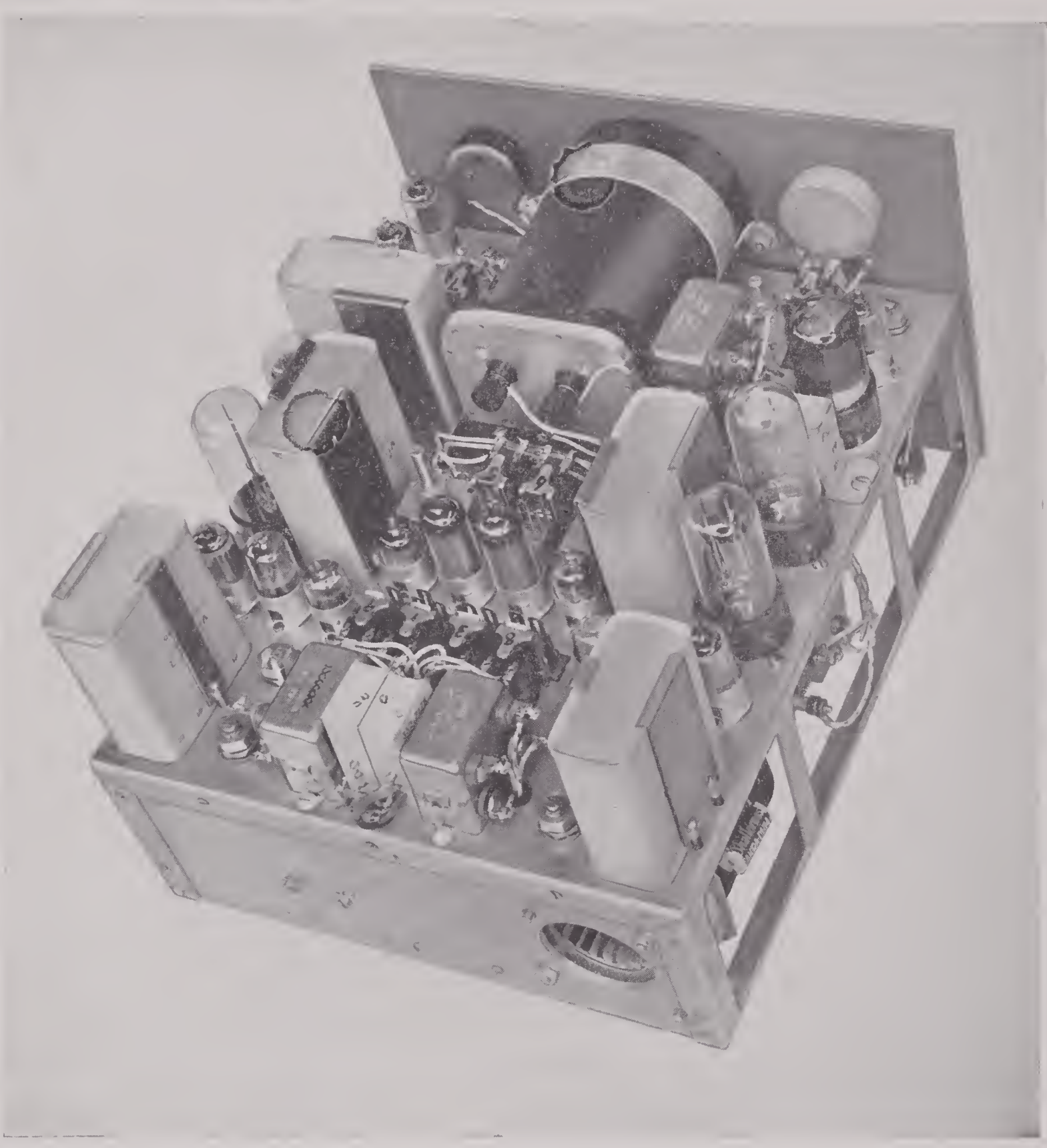

FIGURE 12. Photograph of Mark 3 computer. This and control box comprise complete Mark 3 Model 0 director. Altimeter is shown at center top of panel; accelerometers are mounted below subpanel.

Let the terms in equation (5) be designated by I, II, III and IV, respectively. The voltage output corresponding to these terms is shown as a function of time in Figure 9.

The condition for release of bombs is given by $\mathrm{II} - \mathrm{III} = 0$, and the condition for release of rockets is $(-\mathrm{II} + \mathrm{III}) = (\mathrm{I} - \mathrm{IV})$. The block diagram of Figure 10 shows the manner in which these various voltages are obtained and combined. It should be noted from Chapter 7 that $F_R(K,0) \cong 2\,(K-1)$.

Figure 11 is a circuit diagram of the complete Mark 3 director. The computer has three output circuits, one for releasing bombs or torpedoes and two for firing rockets of different types, all on the same pull-up. The voltages corresponding to the

temperature and lanyard setting are obtained by starting the rocket computer circuits at voltages other than zero; similarly, the voltage corresponding to the desired stick offset setting for bombs or torpedoes is obtained by biasing the bomb computer circuit.

Figure 12 shows a photograph of the Mark 3 computer which includes the altimeter, accelerometer and integrating circuits. The only other component of the Mark 3 director is the control box in which are located all necessary control dials.

8.2.7 Advantage of Mark 3 Bomb Director

The improvements to be expected from the Mark 3 bomb director over the Mark 1 bomb director are as follows:

1. The restrictions on maneuvers are removed since there is no gyro component.

2. The altimeter unit has a continuous voltage output which will allow the timing run to commence at any point. The mechanical construction is simpler since no gearing is used. This should result in better mechanical performance.

3. The accelerometer is lighter, more accurate, and more easily constructed than the accelerometer in the Mark 1 unit.

4. The Mark 3 director provides for the release of a bomb (or torpedo) and two rockets (of different types) on the same pull-up. The rocket channels are individually adjustable and have sufficient latitude to accommodate any type of rocket with or without a lanyard release.

5. A considerable saving in space and weight will be possible with this unit.

6. Partial correction is provided for range winds as well as for deflection winds.

8.3 USE OF THE LEAD-COMPUTING SIGHT[b]

8.3.1 Basic Differential Equations

The use of a gyroscopic *lead-computing sight* [LCS][210a, 238a] such as the Navy Mark 18 or Mark 23 (Army K-14) may be characterized by four reference lines as shown in Figure 13. In this figure the notation is as follows:

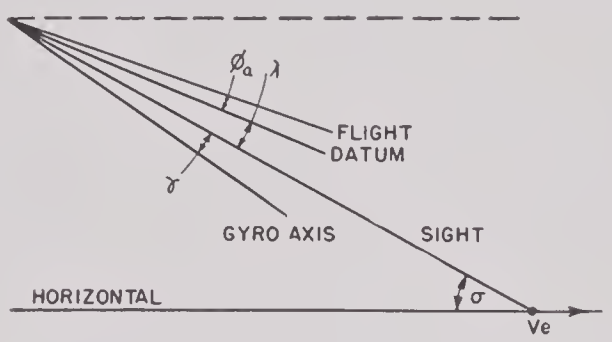

FIGURE 13. Diagram of reference lines in lead-computing sight.

λ = angle by which an arbitrarily chosen datum line in the airplane leads the sight line at any instant.

γ = angle between sight line and gyro axis at any instant.

σ = angle between sight line and horizontal at any instant.

ϕ_a = angle between flight line and datum line at any instant; this is the angle of attack.

V_e = velocity of target, assumed horizontal.

S = distance from airplane to target at any instant. The angles λ and γ are considered positive when the datum and the gyro axis respectively are above the sight line; in the figure λ is positive and γ is negative.

The sight itself is characterized by two constants; (1) the fixed constant a, which determines the relationship between the motion of the sight line with respect to the gyro axis and the motion of the datum line with respect to the gyro axis, and (2) the adjustable sensitivity constant u, which may be caused to vary with range instrumentally and which in the case of the LCS as a gunsight is the time-of-flight at any instant which the bullet would take to reach the target.

The sight line (sight pip of the LCS) is coupled optically to the gyro in such a way that

$$\gamma = a\lambda. \tag{6}$$

Usually a is negative, having a value of -0.43 for the Mark 23. Hence the sight line will always be located between the datum line and the gyro axis, as shown in Figure 13. The angle between the datum line and the gyro axis is

$$\lambda - \gamma = (1 - a)\lambda.$$

[b] Section 8.3 was written by Dr. Albert London of the National Bureau of Standards, and Dr. L. E. Ward, of Naval Ordnance Training Station, Inyokern, California.

It follows from equation (6) that

$$\gamma = \frac{a}{1 - a}(\lambda - \gamma),$$

or, the angular displacement of the sight line from the gyro axis is always $a/(1 - a)$ of the angular displacement of the datum line from the gyro axis. For the Mark 23, the gyro is displaced 3.33 times as much from the datum line as the sight line is from the datum line.

If the effect of angle of attack variations is neglected for the time being, the flight line may be considered as coincident with the datum line. Consider the case where the datum line (or flight line), the sight line, and the gyro axis are initially coincident, and the target is at rest. If the target starts moving, and the pilot starts to track the target, then the gyro axis tends to remain fixed in space, and the sight line will change by an angle $d\gamma$. In order to do this, the pilot must fly the airplane in such a way as to make the flight line change by an angle $d(\lambda - \gamma) = -3.33\ d\gamma$, that is, the airplane will start turning at a rate 3.33 times as fast as the sight line turns.

As the computed lead angle approaches the collision course lead angle, the rate of turn will decrease and will vanish when the correct collision course lead is attained. Consequently the differential equation which the sight must satisfy must be such that the required lead angle λ^* is obtained when $\dot{\lambda}$ is zero. This is accomplished by introducing a precessional force on the gyro such that the velocity of precession is proportional to the displacement of the gyro axis from the datum line and is in such a direction as to return the gyro axis to the datum line, that is:

$$-\frac{d}{dt}(\sigma - \gamma) = b\ (\lambda - \gamma), \tag{7}$$

where b is an instrumental design constant related to u and a by the equation

$$b = \frac{1}{u(1 - a)}.$$

Substituting for b in equation (7) and eliminating γ by use of equation (6) results in the differential equation of the sight, namely

$$-au\,\dot{\lambda} + \lambda = -u\dot{\sigma}. \tag{8}$$

Figure 14 represents the change in positions of the airplane and target in time Δt. By projecting the three other sides of the quadrilateral onto S the relation

$$V\Delta t \cos\lambda + (S + \Delta S)\cos\Delta\sigma - V_e\Delta t\cos\sigma = S \tag{9}$$

is obtained, and by projecting the same three sides onto a line perpendicular to S,

$$V\Delta t \sin\lambda = V_e\Delta t \sin\sigma + (S + \Delta S)\sin\Delta\sigma. \tag{10}$$

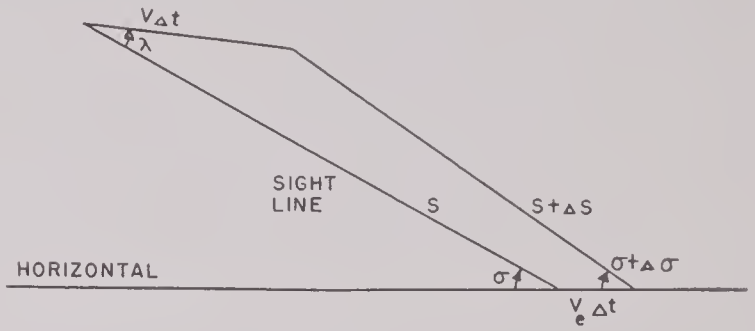

FIGURE 14. Diagrammatic representation of changes in position of airplane and target in time Δt.

From equations (9) and (10), dividing by Δt and then making $\Delta t > 0$, the relations (11) are deduced.

$$\begin{aligned} V\cos\lambda - V_e\cos\sigma + \dot{S} &= 0 \\ V\sin\lambda - V_e\sin\sigma &= S\dot{\sigma}. \end{aligned} \tag{11}$$

Equations (8) and (11) constitute three differential equations for the three dependent variables λ, σ, and S as functions of t. It is desired to obtain from these equations information concerning the rapidity with which the lead-computing sight puts the airplane on a collision course.

8.3.2 Solution for Collision Course

In Figure 15 is shown the collision course, point C being where collision would occur if the airplane were to fly a straight course in dive angle α. T is the time from the instant when λ becomes equal to λ^*

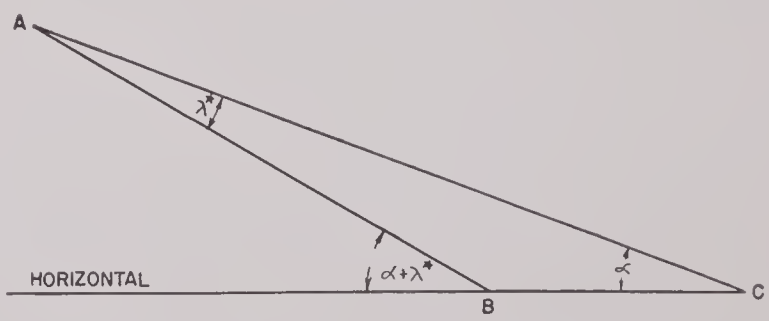

FIGURE 15. Diagrammatic representation of lead angle for collision course approach.

to the time of collision. By projecting the lines AC and BC onto a line perpendicular to AB the relation $VT \sin\lambda^* = V_eT \sin(\alpha + \lambda^*)$ is obtained.

This reduces to $V \sin \lambda^* = V_e \sin (\alpha + \lambda^*)$ or

$$\tan \lambda^* = \frac{V_e \sin \alpha}{V - V_e \cos \alpha}. \tag{12}$$

When solved for the three derivatives, equations (8) and (11) take the form

$$\begin{aligned} \dot{\lambda} &= \frac{\lambda}{au} + \frac{V \sin \lambda - V_e \sin \sigma}{aS}, \\ \dot{\sigma} &= \frac{V \sin \lambda - V_e \sin \sigma}{S}, \\ \dot{S} &= V_e \cos \sigma - V \cos \lambda. \end{aligned} \tag{13}$$

When the quantity dt is eliminated, the pair of equations (14) remains. In these equations it is convenient to regard S as the independent variable, λ and σ being dependent variables.

$$\begin{aligned} \frac{d\lambda}{dS} &= \frac{\lambda S + uV \sin \lambda - uV_e \sin \sigma}{-auS(V \cos \lambda - V_e \cos \sigma)} \\ \frac{d\sigma}{dS} &= \frac{V_e \sin \sigma - V \sin \lambda}{S(V \cos \lambda - V_e \cos \sigma)}. \end{aligned} \tag{14}$$

The first of equation (14) can be rewritten in a form which permits the integration of the important terms, the less important terms being treated as constants.

Since λ remains close to zero while the airplane is still far from the target, and at the same time σ changes but little, one approximation is to replace $\sin \lambda$ by λ, $\cos \lambda$ by unity, and to treat σ as though it were constant. If this is done, the first of equation (14) becomes

$$\frac{d\lambda}{dS} + \frac{(S + uV)\lambda}{auS(V - V_e \cos \sigma)} = \frac{V_e \sin \sigma}{aS(V - V_e \cos \sigma)}. \tag{15}$$

An integrating factor of this is

$$e^{\frac{S + uV \ln S}{au(V - V_e \cos \sigma)}}$$

and the solution of the differential equation is

$$\lambda = \lambda_0 e^{\frac{S_0 - S + uV \ln S_0/S}{au(V - V_e \cos \sigma)}} + e^{\frac{S + u \ln S}{-au(V - V_e \cos \sigma)}} \times \int_S^{S_0} \frac{V_e \sin \sigma}{-aS(V - V_e \cos \sigma)} e^{\frac{S + uV \ln S}{au(V - V_e \cos \sigma)}} dS, \tag{16}$$

where λ_0 and S_0 are initial values.

This solution has been investigated by the Applied Mathematics Group, NDRC.[209a, 209b]

For the numerical case $S_0 = 8{,}100$ feet, $u = 15$ seconds, $V = 450$ feet/second, $V_e = 45$ feet/second, $\sigma_0 = 36.87$ ($\cos \sigma_0 = 4/5$), and the values of a shown in Table 1, it is found that when $S = 5/6, S_0 = 6{,}750$ feet, λ has the values shown.

This table indicates that as $a \longrightarrow 0$ from the negative side, up to 50 per cent of λ^* may be obtained, while the term containing the contribution due to λ_0 is minimized. This term can be made zero, of course, by uncaging the gyro at $S = S_0$ so that $\lambda_0 = 0$. Very small values of a are impracticable since the rate of turn of the airplane is $(1 - a)/a$ times that of the sight line.

8.3.3 Aiming Procedures

The Mark 23 sighting head contains a fixed pip in the form of a cross, which may be considered as fixed rigidly on the datum line, and a movable or gyro pip consisting of a dot. In addition there is associated with the dot and the movable gyro sight field a ring of diamond-shaped points centrally located about the dot. Consequently it is possible to have various aiming procedures involving aiming with the cross, dot, or diamonds in certain specified sequences.

Before describing such procedures, it is advisable to state that from a tactical viewpoint, changing the aim of the plane during the run requires too much

TABLE 1

a	λ calculated from equation (16)
$-1.$	$0.660\ \lambda_0 + \frac{V_e \sin \sigma_0}{V}(0.1629) = 0.660\ \lambda_0 + \frac{V_e \sin \sigma_0}{V - V_e \cos \sigma_0}(0.1499)$
-0.5	$0.436\ \lambda_0 + \frac{V_e \sin \sigma_0}{V}(0.2712) = 0.436\ \lambda_0 + \frac{V_e \sin \sigma_0}{V - V_e \cos \sigma_0}(0.2495)$
-0.1	$0.016\ \lambda_0 + \frac{V_e \sin \sigma_0}{V}(0.4818) = 0.016\ \lambda_0 + \frac{V_e \sin \sigma_0}{V - V_e \cos \sigma_0}(0.4433)$

time and increases the number of operations which the pilot must perform. In some preliminary field tests of these procedures,[137] it was found that using the Mark 23 would require a very skilled pilot, and would deprive the bomb director of one of its principal merits, namely, simplicity of operation from the pilot's point of view.

One such procedure requires tracking the target with the fixed cross for one-sixth of the initial slant range. It will be shown below that this results in approximately 12 per cent of the correct lead angle; let $\lambda = 0.12\lambda^*$ (see Figure 16).

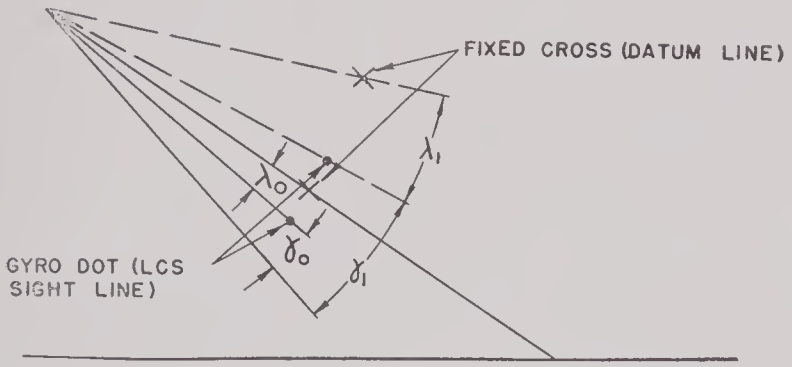

FIGURE 16. Diagrammatic representation of orientation of datum and sight lines in tracking the target during timing run. (For explanation of symbols, see text.)

After tracking the target with the fixed cross for one-sixth of the initial slant range, let the dot be displaced to a symmetrical position on the other side of the line of the fixed cross, as shown in Figure 16. If the gyro axis remains fixed in space, a condition approximately realizable by turning off the range coils, the angle γ between the new sight line and the gyro axis will be $-\gamma_1 = 2\lambda_0 - \gamma_0 = (2 - a)\lambda_0$, and the new lead angle will be

$$\lambda_1 = \frac{1}{a}\gamma_1 = -\frac{2-a}{a}\lambda_0$$

$$= -\frac{2-a}{a}(0.12)\lambda^* \cong 0.68\lambda^*.$$

If the dot is displaced to a position twice as far on the other side of the fixed cross, the new lead angle λ_2 will be

$$\lambda_2 = -\frac{3-a}{a}(0.12)\lambda^* \cong 0.96\lambda^*.$$

It also is possible to track with the fixed cross for a larger fraction of the original range, thus accumulating a larger initial value of λ_0. The solution obtained as a function of the slant range tracking fraction will now be obtained.

With Figure 17 for reference, the differential equation which the sight solves when tracking with the fixed cross will be derived.

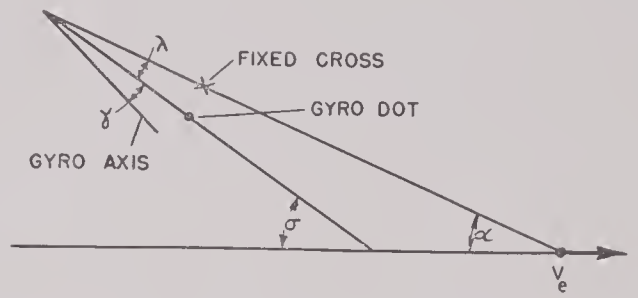

FIGURE 17. Diagrammatic representation of orientation of datum and sight lines in tracking with fixed cross. (For explanation of symbols, see text.)

Here $S\dot{\alpha} = -V_e \sin\alpha$ and $\sigma = \alpha + \lambda$.

Hence

$$\dot{\sigma} = \dot{\alpha} + \dot{\lambda} = \dot{\lambda} - \frac{V_e \sin\alpha}{S} = \lambda - \frac{V_e}{S}\sin(\sigma - \lambda),$$

or, using equation (12) in the approximate form,

$$\lambda^* \cong \frac{V_e}{V}\sin\sigma,$$

$$\dot{\sigma} = \dot{\lambda} - \frac{V\lambda^*}{S} + \frac{V_e\lambda\cos\sigma}{S}. \qquad (17)$$

Combination of equations (17) and (8) so as to eliminate $\dot{\sigma}$ yields

$$(1-a)\dot{\lambda} + \left(\frac{V_e\cos\sigma}{S} + \frac{1}{u}\right)\lambda = \frac{V\lambda^*}{S} \qquad (18)$$

where the term $(V_e\cos\sigma)/S$ is less than V_e/S while $1/u \geq 1/15$. For this reason the term in V_e will be omitted, leaving

$$(1-a)\dot{\lambda} + \frac{\lambda}{u} = \frac{V\lambda^*}{S}$$

or, since

$$\dot{\lambda} = \dot{S}\frac{d\lambda}{dS} \cong -V\frac{d\lambda}{dS},$$

it follows that

$$\frac{d\lambda}{dS} - \frac{\lambda}{u(1-a)V} = -\frac{\lambda^*}{(1-a)S}. \qquad (19)$$

The solution of equation (19) which reduces to λ_0 when $S = S_0$ is

$$\lambda = \lambda_0 e^{-\frac{S_0 - S}{u(1-a)V}} + \frac{\lambda^*}{1-a}\, e^{\frac{S}{u(1-a)V}}\left[\int_{\frac{S}{u(1-a)V}}^{\infty} e^{-x}\frac{dx}{x} - \int_{\frac{S_0}{u(1-a)V}}^{\infty} e^{-x}\frac{dx}{x}\right]. \qquad (20)$$

This solution is not capable of being represented in closed form by means of elementary functions, and the integrals are written with infinity as a limit because the exponential integral

$$-Ei(-z) = \int_z^\infty e^{-x}\frac{dx}{x}$$

is a tabulated function (for instance, the WPA "Tables of Sine, Cosine, and Exponential Integrals").

In the terms of $Ei(-z)$ equation (20) is

$$\lambda = \lambda_0 e^{-(z_0 - z)} + \frac{\lambda^*}{1-a} e^z \left[-Ei(-z) + Ei(-z_0) \right], \tag{21}$$

where

$$z = \frac{S}{u(1-a)V}.$$

If $S/S_0 = \rho$, the quantity $1 - \rho = (S_0 - S)/S_0$ is called the tracking ratio. Suppose $\lambda_0 = 0$ and $\lambda, \lambda^* = 0.1$. Then from equation (21)

$$-Ei(-z) + Ei(-z_0) = \frac{1-a}{10} e^{-z}. \tag{22}$$

This is the relation between z and z_0, i.e., between S and S_0, which makes $\lambda/\lambda^* = 0.1$. Table 2 shows a set of values of z and z_0 which satisfy equation (22) together with the corresponding values of ρ and $1 - \rho$. From this table it is seen that a 15 per cent change in slant range results in an accumulation of 10 per cent of the desired lead angle.

TABLE 2. Fraction of initial slant range for which 10 per cent of the desired lead angle is obtained when tracking with fixed cross in Mark 23 sight.

z	z_0	ρ	$1-\rho$
0.2	0.231	0.865	0.135
0.4	0.464	0.863	0.137
0.6	0.697	0.861	0.139
0.8	0.932	0.859	0.141
1.0	1.168	0.856	0.144
1.2	1.405	0.854	0.146
1.4	1.644	0.852	0.148
1.6	1.884	0.849	0.151
1.8	2.127	0.846	0.153
2.0	2.371	0.844	0.156

For an estimation of the per cent of required solution obtained as function of the fraction of the initial slant range during which the solution is computed, Table 3 is useful. It gives values of λ/λ^* for various values of $1 - \rho$ and for $z = 1.0$ and $z = 0.3$.

TABLE 3. λ/λ^* as a function of tracking ratio.

$1-\rho$	0.144	0.167	0.305	0.5	0.7	0.9	
λ/λ^*	0.100	0.116	0.209	0.324	0.392	0.417	$z = 1.0$
λ/λ^*	0.105	0.124	0.240	0.426	0.648	0.843	$z = 0.3$

It should be noted that for $V = 500$ feet/sec, $u = 15$ sec, and $a = -0.43$, the value $z = 1.0$ corresponds to a slant range at the end of the tracking run of 10,700 feet, while $z = 0.3$ corresponds to a slant range of 3,200 feet for the same values of V, u, and a.

Table 3 shows also that for small values of the tracking ratio $1 - \rho$, the per cent of solution obtained is relatively independent of z, while for large tracking ratios more of the solution is obtained for small values of z. From the definition of z it is seen that z can be made small by decreasing S, increasing u and V, and decreasing a, i.e., making a more negative. For instance, if $a = -1$, then $z = 0.3$ corresponds to $S = 4{,}500$ feet, $V = 500$ feet/sec, and $u = 15$ sec. If $1 - \rho$ is taken as 0.5, then $S_0 = 9{,}000$ feet, $z_0 = 0.6$, and

$$\frac{\lambda}{\lambda^*} = \frac{e^{-3}}{2}\left[-Ei(-0.3) + Ei(-0.6) \right] = 0.305.$$

If, at the end of this tracking run, the dot is displaced to the symmetrical position on the other side of the fixed cross, the lead angle which will be obtained will be $0.91\lambda^*$. Again, if $a = -0.43$, $S_0 = 9{,}000$ feet, $S = 4{,}500$ feet, $u = 6.3$ seconds, and $V = 500$ feet/sec, then $z = 1$, $\lambda = 0.324\ \lambda^*$ and the transposition of the dot to the symmetrical position on the other side of the cross results in a lead angle of $1.1\lambda^*$. Various other operational combinations can, of course, be established.

The amount of correction obtained by tracking with a free gyro, using the optical linkage of the Mark 23, will now be determined. This is nearly the situation when tracking with the gyro pip of the sight with the range coils turned off.

Let Γ (see Figure 18) be the angle between the gyro axis and the horizontal at the instant when the gyro becomes free, i.e., the range coils are turned off. The gyro axis will retain this orientation in space.

From Figure 18, it is seen that, since γ is negative,

$$\Gamma = \sigma - \gamma = \sigma_0 - \gamma_0, \tag{23}$$

where σ_0 and γ_0 are initial values. By use of equation (6), equation (23) becomes

$$a(\lambda_0 - \lambda) = \sigma_0 - \sigma,$$

whence

$$a\dot{\lambda} = \dot{\sigma}. \tag{24}$$

It should be noticed that equation (24) is equivalent to equation (8) when u is extremely large, which

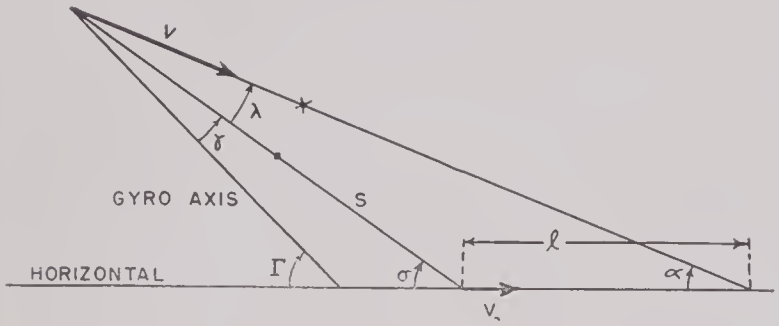

FIGURE 18. Diagrammatic representation of orientation of datum and sight lines in tracking while gyro is free.

is possible only if frictional forces are made negligible. Taking σ from the second of equation (11), equation (24) becomes

$$a\dot{\lambda} = \frac{V \sin \lambda - V_e \sin \sigma}{S} \cong \frac{V}{S}(\lambda - \lambda^*). \tag{25}$$

If equation (25) is associated with the approximate equation $V \cong dS/dt$, the elimination of the quantity dt leads to the differential equation

$$\frac{d\lambda}{dS} + \frac{\lambda}{aS} = \frac{\lambda^*}{aS}. \tag{26}$$

The solution of this equation is

$$\lambda = \lambda_0 \left(\frac{S}{S_0}\right)^{-\frac{1}{a}} + \lambda^* \left[1 - \left(\frac{S}{S_0}\right)^{-\frac{1}{a}}\right]$$

or, if $\lambda_0 = 0$,

$$\frac{\lambda}{\lambda^*} = 1 - \left(\frac{S}{S_0}\right)^{-\frac{1}{a}} = 1 - \rho^{-\frac{1}{a}}. \tag{27}$$

Table 4 shows how λ/λ^* varies with the tracking ratio $1 - \rho$ for $a = -0.43$ and $a = -0.215$.

It is seen from Table 4 that a large part of the solution would be obtained for a tracking ratio of 0.3 if friction could be reduced to a negligible amount in the Mark 23. This would be especially true if an optical linkage constant of $a = -0.215$ were feasible.

8.3.4

Wind Correction

Two other possibilities involving the rate of turn of the airplane caused by the use of the Mark 23 may be considered. As has been shown in Section 6.6.9, the range-wind correction obtained from the photoelectric accelerometer is of the order of 30 per cent.[81] If the rate of turn of the airplane were increased by a factor of 3, the total wind correction would be obtained. At the instant of uncaging the gyro, the airplane begins turning at a rate 3.33 times as fast as the sight line turns, and the whole wind correction would result if this rate of turn were continued for one-sixth of T_c. However, as the tracking ratio increases, and the airplane approaches the collision course lead angle, the rate of turn decreases as lead angle is accumulated. The net effect has been investigated in reference 105, with the conclusion that approximately 65 per cent wind correction will result from the increased rate of turn of the airplane.

The other possibility concerns the crosswind approach. In reference 209 it is shown that in a crosswind approach, the angle of bank is such that the bomb is given a component of velocity in a direction parallel to wind direction, sufficient to give approximately 50 per cent wind correction. It is assumed in this analysis that bombing is accomplished without slipping or skidding. If the rate of turn of the airplane could be increased by a factor of two, the angle of bank should be correspondingly increased so that the entire wind correction would

TABLE 4. λ/λ^* for a free gyro ($\lambda_0 = 0$) with the Mark 23 optical linkage.

$1 - \rho$	0 1	0.144	0.167	0.305	0.5	0.7	0 9	
$\rho^{-1\ a}$	0.783	0.697	0.654	0.429	0.199	0.061	0.0047	$a = -0.43$
λ/λ^*	0.217	0.303	0.346	0.571	0.801	0.939	0.995	
$\rho^{-1/a}$	0.613	0.485	0.427	0.184	0.040	0.004	.....	$a = -0.215$
λ/λ^*	0.387	0.515	0.573	0.816	0.960	0.996	.....	

be obtained. The possibility of increasing the aircraft's rate of turn by a suitably designed LCS is immediately evident.

A word of caution is necessary with respect to the interpretation of the theoretical results presented here. The lead angle and the angle involved in tracking with an LCS are quite small. Consequently, pilot aiming accuracy becomes quite important, since small changes in the pilot's aim may cause "wander" in the flight attitude of the aircraft, thus masking to a considerable extent the "intelligent" part of the LCS output. The feasibility of using the LCS in bomb tossing had not been tried in field tests at the end of the war.

8.4 ANALYTICAL REDUCTION OF SYSTEMATIC ERRORS; REVISION OF THE ψ FUNCTION[c]

8.4.1 Introduction

In the course of the development of the bomb tossing technique, there has appeared and reappeared the problem of elimination or reduction of systematic errors, i.e., errors following known physical laws, as opposed to random errors. The fact that the angle of attack is not constant, for example, calls for a standardized flight calibration procedure; the effect of air resistance must be allowed for; the formulas valid for small pull-up angles require revision for larger pull-ups. The general problem is, in fact, equivalent to that of revising the theory to take into account secondary physical phenomena neglected in the original basic assumptions.

The method used most frequently in Mark 1 equipment for reduction of errors is that of manual setting of the MPI adjustment dial (Section 6.4.9) which produces a change in the effective input time (time-to-target) T_c and consequently alters the pull-up time T_p. The chief disadvantages of this method are as follows:

1. The proper value of the setting depends generally on such unpredictable parameters as altitude and dive angle, and is usually very sensitive to changes in such parameters.

2. When the MPI adjustment is determined according to a formula designed for average conditions, departures from the average often yield large errors.

3. The magnitude of the total required adjustment often exceeds the maximum attainable dial setting.

4. The MPI dial was primarily intended for special adjustments to meet conditions not encountered in the general case, or to correct for extreme departures from average conditions. When systematic errors, which always affect the impact according to a definite law, are not elsewhere allowed for, the MPI setting is no longer a special adjustment, but rather a required step whose omission always causes biased results.

In Section 8.4.1 a method of systematic error correction is developed with the aim of eliminating or minimizing these disadvantages, i.e., (1) rendering all manual settings dependent only on *known or predictable* quantities, so that an accurate setting may be made prior to each flight, (2) reducing greatly the effect of errors of estimation of these quantities, (3) reducing the total required adjustment to a magnitude which is always well within instrumental limits, and (4) incorporating the major portion of the correction in the bomb director itself (ψ function), so that the MPI adjustment need be used only as a secondary correction for deviations from average conditions. The theoretical implications of this method, namely, that the systematic errors in question are automatically eliminated (except for small second-order errors) for average values of the known or predictable quantities, that such errors are so greatly reduced for all values that the manual adjustment is generally optional, and that use of the latter generally reduces the errors to almost negligible magnitude, remain to be put to practical test.

In bomb tossing the pull-up time T_p is determined according to a formula of the form [cf. equation (19) of Chapter 2]:

$$T_p = \frac{T_c \psi}{F(K)} \tag{28}$$

where T_c is the time-to-target.

$F(K)$ is a function of the normal pull-up acceleration Kg, and of its mode of variation with time; and ψ is chiefly a function of the dive angle α. The ψ

[c] Section 8.4 was written by S. H. Lachenbruch of the Ordnance Development Division of the National Bureau of Standards. It covers work initiated under Division 4 sponsorship but completed after the toss bombing project was taken over by the Navy. For this reason the development of the theory is not given in as much detail as the treatment in Chapter 6. It was considered pertinent to include the essential results because of their importance to the project. Reference is made to source material [116] for further derivation of the functions used.

function also depends somewhat on T_c/V, V being the airspeed, and in most bomb directors this variation is taken into account by means of an airspeed dial which is preset (see Section 2.1.3). The variation of ψ with K is negligible.

The method, whose mathematical derivation is given in reference 116, is applied to errors due to *air resistance* and to errors resulting from variation in *angle of attack*, but may be extended to other systematic errors. A brief outline of the method follows:

1. The formula for the systematic error δ in question is converted into a formula for the change ΔT_p in T_p required to offset that error.

2. A quantity ϵ_ψ, depending only on α and T_c/V, is determined such that when V and other predictable parameters assume their *average or modal values*, changing ψ by an amount $\epsilon_\psi \times \psi$ will change T_p by the amount ΔT_p determined in (1), and therefore, theoretically eliminate the error in question for such modal values. This procedure is carried out for each systematic error in turn, and the corrections ϵ_ψ so determined are applied to the most accurate of the ψ functions derived to date, yielding a revised ψ function.

3. To correct for departure of these parameters from their modal values, a quantity ϵ_c, depending only on V and other known or predictable quantities such as ballistic coefficient, is determined such that changing T_c by an amount $\epsilon_c \times T_c$ will eliminate most of the residual error not eliminated by revision of the ψ function. This correction may be applied by means of the MPI adjustment dial prior to each flight, using the known values of the parameters involved.

Thus, theoretically, the revision of the ψ function completely offsets the systematic errors, for all values of α and T_c/V, and for modal values of V and other predictable parameters; and the MPI adjustment in turn offsets the effect of deviations of these predictable parameters from their modal values.

In addition to the corrections for air resistance and angle of attack by the method outlined above, corrections for large pull-ups and for nonconstant pull-up acceleration are made by means of relations derived in Chapter 6.

8.4.2 The Revised ψ Function (ψ_r)

The new theoretical ψ function, as derived in reference 116, is given by

$$\begin{aligned}\psi_r(\alpha, T_c/V) &= \psi_e(1 + \epsilon_{\psi \cdot ar} + \epsilon_{\psi \cdot aa}) + \Delta_k \\ &= \psi_e + \Delta_{ar} + \Delta_{aa} + \Delta_k,\end{aligned} \tag{29}$$

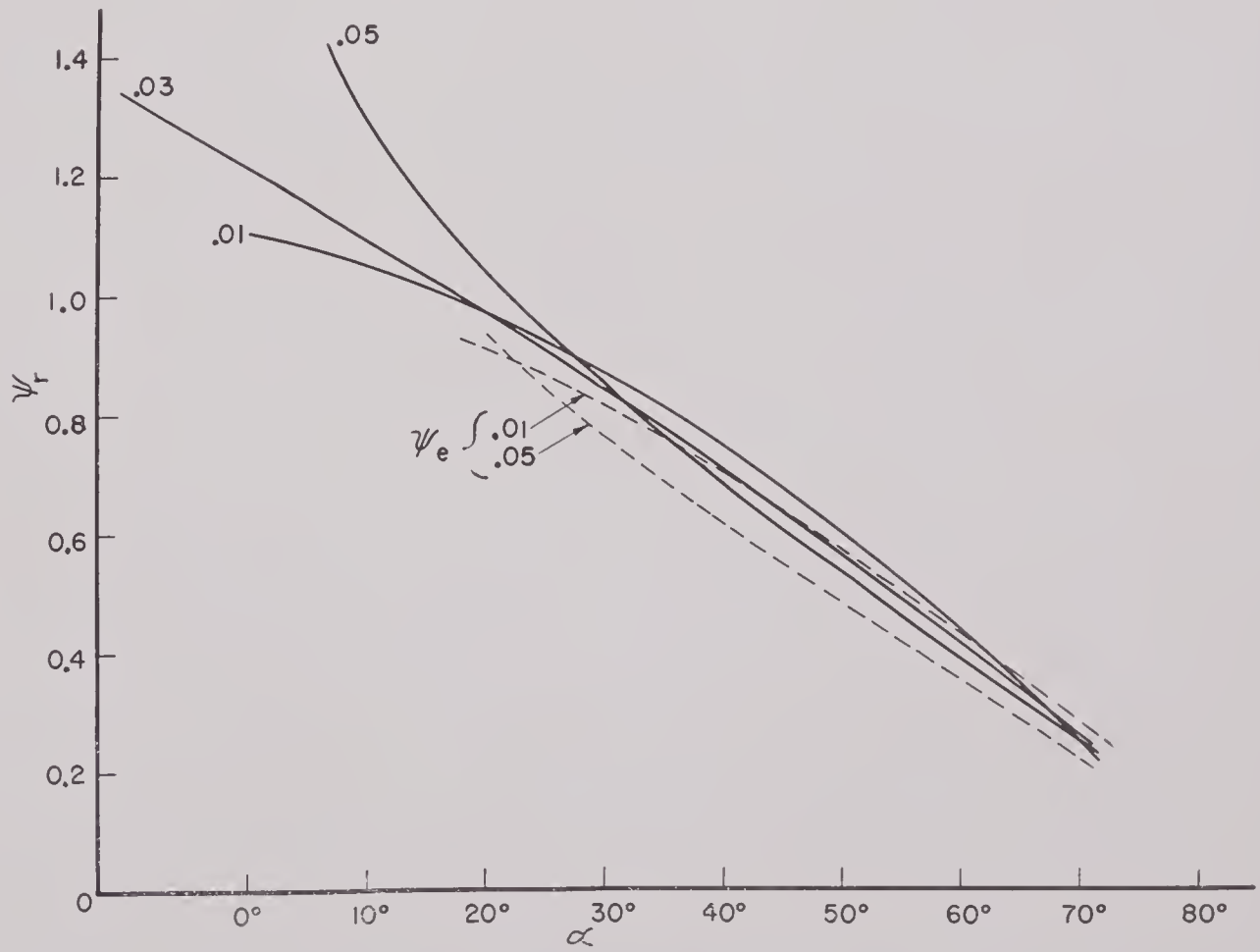

FIGURE 19. Revised ψ function (ψ_r) versus α, for different values of T_c/V (= 0.01, 0.03, and 0.05). For purposes of comparison, the ψ_e function versus α is given by dashed lines for T_c/V = 0.01 and 0.05.

where

ψ_e is the ψ function resulting from the exact solution of the toss bombing equations for circular pull-up (ψ_e is derived, tabulated, and plotted in Sections 6.1.3, 6.1.4, and 6.1.5),

Δ_k is a correction term to allow for nonconstant pull-up acceleration,[93,116]

$\Delta_{ar} = \epsilon_{\psi \cdot ar} \psi_e$ is an allowance for the effect of air resistance on the bomb,[55,116] and

$\Delta_{aa} = \epsilon_{\psi \cdot aa} \psi_e$ is a similar allowance for variation in angle of attack.[101,116]

The quantities $\epsilon_{\psi \cdot ar}$ and $\epsilon_{\psi \cdot aa}$ are given by the following equations:

$$\epsilon_{\psi \cdot ar} = (\overline{V}^2/\bar{c}) \cdot b_{pc} \cdot a \cdot T_c/V \qquad (30)$$

$$\epsilon_{\psi \cdot aa} = (\overline{CW}/1{,}000\,\overline{V}^2) \cdot b_p \cdot (\cos\alpha - \cos\overline{\alpha})/\sin\alpha \qquad (31)$$

where b_p, b_{pc}, and a are functions of T_c/V and α, and the barred symbols represent mean values, and therefore constants. Here $\bar{c}$ is an average bomb ballistic coefficient, and $\overline{CW}$ is the average value of a coefficient determining a plane's rate of change of angle of attack.

The revised theoretical ψ function (ψ_r) is plotted in Figure 19 as a function of α for different values of T_c/V, and is tabulated in Table 5.

TABLE 5. Values of ψ_r ($K = 3$).

α \ T_c/V	0.01	0.02	0.03	0.04	0.05
10°	1.054	1.063	1.097	1.162	1.295
20°	0.973	0.962	0.971	0.995	1.045
30°	0.872	0.852	0.845	0.847	0.856
40°	0.747	0.726	0.711	0.701	0.689
50°	0.603	0.584	0.567	0.553	0.543
60°	0.438	0.432	0.419	0.406	0.395

In the evaluation of ψ_r, K has been set equal to a modal value $\bar{K} = 3$, except in the term Δ_k which is evaluated from reference 93. The variation of ψ_r with K is generally negligible. No calculations have been made for dive angles beyond the operating extremes of 10 and 60 degrees. In fact, an absurd result is obtained at $\alpha = 0$ degrees, at which Δ_{aa} and therefore ψ_r are infinite.

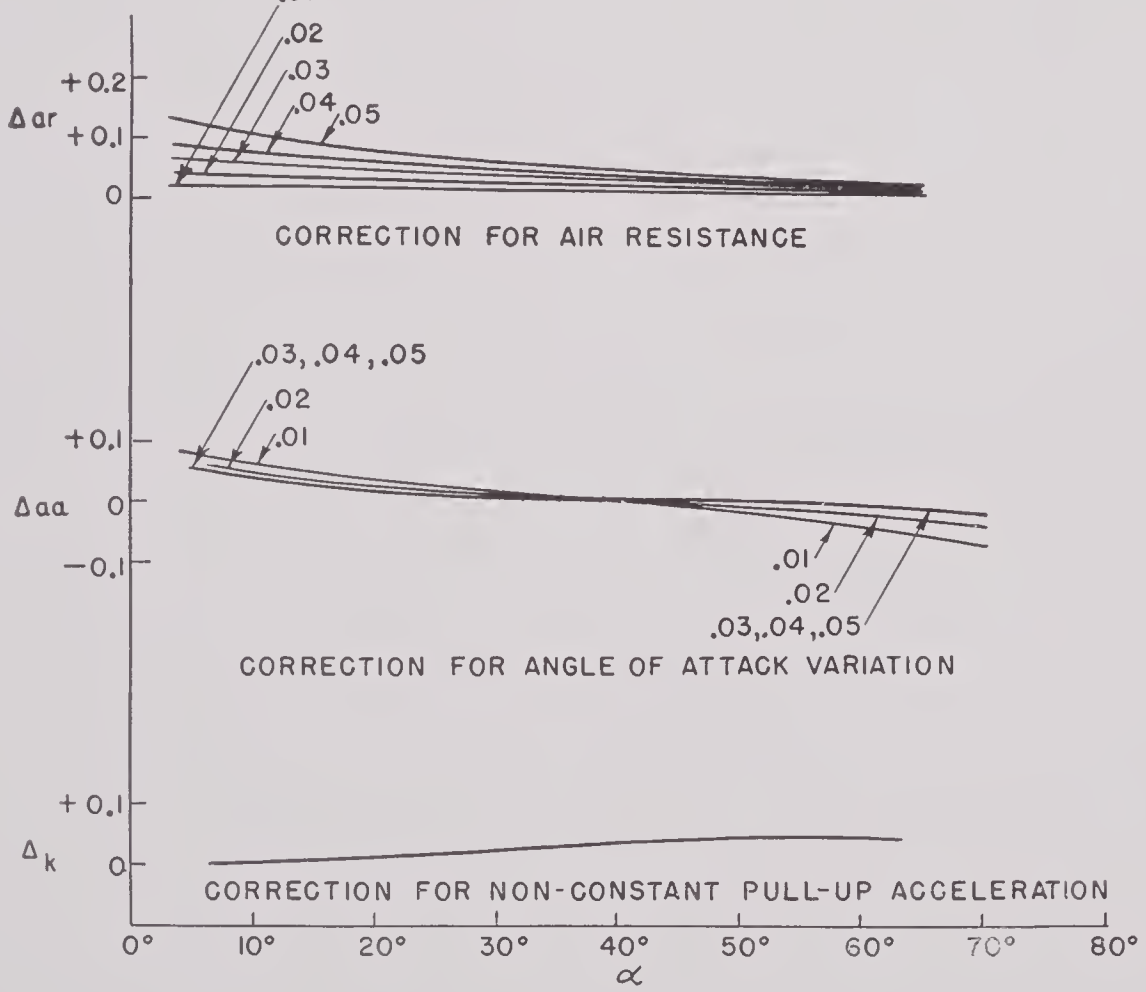

FIGURE 20. Correction terms added to ψ_e to obtain ψ_r, plotted versus dive angle for different values of T_c/V. Δ_k is practically independent of T_c/V.

By comparison it is seen that the curves of Figure 18 are appreciably denser than any of the sets of earlier ψ curves (see Figure 2, Chapter 2, and Section 6.1), at least for dive angles greater than 20 degrees. In other words ψ_r is less dependent on T_c/V than were the earlier ψ functions.

Each of the correction components Δ_{ar}, Δ_{aa}, and Δ_k is plotted separately in Figure 20. The ψ_r function of Figure 19 has been obtained by adding all these components to the ψ_e function of Section 6.1.3.

An important consequence of the use of the ψ_e function as a base (to which the three correction terms are applied) is the removal of all range limitations imposed by the so-called 100-foot error curves of Figure 11 of Chapter 2, and Figure 7 of Chapter 6, which result from approximations implicit in the ψ_0 and ψ_1 functions, and which have been used as criteria determining operating limits.

The degree to which systematic errors are reduced by the revision of the ψ function is discussed in reference 116.

In designing a gyro potentiometer ψ card based on a given theoretical ψ function, the usual procedure is to fit the ψ curve for a modal value of T_c/V by means of a series of straight line segments, thus obtaining an instrumental ψ function which may be made to vary instrumentally with T_c/V in a manner comparable with theory. The complete procedure, involving calculation of voltages according to exponential formulas, is outlined in Section 6.3 for the ψ_1 function.

In the instrumentalization of the ψ_r function there is some leeway in the choice of a modal value of T_c/V. A value $\overline{T_c/V} = 0.025$, however, would be the choice most consistent with the remainder of the theory. This is the value of $\overline{T_c/V}$ used in all formulas given here, being based on a modal slant range $\overline{S} = 7{,}500$ feet and a modal air speed $\overline{V} = 325$ knots

TABLE 6. Values of supplementary MPI adjustments for air resistance ($\epsilon_{c\cdot ar}$) (for use with ψ_r function).

Ballistic coeff. (c) \ True airspeed knots	225	250	275	300	325*	350	375	400	425	450	475	Reciprocal $1/c$
	%	%	%	%	%	%	%	%	%	%	%	
0.75	+3.1	+5.0	+7.1	+9.4	+11.9	+14.6	+17.6	+20.7	+24.0	+27.6	+31.3	1.33
1.00	+1.0	+2.5	+4.0	+5.8	+7.7	+9.7	+11.9	+14.2	+16.7	+19.4	+22.2	1.00
1.25	−0.2	+0.9	+2.2	+3.6	+5.1	+6.7	+8.5	+10.4	+12.4	+14.5	+16.7	0.80
1.50	−1.0	−0.1	+1.0	+2.1	+3.4	+4.8	+6.2	+7.8	+9.5	+11.2	+13.1	0.67
1.75	−1.6	−0.8	+0.1	+1.1	+2.2	+3.4	+4.6	+5.9	+7.4	+8.9	+10.5	0.57
2.00	−2.0	−1.3	−0.5	+0.3	+1.3	+2.3	+3.4	+4.6	+5.8	+7.1	+8.5	0.50
2.25	−2.4	−1.7	−1.0	−0.3	+0.6	+1.5	+2.5	+3.5	+4.6	+5.8	+7.0	0.44
2.50*	−2.7	−2.1	−1.5	−0.8	0.0	+0.8	+1.7	+2.6	+3.6	+4.7	+5.8	0.40
2.75	−2.9	−2.4	−1.8	−1.2	−0.5	+0.3	+1.1	+1.9	+2.8	+3.8	+4.8	0.36
3.00	−3.1	−2.6	−2.1	−1.5	−0.9	−0.2	+0.6	+1.3	+2.2	+3.1	+4.0	0.33
3.25	−3.2	−2.8	−2.3	−1.8	−1.2	−0.6	+0.1	+0.8	+1.6	+2.4	+3.3	0.31
3.50	−3.4	−3.0	−2.5	−2.0	−1.5	−0.9	−0.2	+0.4	+1.1	+1.9	+2.7	0.29
4.00	−3.6	−3.2	−2.8	−2.4	−1.9	−1.4	−0.9	−0.3	+0.4	+1.0	+1.7	0.25
4.50	−3.7	−3.4	−3.1	−2.7	−2.3	−1.8	−1.3	−0.8	−0.3	+0.3	+1.0	0.22
∞	−5.1	−5.1	−5.1	−5.1	−5.1	−5.1	−5.1	−5.1	−5.1	−5.1	−5.1	0.00

*Modal values as used in ψ_r calculations.

[redacted]

Furthermore, the ψ_r curve for that value (very close to the 0.03 curve of Figure 19) has only slight curvature, so that it may be fitted satisfactorily with relatively few line segments — probably only two.

8.4.3 The MPI Adjustment

The components $\epsilon_{\psi \cdot ar}$ and $\epsilon_{\psi \cdot aa}$ of the ψ_r function do not represent a theoretically complete correction for air resistance and angle of attack variation unless all the known or predictable quantities V, c, CW assume their mean or modal values. Deviations from such means may be corrected by setting the MPI adjustment dial in an amount which depends on these quantities and which may therefore be evaluated from known or predicted values of these quantities prior to each flight.

A fixed setting of the MPI adjustment dial causes a fixed fractional or per cent change $\epsilon_c = \Delta T_c / T_c$ in the effective value of T_c, the calibrations on the dial being proportional to ϵ_c (see Section 6.4).

The optimum values of the MPI setting $\epsilon_{c \cdot ar}$ for use in conjunction with the ψ_r function to offset the effect of air resistance are tabulated in Table 6 for different values of V and c. Similarly Table 7 gives the values of the MPI setting $\epsilon_{c \cdot aa}$ used to offset angle of attack variations, for different values of V and CW. The values of C and the nominal (average) values of W are tabulated for several types of planes in Table 8. The optimum net or total adjustment for these two sources of error is $\epsilon_{c \cdot ar} + \epsilon_{c \cdot aa}$. In equation form, as derived in reference 116, these terms are

$$\epsilon_{c \cdot ar} = \overline{a}\, \frac{\overline{T}_c}{\overline{V}} \left(\frac{V^2}{c} - \frac{\overline{V}^2}{\overline{c}} \right), \tag{32}$$

and

$$\epsilon_{c \cdot aa} = \frac{\overline{b}_c}{1{,}000\ \overline{V}^2 \tan \overline{\alpha}} \cdot CW \left(\frac{\overline{V}^2}{V^2} - 1 \right). \tag{33}$$

The use of the tables to determine the MPI adjustment is illustrated by the following example: A TBM plane at nominal weight, whose bomb director operates according to the ψ_r function, is about to toss a bomb whose ballistic coefficient is 3.0, with a

TABLE 7. Values of supplementary MPI adjustment for angle of attack variation ($\epsilon_{c \cdot aa}$). (For use with ψ_r function.)

CW \ True air-speed knots	225	250	275	300	325*	350	375	400	425	450	475
	%	%	%	%	%	%	%	%	%	%	%
1.4×10^6	+ 7.4	+ 4.7	+ 2.7	+ 1.2	0.0	— 0.9	— 1.7	— 2.3	— 2.8	— 3.3	— 3.6
1.6	+ 8.5	+ 5.4	+ 3.1	+ 1.4	0.0	— 1.1	— 1.9	— 2.7	— 3.2	— 3.7	— 4.2
1.8	+ 9.5	+ 6.1	+ 3.5	+ 1.5	0.0	— 1.2	— 2.2	— 3.0	— 3.6	— 4.2	— 4.7
2.0	+ 10.6	+ 6.7	+ 3.9	+ 1.7	0.0	— 1.3	— 2.4	— 3.3	— 4.1	— 4.7	— 5.2
2.2	+ 11.7	+ 7.4	+ 4.3	+ 1.9	0.0	— 1.5	— 2.7	— 3.6	— 4.5	— 5.1	— 5.7
2.4*	+ 12.7	+ 8.1	+ 4.6	+ 2.0	0.0	— 1.6	— 2.9	— 4.0	— 4.9	— 5.6	— 6.2
2.6	+ 13.8	+ 8.7	+ 5.0	+ 2.2	0.0	— 1.7	— 3.2	— 4.3	— 5.3	— 6.1	— 6.8
2.8	+ 14.8	+ 9.4	+ 5.4	+ 2.4	0.0	— 1.9	— 3.4	— 4.6	— 5.7	— 6.5	— 7.3
3.0	+ 15.9	+ 10.1	+ 5.8	+ 2.5	0.0	— 2.0	— 3.6	— 5.0	— 6.1	— 7.0	— 7.8
3.2	+ 17.0	+ 10.8	+ 6.2	+ 2.7	0.0	— 2.2	— 3.9	— 5.3	— 6.5	— 7.5	— 8.3
3.4	+ 18.0	+ 11.4	+ 6.6	+ 2.9	0.0	— 2.3	— 4.1	— 5.6	— 6.9	— 7.9	— 8.8
3.6×10^6	+ 19.1	+ 12.1	+ 7.0	+ 3.0	0.0	— 2.4	— 4.4	— 6.0	— 7.3	— 8.4	— 9.3

*Modal values as used in ψ_r calculations.

true airspeed of approximately 275 knots in the dive. From Table 8, $C = 132$ and $W = 15{,}500$ lb, hence $CW = 2.05 \times 10^6$. Also $c = 3.0$ and $V = 275$ knots. With $V = 275$ knots and $c = 3.0$, Table 6 gives $\epsilon_{c \cdot ar} = -2.1$ per cent. Similarly, with $V = 275$ knots and $CW = 2.05 \times 10^6$ (interpolating between 2.0 and 2.2), Table 7 gives $\epsilon_{c \cdot aa} = +4.0$ per cent. Hence the optimum net MPI adjustment is $-2.1 + 4.0 = +1.9$ per cent.

TABLE 8. Aircraft coefficients (C) and nominal weights (W) of most frequently used planes. [214]

Plane	C*	Nominal W (lb)	Nominal CW	Nominal $CW - \overline{CW}$
F4U (FG)	227	12,000	2.72×10^6	$+0.33 \times 10^6$
SB2C	165	15,000	2.47	+0.08
F6F	193	12,400	2.39	0.00
TBM (TBF)	132	15,500	2.05	−0.34
FM (F4F)	250	7,500	1.87	−0.52
P-38 L	205	17,200	3.53×10^6	$+1.14 \times 10^6$
P-51 K	350	9,500	3.32	+0.93

*C appears in the formula:

$$\text{Angle of attack} = CW \frac{\cos \alpha}{V^2} - k,$$

and is here tabulated in units corresponding to angle of attack in mils, W in pounds, and V in knots.

Examination of Tables 6 and 7 and equations (32) and (33) indicates that all four of the disadvantages cited in Section 8.4.1 are theoretically overcome under this system. It is to be noted that $\epsilon_{c \cdot ar}$ and $\epsilon_{c \cdot aa}$ vary in opposite directions with V, thus imposing an additional limit on the magnitude and degree of variation of their sum.

8.4.4 Advantages and Comments

The revision of the ψ function — with optional MPI adjustment — appears to be a considerably more effective method of correcting for systematic errors than purely manual adjustment methods. The effectiveness of the method in practice remains to be determined from experiments involving the design and installation of a revised ψ card, its testing in the field, and a rigid statistical analysis of the results.

The formulas and curves so far derived[116] may be somewhat improved upon by revising the modal values, from which calculations were made, to fit actual conditions more closely. The possibility of fitting a somewhat different ψ_r function to each type of plane, based on the value of C and the average values of W and V for such plane, might also be considered. The correction terms in ψ_r plotted separately in Figure 20 facilitate the adjustment of any single term.

It has been found that reasonable changes in the assumed modal values $\overline{V}$, $\overline{c}$, $\overline{CW}$ may cause appreciable changes in the density of the ψ_r curves, i.e., in the dependency of ψ_r on T_c/V. Since, furthermore, the MPI adjustment may be used to offset deviations from such modal values, the question arises as to whether some reasonable combination of values $\overline{V}$, $\overline{c}$, and $\overline{CW}$ might render ψ_r practically independent of T_c/V, making it a function of α alone. This would be especially advantageous in bomb directors such as the Mark 3. It has been noted that ψ_r is itself considerably less dependent on T_c/V than ψ_0, ψ_1 and ψ_e.

The extension of the method to include other systematic errors, such as that due to nonconstant airspeed in the dive, is entirely feasible. Such extension would involve an additional correction term in the ψ_r function, and an additional MPI adjustment table.

Furthermore, systematic errors which depend on the pull-up acceleration K, may be offset by revision of the $F(K)$ function for average values of other parameters, since $1/F$, like ψ and T_c, is a factor of T_p, and the analysis in reference 116 may be extended to include changes in this factor.

One important consequence of this method of correction is a greatly simplified flight calibration procedure (see Chapter 4). When the ψ_r function is used, an accurate sight setting may be attained by (1) adjusting the MPI dial according to Tables 6 and 7, and (2) tossing bombs at any convenient range, at an airspeed as close as possible to 325 knots, and at a dive angle of at least 15 degrees (at least 20 degrees if 325 knots cannot be approximated closely; actually somewhat higher dive angles will yield more accurate results) — and adjusting the sight after each such run until impact is consistently near the target. The errors at other values of S, α, and V will be very slight.

BIBLIOGRAPHY

Numbers such as Div. 4-326.3-M1 indicate that the document has been microfilmed and that its title appears in the microfilm index printed in a separate volume. For access to the index volume and to the microfilm, consult the Army or Navy agency listed on the reverse of the half-title page.

NDRC ARMOR AND ORDNANCE REPORTS

1. *A Preliminary Analysis of the Effect of Air Resistance on Certain Aspects of Toss Bombing*, S. H. Lachenbruch, OSRD 4589, Service Projects AC-62 and NO-185, Report A-308, NBS, Ordnance Development Division, September 1944. Div. 4-312.5-M1

NDRC DIVISION 4 — NBS REPORTS

2. *Test of Integrating Aeceleromcters at Aberdeen, February 27, 1943*, F. R. Kotter, NDRC-4, Service Project OD-27, Memorandum Report 98-T, NBS, Ordnance Development Division, Mar. 17, 1943. Div. 4-326.3-M1
3. *Test of Bomb Release Mechanism*, William B. McLean and Jacob Rabinow, NDRC-4, Service Project OD-27, Memorandum Report 48, NBS, Ordnance Development Division, Mar. 19, 1943. Div. 4-328.5-M1
4. *Tests of Aeccleromcters at Aberdeen, March 12, 1943*, F. R. Kotter and T. C. Hellmers, NDRC-4 Service Project OD-27, Memorandum Report 112-T, NBS, Ordnance Development Division, Mar. 23, 1943. Div. 4-326.3-M2
5. *Mathematical Invcstigation of Somc Phases of Toss Bombing*, Phillip R. Karr, NDRC-4, NBS, Ordnance Development Division, Mar. 26, 1943. Div. 4-311-M1
6. *Test of Integrating Accelerometers, April 6, 1943* [Preliminary Report], F. R. Kotter, NDRC-4, Service Project OD-112, Memorandum Report 152-T, NBS, Ordnance Development Division, Apr. 10, 1943. Div. 4-326.3-M3
7. *Test of Mechanical Integrating Aeeelerometer*, D. A. Worcester and F. R. Kotter, NDRC-4, Service Project OD-112, Memorandum Report 166-T, NBS, Ordnance Development Division, Apr. 15, 1943. Div. 4-326.3-M4
8. *Toss Bombing: Acceleration-Integrator Bomb Relcase*, William B. McLean, William L. Whitson, and Jacob Rabinow, NDRC-4, Service Project AC-62, Memorandum Report 5S, NBS, Ordnance Development Division, May 16, 1943. Div. 4-324.11-M1
9. *Toss Bombing: Compcnsating Acceleration-Integrator Bomb Release, Including Field Test Data*, William B. McLean and William L. Whitson, NDRC-4, Service Project AC-62, Memorandum Report 7S, NBS, Ordnance Development Division, Aug. 14, 1943. Div. 4-324.11-M2

NBS REPORTS

10. *Toss Bombing Tests at Cedar Point Naval Air Station, Oct. 9–Nov. 4, 1943*, F. R. Kotter, Report OD-1-57, NBS, Ordnance Development Division, Nov. 18, 1943. Div. 4-330-M1
11. *Toss Bombing: Summary of Proof Data*, William B. McLean and William L. Whitson, Report OD-4-10, NBS, Ordnance Development Division, Nov. 30, 1943. Div. 4-311-M3
12. *Displaced-Image Rangefinder Goggles*, William L. Whitson, Report OD-4-33, NBS, Ordnance Development Division, Feb. 14, 1944. Div. 4-720-M1
13. *Toss Bombing Field Data Using AYF Altimeter and Gyro Dive Angle Attachment*, William L. Whitson, Report OD-4-34, NBS, Ordnance Development Division, Feb. 14, 1944. Div. 4-330-M2
14. *Toss Bombing Field Data Using AYF Altimeter and Gyro Dive Angle Attachment*, William L. Whitson, Report OD-4-39, NBS, Ordnance Development Division, Mar. 16, 1944. Div. 4-330-M2
15. *Toss Bombing Tests at Patuxent*, William L. Whitson, Report OD-4-64, NBS, Ordnance Development Division, May 10, 1944. Div. 4-330-M3
16. *Reversing Integrator with Hyperbolic Slidewire*, William L. Whitson, Report OD-4-57, NBS, Ordnance Development Division, May 22, 1944. Div. 4-324.12-M1
17. *Toss Bombing Tests at Patuxent Using Kollsman Altimeter in SB2C-3 Plane*, William L. Whitson, Report OD-4-67, NBS, Ordnance Development Division, May 25, 1944. Div. 4-330-M4
18. *Toss Bombing Tests at Patuxent Using Kollsman Altimeter in SB2C-3 Plane*, William L. Whitson, Report OD-4-70, NBS, Ordnance Development Division, May 29, 1944. Div. 4-330-M4
19. *Dive Toss Bombing*, William L. Whitson, Report OD-4-58, NBS, Ordnance Development Division, June 1, 1944. Div. 4-311-M4
20. *Field Test, Toss-Bombing, Patuxent, June 23, 1944*, D. C. Friedman, Report OD-1-401, NBS, Ordnance Development Division, July 14, 1944. Div. 4-330-M5
21. *Toss Bombing with a TBM Airplane Using a Fixed-Time Integrator*, F. R. Kotter, Report OD-TB-10, NBS, Ordnance Development Division, Aug. 21, 1944. Div. 4-324.13-M1
22. *The Use of a Reversing Electrieal Integrator in Low Level Toss Bombing with a TBM Airplane*, F. R. Kotter, Report OD-TB-15, NBS, Ordnance Development Division, Aug. 25, 1944. Div. 4-324.12-M2
23. *Toss Bombing with an F6F Airplane at the Naval Proving Ground, Dahlgren, Va.*, F. R. Kotter, Report OD-TB-17, NBS, Ordnance Development Division, Aug. 25, 1944. Div. 4-330-M6
24. *Equations for Toss Bombing for the Horizontal Case Assuming Acceleration is a Function of Time*, William B. McLean, Report OD-TB-19, NBS, Ordnance Development Division, Aug. 31, 1944. Div. 4-311.3-M1
25. *Procedure for Altering and Rebalancing the Gyro*, Frank E. Inman, Report OD-TB-21, NBS, Ordnance Development Division, Sept. 18, 1944. Div. 4-325.1-M1

26. *Bridge for Cheeking Gyro Angle versus Voltage,* Harold N. Cones, Report OD-TB-25, NBS, Ordnance Development Division, Sept. 21, 1944. Div. 4-325.1-M2

27. *Bridge for Adjustment of ψ for Different Plane Veloeities,* Harold N. Cones, Report OD-TB-33, NBS, Ordnance Development Division, Sept. 28, 1944. Div. 4-312.2-M1

Addendum: *Revised Computations of Gyro Output Voltage at 40° Dive Angle for Different Plane Velocities,* S. H. Lachenbruch, Report OD-TB-33A, NBS, Ordnance Development Division, Oct. 25, 1944. Div. 4-312.2-M2

28. *Effeet of Changing Integrator RC Ratio to Correct for an Error in Alignment of Sight With Line of Flight,* William B. McLean, Report OD-SP-40, NBS, Ordnance Development Division, Oct. 26, 1944. Div. 4-312.1-M1

29. *Variation of Integrator ψ Funetion with Velocity, Negleeting Air Resistance,* R. DeAmicis, Report OD-SP-41, NBS, Ordnance-Development Division, Nov. 14, 1944. Div. 4-312.2-M4

30. *Comparison between Actual and Theoretieal Values of Output Voltage from Gyro Potentiometer,* R. DeAmicis, Report OD-SP-42, NBS, Ordnance Development Division, Nov. 3, 1944. Div. 4-325-M1

31. *Test Set for Measuring Closing Time of Relays,* Harold N. Cones, Report OD-SP-43, NBS, Ordnance Development Division, Oct. 17, 1944. Div. 4-328.41-M2

32. *Analysis of Hortizontal Range Error Resulting from Neglect of Pull-up Angle,* S. H. Lachenbruch, Report OD-SP-45, NBS, Ordnance Development Division, Nov. 7, 1944. Div. 4-311.1-M2

33. *Use of the 100-Ft Horizontal Error Curves for Errors of Other Magnitudes,* S. H. Lachenbruch, Report OD-SP-46, NBS, Ordnance Development Division, Nov. 8, 1944. Div. 4-312.2-M3

33a. *Temperature Cyeling of IRC BW-1 and Other Resistors,* A. E. Peterson and F. O. Harrer, Report OD-SP-47, NBS, Ordnance Development Division, Oct. 27, 1944. Div. 4-236-M5

Addendum: *Temperature Cycling of IRC BW-1 Resistors,* Report OD-SP-47a, Nov. 28, 1944. Div. 4-236-M6

34. *General Toss Bombing Solution for the Case of a Non-Constant Accelcration, Ineluding the Effect of the Pull-up Angle,* Albert London, Report OD-SP-48, NBS, Ordnance Development Division, Nov. 3, 1944. Div. 4-311.1-M1

35. *Relationship among Important Angles in Toss Bombing Trajeetories,* S. H. Lachenbruch, Report OD-SP-49, NBS, Ordnance Development Division, Nov. 10, 1944. Div. 4-311.1-M3

36. *Vibration Tests on Integrator During Actual Flights,* Leroy R. Sweetman, Report OD-SP-50, NBS, Ordnance Development Division, Nov. 6, 1944. Div. 4-324.3-M1

37. *Gun Sight Setting on P-47 Airplane for Toss Bombing,* William L. Whitson, Report OD-SP-51, NBS, Ordnance Development Division, Nov. 10, 1944. Div. 4-323.2-M1

37a. *Report on Integrator Brushes and Commutator,* Forest K. Harris, Report OD-SP-52, NBS, Ordnance Development Division, Nov. 15, 1944. Div. 4-324.22-M1

38. *Measurements of Wind Veloeity with the Directional Gyro,* William L. Whitson, Report OD-SP-53, NBS, Ordnance Development Division, Nov. 22, 1944. Div. 4-312.4-M1

38a. *Relay Tests,* Harold N. Cones and F. O. Harrer, Report OD-SP-54, NBS, Ordnance Development Division, Nov. 22, 1944. Div. 4-328.41-M3

39. *Bomb Director Performanee, Patuxent River Station, November 7–14, 1944,* P. V. Johnson, Report OD-SP-55, NBS, Ordnance Development Division, Nov. 22, 1944. Div. 4-321.3-M1

40. *Application of Toss Bombing Equipment to Torpedo Tossing,* Albert London, Report OD-SP-56, NBS, Ordnance Development Division, Nov. 28, 1944. Div. 4-340-M2

41. *Modified Kollsman Altimeter for Toss Bombing Equipment,* B. L. Wilson and Arnold Wexler, Report OD-SP-58, NBS, Ordnance Development Division, Dec. 2, 1944. Div. 4-322.1-M1

42. *Determination of Proper RF Filter for the Thyratron in the Integrator,* Joseph H. Hibbs, Report OD-SP-57, NBS, Ordnance Development Division, Dec. 4, 1944. Div. 4-324.22-M2

43. *Operation of Toss-Bombing Integrator Cireuit,* Albert London, Report OD-SP-60, NBS, Ordnance Development Division, Dec. 7, 1944. Div. 4-324.21-M2

44. *Setting of the Intervalometer for Toss Bombing,* S. H. Lachenbruch, Report OD-SP-61, NBS, Ordnance Development Division, Jan. 1, 1945. Div. 4-328.1-M1

45. *Operating Time of Relay,* Harold N. Cones, Report OD-SP-62, NBS, Ordnance Development Division, Dec. 7, 1944. Div. 4-328.41-M4

46. *Bomb Director Performance, Patuxent River Station, November 15–25, 1944,* P. V. Johnson, Report OD-SP-63, NBS, Ordnance Development Division, Dec. 8, 1944. Div. 4-321.3-M1

47. *Effect of Variation in Dive Angle and Release Altitude on Bomb Director Operation in SB2C Planes,* P. V. Johnson and John H. Park, Report OD-SP-65, NBS, Ordnance Development Division, Dec. 27, 1944. Div. 4-321.3-M2

48. *Progress of Development of Electrieal Indieating Altimeter,* Joseph H. Hibbs, Report OD-SP-66, NBS, Ordnance Development Division, Dec. 19, 1944. Div. 4-322.2-M2

49. *Introduction to Operation of Bomb Director, AN/ASG-10 (XN),* W. S. Hinman, Jr., Report OD-SP-67, NBS, Ordnance Development Division, Dec. 15, 1944. Div. 4-321.1-M1

49a. *Further Temperature Tests on Sprague Vitamin Q Capacitors,* A. E. Peterson and F. O. Harrer, Report OD-SP-68, NBS, Ordnance Development Division, Dec. 16, 1944. Div. 4-328.3-M1

50. *Bomb Direetor Performance, Patuxent River Station, November 28–December 7, 1944,* P. V. Johnson, Report OD-SP-69, NBS, Ordnance Development Division, Dec. 16, 1944. Div. 4-321.3-M1

51. *Tests on Effect of Aircraft Radio and Intercommunication System on Operation of Mk 1 Bomb Direetor,* A. E. Peterson and C. Weaver Creed, Report OD-SP-71, NBS, Ordnance Development Division, Dec. 29, 1944. Div. 4-321.2-M1

52. *Effect of Variation in Dive Angle and Altitude of Release on Bomb Director Performance in an F6F-5 Airplane*, John H. Park, Report OD-SP-72, NBS, Ordnance Development Division, Dec. 30, 1944. Div. 4-321.3-M3

53. *Bomb Director Performance, Patuxent River Station, December 8 to December 28, 1944*, P. V. Johnson, Report OD-SP-73, NBS, Ordnance Development Division, Dec. 30, 1944. Div. 4-321.3-M1

54. *Preliminary Report on the Photo-Electric Dive Angle Meter*, William B. McLean, Joseph H. Hibbs, and McKay R. Bradley, Report OD-SP-74, NBS, Ordnance Development Division, Jan. 8, 1945. Div. 4-327-M2

54a. *Temperature Cycling of Precision Wire-Wound Resistors, December 30, 1944 to January 6, 1945*, F. O. Harrer and Harold N. Cones, Report OD-SP-75, NBS, Ordnance Development Division, Jan. 11, 1945. Div. 4-236-M8

55. *Correction of the Acceleration Integrator for Air Resistance*, S. H. Lachenbruch, Report OD-SP-76, NBS, Ordnance Development Division, Jan. 12, 1945. Div. 4-312.5-M2

56. *Tables of New ψ Functions and Other Related Quantities*, C. F. Eve and Albert London, Report OD-SP-77, NBS, Ordnance Development Division, Jan. 15, 1945. Div. 4-312.2-M5

57. *New ψ Card Design*, Albert London and A. E. Willgoos, Report OD-SP-78, NBS, Ordnance Development Division, Jan. 17, 1945. Div. 4-312.2-M6

58. *Vibration Tests of Modified Kollsman Altimeter for Toss-Bombing Equipment*, B. L. Wilson and Arnold Wexler, Report OD-SP-79, NBS, Ordnance Development Division, Jan. 17, 1945. Div. 4-322.1-M2

59. *Horizontal Range Errors Resulting from Altitude Ratio Errors*, Arnold Wexler and Albert London, Report OD-SP-80, NBS, Ordnance Development Division, Jan. 18, 1945. Div. 4-312.3-M1

60. *Bomb Director Performance, Patuxent River Station, December 29, 1944 to January 31, 1945*, John H. Park, Report OD-SP-82, NBS, Ordnance Development Division, Feb. 16, 1945. Div. 4-321.3-M1

61. *Minimum-Segment K-Block Design*, Albert London and Ray F. Smith, Jr., Report OD-SP-83, NBS, Ordnance Development Division, Feb. 9, 1945. Div. 4-236-M10

62. *Grid Current in the 2050 Thyratron Tube*, Harold N. Cones, R. W. Gustafson, and Robert L. Nutter, Report OD-SP-84, NBS, Ordnance Development Division, Feb. 8, 1945. Div. 4-231.1-M10

63. *Laboratory Tests of an Altitude-Switch for Use with Toss-Bombing Equipment*, Arnold Wexler, B. L. Wilson, and F. O. Harrer, Report OD-SP-85, NBS, Ordnance Development Division, Feb. 16, 1945. Div. 4-322.42-M1

64. *Flight Tests of Iowa Integrator Mounted on A-1-A and New Design Shock Mount*, Leroy R. Sweetman, Report OD-SP-86, NBS, Ordnance Development Division, Feb. 8, 1945. Div. 4-324.3-M4

65. *Description of Test Unit Mk 16 Mod 0*, V. W. Cohen, Report OD-SP-87, NBS, Ordnance Development Division, Mar. 1, 1945. Div. 4-321.4-M1

66. *Rocket-Tossing Theory*, Albert London and C. F. Eve, Report OD-SP-90, NBS, Ordnance Development Division, Feb. 24, 1945. Div. 4-421-M2

67. *Bench Tests on Magnavox Computers*, R. W. Gustafson, Report OD-SP-91, NBS, Ordnance Development Division, Feb. 24, 1945. Div. 4-324.14-M1

68. *Bomb Director Performance, Patuxent River Station, February 1, 1945 to February 28, 1945*, John H. Park, Report OD-SP-93, NBS, Ordnance Development Division, Mar. 10, 1945. Div. 4-321.3-M1

69. *Tests on 2050 Thyratrons in Magnavox and NBS Test Units; Effectiveness of Heat Curing the Thyratrons*, Harold N. Cones, Report OD-SP-95, NBS, Ordnance Development Division, Apr. 16, 1945. Div. 4-231.11-M2

70. *Humidity Tests on Production AN/ASG-10 and Various Cables*, J. L. Pike and Joseph Johansen, Report OD-SP-96, NBS, Ordnance Development Division, Mar. 12, 1945. Div. 4-321.11-M1

Addendum: *Further Humidity Tests on AN/ASG-10 Computer, Cables, Connectors, and Altimeter*, J. L. Pike and Joseph Johansen, Report OD-SP-96A, Apr. 13, 1945. Div. 4-321.11-M3

Second Addendum: *Humidity Tests on AN/ASG-10 Computer, Pilot's Control Box, Altimeter, and Sealed Chamber Terminals*, Report OD-SP-96B, J. L. Pike and Joseph Johansen, May 14, 1945. Div. 4-321.11-M5

71. *Wind Correction for Toss Bombing*, T. H. Nicholl, Report OD-SP-97, NBS, Ordnance Development Division, Mar. 14, 1945. Div. 4-312.4-M2

72. *Exact Solution of Toss Bombing Equations for Circular Pull-up*, S. H. Lachenbruch, Albert London, and C. F. Eve, Report OD-SP-98, NBS, Ordnance Development Division, Mar. 23, 1945. Div. 4-311.1-M5

73. *Laboratory Tests of Electrical Altimeter No. 2 for Use with Toss Bombing Equipment*, Arnold Wexler and Ray F. Smith, Jr., Report OD-SP-99, NBS, Ordnance Development Division, Mar. 24, 1945. Div. 4-322.2-M3

74. *Summary of Time in Air for all Toss Bombing Equipment at Patuxent from 28 October 1944 to 19 March 1945, Listing All Faults in Equipment and Adjustments Made*, John H. Park, Report OD-SP-100, NBS, Ordnance Development Division, Mar. 27, 1945. Div. 4-321.11-M2

75. *Rocket and Bomb Tossing Circuit for Use with Photoelectric Accelerometer*, William B. McLean, Preliminary Report OD-SP-101, NBS, Ordnance Development Division, Apr. 3, 1945. Div. 4-326.1-M1

76. *Bomb Director Performance, Naval Air Station, Patuxent River, Md., March 1–31, 1945*, W. Q. Hull, Report OD-SP-102, NBS, Ordnance Development Division, Apr. 10, 1945. Div. 4-321.3-M1

77. *First Button Releases in SB2C Planes, Their Cause and Probable Cure*, John H. Park, Report OD-SP-103, NBS, Ordnance Development Division, Apr. 11, 1945. Div. 4-328.5-M2

78. *Angle of Attack of Thrust Line, Plane SB2C-4 Ser. 20354*, John H. Park, Report OD-SP-104, NBS, Ordnance Development Division, Apr. 14, 1945. Div. 4-311.4-M2

79. *Range Limitations Resulting from Approximations in Toss Bombing Equations*, S. H. Lachenbruch, Report OD-SP-105, NBS, Ordnance Development Division, Apr. 16, 1945. Div. 4-314-M1

80. *Wind Correction Sighting Grids for Toss Bombing*, Albert London and A. E. Willgoos, Report OD-SP-106, NBS, Ordnance Development Division, May 11, 1945. Div. 4-312.4-M3

81. *Range Wind Correction for Toss Bombing*, Albert London and C. F. Eve, Report OD-SP-107, NBS, Ordnance Development Division, June 5, 1945. Div. 4-312.4-M4

82. *Maintenance Notes on AN/ASG-10 (XN) Equipment*, F. M. Defandorf, Report OD-SP-109, NBS, Ordnance Development Division, May 1, 1945. Div. 4-321.11-M4

83. *Protek (Silica Gel) Dryer Plugs Used in Computer for AN/ASG-10*, Harold N. Cones, Report OD-SP-111, NBS, Ordnance Development Division, May 2, 1946. Div. 4-324.15-M1

84. *Angle of Attack of Thrust Line, Plane F6F, 77555*, L. J. Jelsch, Report OD-SP-112, NBS, Ordnance Development Division, May 7, 1945. Div. 4-311.4-M3

85. *Bomb Director Performance Naval Air Station, Patuxent River, Md., April 1–30, 1945*, John H. Park, Report OD-SP-113, NBS, Ordnance Development Division, May 8, 1945. Div. 4-321.3-M1

86. *Construction on Dive Angle Indicators (Gyro Repeaters) for Use with AN/ASG-10 Gear*, A. E. Peterson, Report OD-SP-116, NBS, Ordnance Development Division, May 21, 1945. Div. 4-327-M4

87. *Dependence of Range on the Allowable Sight Depression in Dive Bombing*, S. H. Lachenbruch, Report OD-SP-117, NBS, Ordnance Development Division, May 11, 1945. Div. 4-311.2-M1

88. *Bomb Director Performance Naval Air Station, Patuxent River, Md., May 1–31, 1945*, John H. Park, Report OD-SP-118, NBS, Ordnance Development Division, June 14, 1945. Div. 4-321.3-M1

89. *Toss Director using Photoelectric Accelerometer, Continuous Take-off Altimeter, and a Linear Condenser Charging Circuit*, William B. McLean, Report OD-SP-119, NBS, Ordnance Development Division, June 22, 1945. Div. 4-326.1-M2

90. *Thyratron Tube Tester*, V. W. Cohen, Report OD-SP-120, NBS, Ordnance Development Division, June 23, 1945; Addendum, July 10, 1945. Div. 4-231.11-M3

91. *Vibration Tests of Magnavox Computers*, C. Weaver Creed and J. L. Pike, Report OD-SP-121, NBS, Ordnance Development Division, July 24, 1945. Div. 4-324.3-M7

92. *Test Unit Mk 17 for Thyratron Tests*, V. W. Cohen, Report OD-SP-122, NBS, Ordnance Development Division, July 9, 1945. Div. 4-231.11-M4

93. *ψ Function for Non-Constant Pull-up Acceleration*, C. F. Eve and Albert London, Report OD-SP-123, NBS, Ordnance Development Division, July 10, 1945. Div. 4-311.1-M7

94. *Angle of Attack of Bore-Sight Datum Line for SB2C-5, F4U, and F6F-5 Airplanes*, John H. Park, Report OD-SP-124, NBS, Ordnance Development Division, June 22, 1945. Div. 4-311.4-M4

95. *Gyroscope Turn Error Compensation*, Forest K. Harris and Frank E. Inman, Report OD-SP-125, NBS, Ordnance Development Division, July 11, 1945. Div. 4-325-M5

96. *Résumé of AIBR Project in ETO Covering Period July 1, 1944 to June 6, 1945*, William L. Whitson, Report OD-SP-126, NBS, Ordnance Development Division, July 12, 1945. Div. 4-221-M1

97. *Bomb Director Performance, Naval Air Station, Patuxent River, Md., June 1–30, 1945*, John H. Park, Report OD-SP-127, NBS, Ordnance Development Division, July 12, 1945. Div. 4-321.3-M1

98. *A Photoelectric Altimeter for Use with Toss Bombing Equipment*, Arnold Wexler, Harold N. Cones, and Fred Nemir, Report OD-SP-128, NBS, Ordnance Development Division, Aug. 7, 1945. Div. 4-322.3-M1

99. *Installation of Toss Bombing Equipment in an F7F-1 Airplane*, J. L. Pike, Report OD-SP-129, NBS, Ordnance Development Division, July 27, 1945. Div. 4-340-M3

100. *Altimeter Shock Mounts*, Arnold Wexler, Report OD-SP-130, NBS, Ordnance Development Division, July 23, 1945. Div. 4-322.1-M3

101. *The Effect of Sight Misalignment and Angle of Attack Variation*, S. H. Lachenbruch, Report OD-SP-131, NBS, Ordnance Development Division, July 23, 1945. Div. 4-312.1-M3

102. *Tests of Pitch Indicating Gyro with Added Freedom about the Roll Axis*, Frank E. Inman, Report OD-SP-132, NBS, Ordnance Development Division, July 25, 1945. Div. 4-325.1-M6

103. *An Improved Altimeter Unit Circuit for AN/ASG-10*, J. L. Pike, Report OD-SP-133, NBS, Ordnance Development Division, Aug. 1, 1945. Div. 4-322.1-M4

104. *Flight Test of Conn Pitch-Indicating Gyro with Added Freedom about the Roll Axis*, Forest K. Harris, Report OD-SP-134, NBS, Ordnance Development Division, Aug. 11, 1945. Div. 4-325.1-M7

105. *Wind Compensation of the Photoelectric Accelerometer when Used with a Lead-Computing Sight*, Albert London, Report OD-SP-135, NBS, Ordnance Development Division, Aug. 21, 1945. Div. 4-326.1-M4

106. *Rack Lag Time for Mk 50 and Mk 46 Mod 1 Racks with AN/ASG-10 Gear*, A. E. Peterson, Report OD-SP-136, NBS, Ordnance Development Division, Aug. 23, 1945. Div. 4-317-M1

107. *Instructions for Test of Bomb Director Mk 1 Mod 1, Prior to Installation*, V. W. Cohen, Report OD-SP-137, NBS, Ordnance Development Division, Aug. 25, 1945. Div. 4-321.4-M2

108. *Photoelectric Accelerometer to Replace Gyro in Mk 1 Mod 1 and 2 Bomb Directors*, William B. McLean, Report OD-SP-138, NBS, Ordnance Development Division, Aug. 12, 1945. Div. 4-326.1-M3

109. *Construction and Method of Operation of the Apparatus and its Component Elements* (Translation from German of Paper by Zeiss on TAS), F. B. Silsbee, Report OD-SP-140, NBS, Ordnance Development Division, Aug. 31, 1945. Div. 4-321.4-M3

110. *Portable DC Operated Test Unit*, V. W. Cohen, Report OD-SP-141, NBS, Ordnance Development Division, Sept. 4, 1945. Div. 4-321.4-M4

111. *Calibration of Two Altimetrie Slides*, Arnold Wexler, and Robert L. Nutter, Report OD-SP-142, NBS, Ordnance Development Division, Sept. 6, 1945. Div. 4-322.3-M2

112. *Instructions for the Modifieation of Gyro Unit Mk 20 Mod 1*, Frank E. Inman, Report OD-SP-144, NBS, Ordnance Development Division, Oct. 4, 1945. Div. 4-325-M7

113. *Analysis of Resistor Values Needed for Mk 3 Circuit*, Martha Cox, Ray F. Smith, Jr., and A. E. Willgoos, Report OD-SP-145, NBS, Ordnance Development Division, Sept. 20, 1945. Div. 4-328.2-M3

114. *Tactical Limitations of the Modified Altimeter Circuit*, Albert London and S. H. Lachenbruch, Report OD-SP-146, NBS, Ordnance Development Division, Oct. 2, 1945. Div. 4-322.42-M2

115. *Short Deseription of the Technique of Dynamic Testing of Aneroid Altimeters and Barometers*, Arnold Wexler, Report OD-SP-147, NBS, Ordnance Development Division, Oct. 11, 1945. Div. 4-322.3-M3

116. *An Analytieal Method for Correeting Systematic Toss Bombing Errors, Involving Revision of the ψ Function*, S. H. Lachenbruch, Report OD-SP-150, NBS, Ordnance Development Division, Nov. 30, 1945. Div. 4-312.2-M7

117. *The Modified Linderman Dive Angle Indicator*, McKay R. Bradley and F. L. Hermach, Report OD-SP-151, NBS, Ordnance Development Division, Dec. 31, 1945. Div. 4-327-M5

118. *Effect of Variation in Dive Angle and Release Altitude on Operation of Mk 1 Mod 1 Bomb Director in an SB2C-4 Airplane*, E. U. Rotor, Report OD-SP-152, NBS, Ordnance Development Division, Jan. 10, 1946. Div. 4-321.2-M4

119. *Relay Lag Timing Errors in the Mk 20 Mod 2 Computer*, F. R. Kotter, Report OD-SP-153, NBS, Ordnance Development Division, Jan. 31, 1946. Div. 4-324.14-M2

120. *Toss Bombing Trajectories*, F. L. Celauro and D. Fisher, Memorandum OD-OAG-32, NBS, Ordnance Development Division, Sept. 6, 1944. Div. 4-313-M1

121. *Field Tests with Toss Bombing Equipment Adjusted for Tossing Torpedoes, July 4 to September 9, 1944, at Patuxent, Md.*, F. R. Kotter, Memorandum OD-SP-24M, NBS, Ordnance Development Division, Sept. 29, 1944. Div. 4-340-M1

122. *Sight Line Adjusted Off Line of Flight*, William L. Whitson, Memorandum OD-SP-43M, NBS, Ordnance Development Division, Nov. 11, 1944. Div. 4-323.2-M2

123. *Sight Settings*, P. V. Johnson, Memorandum OD-SP-44M, NBS, Ordnance Development Division, Nov. 13, 1944. Div. 4-323.2-M3

124. *Method of Checking the Alignment of the Sight with the Flight Line in a Dive*, William B. McLean, Memorandum OD-SP-47M, NBS, Ordnance Development Division, Nov. 16, 1944. Div. 4-312.1-M2

125. *Alternative Integrator Circuit*, F. B. Silsbee, Memorandum OD-SP-58M, NBS, Ordnance Development Division, Dec. 2, 1944. Div. 4-324.21-M1

126. *Flight Curves for Patuxent Planes*, F. R. Kotter, Memorandum OD-SP-61M, NBS, Ordnance Development Division, Nov. 25, 1944. Div. 4-318-M1

127. *Solenoid Operating Air Valve for Use with Dive Angle Indicator*, F. M. Defandorf, Memorandum OD-SP-62M, NBS, Ordnance Development Division, Dec. 8, 1944. Div. 4-327-M1

128. *Results of Field Test of Electrical Indicating Altimeter*, Joseph H. Hibbs, Memorandum OD-SP-64M, NBS, Ordnance Development Division, Dec. 14, 1944. Div. 4-322.2-M1

129. *Change of Shape of Gyro Card for Magnavox Production*, William B. McLean, Memorandum OD-SP-67M, NBS, Ordnance Development Division, Dec. 26, 1944. Div. 4-325-M2

130. *Differenee between Bomb Directors Mk 1 Mod 0 and Mk 1 Mod 1*, F. B. Silsbee, Memorandum OD-SP-73M, NBS, Ordnance Development Division, Jan. 9, 1945. Div. 4-321.2-M2

131. *Angle of Attack of the Bore-Sight Datum Line in the F6F-5*, Robert E. Holland, Memorandum OD-SP-74M, NBS, Ordnance Development Division, Jan. 1, 1945. Div. 4-311.4-M1

132. *Sight Setting for TBM-1C as Determined with the Aid of a Theodolite on Dec. 6, 1944 at Patuxent, Md.*, Albert G. Hoyem, Memorandum OD-SP-75M, NBS, Ordnance Development Division, Jan. 1, 1945. Div. 4-323.2-M4

133. *Specifications of a Humidity Test Chamber*, V. W. Cohen, Memorandum OD-SP-81M, NBS, Ordnance Development Division, Jan. 24, 1945. Div. 4-619-M3

134. *Cycling Test of Raymond Modified Altimeter with New Whisker Design*, Arnold Wexler, Memorandum OD-SP-84M, NBS, Ordnance Development Division, Jan. 31, 1945. Div. 4-322.41-M1

135. *Conversion of Jack and Heintz Horizon to Dive Angle Indicator*, Forest K. Harris, Memorandum OD-SP-85M, NBS, Ordnance Development Division, Feb. 12, 1945. Div. 4-327-M3

136. *Report of Visit to MIT, February 16, 1945*, [The K-11, or Mark 21 Sight as an Aid to Toss Bombing] William B. McLean, Memorandum OD-SP-87M, NBS, Ordnance Development Division, Feb. 23, 1945. Div. 4-323.1-M2

136a. *Recommendations on Gyro Processing at Magnavox on Basis of Visit to Ft. Wayne during Week of April 2, 1945*, Frank E. Inman, Memorandum OD-SP-104M, NBS, Ordnance Development Division, Apr. 16, 1945. Div. 4-325-M3

137. *Trip to Eglin Field, March 3–8, 1945*, William B. McLean, Memorandum OD-8-92M, NBS, Ordnance Development Division, Mar. 16, 1945. Div. 4-323.1-M3

137a. *Report on Visit to Groves, Siekle, and Sperry Plants, June 4–7, 1945*, Frank E. Inman, Memorandum OD-SP-114M, NBS, Ordnance Development Division, June 15, 1945. Div. 4-325-M4

137b. *Report on Magnavox Gyro Test Fixtures and Proeedures*, Forest K. Harris, Memorandum OD-SP-116M, NBS, Ordnance Development Division, June 27, 1945. Div. 4-325.1-M5

138. *Bomb Director Mk 1 Mod 1 Speeifications*, F. B. Silsbee, Memorandum OD-SP-112M, NBS, Ordnance Development Division, June 11, 1945. Div. 4-321.2-M3

139. *Altimeter Contacts*, F. M. Defandorf, Memorandum OD-SP-119M, NBS, Ordnance Development Division, July 11, 1945. Div. 4-322.41-M2

Addendum: *Variations in Overhang of Altimeter Whisker*, Aug. 13, 1945. Div. 4-322.41-M3

140. *Tables of MPI Settings Required for Different Bomb Ballistic Coefficients*, C. F. Eve, Memorandum OD-SP-123M, NBS, Ordnance Development Division, July 20, 1945. Div. 4-242.14-M3

141. *Tests of the Linderman Aceelerometer*, V. W. Cohen, Memorandum OD-SP-124M, NBS, Ordnance Development Division, July 30, 1945. Div. 4-326.2-M1

142. *A List of Unsatisfaetory Features in Mod 1 and 2 Equipment and Some Remedies*, F. M. Defandorf, Memorandum OD-SP-126M, NBS, Ordnance Development Division, Aug. 14, 1945. Div. 4-321.11-M6

143. *Comments on Report on 2050 Tubes by G. E. Johnson to Lt. Bolser, July 20, 1945*, V. W. Cohen, Memorandum OD-SP-130M, NBS, Ordnance Development Division, Aug. 27, 1945. Div. 4-231.1-M12

144. *Stick Offset Setting Nomograph*, C. F. Eve, Memorandum OD-SP-133M, NBS, Ordnance Development Division, Aug. 30, 1945. Div. 4-328.1-M2

145. *Modification of Gyros with CAG-93*, Frank E. Inman, Memorandum OD-SP-135M, NBS, Ordnance Development Division, Sept. 17, 1945. Div. 4-325-M6

146. *Change in Drag Tolerances of Altimeter Unit*. Arnold Wexler, Memorandum OD-SP-136M, NBS, Ordnance Development Division, Oct. 11, 1945. Div. 4-322.5-M2

146a. *K-Bob Springs*, Arnold Wexler, Memorandum OD-SP-141M, NBS, Ordnance Development Division, Nov. 1, 1945. Div. 4-324.22-M4

147. *Tables of Operational Limits in Toss Bombing*, C. F. Eve, Memorandum OD-SP-140M, NBS, Ordnance Development Division, Oct. 29, 1945. Div. 4-314-M2

148. *Elimination of Gyro-Turn Error, and Automatic Caging of Gyro*, Frank E. Inman, Memorandum OD-SP-142M, NBS, Ordnance Development Division, Nov. 8, 1945. Div. 4-325-M8

149. *The Electrically Driven Attitude Gyro*, Frank E. Inman, Memorandum OD-SP-144M, NBS, Ordnance Development Division, Nov. 26, 1945. Div. 4-325-M9

150. *Progress Reports of Speeial Group on Toss Bombing, July 24, 1944 to January 31, 1946*, W. S. Hinman, Jr., and William B. McLean, NBS, Ordnance Development Division, NDRC-4. Div. 4-311-M5

NDRC DIVISION 4 CONTRACTORS' REPORTS

State University of Iowa

151. *Mathematieal Study of Toss Bombing in the General Case*, Irvin H. Swift, OEMsr-769, Interim Report 7, State University of Iowa, May 22, 1943. Div. 4-311-M2

152. *Preliminary Discussion on Electronie Timer*, REI-1, State University of Iowa, Dec. 1, 1943.

153. *Excerpts from University of Iowa Report Coneerning the Theory of Toss Bombing*, OEMsr-769, Report A-S117BT, State University of Iowa, Aug. 5, 1944. Div. 4-311-M6

154. *A Discussion of Toss Bombing Data Taken at Wright Field*, Robert E. Holland, OEMsr-769, Technical Paper A-S120 ERDS, State University of Iowa, Aug. 11, 1944. Div. 4-311-M7

155. *Checking and Adjusting Procedure for Clare A-16494 Relays*, OEMsr-769, Report A-S138A, State University of Iowa, Oct. 17, 1944. Div. 4-328.41-M1

156. *The Elements of Toss Bombing*, Irvin H. Swift, OEMsr-769, Technical Paper REI-TMD-115, Rev. 1, State University of Iowa, Nov. 4, 1944. Div. 4-311-M9

157. *Test Program on Rocket Tossing at Patuxent*, Irvin H. Swift, and James A. Jacobs, Report A-S-146 EP, State University of Iowa, Nov. 4, 1944. Div. 4-423-M1

158. *Leakage Effect with Combination Integrator and PCB* Irvin H. Swift, OEMsr-769, Memorandum MC-1-1-45 State University of Iowa, Revised: Mar. 31, 1945. Div. 4-324.3-M6

159. *An Upper Limit for Angular Mil Separation in Range between Two Rockets Launched Simultaneously*, Carl E. Noble, OEMsr-769, Report MC-1-2-45, State University of Iowa, Jan. 6, 1945. Div. 4-412.4-M5

160. *Rocket Tossing — Results of SP-5 Tests with the TBM-1C at Patuxent*, Albert C. Hoyem, OEMsr-769, Memorandum MC-1-3-45, State University of Iowa, Jan. 13, 1945. Div. 4-421.2-M1

161. *The Effect of Certain Modifications in the Integrator Circuit*, Irvin H. Swift, OEMsr-769, Memorandum MC-2-1-45, State University of Iowa, Feb. 17, 1945. Div. 4-324.21-M3

162. *The Method of Reducing Aircraft Data Used by the University of Iowa Rocket Tossing Group at the Naval Ordnance Test Station, Inyokern, California*, Carl E. Noble, OEMsr-769, Memorandum MC-2-2-45, State University of Iowa, Feb. 17, 1945. Div. 4-421.2-M2

163. *Results of Tests on Switches of the Miero Switch Type*, T. C. Stephens, OEMsr-769, Memorandum MC-2-3-45, State University of Iowa, Feb. 24, 1945. Div. 4-324.22-M3

164. *Pull-up Aeceleration as a Function of Time for F6F and TBM Flights Releasing Rockets and Bombs*, A. H. Crippen, OEMsr-769, Memorandum MC-2-4-45, State University of Iowa, Feb. 24, 1945. Div. 4-316-M1

165. *Theodolite Measurement of Sight Setting for SB2C-4 No. 19717*, A. H. Crippen, OEMsr-769, Memorandum MC-3-1-45, State University of Iowa, Mar. 10, 1945. Div. 4-323.2-M5

166. *The Effect of Plane Velocity on MPI in Tossing Rockets at Patuxent*, Robert E. Holland, OEMsr-769, Memorandum MC-4-1-45, State University of Iowa, Apr. 14, 1945. Div. 4-421.2-M3

167. *Shift in MPI with Change in A Factor in Rocket Tossing*, Irvin H. Swift, OEMsr-769, Memorandum MC-4-2-45, State University of Iowa, Apr. 28, 1945. Div. 4-421.2-M4

168. *Sight Settings for Tossing Compared with CIT Attack Angle Values*, T. C. Stephens, OEMsr-769, Memorandum M7-5-1-45, State University of Iowa, May 5, 1945. Div. 4-422.1-M4

169. *Empirical Equation for the Trajectory Drop of Present Model 11.75" Aircraft Rocket*, M. E. Rolfs, OEMsr-769, Memorandum M7-6-1-45, State University of Iowa, June 6, 1945. Div. 4-412.1-M9

170. *Revision of Empirical Equation for Trajectory Drop of 5.0"AR*, M. E. Rolfs, OEMsr-769, Memorandum M7-6-2-45, State University of Iowa, June 6, 1945. Div. 4-412.1-M10

171. *Note Concerning the Function F* (α), L. E. Ward, OEMsr-769, Memorandum M7-6-3-45, State University of Iowa, June 13, 1945. Div. 4-412.1-M11

172. *An Empirical Equation for Trajectory Drops of 3.5" Aircraft Rocket*, M. E. Rolfs, OEMsr-769, Technical Paper TC-1-1-45, State University of Iowa, Revised: Jan. 20, 1945. Div. 4-412.1-M5

173. *The Motion of Aircraft Rockets During Burning*, L. E. Ward, OEMsr-769, Technical Paper TC-1-2-45, State University of Iowa, Jan. 13, 1945. Div. 4-412.2-M4

174. *Empirical Equations for Trajectory Drops of 11.75" Aircraft Rocket and 5.0" High Velocity Aircraft Rocket*, M. E. Rolfs, OEMsr-769, Technical Paper TC-1-3-45, State University of Iowa, Jan. 27, 1945. Div. 4-412.1-M6

175. *Effect of a Constant Angle between the Sight Line and the Flight Line in Tossing Projectiles*, M. E. Rolfs, OEMsr-769, Technical Paper TC-2-1-45, State University of Iowa, Feb. 24, 1945. Div. 4-311.1-M4

176. *An Equation for the Rocket Tossing Pull-Up Time T_p*, L. E. Ward, OEMsr-769, Technical Paper TC-2-2-45, State University of Iowa, Feb. 24, 1945. Div. 4-421.1-M1

177. *Empirical Equations for Trajectory Drops of 2.25" AR (fast), RP-3, 3.5", 5.0" AR, and RP-3, 5.0"*, M. E. Rolfs, OEMsr-769, Technical Paper TC-3-1-45, State University of Iowa, Mar. 31, 1945. Div. 4-412.1-M7

178. *The Results Obtained from Firing 5.0" HVAR with the Toss Sight in an F6F-5 at Inyokern*, Carl E. Noble, OEMsr-769, Technical Paper TC-4-1-45, State University of Iowa, Revised: July 18, 1945. Div. 4-422.1-M6

179. *Values of the A Factor for Rocket Tossing*, Irvin H. Swift, OEMsr-769, Technical Paper TC-4-2-45, State University of Iowa, Apr. 7, 1945. Div. 4-421.1-M2

180. *An Equation for the Rocket Tossing Pull-Up Time T_p, when Spatial Acceleration Varies with Time*, L. E. Ward, OEMsr-769, Technical Paper TC-4-3-45, State University of Iowa, Apr. 7, 1945. Div. 4-421.1-M3

181. *Summary of Data of Tossing 3.5" AR's Obtained with TBM-1C 45473 at Patuxent*, Albert G. Hoyem, OEMsr-769, Technical Paper TC-4-4-45, State University of Iowa, Apr. 14, 1945. Div. 4-422.1-M2

182. *Wind Corrections for the Toss Sight in Forward Firing of Rockets from Aircraft*, M. E. Rolfs, OEMsr-769, Technical Paper TC-4-5-45, State University of Iowa, Apr. 21, 1945. Div. 4-422.1-M3

183. *Pull-Up Angle at Start of Integration*, Phillip G. Hubbard, OEMsr-769, Technical Report TC-4-6-45, State University of Iowa, Revised: July 4, 1945. Div. 4-311.1-M6

184. *Actual Operation of an REIX Combination Unit when Spatial Acceleration Varies with Time*, Phillip G. Hubbard, OEMsr-769, Technical Paper T7-5-1-45, State University of Iowa, May 5, 1945. Div. 4-422.3-M1

185. *The Effect of Change of Angle of Attack of an Airplane on Rocket Tossing Pull-Up Time*, L. E. Ward, OEMsr-769, Technical Paper No. T7-5-2-45, State University of Iowa, May 30, 1945. Div. 4-421.1-M4

186. *Operation of the AN/ASG-10 Mk 1 Mod 2 Bomb Rocket Director for Rocket Tossing*, Irvin H. Swift, OEMsr-769, Technical Report T7-6-1-45, State University of Iowa, June 13, 1945. Div. 4-422.2-M1

187. *The Results Obtained from Launching 5.0" HVAR with the Toss Sight in an F4U-1D at Inyokern*, Phillip G. Hubbard, OEMsr-769, Technical Report T7-6-2-45, State University of Iowa, June 20, 1945. Div. 4-422.1-M5

188. *Summary Report on Rocket Tossing Theory*, Irvin H. Swift, OEMsr-769, Technical Report T7-7-2-45, State University of Iowa, July 25, 1945. Div. 4-421-M3

189. *General Summary of Rocket Tossing Field Tests*, Albert G. Hoyem, OEMsr-769, Technical Report T7-7-3-45, State University of Iowa, July 25, 1945. Div. 4-423-M2

190. *Iowa Experience with Vibration Tests on REIX-T4 Units*, George S. Carson, OEMsr-769, Memorandum MA-11-1-44, State University of Iowa, Nov. 21, 1944. Div. 4-324.3-M2

191. *Preliminary Test Procedure for REIX-T4 Revised for Circuit 326*, George S. Carson, OEMsr-769, Memorandum MA-12-1-44, State University of Iowa, Revised: Feb. 10, 1945. Div. 4-324.3-M5

192. *Temperature Cycling Tests on Shallcross Resistors*, George S. Carson, OEMsr-769, Memorandum MA-12-2-44, State University of Iowa, Revised: Jan. 27, 1945. Div. 4-236-M9

193. *Investigation of Thyratron 2050 Filament Voltage*, John I. Gansert, OEMsr-769, Memorandum MA-1-1-45, State University of Iowa, Jan. 20, 1945. Div. 4-328.2-M1

194. *Investigation of U-Block Vibration*, A. H. Youmans, OEMsr-769, Memorandum MA-1-2-45, State University of Iowa, Jan. 20, 1945. Div. 4-238.6-M1

195. *Integrator Test Procedure*, Lloyd O. Herwig, OEMsr-659, Memorandum MA-1-3-45, State University of Iowa, Jan. 27, 1945. Div. 4-324.3-M3

196. *Supplementary Data on U-Bloek Vibration*, A. H. Youmans and George S. Carson, OEMsr-769, Memorandum MA-2-2-45, State University of Iowa, Feb. 24, 1945. Div. 4-238.6-M2

197. *Summary Technical Report, Contract OEMsr-769*, Chap. 1, State University of Iowa, Sept. 29, 1945. Div. 4-100-M7

198. Progress Reports, State University of Iowa, NDRC-4.

The Magnovox Company

199. *Type Test of AN/ASG-10, Serial 1004 and 1555 July 6 to August 13, 1945*, Magnavox Company. Div. 4-321.1-M3

200. *Quality Control Report for Bomb Director Test Equipment Mk 17 Mod 0, TS-362/ASG-10, Serial 204 and 212*, C. B. Fine and W. Harl, Magnavox Company, Sept. 25 and Sept. 26, 1945. Div. 4-321.4-M5

201. *Type Test of AN/ASG-10A November 26 to 29, 1945*, C. B. Fine and W. Harl, Magnavox Company, November 1945. Div. 4-321.1-M4

202. *Report on AN/ASG-10 Bomb Director Development, Design, and Production* (includes: *Pilot's Operating Manual for Bomb Director Mk 1 Mod 1, AN/ASG-10*, Report CO-NAVAER 08-5S-501, January 17, 1945; *Operator's Manual for Bomb Director Mk 1 Mod 2, AN/ASG-10A*, Report CO-NAVAER 16-5S-524, June 15, 1945; *Handbook of Maintenanee Instructions for Bomb Dirccior Mk 1 Mod 1 AN/ASG-10*, Report CO-AN 16-30 ASG10-7, August 1, 1945), R. H. Dreisbach and N. F. Martin, OSRD Contract OEMsr-1417, Magnavox Company, May 9, 1946. Div. 4-321.1-M5

Raymond Engineering Laboratory, Inc.

203. *A Study of the Properties of Electrical Contact Resistanee under Very Light Pressures and Under Light Electrieal Load*, Lloyd E. Stein [OEMsr-1378], Engineering Report 225, Raymond Engineering Laboratory, Inc., Jan. 6, 1945. Div. 4-750-M1

204. *Test of Electric Gyro Caging Mechanism*, H. H. Raymond, [OEMsr-1378], Report 230, Raymond Engineering Laboratory, Inc., Jan. 27, 1945. Div. 4-325.1-M3

205. *Test of X-2 Altimeter* (A to D), T. H. Carter, [OEMsr-1378], Report 226, Raymond Engineering Laboratory, Inc., Jan. 18, 20, 26, and Feb. 2, 1945. Div. 4-322.5-M1

206. *Tests of Electrie Gyro Caging Mechanism with Electromagnetic Brake*, K. G. Bacheller, [OEMsr-1378], Report 232, Raymond Engineering Laboratory, Inc., Mar. 15, 1945. Div. 4-325.1-M4

207. *Final Technical Report of Raymond Engineering Laboratory, Inc., on Work Done under Contract OEMsr-1378*, Report 238, Raymond Engineering Laboratory, Inc., Oct. 29, 1945. Div. 4-100-M8

Bowen and Company

208. *Pilot Production of Toss Bombing Equipment*, [OEMsr-1227], Electronics Division, Bowen and Company, Inc., May 1945. Div. 4-321.1-M2

OTHER NDRC DIVISION REPORTS

Applied Mathematics Group

209. *Toss Bombing with Target Motion*, Harry Pollard, AMG Working Paper 293, Study 146, AMG-Columbia, Oct. 24, 1944 Div. 4-311-M8

209a. *The Transient of a Single Gyro Sight with Fixed Sensitivity*, Harry Pollard, OEMsr-1007, AMG Working Paper 406, AMG-Columbia, Apr. 24, 1945. AMP-502.1-M22

209b. *The Failure of the Mark 18 as a Collision Course Determiner*, Harry Pollard, AMG Report 371, AMG-Columbia, Feb. 20, 1945. Div. 4-422.1-M1

210. *A Particular Method of Aiming Bombs and Roekets*, Hassler Whitney, OEMsr-1007, AMG Report 335, Study 124, AMG-Columbia, Dec. 15, 1944. AMP-601. 2-M4

210a. *An Introduction to the Analytieal Principles of Lead Computing Sights*, Saunders MacLane, NDRC, AMP Memo 55.1, Mar. 27, 1944. Div. 4-323.1-M1

211. *A Solution of the Azimuth Problem in Toss Bombing*, Harry Pollard, OEMsr-1007, AMG Working Paper 438, Study 146, AMG-Columbia, June 9, 1945. AMP-803.5-M9

California Institute of Technology

212. *A Theory of Toss Bombing*, Harry Pollard, OEMsr-1007, AMP Report 146-IR, AMG Working Paper 411, AMG-Columbia, September 1945. Div. 4-311-M10

213. *Bore Sighting and Effective Angle of Attack Data for Various Aircraft*, OEMsr-418, OSRD 2254, Service Projects OD-162, OD-164, and NO-170, Div. 3 Report CIT/UNC-2, CIT, Oct. 25, 1944. Div. 4-411.4-M1

214a. *F4U-1, F4U-1D, FG-1: Sight Settings for 2.25", 3.5", and 5.0" Aircraft Rockets*, OEMsr-418, OSRD-2271, Div. 3 Report CIT/UNC-4, CIT, Nov. 14, 1944. Div. 4-411.4-M2

214b. *F6F-3, F6F-5: Sight Settings for 2.25", 3.5", and 5.0" Aircraft Rockets*, OEMsr-418, OSRD 2272, Service Projects OD-162, OD-164, and NO-170, Div. 3 Report CIT/UNC-5, CIT, Nov. 18, 1944. Div. 4-411.4-M3

214c. *TBM-1, TBF-1: Sight Settings for 2.25", 3.5", and 5.0" Aircraft Rockets*, OEMsr-418, OSRD 2273, Div. 3 Report CIT/UNC-6, CIT, Nov. 28, 1944. Div. 4-411.4-M5

214d. *TBM-1C, TBF-1C: Sight Settings for 2.25", 3.5", and 5.0" Aircraft Rockets*, OEMsr-418, OSRD 2274, Div. 3 Report CIT/UNC-7, CIT, Dec. 1, 1944. Div. 4-411.4-M6

214e. *SB2C-1, SB2C-1C, SB2C-3, SB2C-4: Sight Settings for 2.25", 3.5", and 5.0" Aircraft Roekets*, OEMsr-418, OSRD 2275, Service Projects OD-162, OD-164, and NO-170, Div. 3 Report CIT/UNC-8, CIT, Nov. 23, 1944. Div. 4-411.4-M4

215. *Method of Computing Trajectories and Sighting Tables for Forward Firing Aircraft Rockets*, L. Blitzer and L. Davis, Jr., OEMsr-418, OSRD 3361, Service Projects NO-33 and NO-170, Div. 3 Report CIT/JPC-17, CIT, Feb. 20, 1944. Div. 4-412.1-M1

216. *Trajectories of Aircraft Rockets: 3.5" and 5.0"*, OEMsr-418, OSRD 2225, Service Projects OD-162, OD-164, and NO-170, Div. 3 Report CIT/UBC-27, CIT, Sept. 25, 1944. Div. 4-412.1-M2

217. *Trajectories of 11.75" Aircraft Rockets*, OEMsr-418, OSRD 2290, Div. 3 Report CIT/UBC-30, CIT, Nov. 17, 1944; Supplementary Data on Improved 11.75" Aircraft Rocket, May 1945. Div. 4-412.1-M3

218. *Trajectories of 5.0" High Velocity Aircraft Rocket and 2.25" Practice Round*, OEMsr-418, OSRD 2314, Div. 3 Report CIT/UBC-32, CIT, Dec. 15, 1944. Div. 4-412.1-M4

Radiation Laboratory, MIT

219. *Use of Radar Range for Toss Bombing*, J. R. Rogers and J. W. Gray, Div. 14 Report 63, [MIT, Radiation Laboratory], Apr. 21, 1943. Div. 4-315-M1

NAVY

Bureau of Ordnance

220. *Bomb Director Mk 1 Mod 0 (AN/ASG-10 (XN))*, *Description and Instructions for Use*, Bur. of Ord. OP 1306 (Preliminary), Apr. 6, 1945.

221. *Ordnance Specifications, Bomb Director Mk 1 Mod 1*, Bureau of Ordnance, NAVORD OS 3606, June 23, 1945 — Modifications: Letter Bu. Ord. (Pr2b), Aug. 7, 1945; Letter Bu. Ord. (Pr2b) Oct. 1, 1945; Letter Bu. Ord. (Pr2b) Nov. 2, 1945.

222. *Ordnance Specifications, Bomb Director Mk 1 Mod 2*, Bureau of Ordnance, NAVORD OS 3892, Nov. 13, 1945 — Modifications: Letter Bu Ord (Pr2b) Nov. 13, 1945; Letter Bu Ord (Pr2b) Jan. 7, 1946.

Bureau of Aeronautics

223. *Installation Specification, Model AN/ASG-10 (XN-1) Airborne Bomb Director Equipment*, Bureau of Aeronautics, NAVAER-EI-144A, May 9, 1945.

224. *Installation Specification Model AN/ASG-10 Airborne Bomb Director Equipment*, Bureau of Aeronautics, NAVAER-EI-153A, June 20, 1945.

225. *Installation Specification for Bomb Director Mk 1 Mod 2 AN/ASG-10A Airborne Installation*, Bureau of Aeronautics, NAVAER-EI-169, July 21, 1945.

226. *Descriptive and Performance Specifications for AN/ASG-10 (XN) Computing Set*, Bureau of Aeronautics, NAVAER-EP-216A, Dec. 22, 1944.

227 *Descriptive and Performance Specifications for AN/ASG-10 Computing Set*, Bureau of Aeronautics, NAVAER-EP-254, Jan 4, 1945 — Modification I, Feb. 12, 1945; Modification II, Apr. 21, 1945.

228. *Descriptive and Performance Specifications for AN/ASG-10A Computing Set*, Bureau of Aeronautics, NAVAER-EP-281, Mar. 5, 1945.

229. *Descriptive and Performance Specifications for AN/ASG-10B Computing Set (Mk 3)*, Bureau of Aeronautics, NAVAER-EP-282A, June 27, 1945.

230. *Test Specification for Bomb Director Mk 1 Mod 0 AN/ASG-10 (XN-1) Airborne Installation*, Bureau of Aeronautics, NAVAER-ET-135, Mar. 31, 1945.

231. *Test Specification for Bomb Director Mk 1 Mod 1, AN/ASG-10 Airborne Installation*, Bureau of Aeronautics, NAVAER-ET-137A, May 7, 1945.

232. *Test Specification for Bomb Director Mk 1 Mod 2, AN/ASG-10A Airborne Installation*, Bureau of Aeronautics, NAVAER-ET-142, Aug. 13, 1945.

232a. *Pilot's Operating Manual for Bomb Director Mk 1 Mod 1, AN/ASG-10*, Report CO-NAVAER 08-5S-501, Jan. 17, 1945. Div. 4-321.1-M5

232b. *Operator's Manual for Bomb Director Mk 1 Mod 2, AN/ASG-10A*, Report CO-NAVAER 16-5S-524, June 15, 1945. Div. 4-321.1-M5

232c. *Handbook of Maintenance Instructions for Bomb Director Mk 1 Mod 1, AN/ASG-10*, Report CO-AN 16-30ASG10-7, Aug. 1, 1945. Div. 4-321.1-M5

Naval Research Laboratory

233. *Final Report on Type Test of AN/ASG-10 (XN) Equipment*, Naval Research Lab., Report C-F42-5 (311-1: IWF-MLB), Serial No. C-310-28/45 (lbr), Feb. 20, 1945.

234. *Final Report on Tests of AN/ASG-10 Cable Insulation Resistance*, Naval Research Lab. Report C-F42-5/A62 (311-1:FWB) Serial No. C-310-102/45 (rab), May 12, 1945.

235. *Interim Report on Type Test of AN/ASG-10*, I. W. Fuller and M. L. Burnett, Naval Research Laboratory R-2609, Aug. 2, 1945.

236. *Final Report on Type Test of TS-362/ASG-10*, Naval Research Lab. Report C-F42-5 (311-1:IWF:MLB), Serial No. C-310-186/45 (mec), Sept. 22, 1945.

237. Excerpts from ACG Field Reports, Airborne Coordinating Group, Naval Research Lab.

Naval Ordnance Plant

238. *Toss Bomb Memoranda*, Naval Ordnance Plant, Lukas-Harold Corp., September 1944–February 1945.

238a. *Gunsight Mark 23*, Research Technical Report No. 18, Naval Ordnance Plant, Lukas-Harold Corp., Mar. 5, 1945.

Naval Air Station, Patuxent River

239. *Preliminary Report of Tests of Toss Bombing with Modified AIBR Equipment and AYF Altimeter, Tactical Test*, Naval Air Station, Patuxent River, Md., Project TED No. PTR-31A11, Mar. 22, 1944.

240. *Final Report on Evaluation of Toss Bombing Equipment, Tactical Test*, Naval Air Station, Patuxent River, Md., Project TED No. PTR-31A11, Serial S-066, Jan. 19, 1945.

241. *Preliminary Report on Comparison of the Tactical Test Toss Bombing Integrator with the Bureau of Standards Integrator* and *Report on Preliminary Flight Tests of the Tactical Test Integrator, Tactical Test*, Naval Air Station, Patuxent River, Md., Project TED No. PTR-31A75, Serial S-070, Feb. 20, 1945.

242 *Requirements and Recommendations for A Sight to be Used with AN/ASG-10 Equipment. Tactical Test*, Naval Air Station, Patuxent River, Md., Project TED No. PTR-31A75, Serial C-0106, Feb. 24, 1945.

243. *Interim Report on Development of AN/ASG-10 (XN) and AN/ASG-10, Taetieal Test,* Naval Air Station, Patuxent River, Md., Project TED No. PTR-31A75, Serial C-0114, Apr. 10, 1945.

244. *Final Report on Test of Toss Bombing Equipment in the F4U Airplane, Taetieal Test,* Naval Air Station, Patuxent River, Md., Project TED No. PTR-31A52, Serial S-076, Apr. 27, 1945.

245. *Final Report on Taetieal Evaluation of Computing Set AN/ASG-10 (XN) in SB2C-3, -4 Airplanes, Taetieal Test,* Naval Air Station, Patuxent River, Md., Project TED No. PTR-31A68, Serial S-081, May 28, 1945.

246. *Interim Report on Taetieal Evaluation of AN/ASG-10 at Safest Attacking Conditions, Taetical Test,* Naval Air Station, Patuxent River, Md., Project TED No. PTR-31A91, Serial C-762, June 22, 1945.

247. *Interim Report on Taetical Evaluation of AN/ASG-10 at Safest Attaeking Conditions in the F4U-4 Airplane, Tactical Test,* Naval Air Station, Patuxent River, Md., Project TED No. PTR-31A91, Serial C-711, July 26, 1945.

248 *Interim Report on Taetieal Evaluation of AN/ASG-10 in the SB2C-5 Airplane at Attaeking Conditions whieh will Afford a High Degree of Safety, Taetieal Test,* Naval Air Station, Patuxent River, Md., Project TED No. PTR-31A91, Serial C-782, Sept. 13, 1945.

249. *Final Report on Tactical Evaluation of Roeket Tossing with Modified AN/ASG-10 (XN) Computing Set, Tactieal Test,* Naval Air Station, Patuxent River, Md., Project TED No. PTR-31A70, Serial S-088, Sept. 26, 1945.

249a. Letter, Serial C-0105, Tactical Test, Naval Air Station, Patuxent River, Md., Feb. 20, 1945.

250. *Installation of AN/ASG-10(XN) in TBM-3 Airplane No. 22875, Radio Test,* Naval Air Station, Patuxent River, Md., Project TED No. PTR-31733.0, Dec. 4, 1944.

251. *Prototype Installation and Flight Test of AN/ASG-10 (XN) Equipment in SB2C-4 Airplane, Radio Test,* Naval Air Station, Patuxent River, Md., Project TED No. PTR-31723.0, Mar. 17, 1945.

252. *Flight Test of Prototype Installation of Bomb Direetor Mk 1 Mod 1, AN/ASG-10 in TBM-3E Airplane No. 69172, Radio Test,* Naval Air Station, Patuxent River, Md., Project No. PTR-31803.1, Apr. 14, 1945.

253. *Flight Test of Bomb Director Mk 1 Mod 1, AN/ASG-10, in TBM-3E Airplane BuNo 85510, Radio Test,* Naval Air Station, Patuxent River, Md., Project No. PTR-31803.2, May 7, 1945.

254. *Flight Test of Bomb Direetor Mk 1 Mod 1, AN/ASG-10 in FG-1-D Airplane BuNo 76628, Radio Test,* Naval Air Station, Patuxent River, Md., Project TED No. PTR-31818.0, May 12, 1945.

Naval Air Station, Asdevlant, Quonset Pt.

255. *Toss Bombing at Low Altitude,* Project 538, Asdevlant, Naval Air Station, Quonset Pt., R. I., letter ASDD/F41, Serial 00118, Oct. 6, 1944.

255a. *Toss Bombing Combined with Ballistic Aiming,* Asdevlant, Naval Air Station, Quonset Pt., R. I., Letter ASDD/F41, Serial 118, Oct. 16, 1944.

256. *Interim Report on Bomb (Roeket) Direetor Mk 1 Mod 0,* Asdevlant Naval Air Station, Quonset Pt., R. I., Project 538, Serial 099, Mar. 1, 1945.

257. *Report on Bomb Direetor Mk 1 Mod 0 (AN/ASG-10),* Asdevlant, Naval Air Station, Quonset Pt., R. I., Project 538, Serial 0256, May 23, 1945.

258. *Report on Toss-Roekets (Bomb Direetor Mk 1 Mod 0, AN/ASG-10XN),* Asdevlant, Naval Air Station, Quonset Pt., R. I., Project 538, Serial 0286, June 11, 1945.

259. *Report on Simultaneous Tossing of Bombs and Roekets with Bomb Director Mk 1 Mod 0 (AN/ASG-10XN),* Asdevlant, Naval Air Station, Quonset Pt., R. I., Project 538, Serial 0487, Sept. 20, 1945.

Naval Ordnance Test Station, Inyokern, California

259a. *Interim Report on Test of Bomb Direetor Mark 1 Mod. 0, AN/ASG-10 for Roeket Fire Direetion (F6F-5 Plane),* NOTS Project No. 23.3 AS.

259b. *Interim Report on Test of Bomb Direetor Mark 1 Mod. 0, AN/ASG-10 for Rocket Fire Direetion (F4U-1D Plane),* NOTS Project No. 23.3 AS.

ARMY

Ordnanee Department

260. *A Simplified Method of Sighting and Releasing Bombs from Airplanes,* Lt. Col. H. S. Morton, Ordnance Department, Feb. 13, 1943.

261. *Preliminary Mathematieal Analysis of Toss Bombing,* Lt. Col. H. S. Morton, Ordnance Department, Feb. 13, 1943.

262. *General Teehnique for Bombing Stationary or Moving Targets,* Lt. Col. H. S. Morton, Ordnance Department, Feb. 22, 1943.

263. *Plane-to-Plane Bombing: Mathematieal Study of the Timing Funetion of the Aeeeleration Integrator,* Lt. Col. H. S. Morton, Ordnance Dept., Feb. 25, 1943.

264. *Eleetrieal Integrator and Timer,* Lt. Col. H. S. Morton, Ordnance Dept., June 16, 1944.

AAF

265. *Preliminary Report on Test of Bombing Attaek on Airplanes in Formation; Toss Bombing with Radar Range Phase,* Proof Department, AAF Proving Ground Command, Eglin Field, Fla., Serial No. 1-42-60, Aug. 19, 1943.

266. *Air-to-Ground Toss Bombing Using Aeeeleration Integrator,* AAF Center, Orlando, Fla. (AAF Proving Ground Command, Eglin Field, Fla.), AAF Board Project No. Q3648, Aug. 8, 1945.

267. *Fighter Bomber Aecuraey Against Ground Targets,* AAF Center, Orlando, Fla. (AAF Proving Ground Command, Eglin Field, Fla.), AAF Board Project No. 4296C373.11, Oct. 29, 1945.

268. *Final Report on Training Method and Evaluation of the Aeeeleration Integrator Bomb Release,* Training Research and Liaison Section, Williams Field, Chandler, Arizona, Project No. 7-2-45, Nov. 27, 1945.

ORS, 9th AF Hq.

269. *A Report on the Aeceleration Integrator Bomb Release (AIBR) in the Ninth Air Force*, Operational Research Section, 9th AF Headquarters, No. 107, Mar. 26, 1945.

270. *Flight Calibration of Toss Bombing Equipment in P-47 Airplane*, Research Section, 9th AF Headquarters, No. PWA-28-4A, Apr. 5, 1945, revised May 8, 1945.

271. *Operations of Toss Bombing Equipment in P-47-D Airplane*, Research Section, 9th AF Headquarters, No. PWA-28-4A(1), Apr. 5, 1945, revised May 8, 1945.

272. *Notes on the Inspection and Testing of Toss Bombing Equipment for Installation*, Research Section, 9th AF Headquarters, No. PWA-28-4A (2), Apr. 5, 1945, revised May 8, 1945.

273. *Maintenance Notes for AIBR (AN/ASG-10(XN))*, Research Section, 9th AF Headquarters, No. PWA-28-4A(3), Apr. 5, 1945, revised May 8, 1945.

274. *Instructions for Installation: Bomb Director Mk 1 Mod 0 (AN/ASG-10XN) in P-47D Airplane*, WF-O-1, 150, W16609, August 1945.

OSRD APPOINTEES

Division 4

Chief

Alexander Ellett

Technical Aides

A. S. Clarke
Sebas'ian Karrer
Cathryn Pike
John S. Rinehart
E. R. Shaeffer
A. G. Thomas
R. M. Zabel

Members

L. J. Briggs
W. D. Coolidge
Harry Diamond
F. L. Hovde
J. T. Tate

Special Assistants

M. G. Domsitz
W. E. Elliott
Wendell Gould
W. S. Hinman, Jr.
Joseph Kaufman
J. L. Thomas
E. A. Turner
F. C. Wood

Consultants

A. V. Astin
R. A. Becker
R. M. Bowie
Cledo Brunetti
J. W. DuMond
Saul Dushman
Wm. Fondiller
T. B. Godfrey
L. R. Hafstad
J. E. Henderson
R. D. Huntoon
J. A. Jacobs
R. B. Janes
T. Lauritsen
D. H. Loughridge
W. B. McLean
F. L. Mohler
S. H. Neddermeyer
H. F. Olsen
C. H. Page
W. J. Shackelton
F. B. Silsbee
K. D. Smith
G. W. Stewart
J. F. Streib
L. S. Taylor
G. W. Vinal
W. L. Whitson
R. M. Zabel

Contract Number	*Name and Address of Contractor**	*Subject*
OEMsr-769	University of Iowa Iowa City, Iowa	Studies and experimental investigations in connection with development work on special electronic devices and associated equipment.
OEMsr-1227	Bowen and Company, Inc. Bethesda, Maryland	Furnish necessary machine shop and assembly facilities for the development of special electronic devices.
OEMsr-1378	Raymond Engineering Laboratory Berlin, Connecticut	Studies and experimental investigations in connection with development of special electronic devices.
OEMsr-1417	The Magnavox Company Fort Wayne, Indiana	Design toss bombing equipment for production.

* The National Bureau of Standards, which served as the central laboratories for Division 4, NDRC, did not operate under a contract but as a government agency under a direct transfer of funds from OSRD.

SERVICE PROJECT NUMBERS

The projects listed below were transmitted to the Executive Secretary, NDRC, from the War or Navy Department through either the War Department Liaison Officer for NDRC or the Office of Research and Inventions (formerly the Coordinator of Research and Development), Navy Department.

Service Project Number	*Subject*
Army Air Forces AC-62	Development of toss bombing equipment.
Navy NO-185	Development of toss bombing equipment.
Ordnance Department OD-112	Development of toss bombing equipment and techniques.

INDEX

The subject indexes of all STR volume are combined in a master index printed in a separate volume. For access to the index volume consult the Army or Navy Agency listed on the reverse of the half-title page.